Distribution Agreement

In presenting this thesis or dissertation as a partial fulfillment of the requirements for an advanced degree from Emory University, I hereby grant to Emory University and its agents the non-exclusive license to archive, make accessible, and display my thesis or dissertation in whole or in part in all forms of media, now or hereafter known, including display on the world wide web. I understand that I may select some access restrictions as part of the online submission of this thesis or dissertation. I retain all ownership rights to the copyright of the thesis or dissertation. I also retain the right to use in future works (such as articles or books) all or part of this thesis or dissertation.

Signature:

_____ _____

Andrew R. Mahoney Date

Overcoming Antibacterial Resistance through Synthesis of Small Molecules Targeting Efflux Mechanisms

By

Andrew R. Mahoney
Doctor of Philosophy

Chemistry

William M. Wuest, Ph.D.
Advisor

Frank McDonald, Ph.D.
Committee Member

Huw M. L. Davies, Ph.D.
Committee Member

Accepted:

Kimberly Jacob Arriola, Ph.D.
Dean of the James T. Laney School of Graduate Schools

Date

Overcoming Antibacterial Resistance through Synthesis of Small Molecules Targeting Efflux Mechanisms

By

Andrew R. Mahoney

B.S., Gettysburg College, 2017

Advisor: William M. Wuest, Ph.D.

An abstract of
A dissertation submitted to the Faculty of the
James T. Laney School of Graduate Studies of Emory University
in partial fulfillment of the requirements for the degree of
Doctor of Philosophy
in Chemistry
2023

Abstract

Overcoming Antibacterial Resistance through Synthesis of Small Molecules Targeting Efflux Mechanisms

By Andrew R. Mahoney

Antibiotic resistance remains a dire threat to humanity. Mechanisms through which this resistance occurs in bacteria are intricate but warrant extensive study due to the widespread ramifications of this crisis. Efflux of small molecule antibiotics is a particularly understudied mechanism due to limitations in structural biology and screening techniques, but has been identified for virtually every class of antibiotic. This thesis details efforts to probe structural features and substrate recognition of bacterial efflux systems, and to examine potential ways to circumvent them.

The first chapter contextualizes bacterial resistance development, presented first from an evolutionary standpoint, detached from its implications on human health. It is followed by an anthropocentric perspective, analyzing humanity's understanding of microorganisms' roles in disease throughout history. It concludes with analysis of the prevalence of bacterial resistance development and strategies for slowing this phenomenon.

The second chapter details synthetic efforts towards novel promysalin analogs. This natural product is a potent metabolic inhibitor of *Pseudomonas aeruginosa*, but suffers from several key structural liabilities, allowing for bacterial resistance development. Methods to synthesize and biologically examine analogs designed to circumvent two hypothesized mechanisms (efflux and hydrolysis) of promysalin resistance are described.

The third chapter describes investigations into the *P. aeruginosa* efflux pump MexXY-OprM. Because of the relative lack of information regarding substrate recognition and efflux by MexXY-OprM, we undertook collaborative efforts to understand this system, entailing computational screening, biological analysis, and synthesis of a number of berberine analogs with potential as efflux pump inhibitors.

The fourth chapter explores natural product tricepyridinium, a molecule whose antibiotic activity may be attributed either to membrane permeabilization or DNA intercalation. Biological and computational analysis of the natural product and four synthetic analogs designed to investigate this class of molecules' cellular target revealed that several of these analogs showed evasion of bacterial efflux.

The fifth chapter investigates inhibition of bacterial metal chelation, a promising avenue for treatment. Synthesis of ten recently-identified lumazine peptides hypothesized to function as fungal metallophores was thus pursued. While inhibition assays revealed no antibacterial activity for these molecules, efforts are ongoing to determine the role of these compounds in the producing species.

Overcoming Antibacterial Resistance through Synthesis of Small Molecules Targeting Efflux Mechanisms

By

Andrew R. Mahoney

B.S., Gettysburg College, 2017

Advisor: William M. Wuest, Ph.D.

A dissertation submitted to the Faculty of the
James T. Laney School of Graduate Studies of Emory University
in partial fulfillment of the requirements for the degree of
Doctor of Philosophy
in Chemistry
2023

Acknowledgements

The people I wish to thank are innumerable. We are all products of our interactions with others, defined by the experiences we share with friends, enemies, colleagues, lovers, and family. I would not be the person I am today if not for every person with whom I have shared a smile, a laugh, or a tear. The following list of acknowledgements is therefore woefully incomplete. Nevertheless, there are some who deserve recognition above all others.

I would first like to thank my sister Elaine. Her constant wisdom and support have been singlehandedly the most powerful guides I have had, and without them I would have left the graduate program years ago. My father, through incessant chemistry and physics discussions, undoubtedly drove me to pursue a career in the natural sciences in the first place. My late sister Kate always provided me with smiles at our family gatherings, and gave me my competitive spirit. In addition, my late mother Janet sacrificed everything for my siblings and me, and instilled many of the positive traits I retain today, such as my sense of humour, my attention to detail, and my ability to always find things to smile about.

It nearly goes without saying, but I must acknowledge the tremendous support I have been given by my chemistry mentors. My first advisor, Dr. Timothy Funk, instilled a drive and passion for chemistry that persists to this day. Kathryn Zimmerman was my first labmate in Dr. Funk's lab, and was simultaneously incredibly brilliant and endlessly patient with me struggling to learn the basics of existence in an organic chemistry laboratory. My PhD advisor, Dr. William Wuest, in addition to providing me a stage on which to perform for the last several years, also taught me the importance of balancing scientific independence with mentorship. My committee members, Dr. Frank McDonald and Dr. Huw Davies, also drove me to think more critically than I thought possible, and their discussions at my milestones contributed to many of the hypotheses herein.

My friends within and without the chemistry department made the past five years enjoyable, a miraculous feat in graduate school. In particular, Christian Sanchez and Hannah Gold have always been willing to banter and crack jokes to lighten the mood when spirits are low, or have meaningful discussions when times demand it. Ingrid Wilt and Maizie Lee provided me with much-needed distractions in the form of coffee trips to Emory Village. Marina Michaud and Amber Scharnow reminded me that there is a life outside of graduate school, and I miss our nights watching trashy shows together. The boundless enthusiasm of my mentees, Drason Zhang and Michelle Garrison, refreshed my own passions for chemistry, and I wish them both the best. I am grateful to have shared the lab with fellow cohort and dear friends Adrian Demeritte, Ryan Allen, Cassie Zaremba, for pursuing this journey with me. I must also begrudgingly acknowledge those who were not supportive of me, as they nevertheless drove me to complete my doctorate out of sheer spite.

I would like to thank my cat, Gobi, who has enjoyed the past month having me at my apartment to write and cuddle with him. I am grateful that he is now fonder of biting his toys than biting me.

I would like to thank the developers of the Microsoft Windows Snipping Tool, unsung heroes who have undoubtedly saved me countless hours saving and cropping images, especially for this dissertation.

And lastly, reader, I would like to thank you.

Table of Contents

Table of Figures

Table of Schemes

Table of Tables

Chapter 1 - Introduction to Bacterial Infections and Resistance

1.1 An Evolutionary Perspective

1.1.1 The origin of life and evolution of early bacteria.

In an observable universe estimated to encompass 93 billion light years, 125 billion galaxies, and an incalculable number of planets, Earth (as of March 2023) remains the only planet known to harbor life.[1] The origin of life on Earth is subject to intense debate but is largely accepted by the scientific community to have begun between 3.77 and 4.28 billion years ago, shortly – on a cosmic timescale – after the formation of Earth itself (**Figure 1.1**).[2-3] The earliest forms of life are posited to be aquatic extremophiles, utilizing thermal energy from sources such as oceanic hydrothermal vents or geothermal springs to drive biochemical processes, contrasting from many modern organisms whose energy source is solar in origin.[4–6] In this early environment, mineral-rich (e.g. FeS and NiS) sediments can catalyze the formation of biomolecules from the abundance of methane, ammonia, CO_2, and H_2S present.[7,8] Accumulation of these biomolecules to form what scientists lovingly refer to as "prebiotic soup" was necessary for more complex interactions. When the right combination of these biomolecules became encapsulated in a micelle of amphiphilic molecules such as phospholipids (but more likely fatty acids), the first cells came into being.[9–11]

It is generally accepted that all current life on Earth originated from a common ancestor, supported by a variety of evidence including the universal chirality of amino acids, the use of ATP as an energy source, and a universal genetic code. The first organisms were anaerobic and prokaryotic (lacking nuclei and other membrane-bound organelles) but due to the morphological similarity of their fossils, it is unclear which of the domains Bacteria and Archaea diverged first from their common ancestor.[6,12,13] This is further obscured by the process of horizontal gene transfer, a mechanism by which organisms can directly share genetic information with each other. This

phenomenon complicates the task of retrospectively assembling an evolutionary history, as much of the genetic information has been swapped innumerable times between cells.[14,15]

Despite their outward similarity in appearance, bacteria and archaea are less evolutionarily related than eukarya and archaea.[16] One readily apparent difference between bacteria and archaea is the former's incorporation of the protein-sugar complex peptidoglycan into their cell walls. Another key difference between the two domains is in that of metabolism – archaea cannot use light as a source of energy to produce oxygen, whereas many photosynthetic bacteria (cyanobacteria) exist.[17] Indeed, the evolution of photoautotrophic bacteria some 2.7 billion years ago had catastrophic effects on Earth's biosphere; oxygen was a toxic byproduct to many organisms and its rapid accumulation turned Earth's atmosphere from a weakly reducing environment to a strongly oxidizing one.[16–18] This so-called Great Oxidation Event lasted roughly 400 million years and is speculated to have caused the first of Earth's mass extinctions (**Figure 1.1**).[19]

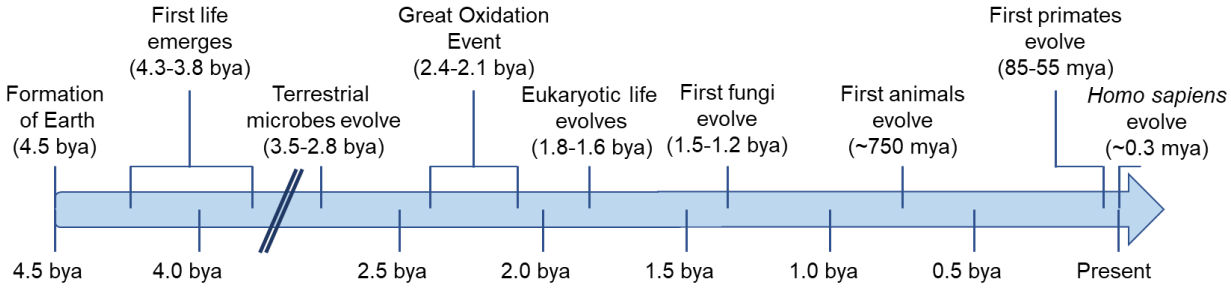

Figure 1.1. Timeline of the history of evolution

However, the increase in free energy available to organisms following the Great Oxidation Event also led to a rapid diversification of life. Bacteria developed pathways to utilize either aerobic or anaerobic metabolism depending on their species and their environment (in contrast, nearly all archaea are anaerobic and live in regions where oxygen is scarce or nonexistent).[20] Eukaryotic organisms evolved, containing an endomembrane network and nuclei, allowing for greater cell size and complexity.[21,22] All eukaryotic organisms contain at least one mitochondrion (with the

exception of *Monocercomonoides*), the likely result of an endosymbiotic relationship between a redox-capable bacterial organism which was later engulfed.[23,24] Due to the advantages of cooperative living (see below for a description of quorum sensing and biofilm formation in bacteria) in a harsh, toxic environment such as a hydrothermal vent or graduate school, multicellular life has evolved independently many times, giving rise to fungi, plants, and animals.[25] In some species of fungi and plants, a second endosymbiotic relationship with bacteria has evolved, giving rise to a photosynthetically-active organelle known as a chloroplast.[26,27]

The Gram stain is an assay by which bacteria are often divided into two classes. In this assay, crystal violet and iodine are applied to a culture of bacteria, staining the cells purple. Washing these cells with ethanol or acetone removes the coloration from one class of bacteria, referred to as gram-negative bacteria (often, a counterstain such as safranin is used to stain these cells a different color to facilitate visualization). Cells remaining purple after the washing step are called gram-positive bacteria. Gram-positive bacteria are generally characterized by a single outer membrane surrounded by a thick layer of peptidoglycan, a substance composed of sugars and amino acids. In contrast, gram-negative bacteria contain an inner (cytoplasmic) membrane as well as a second bacterial outer membrane coated in lipopolysaccharide (an antigen and immunogen). Between these two membranes is a region called the periplasm, containing a variety of enzymes, ions, and a very thin layer of peptidoglycan (**Figure 1.2**).[28,29]

The Gram stain classification of bacteria, though useful in understanding bacterial structure, is not an indicator of taxonomic lineage. It is generally believed that ancestral bacteria were gram positive, and that the evolution of a second membrane allowed for a fitness advantage in the presence of chemical toxins.[30] However, this evolution is known to have occurred multiple times, meaning that two species of gram-negative bacteria are not always more evolutionarily related to each other than to a gram-positive species.[31,32] Nevertheless, due to its utility and relative ease of determination in an unknown species, this classification system has been widely adopted by the scientific community.

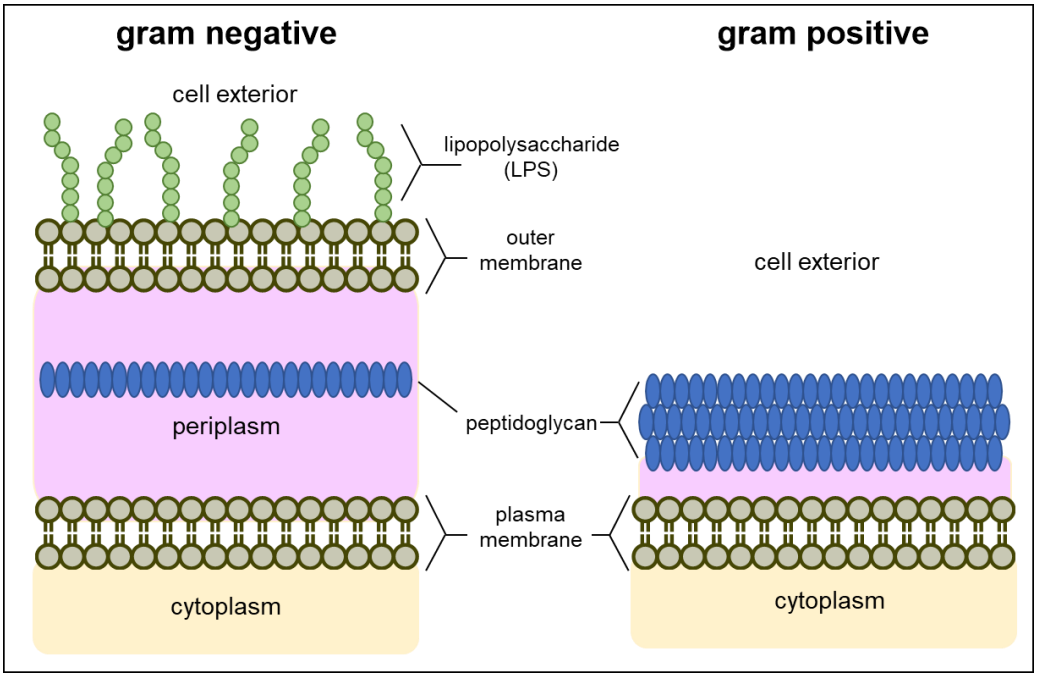

Figure 1.2. Structural characteristics of gram positive and gram negative bacterial membranes

1.1.2 Bacterial communities and evolutionary pressures.

Outside of laboratory settings, microbes exist in a wide variety of environments as complex consortia. These communities usually consist of many species of bacteria, as well as fungi and other unicellular eukaryotes (protists and some plants). This allows multiple species to operate to fill separate ecological niches for which they are particularly well-suited.[33,34] For example, in a

plant rhizosphere (the layer of soil containing the plant's root system, bacteria may serve to fix nitrogen into ammonia, and fungi may form symbiotic or parasitic relationships with plants to absorb or channel nutrients. These communities often exhibit high selective pressure due to the number of species present and competition for limited resources.[35] As a result, these species must be able to quickly adapt to minute changes in the environmental conditions in order to survive.[36]

Communication between or within organisms is a fundamental property of all life. This communication can take many forms and can be on scales as minute as cellular signaling. Bacteria rely on communication in order to adapt to changing conditions in their environment.[37,38] One predominant mechanism by which bacteria communicate with one another is via quorum sensing. This specific process allows cells to detect and respond to changes in population density and relies on secretion of a small molecule (auto-inducing peptides in gram-positive bacteria or N-acyl homoserine lactone in gram-negative bacteria) into the surrounding environment.[39,40] Bacteria express a number of receptors for these signaling molecules on their cell exteriors; when these receptors are bound to their substrates in sufficient quantities - that is, when the density of a population secreting these molecules is high - a signaling cascade results in a standardized phenotypic change in the bacterium. These phenotypes can vary according to species, but often include factors governing cell motility, expression of virulence factors, and formation of biofilms.[41–43]

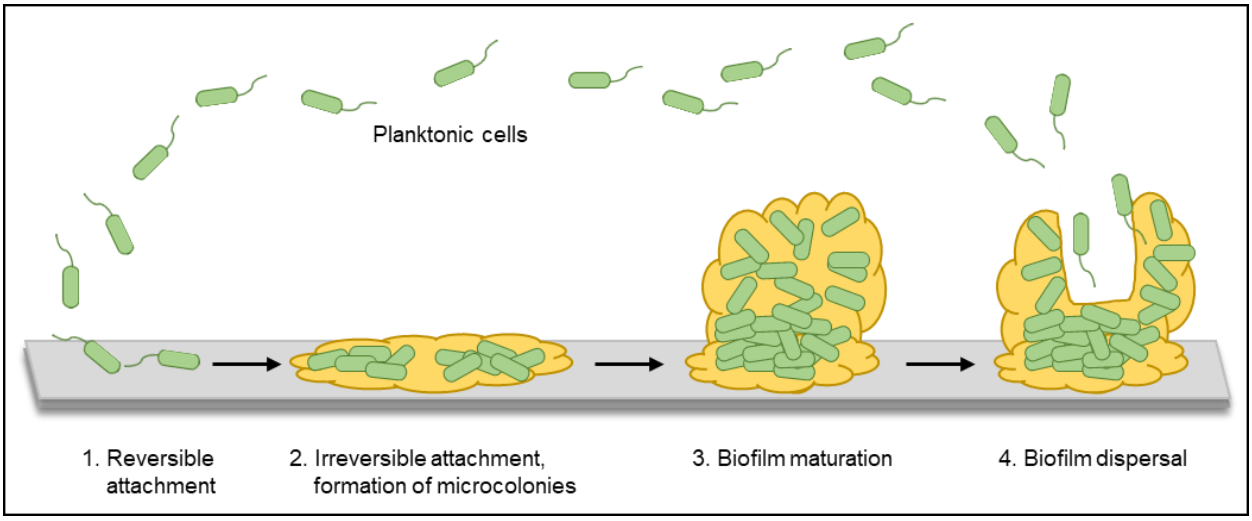

Figure 1.3. Life cycle of biofilm formation and dispersal

Biofilms are another type of complex microbial community, usually consisting of a variety of different microorganisms (**Figure 1.3**).[44] In this state, cell density is high, with the cells adhered to one another and to a solid surface via a sticky matrix consisting of extracellular polymeric substances (EPS).[45] These biofilms can form on virtually any surface and confer a number of advantages to their constituent cells.[45,46] As in rhizospheral communities, different microbial species may play different roles overall contributing to continued success of the biofilm.[44]

Due to the constant force of natural selection and competition for resources in many biological communities, microorganisms evolve diverse ways of improving their own fitness or decreasing the fitness of others. One way the latter occurs is via the targeted secretion of toxic metabolites in the presence of particular species (**Figure 1.4**).[47–49] Antibiotic production is ubiquitous across biological kingdoms, and these molecules can operate in a number of ways to disrupt vital cell processes in their target organisms. The production of these molecules can be quite complex, utilizing intricate biochemical machinery in a controlled manner so as not to subject the producing organism to the compound's toxic effects.[50,51] In response, target organisms may develop

resistance to these antibiotics. There is therefore a constant, microscopic evolutionary dance between the development of more powerful antibiotics and more elegant ways of evading them.

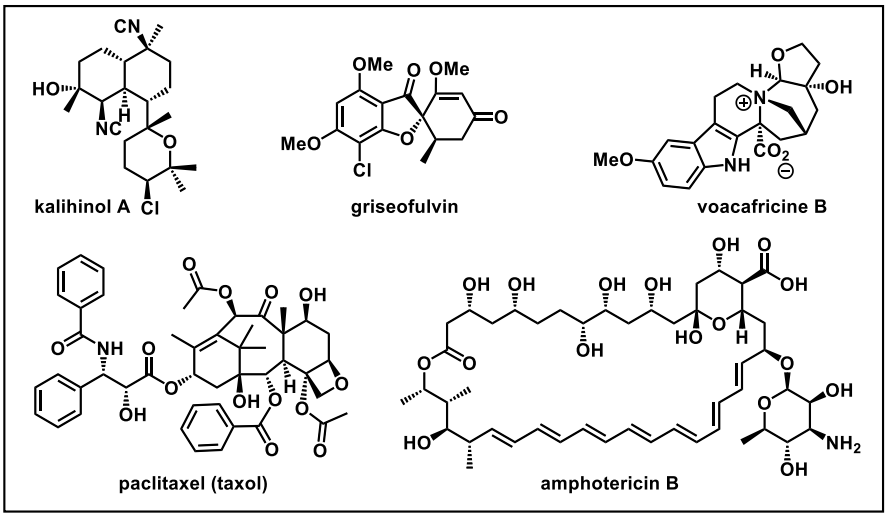

Figure 1.4. Diverse chemical scaffolds of naturally produced secondary metabolites

1.2 An Anthropocentric Perspective

The relationship between humans and microorganisms has historically been complex. Humans have always relied on bacteria and fungi as direct food sources, in fermentation to create bread, cheeses, and alcoholic beverages, and for breaking down organic matter.[50] Similarly, we ourselves are colonized by a vast number of bacteria (estimates reveal about a 1:1 proportion of bacterial cells to human cells), archaea, and fungi most of which are either commensal or mutualistic.[51] Mutualistic intestinal microorganisms have been implicated in numerous roles such as helping host metabolism, targeted immune response, and promotion of angiogenesis.[52,53] However, invasive bacteria have also been implicated in a large number of diseases; for the vast majority of human existence, infections were the leading cause of death. These pathogenic bacteria can have a variety of deleterious effects on human physiology, often producing toxins to cause direct damage to tissues and sequestering nutrients.

For much of human existence, the biological cause of disease was unknown. The first recorded example of medicinal treatment of infection dates back to the 3rd millennium BCE, when ancient Egyptian physicians such as the famed Imhotep would wrap wounds with poultices made with natural sources such as honey, dates, cannabis, or incense.[54,55] Some ancient infections were treated using moldy bread, providing evidence that though the causative agent of disease was unknown, natural products and extracts have been identified as potential therapies for ailments since the dawn of civilization.[55] Similarly, traditional Chinese medicine dates back thousands of years and frequently employs herbal extracts; though the efficacy of such medicinal practices compared to Western medicine remains hotly contested, several examples have been accepted as effective treatments, such as the use of artemisinin as an antimalarial.[56]

The discovery of germ theory (that many diseases are caused by infectious agents such as microoorganisms and viruses) evolved over many centuries. The ancient Indian medical treatise the Sushruta Samhita is the first written text referencing the notion that diseases can be transmitted from one person to another, and advocated for practices of good hygiene to prevent the spread of contagion.[57] Much later (ca. 13th century CE), Islamic scholars correctly identified that a sickness could be transmitted from one person to another via contaminated water, food, and clothing, implying that some unseen force or entity was lingering in these places.[58] The advent of microscopy in the 1600s allowed for identification of this entity: microorganisms present in virtually every substance, the discovery of which is often credited to Kircher and van Leeuwenhoek.[59] About a century later, Louis Pasteur provided conclusive evidence that these microorganisms were the causative agents of diseases, and that destruction of these microorganisms could cure these diseases.[60]

Shortly after the scientific community's acceptance of germ theory following Pasteur's experiments in the late 19th century, the development of novel treatments for the killing of microorganisms (antibiotics) began. The first example of this process was conducted in the 1890s, in which German physicians isolated infectious bacteria (*Pseudomonas aeruginosa*) from a wound and found that by co-culturing this bacterium with other known infectious agents (the bacteria causing either cholera, typhoid, diphtheria, or anthrax), *P. aeruginosa* was able to inhibit the growth of the other species. Extracts of the isolated *P. aeruginosa* strain and purification of the chemical compounds responsible for these effects resulted in the first antibiotic, pyocyanase (**Figure 1.5, left**).[61] While clinical use of this drug was later abandoned due to its toxicity (likely caused by impure samples contaminated with toxic phenazines also produced by *P. aeruginosa*), the pyocyanase story demonstrated that one infectious agent could kill another, and that naturally-produced compounds are a promising therapeutic avenue.

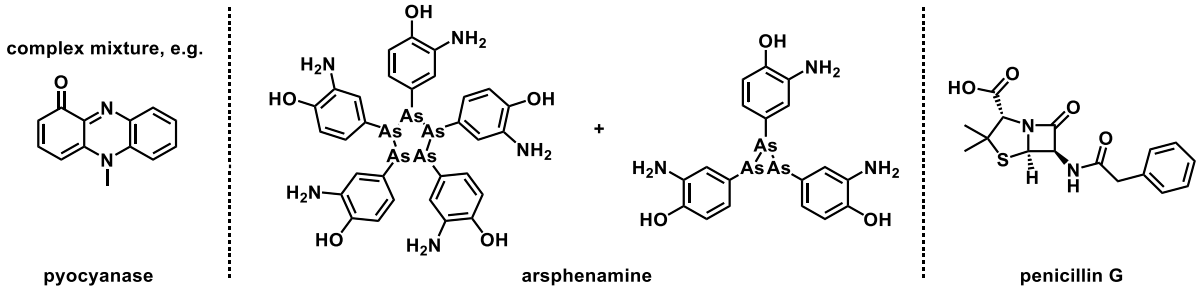

Figure 1.5. Active components of the first three clinical antibiotics

Scientific groups began pursuing the development of new antibiotics, particularly ones that had high selectivity for bacterial cells while leaving human cells unaffected. In 1909, Paul Ehrlich's laboratory performed the first example of a successful structure-activity relationship study, synthesizing a series of arsenic-based compounds which ultimately resulted in the discovery of a cure for syphilis in the form of arsphenamine (Salvarsan, **Figure 1.5, middle**).[62]

The serendipitous discovery of penicillin by Alexander Fleming (**Figure 1.5, right**) and subsequent improvements in its isolation and purification propelled the world into what has been described the "golden era of antibiotics." The clinical success of this drug inspired the development of many other antibiotics; use of a co-culturing strategy of two microorganisms to encourage production of antibiotics (mimicking the natural production of these compounds in microbial consortia) was common.[63] Novel classes of antibiotics targeting different cell processes were discovered, including aminoglycosides (protein synthesis inhibitors), macrolides (RNA synthesis inhibitors), and fluoroquinolones (DNA replication inhibitors) (**Figure 1.6**).[64]

Due to the advent of antibiotics, death rate due to infection fell dramatically and overall life expectancy of humans increased considerably. Unfortunately, the successes of the 1900s did not ultimately eliminate the universal threat of bacterial infection. Despite countless successful treatments over the next hundred years and innumerable saved lives, the co-culture strategy for the discovery of novel antibiotics saw diminishing returns, with the same compounds being isolated

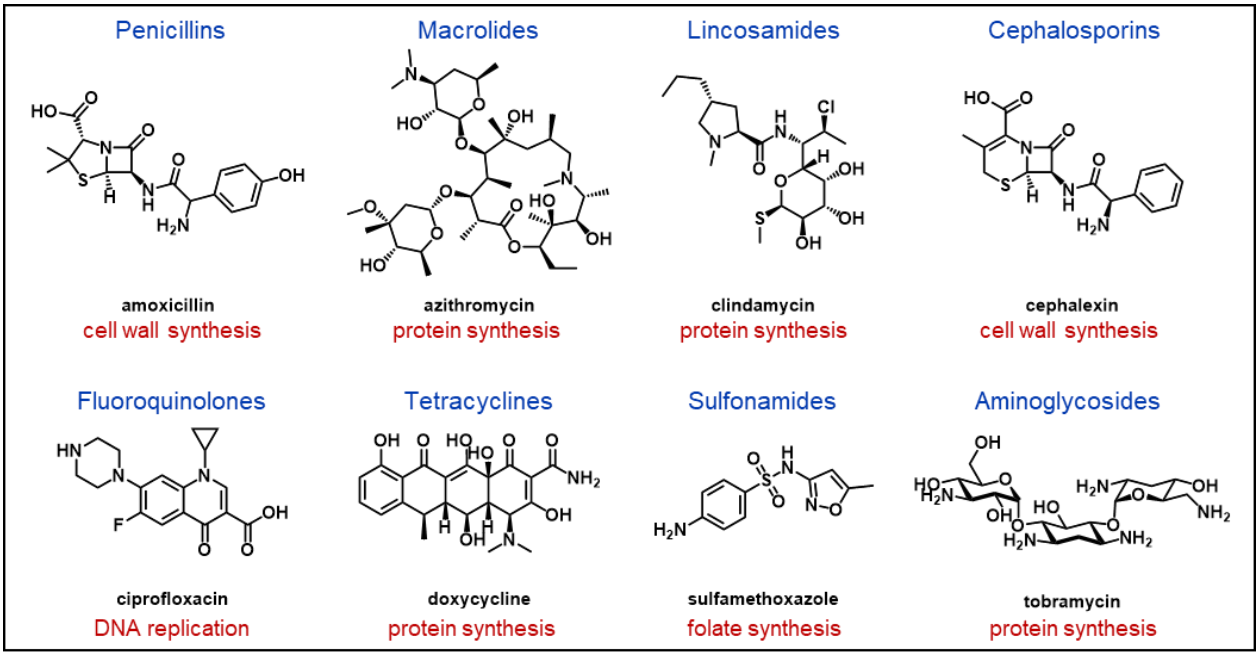

Figure 1.6. Major classes of antibiotics, representative examples, and intracellular targets of inhibition

again and again.[63] A corresponding decrease in financial incentive (reinforced by disincentives for approval of antibiotics by the FDA and a shift towards development of profitable treatments for cancer and chronic disease) for the research into development of novel antibiotics led to the downsizing and shuttering of many pharmaceutical antibiotic programs.[65,66] Furthermore, the ever worsening threat of bacterial resistance to antibiotic treatment has begun to severely limit their usage in clinical contexts.

1.3 Antibiotic Resistance

As is the case in natural microenvironments, exposure of a bacterial species to an antibiotic compound introduces an aspect of high selective pressure. At sub-inhibitory concentrations, there is a large advantage conferred to a bacterial population that can withstand the effects of a toxin. As a result, the use of antibiotics to treat against infections inherently selects for resistance against that treatment. The first report of clinical antibiotic resistance came in 1924, when a strain of syphilis-causing bacteria was found to no longer be susceptible to Salvarsan.[67] Fleming himself predicted the rise of antibiotic resistance, being quoted as saying "The time may come when penicillin can be bought by anyone in the shops. Then there is the danger that the ignorant man may easily under-dose himself and by exposing his microbes to nonlethal quantities of the drug make them resistant."[68] Indeed, resistance has been observed for every class of antibacterial drug used clinically. This resistance often develops within years of its introduction as a treatment (in some case, even predating its clinical use) (**Figure 1.9**). This is of no surprise, as most antibiotics are natural products or derivatives thereof, and likely were being produced by their native species countless years ago to combat bacteria, which have had equal time to evolve mechanisms of resistance. Clinical resistance therefore often results from a combination of these resistance genes

developing via *de novo* mutations and being acquired via horizontal gene transfer from other strains or species.

The biochemical mechanisms of bacterial antibiotic resistance are complex but can generally be divided into three categories (**Figure 1.7**).[69] First, bacteria can modify or degrade the antibiotic molecule itself, causing structural changes that render it ineffective at killing the cell. Second, bacteria can modify the target of the antibiotic. For example, if the target is an enzyme, a mutation in the binding site may cause resistance. Finally, bacteria may transport the antibiotic to a location where it is no longer effective. This can either be done via sequestration of the antibiotic using specialized drug-binding proteins, or via incorporation of efflux pumps.

Efflux-mediated antibiotic resistance is a particularly large concern for a number of reasons. Many classes of pumps have low substrate specificity, being able to export a variety of structurally dissimilar small molecules. This is because unlike an enzyme, which may utilize a well-defined active site to bind a compound with high specificity, substrate recognition in efflux pumps is more dependent on physicochemical properties (polarity, aromaticity, etc.), by which parameters many current antibiotic classes are similar.[70,71] This in turn can confer resistance to many antibiotics

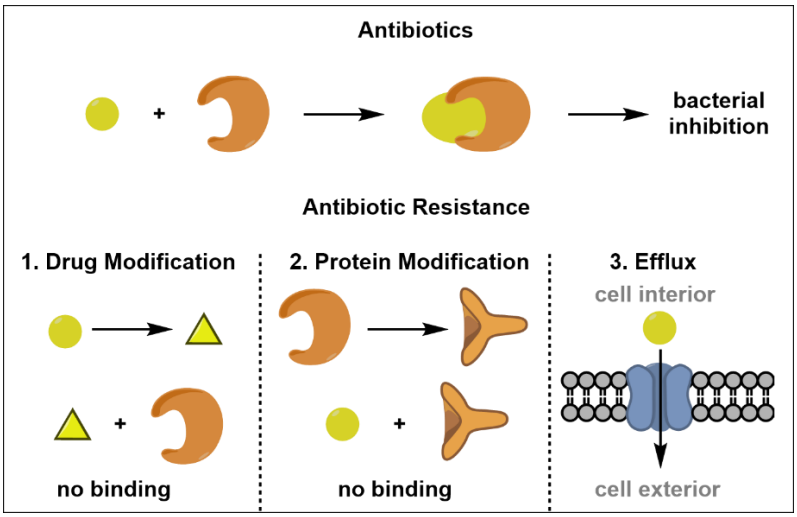

Figure 1.7. Major mechanisms of bacterial antibiotic resistance

simultaneously, quickly rendering an infection difficult to treat.[71] In addition, expression of genes encoding these pumps can often be directly induced by the presence of antibiotic compounds, meaning that chronic exposure to antibiotics rapidly causes resistance in cells which have incorporated these genes.[72] Finally, the genes encoding efflux pumps can be located either chromosomally or on mobile genetic elements such as plasmids and transposons.[73] Chromosomal efflux pumps allow for these genes to confer a high fitness advantage to cells in toxic environments, while efflux pumps encoded on plasmids allow for these genes to be easily transmitted between cells (even of distantly related bacterial species), in a process called horizontal gene transfer.[73]

Horizontal gene transfer (HGT) or lateral gene transfer, is a mechanism by which organisms can exchange genetic information and is often discussed in the context of bacterial sharing of genes that confer antibiotic resistance. There are three major ways that HGT is known to happen (**Figure 1.8**). Most simply, free mobile genetic elements in the extracellular environment can be imported, in a process called transformation (this process is often exploited in biochemical genetic manipulation studies). In transduction, these genes are exchanged through a bacteriophage intermediary. Finally, bacterial conjugation involves the physical contact of two cells using an appendage known as a sex pilus. After formation of a mating bridge (a type of pore) between the bacteria, a plasmid can be transported from one cell to the other. In this manner, in the presence of selective pressure such as antibiotic stress, genes conferring resistance can be disseminated very rapidly within cellular populations.[74]

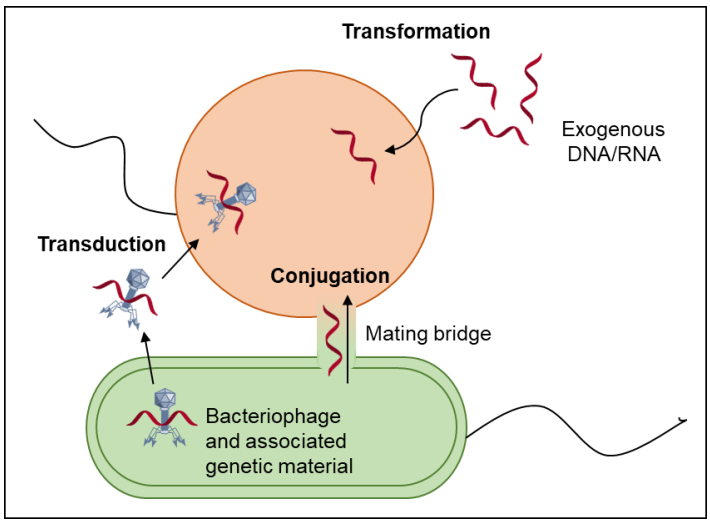

Figure 1.8. Mechanisms of horizontal gene transfer

According to the Centers for Disease Control's 2019 Antibiotic/Antimicrobial Resistance Threats report, over 3 million infections caused by antimicrobial resistant bacteria and fungi occur in the United States each year, resulting in 48,000 deaths annually.[75] The financial burden of antimicrobial resistance is also extensive, costing an estimated $55 billion annually for healthcare and lost productivity. The onset of the COVID-19 pandemic has only worsened the issue, reversing progress made in addressing underlying causes of the resistance crisis such as over prescription (about 80% of patients hospitalized with COVID-19 were prescribed a prophylactic antibiotic) and misuse of antibiotics, leading to a further 15% increase in antimicrobial-resistant infections and deaths in 2020.[76,77] Antimicrobial resistance also disproportionately affects developing countries, associated with a global death toll of over 5 million people in 2019 alone.[78]

Several factors have contributed to increasing the rate at which bacteria develop resistance. An increase in global travel has allowed for the mingling of genetically distinct strains of bacteria, allowing them to exchange resistance genes.[79] The overprescription of antibiotics is well-documented, occurring when patients seek treatments for minor ailments or when healthcare providers do not accurately diagnose bacterial infections prior to prescription.[80] Finally, the misuse

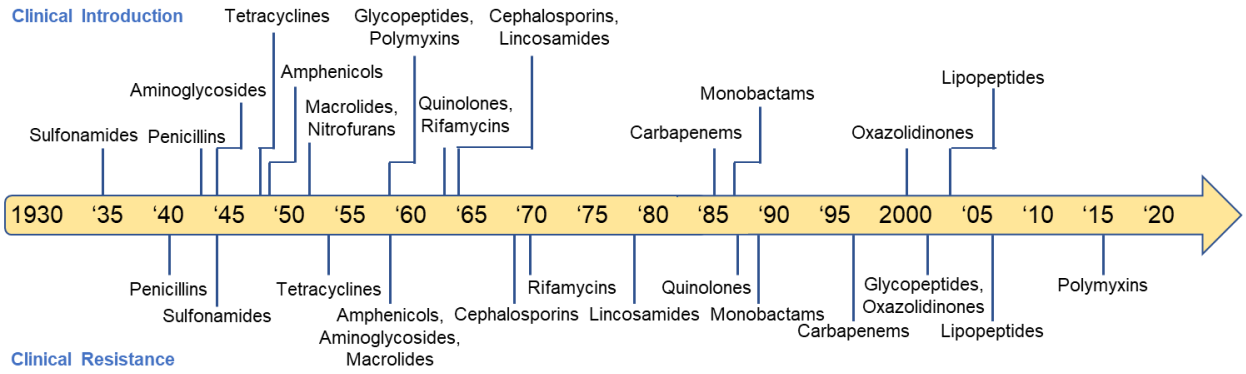

Figure 1.9. Timeline of introduction of major classes of antibiotics (top) and first observation of clinical resistance to these classes of antibiotics (bottom)

of antibiotics, such as in the case of patients not following treatment regimens or the agricultural use of antibiotics in some countries to increase the weight of livestock, has further exacerbated the antibiotic resistance crisis. It is estimated that by 2050, bacterial infections will once again become the leading cause of death. A 2016 report estimated an annual global death toll of 10 million people by 2050, a revised estimate in 2019 found that barring major policy change and a concerted global effort, we are likely to hit that death toll much sooner.[81,82]

Several strategies have been proposed to mitigate or reverse the antimicrobial resistance crisis.[76,83,84] First, improved scientific communication to the general public and to government agencies must be had regarding the dire threat antimicrobial resistance poses. Sweeping regulatory changes must be made to facilitate the process of antibiotic development and approval, and incentives must be placed on these research areas to encourage investment of resources by pharmaceutical companies. Development of antibacterials and antifungals functioning through novel mechanisms of action can prevent cross-resistance and extend the useful clinical lifespan of these drugs. Resistance mechanisms can be directly targeted in combination therapies to potentiate the activities of currently used antibiotic compounds. Finally, advancements in point-of-care diagnostic technologies to both quickly and accurately identify infectious pathogens can be made

to reduce unnecessary prescription of antibiotics, and can be coupled with the development of selective, narrow-spectrum antibiotics. These narrow-spectrum antibiotics are enticing, as they do not disrupt patients' commensal and mutualistic microbiota and generate less selective pressure for pan-resistance development. Research into the mechanisms by which bacteria develop resistance to antibiotics is also vital. The following thesis details efforts to probe one of the significant ways by which this occurs – drug efflux – and investigate possible methods to circumvent this mechanism.

1.4 Chapter 1 References

(1) Lauer, T. R.; Postman, M.; Weaver, H. A.; Spencer, J. R.; Stern, S. A.; Buie, M. W.; Durda, D. D.; Lisse, C. M.; Poppe, A. R.; Binzel, R. P.; Britt, D. T.; Buratti, B. J.; Cheng, A. F.; Grundy, W. M.; Horányi, M.; Kavelaars, J. J.; Linscott, I. R.; McKinnon, W. B.; Moore, J. M.; Núñez, J. I.; Olkin, C. B.; Parker, J. W.; Porter, S. B.; Reuter, D. C.; Robbins, S. J.; Schenk, P.; Showalter, M. R.; Singer, K. N.; Verbiscer, A. J.; Young, L. A. New Horizons Observations of the Cosmic Optical Background. *Astrophys. J.* **2021**, *906* (2), 77. https://doi.org/10.3847/1538-4357/abc881.

(2) Dalrymple, G. B. The Age of the Earth in the Twentieth Century: A Problem (Mostly) Solved. *Geol. Soc. Lond. Spec. Publ.* **2001**, *190* (1), 205–221. https://doi.org/10.1144/GSL.SP.2001.190.01.14.

(3) Pearce, B. K. D.; Tupper, A. S.; Pudritz, R. E.; Higgs, P. G. Constraining the Time Interval for the Origin of Life on Earth. *Astrobiology* **2018**, *18* (3), 343–364. https://doi.org/10.1089/ast.2017.1674.

(4) Deamer, D. Where Did Life Begin? Testing Ideas in Prebiotic Analogue Conditions. *Life* **2021**, *11* (2), 134. https://doi.org/10.3390/life11020134.

(5) Damer, B.; Deamer, D. The Hot Spring Hypothesis for an Origin of Life. *Astrobiology* **2020**, *20* (4), 429–452. https://doi.org/10.1089/ast.2019.2045.

(6) Weiss, M. C.; Sousa, F. L.; Mrnjavac, N.; Neukirchen, S.; Roettger, M.; Nelson-Sathi, S.; Martin, W. F. The Physiology and Habitat of the Last Universal Common Ancestor. *Nat. Microbiol.* **2016**, *1* (9), 1–8. https://doi.org/10.1038/nmicrobiol.2016.116.

(7) Colín-García, M. Hydrothermal Vents and Prebiotic Chemistry: A Review. *Bol. Soc. Geológica Mex.* **2016**, *68* (3), 599–620. https://doi.org/10.18268/BSGM2016v68n3a13.

(8) Roldan, A.; Hollingsworth, N.; Roffey, A.; Islam, H.-U.; Goodall, J. B. M.; Catlow, C. R. A.; Darr, J. A.; Bras, W.; Sankar, G.; Holt, K. B.; Hogarth, G.; Leeuw, N. H. de. Bio-Inspired

CO2 Conversion by Iron Sulfide Catalysts under Sustainable Conditions. *Chem. Commun.* **2015**, *51* (35), 7501–7504. https://doi.org/10.1039/C5CC02078F.

(9) Milshteyn, D.; Damer, B.; Havig, J.; Deamer, D. Amphiphilic Compounds Assemble into Membranous Vesicles in Hydrothermal Hot Spring Water but Not in Seawater. *Life* **2018**, *8* (2), 11. https://doi.org/10.3390/life8020011.

(10) Deamer, D. The Role of Lipid Membranes in Life's Origin. *Life* **2017**, *7* (1), 5. https://doi.org/10.3390/life7010005.

(11) Lane, N.; Martin, W. F. The Origin of Membrane Bioenergetics. *Cell* **2012**, *151* (7), 1406–1416. https://doi.org/10.1016/j.cell.2012.11.050.

(12) Weiss, M. C.; Preiner, M.; Xavier, J. C.; Zimorski, V.; Martin, W. F. The Last Universal Common Ancestor between Ancient Earth Chemistry and the Onset of Genetics. *PLOS Genet.* **2018**, *14* (8), e1007518. https://doi.org/10.1371/journal.pgen.1007518.

(13) Xavier, J. C.; Gerhards, R. E.; Wimmer, J. L. E.; Brueckner, J.; Tria, F. D. K.; Martin, W. F. The Metabolic Network of the Last Bacterial Common Ancestor. *Commun. Biol.* **2021**, *4* (1), 1–10. https://doi.org/10.1038/s42003-021-01918-4.

(14) Boto, L. Horizontal Gene Transfer in Evolution: Facts and Challenges. *Proc. R. Soc. B Biol. Sci.* **2010**, *277* (1683), 819–827. https://doi.org/10.1098/rspb.2009.1679.

(15) Daubin, V.; Szöllősi, G. J. Horizontal Gene Transfer and the History of Life. *Cold Spring Harb. Perspect. Biol.* **2016**, *8* (4), a018036. https://doi.org/10.1101/cshperspect.a018036.

(16) Kasting, J. F. Earth's Early Atmosphere. *Science* **1993**, *259* (5097), 920–926. https://doi.org/10.1126/science.11536547.

(17) Shaw, G. H. Earth's Atmosphere – Hadean to Early Proterozoic. *Geochemistry* **2008**, *68* (3), 235–264. https://doi.org/10.1016/j.chemer.2008.05.001.

(18) Schirrmeister, B. E.; de Vos, J. M.; Antonelli, A.; Bagheri, H. C. Evolution of Multicellularity Coincided with Increased Diversification of Cyanobacteria and the Great Oxidation Event. *Proc. Natl. Acad. Sci.* **2013**, *110* (5), 1791–1796. https://doi.org/10.1073/pnas.1209927110.

(19) Hodgskiss, M. S. W.; Crockford, P. W.; Peng, Y.; Wing, B. A.; Horner, T. J. A Productivity Collapse to End Earth's Great Oxidation. *Proc. Natl. Acad. Sci.* **2019**, *116* (35), 17207–17212. https://doi.org/10.1073/pnas.1900325116.

(20) Soo, R. M.; Hemp, J.; Parks, D. H.; Fischer, W. W.; Hugenholtz, P. On the Origins of Oxygenic Photosynthesis and Aerobic Respiration in Cyanobacteria. *Science* **2017**, *355* (6332), 1436–1440. https://doi.org/10.1126/science.aal3794.

(21) Sperling, E. A.; Frieder, C. A.; Raman, A. V.; Girguis, P. R.; Levin, L. A.; Knoll, A. H. Oxygen, Ecology, and the Cambrian Radiation of Animals. *Proc. Natl. Acad. Sci.* **2013**, *110* (33), 13446–13451. https://doi.org/10.1073/pnas.1312778110.

(22) Gross, J.; Bhattacharya, D. Uniting Sex and Eukaryote Origins in an Emerging Oxygenic World. *Biol. Direct* **2010**, *5* (1), 53. https://doi.org/10.1186/1745-6150-5-53.

(23) Cavalier-Smith, T. Origin of Mitochondria by Intracellular Enslavement of a Photosynthetic Purple Bacterium. *Proc. R. Soc. B Biol. Sci.* **2006**, *273* (1596), 1943–1952. https://doi.org/10.1098/rspb.2006.3531.

(24) Karnkowska, A.; Vacek, V.; Zubáčová, Z.; Treitli, S. C.; Petrželková, R.; Eme, L.; Novák, L.; Žárský, V.; Barlow, L. D.; Herman, E. K.; Soukal, P.; Hroudová, M.; Doležal, P.; Stairs, C. W.; Roger, A. J.; Eliáš, M.; Dacks, J. B.; Vlček, Č.; Hampl, V. A Eukaryote without a Mitochondrial Organelle. *Curr. Biol.* **2016**, *26* (10), 1274–1284. https://doi.org/10.1016/j.cub.2016.03.053.

(25) Parfrey, L. W.; Lahr, D. J. G. Multicellularity Arose Several Times in the Evolution of Eukaryotes (Response to DOI 10.1002/Bies.201100187). *BioEssays* **2013**, *35* (4), 339–347. https://doi.org/10.1002/bies.201200143.

(26) Campbell, N. A.; Reece, J. B. *Biology*, 8th ed.; Pearson Benjamin Cummings: San Francisco, 2008.

(27) McFadden, G. I.; Dooren, G. G. van. Evolution: Red Algal Genome Affirms a Common Origin of All Plastids. *Curr. Biol.* **2004**, *14* (13), R514–R516. https://doi.org/10.1016/j.cub.2004.06.041.

(28) *Medical Microbiology*, 4th ed.; Baron, S., Ed.; University of Texas Medical Branch at Galveston: Galveston, Tex, 1996.

(29) Madigan, M. T.; Martinko, J. M.; Brock, T. D.; Madigan, M. T. *Brock Biology of Microorganisms*, 11. ed., international ed.; Pearson, Prentice Hall: Upper Saddle River, NJ, 2006.

(30) Gupta, R. S. Origin of Diderm (Gram-Negative) Bacteria: Antibiotic Selection Pressure Rather than Endosymbiosis Likely Led to the Evolution of Bacterial Cells with Two Membranes. *Antonie Van Leeuwenhoek* **2011**, *100* (2), 171–182. https://doi.org/10.1007/s10482-011-9616-8.

(31) Gupta, R. S. Protein Phylogenies and Signature Sequences: A Reappraisal of Evolutionary Relationships among Archaebacteria, Eubacteria, and Eukaryotes. *Microbiol. Mol. Biol. Rev. MMBR* **1998**, *62* (4), 1435–1491. https://doi.org/10.1128/MMBR.62.4.1435-1491.1998.

(32) Gupta, R. S. The Natural Evolutionary Relationships among Prokaryotes. *Crit. Rev. Microbiol.* **2000**, *26* (2), 111–131. https://doi.org/10.1080/10408410091154219.

(33) Walker, T. S.; Bais, H. P.; Grotewold, E.; Vivanco, J. M. Root Exudation and Rhizosphere Biology. *Plant Physiol.* **2003**, *132* (1), 44–51. https://doi.org/10.1104/pp.102.019661.

(34) Brachmann, A.; Parniske, M. The Most Widespread Symbiosis on Earth. *PLOS Biol.* **2006**, *4* (7), e239. https://doi.org/10.1371/journal.pbio.0040239.

(35) Weller, D. M. Biological Control of Soilborne Plant Pathogens in the Rhizosphere with Bacteria. *Annu. Rev. Phytopathol.* **1988**, *26* (1), 379–407. https://doi.org/10.1146/annurev.py.26.090188.002115.

(36) Jousset, A.; Rochat, L.; Scheu, S.; Bonkowski, M.; Keel, C. Predator-Prey Chemical Warfare Determines the Expression of Biocontrol Genes by Rhizosphere-Associated Pseudomonas Fluorescens. *Appl. Environ. Microbiol.* **2010**, *76* (15), 5263–5268. https://doi.org/10.1128/AEM.02941-09.

(37) Federle, M. J.; Bassler, B. L. Interspecies Communication in Bacteria. *J. Clin. Invest.* **2003**, *112* (9), 1291–1299. https://doi.org/10.1172/JCI200320195.

(38) Waters, C. M.; Bassler, B. L. Quorum Sensing: Cell-to-Cell Communication in Bacteria. *Annu. Rev. Cell Dev. Biol.* **2005**, *21*, 319–346. https://doi.org/10.1146/annurev.cellbio.21.012704.131001.

(39) Miller, M. B.; Bassler, B. L. Quorum Sensing in Bacteria. *Annu. Rev. Microbiol.* **2001**, *55* (1), 165–199. https://doi.org/10.1146/annurev.micro.55.1.165.

(40) Pena, R. T.; Blasco, L.; Ambroa, A.; González-Pedrajo, B.; Fernández-García, L.; López, M.; Bleriot, I.; Bou, G.; García-Contreras, R.; Wood, T. K.; Tomás, M. Relationship Between Quorum Sensing and Secretion Systems. *Front. Microbiol.* **2019**, *10*.

(41) dos Reis Ponce-Rossi, A.; Pinto, U. M.; de Oliveira Barros Ribon, A.; Bazzolli, D. M. S.; Vanetti, M. C. D. Quorum Sensing Regulated Phenotypes in Aeromonas Hydrophila ATCC 7966 Deficient in AHL Production. *Ann. Microbiol.* **2016**, *66* (3), 1117–1126. https://doi.org/10.1007/s13213-016-1196-4.

(42) Striednig, B.; Hilbi, H. Bacterial Quorum Sensing and Phenotypic Heterogeneity: How the Collective Shapes the Individual. *Trends Microbiol.* **2022**, *30* (4), 379–389. https://doi.org/10.1016/j.tim.2021.09.001.

(43) Sauer, K.; Camper, A. K.; Ehrlich, G. D.; Costerton, J. W.; Davies, D. G. Pseudomonas Aeruginosa Displays Multiple Phenotypes during Development as a Biofilm. *J. Bacteriol.* **2002**, *184* (4), 1140–1154. https://doi.org/10.1128/jb.184.4.1140-1154.2002.

(44) Nadell, C. D.; Xavier, J. B.; Foster, K. R. The Sociobiology of Biofilms. *FEMS Microbiol. Rev.* **2009**, *33* (1), 206–224. https://doi.org/10.1111/j.1574-6976.2008.00150.x.

(45) Hall-Stoodley, L.; Costerton, J. W.; Stoodley, P. Bacterial Biofilms: From the Natural Environment to Infectious Diseases. *Nat. Rev. Microbiol.* **2004**, *2* (2), 95–108. https://doi.org/10.1038/nrmicro821.

(46) O'Toole, G.; Kaplan, H. B.; Kolter, R. Biofilm Formation as Microbial Development. *Annu. Rev. Microbiol.* **2000**, *54* (1), 49–79. https://doi.org/10.1146/annurev.micro.54.1.49.

(47) Newman, D. J.; Cragg, G. M. Natural Products as Sources of New Drugs over the Nearly Four Decades from 01/1981 to 09/2019. *J. Nat. Prod.* **2020**, *83* (3), 770–803. https://doi.org/10.1021/acs.jnatprod.9b01285.

(48) Clardy, J.; Fischbach, M.; Currie, C. The Natural History of Antibiotics. *Curr. Biol. CB* **2009**, *19* (11), R437–R441. https://doi.org/10.1016/j.cub.2009.04.001.

(49) Schneider, Y. K. Bacterial Natural Product Drug Discovery for New Antibiotics: Strategies for Tackling the Problem of Antibiotic Resistance by Efficient Bioprospecting. *Antibiotics* **2021**, *10* (7), 842. https://doi.org/10.3390/antibiotics10070842.

(50) Lorenzo, J. M.; Munekata, P. E.; Dominguez, R.; Pateiro, M.; Saraiva, J. A.; Franco, D. Main Groups of Microorganisms of Relevance for Food Safety and Stability. *Innov. Technol. Food Preserv.* **2018**, 53–107. https://doi.org/10.1016/B978-0-12-811031-7.00003-0.

(51) Sender, R.; Fuchs, S.; Milo, R. Are We Really Vastly Outnumbered? Revisiting the Ratio of Bacterial to Host Cells in Humans. *Cell* **2016**, *164* (3), 337–340. https://doi.org/10.1016/j.cell.2016.01.013.

(52) Bull, M. J.; Plummer, N. T. Part 1: The Human Gut Microbiome in Health and Disease. *Integr. Med. Clin. J.* **2014**, *13* (6), 17–22.

(53) Schirbel, A.; Kessler, S.; Rieder, F.; West, G.; Rebert, N.; Asosingh, K.; McDonald, C.; Fiocchi, C. Pro-Angiogenic Activity of TLRs and NLRs: A Novel Link Between Gut Microbiota and Intestinal Angiogenesis. *Gastroenterology* **2013**, *144* (3), 613-623.e9. https://doi.org/10.1053/j.gastro.2012.11.005.

(54) Metwaly, A. M.; Ghoneim, M. M.; Eissa, Ibrahim. H.; Elsehemy, I. A.; Mostafa, A. E.; Hegazy, M. M.; Afifi, W. M.; Dou, D. Traditional Ancient Egyptian Medicine: A Review. *Saudi J. Biol. Sci.* **2021**, *28* (10), 5823–5832. https://doi.org/10.1016/j.sjbs.2021.06.044.

(55) Gould, K. Antibiotics: From Prehistory to the Present Day. *J. Antimicrob. Chemother.* **2016**, *71* (3), 572–575. https://doi.org/10.1093/jac/dkv484.

(56) Krishna, S.; Bustamante, L.; Haynes, R. K.; Staines, H. M. Artemisinins: Their Growing Importance in Medicine. *Trends Pharmacol. Sci.* **2008**, *29* (10), 520–527. https://doi.org/10.1016/j.tips.2008.07.004.

(57) Bhishagratna, K. *An English Translation of the Sushruta Samhita: Based on Original Sanskrit Text*; 1907.

(58) Reid, M. H. *Law and Piety in Medieval Islam*, First paperback edition.; Cambridge studies in Islamic civilization; Cambridge University Press: Cambridge, 2017.

(59) Ledermann, W. [Who saw them the first?]. *Rev. Chil. Infectologia Organo Of. Soc. Chil. Infectologia* **2012**, *29* (3), 348–352. https://doi.org/10.4067/S0716-10182012000300017.

(60) Smith, K. A. Louis Pasteur, the Father of Immunology? *Front. Immunol.* **2012**, *3*, 68. https://doi.org/10.3389/fimmu.2012.00068.

(61) Emmerich, R.; Löw, O. Bakteriolytische Enzyme als Ursache der erworbenen Immunität und die Heilung von Infectionskrankheiten durch dieselben. *Z. Für Hyg. Infekt.* **1899**, *31* (1), 1–65. https://doi.org/10.1007/BF02206499.

(62) Vernon, G. Syphilis and Salvarsan. *Br. J. Gen. Pract.* **2019**, *69* (682), 246. https://doi.org/10.3399/bjgp19X702533.

(63) Ueda, K.; Beppu, T. Antibiotics in Microbial Coculture. *J. Antibiot. (Tokyo)* **2017**, *70* (4), 361–365. https://doi.org/10.1038/ja.2016.127.

(64) Kapoor, G.; Saigal, S.; Elongavan, A. Action and Resistance Mechanisms of Antibiotics: A Guide for Clinicians. *J. Anaesthesiol. Clin. Pharmacol.* **2017**, *33* (3), 300–305. https://doi.org/10.4103/joacp.JOACP_349_15.

(65) Årdal, C.; Balasegaram, M.; Laxminarayan, R.; McAdams, D.; Outterson, K.; Rex, J. H.; Sumpradit, N. Antibiotic Development — Economic, Regulatory and Societal Challenges. *Nat. Rev. Microbiol.* **2020**, *18* (5), 267–274. https://doi.org/10.1038/s41579-019-0293-3.

(66) Simpkin, V. L.; Renwick, M. J.; Kelly, R.; Mossialos, E. Incentivising Innovation in Antibiotic Drug Discovery and Development: Progress, Challenges and next Steps. *J. Antibiot. (Tokyo)* **2017**, *70* (12), 1087–1096. https://doi.org/10.1038/ja.2017.124.

(67) MILLER, T. H. THE PROBLEM OF ARSPHENAMINE-RESISTANT SYPHILIS: REPORT OF A CASE. *J. Am. Med. Assoc.* **1931**, *97* (1), 11–14. https://doi.org/10.1001/jama.1931.02730010015004.

(68) Yap, M.-N. F. The Double Life of Antibiotics. *Mo. Med.* **2013**, *110* (4), 320–324.

(69) Reygaert, W. C. An Overview of the Antimicrobial Resistance Mechanisms of Bacteria. *AIMS Microbiol.* **2018**, *4* (3), 482–501. https://doi.org/10.3934/microbiol.2018.3.482.

(70) Van Bambeke, F.; Balzi, E.; Tulkens, P. M. Antibiotic Efflux Pumps. *Biochem. Pharmacol.* **2000**, *60* (4), 457–470. https://doi.org/10.1016/S0006-2952(00)00291-4.

(71) Du, D.; Wang-Kan, X.; Neuberger, A.; van Veen, H. W.; Pos, K. M.; Piddock, L. J. V.; Luisi, B. F. Multidrug Efflux Pumps: Structure, Function and Regulation. *Nat. Rev. Microbiol.* **2018**, *16* (9), 523–539. https://doi.org/10.1038/s41579-018-0048-6.

(72) Morita, Y.; Sobel, M. L.; Poole, K. Antibiotic Inducibility of the MexXY Multidrug Efflux System of Pseudomonas Aeruginosa: Involvement of the Antibiotic-Inducible PA5471 Gene Product. *J. Bacteriol.* **2006**, *188* (5), 1847–1855. https://doi.org/10.1128/JB.188.5.1847-1855.2006.

(73) Li, X.-Z.; Plésiat, P.; Nikaido, H. The Challenge of Efflux-Mediated Antibiotic Resistance in Gram-Negative Bacteria. *Clin. Microbiol. Rev.* **2015**, *28* (2), 337–418. https://doi.org/10.1128/CMR.00117-14.

(74) Gyles, C.; Boerlin, P. Horizontally Transferred Genetic Elements and Their Role in Pathogenesis of Bacterial Disease. *Vet. Pathol.* **2014**, *51* (2), 328–340. https://doi.org/10.1177/0300985813511131.

(75) Centers for Disease Control and Prevention (U.S.). *Antibiotic Resistance Threats in the United States, 2019*; Centers for Disease Control and Prevention (U.S.), 2019. https://doi.org/10.15620/cdc:82532.

(76) Mahoney, A. R.; Safaee, M. M.; Wuest, W. M.; Furst, A. L. The Silent Pandemic: Emergent Antibiotic Resistances Following the Global Response to SARS-CoV-2. *iScience* **2021**, *24* (4), 102304. https://doi.org/10.1016/j.isci.2021.102304.

(77) *COVID-19: U.S. Impact on Antimicrobial Resistance, Special Report 2022*; National Center for Emerging and Zoonotic Infectious Diseases, 2022. https://doi.org/10.15620/cdc:117915.

(78) Murray, C. J.; Ikuta, K. S.; Sharara, F.; Swetschinski, L.; Aguilar, G. R.; Gray, A.; Han, C.; Bisignano, C.; Rao, P.; Wool, E.; Johnson, S. C.; Browne, A. J.; Chipeta, M. G.; Fell, F.; Hackett, S.; Haines-Woodhouse, G.; Hamadani, B. H. K.; Kumaran, E. A. P.; McManigal, B.; Agarwal, R.; Akech, S.; Albertson, S.; Amuasi, J.; Andrews, J.; Aravkin, A.; Ashley, E.; Bailey, F.; Baker, S.; Basnyat, B.; Bekker, A.; Bender, R.; Bethou, A.; Bielicki, J.; Boonkasidecha, S.; Bukosia, J.; Carvalheiro, C.; Castañeda-Orjuela, C.; Chansamouth, V.; Chaurasia, S.; Chiurchiù, S.; Chowdhury, F.; Cook, A. J.; Cooper, B.; Cressey, T. R.; Criollo-Mora, E.; Cunningham, M.; Darboe, S.; Day, N. P. J.; Luca, M. D.; Dokova, K.; Dramowski, A.; Dunachie, S. J.; Eckmanns, T.; Eibach, D.; Emami, A.; Feasey, N.; Fisher-Pearson, N.; Forrest, K.; Garrett, D.; Gastmeier, P.; Giref, A. Z.; Greer, R. C.; Gupta, V.; Haller, S.; Haselbeck, A.; Hay, S. I.; Holm, M.; Hopkins, S.; Iregbu, K. C.; Jacobs, J.; Jarovsky, D.; Javanmardi, F.; Khorana, M.; Kissoon, N.; Kobeissi, E.; Kostyanev, T.; Krapp, F.; Krumkamp, R.; Kumar, A.; Kyu, H. H.; Lim, C.; Limmathurotsakul, D.; Loftus, M. J.; Lunn, M.; Ma, J.; Mturi, N.; Munera-Huertas, T.; Musicha, P.; Mussi-Pinhata, M. M.; Nakamura, T.; Nanavati, R.; Nangia, S.; Newton, P.; Ngoun, C.; Novotney, A.; Nwakanma, D.; Obiero, C. W.; Olivas-Martinez, A.; Olliaro, P.; Ooko, E.; Ortiz-Brizuela, E.; Peleg, A. Y.; Perrone, C.; Plakkal, N.; Ponce-de-Leon, A.; Raad, M.; Ramdin, T.; Riddell, A.; Roberts, T.; Robotham, J. V.; Roca, A.; Rudd, K. E.; Russell, N.; Schnall, J.; Scott, J. A. G.; Shivamallappa, M.; Sifuentes-Osornio, J.; Steenkeste, N.; Stewardson, A. J.; Stoeva, T.; Tasak, N.; Thaiprakong, A.; Thwaites, G.; Turner, C.; Turner, P.; Doorn, H. R. van; Velaphi, S.; Vongpradith, A.; Vu, H.; Walsh, T.; Waner, S.; Wangrangsimakul, T.; Wozniak, T.; Zheng, P.; Sartorius, B.; Lopez, A. D.; Stergachis, A.; Moore, C.; Dolecek, C.; Naghavi, M. Global Burden of Bacterial Antimicrobial Resistance in 2019: A Systematic Analysis. *The Lancet* **2022**, *399* (10325), 629–655. https://doi.org/10.1016/S0140-6736(21)02724-0.

(79) Bokhary, H.; Pangesti, K. N. A.; Rashid, H.; Abd El Ghany, M.; Hill-Cawthorne, G. A. Travel-Related Antimicrobial Resistance: A Systematic Review. *Trop. Med. Infect. Dis.* **2021**, *6* (1), 11. https://doi.org/10.3390/tropicalmed6010011.

(80) Llor, C.; Bjerrum, L. Antimicrobial Resistance: Risk Associated with Antibiotic Overuse and Initiatives to Reduce the Problem. *Ther. Adv. Drug Saf.* **2014**, *5* (6), 229–241. https://doi.org/10.1177/2042098614554919.

(81) O'Neill, J. *Tackling Drug-Resistant Infections Globally: Final Report and Recommendations*; Report; Government of the United Kingdom, 2016. https://apo.org.au/node/63983 (accessed 2023-03-06).

(82) *No time to Wait: Securing the future from drug-resistant infections*. https://www.who.int/publications-detail-redirect/no-time-to-wait-securing-the-future-from-drug-resistant-infections (accessed 2023-03-06).

(83) Cars, O.; Chandy, S. J.; Mpundu, M.; Peralta, A. Q.; Zorzet, A.; So, A. D. Resetting the Agenda for Antibiotic Resistance through a Health Systems Perspective. *Lancet Glob. Health* **2021**, *9* (7), e1022–e1027. https://doi.org/10.1016/S2214-109X(21)00163-7.

(84) Annunziato, G. Strategies to Overcome Antimicrobial Resistance (AMR) Making Use of Non-Essential Target Inhibitors: A Review. *Int. J. Mol. Sci.* **2019**, *20* (23), 5844. https://doi.org/10.3390/ijms20235844.

Chapter 2 - Investigation of Promysalin Resistance via Rationally Guided Analog Design

2.1 Introduction

Cystic fibrosis (CF) is an often fatal autosomal recessive disorder most commonly afflicting white populations (1 in 2,500-3,500 newborns), but also occurs in African Americans (1 in 17,000 newborns), Asian Americans (1 in 31,000 newborns), Hispanic populations (1 in 4,000-10,000 newborns), and more.[85] The disease is caused by mutations in the CFTR gene encoding for the CF transmembrane conductance regulator, an ABC exporter of chloride ions expressed in epithelial cells.[86] Over 800 missense mutations in CFTR leading to CF have been identified and are classified according to the effect they have on protein production and function. These can range from Class 1 mutations which result in complete lack of CFTR production due to an early translation termination event to Class 6 mutations, in which the exterior surface of the CFTR protein is unstable, leading to poor chloride transport and lower total amount of protein. The most common mutation is F508Δ, a Class 2 mutation resulting in poor trafficking of the CFTR protein from the ribosome where it is synthesized to the cell surface. Regardless of mutation, the resulting

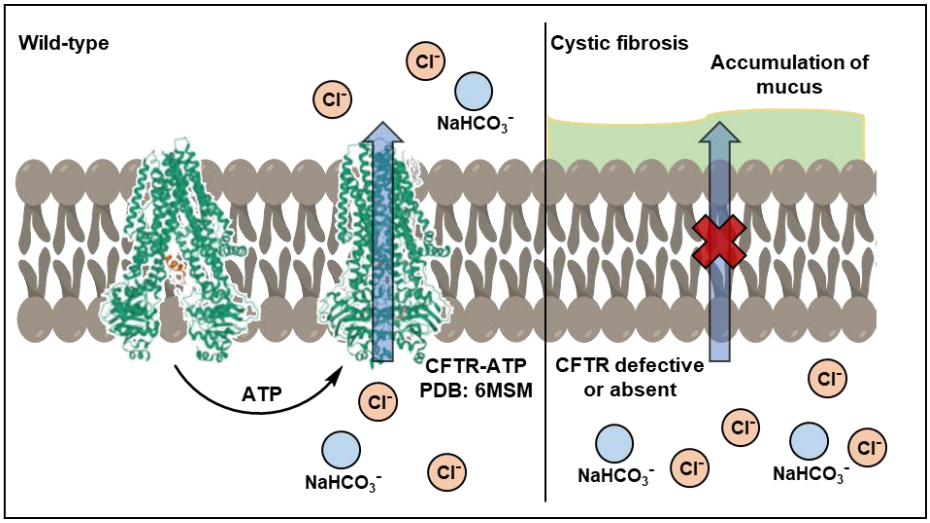

Figure 2.1. Comparison of CFTR in healthy vs. CF-afflicted cells

inefficiency or inability (depending on severity) of cells to export chloride ions results in poor water hydration of the cellular membrane surface (**Figure 2.1**).[86,87]

In patients affected with cystic fibrosis, poor CFTR function displays as a variety of symptoms (**Figure 2.1**). In sweat glands, CFTR is necessary for the reuptake of water into cells; defective CFTR does not allow this process and leads to an accumulation of salt in the sweat of CF patients, an often-used diagnostic marker for the disease. The lack of hydrating water on cell surfaces also causes a buildup of overly viscous mucus in the pancreas, airways, and lungs. While mucus is a natural substance secreted by submucosal glands and serves to lubricate the airways and gastrointestinal tract, in people affected with cystic fibrosis this abnormally thick mucus can affect a variety of bodily functions. For example, in the pancreas this mucus can block pancreatic ducts, leading to pain, vomiting and inflammation while also preventing the production and secretion of digestive enzymes causing malnutrition. In the lungs, thick, sticky mucus accumulation prevents cilial motion, rendering them ineffective at clearing foreign particles, resulting in frequent coughing, difficulty breathing, and chronic bacterial infection.[87]

Respiratory disease associated with inflammation, acute airway damage, and infection is the primary cause of death in CF patients. The thick mucoidal nature of CF lungs serve as an excellent breeding ground for a variety of bacteria. Because of the inability of those afflicted to effectively clear this mucus, CF patients suffer from chronic bacterial respiratory infections. To combat these bacteria, CF patients are typically prescribed broad spectrum antibiotics (typically penicillins, cephalosporins, macrolides, or aminoglycosides). However, the frequency of infections and resulting treatment regimens inherently selects for the development of antibiotic resistance. At young ages, the majority of these infections are caused by *Staphylococcus aureus* and *Haemophilus influenzae*, but as patients approach their early 20s, the prevalence of *Pseudomonas aeruginosa* in percentage of infections becomes dominant (**Figure 2.2**).[87–89]

Pseudomonas aeruginosa is an opportunistic, rod shaped, gram-negative pathogenic bacteria. Besides cystic fibrosis patients, *P. aeruginosa* infections are common in burn victims and immunocompromised populations. This species is typically aerobic but in low oxygen

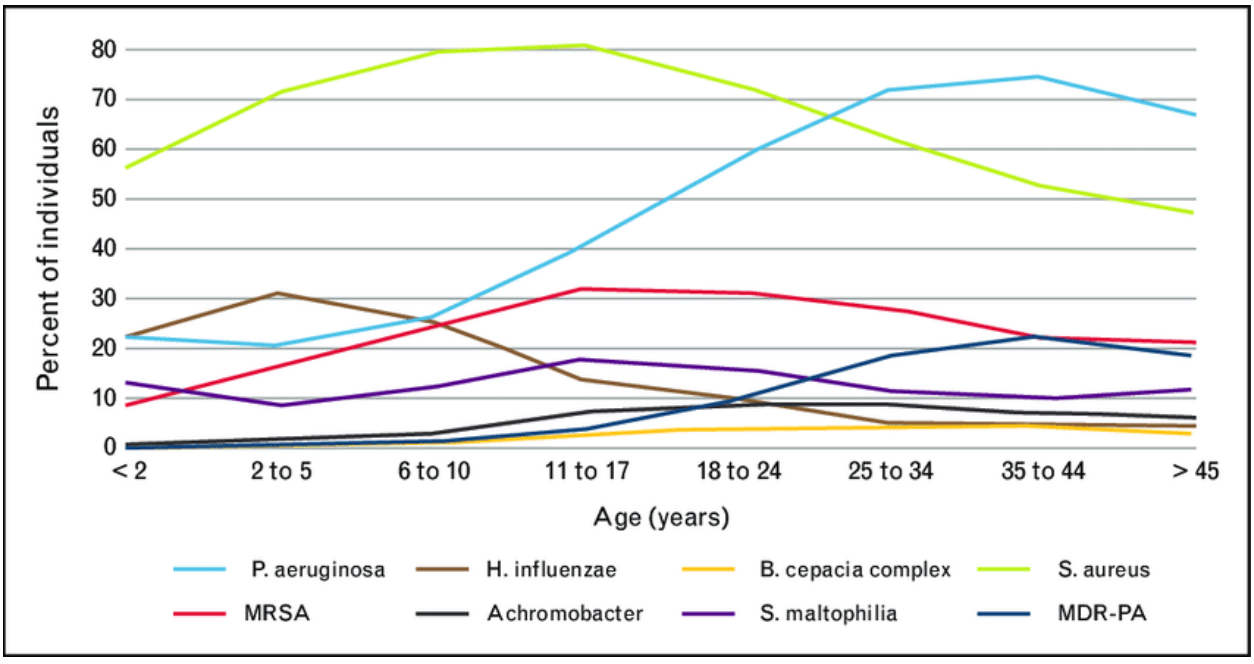

Figure 2.2. Species-specific respiratory infection prevalence in CF patients as a function of their age. Data retrieved from Langan et al.[89]

environments it is an example of a facultative anaerobe, able to switch to the fermentation pathway as its source of ATP. It also has the ability to utilize a wide variety of different carbon sources as food; this combination of traits allows it to be a very effective colonizer, and as a result *P. aeruginosa* is found in most natural and artificial environments around the world. Its ability to thrive even under anaerobic conditions allows it to form very successful biofilms in its hosts. These biofilms in combination with *P. aeruginosa*'s many intrinsic forms of antibiotic resistance makes it a particularly challenging bacterium to treat. Furthermore, diagnosis of a *P. aeruginosa* infection can be complicated by the high propensity of colonization of non-sterilized equipment or surfaces, as well as the variety of morphologies that *P. aeruginosa* colonies can take. However, true pathogenic *P. aeruginosa* infections almost always require some form of treatment.[90]

Treatments for *P. aeruginosa* are limited due to the bacterium's complex mechanisms of antibiotic resistance. It is known to express a number of multidrug efflux pumps such as mexAB and mexXY. Furthermore, *P. aeruginosa* is especially adept at acquiring resistance via horizontal gene transfer, accelerating the rate at which treatments become ineffective. In many cases, the safest course of action to prevent treatment failure is to isolate a sample of the infectious bacteria (e.g. a sputum sample of a cystic fibrosis patient) and assess its susceptibility to different classes of antibiotics *in vitro*. Due to the limited number of currently effective treatments for *P. aeruginosa* infections and the high rate of acquired resistance, it is crucial to develop additional small molecule drugs that function via novel mechanisms of action to prevent cross resistance.[91]

In 2011, the isolation of a novel antibiotic from the rhizosphere of a Sri Lankan rice plant was reported.[92] The rhizospheral environment is an interesting one, as the abundance of nutrients and water around a plant's root systems leads to a complex network of microorganisms competing for resources. Our interest was piqued upon hearing the report of this novel antibiotic due to its

reported species-specific activity against *P. aeruginosa*. The molecule was found to be produced by *Pseudomonas putida* and did not inhibit the growth of any other bacteria tested. The authors also described the biosynthetic gene cluster necessary for this molecule's synthesis, and provided structural elucidation using NMR and mass spectrometry techniques (**Figure 2.3**). Based on the molecular structure containing a proline, 2,8-dihydroxymyristamide, and a salicylate moiety, the authors named the molecule promysalin (**2.01**).[92]

In 2015, the Wuest lab began its work on the total synthesis and biological investigation of promysalin.[93] The diverted synthetic route devised allowed for elucidation of the configuration of the chiral centers on the 2,8-dihydroxymyristamide sidechain via systematic synthesis of all four possible stereoisomers followed by comparison to the spectral data and antibiotic activity of the isolated natural product. These sidechains were synthesized starting from hex-5-en-amide, which was first derivatized with an Evans chiral auxiliary, allowing for subsequent asymmetric Davis oxidation to form **2.04**. The terminal alkene was then subjected to Grubbs-catalyzed olefin metathesis (refer to **Figure 2.4** for catalyst structures and naming conventions used herein) to homoallylic alcohol **2.05** (generated via enantioselective Keck allylation of heptanal). After

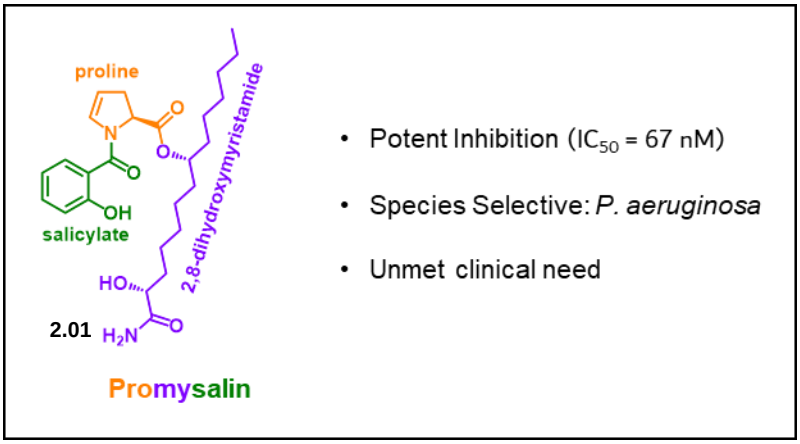

Figure 2.3. Key structural features and biological activity of promysalin

hydrogenation of the alkene and aminolytic cleavage of the Evans auxiliary, a late stage esterification reaction then attached the sidechain to the proline-salicylate fragment.

The proline-salicylate fragment was synthesized from commercially available methyl salicylate. After SEM protection of the phenol group, the ester was hydrolyzed and coupled to trans-4-hydroxy-(L)-proline methyl ester. The hydroxyl group was oxidized using DMP to the ketone, then addition of triflic anhydride and 2,6-lutidine allowed for regioselective enol triflate formation. Use of Stille coupling conditions with tributyltin hydride as the stannane allowed for protode(pseudo)halogenation, affording the desired fragment as its methyl ester (**2.02**). Base-mediated hydrolysis (**2.03**) allowed for successful coupling to the sidechain using EDC. After this esterification, global deprotection was achieved using TBAF to give the natural product (**2.01**).[93]

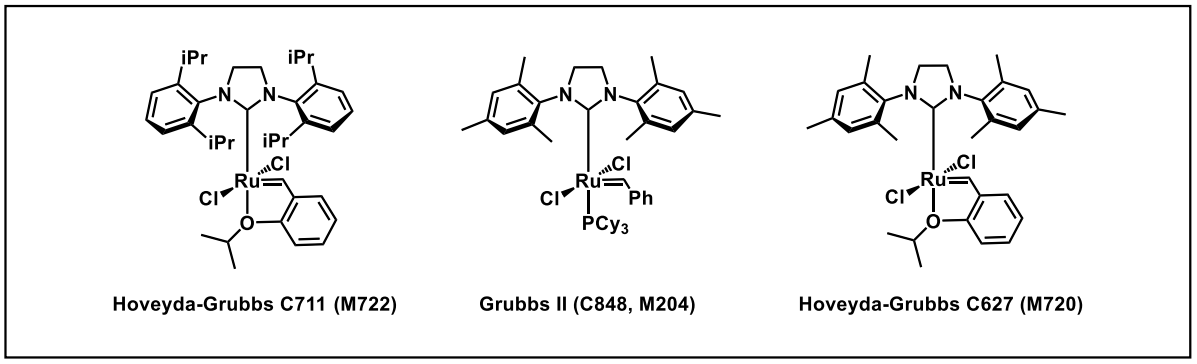

Figure 2.4. Olefin metathesis catalysts used in the synthesis of promysalin and related analogs

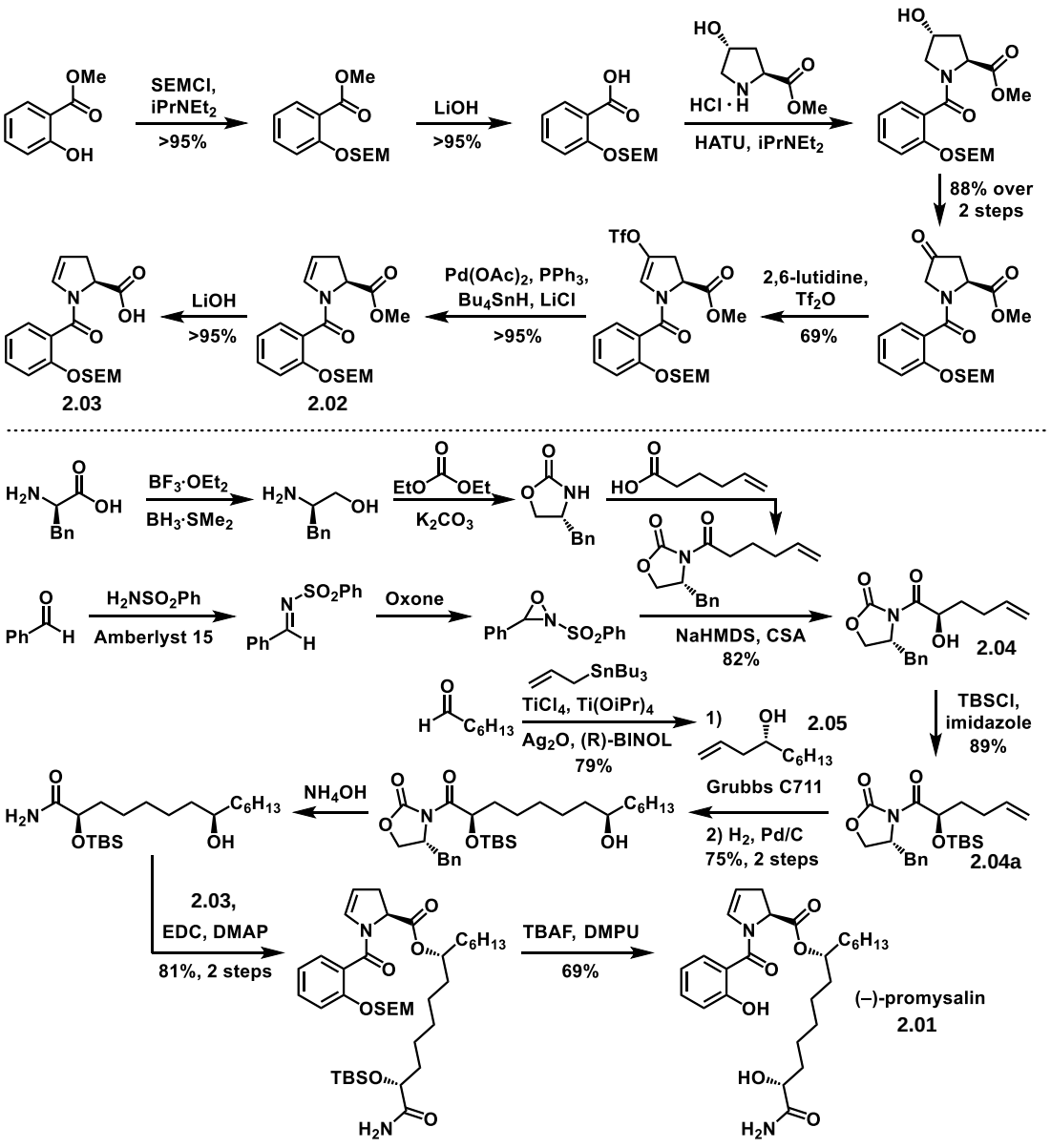

Scheme 2.1. Total synthesis of promysalin by the Wuest lab

In order to develop improved analogs of promysalin, it was important to understand its antibacterial mechanism of action. Lacking the proteomics expertise to deduce this ourselves, we initiated a collaboration with Stephan Sieber's lab at the Technical University of Munich. By developing a promysalin probe containing an aziridine/alkyne moiety (**Figure 2.4A**) for photoinduced crosslinking and biotin-streptavidin pulldown, respectively, we used affinity based protein profiling to discover that promysalin binds to succinate dehydrogenase (Sdh) (**Figure**

2.4B). This membrane-bound enzyme functions in the citric acid cycle, catalyzing the oxidation of succinate to fumarate, coupled to the reduction of ubiquinone to ubiquinol (**Figure 2.4C**). It also serves as complex II in the electron transport chain. Inhibiting this enzyme thus deprives the bacteria of significant amounts of energy, slowing growth. This mechanism of action was confirmed via successful growth of *P. aeruginosa* on plates supplemented with fumarate, as well as from successful serial passage experiments to generate a promysalin-resistant mutant, in which residues in Sdh are altered.[94]

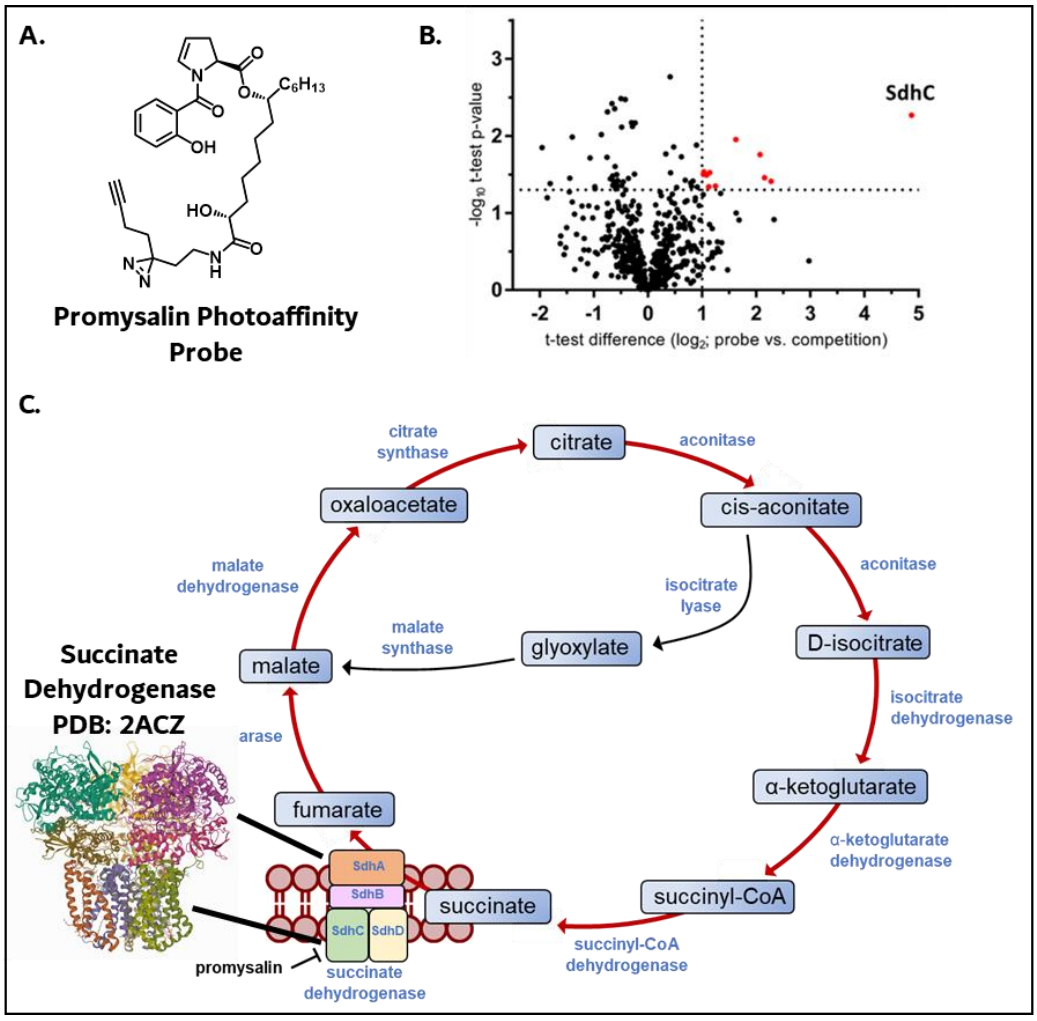

Figure 2.5. A. Structure of photoaffinity probe used in proteomic analysis of promysalin. **B.** Volcano plot showing significant and highly enriched pulldown of SdhC, indicating this is promysalin's target. **C.** Crystal structure of *E. coli* Sdh, and biochemical function of Sdh in the citric acid cycle

Armed with the knowledge that promysalin's antibiotic activity can be attributed to inhibition of Sdh, we wanted to understand the specific binding interactions between the small molecule and its binding site. As Sdh is membrane bound and has never been crystallized in *P. aeruginosa*, an X-ray crystal structure of a bound state was not feasible. We instead relied on computational methods, collaborating with Dr. John Karanicolas at the Fox Chase Cancer Center to develop a computational homology model of *P. aeruginosa* Sdh and docking promysalin into this virtual model (**Figure 2.6, Figure 2.10**).[94]

While Dr. Steele's diverted synthetic route has been effective, allowing the group to generate over 50 promysalin analogs to date (revealing that the proline-salicylate ring is not amenable to modification), none of these compounds have overcome the major liability of promysalin – its large difference between its minimum inhibitory concentration (MIC) and its 50% inhibitory concentration (IC_{50}) (**Figure 6.1**).[95] This difference signifies that while promysalin is extremely capable of inhibiting growth of a significant portion of *P. aeruginosa* cells, total inhibition of the population requires insurmountably large amounts of drug. It remains unclear whether this remaining population is truly resistant to promysalin or if it represents an example of persistence. While drug resistance is defined as a genetic modification of an organism to resist the effects of a drug, persistent cells evade a drug's mechanism of action by becoming metabolically inactive. As promysalin functions by inhibiting primary metabolism, either of these phenomena may be occurring.

We first pursued the hypothesis that a subset of the *P. aeruginosa* population was inherently resistant to promysalin, as resistance selection assays had been successful in the past. If resistance were occurring, there were two likely mechanisms by which this could happen. First, promysalin may be hydrolytically cleaved about its ester linkage into a carboxylic acid fragment and an alcohol

fragment (both of which have been synthesized and shown to be biologically inactive). This hydrolysis may be enzymatic, catalyzed by an ester hydrolase, or it may be pH mediated, as promysalin has been repeatedly shown to be unstable in acidic solutions. The second proposed mechanism of resistance is efflux of promysalin to sublethal intracellular concentration via one of *P. aeruginosa's* many known efflux pumps (**Figure 2.6**).[91]

While we judged ester hydrolysis and efflux to be the most likely mechanisms of resistance, they are by no means the only possibilities. A transcriptomic analysis of the promysalin producing stain of *P. putida* revealed that in addition to upregulating the expression of efflux pumps, it is able to avoid being killed by its own metabolite by altering metabolic flux, downregulating the Entner-Doudoroff pathway and increasing nutrient uptake and the β-ketoadipate pathway in the presence of exogenous promysalin.[96]

In order to combat the proposed promysalin ester hydrolysis mechanism of resistance, we desired a promysalin analog containing an amide linkage. As amides are known to be significantly less

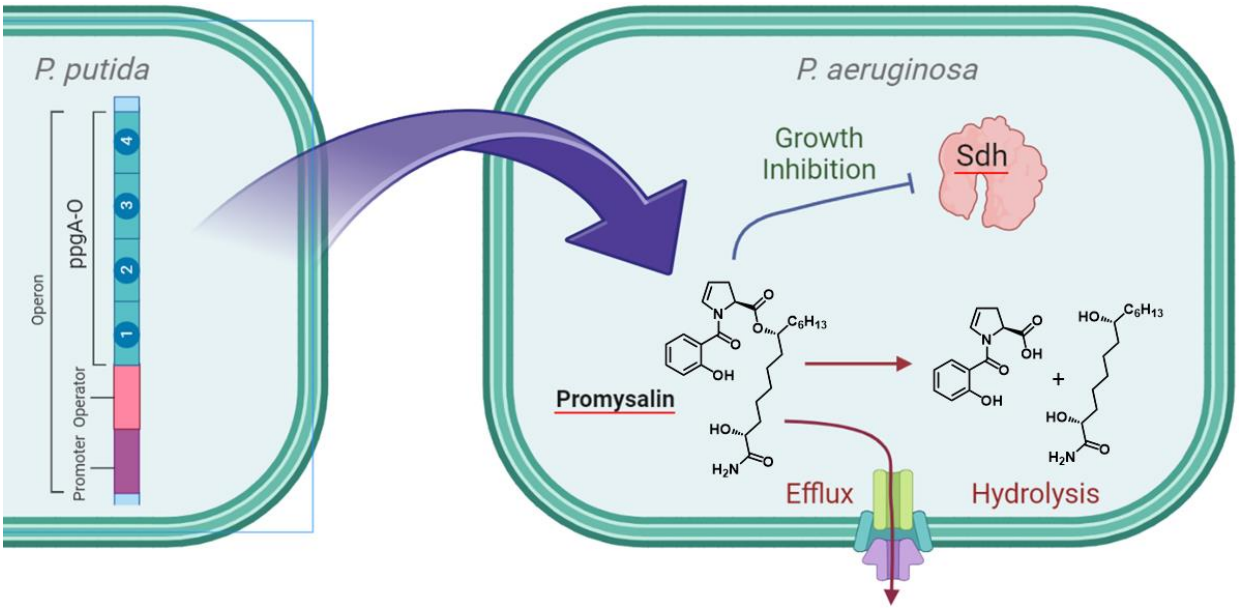

Figure 2.6. Promysalin's biosynthesis by *P. putida*, biological target in *P. aeruginosa*, and two proposed mechanisms of resistance

hydrolytically prone than esters, this seemed an appropriate solution. However, this simple modification removed all biological activity, a surprising outcome. Upon examination of the bound conformation of promysalin in Sdh, we identified a potential hydrogen bonding interaction between promysalin's terminal amide and its linker ester – we therefore reasoned that disruption of this stabilizing effect by replacing the ester with an amide was responsible for the observed loss of potency. To overcome this challenge, we desired an analog in which the moieties were switched, a linker amide to reduce hydrolytic potential and a terminal carboxylic acid to restore the proposed hydrogen bonding effect. We also wanted to further increase binding affinity and stability in the binding pocket by incorporation of aryl groups at the unfunctionalized end of the sidechain, allowing for pi-stacking with a nearby tryptophan residue on the protein (**Figure 2.7**).[97]

To combat the proposed efflux mechanism of *P. aeruginosa* resistance to promysalin, we desired analogs which could utilize a targeted covalent inhibitor (TCI) approach. Targeted covalent inhibition is a strategy employed in some small molecule drugs in which there is a well characterized binding site (**Figure 2.8**). If this binding site contains a particularly reactive amino

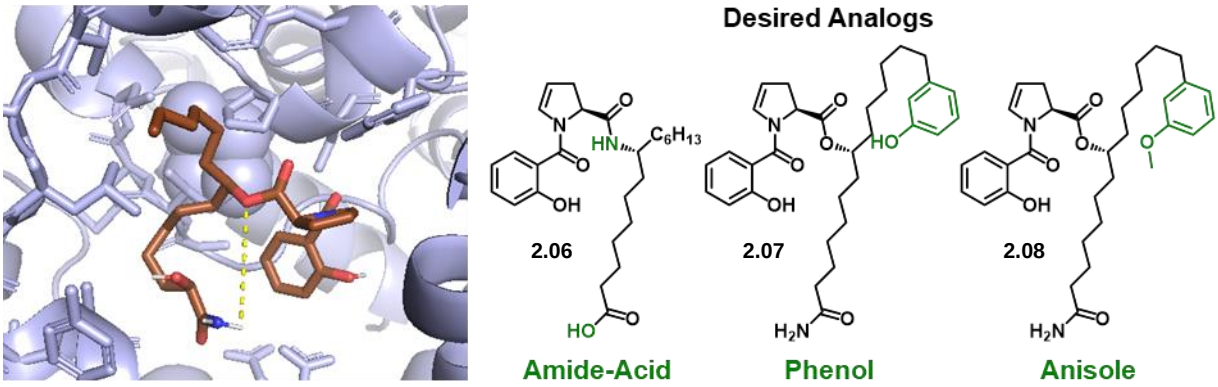

Figure 2.7. Computational docking model of promysalin showing a key intramolecular hydrogen bond

acid (such as a nucleophilic serine, lysine, or cysteine), the drug can be designed to incorporate functionality which will covalently react with the target amino acid.[98,99] Covalently ligating a small molecule drug to its protein of interest can dramatically improve drug potency, but fears of off

target reactivity of strongly electrophilic covalent "warheads" precluded significant efforts by the pharmaceutical industry to pursue this class of drugs until recently. As a result, while many approved drugs are known to function through covalent inhibition of their targets, it was only after common usage that their mechanisms of action were discovered (i.e. targeted covalent inhibition was not a goal of drug design, it was an unintended process that happened to result in a successful medication). Aspirin, β-lactam antibiotics, and omeprazole are all famous examples of covalent drugs that found use long before their exact biological roles were discovered. Luckily, recent improvements in synthetic chemistry and in understanding of reactivity in biological systems has caused a resurgence of this strategy, allowing a medicinal chemist to fine tune the TCI functional group to be only as reactive as necessary to engage with the target, minimizing selectivity issues (**Figure 2.9**).[98,100,101]

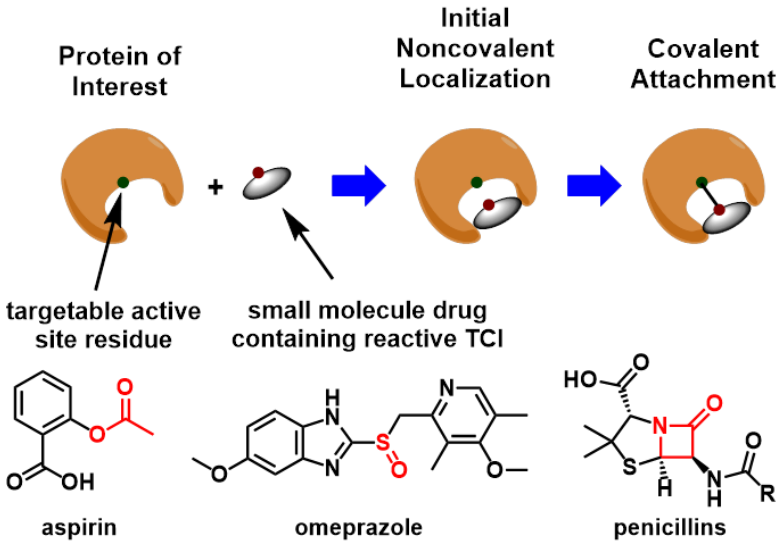

Figure 2.8. General TCI strategy, and popular pharmaceuticals known to function through covalent inhibition

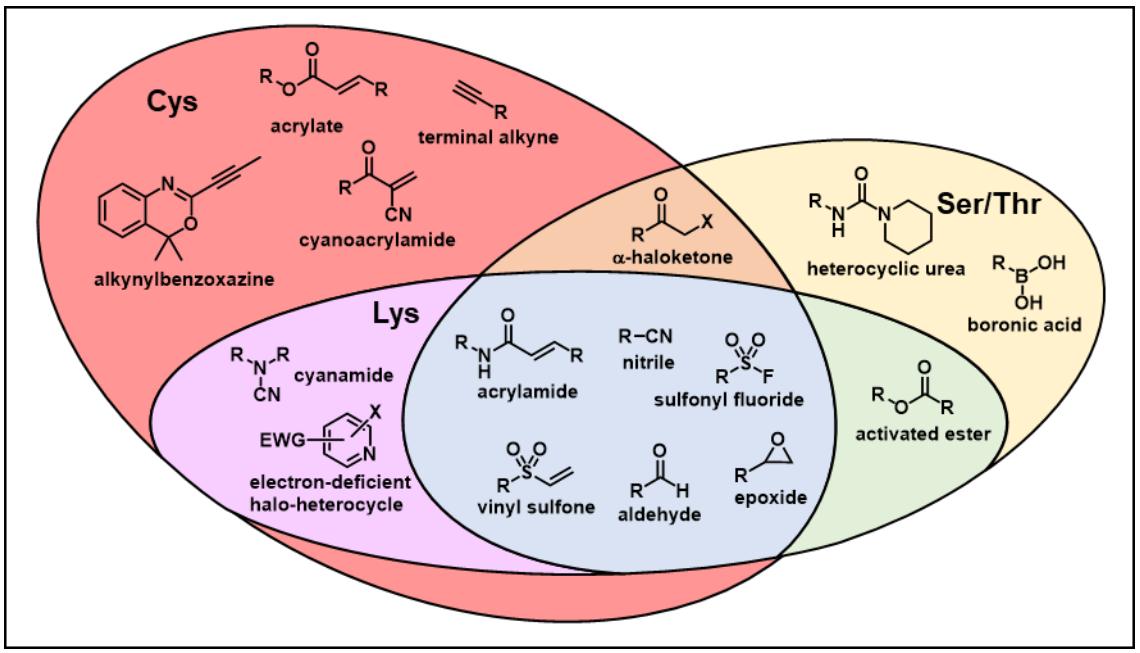

Figure 2.9. Venn diagram of selectivities of some common TCIs towards cysteine (red oval), serine/threonine (yellow oval), or lysine (blue oval)[101]

We rationalized that utilization of a TCI strategy had the potential to overcome the proposed efflux mechanism of resistance in *P. aeruginosa*. Covalently ligating promysalin to Sdh would render the cell unable to efflux the molecule without first degrading the protein or the covalent linkage. Furthermore, the increase in binding affinity and more ordered binding mode granted by utilizing covalent inhibition could be expected to translate to a more potent antibiotic. Incorporation of TCI functionality into promysalin first required identification of a sufficiently reactive residue in *P. aeruginosa* Sdh. Fortunately, we observed a key serine residue in close proximity to the amide terminus of promysalin's sidechain, a region we had previously shown to be amenable to modification.[94,95] We therefore sought to design a series of analogs replacing the terminal amide with a small set of electrophiles commonly used in TCI strategies. Acrylamides are by far the most frequently encountered TCI functional groups, serving as Michael acceptors to irreversibly bind nucleophilic amino acids such as cysteines. TCIs specifically targeting less nucleophilic hydroxyl nucleophiles (Ser, Thr) include nitriles and boronic acids – while reversible covalent inhibitors,

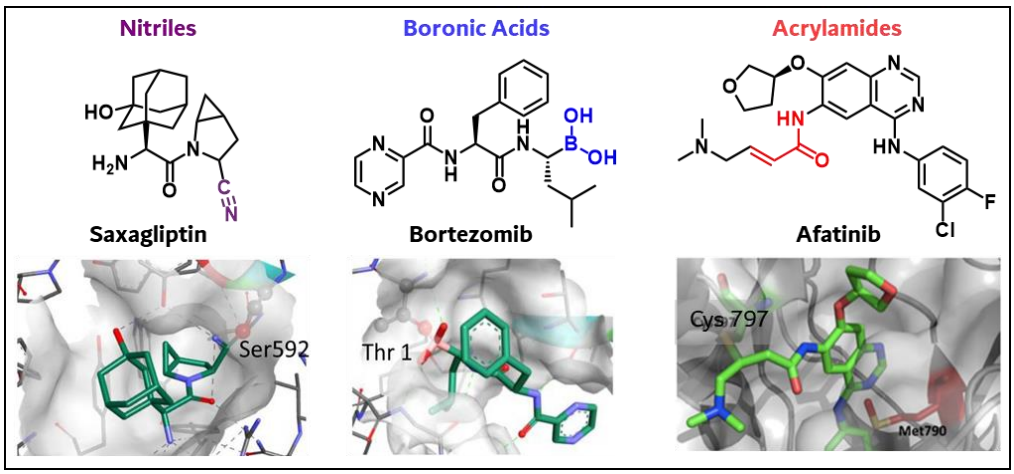

Figure 2.10. Recent successes in incorporation of TCIs to enzyme inhibitors, and depictions of their binding modes

these functionalities have proved successful in the development of covalent protein inhibitors (**Figure 2.10**). We were interested in developing two series of promysalin TCI analogs, one which retained the native length of promysalin's sidechain, and one which extended the sidechain slightly in order to position the TCI functional group in optimal proximity to Ser27 in the binding pocket (**Figure 2.11**).

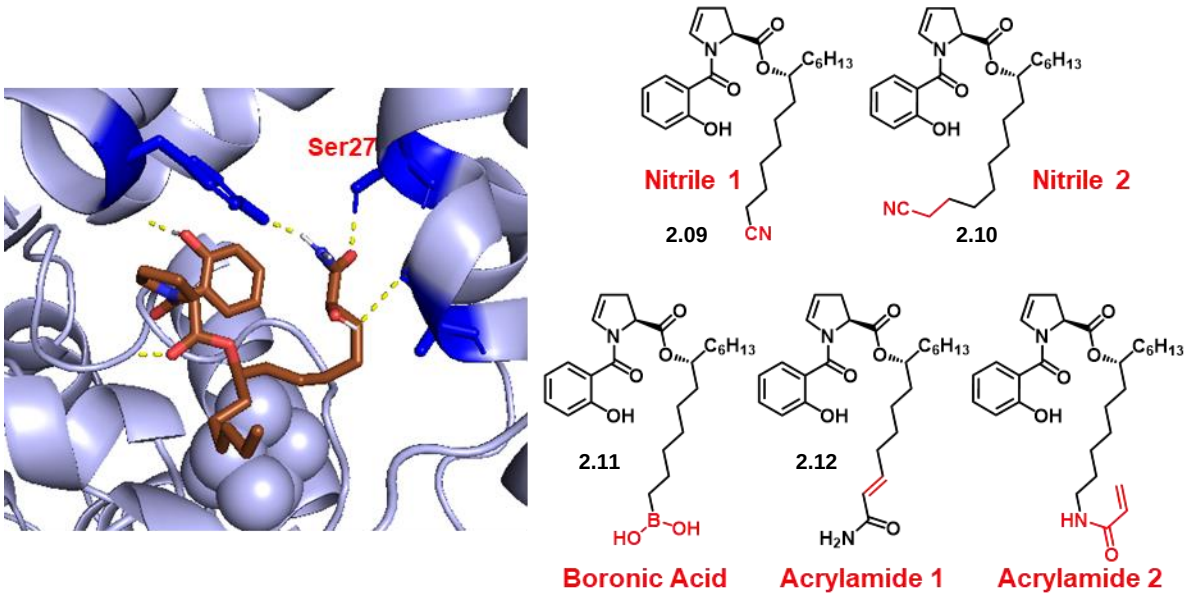

Figure 2.11. Computational docking model of promysalin showing a targetable active site serine, and a series of desired analogs containing Ser-reactive TCIs

2.2 Synthesis

As our lab had already developed a robust diverted total synthesis strategy for the development of promysalin analogs, the synthetic route towards the desired analogs required only the novel sidechains incorporating the necessary functionality.[95] These sidechains could then be coupled to the proline-salicylate pharmacophore, followed by fluoride-mediated desilylation (**Scheme 2.2**).

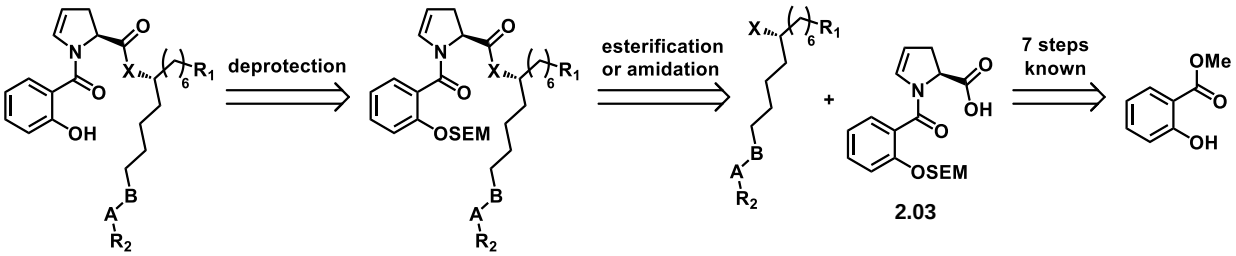

Scheme 2.2. General retrosynthetic strategy towards desired analogs

alcohol required for the other desired analogs, its synthesis was pursued first. Initial attempts to synthesize this compound relied on a Mitsunobu reaction to substitute the known hydroxyl compound **2.14** with an azide, with complete inversion of stereochemistry (**Scheme 2.3**).[95] This reaction proved very challenging, giving irreproducible yields and requiring extensive purification to remove the reduced DIAD and PPh_3O byproducts formed in the reaction, both of which coelute with the product in mixtures of ethyl acetate/hexane eluents. Attempts to carry these impurities through to the following reaction (a simultaneous alkene hydrogenation and azide reduction to the

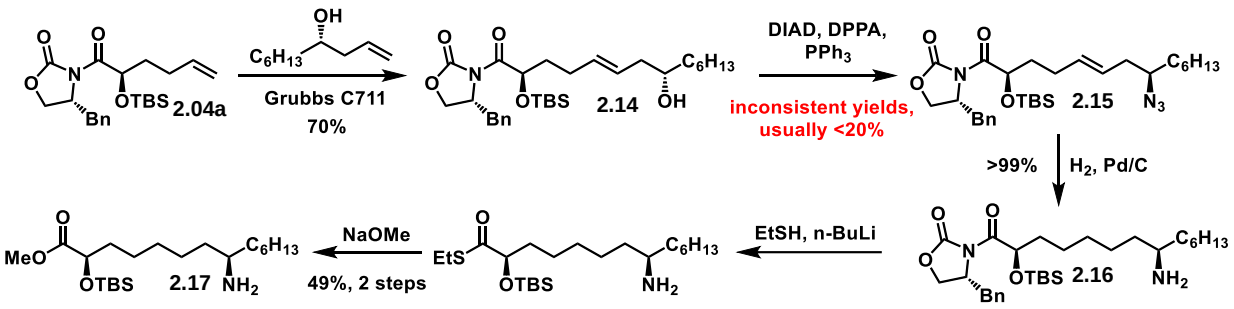

Scheme 2.3. Initial synthetic route to amide acid sidechain, utilizing a Mitsunobu reaction to generate a chiral azide

corresponding primary amine) also proved disastrous, as the newly formed amine (**2.16**) was found to react with reduced DIAD to form conjugated products.

Alternatives to the Mitsunobu reaction were considered, as generation of a chiral homoallylic amine has been reported in the literature. One strategy involves formation of a benzyl imine, followed by asymmetric allylation utilizing a chiral bis-π-allylpalladium catalyst.[102] Alternatively, reports of camphorquinone-based auxiliaries to activate the aldehyde piqued our interest due to the lack of required metal catalysis.[103] The resulting chiral imine can then undergo an aza-Cope rearrangement to deliver the required chiral homoallylic amine (**2.19**, **Scheme 2.4**). This second strategy was attempted and began with synthesis of the necessary chiral auxiliary. Camphorquinone was thus reacted with methanolic ammonia to form the corresponding imine, which was then allylated with pinacol allylboronate. Subsequent condensation of **2.18** onto heptanal did indeed induce aza-Cope rearrangement, leading to low amounts of isolable **2.19** after hydrolysis with hydroxylamine-acetic acid. While this method was relatively facile, allowing for recovery and recycling of the camphorquinone auxiliary, the resulting homoallylic amine (**2.19**) proved challenging to purify, requiring chromatography (whereas the analogous homoallylic alcohol **2.05** could be distilled) and complicated due to its high polarity and streaking on silica. Furthermore, the low amounts of isolated product could not be successfully coupled to the Evans

alkene fragment (**2.04a**) likely due to coordination of the amine with the Grubbs catalyst, leading to deactivation.

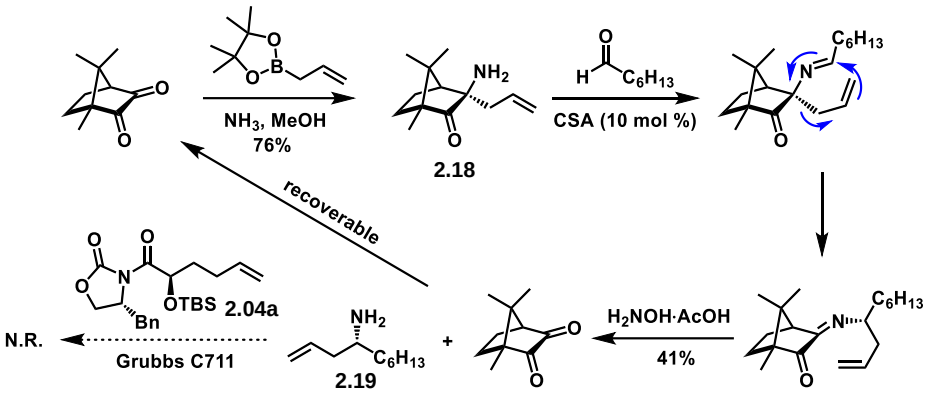

Scheme 2.4. Alternative strategy towards chiral homoallylic amine using a camphorquinone-directed aza-Cope cyclization

Based on this result, it was decided that generation of the chiral amine should be performed after the already-optimized metathesis reaction of the homoallylic alcohol. Due to the high step count required for synthesis of the Evans alkene (**2.04a**), optimization was done instead utilizing the commercially available reagent methyl hex-5-enoate. Our lab's SAR campaign on the promysalin sidechain revealed the α-hydroxyl group is not necessary for activity, so the dehydroxylated amide acid was pursued instead (**Scheme 2.5**).

Use of a Mitsunobu reaction with DIAD and DPPA still proved initially challenging for reliable synthesis and purification of this simplified sidechain (**2.21**). Fortunately, optimization of reaction conditions was successful in remedying these issues for this particular scaffold. In particular, decreasing the temperature and increasing the reaction time limited *in situ* decomposition of DIAD, lowering the number of byproducts that needed to be removed. This allowed for purification utilizing a less arduous method: removal of the bulk of PPh_3 and PPh_3O via column chromatography in a slow gradient of 0-10% EtOAc/hexanes, followed by removal of reduced

DIAD by preparative TLC. While this material still contained residual PPh_3 and PPh_3O, it was found that this did not significantly affect yield in the subsequent hydrogenation/reduction step, giving the completed amide acid sidechain (**2.21**). Alternatively, if purer material was desired, trituration with cold pentane followed by decanting was usually successful in affording product, albeit in a lower yield due to partial solubility of the product in pentane.

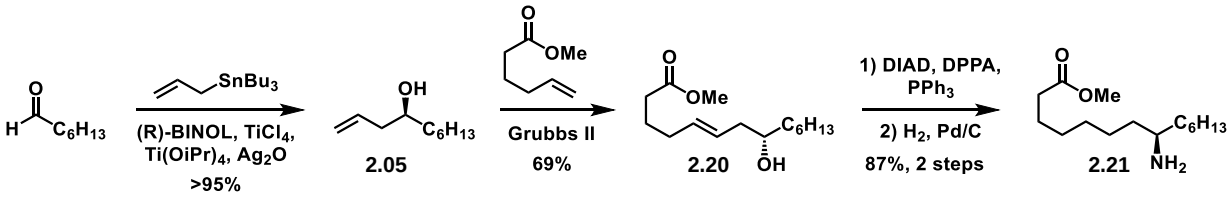

Scheme 2.5. Successful synthesis of amide acid sidechain utilizing a simplified Mitsunobu scaffold

We envisioned that the phenol (**2.07**) and anisole (**2.08**) analogs could be derived from the same starting materials, and that a reaction to cleave the aromatic methyl ether could be used to efficiently derivatize the material at a late stage (**Scheme 2.6**). Utilizing the same approach used by previous lab members to generate a phenyl analog, we first coupled ethyl hept-6-enoate to 3-vinylanisole using cross metathesis.[97] Hydrogenation of the resulting styrene to **2.22** followed by partial ester reduction with DIBAL-H formed our key aldehyde fragment (**2.23**). This aldehyde was subjected to Keck allylation (forming **2.24**), after which point a second Grubbs metathesis was used to couple hex-5-enamide; a second hydrogenation then afforded anisole sidechain **2.25**. Demethylation of the anisole was unsuccessful utilizing Lewis acids such as BBr_3, but a nucleophilic demethylation with sodium ethanethiolate proved more successful, allowing late stage conversion of anisole sidechain **2.25** into phenol sidechain **2.26**.[104]

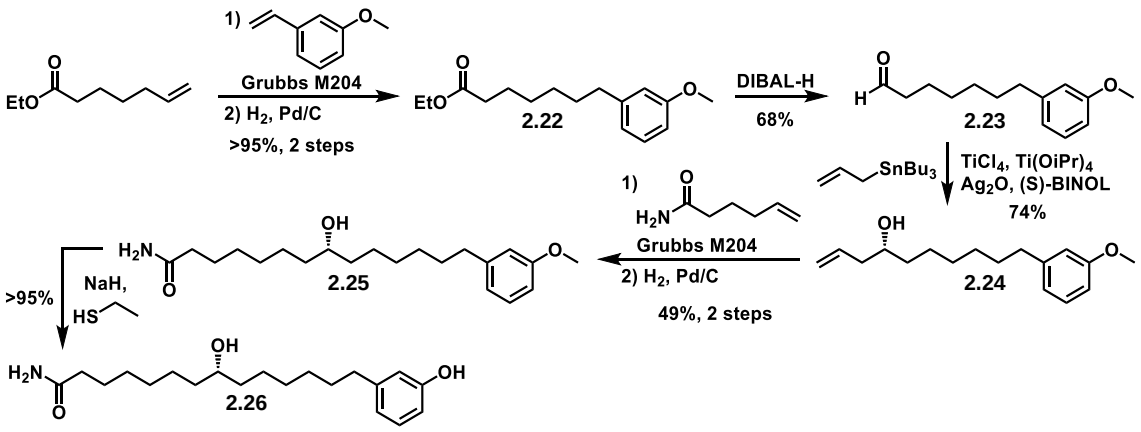

Scheme 2.6. Synthesis of anisole and phenol sidechains

We next turned our attention towards synthesis of the TCI sidechains. We began with synthesis of the sidechain required for nitrile analog **2.09**, as we reasoned that this should be easily accessible via dehydration of the amide present in the sidechain (**2.27**) of dehydroxypromysalin, a previously synthesized analog (**Scheme 2.7**). Due to apprehensions about exposure of the chiral hydroxyl group to dehydrating agents, we first protected this moiety as a silyl ether; subsequent dehydration with thionyl chloride and fluoride-mediated silyl deprotection proved straightforward in formation of **2.28**. The incorporation of a boronic acid TCI required a slightly different approach, as while boron's innate electrophilicity due to its vacant p-orbital renders it an excellent option for medicinal covalent inhibition, it also presents a potential synthetic liability. Fortunately, the development of a robust and general boronic acid protecting group by the Burke lab in the form of N-methyliminodiacetic acid (MIDA) boronates presented a useful solution to our synthetic concerns.[105] MIDA protection of 4-pentenylboronic acid (generated by Grignard addition of 4-pentenylmagnesium bromide to trimethylborane) enabled successful cross metathesis and hydrogenation to afford our desired protected boronic acid side chain (**2.30**, **Scheme 2.7**).

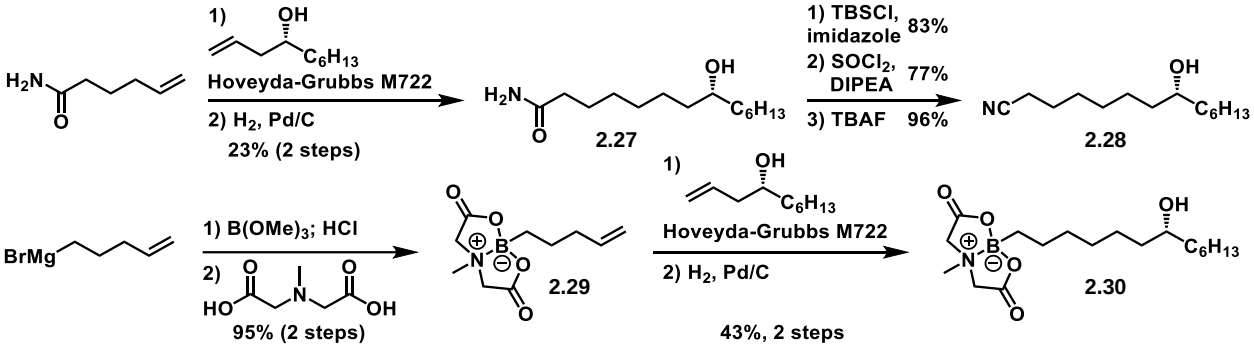

Scheme 2.7. Synthesis of short nitrile and boronic acid analog sidechains

The sidechain for acrylamide 2 analog **2.13** was initially vexing. An initial route was designed in which metathesis of an amine-containing terminal alkene could be followed by reaction of that amine with acryloyl chloride (**Scheme 2.8**). However, attempts to perform this reaction were unsuccessful, as amines are extremely poor metathesis substrates due to their high Lewis basicity. Attempts to mask this basicity by using trifluoroacetic acid or toluenesulfonic anhydride as additives did not remedy the situation. Protection of the amine with a sterically bulky Fmoc group (**2.31**) allowed for metathesis reaction to take place in acceptable yield and deprotection to **2.33** was facile, affording crude product with no aromatic resonances by ^{1}H or ^{13}C NMR. However, upon attempting to acylate with acryloyl chloride, we observed a surprising and undesired selectivity for acylation of the secondary alcohol. Generation of O-acrylated and O,N-diacrylated species **2.33a** and **2.33b**, respectively, occurred in a 3:1 molar ratio, with no isolation of desired N-monoacrylated product, indicating that O-acrylation of **2.33** proceeded first. Protection of this secondary alcohol was undesirable as it added additional steps and required the use of two orthogonal protecting groups. Additionally, we have repeatedly observed that protection of this alcohol immediately after Keck allylation severely lowers yields of subsequent metathesis, presumably due to increased steric bulk about the terminal alkene. As a result, alternative approaches were considered.

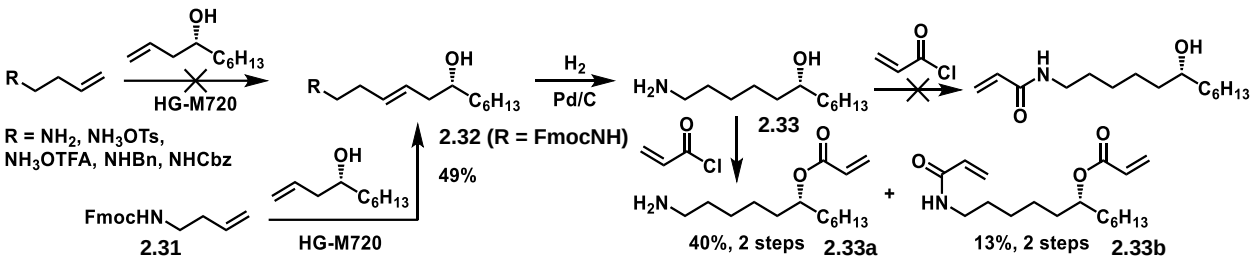

Scheme 2.8. Initial attempts towards synthesis of flipped acrylamide sidechain

While asymmetric Keck allylation had proved successful in the formation of our chiral homoallylic alcohol intermediates, the arduous reaction setup and purification, as well as the high cost and high toxicity of the reagents required led us to desire a more chemist-friendly approach at this point. After considering several options including alternative allylation reactions and chiral reductions, we settled on a sequential Grignard addition approach to commercially available (S)-epichlorohydrin (**Scheme 2.9**). Reports of this approach in the literature drew our attention, as it has been previously utilized to synthesize very similar scaffolds to our desired system.[106] Regioselective copper-catalyzed Grignard addition of 5-pentenylmagnesium bromide to the less hindered face of this chiral epoxide proceeded in high yield to produce **2.34**. Base-mediated epoxide reformation followed by second Grignard addition of pentylmagnesium bromide successfully generated chiral intermediate **2.35** which we envisioned could be derivatized to form

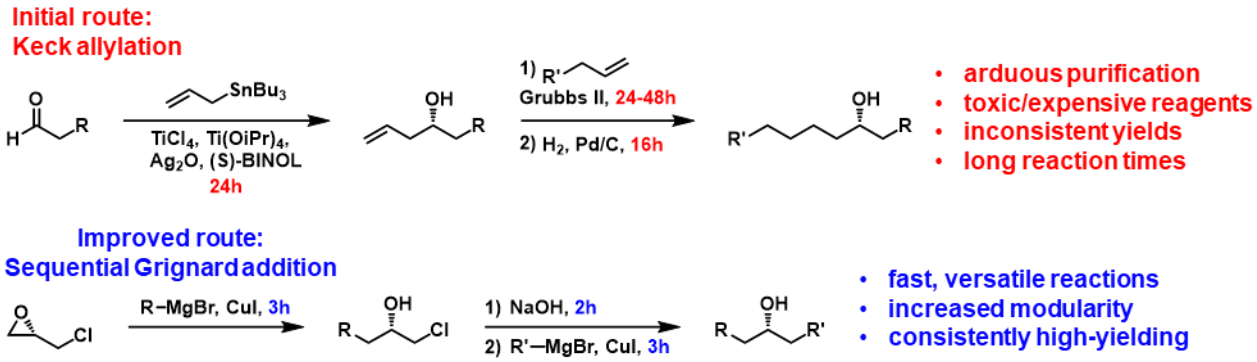

Scheme 2.9. Improved approach for promysalin sidechain synthesis using sequential Grignard addition to (S)-epichlorohydrin

the rest of our desired analogs, in a manner which proved much easier and faster than the Keck allylation approach (**Scheme 2.10**). Cross metathesis of this intermediate with acrylamide thus generated our required acrylamide sidechain (**2.40**, **Scheme 2.12**).

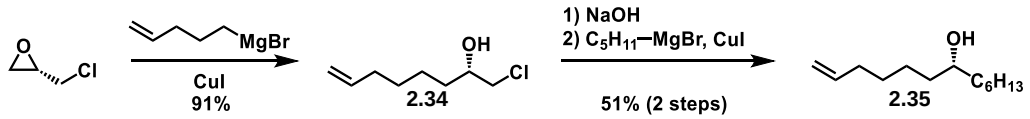

Scheme 2.10. Use of new promysalin sidechain synthesis to generate key chiral intermediate

When utilizing the sequential Grignard addition strategy instead of the initial Keck allylation, the resulting product (**2.35**) contains three additional carbons between the chiral alcohol and the terminal alkene (relative to **2.05**). In the case of the desired flipped acrylamide analog, no additional carbons are necessary so the metathesis reaction could be circumvented altogether. Instead, an anti-Markovnikov hydroamination reaction of the terminal alkene could afford the primary amine.[107] In this case, protection of the secondary alcohol as a tert-butyldiphenyl silyl ether was not burdensome and was not predicted to affect yields for subsequent reactions. Furthermore, this choice of protecting group allowed for incorporation of a chromophore, allowing for easier reaction monitoring and subsequent purification. We were able to encourage successful and regioselective hydroamination first via hydrozirconation of the alkene using Schwartz's reagent (zirconocene hydrochloride) followed by *in situ* displacement of the zirconium with hydroxylamine-O-sulfonic acid. Substitution of the newly generated amine (**2.41**) onto acryloyl chloride was then straightforward, and the silyl ether could be cleaved utilizing hydrofluoric acid (less harsh deprotections using TBAF or KF/18-crown-6 were attempted but did not result in product formation) to deliver the desired deprotected sidechain (**2.42**, **Scheme 2.12**).

Synthesis of our extended nitrile analog (**2.10**) also proved initially challenging (**Scheme 2.11**). While shortened nitrile sidechain **2.28** could simply be made from dehydration of the amide in the

dehydroxypromysalin sidechain, the required methyl oct-7-enoate (or the corresponding acid) required for synthesis of the analogous lengthened sidechain is not commercially available. Utilizing the new sequential Grignard approach overcame this problem, as additional carbons on alcohol fragment **2.35** (relative to **2.05**) meant that shorter, commercially available methyl pent-5-enamide was required instead. Unfortunately, Grubbs metathesis gave low yields of product, attributable to very low solubility of this amide in appropriate metathesis solvents and/or coordination and subsequent deactivation of the ruthenium catalyst to the amide. Dibenzylation of the amide to **2.38** overcame both of these issues, allowing for a significant improvement in metathesis yield, however attempts at subsequent removal of these benzyl groups either by hydrogenolysis or by direct von Braun degradation to the nitrile proved futile. Indeed, literature reports of successful debenzylation of tertiary amides are scarce. We were therefore forced to abandon an amide dehydration strategy for generation of our extended nitrile analog.

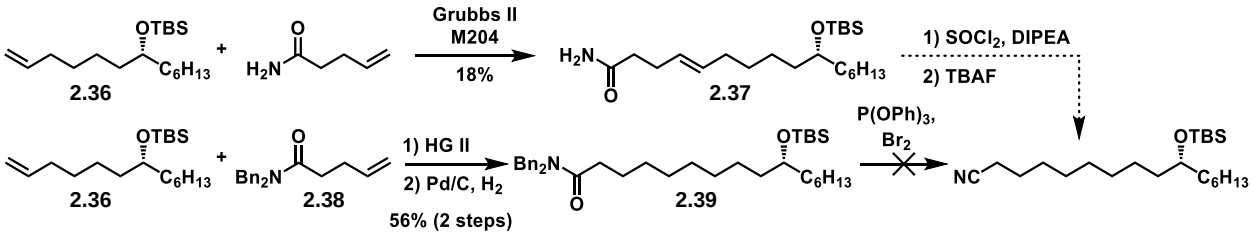

Scheme 2.11. Initial strategies towards the extended nitrile sidechain using an amide dehydration approach

We next considered alternative methods of nitrile formation. For example, the oxidative transformation of terminal alcohols to nitriles has been reported using a variety of systems.[108–110] However, test reactions using these conditions on simple aliphatic alcohols did not in our hands reliably generate the desired nitrile, and it was hypothesized that the functionalized sidechain would fare no better. In addition, this oxidative strategy would likely require protection of the chiral secondary alcohol, further increasing the number of synthetic steps. Fortunately, we

discovered a successful method of generating our desired analog through direct metathesis of homoallyl cyanide.[111] This result was surprising, as nitriles are notoriously poor metathesis substrates due to their ability to coordinate to metals, and because initial test reactions using this approach had not proved successful. Optimization of reaction conditions nevertheless was able to generate the desired product in satisfactory yield. Chemoselective hydrogenation of the internal alkene also required optimization – initial attempts to perform this reduction using homoallyl cyanide as a test substrate resulted in formation of a mixture of primary, secondary, and tertiary amines – but was successful when very low catalyst loadings and short reaction times were employed, thus generating extended nitrile sidechain **2.43** (**Scheme 2.12**).

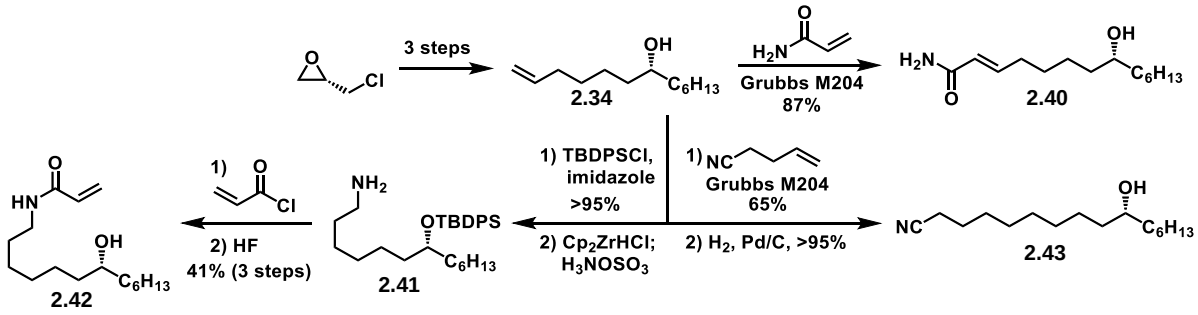

Scheme 2.12. Use of key synthetic intermediate from novel sequential Grignard strategy in the rapid synthesis of remaining desired analog sidechains

In general, EDC coupling of the promysalin analog sidechains to proline-salicylate fragment **2.03** followed by SEM deprotection with TBAF was straightforward, following reports by past members of our lab (**Scheme 2.13**). In the case of boronic acid analog **2.11**, the incompatibility of MIDA boronates with hard nucleophiles such as fluoride necessitated SEM deprotection of **2.02** prior to hydrolysis and EDC coupling. Rapid boronate deprotection was then achieved under basic conditions. In the case of **2.06**, a final base-mediated saponification of the methyl ester present in sidechain **2.21** after coupling was necessary to afford the completed amide-acid analog.

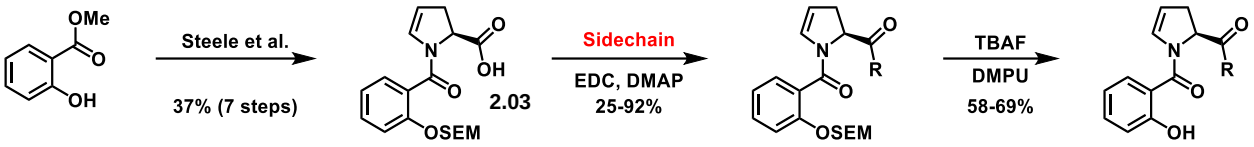

Scheme 2.13. Final coupling and deprotection steps for desired promysalin analogs

2.3 Biological Investigation

With our set of desired promysalin analogs in hand, we next turned our attention towards biological analysis of these compounds. IC_{50} assays were performed to assess the inhibitory activity of our compounds against *P. aeruginosa* strains PAO1 and PA14 (**Table 2.1, Table 6.4, Figure 6.3**). Previously reported noncovalent analog and best-in-class lead compound dehydroxypromysalin was used as a positive control, in addition to gentamicin. The newly-synthesized phenol (**2.07**) and anisole (**2.08**) promysalin analogs were not tested in this panel but will be tested by other members of the group alongside other aryl-substituted analogs within the next six months.

Table 2.1. IC_{50} values of amide acid and TCI analogs against *P. aeruginosa*, as well as previously published noncovalent analog NC used as positive control

Analog	PA14	PAO1
amide acid (2.06)	>250	>250
nitrile 1 (2.09)	1.58	2.04
nitrile 2 (2.10)	3.67	2.56
boronic acid (2.11)	21.6	42.2
acrylamide 1 (2.12)	5.24	15.2
acrylamide 2 (2.13)	5.58	7.69
gentamicin	6.16	4.90
dehydroxy-2.01	0.516	3.29

Of the newly synthesized analogs, nitrile **2.09** proved most potent, with IC_{50} values of 1.58 µM and 2.04 µM against PA14 and PAO1, respectively. The extended analogs both proved equipotent to their shortened counterparts (**2.10** compared to **2.09**, or **2.13** compared to **2.12**), indicating a lack of steric or electronic constraints in that sector of the Sdh binding pocket. Interestingly, the amide acid analog (**2.06**) was completely inactive against either strain. One potential explanation

for this result is that increased conformational strain about the amide linker relative to that of the ester-containing analogs and natural product prevents these molecules from adopting the twisted conformation observed in our docking model. The boronic acid-containing analog (**2.11**) also saw drastically decreased activity relative to the other analogs, this may be due to an observed reversible macrocyclization resulting from nucleophilic addition of the salicylate phenol into the boronic acid, confirmed by variable temperature NMR and mass spectrometry studies (**Figure 2.12**). As we have previously identified that the salicylate phenol is crucial for biological activity, this macrocyclization may be deleterious and sufficiently decrease Sdh binding affinity to result in the observed reduced *P. aeruginosa* inhibition.

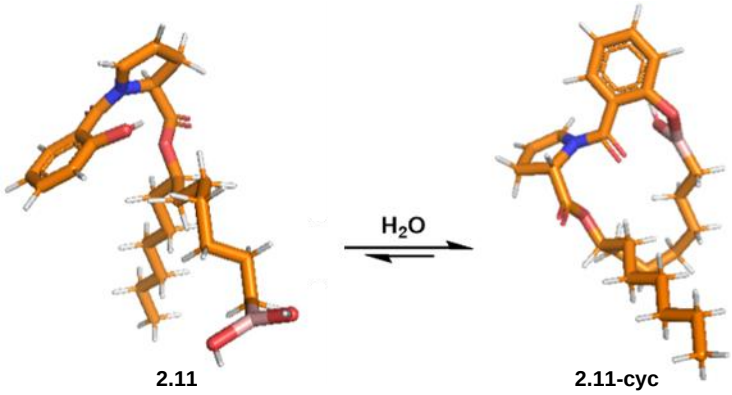

Figure 2.12. Reversible macrocyclization observed in boronic acid analog

Unfortunately, none of our newly synthesized analogs had improved MIC values against any tested PA strain relative to that of promysalin (MIC values >250 μM for all analogs reported herein), indicating that we were unsuccessful in fully overcoming PA resistance mechanisms. We were, however, still interested in investigation of whether *P. aeruginosa*'s resistance to promysalin was occurring through an efflux mechanism. To answer this question, we collaborated with Genentech (Dr. Kelly Storek) to develop a *P. aeruginosa* strain harboring gene deletions of eight efflux pumps

and porins (mexXY, mexCD-oprJ, mexJK, opmH, mexEF-oprN, oprD, mexGHI-opmD, and mexAB) (**Table 6.3**).

To assess whether our targeted covalent inhibitor-containing analogs were less susceptible to the hypothesized efflux mechanism of *P. aeruginosa* promysalin resistance, we tested our four best analogs (**2.09, 2.10, 2.12,** and **2.13**) against this novel efflux knockout strain (**Table 2.2, Table 6.4, Figure 6.3**). As expected, all analogs showed an increase in potency, including control compound dehydroxypromysalin which possesses a 74 picomolar IC_{50}, suggesting that efflux through one or more of these pumps is in fact playing at least some role in promysalin resistance in wild-type *P. aeruginosa*. Of the newly synthesized analogs, the shortened acrylamide (**2.12**) showed the most marked increase in activity, with a 1000-fold decrease in IC_{50} value relative to the parent PA14 strain and displaying single digit nanomolar inhibitory activity. This may indicate that **2.12**, while a very potent inhibitor of *P. aeruginosa* Sdh, is particularly sensitive to efflux.

Table 2.2. Summary of IC_{50} data for amide acid and TCI analogs against *P. aeruginosa*, including a newly generated efflux-incapable strain

Analog	PA14	PAO1	PA14 efflux knockout
amide acid (2.06)	>250	>250	N.T.
nitrile 1 (2.09)	1.58	2.04	0.267
nitrile 2 (2.10)	3.67	2.56	1.28
boronic acid (2.11)	21.6	42.2	N.T
acrylamide 1 (2.12)	5.24	15.2	0.00299
acrylamide 2 (2.13)	5.58	7.69	0.388
gentamicin	6.16	4.90	3.50
dehydroxy-2.01	0.516	3.29	0.0000744

We were also interested in investigating whether these analogs retain the species selectivity reported by the initial isolation group. *Pseudomonas syringae* is another well-studied bacterial species and displays pathogenicity towards plants. It receives particular attention in the agrochemical industry, in which *P. syringae* can affect a wide variety of dissimilar crops including

wheat, tomato, horse chestnut, and kiwifruit plants.[112,113] Due to these effects, *P. syringae* presents a major economic hurdle; recent outbreaks in Italy and New Zealand cost an estimated $2 million and $2 billion, respectively.[112] Examination on the effects of promysalin analogs on this pathogen therefore presented an interesting opportunity, as potent inhibition of this species would provide a much-needed treatment option, whereas a lack of inhibition would mean that these analogs are exquisitely selective for *P. aeruginosa*.

None of the tested analogs showed any activity against *P. syringae*, highlighting that these compounds have increased species specificity relative to that of the natural product itself, which was reported active against this bacterium. The precise biochemical mechanisms by which this selectivity arises are yet to be understood but are likely a combination of differences in the metabolic flux between these species. For example, in the citric acid cycle, a known glyoxylate shunt pathway can circumvent the need for Sdh by conversion of isocitrate to malate (**Figure 2.4C**), bypassing fumarate (the normal product of Sdh). If *P. syringae* is more competent in diverting carbon flux to this pathway than *P. aeruginosa*, it could provide one explanation for why inhibition of Sdh is effective in the latter, but not the former. Differences in nutrient absorption rate and metabolic flux, in addition to upregulation of efflux pumps, have indeed been shown to account for the selectivity of promysalin for *P. aeruginosa* over the producing strain of *P. putida*.[96]

2.4 Chapter 2 Concluding Remarks and Future Directions

Our lab has been invested in the study of promysalin and related compounds for eight years. Over that time, we have generated a great deal of information: elucidation of promysalin's absolute stereochemistry, identification of its antibiotic mechanism of action, and identification of the regions of the molecule most amenable to structural modification. The present studies contribute to this knowledge in a number of ways.

First, we have identified an improved approach to the synthesis of promysalin sidechains. This sequential Grignard strategy is more modular, presents fewer safety concerns, and is substantially less arduous than the initial Keck allylation strategy. Furthermore, as evidenced by synthesis of acrylamide analog **2.13**, the Grignard strategy allows for the introduction of functionality which would not otherwise be possible using known methods. We successfully used a combination of these two approaches to synthesize eight novel promysalin analogs. Second, through testing of six of these analogs in a novel efflux knockout strain (generated through a successful academia-industry collaboration), we identified that efflux is a significant contributor to promysalin resistance in *P. aeruginosa*. Further, we identify that a TCI strategy, which has shown promise in other pharmaceuticals, is not sufficient to overcome this resistance in this particular scenario. Finally, we demonstrate that the newly synthesized analogs are more selective towards *P. aeruginosa* than the natural product itself; as narrow-spectrum antibiotics are less prone to resistance development, this insight could prove useful.

Future studies into promysalin will involve examination of other potential mechanisms of resistance which may be working in concert with the efflux mechanism observed herein. Evaluation of synergistic potential of promysalin with clinically approved drugs is ongoing, as are assays to examine the formation of persister cells in promysalin-treated populations of *P. aeruginosa*. Finally, examination of the final two analogs (phenol **2.07** and anisole **2.08**) alongside a panel of additional aryl analogs may provide insights into the potential for stabilizing binding interactions through π-stacking interactions between promysalin and Sdh. We ultimately hope to utilize a combination of our SAR results to synthesize a best-in-class analog of promysalin.

2.5 Chapter 2 References

(85) *Cystic fibrosis: MedlinePlus Genetics*. https://medlineplus.gov/genetics/condition/cystic-fibrosis/ (accessed 2023-03-07).

(86) Davies, J. C.; Alton, E. W. F. W.; Bush, A. Cystic Fibrosis. *BMJ* **2007**, *335* (7632), 1255–1259. https://doi.org/10.1136/bmj.39391.713229.AD.

(87) Chen, Q.; Shen, Y.; Zheng, J. A Review of Cystic Fibrosis: Basic and Clinical Aspects. *Anim. Models Exp. Med.* **2021**, *4* (3), 220–232. https://doi.org/10.1002/ame2.12180.

(88) Fodor, A. A.; Klem, E. R.; Gilpin, D. F.; Elborn, J. S.; Boucher, R. C.; Tunney, M. M.; Wolfgang, M. C. The Adult Cystic Fibrosis Airway Microbiota Is Stable over Time and Infection Type, and Highly Resilient to Antibiotic Treatment of Exacerbations. *PLOS ONE* **2012**, *7* (9), e45001. https://doi.org/10.1371/journal.pone.0045001.

(89) Langan, K. M.; Kotsimbos, T.; Peleg, A. Y. Managing Pseudomonas Aeruginosa Respiratory Infections in Cystic Fibrosis. *Curr. Opin. Infect. Dis.* **2015**, *28* (6), 547. https://doi.org/10.1097/QCO.0000000000000217.

(90) *Pseudomonas aeruginosa Infection | HAI | CDC*. https://www.cdc.gov/hai/organisms/pseudomonas.html (accessed 2023-03-07).

(91) Pang, Z.; Raudonis, R.; Glick, B. R.; Lin, T.-J.; Cheng, Z. Antibiotic Resistance in Pseudomonas Aeruginosa: Mechanisms and Alternative Therapeutic Strategies. *Biotechnol. Adv.* **2019**, *37* (1), 177–192. https://doi.org/10.1016/j.biotechadv.2018.11.013.

(92) Li, W.; Estrada-de los Santos, P.; Matthijs, S.; Xie, G.-L.; Busson, R.; Cornelis, P.; Rozenski, J.; De Mot, R. Promysalin, a Salicylate-Containing Pseudomonas Putida Antibiotic, Promotes Surface Colonization and Selectively Targets Other Pseudomonas. *Chem. Biol.* **2011**, *18* (10), 1320–1330. https://doi.org/10.1016/j.chembiol.2011.08.006.

(93) Steele, A. D.; Knouse, K. W.; Keohane, C. E.; Wuest, W. M. Total Synthesis and Biological Investigation of (−)-Promysalin. *J. Am. Chem. Soc.* **2015**, *137* (23), 7314–7317. https://doi.org/10.1021/jacs.5b04767.

(94) Keohane, C. E.; Steele, A. D.; Fetzer, C.; Khowsathit, J.; Van Tyne, D.; Moynié, L.; Gilmore, M. S.; Karanicolas, J.; Sieber, S. A.; Wuest, W. M. Promysalin Elicits Species-Selective Inhibition of Pseudomonas Aeruginosa by Targeting Succinate Dehydrogenase. *J. Am. Chem. Soc.* **2018**, *140* (5), 1774–1782. https://doi.org/10.1021/jacs.7b11212.

(95) Steele, A. D.; Keohane, C. E.; Knouse, K. W.; Rossiter, S. E.; Williams, S. J.; Wuest, W. M. Diverted Total Synthesis of Promysalin Analogs Demonstrates That an Iron-Binding Motif Is Responsible for Its Narrow-Spectrum Antibacterial Activity. *J. Am. Chem. Soc.* **2016**, *138* (18), 5833–5836. https://doi.org/10.1021/jacs.6b03373.

(96) Giglio, K. M.; Keohane, C. E.; Stodghill, P. V.; Steele, A. D.; Fetzer, C.; Sieber, S. A.; Filiatrault, M. J.; Wuest, W. M. Transcriptomic Profiling Suggests That Promysalin Alters the

Metabolic Flux, Motility, and Iron Regulation in Pseudomonas Putida KT2440. *ACS Infect. Dis.* **2018**, *4* (8), 1179–1187. https://doi.org/10.1021/acsinfecdis.8b00041.

(97) Post, S. J.; Keohane, C. E.; Rossiter, L. M.; Kaplan, A. R.; Khowsathit, J.; Matuska, K.; Karanicolas, J.; Wuest, W. M. Target-Based Design of Promysalin Analogues Identifies a New Putative Binding Cleft in Succinate Dehydrogenase. *ACS Infect. Dis.* **2020**, *6* (6), 1372–1377. https://doi.org/10.1021/acsinfecdis.0c00024.

(98) Singh, J.; Petter, R. C.; Baillie, T. A.; Whitty, A. The Resurgence of Covalent Drugs. *Nat. Rev. Drug Discov.* **2011**, *10* (4), 307–317. https://doi.org/10.1038/nrd3410.

(99) Boike, L.; Henning, N. J.; Nomura, D. K. Advances in Covalent Drug Discovery. *Nat. Rev. Drug Discov.* **2022**, *21* (12), 881–898. https://doi.org/10.1038/s41573-022-00542-z.

(100) Gehringer, M.; Laufer, S. A. Emerging and Re-Emerging Warheads for Targeted Covalent Inhibitors: Applications in Medicinal Chemistry and Chemical Biology. *J. Med. Chem.* **2019**, *62* (12), 5673–5724. https://doi.org/10.1021/acs.jmedchem.8b01153.

(101) Martin, J. S.; MacKenzie, C. J.; Fletcher, D.; Gilbert, I. H. Characterising Covalent Warhead Reactivity. *Bioorg. Med. Chem.* **2019**, *27* (10), 2066–2074. https://doi.org/10.1016/j.bmc.2019.04.002.

(102) Fernandes, R. A.; Yamamoto, Y. The First Catalytic Asymmetric Allylation of Imines with the Tetraallylsilane−TBAF−MeOH System, Using the Chiral Bis-π-Allylpalladium Complex. *J. Org. Chem.* **2004**, *69* (3), 735–738. https://doi.org/10.1021/jo035453b.

(103) Sugiura, M.; Mori, C.; Kobayashi, S. Enantioselective Transfer Aminoallylation: Synthesis of Optically Active Homoallylic Primary Amines. *J. Am. Chem. Soc.* **2006**, *128* (34), 11038–11039. https://doi.org/10.1021/ja064106r.

(104) Dodge, J. A.; Stocksdale, M. G.; Fahey, K. J.; Jones, C. D. Regioselectivity in the Alkaline Thiolate Deprotection of Aryl Methyl Ethers. *J. Org. Chem.* **1995**, *60* (3), 739–741. https://doi.org/10.1021/jo00108a046.

(105) Knapp, D. M.; Gillis, E. P.; Burke, M. D. A General Solution for Unstable Boronic Acids: Slow-Release Cross-Coupling from Air-Stable MIDA Boronates. *J. Am. Chem. Soc.* **2009**, *131* (20), 6961–6963. https://doi.org/10.1021/ja901416p.

(106) Purino, M. A.; Ramírez, M. A.; Daranas, A. H.; Martín, V. S.; Padrón, J. I. Iron(III) Catalyzed Direct Synthesis of Cis-2,7-Disubstituted Oxepanes. The Shortest Total Synthesis of (+)-Isolaurepan. *Org. Lett.* **2012**, *14* (23), 5904–5907. https://doi.org/10.1021/ol3028016.

(107) Strom, A. E.; Hartwig, J. F. One-Pot Anti-Markovnikov Hydroamination of Unactivated Alkenes by Hydrozirconation and Amination. *J. Org. Chem.* **2013**, *78* (17), 8909–8914. https://doi.org/10.1021/jo401498w.

(108) Yin, W.; Wang, C.; Huang, Y. Highly Practical Synthesis of Nitriles and Heterocycles from Alcohols under Mild Conditions by Aerobic Double Dehydrogenative Catalysis. *Org. Lett.* **2013**, *15* (8), 1850–1853. https://doi.org/10.1021/ol400459y.

(109) Vatèle, J.-M. One-Pot Oxidative Conversion of Alcohols into Nitriles by Using a TEMPO/PhI(OAc)2/NH4OAc System. *Synlett* **2014**, *25* (9), 1275–1278. https://doi.org/10.1055/s-0033-1341124.

(110) Shimojo, H.; Moriyama, K.; Togo, H. Simple One-Pot Conversion of Alcohols into Nitriles. *Synthesis* **2013**, 2155–2164. https://doi.org/10.1055/s-0033-1338489.

(111) Abel, G.; Nguyen, K.; Viamajala, S.; Varanasi, S. Cross-Metathesis Approach to Produce Precursors of Nylon 12 and Nylon 13 from Methyl Oleate. *RSC Adv.* **2012**, 7.

(112) Vanneste, J. L. The Scientific, Economic, and Social Impacts of the New Zealand Outbreak of Bacterial Canker of Kiwifruit (Pseudomonas Syringae Pv. Actinidiae). *Annu. Rev. Phytopathol.* **2017**, *55* (1), 377–399. https://doi.org/10.1146/annurev-phyto-080516-035530.

(113) Xin, X.-F.; Kvitko, B.; He, S. Y. Pseudomonas Syringae: What It Takes to Be a Pathogen. *Nat. Rev. Microbiol.* **2018**, *16* (5), 316–328. https://doi.org/10.1038/nrmicro.2018.17.

Chapter 3 - Optimization of berberine-derived alkaloids as MexXY-OprM Inhibitors and Aminoglycoside Adjuvants

3.1 Introduction

The incorporation of proteins into cell membranes is ubiquitous across all kingdoms of life, and can serve many functions. Depending on the nature of the protein-membrane interaction, these proteins are divided into categories (**Figure 3.1**). Peripheral membrane proteins can reversibly coordinate using noncovalent interactions to the membrane, while integral membrane proteins are permanent membrane incorporations. If an integral membrane protein exists only on one face of the lipid bilayer (towards the cytoplasm, periplasm, or extracellular matrix), it is categorized as an integral monotopic protein; these often function as receptors for signal transduction pathways, in immune response, or to catalyze a particular chemical reaction (such as the cyclooxygenases COX1 and COX2 involved in prostaglandin synthesis and often targeted by inflammation and pain

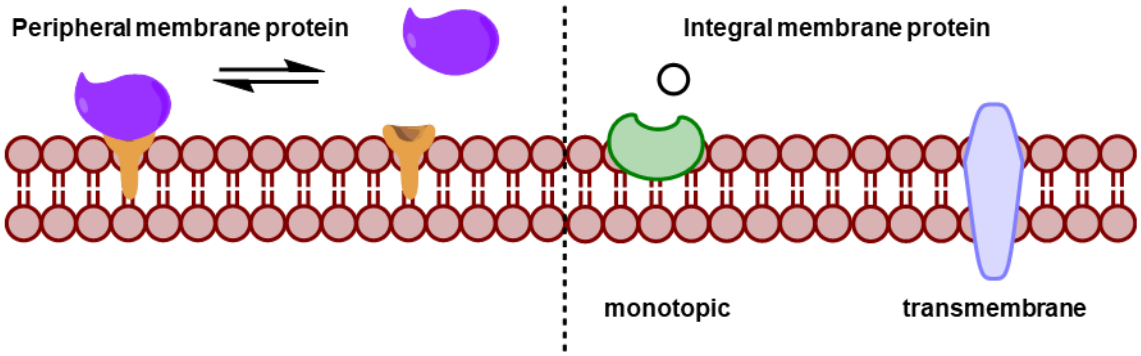

Figure 3.1 Classes of proteins temporarily attached (peripheral) or permanently incorporated (integral) into cell membranes

medication). A protein that spans the entire membrane is referred to as an integral polytopic protein, or a transmembrane protein; these can either be enzymatic (as in the case of succinate dehydrogenase) or can function as transporters of ions, small molecules, or macromolecules into or out of a cell.[114]

One important class of active (requiring energy input) membrane transporters in bacteria and eukaryotes are efflux pumps. Many classes of efflux pump have been characterized, but all are involved in exporting compounds from the cell – these can be nontoxic compounds such as quorum sensing molecules or other metabolites, or they can be compounds normally toxic to a cell such as heavy metals, cellular waste products, or antibiotics. Antibiotic efflux is an effective mechanism by which bacteria develop resistance to drugs, expending energy to decrease the intracellular concentration of these molecules to sublethal levels.[70,71]

In bacteria, there are five categories of efflux pump: the ATP-binding cassette superfamily (ABC), the major facilitator superfamily (MFS), the small multidrug resistance family (SMR), the multi antimicrobial extrusion protein family (MATE), and the resistance-nodulation-cell division superfamily (RND), which all function by slightly different mechanisms, have different substrate scopes, and/or are structured differently. The RND superfamily of efflux pump is a class of secondary active transporter utilizing the energy from the proton gradients across the membrane

to efflux its substrates (rather than utilizing energy from ATP as in the ABC family) and are especially prevalent in gram-negative bacteria. In this class, the AcrAB-TolC pump in *E. coli* is the most well-characterized and has homologs in a number of species. RND efflux pumps consist of three identical protomers that come together to form a tube shape, and each protomer is composed of three proteins: a homotrimeric outer membrane channel, homohexameric periplasm adaptor protein, and a homotrimeric inner membrane transporter (**Figure 3.2A**).[71]

The inner membrane transporter is posited to be the site of substrate recognition in RND efflux pumps. In this system, the mechanism of substrate recognition involves a cycle of three conformational states (access (A), binding (B), and extrusion (E)), which occurs interdependently in each protomer and is required for both substrate entry into the transporter and translocation to the periplasmic protein. In the A-state, substrates enter a region called the proximal binding pocket (PBP), activating the first conformational change. As the protomer cycles to the B-state, substrates move into the distal binding pocket (DBP). The final conformational state is reached when

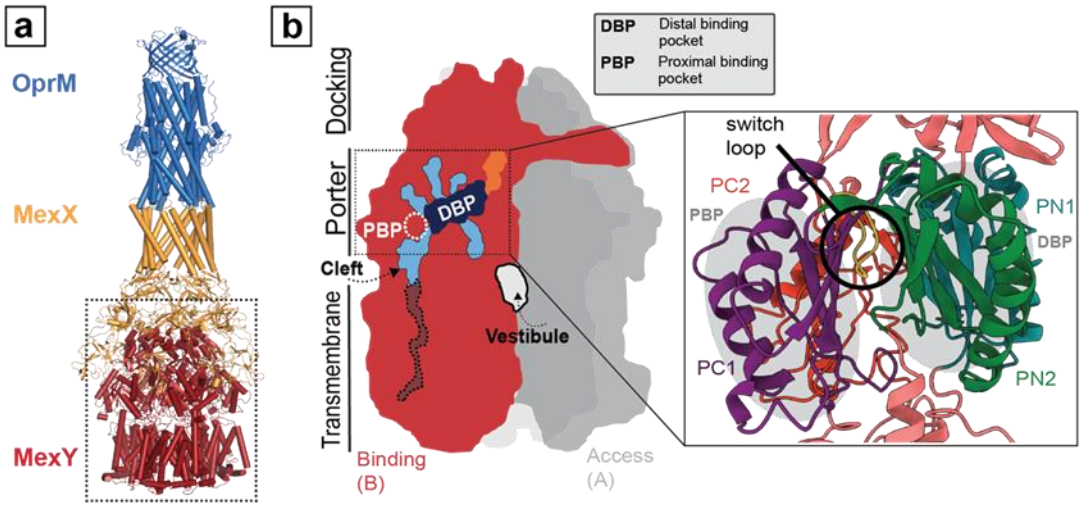

Figure 3.2. A. Structure of RND efflux pump MexXY-OprM, including inner membrane transporter MexY (red), periplasmic adaptor protein MexX (gold) and outer membrane protein OprM (blue). **B.** Structure of MexY cycling between three conformational states: access (dark grey), binding (red), and extrusion (light grey), alongside a zoomed in region of the binding domains DBP and PBP

substrates leave the DBP and enter the now open efflux tunnel in the E-state. The compound thus is moved out of the cell interior and can then be effluxed by the OprM protein on the bacterial outer membrane (**Figure 3.2B**).

In *Pseudomonas aeruginosa*, 12 efflux pumps in the RND superfamily are encoded, of which MexAB-OprM, MexCD-OprJ, MexEF-OprN, and MexXY-OprM are associated with clinical antibiotic resistance.[115] While the substrate profiles of these four efflux pumps are similar and overlapping, MexXY-OprM is the only one which possesses the ability to export aminoglycoside antibiotics (**Figure 3.3**).[116] This class of drug is a frontline treatment in therapeutic regimens for chronic *P. aeruginosa* infections (e.g., CF patients); efflux via MexXY-OprM is therefore one of the primary causes of treatment failure in these situations. Research investigating the specific mechanisms of aminoglycoside recognition and efflux by this pump is therefore highly important in order to allow development of future generations of antibiotics.

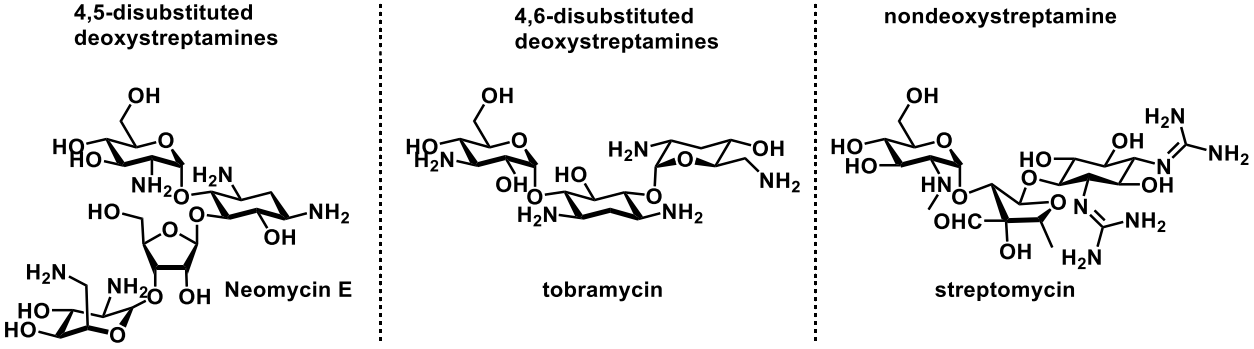

Figure 3.3. Structure of aminoglycoside antibiotics, divided into their three subclasses

Because all three proteins in an RND efflux pump must work in concert, inhibition of any one protein is sufficient to prevent efflux from occurring (**Figure 3.4**). Efflux pump inhibitors (EPIs) are chemical compounds that interfere with the ability of an efflux pump to recognize, bind, or export its natural substrates. By definition, these compounds are not antibiotic in nature, meaning

that in the absence of additional toxins, these compounds should not cause cell death (except in the cases in which an efflux pump is inhibited whose substrate is a toxic byproduct of a normal cellular function). The ideal EPI is specific for a particular efflux pump, this often requires inhibition of the inner membrane transporter as many pumps can utilize the same outer membrane channel (e.g., MexAB and MexXY both utilize the OprM channel, an inhibitor of OprM would therefore not be specific).[117]

A combination therapy approach utilizing a potent antibiotic as well as an EPI would seem to be a logical therapeutic avenue. Pharmaceutical combination therapies for the treatment of bacterial infections date back to the discovery of the synergistic effects between amoxicillin and clavulanic acid by British scientists in the 1970s.[118] These approaches are often used in the case of multidrug resistant infections, in which single antibiotics are ineffective. Synergistic drugs often function via

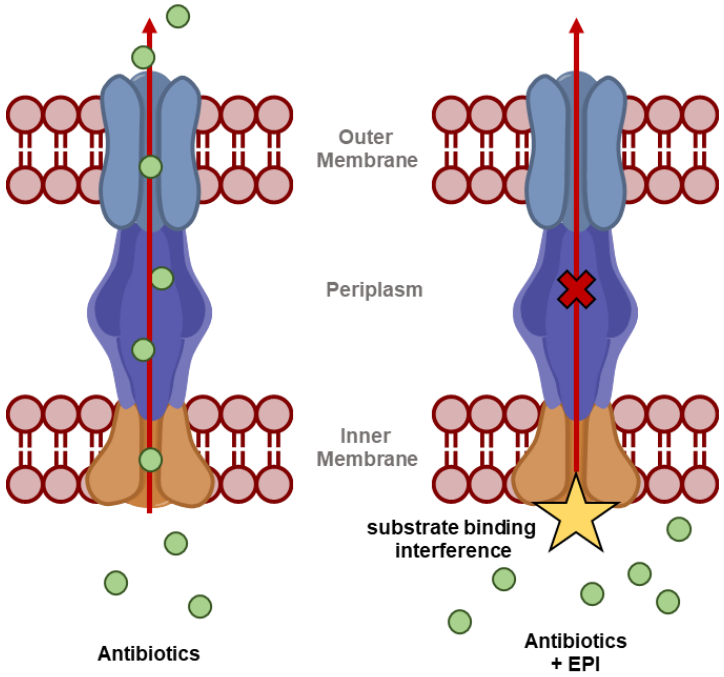

Figure 3.4. Efflux pump inhibition strategy for antibiotic potentiation

different mechanisms of action, such as a bacteriostatic compound being used in concert with a bactericidal antibiotic.[119] Alternatively, one compound may function by inhibiting a protein or

process that confers resistance to the second compound, such as the combination of penicillins with β-lactamase inhibitors.[118] To that end, if an antibiotic were a known substrate of a bacterial efflux pump, one could expect the addition of a therapeutic EPI to improve bacterial clearance. Natural product EPIs have been identified, such as reserpine (an inhibitor of both mammalian and bacterial efflux pumps) and baicalein (an inhibitor of MDR pumps, isolated from thyme).[120] Synthetic EPIs of note include Phe-Arg-β-naphthylamide (PAβN), an inhibitor of MexAB, MexCD, and MexEF pumps (but not MexXY) in *P. aeruginosa* and cyanide 3-chlorophenylhydrazone (CCCP) (**Figure 3.5**).[121]

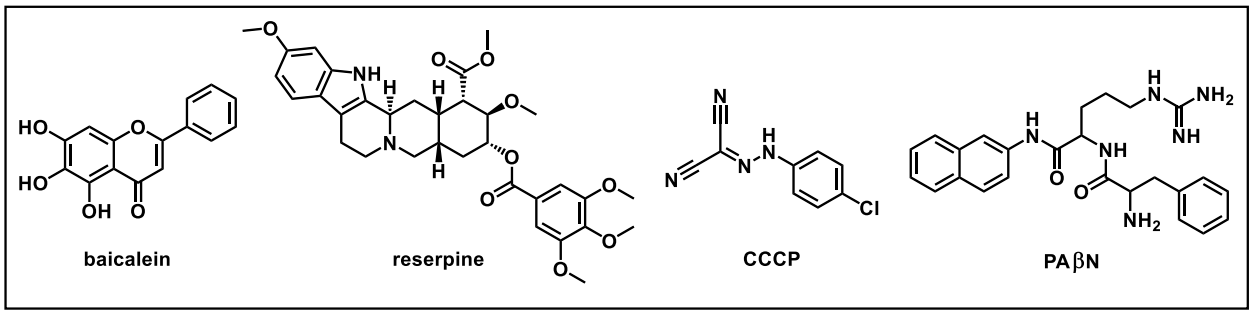

Figure 3.5. Structures of known natural (baicalein and reserpine) and synthetic (CCCP and PAβN) efflux pump inhibitors

therapeutic use. Regulatory hurdles with the approval of non-antibiotics to treat bacterial infections notwithstanding, there are a number of challenges associated with the development of clinically useful EPIs. For example, the inherent complex structure of efflux pumps makes their study remarkably difficult. Transmembrane proteins are notoriously difficult to purify and crystallize due to their incorporation into cellular membranes and their tendency to adopt rather different conformations when not membrane associated. As a result, structural information on these pumps in their native environments is limited, and guided design of specific inhibitors is therefore challenging. In addition, differential binding modes of disparate classes of antibiotics to multidrug efflux pumps mean that EPIs targeting these pumps often do not equally potentiate the activity of

all substrate classes (for example, while PAβN is a known inhibitor of MexAB-OprM and can potentiate fluroquinolones, it does not potentiate carbenicillin or ethidium bromide, despite them being substrates of this pump).[122] Finally, many known EPIs have very poor pharmacological profiles and are often toxic to eukaryotes, rendering them useless in the clinic.

Berberine (**3.01**) is a natural product known to weakly inhibit the MexXY-OprM efflux pump in *P. aeruginosa*.[123] It is a planar polycyclic aromatic compound containing a benzylisoquinoline core, quaternary nitrogen salt, methylenedioxy bridge, and two methoxy substituents. It is produced by a number of plants around the world such as *Berberis vulgaris*, *Eschscholzia californica*, and *Coptis chinensis*, the last of which is a fundamental plant in traditional Chinese medicines. Pure berberine is a bright yellow powder and plants which produce it have historically been used to dye fibrous textiles such as wool.[124] Berberine (**3.01**) is the parent compound of a family known as protoberberine alkaloids, a class which also contains compounds such as palmatine, jatrorrhizine, and coptisine, all containing the same fundamental connectivity but with different substitution patterns on the oxygen atoms.

Biosynthesis of protoberberine alkaloids has been studied due to their historical importance (**Scheme 3.1**). Starting from L-tyrosine, hydroxylation and decarboxylation forms (L)-dopamine. An additional molecule of L-tyrosine is decarboxylated, oxidized, and hydrolyzed to form 4-hydroxyphenylacetaldehyde. These two tyrosine-derived compounds are then joined in a biocatalyzed Pictet Spengler-type reaction. Methylation of the nitrogen via a radical SAM enzyme forms (S)-reticuline, the common precursor to all protoberberine alkaloids.[125]

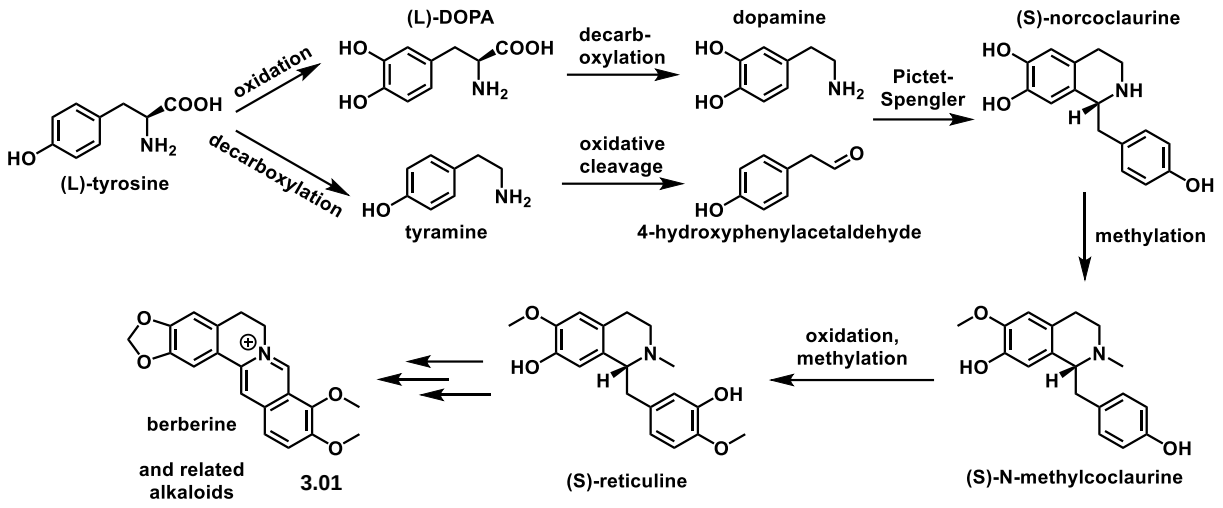

Scheme 3.1. Biosynthesis of berberine and other protoberberine alkaloids[125]

Due to its well-studied nature and long history, there are a variety of known physiological effects of berberine (**3.01**) in humans. Many studies and metastudies have reported that berberine is a promising treatment for cancer, diabetes, Alzheimer's disease, diarrhea, cardiovascular disease, atherosclerosis, and microbial infections caused by bacteria, fungal, protozoal, and viral pathogens.[126–136] Its antimicrobial properties have been studied in detail, and berberine's mechanism of action has been determined to be a combination of membrane depolarization, formation of reactive oxygen species (ROS), and disruption of metabolic pathways including the shikimate and peptidoglycan biosynthesis pathways.[137,138]

Despite these seemingly miraculous data on berberine's health benefits, it has not been approved for therapeutic treatment of any condition by the FDA (though it is available over the counter or as a dietary supplement). This is at least partially due to the fact that berberine exhibits several physiological liabilities. The pharmacological profile of berberine in particular is exceptionally poor, having low water solubility and bioavailability due to poor intestinal absorption and its extensive metabolism after oral administration. Metabolite studies indicate the main reactions

occurring on berberine in first-pass metabolism are ether cleavage (at both the methoxy positions and the methylenedioxy bridgehead) and nonselective hydroxylation at a variety of positions on the scaffold. These metabolites can then be conjugated to a variety of groups in phase-II metabolism and excreted in urine and bile.[138] A pilot study of 20 volunteers found that a 400 mg oral dose of berberine chloride resulted in a mean maximum concentration in plasma (C_{max}) of an abysmal 0.4 ng/mL, far below than the concentrations at which the physiological effects previously described had been observed.[139] Furthermore, berberine has been shown to inhibit cytochrome P450 enzymes CYP2D6 and CYP3A4, leading to the potential for adverse drug-drug interactions.[140,141] Nevertheless, the study of berberine and other protoberberine alkaloids is ongoing in many labs in an effort to produce compounds with well-defined activities, improved pharmacological profiles, and lower potential risks of adverse effects.

3.2 Computational Screening

Due to the severe threat caused by efflux-mediated antibiotic resistance, a collaborative initiative was launched in 2020 between the Wuest and Conn labs to identify potential scaffolds which could bind and/or inhibit the MexXY-OprM efflux pump in *P. aeruginosa*. Based on berberine's reported weak binding to this pump, as well as the well-studied nature of its synthesis, derivatization, and chemical properties, we regarded it as a promising starting point for SAR study. Using the Schrodinger LiveDesign Suite and Discovery platform, a computational high-throughput screen was performed by Dr. Debayan Dey (Conn Lab, Emory University). In this screen, approximately 10,000 compounds with structural similarity to berberine (Tanimoto coefficient > 0.8) were assembled into a custom-made virtual dataset. These compounds were sequentially docked into the proximal and distal binding pockets of a PAO1 MexY homology model (in its B conformation) using the Glide program.

After ranking the docked compounds according to their HTVS GLIDE docking scores, the top 1,000 compounds were re-docked using Glide SP for increased precision. The resulting compounds were K-means clustered, a statistical technique for clustering a dataset based in this case on similarity of structure and chemical properties. The compounds predicted to bind with highest affinity to MexY fell into three categories: berberine conjugated with piperazine motifs (**3.02** and **3.03**), berberine conjugated to propanamines (**3.06 and 3.07**), and dimeric berberines linked with an alkyl chain (**3.05**, **Figure 3.6**).

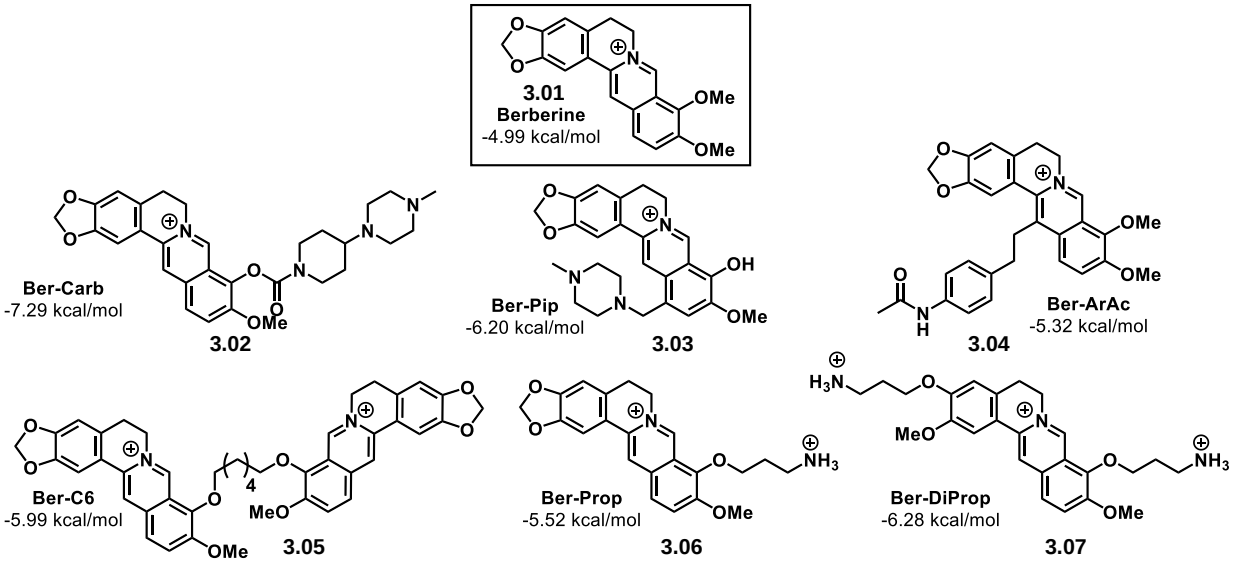

Scheme 3.2. Structures of computational hits from structure-guided docking into MexY

3.3 Synthesis

In order to assess the validity of our computational modeling data, synthesis of the predicted hits and biochemical analysis of their interaction with the MexY inner membrane pump was necessary. In addition, we were interested in examining the potential of a successful MexY inhibitor to potentiate the antibiotic activity of aminoglycosides, as they are uniquely effluxed by MexXY/OprM and bacterial resistance to aminoglycosides presents an urgent unmet medical need.

As the virtual library used in our computational screen was created from known scaffolds, the desired analogs and their syntheses have previously been reported in the chemical literature.[141–143] The majority of these compounds can be derived from berberrubine (**3.08**), a protoberberine analog in which the C9 methoxy substituent is replaced with a hydroxyl moiety. While berberrubine is prohibitively expensive from commercial vendors, the selective demethylation of the more affordable berberine chloride (**3.01**) via vacuum pyrolysis to form berberrubine (**3.08**, **Scheme 3.2**) is known in the literature. A semisynthetic approach from commercial berberine chloride (**3.01**) was thus utilized to access the desired analogs.

Vacuum pyrolysis of berberine chloride (**3.01**) to form berberrubine (**3.08**) is frequently employed in the study of protoberberine alkaloid natural products and synthetic analogs, as the added electron density of the free phenol of berberrubine allows for a variety of chemical manipulations.[142–144] This reaction was first reported in 1903, when German chemists heated an extract of the Berberis plant in urea over an open flame and observed a stark color change from yellow (**3.01**) to red (**3.08**).[145] A number of improvements to the technique have been made to the reaction in the last 120 years; screening of a variety of literature conditions revealed that in our hands a near quantitative conversion could be obtained using solvent-free conditions in an oil bath preheated to 190°C. Because this reaction was run neat, utilization of a reaction vessel with a large surface area was important to ensure even heating of the berberine powder.

The free phenol of **3.08** was derivatized in a number of ways (**Scheme 3.2**). To generate **Ber-Carb** (**3.02**), triphosgene was reacted with 1-methyl-4-(piperidin-4-yl)piperazine, and the resulting carbamic chloride was substituted with berberrubine. Similarly, two equivalents of berberrubine (**3.08**) could be utilized in a dimerization reaction with 1,6-diiodohexane, generating **Ber-C6** (**3.05**) in moderate yield. The major byproduct of this reaction resulted from

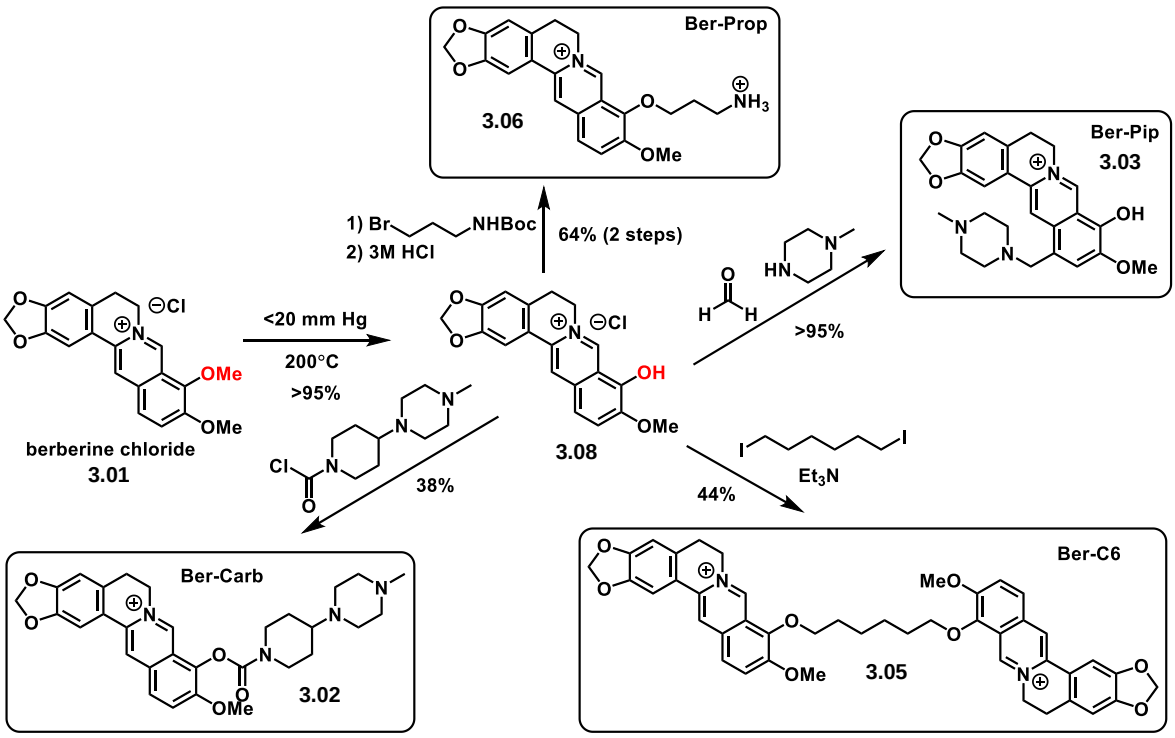

Scheme 3.3. Semisynthetic strategy towards four berberine analogs

wherein the chloride counterion displaced the terminal iodide. This newly formed terminal chloride was not sufficiently electrophilic to undergo the second substitution required for dimer formation under the tested conditions. Initial investigations to determine if this byproduct could be used in a facile manner to generate desired analog **Ber-Prop** (**3.06**) via substitution with methanolic ammonia also proved unsuccessful. Instead, **Ber-Prop** (**3.06**) was generated via addition of berberrubine to 3-(Boc-amino)propyl bromide, followed by hydrochloric acid-mediated deprotection, providing the desired analog as its hydrochloride salt. Finally, condensation of N-methylpiperazine onto formaldehyde to generate the corresponding imine, followed by *in situ* addition of berberrubine provided compound **Ber-Pip** (**3.03**) in which substitution occurs at C-12 rather than at the phenolic position. This is possibly due to HSAB theory, with the imine acting as a "soft" electrophile and therefore preferentially reacting in a

conjugate addition fashion. Thus, the first four of our computational hits could be synthetically generated in short order with little need for optimization.

In contrast, attempts to synthesize **Ber-ArAc** (**3.04**) proved less fruitful. While all other desired compounds had been previously published in peer-reviewed journals, the only report of this compound is from a patent issued to Italian pharmaceutical company Naxospharma in 2011.[146] Experimental details for the formation of **Ber-ArAc** (**3.04**) are limited, but the general synthetic strategy seems to involve reduction of the quinolinium ring via hydride addition to C8, followed by nucleophilic addition of the resulting enamine to an electrophile, derivatization of this new C13 moiety to the desired phenethylacetamide, further reduction of the iminium ion to the tetrahydroberberine, then subsequent reoxidation to restore aromaticity of the core scaffold (**Scheme 3.3**). When this inelegant strategy was attempted, we immediately discovered that the enamine was so prone to spontaneous oxidation to reform berberine chloride (**3.01**) that no successful nucleophilic addition could be observed.

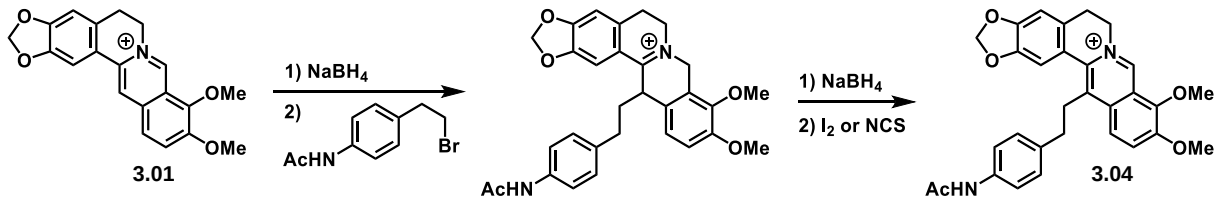

Scheme 3.4. Patented route to synthesis of 13-substituted berberine compounds

As the patent conditions for preparation of **Ber-ArAc** (**3.04**) were deemed insufficiently detailed, alternate literature-based approaches were desired. For example, Bremner and Samnosern reported successful C13 derivatization of berberine with a variety of similar substituents by first reacting berberine (**3.01**) with allyltributylstannane in superheated dichloromethane, affording 8-allyldihydroberberine (**3.09**). This precursor could then be reacted with electrophiles in an

interesting mechanism which the authors rationalize as a one pot enamine addition, 3,3-sigmatropic rearrangement, and retro-ene reaction to give the 13-substituted berberine compounds (**Scheme 3.4**).[147]

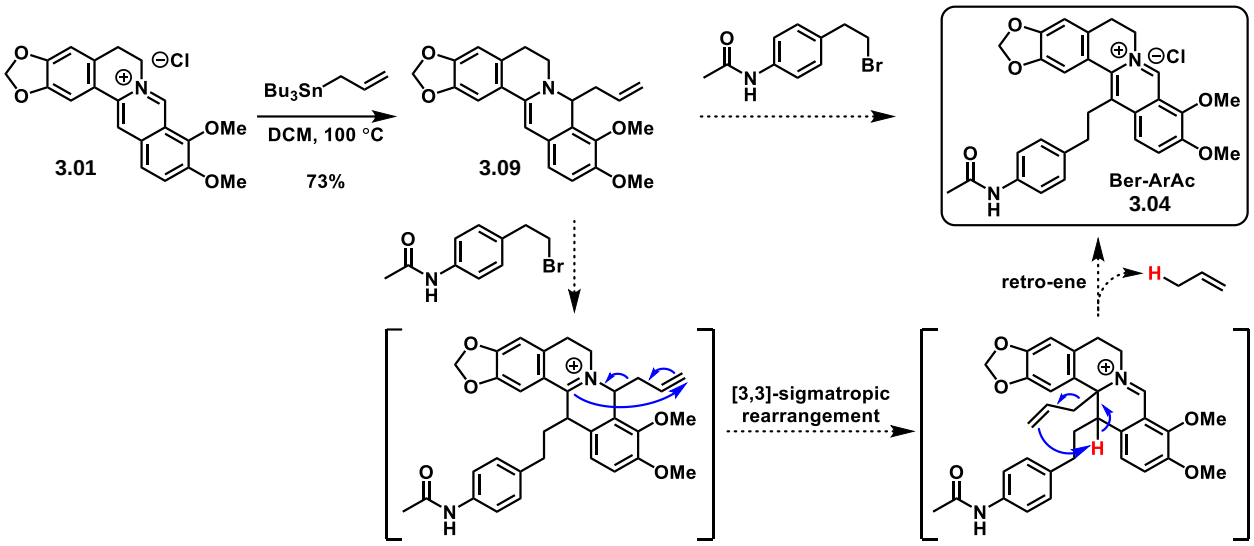

Scheme 3.5. Strategy for synthesis of 13-substituted berberine compounds using 8-allyldihydroberberine as a functional handle to allow enamine addition, 3,3-sigmatropic rearrangement, and retro-ene reaction

Preparation of 8-allyldihydroberberine (**3.09**) in our hands was reproducible, and we were pleased to observe that this compound was substantially more stable than the original dihydroberberine. However, repeated attempts to react this precursor with N-(4-(2-bromoethyl)phenyl)acetamide to generate **Ber-ArAc** (**3.04**) were unsuccessful. Indeed, the publication from which this strategy was developed only reported derivatization with activated (benzylic or α-keto) electrophiles.[147] It would therefore appear that this strategy (and likely, all berberine enamine addition strategies) are not appropriate for 13-substitution with simple unactivated electrophiles. In addition, the hazardous conditions required for the formation of the 8-allyldihydroberberine (**3.09**) precursor led us to devise a safer approach.

As regioselective C-13 halogenation of berberine (**3.01**) has been reported in the literature, we were next interested in the development of a transition metal-catalyzed cross coupling approach.[148]

This could facilitate future incorporation of a large number or aryl, heteroaryl, vinyl, or alkyl substituents and complement the limitations in the other approaches used in substitution at this position. A Suzuki approach was first attempted due to this reaction's broad substrate scope (**Scheme 3.5**); though Suzuki cross coupling of pyridinium halides is rare in the literature, it was first successfully reported in 2006 by the Alvarez-Builla lab.[149] While formation of 13-bromoberberine (**3.10**) and 13-iodoberberine (**3.14**) proceeded in good yields and regioselectivity, attempts to generate the required boronic acid were less successful.

We first attempted formation of the boronic acid via Miyaura-type borylation of N-(4-(2-bromoethyl)phenyl)acetamide (**3.12**, **Scheme 3.5**). Synthesis of this starting material began from double acylation of 2-(4-aminophenyl)ethanol followed by base-mediated ester hydrolysis to generate monoacylated intermediate **3.11**, which could then be subjected to Appel conditions to afford the necessary halide. Unfortunately, screening variable temperatures, bases, solvents, and catalysts for the borylation reaction did not result in identification of conditions that could generate the desired product (**Table 3.1**). Preparation of the alkyl iodide (**3.13**) was performed to increase reactivity but also did not allow for subsequent Miyaura borylation. Similarly, a lithium halogen exchange followed by borylation was attempted for both bromide (**3.12**) and iodide (**3.13**) substrates but was equally unsuccessful (see Chapter 4 for a successful example of replacing a Miyaura borylation approach with lithiation-borylation).

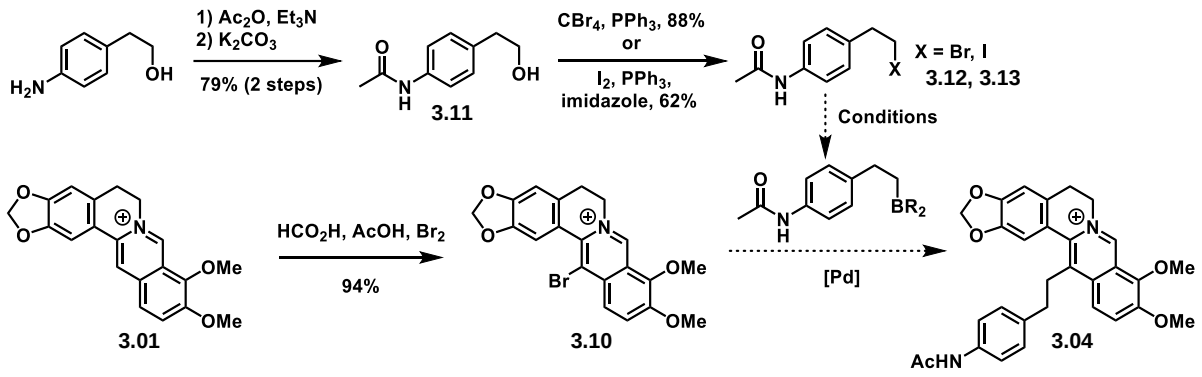

Scheme 3.6. Suzuki strategy for synthesis of Ber-ArAc

Reasoning that the amide functionality may be coordinating to and deactivating the palladium catalysts used in Miyaura borylation, we instead tried anti-Markovnikov hydroboration of N-(4-vinylphenyl)acetamide (**3.15**, formed via acylation of 4-vinylaniline) to produce the boronic acid required for our desired Suzuki approach (**Table 3.1**). Sadly, no reaction was observed utilizing catecholborane, 9-BBN or B_2pin_2 as the boron source at a variety of temperatures. It is possible that **3.15** is too electron-deficient to engage in the desired reaction. Final attempts at a Suzuki strategy were dashed upon attempting to form the boronic acid on the berberine scaffold instead, resulting in an unidentifiable conglomeration of byproducts that could not be separated.

In general, purification of berberine derivatives poses several complicating factors. First, the charged isoquinolinium renders the molecule extremely polar, limiting chromatographic eluents that can successfully remove the compounds from silica. Use of reverse-phase silica usually results in near immediate coelution of all compounds. Second, the high planarity of these compounds further complicates separation by chromatography or by crystallization, as pi-stacking interactions between molecules frequently causes coelution (or cocrystallization) of impurities with the desired material. Finally, the excellent dyeing properties of berberine (**3.01**) and its derivatives leads to

Table 3.1. Attempts at synthesis of boronate required for Ber-ArAc Suzuki coupling, using either Miyaura borylation, lithiation-borylation, or hydroboration strategies

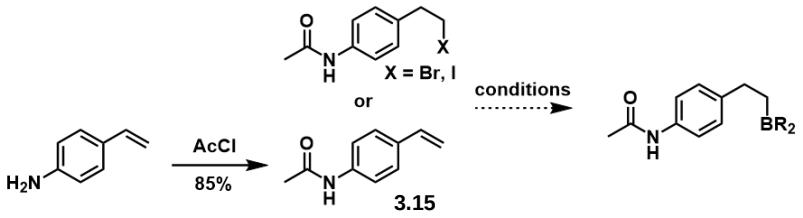

Substrate	Boron Source	Catalyst	Solvent	Temperature	Result
Bromide	B_2pin_2	$Pd(dppf)_2Cl_2$	1,4-dioxane	reflux	no rxn
Bromide	B_2pin_2	$Pd(dppf)_2Cl_2$	toluene	reflux	no rxn
Bromide	B_2pin_2	$Pd(OAc)_2$	1,4-dioxane	reflux	no rxn
Bromide	B_2pin_2	$Pd(PPh_3)_4$	1,4-dioxane	reflux	no rxn
Bromide	B_2pin_2	t-Buli (2.5 eq.)	DCM	-78°C	degradation
Iodide	B_2pin_2	$Pd(dppf)_2Cl_2$	1,4-dioxane	80°C	no rxn
Iodide	iPrOBpin	t-Buli (2.5 eq.)	THF	-78°C	degradation
Alkene	HBcat	None	toluene	100°C	no rxn
Alkene	HBcat	N,N-DMA	DMF	60°C	no rxn
Alkene	9-BBN	None	THF	23°C	no rxn
Alkene	9-BBN	None	THF	reflux	no rxn
Alkene	9-BBN	None	THF	80°C (sealed)	no rxn
Alkene	B_2pin_2	None	THF	reflux	no rxn
Alkene	B_2pin_2	CuCl	MeOH	40°C	no rxn

staining of solid phase reagents (silica, celite, etc.) and corresponding substantial decreases in yield.[124,150] Indeed, dilute alcoholic solutions of berberine (**3.01**) can be used as an irreversible TLC stain for visualization of compounds.[151] Because of these factors, synthetic routes towards berberine derivatives that require the fewest purification steps are in our hands almost always the highest yielding. We therefore abandoned the search for Suzuki conditions, as optimization of this approach would require too many reaction steps on the berberine scaffold itself (for example, a differentially protected nitrogen could in theory allow successful Miyaura borylation and coupling, but the charged coupling product would need to be further reacted in deprotection and reacylation steps).

Since we had built up a stockpile of acylated styrene **3.15** for use in our hydroboration approach, a Heck strategy was next attempted (**Scheme 3.6**). Fortunately, this coupling proved successful on our first attempt, providing a product resembling the fully unsaturated version (**3.04a**) of our

desired **Ber-ArAc** analog. However, due to time constraints and resource limitations, analogous reductive Heck conditions to generate the true analog (**3.04**) were not fully explored, though this remains a promising approach for the generation of this compound. It is possible that, similar to the results seen for dihydroberberine, **Ber-ArAc** (**3.04**) may be unstable due to spontaneous oxidation in air to desaturate the ethyl linkage to produce a fully conjugated system, though this theory would need to be subjected to further scrutiny. To our knowledge, these results are the first example of a successful Heck coupling to a charged heterocycle.

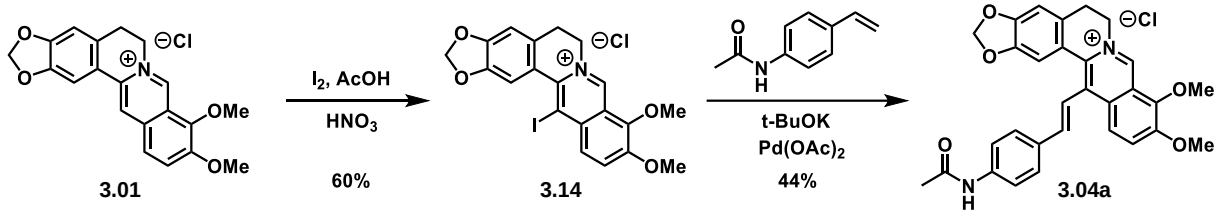

Scheme 3.7. Successful synthesis of unsaturated Ber-ArAc using a Heck strategy

Ber-DiProp (**3.07**) has been semisynthesized in the literature from protoberberine compound jatrorrhizine, featuring a guaiacol moiety in place of berberine's methylenedioxy ring.[152] Unfortunately, unlike berberine, jatrorrhizine is unavailable commercially, necessitating an alternate approach. An initial strategy was developed, in which selective Lewis acid-mediated cleavage of the methylenedioxy bridge could be followed by realkylation to the desired substitution pattern, followed by the known vacuum pyrolysis and amination. This had precedent in the literature, in which the Brossi lab were able to chemoselectively cleave a methylenedioxy bridge of a similar scaffold using boron trichloride while leaving methoxy ethers intact (**Scheme 3.7, top**).[153] Unfortunately, we were unable to reproduce these results on the berberine (**3.01**) system, producing instead an inseparable mixture of methylated and demethylated isomers. Use of

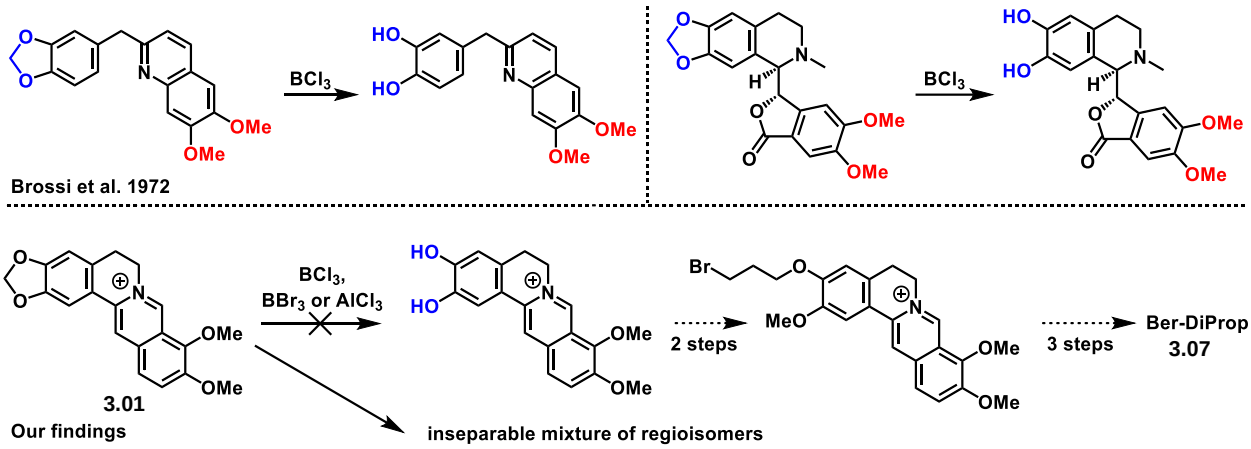

Scheme 3.8. Top: Literature precedent for selective Lewis acid-mediated cleavage of methylenedioxy bridge in the presence of aromatic methyl ether. Bottom: Unsuccessful attempts at reproducing this strategy on the berberine scaffold

Because of challenges accessing **Ber-ArAc** (**3.04**) and **Ber-DiProp** (**3.07**) semisynthetically, a total synthesis route to these compounds was desired. Previous work has been performed on the total synthesis of berberine and related compounds. The first reported total synthesis of berberine (**3.01**) was performed in 8 steps in 1969 by Kametani et al. and featured condensation of 3,4-methylenedioxyphenethylamine with methyl 2-(5-benzyloxy)-2-bromo-4-methoxyphenylacetate followed by cyclization, as well as a key Mannich reaction using formaldehyde (**Scheme 3.8**).[154] Yields for this synthesis were generally low however, and several improved berberine syntheses have since been published.[155–157] In particular, a 2018 publication by the Clift lab detailed a succinct four step route to berberine affording **3.01** in a reported 53% overall yield.[155] Furthermore, the authors showcased this route's modularity by using it to synthesize coptisine (4 steps, 39% yield) and jatrorrhizine (**3.19**, 4 steps, 20% yield), the latter of which had utility for synthesis of our desired **Ber-DiProp** (**3.07**) analog.

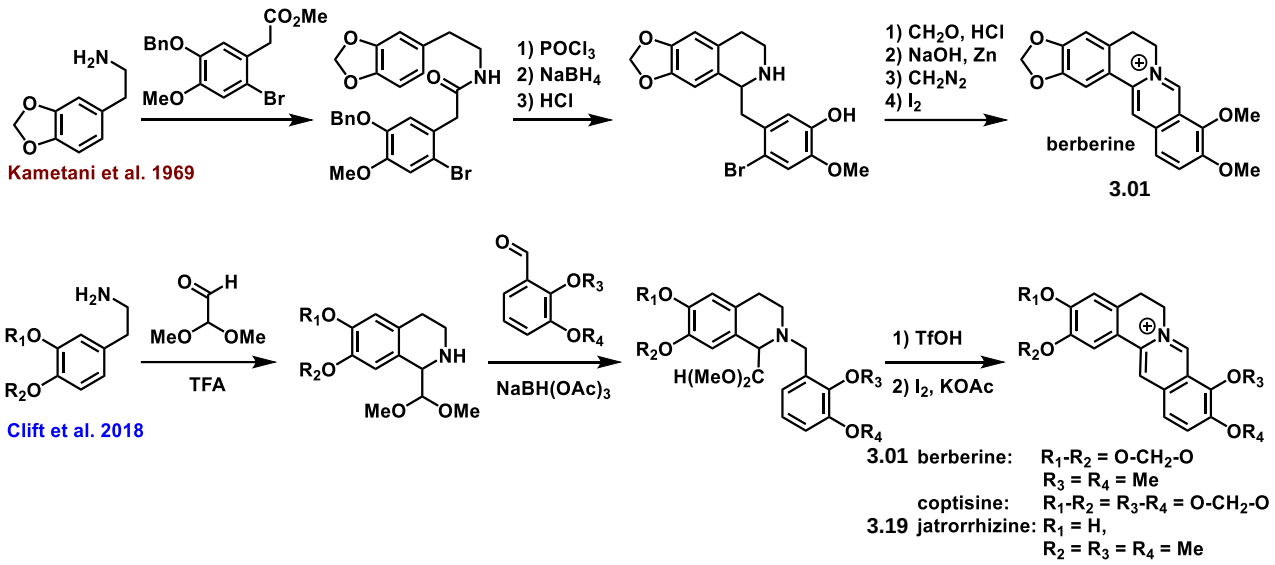

Scheme 3.9. Comparison of synthetic strategies towards berberine and related compounds published by Kametani and Clift

reported. Starting from 5-(2-aminoethyl)-2-methoxyphenol (**3.16**), a regioselective Pictet Spengler reaction with 2,2-dimethoxyacetaldehyde afforded a bicyclic secondary amine (**3.17**). This amine could be utilized in a reductive amination with 2-hydroxy-3-methoxybenzaldehyde to append the rest of the carbons of the molecule, forming **3.18**. Triflic acid mediated acetal cleavage and Friedel Crafts-type acylation then successfully generated the tetracyclic scaffold which could be aromatized to jatrorrhizine (**3.19**) using iodine in 22% overall yield over four steps (**Scheme 3.9**).

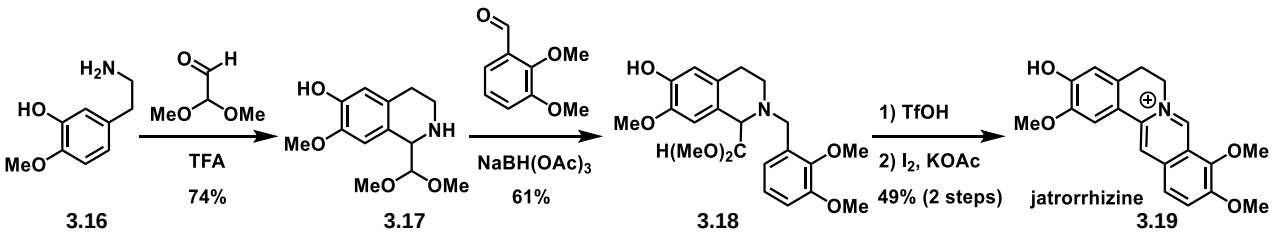

Scheme 3.10. Total synthesis of jatrorrhizine, following the synthetic strategy of Clift et al.

Initial biological results for **Ber-Carb** (**3.02**), **Ber-Pip** (**3.03**), **Ber-C6** (**3.05**), **Ber-Prop** (**3.06**), and berberine itself (**3.01**), were obtained **(Table 6.1)**. These checkerboard assays, performed by Logan Kavanaugh (Conn Lab, Emory University), entailed assessment of synergistic interaction

between berberine compounds and aminoglycoside antibiotics in growth inhibition of *P. aeruginosa* strain PAO1. Results of these assays confirmed previous literature reports of berberine's weak inhibition of MexXY-OprM, reducing the MIC of kanamycin and gentamycin in these cells twofold.[123] Piperazine analogs **Ber-Carb** (**3.02**) and **Ber-Pip** (**3.03**) did not show any synergistic ability, while **Ber-Prop** (**3.06**, FIC = 0.44 for both aminoglycosides) showed synergy on par with berberine (FIC = 0.5 for both aminoglycosides). However, **Ber-C6** (**3.05**) gave promising results, potentiating the activity of kanamycin and gentamicin two- to six-fold, with FIC values of 0.38 and 0.48 for kanamycin and gentamicin respectively. Due to this finding, combined with synthetic difficulties in accessing the remaining **Ber-ArAc** (**3.04**) and **Ber-DiProp** (**3.07**) analogs, we prioritized optimization of this dimeric scaffold.

The first way in which we sought to optimize **Ber-C6** (**3.05**) was by altering the length of its alkyl linker. Computational docking results (Dr. Debayan Dey, Conn Lab, Emory University) indicated that one of the berberine monomers made a number of important polar contacts with the MexY DBP, but the other did not (**Figure 3.7**). This led to a structural hypothesis for efflux pump inhibition by **Ber-C6** (**3.05**) in which one monomer could effectively bind to the substrate recognition site of the MexY DBP, and the alkyl linker would tether the remaining monomer within the cell. Modification of the linker length was therefore predicted to alter the effectiveness of this tethering. Due to the concise nature of the semisynthetic route used to access **Ber-C6** (**3.05**), we additionally anticipated that synthesis of a small library of dimers with variable alkyl linker length would be relatively straightforward.

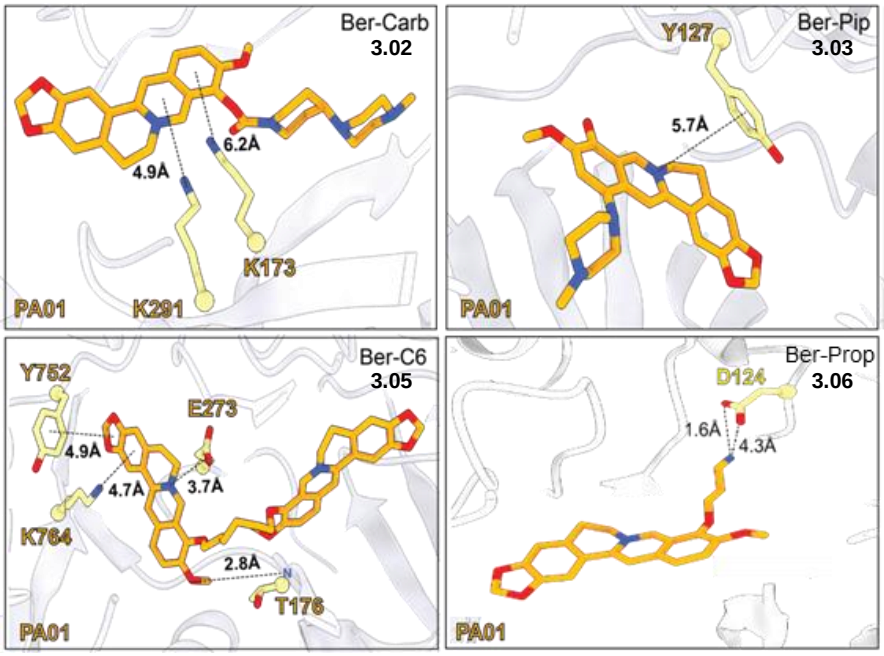

Figure 3.6. Predicted binding poses for the first four synthesized berberine analogs

Synthesis of this second generation of analogs (**3.20 – 3.24**) proceeded by reaction of berberrubine chloride (**3.08**) with commercially available dialkyl halides of varied length, from 1,3-diiodopropane to 1,12-dibromohexane (**Scheme 3.10**).[142] Yields were moderate and increased consistently with alkyl length, suggesting that the dimerization reaction is slowed either by the steric repulsion of the bulky polycyclic rings or the electronic repulsion of the charged quaternary nitrogen atoms as they approach one another. This hypothesis is additionally supported by the observation that addition of a single berberrubine monomer to the alkyl halide was relatively rapid, leading to isolable monoalkylated product in less than one hour (as described above for Ber-C6), but complete addition of a second berberrubine molecule took up to 72 hours. Longer dialkyl halides are typically only available as bromides; to facilitate dimerization onto these worse leaving groups sodium iodide was used as an additive.

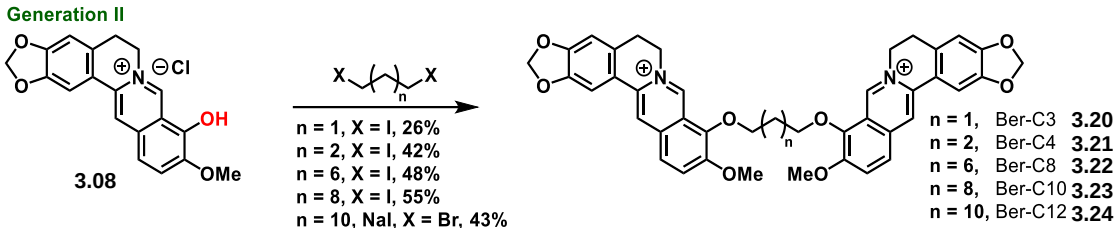

Scheme 3.11. Synthesis of second-generation berberine analogs, modifying alkyl linker length

Biological analysis of the generation 2 analogs (**3.20 – 3.24,** Logan Kavanaugh, Conn Lab, Emory University) revealed a consistent trend wherein increased dimer linker length was positively correlated with synergism (**Figure 3.8, Table 6.1**). **Ber-C3** (**3.20**) was weakly synergistic (kanamycin FIC = 0.4, gentamicin FIC = 0.38) to the more synergistic **Ber-C10** (**3.23**, kanamycin FIC = 0.31, gentamicin FIC = 0.33). Extending the linker further to C12 (**3.24**) saw the synergistic effects begin to decrease again, so alkyl linkers longer than this were not pursued. Importantly, long-chain berberine alkyl dimers also showed an aminoglycoside-independent killing effect of *P. aeruginosa*, revealing that these compounds were no longer selective for MexY inhibition. This was further confirmed via observation that adding 64 µg/mL of either **Ber-C8** (**3.22**), **Ber-C10** (**3.23**), or **Ber-C12** (**3.24**) in a time-kill assay resulted in a lower aminoglycoside MIC against PAO1 than for an aminoglycoside alone against a PAO1Δ*mexXY* strain (**Table 3.2, Table 6.2**). As aminoglycosides are known to be solely exported by MexXY, their MIC in a *mexXY* knockout strain should theoretically be the limit to which an efflux pump inhibitor such as our berberine dimers can synergize. We thus reasoned that in addition to inhibiting the MexY protein, the long-chain dimers were acting via some other mechanism to inhibit *P. aeruginosa*.

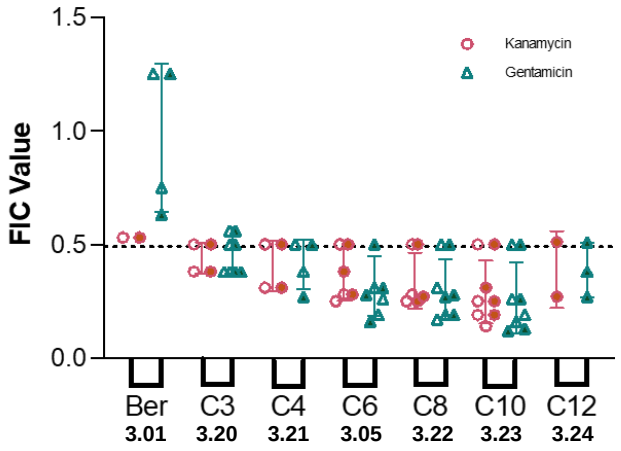

Figure 3.7. Fractional inhibitory concentration (FIC) values for alkyl-linked berberine dimers

We reasoned that due to the structure of long-chain berberine dimers containing charged quaternary ammoniums and long hydrophobic interiors, these compounds could be acting as membrane permeabilizers, associating with the similarly amphipathic phospholipid bacterial membranes and causing cell lysis at sufficiently high concentrations (see chapter 4 for a more detailed description of the antimicrobial mechanisms of quaternary ammonium compounds). In an effort to develop compounds with the same high synergistic potential but with heightened specificity towards efflux pump inhibition, we desired analogs containing linkers utilizing

Table 3.2. Checkerboard synergy assay results utilizing kanamycin, amikacin, gentamicin, or tobramycin with synthetic berberine analogs in an efflux competent (PAO1) or incompetent (PAO1Δ*mexXY*) strain of *P. aeruginosa*

			Aminoglycosides (μg/mL)			
			Kan	**Ami**	**Gen**	**Tob**
Bacterial Strain	PAO1		64	1	1	0.5
	PAO1Δ*mexXY*		16	0.25	0.25	0.25
Compound [64 μg/mL]	**BER**	**3.01**	32	0.5	0.5	0.25
	Ber-Pip	**3.03**	64	ND*	1	ND
	Ber-Carb	**3.02**	32	ND	0.5	ND
	Ber-Prop	**3.06**	32	ND	0.5	ND
	Ber-C3	**3.20**	16	0.25	0.25	0.25
	Ber-C4	**3.21**	16	0.5	0.25	0.25
	Ber-C6	**3.05**	16	ND	0.25	ND
	Ber-C8	**3.22**	16	ND	0.125	ND
	Ber-C10	**3.23**	8	0.125	0.0625	0.0625
	Ber-C12	**3.24**	8	0.125	0.125	0.125

alternative chemical motifs that should disfavor membrane intercalation. For example, incorporation of a PEG linker was predicted to increase the hydrophilicity of the linker, disfavoring association with hydrophobic phospholipid tails. Alternatively, rigidification of the berberine dimer scaffold could be achieved by utilizing aryl hydrocarbon linkers and would similarly be predicted to limit interaction with the membrane interior.

A third generation of compounds (**3.25 - 3.28**) was thus synthesized, again starting from commercially available dihalides (**Scheme 3.11**). Yields were low (which was somewhat surprising due to the heightened electrophilicity of the benzylic halides) due to difficulty in purification of these products from their monoalkylated byproducts, though no significant attempts were made for their optimization. However, sufficient material was nevertheless generated to allow biological analysis. While we identified that this third generation of berberine dimers returned specificity towards inhibition of MexY, the compounds themselves were only weakly synergistic, with FIC values higher than those of the alkyl dimers of equivalent length (Logan Kavanaugh, Conn Lab, Emory University, **Table 6.1**).

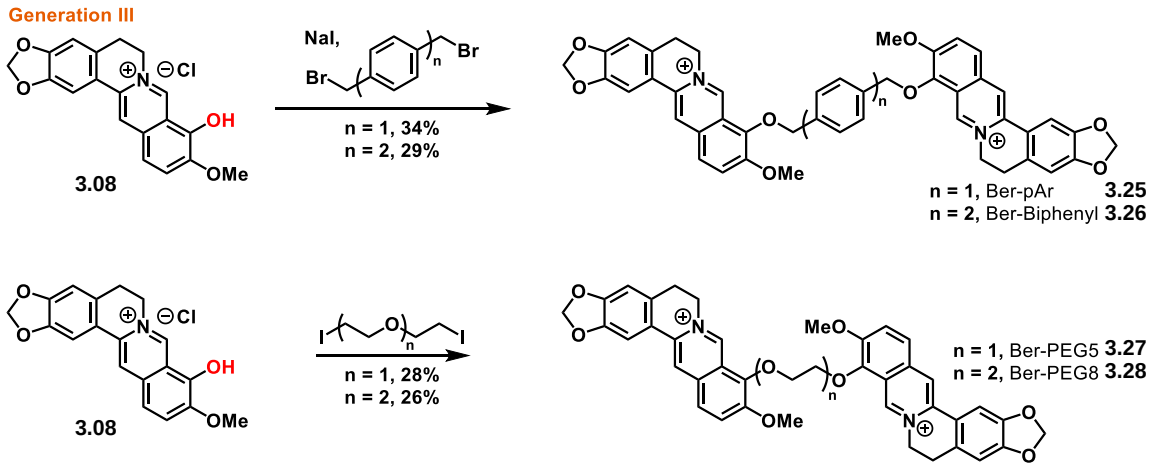

Scheme 3.12. Synthesis of third-generation berberine analogs, modifying alkyl linker composition

Insights into the specific binding interactions between berberine dimers and the DBP of the MexY protein were explored computationally (Dr. Debayan Dey, Conn Lab, Emory University). Molecular dynamics simulations of lead compounds **Ber-C3** (**3.20**), **Ber-C12** (**3.24**), and **Ber-pAr** (**3.25**), as well as berberine (**3.01**), were performed in Schrodinger Desmond, and revealed that the dimeric analogs had significantly greater predicted binding score after a 50 ns simulation (**Table 3.3, Figure 6.2**). **Ber-C3** (**3.20**) showed the lowest ligand strain energy and highest π-packing score, revealing that a combination of aryl moieties and flexibility was important for binding interactions with MexY. To investigate biochemically whether these compounds bound in the same spot as berberine (**3.01**), a three-way synergy assay was performed (Conn Lab) utilizing berberine (**3.01**), **Ber-C3** (**3.20**), and amikacin. We predicted that if berberine and **Ber-C3** (**3.20**) bound in overlapping regions of the DBP, they should compete for binding instead of showing increased synergy with amikacin. This is what was observed, wherein concentrations above 128 μg/mL, **Ber-C3** (**3.20**) could outcompete berberine (64 μg/mL) for binding resulting in the synergistic MIC of **Ber-C3** (**3.20**) and amikacin. At concentrations of **Ber-C3** (**3.20**) below 128 μg/mL, berberine (64 μg/mL) outcompeted **Ber-C3** (**3.20**), resulting in the synergistic MIC of berberine and amikacin.

To examine whether linear alkyl dimers such as **Ber-C12** (**3.24**) were inhibiting *P. aeruginosa* through a membrane permeabilization mechanism, a hemolysis assay was performed (by myself

Ligand	0 ns	50 ns
Ber	n/a	F601
Ber-C3 **3.20**	R116, Y127, K173, E175, K291, F601	R67, D124, E175, F276 K291, F601, S671, K76
Ber-C12 **3.24**	Y127, Q163, R763	K291, Y326
Ber-pAr **3.25**	R166, E273, F276, F601, S671, Q761	R67, F276, K291, F601, S

Table 3.3. Polar contacts of four berberine compounds before and after a 50 ns molecular dynamics simulation in the DBP of MexY, performed in Schrodinger Desmond

and Logan Kavanaugh, Conn Lab, Emory University), in which berberine compounds were incubated with ovine erythrocytes for one hour (**Figure 3.9A**). This assay reveals the membrane lytic potential of compounds in a visually apparent way, as the cell lysate (if any is present) turns the solution red in a quantifiable manner. However, the hemolysis assay revealed that berberine, **Ber-C4** (**3.21**), **Ber-C10** (**3.23**), and **Ber-C12** (**3.24**) all showed minimal lytic activity (LC_{20} all >128 μg/mL). To further assess this hypothesis (as ovine erythrocytes are not always ideal models for bacterial cell lysis), Logan Kavanaugh (Conn Lab, Emory University) performed a vancomycin susceptibility assay (**Figure 3.9B, Figure 3.9C**). Vancomycin acts to kill gram positive bacteria via inhibition of cell wall synthesis but is unable to access the inner membrane of gram negative bacteria and therefore normally has no potent effects on species like *P. aeruginosa*. However, in the presence of a membrane permeabilizer vancomycin is able to reach the inner membrane and shows a killing effect even for gram negative bacteria.[158] We therefore predicted that if long-chain berberine dimers were acting to permeabilize PAO1 membranes, vancomycin should show a reduced MIC. However, this was not observed, as vancomycin retained the same high MIC (128 μg/mL) in both PAO1 and its isogenic *mexXY* knockout in either the presence or absence of **Ber-C12** (**3.24**) additive (at 64 μg/mL). The results of these assays show that the mechanism of bacterial inhibition by compounds like **Ber-C12** (**3.24**) is not membrane permeabilization. Further investigation into these compounds' true inhibitory mechanism is ongoing.

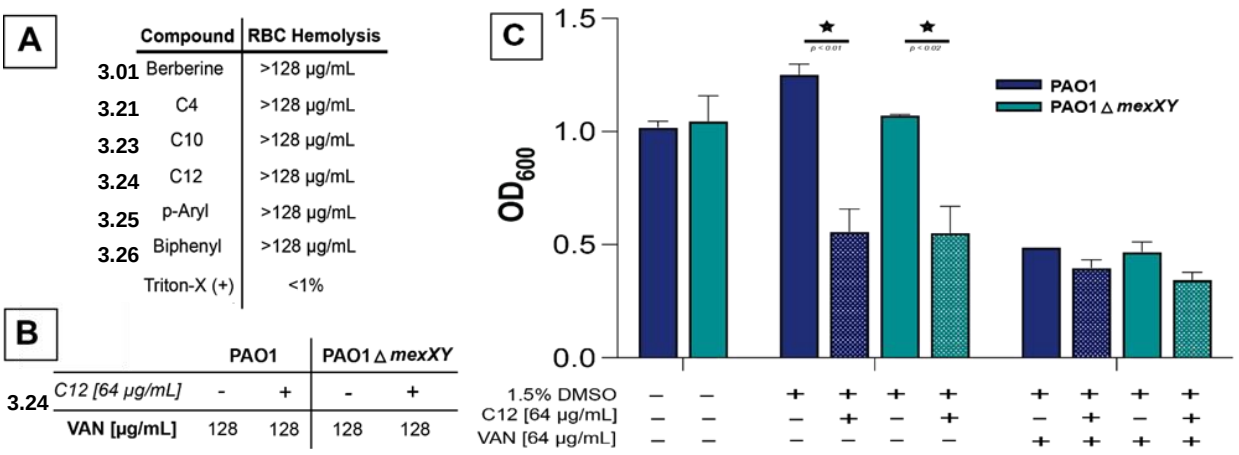

Figure 3.8. Results of assays to examine hypothesis of membrane perturbation for berberine dimers. A. LC_{20} values obtained for representative compounds and controls in hemolysis of ovine erythrocytes. B. Vancomycin sensitization assay MIC values. C. Vancomycin sensitization assay OD_{600} values

3.4 Concluding Remarks and Future Directions

Berberine (**3.01**) has been the subject of much study, due to its long history of use in traditional medicines and dyes, and for the conflicting reports of its efficacy in treatment of a wide variety of ailments. We here conclusively show that berberine and berberine-derived compounds can be used as efflux pump inhibitors selective for MexXY-OprM. This inhibition, though not at a potency which is likely to be clinically relevant without significant further optimization, can allow for structural investigation of interactions within the DBP of MexY as it pertains to aminoglycoside efflux. We have shown that this efflux pump inhibition confers synergism with all tested aminoglycosides (amikacin, gentamicin, tobramycin, and kanamycin), and occurs in both laboratory *P. aeruginosa* strains PAO1, PA7, PA14 as well as clinical isolates, including pan-aminoglycoside resistant isolates K2156 and K2161 (**Table 6.2**). Using **Ber-C3** (**3.20**) as an adjuvant, we were able to restore aminoglycoside MIC in these resistant isolates to knockout levels, highlighting the effectiveness of efflux pump inhibitors as a viable clinical solution to efflux-mediated antibiotic resistance.

Future efforts with this project will aim to develop further insights into the nature of the interactions between berberine compounds and MexY. Work is ongoing in the Conn lab to develop a reliable method of crystallization of the MexY protein subunit; this may allow cocrystallization with an EPI like berberine (**3.01**) which could provide tremendous structural insights into the design of improved inhibitors and gain understanding into the precise mechanisms of aminoglycoside resistance. We additionally remain interested in the mechanisms by which **Ber-C8** (**3.22**), **Ber-C10** (**3.23**), and **Ber-C12** (**3.24**) were able to inhibit growth of *P. aeruginosa* in an aminoglycoside-independent manner. While our initial hypothesis of membrane permeabilization does not appear to be correct based on the results of our hemolysis and vancomycin sensitization assays, knowledge of how these compounds are acting could provide interesting insights, especially if they function through a novel mechanism of action unutilized by other drug classes.

3.5 Chapter 3 References

(114) Hedin, L. E.; Illergård, K.; Elofsson, A. An Introduction to Membrane Proteins. *J. Proteome Res.* **2011**, *10* (8), 3324–3331. https://doi.org/10.1021/pr200145a.

(115) Fernández, L.; Hancock, R. E. W. Adaptive and Mutational Resistance: Role of Porins and Efflux Pumps in Drug Resistance. *Clin. Microbiol. Rev.* **2012**, *25* (4), 661–681. https://doi.org/10.1128/CMR.00043-12.

(116) Okamoto, K.; Gotoh, N.; Nishino, T. Alterations of Susceptibility of Pseudomonas Aeruginosa by Overproduction of Multidrug Efflux Systems, MexAB-OprM, MexCD-OprJ, and MexXY/OprM to Carbapenems: Substrate Specificities of the Efflux Systems. *J. Infect. Chemother.* **2002**, *8* (4), 371–373. https://doi.org/10.1007/s10156-002-0193-7.

(117) Alenazy, R. Drug Efflux Pump Inhibitors: A Promising Approach to Counter Multidrug Resistance in Gram-Negative Pathogens by Targeting AcrB Protein from AcrAB-TolC Multidrug Efflux Pump from Escherichia Coli. *Biology* **2022**, *11* (9), 1328. https://doi.org/10.3390/biology11091328.

(118) White, A. R.; Kaye, C.; Poupard, J.; Pypstra, R.; Woodnutt, G.; Wynne, B. Augmentin (Amoxicillin/Clavulanate) in the Treatment of Community-Acquired Respiratory Tract Infection: A Review of the Continuing Development of an Innovative Antimicrobial Agent. *J. Antimicrob. Chemother.* **2004**, *53 Suppl 1*, i3-20. https://doi.org/10.1093/jac/dkh050.

(119) Bush, K. Synergistic Antibiotic Combinations. In *Antibacterials: Volume I*; Fisher, J. F., Mobashery, S., Miller, M. J., Eds.; Topics in Medicinal Chemistry; Springer International Publishing: Cham, 2018; pp 69–88. https://doi.org/10.1007/7355_2017_23.

(120) Stavri, M.; Piddock, L. J. V.; Gibbons, S. Bacterial Efflux Pump Inhibitors from Natural Sources. *J. Antimicrob. Chemother.* **2007**, *59* (6), 1247–1260. https://doi.org/10.1093/jac/dkl460.

(121) Lamut, A.; Peterlin Mašič, L.; Kikelj, D.; Tomašič, T. Efflux Pump Inhibitors of Clinically Relevant Multidrug Resistant Bacteria. *Med. Res. Rev.* **2019**, *39* (6), 2460–2504. https://doi.org/10.1002/med.21591.

(122) Jamshidi, S.; Sutton, J. M.; Rahman, K. M. Computational Study Reveals the Molecular Mechanism of the Interaction between the Efflux Inhibitor PAβN and the AdeB Transporter from Acinetobacter Baumannii. *ACS Omega* **2017**, *2* (6), 3002–3016. https://doi.org/10.1021/acsomega.7b00131.

(123) Su, F.; Wang, J. Berberine Inhibits the MexXY-OprM Efflux Pump to Reverse Imipenem Resistance in a Clinical Carbapenem-resistant Pseudomonas Aeruginosa Isolate in a Planktonic State. *Exp. Ther. Med.* **2018**, *15* (1), 467–472. https://doi.org/10.3892/etm.2017.5431.

(124) Leona, M.; Lombardi, J. R. Identification of Berberine in Ancient and Historical Textiles by Surface-Enhanced Raman Scattering. *J. Raman Spectrosc.* **2007**, *38* (7), 853–858. https://doi.org/10.1002/jrs.1726.

(125) Yamada, Y.; Yoshimoto, T.; Yoshida, S. T.; Sato, F. Characterization of the Promoter Region of Biosynthetic Enzyme Genes Involved in Berberine Biosynthesis in Coptis Japonica. *Front. Plant Sci.* **2016**, *7*.

(126) Khosla, P. K.; Neeraj, V. I.; Gupta, S. K.; Satpathy, G. Berberine, a Potential Drug for Trachoma. *Rev. Int. Trach. Pathol. Ocul. Trop. Subtrop. Sante Publique Organe Ligue Contre Trach. Avec Collab. Int. Organ. Trach. Organ.* **1992**, *69*, 147–165.

(127) Wang, Y.; Liu, Y.; Du, X.; Ma, H.; Yao, J. The Anti-Cancer Mechanisms of Berberine: A Review. *Cancer Manag. Res.* **2020**, *12*, 695–702. https://doi.org/10.2147/CMAR.S242329.

(128) Wang, Y.; Liu, H.; Zheng, M.; Yang, Y.; Ren, H.; Kong, Y.; Wang, S.; Wang, J.; Jiang, Y.; Yang, J.; Shan, C. Berberine Slows the Progression of Prediabetes to Diabetes in Zucker Diabetic Fatty Rats by Enhancing Intestinal Secretion of Glucagon-Like Peptide-2 and Improving the Gut Microbiota. *Front. Endocrinol.* **2021**, *12*.

(129) Xie, W.; Su, F.; Wang, G.; Peng, Z.; Xu, Y.; Zhang, Y.; Xu, N.; Hou, K.; Hu, Z.; Chen, Y.; Chen, R. Glucose-Lowering Effect of Berberine on Type 2 Diabetes: A Systematic Review and Meta-Analysis. *Front. Pharmacol.* **2022**, *13*.

(130) Yin, J.; Xing, H.; Ye, J. Efficacy of Berberine in Patients with Type 2 Diabetes. *Metabolism.* **2008**, *57* (5), 712–717. https://doi.org/10.1016/j.metabol.2008.01.013.

(131) Ji, H.-F.; Shen, L. Berberine: A Potential Multipotent Natural Product to Combat Alzheimer's Disease. *Molecules* **2011**, *16* (8), 6732–6740. https://doi.org/10.3390/molecules16086732.

(132) Yu, M.; Jin, X.; Liang, C.; Bu, F.; Pan, D.; He, Q.; Ming, Y.; Little, P.; Du, H.; Liang, S.; Hu, R.; Li, C.; Hu, Y. J.; Cao, H.; Liu, J.; Fei, Y. Berberine for Diarrhea in Children and Adults: A Systematic Review and Meta-Analysis. *Ther. Adv. Gastroenterol.* **2020**, *13*, 1756284820961299. https://doi.org/10.1177/1756284820961299.

(133) Lau, C. W.; Yao, X. Q.; Chen, Z. Y.; Ko, W. H.; Huang, Y. Cardiovascular Actions of Berberine. *Cardiovasc. Drug Rev.* **2001**, *19* (3), 234–244. https://doi.org/10.1111/j.1527-3466.2001.tb00068.x.

(134) Rui, R.; Yang, H.; Liu, Y.; Zhou, Y.; Xu, X.; Li, C.; Liu, S. Effects of Berberine on Atherosclerosis. *Front. Pharmacol.* **2021**, *12*, 764175. https://doi.org/10.3389/fphar.2021.764175.

(135) Kosalec, I.; Jembrek, M. J.; Vlainić, J. The Spectrum of Berberine Antibacterial and Antifungal Activities. In *Promising Antimicrobials from Natural Products*; Rai, M., Kosalec, I., Eds.; Springer International Publishing: Cham, 2022; pp 119–132. https://doi.org/10.1007/978-3-030-83504-0_7.

(136) Warowicka, A.; Nawrot, R.; Goździcka-Józefiak, A. Antiviral Activity of Berberine. *Arch. Virol.* **2020**, *165* (9), 1935–1945. https://doi.org/10.1007/s00705-020-04706-3.

(137) Wu, S.; Yang, K.; Hong, Y.; Gong, Y.; Ni, J.; Yang, N.; Ding, W. A New Perspective on the Antimicrobial Mechanism of Berberine Hydrochloride Against Staphylococcus Aureus Revealed by Untargeted Metabolomic Studies. *Front. Microbiol.* **2022**, *13*.

(138) Wang, K.; Feng, X.; Chai, L.; Cao, S.; Qiu, F. The Metabolism of Berberine and Its Contribution to the Pharmacological Effects. *Drug Metab. Rev.* **2017**, *49* (2), 139–157. https://doi.org/10.1080/03602532.2017.1306544.

(139) Hua, W.; Ding, L.; Chen, Y.; Gong, B.; He, J.; Xu, G. Determination of Berberine in Human Plasma by Liquid Chromatography-Electrospray Ionization-Mass Spectrometry. *J. Pharm. Biomed. Anal.* **2007**, *44* (4), 931–937. https://doi.org/10.1016/j.jpba.2007.03.022.

(140) Guo, Y.; Chen, Y.; Tan, Z.-R.; Klaassen, C. D.; Zhou, H.-H. Repeated Administration of Berberine Inhibits Cytochromes P450 in Humans. *Eur. J. Clin. Pharmacol.* **2012**, *68* (2), 213–217. https://doi.org/10.1007/s00228-011-1108-2.

(141) Kim, H. G.; Lee, H. S.; Jeon, J. S.; Choi, Y. J.; Choi, Y. J.; Yoo, S.-Y.; Kim, E.; Lee, K.; Park, I.; Na, M.; Park, H.-J.; Cho, S.-W.; Kim, J.-H.; Lee, J.-Y.; Kim, S. K. Quasi-Irreversible Inhibition of CYP2D6 by Berberine. *Pharmaceutics* **2020**, *12* (10), 916. https://doi.org/10.3390/pharmaceutics12100916.

(142) Chen, W.-H.; Pang, J.-Y.; Qin, Y.; Peng, Q.; Cai, Z.; Jiang, Z.-H. Synthesis of Linked Berberine Dimers and Their Remarkably Enhanced DNA-Binding Affinities. *Bioorg. Med. Chem. Lett.* **2005**, *15* (10), 2689–2692. https://doi.org/10.1016/j.bmcl.2004.10.098.

(143) Huang, M.-Y.; Lin, J.; Huang, Z.-J.; Xu, H.-G.; Hong, J.; Sun, P.-H.; Guo, J.-L.; Chen, W.-M. Design, Synthesis and Anti-Inflammatory Effects of Novel 9-O-Substituted-Berberine Derivatives. *MedChemComm* **2016**, *7* (4), 658–666. https://doi.org/10.1039/C5MD00577A.

(144) Li, R.; Wu, J.; He, Y.; Hai, L.; Wu, Y. Synthesis and in Vitro Evaluation of 12-(Substituted Aminomethyl) Berberrubine Derivatives as Anti-Diabetics. *Bioorg. Med. Chem. Lett.* **2014**, *24* (7), 1762–1765. https://doi.org/10.1016/j.bmcl.2014.02.032.

(145): None. Apotheker-Zeitung 18. Jg. 1903. *Apoth.-Ztg. Organ Dtsch. Apoth. - Standesztg. Dtsch. Apoth.* **1903**, *18*, 1903. https://doi.org/10.24355/DBBS.084-201104191712-0.

(146) Lombardi, P.; Buzzetti, F.; Arcamone, A. G. Benzoquinolizinium Salt Derivatives as Anticancer Agents, January 27, 2011. https://patentscope.wipo.int/search/en/detail.jsf?docId=WO2011009714 (accessed 2023-03-07).

(147) Bremner, J. B.; Samosorn, S. 8-Allyldihydroberberine as an Alternative Precursor for the Synthesis of 13-Substituted Berberine Derivatives. *Aust. J. Chem.* **2003**, *56* (9), 871–873. https://doi.org/10.1071/ch03054.

(148) Ding, Y.; Ye, X.; Zhu, J.; Zhu, X.; Li, X.; Chen, B. Structural Modification of Berberine Alkaloid and Their Hypoglycemic Activity. *J. Funct. Foods* **2014**, *7*, 229–237. https://doi.org/10.1016/j.jff.2014.02.007.

(149) Reyes, M. J.; Castillo, R.; Izquierdo, M. L.; Alvarez-Builla, J. Regioselective Suzuki Coupling on Pyridinium N-(3,5-Dibromoheteroar-2-Yl)Aminides. *Tetrahedron Lett.* **2006**, *47* (36), 6457–6460. https://doi.org/10.1016/j.tetlet.2006.06.097.

(150) Liu, Y.; Cao, J.; Niu, W.; Liu, M.; Guo, X. Studies on the Dyeing and Functional Properties of Modified Berberine for a Variety of Fabrics. *AATCC J. Res.* **2019**, *6* (4), 8–14. https://doi.org/10.14504/ajr.6.4.2.

(151) *How To: Run a Prep TLC*. http://www.chem.rochester.edu/notvoodoo/pages/how_to.php?page=run_prep_tlc (accessed 2023-03-07).

(152) Pang, J.-Y.; Long, Y.-H.; Chen, W.-H.; Jiang, Z.-H. Amplification of DNA-Binding Affinities of Protoberberine Alkaloids by Appended Polyamines. *Bioorg. Med. Chem. Lett.* **2007**, *17* (4), 1018–1021. https://doi.org/10.1016/j.bmcl.2006.11.037.

(153) Teitel, S.; O'Brien, J.; Brossi, A. Preferential Cleavage of an Aromatic Methylenedioxy Group in the Presence of Methoxyls with Boron Trichloride. *J. Org. Chem.* **1972**, *37* (21), 3368–3369. https://doi.org/10.1021/jo00986a046.

(154) Kametani, T.; Noguchi, I.; Saito, K.; Kaneda, S. Studies on the Syntheses of Heterocyclic Compounds. Part CCCII. Alternative Total Syntheses of (±)-Nandinine, (±)-Canadine, and

Berberine Iodide. *J. Chem. Soc. C Org.* **1969**, No. 15, 2036–2038. https://doi.org/10.1039/J39690002036.

(155) Mori-Quiroz, L. M.; Hedrick, S. L.; De Los Santos, A. R.; Clift, M. D. A Unified Strategy for the Syntheses of the Isoquinolinium Alkaloids Berberine, Coptisine, and Jatrorrhizine. *Org. Lett.* **2018**, *20* (14), 4281–4284. https://doi.org/10.1021/acs.orglett.8b01702.

(156) Reddy, V.; Jadhav, A. S.; Anand, R. V. A Room-Temperature Protocol to Access Isoquinolines through Ag(I) Catalysed Annulation of o-(1-Alkynyl)Arylaldehydes and Ketones with NH4OAc: Elaboration to Berberine and Palmatine. *Org. Biomol. Chem.* **2015**, *13* (12), 3732–3741. https://doi.org/10.1039/C4OB02641A.

(157) Gatland, A. E.; Pilgrim, B. S.; Procopiou, P. A.; Donohoe, T. J. Short and Efficient Syntheses of Protoberberine Alkaloids Using Palladium-Catalyzed Enolate Arylation. *Angew. Chem. Int. Ed Engl.* **2014**, *53* (52), 14555–14558. https://doi.org/10.1002/anie.201409164.

(158) Lei, E.; Tao, H.; Jiao, S.; Yang, A.; Zhou, Y.; Wang, M.; Wen, K.; Wang, Y.; Chen, Z.; Chen, X.; Song, J.; Zhou, C.; Huang, W.; Xu, L.; Guan, D.; Tan, C.; Liu, H.; Cai, Q.; Zhou, K.; Modica, J.; Huang, S.-Y.; Huang, W.; Feng, X. Potentiation of Vancomycin: Creating Cooperative Membrane Lysis through a "Derivatization-for-Sensitization" Approach. *J. Am. Chem. Soc.* **2022**, *144* (23), 10622–10639. https://doi.org/10.1021/jacs.2c03784.

Chapter 4 - Concise synthesis of tricepyridinium bromide derivatives

4.1 Introduction

Quaternary ammonium compounds (QACs) are a class of molecule characterized by a tetravalent ammonium ion usually bound to four hydrocarbon substituents (of which linear alkane and benzyl are most common). Their amphipathic nature makes them well-suited for a variety of uses, and as such QACs are found ubiquitously in household, industrial, and clinical settings.[159] They are effective surfactants and detergents, forming micelles around hydrophobic molecules and removing them. As fabric softeners, QACs are usually employed as betaine esters, this allows them to perform their role as antistatic agents (neutralizing charge and aligning fabric threads) while being more hydrolytically labile and biodegradable than simple aliphatic QACs.[159–161] In organic chemistry, the amphiphilicity of QACs makes them excellent phase transfer catalysts. If a reaction is run in a biphasic system in which reaction components are poorly soluble in at least one phase (for example, substitution reaction of aqueous sodium cyanide with an ethereal solution of 1-

bromooctane), employing a QAC such as tetrabutylammonium bromide can therefore substantially improve reaction rates, increase yields, and limit the need for specialized solvents.[162]

The antimicrobial potential of quaternary ammonium compounds (QACs) was first identified over a century ago, when researchers at the Rockefeller Institute described the bactericidal activity of a series of hexamethylenetetraminium salts on *Salmonella typhi* in 1916.[163] Since then, QACs have come to constitute one of the largest classes of active ingredients in disinfectant and biocide formulations. The antibiotic mechanism of action of QACs is also related to this class of compounds' amphiphilicity.[164] QACs can disrupt cell membrane stability by initial electrostatic association of the cationic nitrogen with the anionic phosphate head of a lipid bilayer. A poorly-understood "flip" of the molecule then leads to incorporation of the QAC hydrophobic alkyl chains into the nonpolar interior region of the membrane. At sufficient concentrations, incorporation of QAC molecules sufficiently lowers membrane integrity to allow pore formation and/or complete membrane lysis (**Figure 4.1**).[164] Due to their potential for activity against a wide variety of pathogens (bacteria, fungi, enveloped viruses, and amoebae), QACs are recommended for general hospital use in the sterilization of noncritical patient care equipment—any surface that has the potential for contact with skin but not mucous membranes.[165] Outside of hospitals, QACs also see use as surface disinfectants in household and foodservice settings, comprising the active ingredient of many commercially available cleaning sprays and wipes.

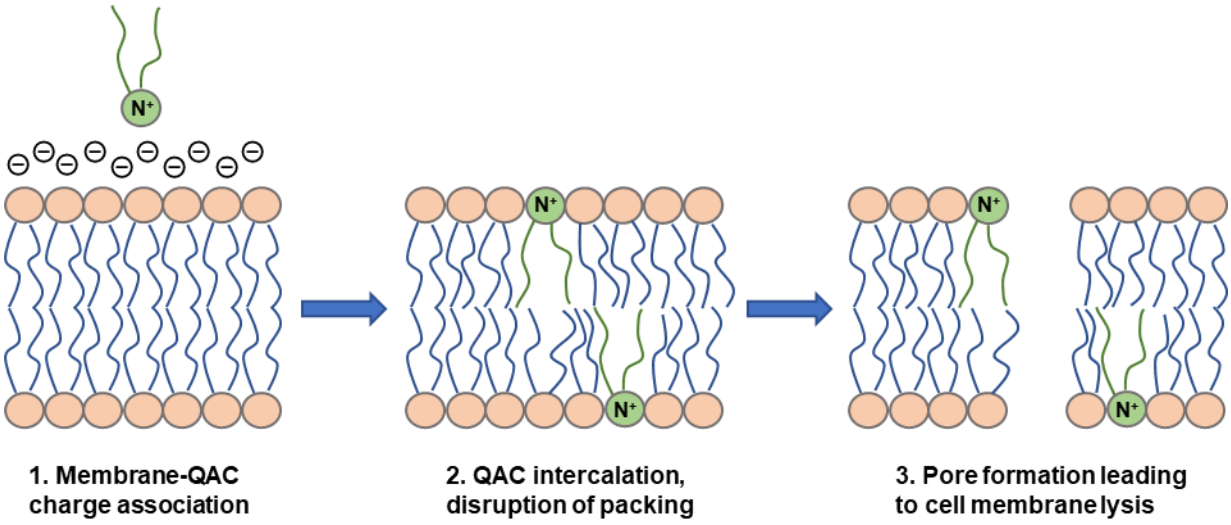

Figure 4.1. Mechanism of action of most antimicrobial QACs

Although the general class of QACs may contain a wide variety of substituents around the ammonium cation, the most commonly employed QACs for sanitization are alkonium chlorides, with benzalkonium (BACs) and dimethyldecyl ammonium chloride (DDAC) being the most common (**Figure 4.2**). The former contains at least one benzyl group in addition to linear or branched alkyl groups ranging from 1 to 18 carbons in length. The most common counterion in QACs by far is chloride, but bromide, saccharide, and acetate are also seen.[166,167] Commercial QAC formulations are often dilute solutions (generally between 0.01% and 1%) and may contain a combination of multiple QACs.

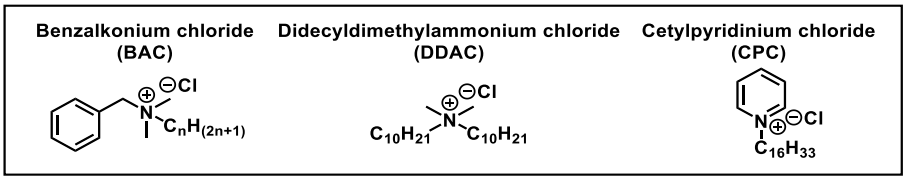

Figure 4.2. Structure of commonly used QAC disinfectants

Although bacterial resistance to QACs was first identified in the 1980s, the precise mechanisms by which this resistance occurs remain significantly understudied.[168–171] As the vast majority of

QAC disinfectants function via membrane permeabilization leading to cell lysis, some bacterial species have intrinsic resistance to QACs caused by the composition of their outer membrane (QAC disifnfectants are almost always more potent against gram-positive bacteria than the dual-membrane gram-negative species).[172,173] However, it is generally accepted that acquired resistance in gram-positive bacteria such as *Staphylococcus* species is the result of the presence of multidrug or QAC-specific efflux pumps (**Figure 4.3, top**). Studies have shown that methicillin-resistant *S. aureus* (MRSA) isolates containing qac genes have significantly higher minimum bactericidal concentrations (MBCs) than those without these genes, confirming that qac genes are indeed likely the true mechanism of resistance in these bacteria.[174] Although QAC resistance in gram-negative bacteria is less common in the literature, 2- to 8-fold changes in minimum inhibitory concentrations (MICs) in gram-negative species were observed from species isolated from drains that had repeated QAC exposure.[174] Additional studies have highlighted the emergence of QAC tolerance in the pathogens *Listeria monocytogenes* and *Pseudomonas aeruginosa*, with the latter noting membrane composition changes that may contribute to this tolerance.[175,176] Indeed, it has been observed that rigidification of bacterial cell membranes via incorporation of a higher percentage of fully saturated fatty acids can allow these species to withstand the effects of QACs (**Figure 4.3, bottom**).

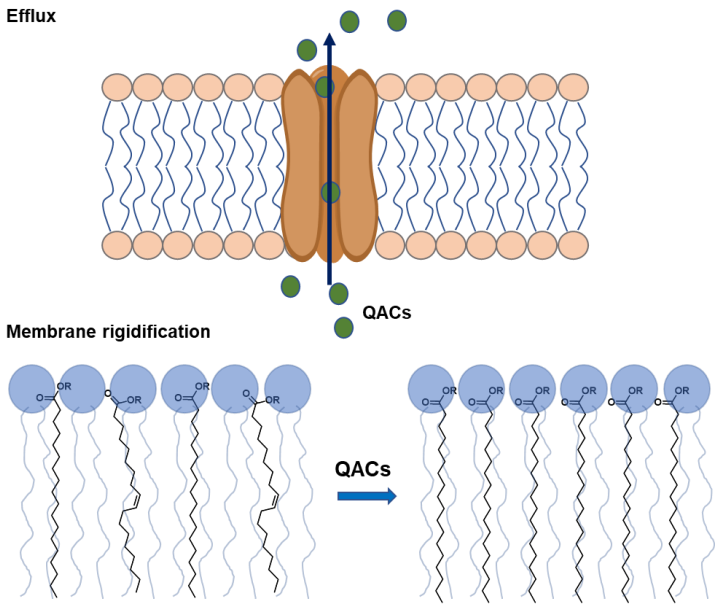

Figure 4.3. Known mechanisms of QAC resistance in bacteria

In *Staphylococcus*, the genes encoding for QAC-transporting efflux pumps are located on mobile genetic elements such as plasmids.[172,173] This allows for efficient horizontal gene transfer, resulting in the potential for the rapid spread of QAC resistance between species. One study found that of 238 human clinical isolates of *Staphylococci* from Norway, 50% were phenotypically resistant to BAC. Furthermore, the authors suggested this resistance to be a direct consequence of selective pressure resulting from the use of disinfectants. Additional studies have shown that *Staphylococci* isolated from surfaces frequently treated with QACs have resistances to BAC (one of the most common QACs), whereas *Staphylococci* isolated from other, nontreated surfaces remained susceptible to this compound, providing additional evidence that it is in fact the use of QACs that drives resistance acquisition.[177]

The ongoing SARS-CoV-2 (COVID-19) pandemic has been implicated in the exacerbation of QAC resistance. As a component of the response to this pandemic, the manufacture, sale, and use of QAC disinfectants have all increased dramatically.[76,166] Of the 654 products on the

Environmental Protection Agency's list of recommended disinfectants against SARS-CoV-2, 306 contain a QAC as the active ingredient.[178] Disinfection is also occurring in more environments during the pandemic; once mostly relegated to indoor high-risk settings, QACs are now being used to disinfect public transportation, public benches, and other outdoor spaces. Critically, QACs are non-volatile and are not generally rinsed off of surfaces after application, enabling these compounds to remain on these surfaces or in the environment at potentially sub-inhibitory levels for extended periods of time.

The bactericidal activity of QACs is highly dependent on the context of use. Factors such as surface composition, temperature, method of application, and dwell time have all been shown to significantly impact the efficacy of sanitizers containing these compounds.[165] It is likely that, due to the overwhelming number of hospital admissions during the COVID-19 pandemic, increased pressure to ensure rapid room turnaround between patients may have led to a relaxation in sanitization protocols; the pandemic has been linked to shortages in PPE, supplies and testing, and logistical support.[179] These challenges have further been linked to increases in hospital-acquired infections and increased rates of sepsis.[179–182] Furthermore, in non-clinical environments, there is much less oversight of proper disinfection guidelines than in hospitals. Thus, QAC resistance has also been detected in non-clinical settings; testing *S. aureus* strains from the surfaces of ATMs in Hong Kong yielded strains containing the QAC resistance genes qacA and qacB.[183] Antibiotic resistance as a whole is well-documented as having been worsened during the pandemic; the CDC estimates that of the bacteria and fungi described as “Urgent Threats,” a 13-78% (dependent on species, 13% is specific for MRSA, up to 78% for carbapenem-resistant *Acinetobacter*) rise of infections between 2019 and 2020 was observed.[77,184]

Our lab's research into QACs aims to probe their structure activity relationship to improve their properties in a variety of ways. Increasing antimicrobial potency, decreasing eukaryotic toxicity, and decreasing bacterial propensity for resistance are all current goals for this project. Our results (further corroborated by other reports) have revealed that incorporation of multiple ammonium cations and decreasing structural rigidity of QACs may lead to improved efficacy and therapeutic indices.[171,185,186] Due to reports of environmental concerns with the use of QACs and subsequent impacts on their presence in surface runoff have led us to take inspiration from the incorporation of ester moieties in QAC-based fabric softeners; the analogous antimicrobial "soft-QACs" show similar potency but are more biodegradable.[161,187] We further believe these may have an added benefit of decreasing total bacterial exposure to QACs in the environment, slowing their resistance development. We have also been interested in substitution of the ammonium cation for phosphonium cations and have been investigating bacterial resistance to this series of compounds (**Figure 4.4**).[188–190]

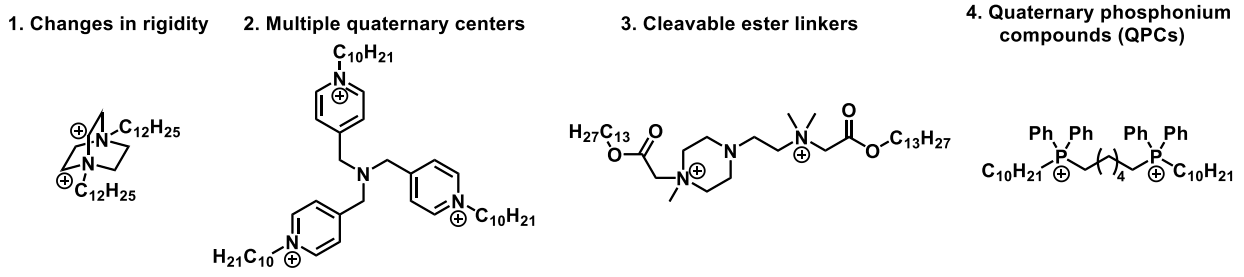

Figure 4.4. Novel classes of quaternary biocides being investigated by the Wuest lab

Due to our lab's longstanding interest in the discovery and development of novel QACs, we were interested when a naturally-produced QAC was isolated from a laboratory strain of *E. coli* transformed with the metagenomic library of *Discodermia calyx* in 2017.[191] Termed "tricepyridinium bromide," this compound features a pyridinium core bound to three indole

moieties at the N, 3, and 5 positions (**4.01**). When tested for antimicrobial properties, the natural product showed potent activity against gram-positive bacteria *B. cereus* (0.78 µg/mL) and *S. aureus* (1.56 µg/mL), as well as the pathogenic yeast *C. albicans* (12.5 µg/mL) (**Table 4.1**). The isolation group confirmed the natural product's structure via total synthesis, and preliminary SAR data showed that while the indoles at the 3 and 5 positions were necessary for antimicrobial activity, the N-ethylindole moiety could be substituted for a simplified ethyl group without significant loss of potency.[191]

Table 4.1. Structure of tricepyridinium bromide and its reported antimicrobial activity

Tricepyridinium bromide

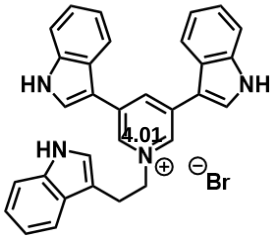

Species	MIC (µg/mL)
B. cereus	0.78
S. aureus	1.56
C. albicans	12.5
E. coli	>100

While most synthetic QACs exhibit antimicrobial properties derived from their amphiphilic nature, tricepyridinium bromide is unusual in its lack of a region with aliphatic, hydrophobic character. It should be noted that while tricepyridinium is not amphiphilic, it is amphoteric, containing electron-rich indole rings as well as an electron-poor pyridinium moiety. Nevertheless, it seems unlikely that this compound would be able to successfully disrupt membrane stability, and so it was reasoned that this molecule's antimicrobial properties may be due to an alternate mechanism of action.

Ethidium bromide is a QAC with structural similarity to tricepyridinium, featuring a quaternized N-ethylpyridinium core and polycyclic aromatic peripheral groups. In contrast to tricepyridinium, ethidium bromide's biological activity has been well-documented. Its high planarity allows it to

intercalate between base pairs of DNA, leading to its use in a biochemistry setting as a fluorescent stain for the detection and visualization of nucleic acids.[192] Its propensity to intercalate also renders ethidium bromide highly toxic, serving as a mutagen by disrupting the process of DNA replication (**Figure 4.5A**). We hypothesized that tricepyridinium bromide may be acting in a similar fashion in bacterial cells. In contrast, if a membrane perturbation mechanism were in play (as supported by the compound's selectivity for gram-positive bacteria), the potency of the compound could be markedly improved via the incorporation of a true hydrophobic aliphatic region. We therefore aimed to synthesize a small library of N-alkyl analogs of varying aliphatic chain length and compare their potencies to that of the natural product. Previous studies in our lab have shown that an alkyl length of 10-14 carbons are optimally suited for membrane permeabilization, as they most

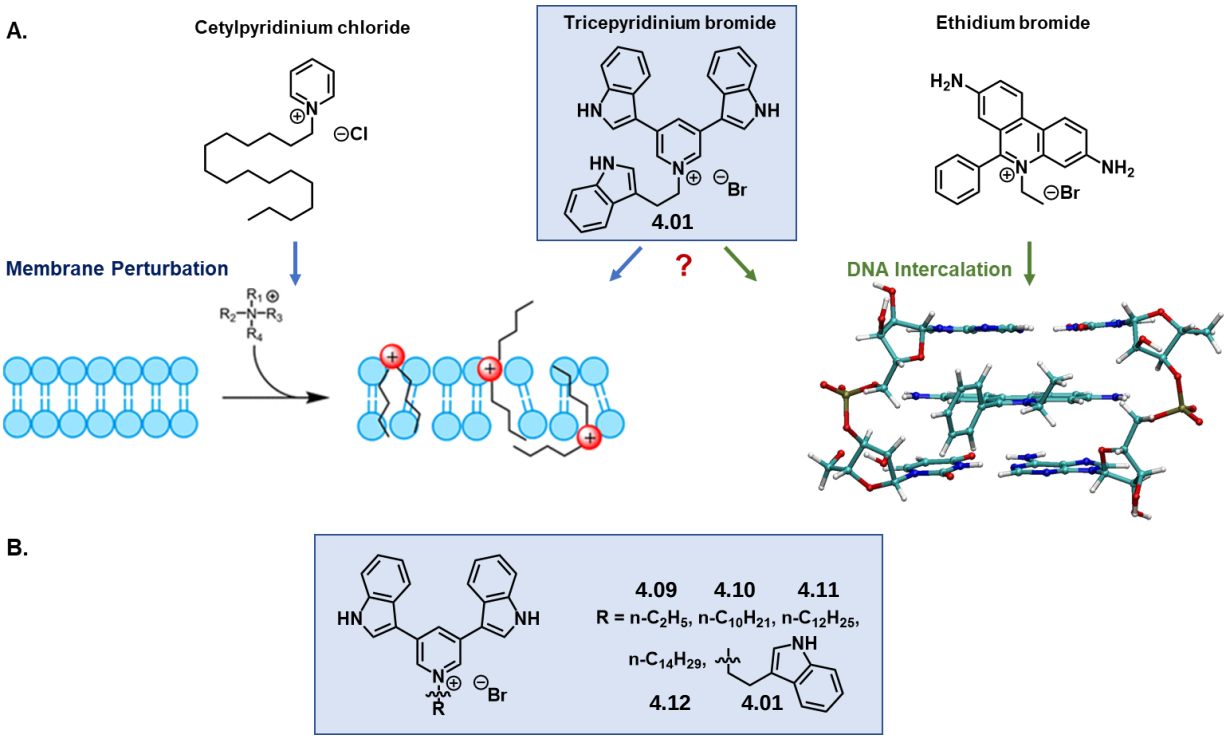

Figure 4.5. A. Proposed mechanisms of action of tricepyridinium bromide, either via membrane perturbation (akin to cetylpyridinium chloride) or DNA intercalation (akin to ethidium bromide). **B**. Structures of desired natural product and N-alkyl analogs to probe the compounds' mechanism of action

closely mimic the lengths of the majority of phospholipid chains that compose bacterial membranes.[193] As a result, we targeted the synthesis of tricepyridinium bromide (**4.01**), an N-ethyl analog previously reported by the isolation group (**4.09**), and analogs containing N-decyl (**4.10**), N-dodecyl (**4.11**), and N-tetradecyl (**4.12**) moieties (**Figure 4.5B**).

4.2 Synthesis

As the tricepyridinium natural product (**4.01**) had been synthesized already by the isolation group, we sought to use their published route to access our N-alkyl analogs and test our mechanistic hypotheses in bacteria (**Scheme 4.1**).[191] This synthetic route begins with Miyaura-type borylation of 3,5-dibromopyridine (**4.02**) to install two pinacolboranes. Next, a reported bis-Suzuki reaction appends N-Boc-3-bromoindole moieties to these positions. After acid-mediated indole deprotection to form **4.05**, the pyridine is then quaternized in a Menshutkin-type reaction using 3-(2-bromoethyl)indole as the electrophile. This concise route, as published, affords the natural product (**4.01**) in a longest linear sequence of four steps (total 6 steps) and 32% overall yield.[191] Importantly, it is also modular, allowing for potential future analog design by Suzuki coupling of other moieties at the 3 and 5 positions

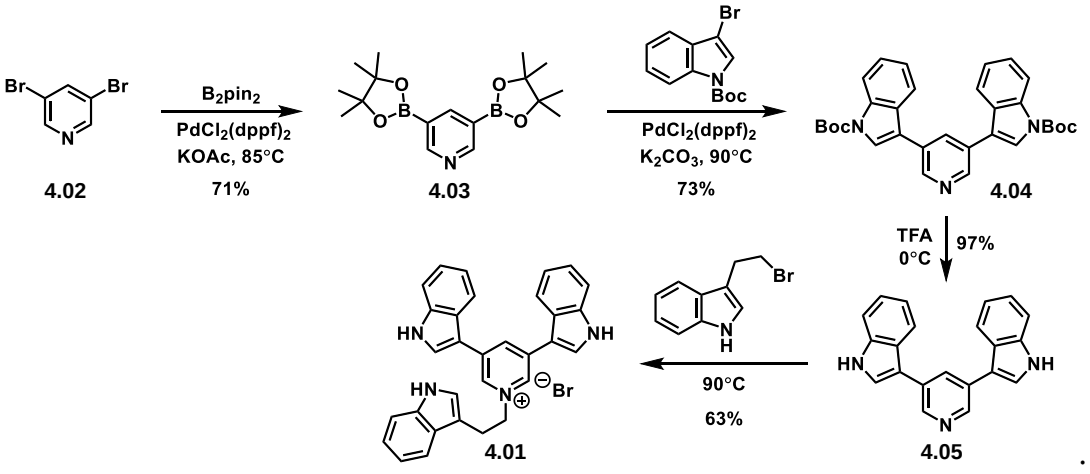

Scheme 4.1. Initial route to tricepyridinium bromide published by Okada et al.

Additionally, quaternization in the final step was ideal for our purposes, allowing us to rapidly derivatize a common intermediate into all of our desired

N-alkyl analogs as well as limiting the number of charged species needing purification.

Unfortunately, initial attempts to reproduce this synthetic route proved unsuccessful. Miyaura borylation of 3,5-dibromopyridine (**4.02**) using the reported conditions did not cleanly afford diborylated product (**4.03**) in reproducibly high yields, often leading to a mixture of monoborylation, varying degrees of protodehalogenation, as well as recovered starting material. Purification of this complex mixture of products proved challenging. Furthermore, what little material could be successfully yielded from this borylation was attempted in the subsequent Suzuki reaction with N-Boc-3-bromoindole and proved equally challenging. To alleviate the foreseen financial burden of optimizing these two palladium-catalyzed steps, an altered route was designed with the intention of being amenable to an undergraduate student's skillset.

Seeking to retain the modularity and late-stage quaternization of the initially published route, a new route was designed to allow for higher reproducibility (**Scheme 4.2**). Most importantly, the key bis-Suzuki step of the first route was inverted, with the intent of coupling commercially available 3,5-dibromopyridine with an indole substituted with a boronic acid at the 3 position (**4.07**). This would limit the need for selectivity in a borylation reaction, as only one aryl halide would be present. Because oxidative addition of electron-rich aryl systems to metal centers is usually slower than electron-poor ones, we decided to utilize the same protecting group for indole as in the initial report, an electron withdrawing Boc group.[194]

While the protected indole-3-boronic acid pinacol ester (**4.07**) is available commercially, it is quite expensive (1g = $53 as of February 20, 2023 from CombiBlocks). Similarly, 3-bromoindole and

any N-protected variants are either commercially unavailable or prohibitively expensive for our purposes, likely due to the instability of 3-haloindoles (in contrast, indoles substituted with halogens at the 4, 5, 6, or 7 positions are readily available from most vendors). Fortunately, laboratory-scale preparation of these materials and their use in subsequent reactions is precedented in the literature, so this approach was chosen for our synthetic route.[195] Starting from indole, protection with di-tert-butyl dicarbonate was facile, and subsequent bromination proceeded regioselectively at the 3-position using N-bromosuccinimide to form **4.06** (**Scheme 4.2**).

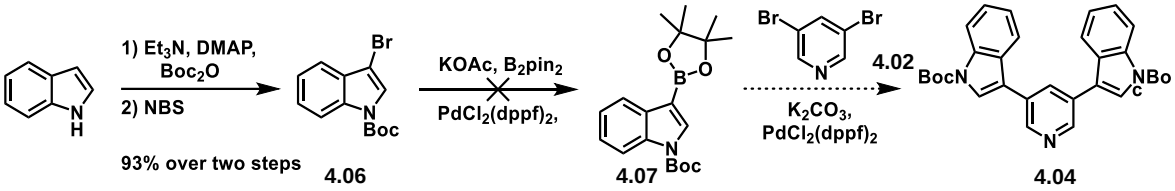

Scheme 4.2. First optimization approach towards key scaffold

Borylation of N-Boc-3-bromoindole to form **4.07** proved more challenging than initially anticipated. Miyaura borylation was unsuccessful and afforded mostly protodehalogenated product. This indicated to us that though oxidative addition of palladium was occurring, the borylation step was not proceeding under the tested conditions. Based on literature reports of successful borylations of indole, the use of a palladium-catalyzed approach was abandoned in favor of a lithiation-borylation strategy.[196–198] We hypothesized that a lithium-halogen exchange followed by addition of an electrophilic boron species would allow for shorter reaction times, higher yields, and more straightforward purification than the use of transition metal catalysis. Unfortunately, the reaction did not proceed as anticipated, leading to little isolable product.

To optimize the borylation, we reasoned that a protected 3-iodoindole would be more reactive under lithiation-borylation conditions. Synthesis of N-Boc-3-iodoindole (**4.08**) as first reported by

Witulksi et al proceeded smoothly, and we found that Boc protection could be performed in high yield without the need for chromatographic purification of the 3-iodoindole intermediate, facilitating this approach.[195] While we discovered that N-Boc-3-iodoindole (**4.08**) was sensitive to light, oxygen, and moisture and would decompose rapidly if kept at ambient temperature, use of this material the same day it was made usually resulted in satisfactory performance. In agreement with the Aggarwal lab's findings, lithiation of N-Boc-3-iodoindole (**4.08**) using n-butyllithium, followed by slow addition of isopropoxy(pinacol)borane then successfully generated our desired borylated indole species (**4.07**) in good yield.[199]

First attempts at our key bis-Suzuki coupling to 3,5-dibromopyridine (**4.02**) using the conditions from the tricepyridinium isolation paper proved only moderately successful, leading mostly to recovered starting material and monoarylation. We found that full conversion of the starting material could be observed when potassium carbonate was replaced with the more soluble cesium carbonate, and when the palladium species used was $Pd(PPh_3)_4$. However, monoarylation byproducts (either still brominated or after protodehalogenation) were still produced in sufficiently large quantities to complicate purification. Fortunately, this hurdle could be overcome simply by increasing the number of stoichiometric equivalents of borylated indole species from the required 2 to a slight excess of 3. This allowed for a gratifying increase in yield of our key step to 88%, allowing for rapid gram-scale synthesis of our required Boc-protected diindolylpyridine (**4.04**).

Indole deprotection using trifluoroacetic acid proved straightforward, though the triaryl product (**4.05**) was insoluble in most organic solvents, with the exception of pyridine. This limited the scalability of this reaction; near-quantitative yields could be obtained on <75 mg scale, but attempts to perform larger-scale reactions resulted in a lower percentage yield of isolated product. Hydrochloric acid-mediated deprotection was also briefly explored in order to isolate the product

as its hydrochloride salt, but this approach proved less successful. Nevertheless, sufficient quantities of **4.05**, the common precursor to our desired analogs, could be produced in this manner. Quaternization of the pyridine nitrogen via substitution onto either linear alkyl bromides or 3-(2-bromoethyl)indole then afforded the desired family of analogs as bromide salts in high yield.

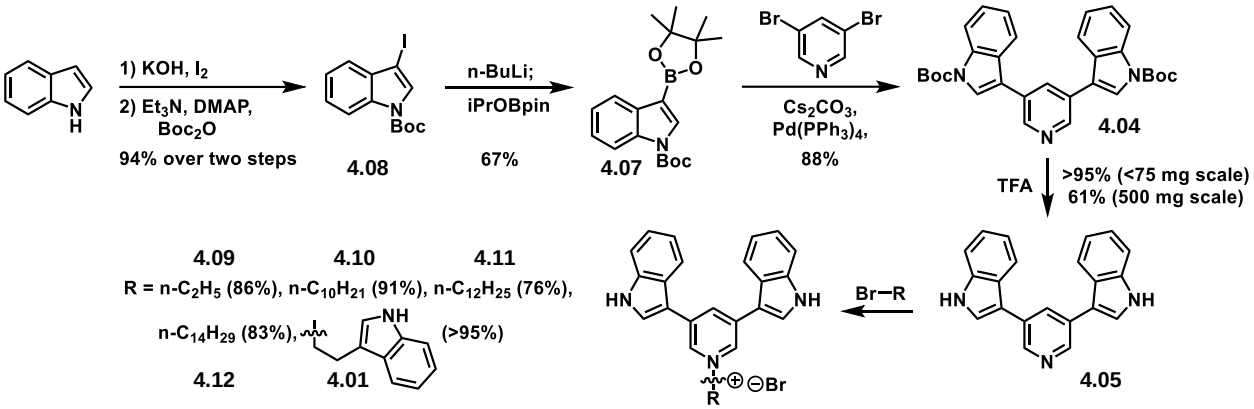

Scheme 4.3. Final optimized synthetic route towards tricepyridinium and N-alkyl analogs

Our optimized route to tricepyridinium (**4.01**) and N-alkyltricepyridinium analogs (**4.09 - 4.12**) has several advantages over the previously published synthesis. We maintain the high modularity and late-stage diversification enjoyed by the initial route, but altering the coupling partners in our hands increased reproducibility of the reactions towards the protected diindolylpyridine common to both strategies (**4.04**). Our route gives a marginally higher overall yield (55% vs 52%) to this common intermediate and allows for its synthesis on larger scale. Purification of intermediates is also more facile with this optimized route; whereas HPLC purification is necessary for intermediates in the original paper. We also delay the need for transition metal catalysis until 4 steps into the synthesis, lowering the cost of our route compared to the initial publication, in which steps 1 and 2 both require the use of palladium. Nevertheless, we acknowledge that the initial route is more concise, requiring only four steps in the longest linear sequence towards the natural product, whereas our more linear route requires six.

4.3 Biological and Computational Investigation

4.3.1 Introduction to assays

Armed with this small array of compounds, attention was directed towards evaluation of their biological activities. As a preliminary assessment of eukaryotic toxicity, examination of the compounds' capability to lyse ovine erythrocytes was desired. Hemolytic activity is usually a reliable indicator that an antibiotic's mechanism of action indeed involves membrane permeabilization or disruption; this assay therefore serves both the purposes of furthering mechanistic understanding of these compounds' activity as well as highlighting any important toxicity concerns against eukaryotic cells. In addition, we sought to confirm the antibacterial activity reported in the initial isolation, as well as assess the biological impact of incorporating N-alkyl chains into the scaffold.

4.3.2 Hemolysis assay

Incubation of tricepyridinium compounds with ovine erythrocytes did not reveal potent hemolytic activity (**Table 4.2, Table 6.5**). In contrast, all tested compounds had LC_{20} values (the concentration of compound at which 20% of red blood cells lyse) of 125 μM or greater. This was exciting, as this shows the synthesized compounds are significantly less hemolytic than even common commercially available QACs such as CPC.

Table 4.2. Results of hemolysis assay (ovine erythrocytes)

Compound	CPC	Tricepyridinium	Ethyl	Decyl	Dodecyl	Tetradecyl
LC_{20} (μM)	16	125	250	125	125	125

4.3.3 MIC assay

The natural product and newly synthesized analogs were then assessed for antibacterial properties. As an additional probe into the potential mechanism of the natural product and synthetic analogs, we extended this antibacterial MIC assay to additional species not tested in the additional isolation report: gram positive oral pathogen *Streptococcus mutans* and gram negative opportunistic pathogen *Pseudomonas aeruginosa*. Results of this inhibition assay confirmed the natural product to be a potent inhibitor of gram positive pathogens. The decyl analog (**4.10**) had comparable activity to the natural product (**4.01**), whereas the ethyl (**4.09**), dodecyl (**4.11**), and tetradecyl analogs (**4.12**) all showed a moderate loss in potency (**Table 4.3**). Importantly, no activity was seen for any tricepyridinium compounds (at concentrations ≤ 250 μM) against gram negative pathogens, and in fact these compounds showed an even greater selectivity towards gram positive bacteria than the tested positive controls, commercial QACs cetylpyridinium chloride and benzalkonium chloride.

Table 4.3. Results of MIC assay. Data were assessed by visual inspection after 24 hours static incubation.

Compound	*S. mutans*	*S. aureus*	*S. aureus*	*S. aureus*	*P. aeruginosa*	*E. coli*
CPC	1	0.5	1	1	250	32
BAC	1	2	4	4	125	64
Tricepyridinium	4	2	4	16	>250	>250
Ethyl (4.09)	125	32	64	250	>250	>250
Decyl (4.10)	2	16	16	16	>250	>250
Dodecyl (4.11)	8	32	32	32	>250	>250
Tetradecyl (4.12)	32	64	64	64	>250	>250

Differential, strain specific activity was observed for the natural product (**4.01**) and ethyl analog (**4.09**) in *S. aureus*, with an 8-fold decreased activity against methicillin resistant strain ATCC33591 as compared to wild type lab strain SH1000. This was not wholly surprising, as strain ATCC33591 is known to harbor QAC resistance genes encoding efflux pumps as described in this chapter's introduction (and **Figure 4.6**). More interesting, however, was the fact that longer N-alkyl analogs (**4.10 - 4.12**) showed no such difference in activity between these two strains. This indicated to us that while strain ATCC33591 displayed inherent efflux-mediated resistance to QACs such as the natural product and short-chain ethyl analog, a longer alkyl chain seems to confer the ability of tricepyridinium compounds to evade this resistance.

4.3.4 Computational docking studies

The QacA efflux pump in *S. aureus* is regulated by trans-acting repressor protein QacR. In the presence of a QAC like tricepyridinium (**4.01**) or BAC, these molecules bind to QacR and disrupt its association to the qacA gene. The resulting expression of the gene acts as a feedback loop to upregulate the production and incorporation of the efflux pump, which can ultimately lead to QAC resistance (**Figure 4.6**).[200]

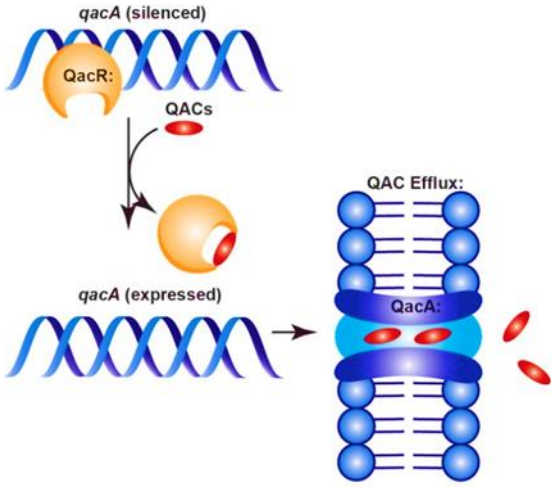

Figure 4.6. Mechanism of QAC resistance via efflux in *S. aureus*

To further probe the observed circumvention of QAC resistance by long chain N-alkyltricepyridinium analogs in *S. aureus*, a computational approach was taken. We hypothesized that either these compounds were not being recognized and effluxed by the QacA pump, or were not binding the transcription factor QacR and thereby not derepressing the QacA gene. The first scenario seems unlikely, as QacA is known to have a broad substrate scope and effluxes compounds with high structural similarity to our long-chain tricepyridinium analogs, such as CPC.[201] In addition, examination of this hypothesis either computationally or biochemically is challenging due to the fact that QacA is membrane bound and no crystal structure has been reported, and that other Qac-family efflux pumps have also been reported and may be implicated. We therefore focused our efforts on evaluation of the second hypothesis. Computational docking of all synthesized compounds into the binding site of QacR was thus performed with AutoDock Vina embedded in PyRx (later reproduced using Schrödinger GLIDE) and visualized using PyMOL (**Figure 4.7**).

The binding pocket of QacR contains a number of tyrosine and tryptophan residues, facilitating π-stacking interactions with the aromatic moieties commonly seen in QACs. Indeed, previous work by our group has shown that monocationic QACs bearing aryl moieties are favorable substrates for resistance development. Computational modeling results reliably localized all of the tested tricepyridinium compounds to this recognition region. Decyl, dodecyl, and tetradecyl compounds (**4.10 - 4.12**) were all predicted to bind in virtually identical modes to QacR, allowing for stabilizing π-stacking interactions of the indole moieties with Y93 (slip-stacking geometry) and Y103 (T-shaped geometry), as well as hydrogen bonding of the indole protons to T89 and N157 and orientation of the long alkyl chains to the hydrophobic interior of the protein. In contrast, the ethyl analog (**4.09**) had a computed binding mode that was rotated nearly 180 degrees in-plane

with respect to analogs with longer alkyl chains; this conformation retained hydrogen bonding to T89 but exchanged its N157 interaction for an additional π-stacking interaction (T-shaped geometry) with W61. The additional indole moiety of the natural product (**4.01**) allows it to adopt a third, lower energy conformation in which the molecule forfeits planarity to allow for an intramolecular π-stacking between two of its indole moieties, as well as to W61, Y93, Y103, and Y123. Hydrogen bonding to T161 is also predicted, though interactions with T89 and N157 are lost. The relative predicted affinities place tricepyridinium (**4.01**) as the strongest binder to QacR (-12.8 kcal/mol), followed by ethyl (**4.09**, -11.1 kcal/mol), decyl (**4.10**, -11.0 kcal/mol), dodecyl (**4.11**, -10.8 kcal/mol), and tetradecyl (**4.12**, -10.7 kcal/mol) analogs.

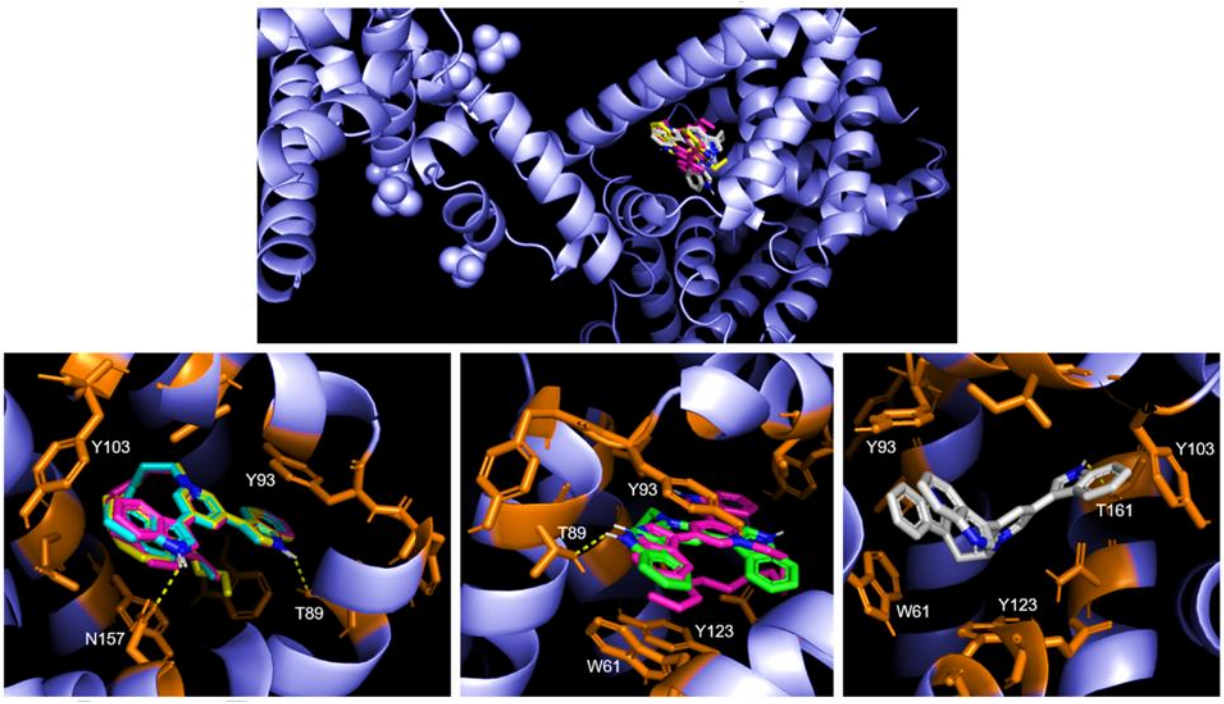

Figure 4.7. Computational docking models of tricepyridinium (4.01, white) ethyl (4.09, green), decyl (4.10, cyan), dodecyl (4.11, magenta), and tetradecyl (4.12, yellow) analogs in *S. aureus* QacR[202]

4.4 Chapter 4 Concluding Remarks and Future Studies

Development of novel quaternary ammonium compounds with interesting mechanisms of action and the potential to overcome resistance remains a top priority for our lab. In this work, we were able to develop a reliable, scalable route to the synthesis of a new class of QAC, N-quaternized pyridinium compounds with indole substitution at the 3 and 5 positions. This synthetic route offers key advantages over the previously published route and allowed for preliminary examination of the biological properties of this family of compounds.

The results of our biological assays complicate the question of the compounds' mechanisms of action in bacteria. High selectivity towards inhibition of gram positive bacteria is one piece of evidence indicative of membrane permeabilization. However, the compounds extremely low hemolytic toxicity and lack of hydrophobic region in the natural product seem to suggest against this mechanism. Further studies to directly elucidate this mechanism may be warranted if additional insight is desired into this class of QACs. For example, membrane permeabilization assays using SYTOX green and orange dyes could directly examine the structural integrity of the bacterial cells. Alternatively, DNA binding assays such as the one designed by Inspiralis could probe our other hypothesized mechanism by which tricepyridinium and its synthetic analogs may be interacting with bacteria.

Interestingly, we serendipitously developed three compounds (**4.10 - 4.12**) with the potential to evade efflux-mediated QAC resistance in *S. aureus*. The decreased computational binding affinity and drastically altered binding confirmation predicted for these compounds relative to the natural product indicate that this resistance circumvention may be due to an inability to bind to transcription factor and resistance mediator protein QacR, preventing efflux of QAC molecules. Further analysis of this interaction via biochemical kinetic binding studies to QacR and

comparative resistance selection assays could provide interesting insights into this potential for structure-guided evasion of QAC resistance in *S. aureus*.

4.5 Chapter 4 References

(159) Bureš, F. Quaternary Ammonium Compounds: Simple in Structure, Complex in Application. *Top. Curr. Chem.* **2019**, *377* (3), 14. https://doi.org/10.1007/s41061-019-0239-2.

(160) Hellberg, P.-E.; Bergström, K.; Holmberg, K. Cleavable Surfactants. *J. Surfactants Deterg.* **2000**, *3* (1), 81–91. https://doi.org/10.1007/s11743-000-0118-z.

(161) Zhang, C.; Cui, F.; Zeng, G.; Jiang, M.; Yang, Z.; Yu, Z.; Zhu, M.; Shen, L. Quaternary Ammonium Compounds (QACs): A Review on Occurrence, Fate and Toxicity in the Environment. *Sci. Total Environ.* **2015**, *518–519*, 352–362. https://doi.org/10.1016/j.scitotenv.2015.03.007.

(162) Starks, C. M. Phase-Transfer Catalysis. I. Heterogeneous Reactions Involving Anion Transfer by Quaternary Ammonium and Phosphonium Salts. *J. Am. Chem. Soc.* **1971**, *93* (1), 195–199. https://doi.org/10.1021/ja00730a033.

(163) Jacobs, W. A.; Heidelberger, M.; Bull, C. G. THE BACTERICIDAL PROPERTIES OF THE QUATERNARY SALTS OF HEXAMETHYLENETETRAMINE : III. THE RELATION BETWEEN CONSTITUTION AND BACTERICIDAL ACTION IN THE QUATERNARY SALTS OBTAINED FROM HALOGENACETYL COMPOUNDS. *J. Exp. Med.* **1916**, *23* (5), 577–599. https://doi.org/10.1084/jem.23.5.577.

(164) Alkhalifa, S.; Jennings, M. C.; Granata, D.; Klein, M.; Wuest, W. M.; Minbiole, K. P. C.; Carnevale, V. Analysis of the Destabilization of Bacterial Membranes by Quaternary Ammonium Compounds: A Combined Experimental and Computational Study. *ChemBioChem* **2020**, *21* (10), 1510–1516. https://doi.org/10.1002/cbic.201900698.

(165) Leas, B. F.; Sullivan, N.; Han, J. H.; Pegues, D. A.; Kaczmarek, J. L.; Umscheid, C. A. *Environmental Cleaning for the Prevention of Healthcare-Associated Infections*; AHRQ Comparative Effectiveness Technical Briefs; Agency for Healthcare Research and Quality (US): Rockville (MD), 2015.

(166) Hora, P. I.; Pati, S. G.; McNamara, P. J.; Arnold, W. A. Increased Use of Quaternary Ammonium Compounds during the SARS-CoV-2 Pandemic and Beyond: Consideration of Environmental Implications. *Environ. Sci. Technol. Lett.* **2020**, *7* (9), 622–631. https://doi.org/10.1021/acs.estlett.0c00437.

(167) Schrank, C. L.; Minbiole, K. P. C.; Wuest, W. M. Are Quaternary Ammonium Compounds, the Workhorse Disinfectants, Effective against Severe Acute Respiratory

Syndrome-Coronavirus-2? *ACS Infect. Dis.* **2020**, *6* (7), 1553–1557. https://doi.org/10.1021/acsinfecdis.0c00265.

(168) Jennings, M. C.; Forman, M. E.; Duggan, S. M.; Minbiole, K. P. C.; Wuest, W. M. Efflux Pumps Might Not Be the Major Drivers of QAC Resistance in Methicillin-Resistant Staphylococcus Aureus. *ChemBioChem* **2017**, *18* (16), 1573–1577. https://doi.org/10.1002/cbic.201700233.

(169) Russell, A. D.; Hammond, S. A.; Morgan, J. R. Bacterial Resistance to Antiseptics and Disinfectants. *J. Hosp. Infect.* **1986**, *7* (3), 213–225. https://doi.org/10.1016/0195-6701(86)90071-X.

(170) Jennings, M. C.; Minbiole, K. P. C.; Wuest, W. M. Quaternary Ammonium Compounds: An Antimicrobial Mainstay and Platform for Innovation to Address Bacterial Resistance. *ACS Infect. Dis.* **2015**, *1* (7), 288–303. https://doi.org/10.1021/acsinfecdis.5b00047.

(171) Jennings, M. C.; Buttaro, B. A.; Minbiole, K. P. C.; Wuest, W. M. Bioorganic Investigation of Multicationic Antimicrobials to Combat QAC-Resistant Staphylococcus Aureus. *ACS Infect. Dis.* **2015**, *1* (7), 304–309. https://doi.org/10.1021/acsinfecdis.5b00032.

(172) Bragg, R.; Jansen, A.; Coetzee, M.; van der Westhuizen, W.; Boucher, C. Bacterial Resistance to Quaternary Ammonium Compounds (QAC) Disinfectants. *Adv. Exp. Med. Biol.* **2014**, *808*, 1–13. https://doi.org/10.1007/978-81-322-1774-9_1.

(173) Sidhu, M. S.; Heir, E.; Leegaard, T.; Wiger, K.; Holck, A. Frequency of Disinfectant Resistance Genes and Genetic Linkage with Beta-Lactamase Transposon Tn552 among Clinical Staphylococci. *Antimicrob. Agents Chemother.* **2002**, *46* (9), 2797–2803. https://doi.org/10.1128/aac.46.9.2797-2803.2002.

(174) McBain, A. J.; Ledder, R. G.; Moore, L. E.; Catrenich, C. E.; Gilbert, P. Effects of Quaternary-Ammonium-Based Formulations on Bacterial Community Dynamics and Antimicrobial Susceptibility. *Appl. Environ. Microbiol.* **2004**, *70* (6), 3449–3456. https://doi.org/10.1128/AEM.70.6.3449-3456.2004.

(175) Xu, D.; Li, Y.; Shamim Hasan Zahid, M.; Yamasaki, S.; Shi, L.; Li, J.; Yan, H. Benzalkonium Chloride and Heavy-Metal Tolerance in Listeria Monocytogenes from Retail Foods. *Int. J. Food Microbiol.* **2014**, *190*, 24–30. https://doi.org/10.1016/j.ijfoodmicro.2014.08.017.

(176) Méchin, L.; Dubois-Brissonnet, F.; Heyd, B.; Leveau, J. Y. Adaptation of Pseudomonas Aeruginosa ATCC 15442 to Didecyldimethylammonium Bromide Induces Changes in Membrane Fatty Acid Composition and in Resistance of Cells. *J. Appl. Microbiol.* **1999**, *86* (5), 859–866. https://doi.org/10.1046/j.1365-2672.1999.00770.x.

(177) He, G.-X.; Landry, M.; Chen, H.; Thorpe, C.; Walsh, D.; Varela, M. F.; Pan, H. Detection of Benzalkonium Chloride Resistance in Community Environmental Isolates of Staphylococci. *J. Med. Microbiol.* **2014**, *63* (5), 735–741. https://doi.org/10.1099/jmm.0.073072-0.

(178) EPA. *Disinfectants Pesticides*. https://cfpub.epa.gov/giwiz/disinfectants/index.cfm (accessed 2021-01-17).

(179) McMullen, K. M.; Smith, B. A.; Rebmann, T. Impact of SARS-CoV-2 on Hospital Acquired Infection Rates in the United States: Predictions and Early Results. *Am. J. Infect. Control* **2020**, *48* (11), 1409–1411. https://doi.org/10.1016/j.ajic.2020.06.209.

(180) Richterman, A.; Meyerowitz, E. A.; Cevik, M. Hospital-Acquired SARS-CoV-2 Infection: Lessons for Public Health. *JAMA* **2020**, *324* (21), 2155–2156. https://doi.org/10.1001/jama.2020.21399.

(181) Liu, D.; Wang, Q.; Zhang, H.; Cui, L.; Shen, F.; Chen, Y.; Sun, J.; Gan, L.; Sun, J.; Wang, J.; Zhang, J.; Cai, Q.; Deng, J.; Jiang, J.; Zeng, L. Viral Sepsis Is a Complication in Patients with Novel Corona Virus Disease (COVID-19). *Med. Drug Discov.* **2020**, *8*, 100057. https://doi.org/10.1016/j.medidd.2020.100057.

(182) Li, H.; Liu, L.; Zhang, D.; Xu, J.; Dai, H.; Tang, N.; Su, X.; Cao, B. SARS-CoV-2 and Viral Sepsis: Observations and Hypotheses. *The Lancet* **2020**, *395* (10235), 1517–1520. https://doi.org/10.1016/S0140-6736(20)30920-X.

(183) Zhang, M.; O'dononghue, M.; Boost, M. V. Characterization of Staphylococci Contaminating Automated Teller Machines in Hong Kong. *Epidemiol. Infect.* **2012**, *140* (8), 1366–1371. https://doi.org/10.1017/S095026881100207X.

(184) Langford, B. J.; Soucy, J.-P. R.; Leung, V.; So, M.; Kwan, A. T. H.; Portnoff, J. S.; Bertagnolio, S.; Raybardhan, S.; MacFadden, D. R.; Daneman, N. Antibiotic Resistance Associated with the COVID-19 Pandemic: A Systematic Review and Meta-Analysis. *Clin. Microbiol. Infect.* **2023**, *29* (3), 302–309. https://doi.org/10.1016/j.cmi.2022.12.006.

(185) Kontos, R. C.; Schallenhammer, S. A.; Bentley, B. S.; Morrison, K. R.; Feliciano, J. A.; Tasca, J. A.; Kaplan, A. R.; Bezpalko, M. W.; Kassel, S. W.; Wuest, W. M.; Minbiole, K. P. C. An Investigation Into Rigidity-Activity Relationships in BisQAC Amphiphilic Antiseptics. *ChemMedChem* **2019**, *14* (1), 83–87. https://doi.org/10.1002/cmdc.201800622.

(186) Leitgeb, A. J.; Feliciano, J. A.; Sanchez, H. A.; Allen, R. A.; Morrison, K. R.; Sommers, K. J.; Carden, R. G.; Wuest, W. M.; Minbiole, K. P. C. Further Investigations into Rigidity-Activity Relationships in BisQAC Amphiphilic Antiseptics. *ChemMedChem* **2020**, *15* (8), 667–670. https://doi.org/10.1002/cmdc.201900662.

(187) Allen, R. A.; Jennings, M. C.; Mitchell, M. A.; Al-Khalifa, S. E.; Wuest, W. M.; Minbiole, K. P. C. Ester- and Amide-Containing MultiQACs: Exploring Multicationic Soft Antimicrobial Agents. *Bioorg. Med. Chem. Lett.* **2017**, *27* (10), 2107–2112. https://doi.org/10.1016/j.bmcl.2017.03.077.

(188) Thierer, L. M.; Petersen, A. A.; Michaud, M. E.; Sanchez, C. A.; Brayton, S. R.; Wuest, W. M.; Minbiole, K. P. C. Atom Economical QPCs: Phenyl-Free Biscationic Quaternary Phosphonium Compounds as Potent Disinfectants. *ACS Infect. Dis.* **2023**. https://doi.org/10.1021/acsinfecdis.2c00575.

(189) Michaud, M. E.; Allen, R. A.; Morrison-Lewis, K. R.; Sanchez, C. A.; Minbiole, K. P. C.; Post, S. J.; Wuest, W. M. Quaternary Phosphonium Compound Unveiled as a Potent Disinfectant against Highly Resistant Acinetobacter Baumannii Clinical Isolates. *ACS Infect. Dis.* **2022**, *8* (11), 2307–2314. https://doi.org/10.1021/acsinfecdis.2c00382.

(190) Sommers, K. J.; Michaud, M. E.; Hogue, C. E.; Scharnow, A. M.; Amoo, L. E.; Petersen, A. A.; Carden, R. G.; Minbiole, K. P. C.; Wuest, W. M. Quaternary Phosphonium Compounds: An Examination of Non-Nitrogenous Cationic Amphiphiles That Evade Disinfectant Resistance. *ACS Infect. Dis.* **2022**, *8* (2), 387–397. https://doi.org/10.1021/acsinfecdis.1c00611.

(191) Okada, M.; Sugita, T.; Wong, C. P.; Wakimoto, T.; Abe, I. Identification of Pyridinium with Three Indole Moieties as an Antimicrobial Agent. *J. Nat. Prod.* **2017**, *80* (4), 1205–1209. https://doi.org/10.1021/acs.jnatprod.6b01152.

(192) Nafisi, S.; Saboury, A. A.; Keramat, N.; Neault, J.-F.; Tajmir-Riahi, H.-A. Stability and Structural Features of DNA Intercalation with Ethidium Bromide, Acridine Orange and Methylene Blue. *J. Mol. Struct.* **2007**, *827* (1), 35–43. https://doi.org/10.1016/j.molstruc.2006.05.004.

(193) Morrison, K. R.; Allen, R. A.; Minbiole, K. P. C.; Wuest, W. M. More QACs, More Questions: Recent Advances in Structure Activity Relationships and Hurdles in Understanding Resistance Mechanisms. *Tetrahedron Lett.* **2019**, *60* (37), 150935. https://doi.org/10.1016/j.tetlet.2019.07.026.

(194) Wang, K.; Fu, Q.; Zhou, R.; Zheng, X.; Fu, H.; Chen, H.; Li, R. Tetraphosphine/Palladium-Catalyzed Suzuki–Miyaura Coupling of Heteroaryl Halides with 3-Pyridine- and 3-Thiopheneboronic Acid: An Efficient Catalyst for the Formation of Biheteroaryls. *Appl. Organomet. Chem.* **2013**, *27* (4), 232–238. https://doi.org/10.1002/aoc.2965.

(195) Witulski, B.; Buschmann, N.; Bergsträßer, U. Hydroboration and Suzuki–Miyaura Coupling Reactions with the Electronically Modulated Variant of an Ynamine: The Synthesis of (E)-β-Arylenamides. *Tetrahedron* **2000**, *56* (43), 8473–8480. https://doi.org/10.1016/S0040-4020(00)00773-0.

(196) Pagano, N.; Maksimoska, J.; Bregman, H.; Williams, D. S.; Webster, R. D.; Xue, F.; Meggers, E. Ruthenium Half-Sandwich Complexes as Protein Kinase Inhibitors: Derivatization of the Pyridocarbazole Pharmacophore Ligand. *Org. Biomol. Chem.* **2007**, *5* (8), 1218–1227. https://doi.org/10.1039/B700433H.

(197) Mizuta, M.; Seio, K.; Miyata, K.; Sekine, M. Fluorescent Pyrimidopyrimidoindole Nucleosides: Control of Photophysical Characterizations by Substituent Effects. *J. Org. Chem.* **2007**, *72* (14), 5046–5055. https://doi.org/10.1021/jo070206j.

(198) Haynes, S. W.; Sydor, P. K.; Stanley, A. E.; Song, L.; Challis, G. L. Role and Substrate Specificity of the Streptomyces Coelicolor RedH Enzyme in Undecylprodiginine Biosynthesis. *Chem. Commun.* **2008**, No. 16, 1865–1867. https://doi.org/10.1039/B801677A.

(199) Watson, C. G.; Aggarwal, V. K. Asymmetric Synthesis of 1-Heteroaryl-1-Arylalkyl Tertiary Alcohols and 1-Pyridyl-1-Arylethanes by Lithiation–Borylation Methodology. *Org. Lett.* **2013**, *15* (6), 1346–1349. https://doi.org/10.1021/ol400289v.

(200) Grkovic, S.; Brown, M. H.; Roberts, N. J.; Paulsen, I. T.; Skurray, R. A. QacR Is a Repressor Protein That Regulates Expression of the Staphylococcus Aureus Multidrug Efflux Pump QacA. *J. Biol. Chem.* **1998**, *273* (29), 18665–18673. https://doi.org/10.1074/jbc.273.29.18665.

(201) Mitchell, B. A.; Brown, M. H.; Skurray, R. A. QacA Multidrug Efflux Pump FromStaphylococcus Aureus: Comparative Analysis of Resistance to Diamidines, Biguanidines, and Guanylhydrazones. *Antimicrob. Agents Chemother.* **1998**, *42* (2), 475–477. https://doi.org/10.1128/AAC.42.2.475.

(202) Garrison, M. A.; Mahoney, A. R.; Wuest, W. M. Tricepyridinium-Inspired QACs Yield Potent Antimicrobials and Provide Insight into QAC Resistance. *ChemMedChem* **2020**, *n/a* (n/a). https://doi.org/10.1002/cmdc.202000604.

Chapter 5 - A bioinspired approach to synthesize metal-chelating lumazine peptides

5.1 Introduction

Of the 118 chemical elements discovered to date, 18 are known to be required in all living organisms, and an additional 17 are required for some taxa.[203,204] Of the former, hydrogen, carbon, oxygen, and nitrogen are found ubiquitously in nearly every biomolecule. The least abundant of these elements are the transition metals, of which manganese, iron, cobalt, copper, zinc, and molybdenum are essential for all known life (as well as vanadium, nickel, cadmium, and tungsten in some organisms). Transition metals play important roles in biological systems, serving primarily as enzymatic cofactors (**Figure 5.1, top**). However, most of these metals are only required in minute quantities, and overexposure can lead to toxicity (**Figure 5.1, bottom**).[205–207] For example, copper plays crucial roles in respiration, transporting both electrons and oxygen in the electron transport chain. However, in larger quantities copper is extremely toxic to microorganisms and has been exploited for its antimicrobial effects, probably stemming from increased oxidative stress and/or improper binding and inactivation of essential proteins.[206,208] Metal toxicity to cells does

not always require their presence in the cell interior; metals can inhibit the function of the membrane-bound electron transport chain in prokaryotes or antagonize the uptake of other nutrients into the cell.[207] Due to this narrow toxicity window, metal homeostasis in biology is an extremely delicate and intricately controlled balance.[209]

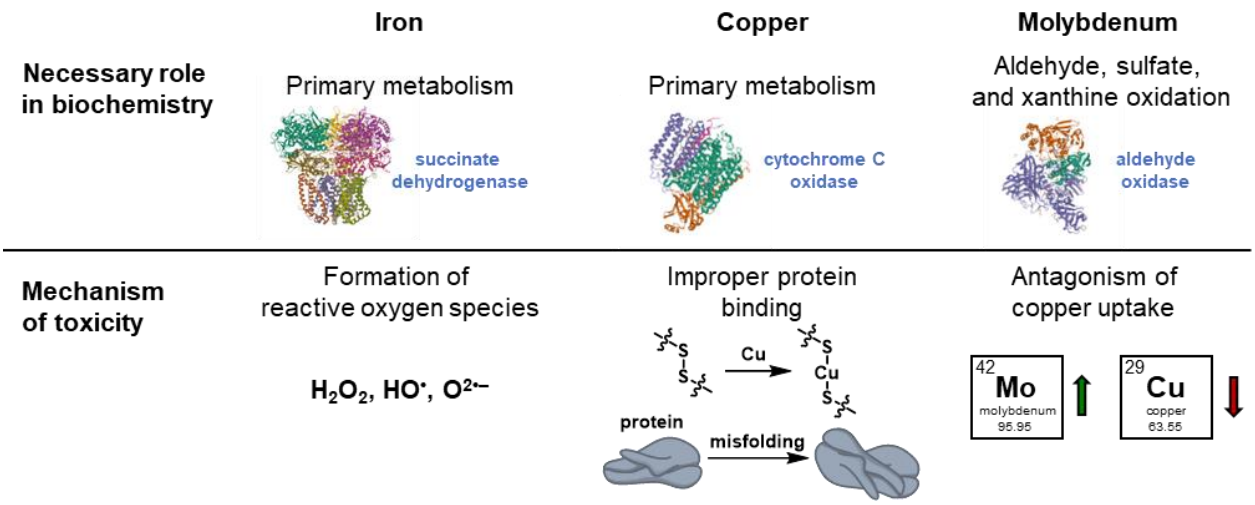

Figure 5.1. Dual role of transition metals in biological systems, causing beneficial or deleterious effects depending on the concentration of metal present

In bacteria, there are many processes at play to ensure that metals are present in sufficient, but not toxic, quantities. This requires elegant mechanisms by which the detection and quantification of these metals by the bacteria can occur. In many cases, genes controlling metal homeostasis pathways (efflux, import, etc.) are regulated by metal-binding transcription factors. When a certain metal is present and binds these proteins in sufficient quantity, the genes will be transcribed, triggering feedback loops. In the case of metal intoxication, these pathways can reduce metal concentration in three major ways (**Figure 5.2**). Prokaryotes can upregulate the expression of efflux pumps that can export metals, such as in the case of copper detoxification in *E. coli* mediated by the RND efflux pump CusA. Alternatively, free metals can be bound by proteins or other molecules (such as histidine or glutathione) in a process called cytosolic buffering. Finally, excess

metal can be temporarily stored within hollow proteins (e.g., the universal protein ferritin, which can sequester up to 4,500 atoms of Fe(III) per protein molecule).[209]

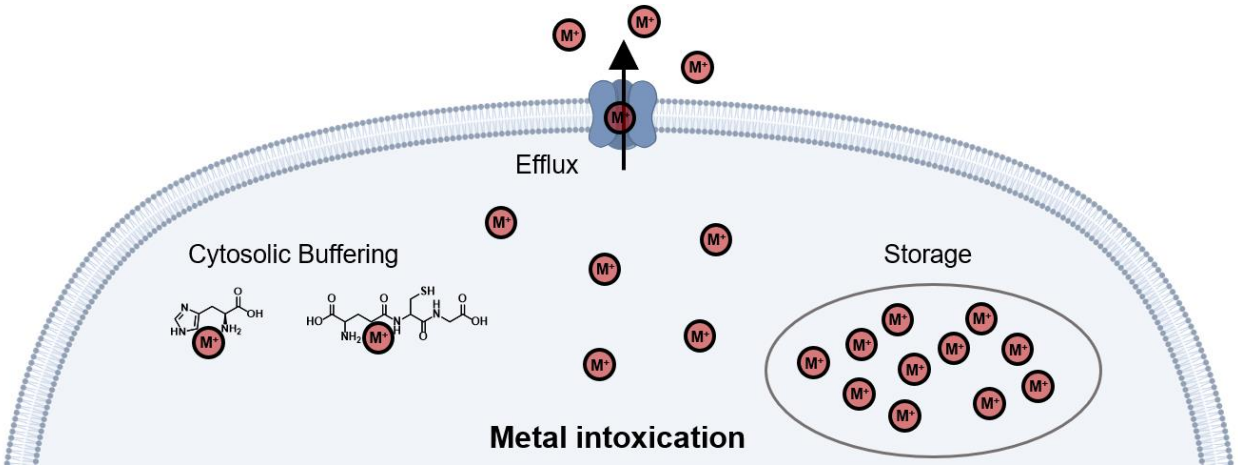

Figure 5.2. Examples of bacterial adaptations to environments containing high concentrations of metals

There are also many mechanisms by which bacteria can adapt under conditions of metal deficiency (**Figure 5.3**). This response often varies according to which metal is limited and that metal's normal function. As is the case for most nutrient deficiencies in prokaryotes, one general solution can be to slow metabolic function, lowering the threshold at which the metals are required for cellular processes.[210] Alternatively, if the metal is involved in binding a certain protein as a cofactor, upregulation of an analogous redundant protein that can function in the absence of that metal, or by chelating an alternate cofactor can occur. Finally, cells can upregulate machinery to import metals at a higher rate. This can take the form of pumps or channels to allow for the uptake of whatever low concentration of metal the environment might contain. It can alternatively be seen through the secretion of metal binding small molecules, which can then be brought back into the cells and released from their metals.[209]

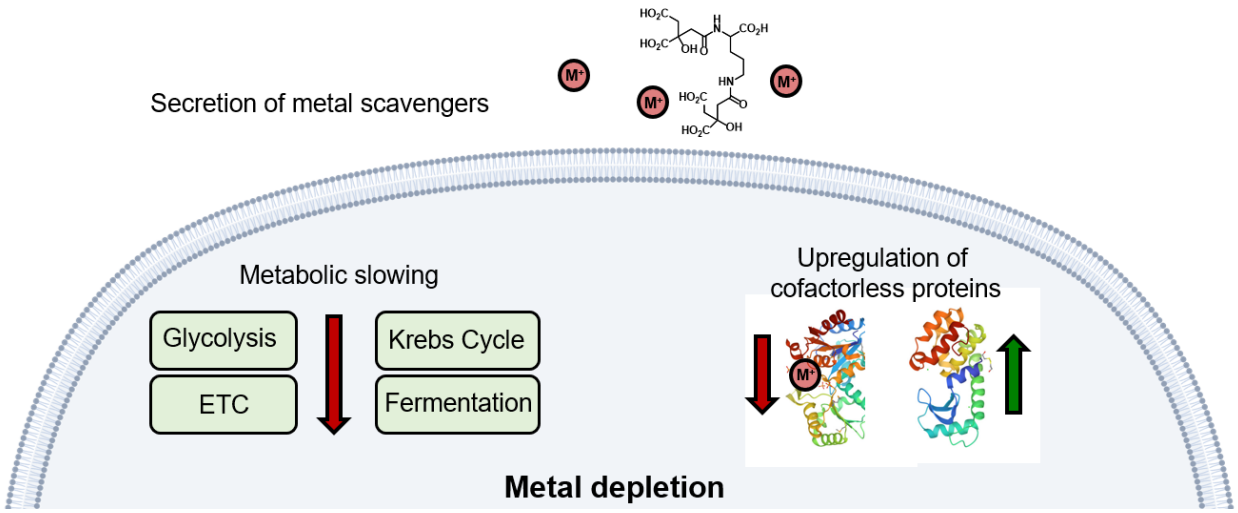

Figure 5.3. Examples of bacterial adaptations to environments containing low concentrations of metals

Secreted metal chelators (metallophores) are often specific for a certain metal, allowing bacteria to closely regulate homeostasis in environments which may be high in concentration of some metals and low in others.[211,212] For example, siderophores are small molecules secreted by bacteria with a high affinity for iron, whereas chalkophores bind strongly to copper. Importantly, bacterial metallophores are known virulence factors – systems by which they display increased pathogenicity and pose larger threats to their hosts. In this case, secreted metal chelators, while not always essential for bacterial function, allow them to obtain nutrients from their hosts and promoting colonization.[212,213]

The inhibition of virulence factors is one proposed way to combat the ever-worsening problem of antibiotic resistance.[214] As virulence factors are not required for cellular life, inhibition of these processes or systems is predicted to generate less selective pressure for the development of resistance, prolonging the drugs' clinical lifespan. In addition, as virulence factors are markers of pathogenic bacteria, antivirulence agents are likely to be selective for invading species and preserve commensal microbiota known to contribute to healthy host metabolism and function.

Inhibition of bacterial metallophores, through inhibition of their production, secretion, or extracellular function, is therefore a viable therapeutic strategy.

Synthetic mimics of metallophores have been proposed as effective antivirulence agents for bacteria.[214,215] These small molecules can take one of three forms: small molecule drugs that bind to and inhibit bacterial import machinery, chelators that bind metals but do not release them inside bacterial cells, and metal binding small molecules conjugated to an antibiotic. One recently-approved therapeutic following the third strategy is Fetroja (cefiderocol), an aptly-named iron "Trojan horse" drug composed of a siderophore conjugated to a cephalosporin.[215] Upon binding extracellular iron, the molecule is imported into the cell. At this point, the cephalosporin moiety can take effect, disrupting bacterial cell wall synthesis by inhibiting penicillin-binding proteins. Unfortunately, the chelator-antibiotic conjugate strategy suffers from the fact that pathogens may develop resistance now in two ways: modification of the siderophore import machinery to exclude this molecule, or via cephalosporin resistance (already prevalent in many species). Indeed, resistance to cefiderocol was observed even prior to its FDA approval, and this resistance has increased in prevalence at an alarming rate.[216] Therefore, the discovery of antivirulence agents which function in the absence of an antibiotic are highly desirable.

There are a number of privileged scaffolds for metal chelation in bacteria. Due to the electropositive nature of transition metals in general, these scaffolds are often electron rich, with coordination of the metal center to multiple oxygen and/or nitrogen atoms. Binding stoichiometry of a metal to its metallophore is not always 1:1. For example, pyochelin, a known metabolite of *Pseudomonas aeruginosa*, is a poorly-selective chelator of Fe(III), Cu(II), and Zn(II). Complexes with Cu(II) and Zn(II) are bischelate in nature (that is, the binding stoichiometry is 2:1 pyochelin : Cu/Zn) (**Figure 5.4**).[217] This is not to be confused with denticity (multiple noncontiguous atoms

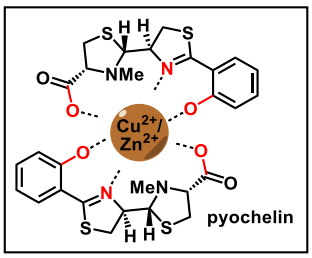

Figure 5.4. Model of pyochelin's bischelate association with Cu(II) and Zn(II) utilizing its phenol, thiazole, and carboxylate

on a metallophore binding to a metal; virtually all biological metallophores are polydentate) or hapticity (multiple contiguous atoms in a ligand binding to a metal).

In the case of siderophores, priviliged scaffolds often include hydroxamates, catecholates, aminocarboxylates, and thiazolines, or some combination of these.[218] Chalkophores are less well-studied, but in the past 20 years a variety of copper-binding compounds produced by methanogenic bacteria have been identified.[219–222] Termed methanobactins, these peptide-derived compounds bind Cu(I) and Cu(II) utilizing oxazolinone and enethiol moieties. A notable chalkophore produced by nonmethanogen *Streptomyces thioluteus* is SF2768, which chelates Cu(I) and Cu(II) using isonitrile (or isocyanide) ligands (**Figure 5.5**).[222]

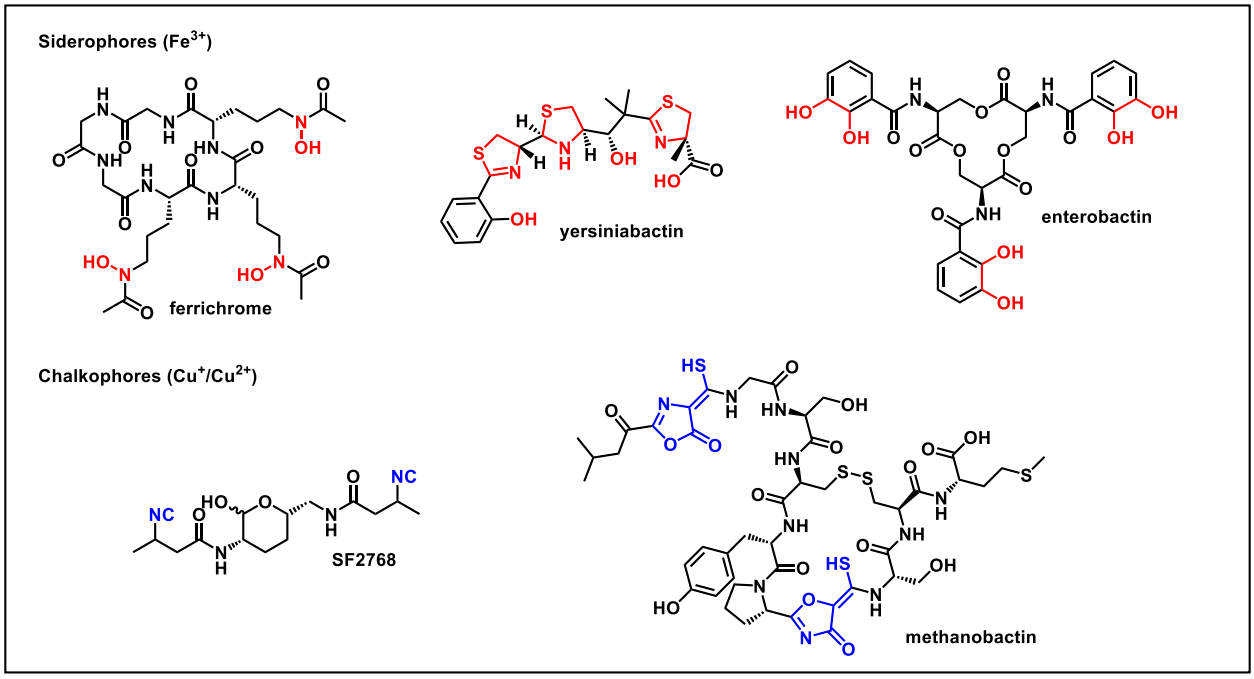

Figure 5.5. Privileged scaffolds for chelation of siderophores and chalkophores

Due to the advantages described above of antivirulence agents targeting metal homeostasis, our group remains particularly interested in isonitrile natural products. The isocyanide functional group is exceedingly rare in nature but compounds containing one or more isocyanides play unique biochemical roles, almost always involved with metal sequestration. For example, Xanthocillin X, the first reported natural isocyanide, is a potent broad-spectrum antibiotic that functions through sequestration of heme and subsequent disruption of iron homeostasis in bacterial cells.[223] Similarly, Wright et al. discovered that a series of terpene-derived isonitrile natural products from marine sponges also function to dysregulate heme, leading to potent antimalarial activity.[224]

In comparison to their terrestrial counterparts, natural products from marine organisms have largely remained unexplored in regard to their antibacterial activity. Due to the drastically altered environmental conditions in which these organisms live, these natural products often have unique structures and may function via novel, unexplored mechanisms of action, thereby presenting new opportunities as drug candidates to treat bacteria that have developed resistance to currently-used therapeutics. Over the last decade, a number of independent natural product isolation groups have reported the discovery of twelve unique lumazine-derived compounds (**5.01 – 5.12**), isolated from marine *Aspergillus sp.* and *Penicilium sp.* fungi (**Figure 5.6**).[225–230] These compounds structurally differ in lumazine N_3-methylation, internal amino acid residue, and *ortho*-functionality on the C-terminal anthranilate moiety. Our group became interested in this class of molecules in 2020 upon the discovery of Penilumamide F, a lumazine peptide containing an alanine linker and a 2-isocyanoaniline moiety in place of the more standard anthranilate C-terminus.[230] Based on previous reports of isocyanide-containing natural products, we were therefore curious if Penilumamide F may exhibit metal binding properties, and whether or not this may translate to antimicrobial activity. Two non-peptidic lumazine natural products were also isolated in 2005 from

the parasitic freshwater leech *Limnatis nilotica*; these in combination with the penilumamides, aspergilumamide A, and terrelumamide B, constitute the only known examples of lumazine incorporation to our knowledge.[231]

Despite the growing number of compounds reported, the biological purpose of this class of lumazine peptides as a whole remains unexplored. A range of physiological effects of these compounds in humans has been identified. For example, terrelumamides A and B (differing only in amino acid composition between a linker Ser and Thr) were shown to bind DNA and to modulate insulin sensitivity.[227] However, the role that these compounds play in the producing fungi is yet to be understood. All isolation reports corroborate that lumazine peptides are noncytotoxic against a variety of eukaryotic cell lines. While all compounds apart from terrelumamides A and B were tested and shown to have no antibacterial activity, the species used in these studies were somewhat limited. In most cases, only gram-positive bacteria were tested, in addition to *E. coli* as the sole gram-negative bacterium. Antibiotic testing of aspergilumamide against a further two gram-negative bacterial species, *Vibrio parahaemolyticus* and *Listonella anguillarum*, was also performed.[229] However, testing against more clinically relevant gram-negative bacteria such as *Acinetobacter baumanii* and *Pseudomonas aeruginosa* was noticeably lacking in all reports. We were therefore interested in investigating the biological function of these compounds.

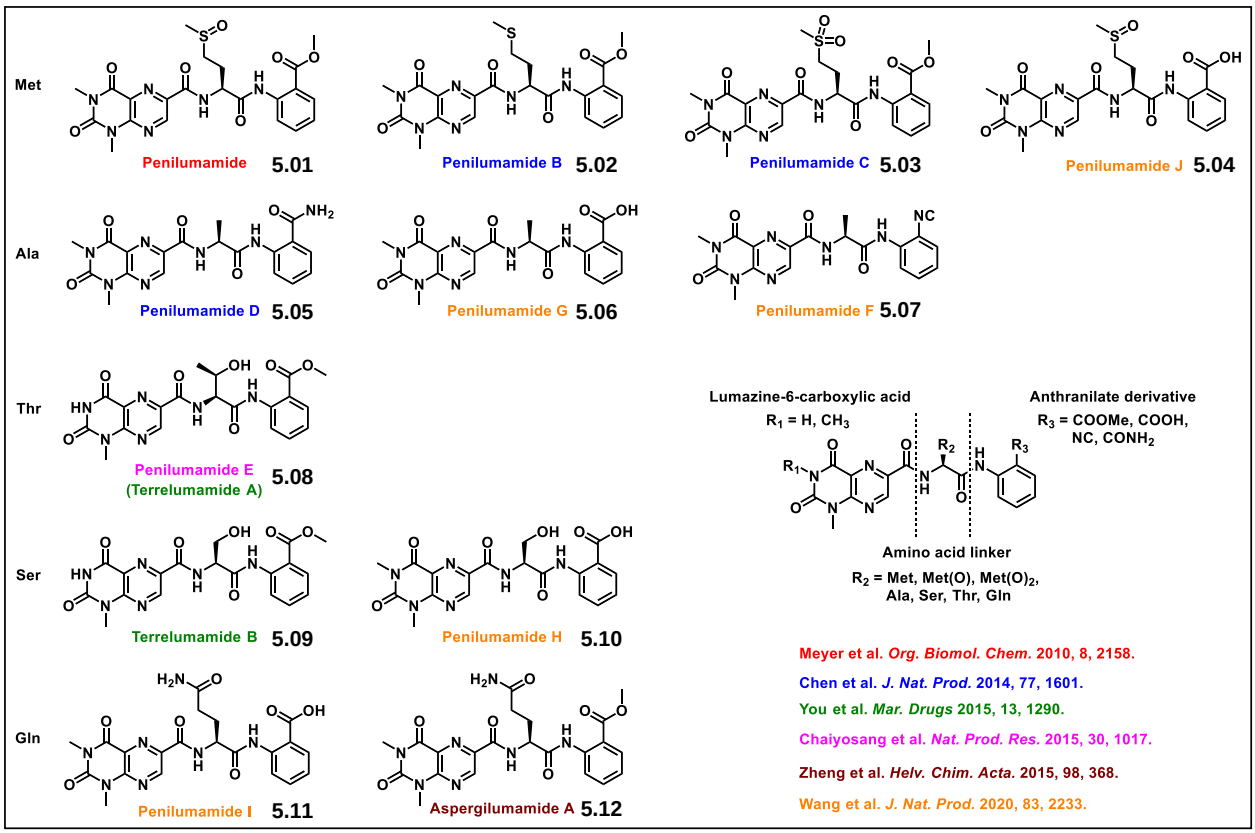

Figure 5.6. Various isolation reports and structural elucidation of lumazine peptide natural products over the last thirteen years

The lumazine heterocycle itself sees use in riboflavin biosynthesis, in which lumazine synthase catalyzes a condensation reaction between GTP-derived 5-amino-6-(D-ribitylamino)uracil and 1-deoxy-L-glycero-tetrulose 4-phosphate, a downstream biosynthetic product of the pentose phosphate pathway. Two molecules of this lumazine derivative then engage in a dismutation reaction catalyzed by riboflavin synthase to produce the essential nutrient riboflavin (**Scheme 5.1**).[232] This process is ubiquitous in plants, fungi, and bacteria, but is absent in animals. Importantly, gram-negative bacteria as well as some fungi are unable to efficiently uptake riboflavin as a nutrient and are therefore dependent on its biosynthesis; this in combination with the lack of analogous enzymes in animal cells mean that therapeutics targeting the riboflavin

synthesis pathway (such as competitive inhibitors shown in **Scheme 5.1**) are therefore promising candidates for inhibition of gram-negative bacteria.[233–236]

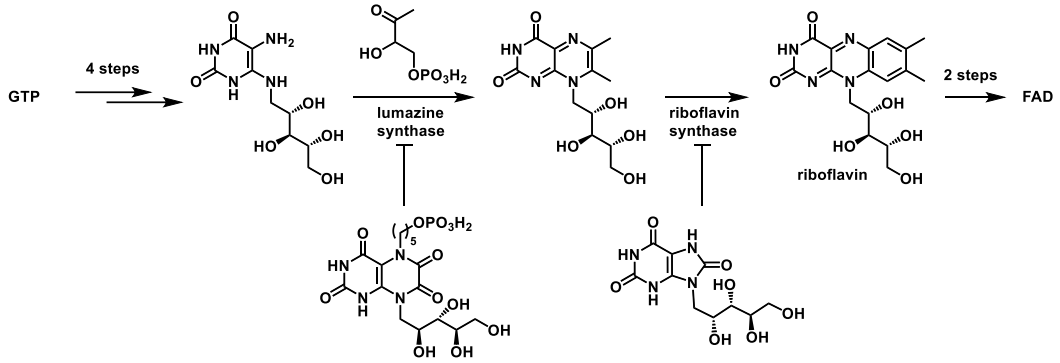

Scheme 5.1. Biosynthesis of riboflavin and FAD, and inhibition of this pathway by synthetic small molecules

While riboflavin biosynthesis has been well understood for many years, the discovery of lumazine incorporation into other secondary metabolites is relatively recent. The biosynthetic gene cluster encoding the fungal NRPS machinery required for production of penilumamide and its derivatives has recently been identified.[237] In *A. flavipes*, this cluster encompasses three NRPS proteins and a total of four adenylation-thiolation-condensation (ATC) modules, one of which is hypothesized to be redundant and is skipped. In the case of penilumamide, a pterin such as lumazine-6-carboxylic acid (**5.13**, either anabolically synthesized from GTP or resulting from enzymatic folic acid degradation) is loaded onto the NRP assembly line, and methionine and anthranilate are then sequentially attached. It remains unclear whether the other naturally-occurring lumazine peptides result from modification at the lumazine and anthranilate termini before or after assembly of the peptide, and whether the internal amino acid residue is incorporated by yet-unidentified analogous NRPSs.

Our main objective in studying the lumazine peptides was in optimization of their chemical synthesis and elucidation of their biological role. We hypothesized that these molecules may serve

as mimics of flavin biosynthesis intermediates due to their incorporation of a lumazine heterocycle and their structural similarity to other known inhibitors of this pathway. Alternatively, based on the recent isolation of Penilumamide F (**5.07**) containing an isocyanide moiety, we hypothesized that these molecules may instead be involved in metal homeostasis. The different members of this family may be involved in sequestration of different metals, or as in the case of methanobactins may simply have different binding affinities for the same metal. One plausible binding mode can be visualized below, using Penilumamide J (**5.04**) as a hexadentate ligand for an unidentified metal ion, in which the lumazine heterocycle itself, C-terminal aniline substituent, and methionine sulfoxide are all able to chelate with reasonable metal geometry (**Figure 5.7**).

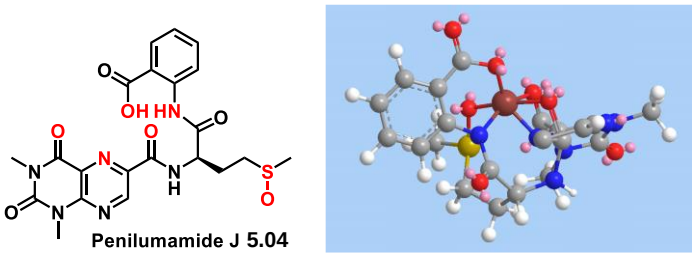

Figure 5.7. Visualization of metal-binding hypothesis with one potential binding confirmation of penilumamide J (5.04) to a metal ion using the functional groups highlighted in red

In order to test our hypothesis of a metallophore role for these compounds, we specifically targeted natural products containing Ala, Ser, Met, and Gln linkers with COOH, COOMe, and NC termini. In addition, we desired synthetic analogs incorporating the isocyanate moiety onto Met, Ser, and Gln-linked lumazine peptides to form likely but undiscovered natural products in the penilumamide family (**Scheme 5.2**). As these compounds are peptidic, retrosynthetic disconnection about the amide bonds seemed the most practical approach towards our desired compounds.

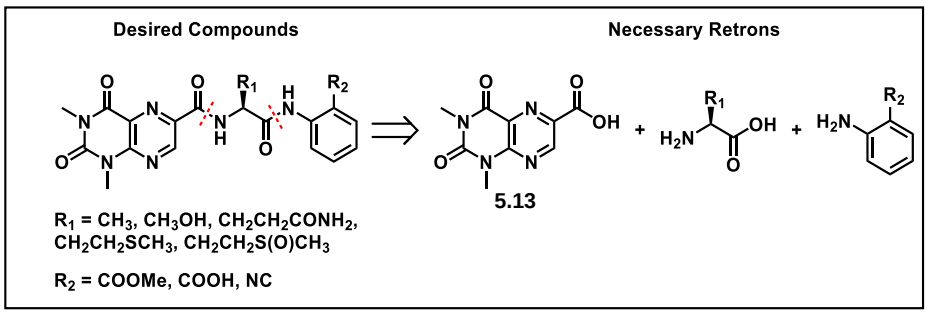

Scheme 5.2. Retrosynthetic analysis of desired lumazine compounds

5.2 Synthesis

DISCLAIMER: Preparation and characterization of compounds **5.15 - 5.18** and **5.33 - 5.36** was performed by previous lab undergraduate member Michelle Garrison. Though these strategies are discussed herein, full experimental details and characterization data for these compounds can instead be found in this student's Honors Thesis. Similarly, compounds **5.37 - 5.41** were prepared and characterized by current staff scientist Wanli Zhang, these experimental details and characterization data will be present in an upcoming manuscript submitted to Med. Chem. Res.

The lumazine heterocycle has been synthesized previously in a number of ways. One of the first methods for its synthesis was utilization of the Gabriel-Isay condensation, which condenses 5,6-diaminouracils onto 1,2-dicarbonyls to give a mixture of regioisomers in a disubstituted lumazine.[238] For regiocontrolled lumazine synthesis, the Timmis pteridine synthesis uses a 1,2-aminonitroso compound to react in a cyclization-condensation with a cyanoacetic acid or ester.[239] Alternatively, a strategy like that developed by Viscontini et al. can be employed, in which two sequential Amadori rearrangements deliver exclusively 6-substituted lumazines via reaction of 5,6-diaminouracils with pentose-substituted hydrazones (**Figure 5.8**).[240]

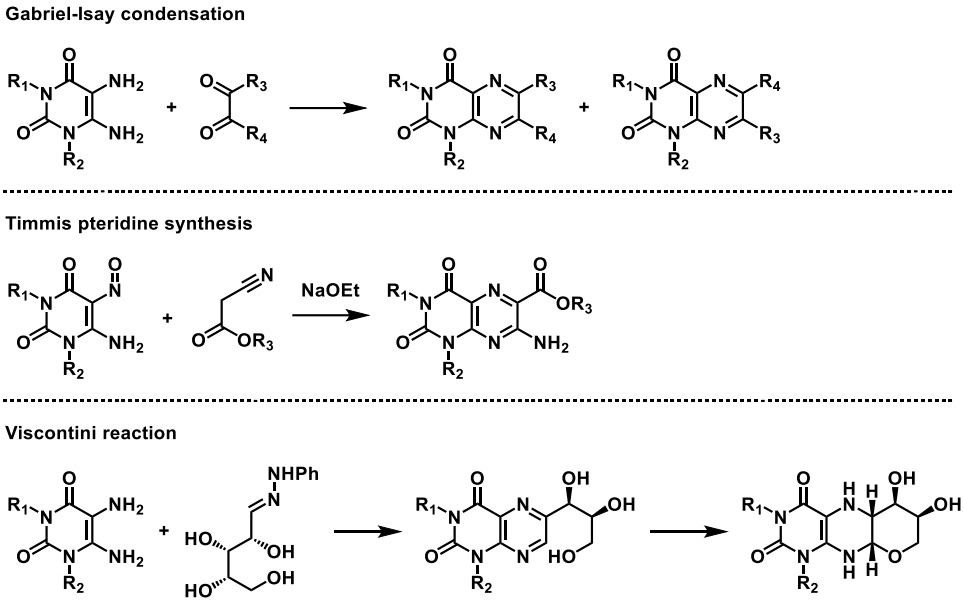

Figure 5.8. Previous synthetic approaches to formation of lumazine heterocycles

In the first reported synthesis of Penilumamides B-D (**5.02 - 5.04**), the authors use an approach to the lumazine heterocycle originally published by Yoneda et al.[241,242] This strategy employs conversion of 6-amino-1,3-dimethyluracil (**5.14**) to a 5-phenylazo substituted derivative (**5.15**), followed by reaction with diethyl acetylenedicarboxylate to give the lumazine heterocycle disubstituted with ethyl esters at the 6 and 7 positions (**5.16**). After this, treatment with a 1:3 mixture of hydrochloric acid and acetic acid is reported to cause ester hydrolysis and monodecarboxylation at the 7 position, delivering 1,3-dimethyllumazine-6-carboxylic acid (**5.13**). This material can then be taken on to sequential amidation reactions utilizing the necessary amino acid (in the case of the original publication, alanine and methionine) and aniline derivative (**Scheme 5.3, black**).

In synthesizing the lumazine heterocycle, we were able to replicate the first two steps of this synthesis, to **5.16**. However, attempts at the acid-mediated decarboxylation reaction were wholly unsuccessful, resulting instead in saponification to the 6,7-dicarboxylic acid (**5.18**). Use of different ratios of acetic and hydrochloric acids and reacting the solution for a longer period of time did not affect the result. In an effort to circumvent the problem of needing to remove functionality, the same cyclization reaction was attempted using methyl propiolate. While the cyclization did occur to deliver lumazine substituted at the 6 position, the final aniline elimination step did not (instead resulting in **5.17**), and attempting to force its elimination via addition of triethylamine or acetic acid was unsuccessful. Comparable results were seen when cyclization with ethyl propiolate or propiolic acid were attempted. A final attempt at reacting the azo compound with methyl bromoacetate followed by base-mediated cyclization resulted in degradation of the scaffold (**Scheme 5.3, blue**).

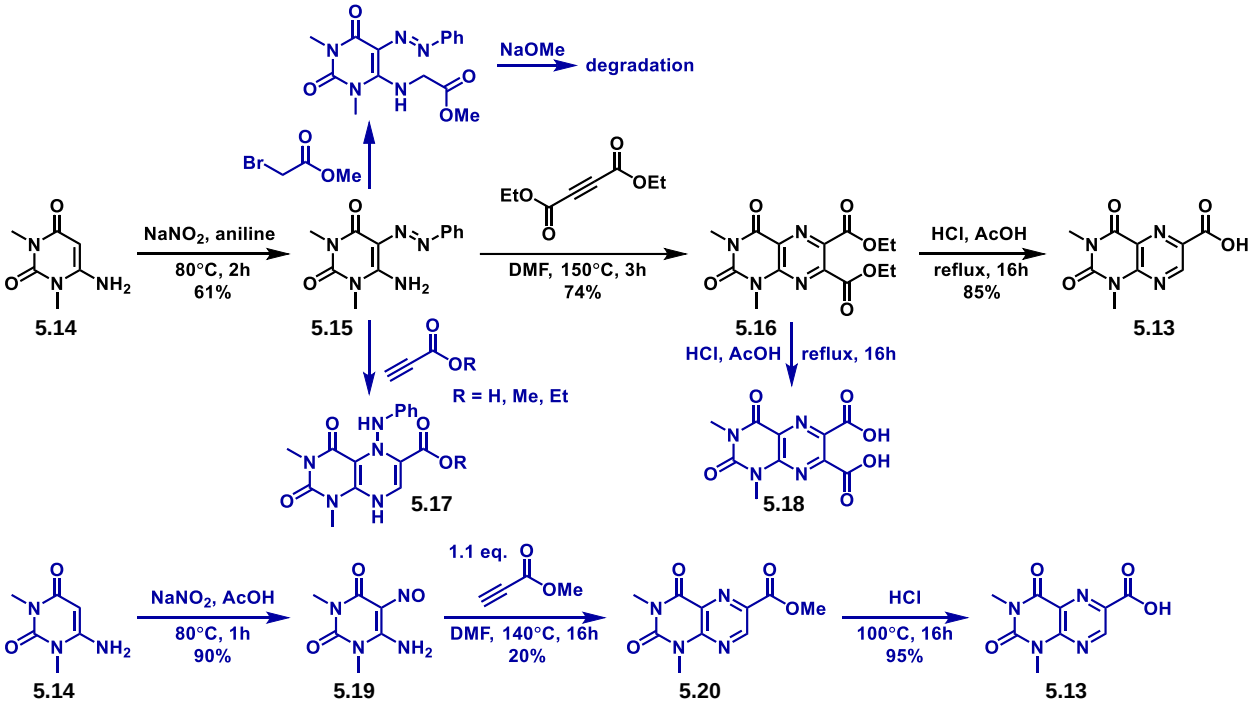

Scheme 5.3. Initial attempts to synthesize lumazine-6-carboxylic acid, showing route previously published by Penjarla et al. (black) and our observed results (blue)

The work reported by Yoneda et al. describes a second approach in which instead of forming the 6-amino-5-phenylazopteridine, the reactive precursor to cyclization is instead a 5-nitroso compound (**5.19**) which can be generated from the same commercially available material using sodium nitrite and acetic acid.[241] While Yoneda's group then reacts this material with diethyl acetylenedicarboxylate, we hypothesized that in our hands the subsequent decarboxylation would fare no better than it did initially. Instead, we combined aspects of our previous two approaches, reacting 6-amino-1,3-dimethyl-5-nitrosouracil (**5.19**) with methyl propiolate, which was successful in producing desired monoester **5.20** at the 6 position. We were surprised to find that this particular methyl ester was quite resistant to saponification but forcing conditions (refluxing in a solvent of concentrated hydrochloric acid overnight) did eventually allow full conversion to the 1,3-dimethyllumazine-6-carboxylic acid (**5.13, Scheme 5.3**).

Due to the challenges we had encountered with synthesis of the lumazine heterocycle, our synthesis follows a different sequence than that of the previously published total synthesis of Penilumamides B-D by Penjarla et al (**Scheme 5.4, top**).[242] In particular, we reversed the order of couplings so as to allow for late stage incorporation of the lumazine heterocycle, which was more challenging to produce. In addition to being more modular, this decision had the added benefit of lowering overall cost of the synthesis, as N-terminal-protected amino acids are generally cheaper than C-terminal-protected amino acids (for example, Boc-Met-OH is less expensive than H_2N-Met-OMe). Initial coupling to the unprotected C terminus therefore allows for a cheaper synthetic route.

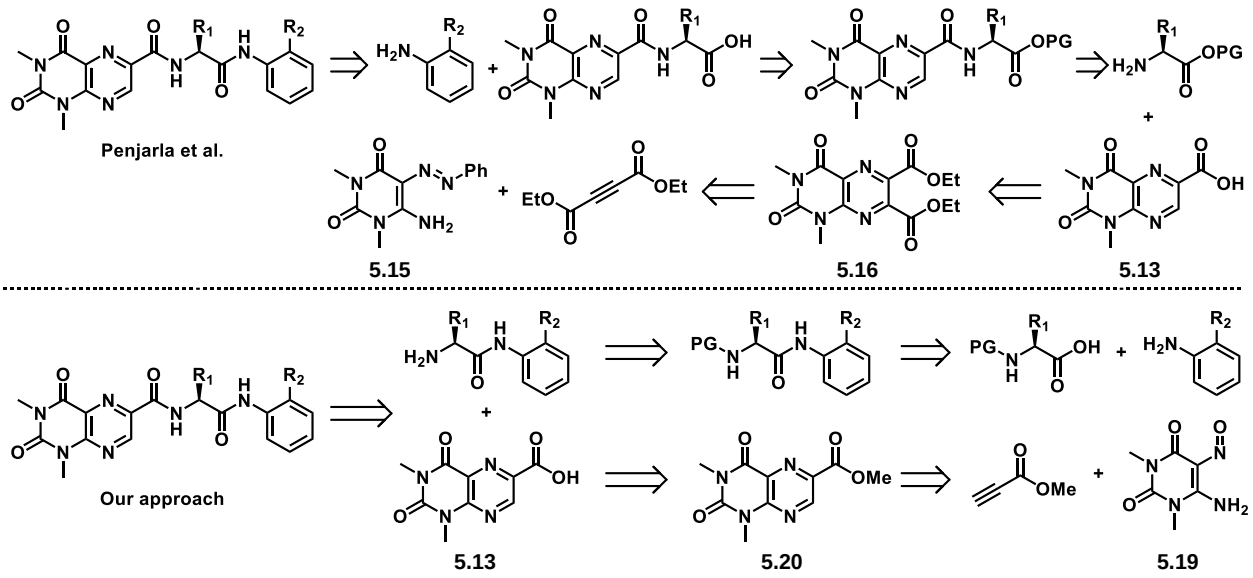

Scheme 5.4. Comparison of Penjarla's retrosynthetic analysis of lumazine peptides (top) with our approach (bottom)

termini, we reasoned that these could be accessed from the same route, with a final saponification step to convert from the former to the latter. We therefore began our synthesis with coupling of methyl anthranilate (**5.21**, a very cheap commodity chemical used to impart grape flavoring and odor to cosmetics and foods) to N-Boc protected amino acids (alanine, serine-OBn, methionine, and glutamine). In contrast to literature reports of anthranilate couplings, in our hands these proceeded in high yields and were remarkably easy to purify, a welcome relief after challenges with the lumazine heterocycle itself (**Scheme 5.5**).[243] However, closer examination of the glutamine coupling product indicated that in addition to the desired amidation, a dehydration reaction had also occurred to deliver a nitrile sidechain. This undesired side reaction has been reported in the literature and is postulated to occur via nucleophilic addition of the amide oxygen to the carbonyl after activation by the coupling rearrangement.[244] The presence of base (common in coupling reactions) can then allow for deprotonation of the resulting imine to reform a carboxylate in a formal dehydration mechanism (**Scheme 5.6**). Literature reports indicate that this side reaction can be prevented by protecting the glutamine amide as a bulky 9-xanthenyl amide.[244]

However, incorporation of this protecting group also severely lowered coupling yields to about 25%. Reasoning that the glutamine analog was unnecessary to test our metal binding hypothesis, we diverted our efforts to completion of the synthesis of the remaining compounds.

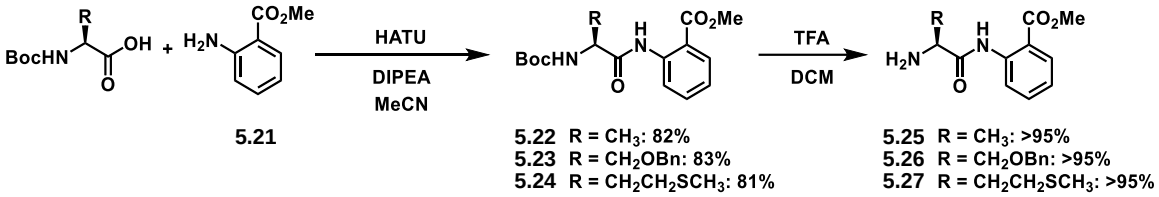

Scheme 5.5. Successful coupling of anthranilate and amino acid fragments, with subsequent deprotection

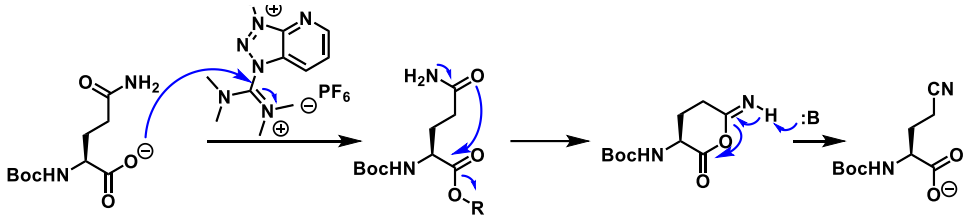

Scheme 5.6. Observed dehydration in anthranilate-glutamine coupling reaction conditions, and proposed mechanism

then coupled with 1,3-dimethyllumazine-6-carboxylic acid (**5.13**). Yields were initially low, which we attributed to impurities present in the lumazine acid fragment. Due to the number of byproducts present after cyclization with methyl propiolate to form **5.20**, in addition to extremely low solubility of **5.13** in most organic solvents, purification of this fragment had been minimal. We therefore began re-optimization of this fragment's synthesis to allow for more facile isolation of the desired product in sufficient purity to allow successful coupling. Attempts were made to isolate and characterize the byproducts formed from the cyclization reaction, however these compounds tended to coelute, making their identification extremely challenging. We found that increasing the number of stoichiometric equivalents of methyl propiolate to 3.5 was deleterious to both yield and purity of **5.20**, indicating that the byproducts generated are likely a result of polymerization reactions of methyl propiolate. In contrast, using **5.19** in excess greatly simplified column chromatography and more than doubled the reaction yield. We also found that instead of

chromatographic purification, recrystallization could also be performed, allowing for substantial scale up of what was once our limiting fragment. The recrystallized material could be hydrolyzed under our forcing conditions to afford **5.13** in much higher purity (though we found it unnecessary, this carboxylic acid was also purifiable via recrystallization). Through these efforts, we have therefore developed a concise, chromatography-free, scalable synthesis of 6-substituted lumazine compounds such as **5.13**, a strategy offering significant advantages over those currently present in the literature (**Scheme 5.7**).

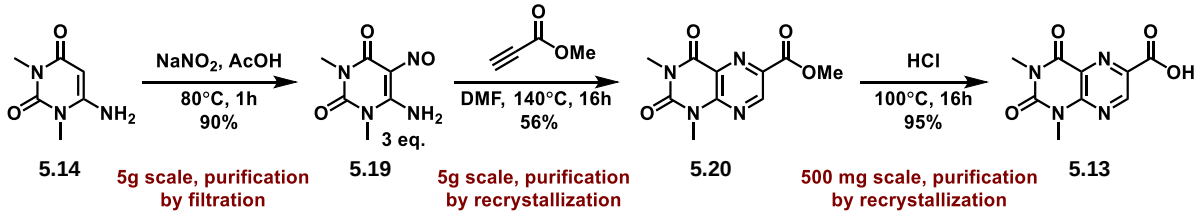

Scheme 5.7. Summary of optimized route to synthesis of lumazine-6-carboxylic acid

Coupling of this new batch of 1,3-dimethyllumazine-6-carboxylic acid (**5.13**) with the deprotected amino acid-anthranilate fragments (**5.25 – 5.27**) proved much more successful, increasing yield and allowing for isolation of sufficient quantities of all three coupled products (including Penilumamide B, **5.02**, for which characterization data was identical to that published in the literature).[226] Attempts to hydrolyze these anthranilate methyl esters under basic conditions did not cleanly afford the corresponding acids, instead degrading the lumazine heterocycle to form an unidentified side product. Examination of literature reports on exposure of lumazine derivatives to lithium hydroxide revealed that this side product was likely a substituted pyrazine (**Scheme 5.8**).[245]

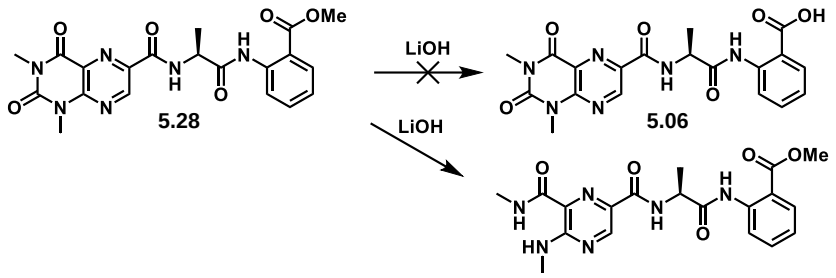

Scheme 5.8. Observed degradation of lumazine heterocycle to trisubstituted pyrazine under basic conditions

Other ester cleavage methods were next attempted, using alanine compound **5.28** as a model substrate (**Scheme 5.9**). Acidic hydrolysis using 1M HCl was tried, but no reaction was observed after 24 hours, so the reaction was quenched and the starting material recovered. It is possible that the aromatic methyl ester is stable to acidic conditions, as had been observed for the lumazine methyl ester (**5.20**) itself, and using forcing conditions was not attempted for fear of amide bond cleavage and/or epimerization of the amino acid chiral center. The Nicolaou lab has previously reported a mild cleavage of aromatic and aliphatic esters with a broad functional group tolerance using trimethyltin hydroxide.[246] However, even with ten equivalents of this reagent, no reaction was observed after refluxing for 24 hours. Electrophilic methyl ester cleavage has been reported with TMS-I, delivering first the silyl ester which undergoes cleavage to the acid during aqueous workup.[247] However, this method has only limited applicability to aryl methyl esters, likely due to the instability of TMS-I at the higher temperatures necessary for their cleavage in this reaction. This, in concert with the fact that TMS-I is not commercially available, is light sensitive, and must be carefully prepared *in situ* made this method undesirable. Nevertheless, we were interested in this general strategy, as nucleophilic approaches had been thus far unsuccessful. A similar reaction using lithium iodide in refluxing pyridine for the cleavage of methyl esters was known in the literature and was utilized at a late stage in Furstner's synthesis of amphidinolide X in 2004.[248,249] Lithium iodide is substantially more stable than TMS-I and can thus be reacted at higher

temperatures. It is also commercially available and quite inexpensive, so the use of this strategy was next attempted. We were relieved to find that the cleavage of Lum-Ala-Ant-OMe (**5.28**) proceeded in acceptable yields with no observable side reactions to afford Penilumamide G (**5.06, Scheme 5.9**). This strategy proved to be general, also successfully cleaving the serine (**5.29**) and methionine-containing (**5.02**) substrates (forming **5.30** and **5.31**, respectively).

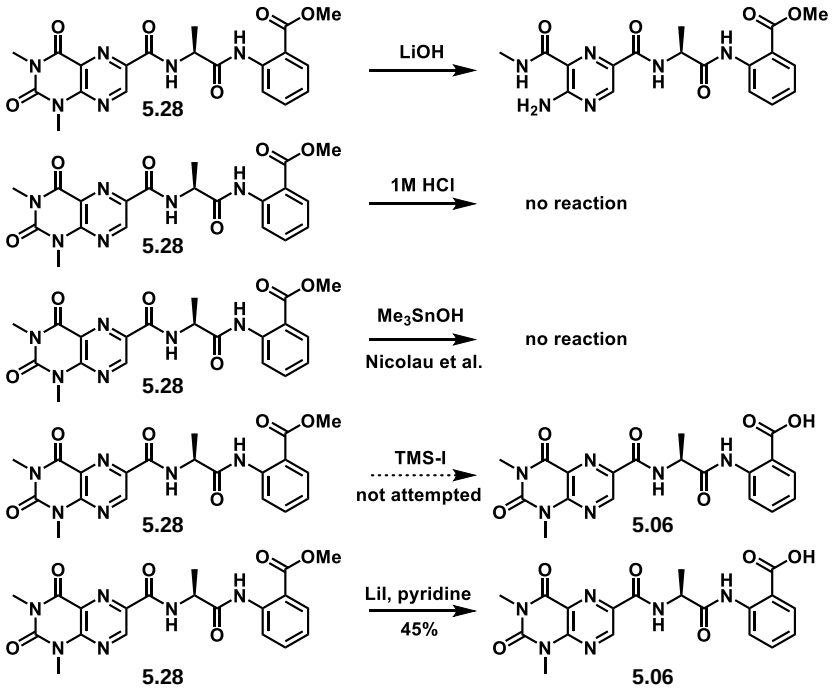

Scheme 5.9. Screening of methods for the hydrolysis of the methyl anthranilate fragment

Deprotection of the benzyl ether used to protect the serine sidechain also proved more difficult than anticipated (**Scheme 5.10**). Hydrogenolysis of **5.30** using palladium on carbon at 1 atm H_2 did not afford any product in ethyl acetate or methanol solvents. Paar bomb hydrogenation was next attempted, but even at pressures as great as 25 atm H_2 did not show any conversion of starting material after 24 hours. A recent photocatalytic method for the oxidative debenzylation of benzyl ethers using DDQ and tert-butyl nitrite published by Cavedon et al. was briefly explored and did deliver the desired Penilumamide H (**5.10**), albeit in low yields.[250] Interestingly, benzyl ether

hydrogenolysis on the anthranilate methyl ester (**5.29**) at 1 atm H_2 afforded product in moderate yields. It remains unclear why this substrate is more amenable to hydrogenolysis than equivalent anthranilic acid **5.30**, perhaps some favorable stabilization of the benzyl ether with the carboxylic acid or its attached aromatic ring prevents its hydrogenolysis. Nevertheless, the methyl ester of Penilumamide H (itself a likely yet-unidentified natural product) was subsequently cleaved with Li-I and the material was combined with that obtained via photocatalytic cleavage.

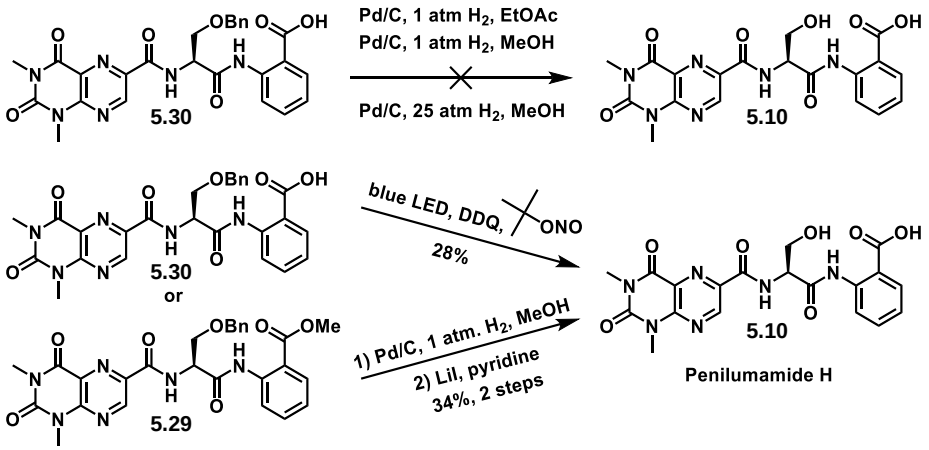

Scheme 5.10. Screen of conditions used for serine debenzylation to form penilumamide H

Isolated methionine-bridged lumazine peptides (penilumamides A-C, J) exist in a number of oxidation states. Methionine oxidation in cells is almost always deleterious, causing protein misfolding or inactivation, and has been linked to symptoms of neurodegeneration and aging in a variety of organisms.[251] This process is usually caused by reactive oxygen species (ROS) such as hydrogen peroxide, which result in the formation of methionine sulfoxide in a non-stereoselective manner. In rare cases, further oxidation to methionine sulfone is also possible in the presence of strong oxidizing species. Most organisms express a variety of methionine sulfoxide reductases to reverse single oxidation events, but formation of methionine sulfone is not known to be biologically reversible.[252] Enzymatic methionine oxidation as a mechanism of protein regulation

has more recently been identified, and results in the stereospecific formation of (R) or (S)-methionine sulfoxide.[253,254]

The isolation reports of methionine sulfoxide-containing penilumamides A (**5.01**) and J (**5.04**) reveal that the sulfur atom exists as a mixture of the (R) and (S) configurations; this indicates that penilumamide methionine oxidation is likely a result of either in vivo ROS exposure or an artifact of the isolation conditions themselves. Methionine sulfone, such as that reported in penilumamide C (**5.03**), is virtually unheard in small molecule natural products of due to the lack of suitable oxidants in most biological systems (to our knowledge, only three such metabolites have been reported in the literature, and in extremely low quantities with little or no characterization of the natural extracts themselves).[226,255,256] We therefore postulated that the sulfone moiety in the previously-synthesized penilumamide C is unrelated to the family's biological role, and omitted this compound from our investigation. Contrary to reports of the oxidative instability of penilumamide (**5.01**) and penilumamide B (**5.02**) and their slow conversion to penilumamide C (**5.03**), we saw neither overoxidation when using hydrogen peroxide to generate the sulfoxide, nor spontaneous oxidation in air from either material to the sulfone (**Scheme 5.11**).[226] Even storing **5.01** in a solution of DMSO for 7 days did not cause any oxidation event to take place.

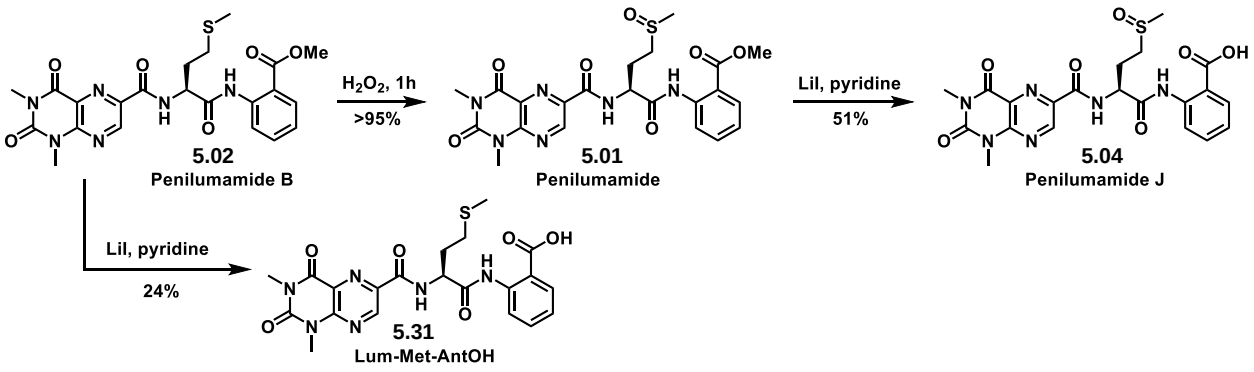

Scheme 5.11. Diverted synthetic route to methionine-containing penilumamide natural products

With our first eight lumazine peptides (penilumamide **5.01**, penilumamide B **5.02**, penilumamide B carboxylic acid **5.31**, penilumamide G **5.06**, penilumamide G methyl ester **5.28**, penilumamide H **5.10**, penilumamide H methyl ester **5.10a**, and penilumamide J **5.04**) and two intermediates (Lum-Ser(OBn)-AntOMe **5.29** and Lum-Ser(OBn)-AntOH **5.30**) in hand, we turned to their biological evaluation. To gain insights into potential for antibiotic activity, these compounds were first screened against a broad panel of bacteria: *E. coli*, *P. aeruginosa*, *A. baumanii*, *E. faecalis*, methicillin-susceptible *S. aureus*, and methicillin-resistant *S. aureus*. In all cases, gentamicin was used as a positive control. Unfortunately, none of our tested compounds showed any inhibitory activity against any of these bacterial species, highlighting that it is unlikely that these biomolecules are produced by fungi in order to combat neighboring species. Somewhat notably, at the highest tested concentration of all compounds (250 μM) we observed a change in color of *P. aeruginosa* from the ordinary blue-green to near colourless. This was particularly interesting as the blue-green pigment normally observed in *P. aeruginosa* is caused by production of pyocyanin and pyoverdine, known iron-binding virulence factors.[257,258]

For our remaining series of analogs, initial attempts at isonitrile formation relied on reaction of 1,2-phenylenediamine (**5.32**) with formic acid and acetic anhydride, with the intent to next dehydrate the resulting formamide (**5.33**) to the desired isonitrile (**Scheme 5.12**). However, on test scale the selectivity for monoamidation was very challenging to control. Attempts to first protect one of the amines using Boc (**5.34**) or benzyl (**5.35**) groups, followed by formamide formation was also unsuccessful, which we attributed to instability of either protecting group to the harsh conditions required. Seeking a milder method for isonitrile installation, we attempted literature reports of one-step conversion of amines to isonitriles using base and either chloroform or sodium chlorodifluoroacetate, the latter of which was successful in forming **5.36**.[259] However, subsequent

efforts to deprotect the remaining amine for its use in coupling invariably led to complete decomposition, indicating that the likely instability of 2-isocyanoaniline made this approach impossible.

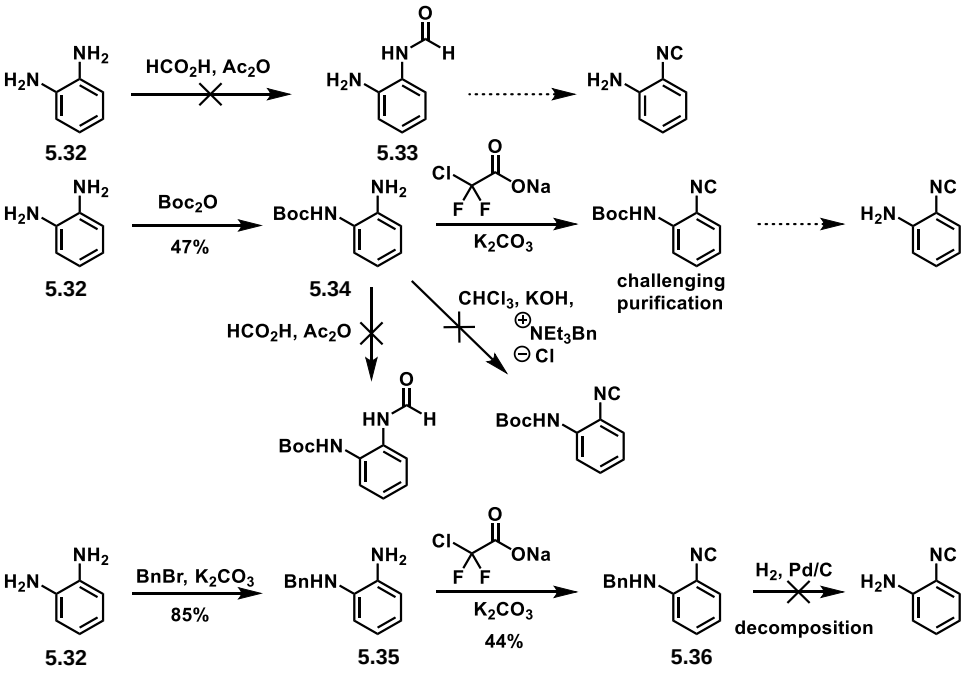

Scheme 5.12. Initial synthetic investigations into formation of 2-isocyanoaniline

Reasoning that the high reactivity of isocyanide moieties necessitated late-stage incorporation, we first coupled 1,2-phenylenediamine (**5.32**) with our desired amino acids. So as to avoid side reactions with the remaining amine, it could now be protected as its formamide, which we reasoned could be dehydrated at a later stage. Unfortunately, we discovered that dehydrating this moiety either before or after coupling to 1,3-dimethyllumazine-6-carboxylic acid (**5.13**), while successful, resulted in the unexpected slow decomposition of the isonitrile to undesired benzimidazole products, likely due to reaction of the isonitrile with the neighboring amide (**Scheme 5.13**). No methods of purification (buffered eluent, low temperatures, various additives) were able to prevent

this degradation, preventing access to isonitrile-substituted C-terminal lumazine peptides in our hands.

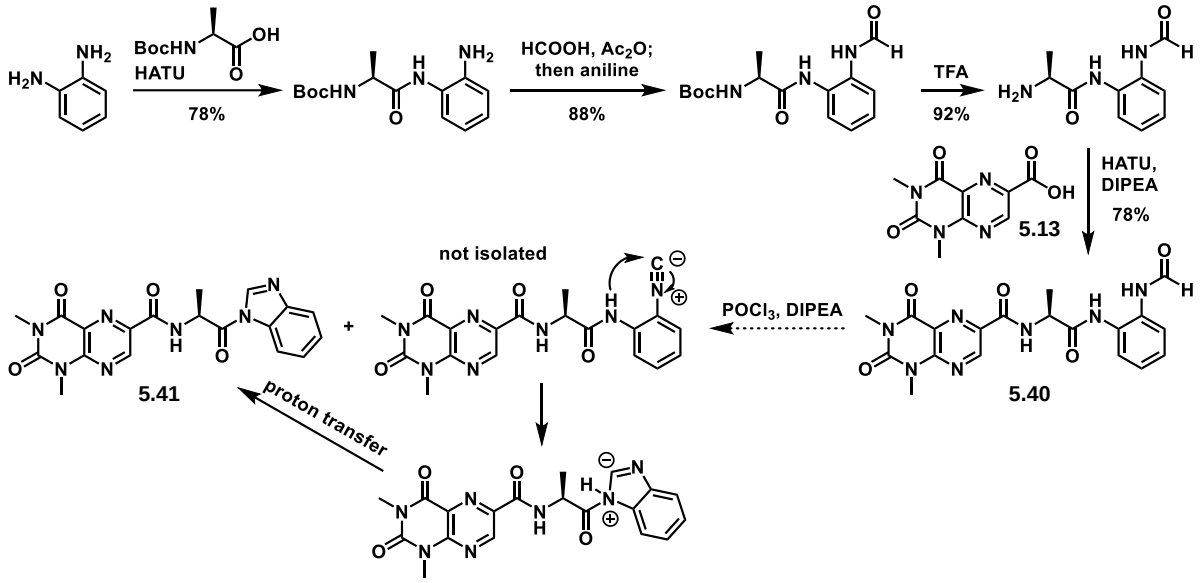

Scheme 5.13. Alternate strategy of isocyanide-containing lumazine peptides, and observed cyclization to benzimidazole products

of the extremely sensitive isonitrile moiety with a separate metal-binding motif may allow us to continue our investigation. As catechols are a privileged scaffold for metal chelation, we hypothesized that incorporating 2,3- or 3,4-dihydroxy motifs onto the C-terminal aromatic ring could provide comparable results with the natural activity of Penilumamide F (**Figure 5.9**).[260] Synthesis of these catechol-substituted lumazine peptide analogs is ongoing in our lab.

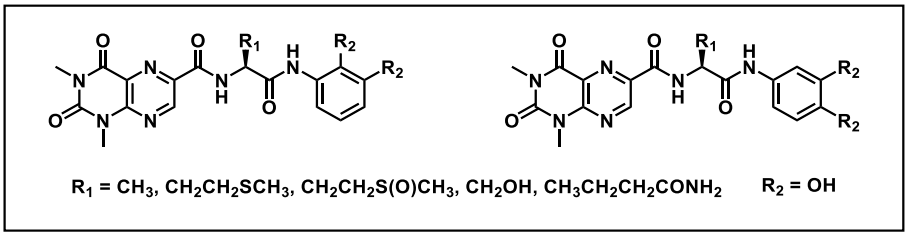

Figure 5.9. Desired catechol-containing lumazine peptides analog to assess metal binding potential

5.4 Chapter 5 Concluding Remarks and Future Directions

We remain interested in the synthesis and biological investigation of lumazine peptide natural products and synthetic analogs. While instability of our desired isonitrile series of analogs necessitated a change in strategy to incorporation of catechol moieties, it is our hope that these new analogs will provide interesting insights into the class's biological role. We hope to finish the synthesis of these compounds shortly and move forward with assessment of their activity. Our first foray into the investigation of these compounds will involve repeating the IC_{50} assay done for the first ten compounds, utilizing the same bacterial strains and controls to allow for their comparison. The observation of reduced phenazine production in *P. aeruginosa* for all tested compounds may support our hypothesis of a metal-binding role for these compounds – that is, supplying these bacterial cells with an exogenous metallophore allows for the downregulation of production of their own metal chelators, a biosynthetic pathway known to be highly energetically costly for the bacteria. We predict that if this is the true mechanism of these compounds, we should see similar or more pronounced results for the catechol-containing lumazine peptide analogs. To obtain further evidence for this biological role, we will conduct fluorimetry-based metal titration assays using a variety of metal ions to obtain a direct measurement of our compounds metal-binding propensity. This will also allow us to determine if lumazine peptides bind particular metal ions with any specificity and indicate the relative binding stoichiometry.

5.4 Chapter 5 References

(203) Kaspari, M.; Powers, J. S. Biogeochemistry and Geographical Ecology: Embracing All Twenty-Five Elements Required to Build Organisms. *Am. Nat.* **2016**, *188* (S1), S62–S73. https://doi.org/10.1086/687576.

(204) Emsley, J. *Nature's Building Blocks: An A-Z Guide to the Elements*, Reprinted with corrections.; Oxford Univ. Press: Oxford, 2003.

(205) Frawley, E. R.; Fang, F. C. The Ins and Outs of Bacterial Iron Metabolism. *Mol. Microbiol.* **2014**, *93* (4), 609–616. https://doi.org/10.1111/mmi.12709.

(206) Greene, N. P.; Koronakis, V. Bacterial Metal Resistance: Coping with Copper without Cooperativity? *mBio 12* (3), e00653-21. https://doi.org/10.1128/mBio.00653-21.

(207) McDevitt, C. A.; Ogunniyi, A. D.; Valkov, E.; Lawrence, M. C.; Kobe, B.; McEwan, A. G.; Paton, J. C. A Molecular Mechanism for Bacterial Susceptibility to Zinc. *PLOS Pathog.* **2011**, *7* (11), e1002357. https://doi.org/10.1371/journal.ppat.1002357.

(208) Solioz, M. Copper Toxicity. In *Copper and Bacteria: Evolution, Homeostasis and Toxicity*; Solioz, M., Ed.; SpringerBriefs in Molecular Science; Springer International Publishing: Cham, 2018; pp 11–19. https://doi.org/10.1007/978-3-319-94439-5_2.

(209) Chandrangsu, P.; Rensing, C.; Helmann, J. D. Metal Homeostasis and Resistance in Bacteria. *Nat. Rev. Microbiol.* **2017**, *15* (6), 338–350. https://doi.org/10.1038/nrmicro.2017.15.

(210) Krüger, B.; Liang, C.; Prell, F.; Fieselmann, A.; Moya, A.; Schuster, S.; Völker, U.; Dandekar, T. Metabolic Adaptation and Protein Complexes in Prokaryotes. *Metabolites* **2012**, *2* (4), 940–958. https://doi.org/10.3390/metabo2040940.

(211) Wichard, T. Identification of Metallophores and Organic Ligands in the Chemosphere of the Marine Macroalga Ulva (Chlorophyta) and at Land-Sea Interfaces. *Front. Mar. Sci.* **2016**, *3*.

(212) Ghssein, G.; Ezzeddine, Z. The Key Element Role of Metallophores in the Pathogenicity and Virulence of Staphylococcus Aureus: A Review. *Biology* **2022**, *11* (10), 1525. https://doi.org/10.3390/biology11101525.

(213) Neumann, W.; Gulati, A.; Nolan, E. M. Metal Homeostasis in Infectious Disease: Recent Advances in Bacterial Metallophores and the Human Metal-Withholding Response. *Curr. Opin. Chem. Biol.* **2017**, *37*, 10–18. https://doi.org/10.1016/j.cbpa.2016.09.012.

(214) Clatworthy, A. E.; Pierson, E.; Hung, D. T. Targeting Virulence: A New Paradigm for Antimicrobial Therapy. *Nat. Chem. Biol.* **2007**, *3* (9), 541–548. https://doi.org/10.1038/nchembio.2007.24.

(215) Repac Antić, D.; Parčina, M.; Gobin, I.; Petković Didović, M. Chelation in Antibacterial Drugs: From Nitroxoline to Cefiderocol and Beyond. *Antibiotics* **2022**, *11* (8), 1105. https://doi.org/10.3390/antibiotics11081105.

(216) Karakonstantis, S.; Rousaki, M.; Kritsotakis, E. I. Cefiderocol: Systematic Review of Mechanisms of Resistance, Heteroresistance and In Vivo Emergence of Resistance. *Antibiotics* **2022**, *11* (6), 723. https://doi.org/10.3390/antibiotics11060723.

(217) Brandel, J.; Humbert, N.; Elhabiri, M.; Schalk, I. J.; Mislin, G. L. A.; Albrecht-Gary, A.-M. Pyochelin, a Siderophore of Pseudomonas Aeruginosa: Physicochemical Characterization of the Iron(III), Copper(II) and Zinc(II) Complexes. *Dalton Trans.* **2012**, *41* (9), 2820–2834. https://doi.org/10.1039/C1DT11804H.

(218) Ahmed, E.; Holmström, S. J. M. Siderophores in Environmental Research: Roles and Applications. *Microb. Biotechnol.* **2014**, *7* (3), 196–208. https://doi.org/10.1111/1751-7915.12117.

(219) Kim, H. J.; Graham, D. W.; DiSpirito, A. A.; Alterman, M. A.; Galeva, N.; Larive, C. K.; Asunskis, D.; Sherwood, P. M. A. Methanobactin, a Copper-Acquisition Compound from Methane-Oxidizing Bacteria. *Science* **2004**, *305* (5690), 1612–1615. https://doi.org/10.1126/science.1098322.

(220) Behling, L. A.; Hartsel, S. C.; Lewis, D. E.; DiSpirito, A. A.; Choi, D. W.; Masterson, L. R.; Veglia, G.; Gallagher, W. H. NMR, Mass Spectrometry and Chemical Evidence Reveal a Different Chemical Structure for Methanobactin That Contains Oxazolone Rings. *J. Am. Chem. Soc.* **2008**, *130* (38), 12604–12605. https://doi.org/10.1021/ja804747d.

(221) Kenney, G. E.; Rosenzweig, A. C. Chalkophores. *Annu. Rev. Biochem.* **2018**, *87*, 645–676. https://doi.org/10.1146/annurev-biochem-062917-012300.

(222) Wang, L.; Zhu, M.; Zhang, Q.; Zhang, X.; Yang, P.; Liu, Z.; Deng, Y.; Zhu, Y.; Huang, X.; Han, L.; Li, S.; He, J. Diisonitrile Natural Product SF2768 Functions As a Chalkophore That Mediates Copper Acquisition in Streptomyces Thioluteus. *ACS Chem. Biol.* **2017**, *12* (12), 3067–3075. https://doi.org/10.1021/acschembio.7b00897.

(223) Hübner, I.; Shapiro, J. A.; Hoßmann, J.; Drechsel, J.; Hacker, S. M.; Rather, P. N.; Pieper, D. H.; Wuest, W. M.; Sieber, S. A. Broad Spectrum Antibiotic Xanthocillin X Effectively Kills Acinetobacter Baumannii via Dysregulation of Heme Biosynthesis. *ACS Cent. Sci.* **2021**, *7* (3), 488–498. https://doi.org/10.1021/acscentsci.0c01621.

(224) Wright, A. D.; Wang, H.; Gurrath, M.; König, G. M.; Kocak, G.; Neumann, G.; Loria, P.; Foley, M.; Tilley, L. Inhibition of Heme Detoxification Processes Underlies the Antimalarial Activity of Terpene Isonitrile Compounds from Marine Sponges. *J. Med. Chem.* **2001**, *44* (6), 873–885. https://doi.org/10.1021/jm0010724.

(225) Meyer, S. W.; Mordhorst, T. F.; Lee, C.; Jensen, P. R.; Fenical, W.; Köck, M. Penilumamide, a Novel Lumazine Peptide Isolated from the Marine-Derived Fungus, Penicillium Sp. CNL-338. *Org. Biomol. Chem.* **2010**, *8* (9), 2158–2163. https://doi.org/10.1039/b910629d.

(226) Chen, M.; Shao, C.-L.; Fu, X.-M.; Kong, C.-J.; She, Z.-G.; Wang, C.-Y. Lumazine Peptides Penilumamides B–D and the Cyclic Pentapeptide Asperpeptide A from a Gorgonian-Derived Aspergillus Sp. Fungus. *J. Nat. Prod.* **2014**, *77* (7), 1601–1606. https://doi.org/10.1021/np5001686.

(227) You, M.; Liao, L.; Hong, S. H.; Park, W.; Kwon, D. I.; Lee, J.; Noh, M.; Oh, D.-C.; Oh, K.-B.; Shin, J. Lumazine Peptides from the Marine-Derived Fungus Aspergillus Terreus. *Mar. Drugs* **2015**, *13* (3), 1290–1303. https://doi.org/10.3390/md13031290.

(228) Chaiyosang, B.; Kanokmedhakul, K.; Boonmak, J.; Youngme, S.; Kukongviriyapan, V.; Soytong, K.; Kanokmedhakul, S. A New Lumazine Peptide Penilumamide E from the Fungus Aspergillus Terreus. *Nat. Prod. Res.* **2016**, *30* (9), 1017–1024. https://doi.org/10.1080/14786419.2015.1101107.

(229) Zheng, C.-J.; Wu, L.-Y.; Li, X.-B.; Song, X.-M.; Niu, Z.-G.; Song, X.-P.; Chen, G.-Y.; Wang, C.-Y. Structure and Absolute Configuration of Aspergilumamide A, a Novel Lumazine

Peptide from the Mangrove-Derived Fungus Aspergillus Sp. *Helv. Chim. Acta* **2015**, *98* (3), 368–373. https://doi.org/10.1002/hlca.201400197.

(230) Wang, C.; Wu, X.; Bai, H.; Zaman, K. A. U.; Hou, S.; Saito, J.; Wongwiwatthananukit, S.; Kim, K. S.; Cao, S. Antibacterial and NF-KB Inhibitory Lumazine Peptides, Aspochalasin, γ-Butyrolactone Derivatives, and Cyclic Peptides from a Hawaiian Aspergillus Flavipes. *J. Nat. Prod.* **2020**, *83* (7), 2233–2240. https://doi.org/10.1021/acs.jnatprod.0c00344.

(231) Voerman, G.; Cavalli, S.; van der Marel, G. A.; Pfleiderer, W.; van Boom, J. H.; Filippov, D. V. 1,3-Dimethyllumazine Derivatives from Limnatis Nilotica. *J. Nat. Prod.* **2005**, *68* (6), 938–941. https://doi.org/10.1021/np049617a.

(232) Averianova, L. A.; Balabanova, L. A.; Son, O. M.; Podvolotskaya, A. B.; Tekutyeva, L. A. Production of Vitamin B2 (Riboflavin) by Microorganisms: An Overview. *Front. Bioeng. Biotechnol.* **2020**, *8*.

(233) Lei, J.; Xin, C.; Xiao, W.; Chen, W.; Song, Z. The Promise of Endogenous and Exogenous Riboflavin in Anti-Infection. *Virulence 12* (1), 2314–2326. https://doi.org/10.1080/21505594.2021.1963909.

(234) Chen, J.; Illarionov, B.; Bacher, A.; Fischer, M.; Haase, I.; Georg, G.; Ye, Q.; Ma, Z.; Cushman, M. A High-Throughput Screen Utilizing the Fluorescence of Riboflavin for Identification of Lumazine Synthase Inhibitors. *Anal. Biochem.* **2005**, *338* (1), 124–130. https://doi.org/10.1016/j.ab.2004.11.033.

(235) Cushman, M.; Yang, D.; Kis, K.; Bacher, A. Design, Synthesis, and Evaluation of 9-D-Ribityl-1,3,7-Trihydro-2,6,8-Purinetrione, a Potent Inhibitor of Riboflavin Synthase and Lumazine Synthase. *J. Org. Chem.* **2001**, *66* (25), 8320–8327. https://doi.org/10.1021/jo010706r.

(236) Cushman, M.; Jin, G.; Illarionov, B.; Fischer, M.; Ladenstein, R.; Bacher, A. Design, Synthesis, and Biochemical Evaluation of 1,5,6,7-Tetrahydro-6,7-Dioxo-9-d-Ribitylaminolumazines Bearing Alkyl Phosphate Substituents as Inhibitors of Lumazine Synthase and Riboflavin Synthase. *J. Org. Chem.* **2005**, *70* (20), 8162–8170. https://doi.org/10.1021/jo051332v.

(237) Heard, S. C.; Winter, J. M. Biosynthesis of the Fungal Nonribosomal Peptide Penilumamide A and Biochemical Characterization of a Pterin-Specific Adenylation Domain. bioRxiv August 30, 2022, p 2022.08.30.505926. https://doi.org/10.1101/2022.08.30.505926.

(238) Isay, O. Eine Synthese Des Purins. *Berichte Dtsch. Chem. Ges.* **1906**, *39* (1), 250–265. https://doi.org/10.1002/cber.19060390149.

(239) Timmis, G. M. A New Synthesis of Pteridines. *Nature* **1949**, *164* (4160), 139. https://doi.org/10.1038/164139a0.

(240) Viscontini, M.; Bosshard, R. Über Pterin-Chemie 87. Mitteilung. Regiospezifische Synthese von (Polyhydroxypropyl)-Pterinen: Herstellung von D-Anapterin Und L-Primapterin. *Helv. Chim. Acta* **1990**, *73* (2), 337–345. https://doi.org/10.1002/hlca.19900730213.

(241) Yoneda, F.; Koga, R.; Nishigaki, S.; Fukazawa, S. A Synthesis of Lumazine Derivatives. *J. Heterocycl. Chem.* **1982**, *19* (4), 949–951. https://doi.org/10.1002/jhet.5570190452.

(242) Reddy Penjarla, T.; Kundarapu, M.; Syed Mohd., B.; Bhattacharya, A. A Straight Forward and First Total Synthesis of Penilumamides B–D. *Tetrahedron Lett.* **2017**, *58* (34), 3347–3349. https://doi.org/10.1016/j.tetlet.2017.07.027.

(243) Xin, D.; Burgess, K. Anthranilic Acid-Containing Cyclic Tetrapeptides: At the Crossroads of Conformational Rigidity and Synthetic Accessibility. *Org. Biomol. Chem.* **2016**, *14* (22), 5049–5058. https://doi.org/10.1039/C6OB00693K.

(244) Isidro-Llobet, A.; Alvarez, M.; Albericio, F. Amino Acid-Protecting Groups. *Chem. Rev.* **2009**, *109* (6), 2455–2504. https://doi.org/10.1021/cr800323s.

(245) Albert, A.; Phillips, J. N. 264. Ionization Constants of Heterocyclic Substances. Part II. Hydroxy-Derivatives of Nitrogenous Six-Membered Ring-Compounds. *J. Chem. Soc. Resumed* **1956**, No. 0, 1294–1304. https://doi.org/10.1039/JR9560001294.

(246) Nicolaou, K. C.; Estrada, A. A.; Zak, M.; Lee, S. H.; Safina, B. S. A Mild and Selective Method for the Hydrolysis of Esters with Trimethyltin Hydroxide. *Angew. Chem. Int. Ed.* **2005**, *44* (9), 1378–1382. https://doi.org/10.1002/anie.200462207.

(247) Jung, M. E.; Lyster, M. A. Quantitative Dealkylation of Alkyl Ethers via Treatment with Trimethylsilyl Iodide. A New Method for Ether Hydrolysis. *J. Org. Chem.* **1977**, *42* (23), 3761–3764. https://doi.org/10.1021/jo00443a033.

(248) Fisher, J. W.; Trinkle, K. L. Iodide Dealkylation of Benzyl, PMB, PNB, and t-Butyl N-Acyl Amino Acid Esters via Lithium Ion Coordination. *Tetrahedron Lett.* **1994**, *35* (16), 2505–2508. https://doi.org/10.1016/S0040-4039(00)77156-5.

(249) Lepage, O.; Kattnig, E.; Fürstner, A. Total Synthesis of Amphidinolide X. *J. Am. Chem. Soc.* **2004**, *126* (49), 15970–15971. https://doi.org/10.1021/ja044130+.

(250) Cavedon, C.; Sletten, E. T.; Madani, A.; Niemeyer, O.; Seeberger, P. H.; Pieber, B. Visible-Light-Mediated Oxidative Debenzylation Enables the Use of Benzyl Ethers as Temporary Protecting Groups. *Org. Lett.* **2021**, *23* (2), 514–518. https://doi.org/10.1021/acs.orglett.0c04026.

(251) Korovesis, D.; Rubio-Tomás, T.; Tavernarakis, N. Oxidative Stress in Age-Related Neurodegenerative Diseases: An Overview of Recent Tools and Findings. *Antioxidants* **2023**, *12* (1), 131. https://doi.org/10.3390/antiox12010131.

(252) Hoshi, T.; Heinemann, S. H. Regulation of Cell Function by Methionine Oxidation and Reduction. *J. Physiol.* **2001**, *531* (1), 1–11. https://doi.org/10.1111/j.1469-7793.2001.0001j.x.

(253) Lim, J. C.; You, Z.; Kim, G.; Levine, R. L. Methionine Sulfoxide Reductase A Is a Stereospecific Methionine Oxidase. *Proc. Natl. Acad. Sci.* **2011**, *108* (26), 10472–10477. https://doi.org/10.1073/pnas.1101275108.

(254) Cao, Z.; Mitchell, L.; Hsia, O.; Scarpa, M.; Caldwell, S. T.; Alfred, A. D.; Gennaris, A.; Collet, J.-F.; Hartley, R. C.; Bulleid, N. J. Methionine Sulfoxide Reductase B3 Requires Resolving Cysteine Residues for Full Activity and Can Act as a Stereospecific Methionine Oxidase. *Biochem. J.* **2018**, *475* (4), 827–838. https://doi.org/10.1042/BCJ20170929.

(255) Okinyo-Owiti, D. P.; Young, L.; Burnett, P.-G. G.; Reaney, M. J. T. New Flaxseed Orbitides: Detection, Sequencing, and 15N Incorporation. *Pept. Sci.* **2014**, *102* (2), 168–175. https://doi.org/10.1002/bip.22459.

(256) Pereira, A. R.; Kale, A. J.; Fenley, A. T.; Byrum, T.; Debonsi, H. M.; Gilson, M. K.; Valeriote, F. A.; Moore, B. S.; Gerwick, W. H. The Carmaphycins, New Proteasome Inhibitors Exhibiting an α,β-Epoxyketone Warhead from a Marine Cyanobacterium. *Chembiochem* **2012**, *13* (6), 810–817. https://doi.org/10.1002/cbic.201200007.

(257) Little, A. S.; Okkotsu, Y.; Reinhart, A. A.; Damron, F. H.; Barbier, M.; Barrett, B.; Oglesby-Sherrouse, A. G.; Goldberg, J. B.; Cody, W. L.; Schurr, M. J.; Vasil, M. L.; Schurr, M. J. Pseudomonas Aeruginosa AlgR Phosphorylation Status Differentially Regulates Pyocyanin and Pyoverdine Production. *mBio* **2018**, *9* (1), e02318-17. https://doi.org/10.1128/mBio.02318-17.

(258) Cornelis, P.; Dingemans, J. Pseudomonas Aeruginosa Adapts Its Iron Uptake Strategies in Function of the Type of Infections. *Front. Cell. Infect. Microbiol.* **2013**, *3*.

(259) Si, Y.-X.; Zhu, P.-F.; Zhang, S.-L. Synthesis of Isocyanides by Reacting Primary Amines with Difluorocarbene. *Org. Lett.* **2020**, *22* (22), 9086–9090. https://doi.org/10.1021/acs.orglett.0c03472.

(260) Ahmed, E.; Holmström, S. J. M. Siderophores in Environmental Research: Roles and Applications. *Microb. Biotechnol.* **2014**, *7* (3), 196. https://doi.org/10.1111/1751-7915.12117.

Chapter 6 - Experimental Details

6.1 Supplementary schemes, figures, and tables

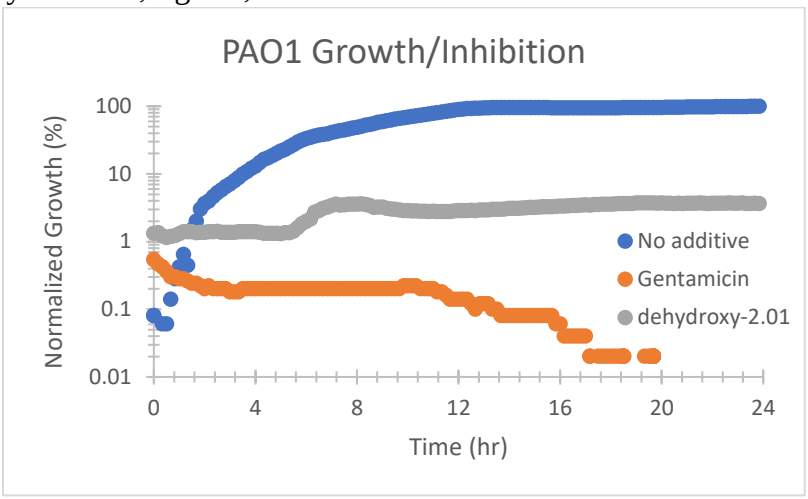

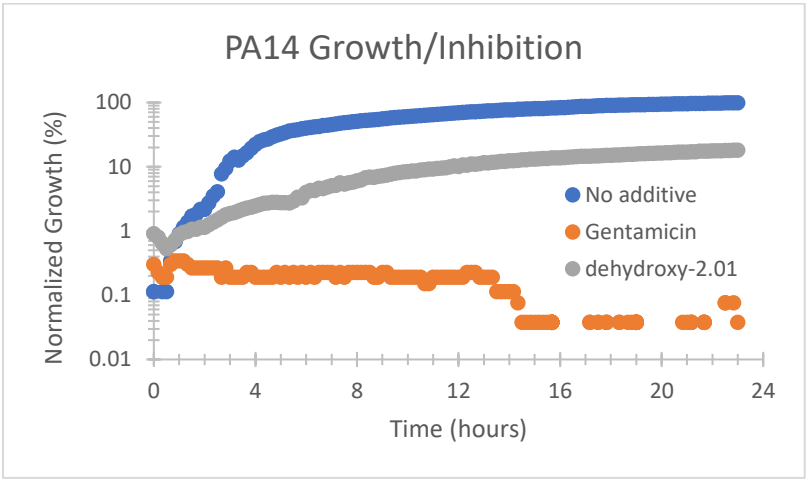

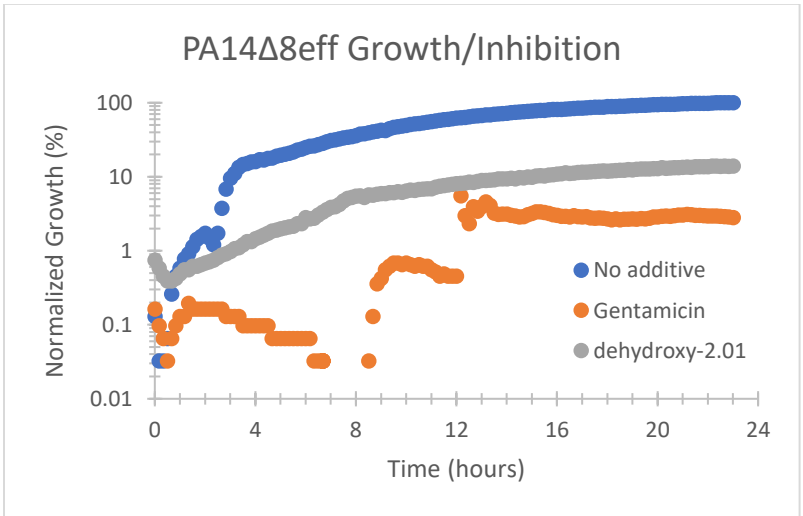

Figure 6.1. Normalized growth and inhibition curves for all PA strains tested against promysalin compounds. Gentamicin and dehydroxy-2.01 were tested at 100 µM for all strains

Table 6.1. Predicted minimum inhibitory concentrations (MICs) and fractional inhibitory concentrations (FICs) for all berberine compounds

	Compound	Predicted MIC [μg/mL]	Antibiotic	FIC Range	Average FIC
	Berberine (3.01)	979	Kan	0.5	0.5
			Gen	0.5	0.5
GENERATION I	Ber-Carb (3.02)	760	Kan	1.67	1.67
			Gen	0.52	0.52
	Ber-Pip (3.03)	3549	Kan	0.50	0.50
			Gen	1.14	1.14
	Ber-Prop (3.06)	947	Kan	0.39-0.5	0.44
			Gen	0.39-0.5	0.44
	Ber-C6 (3.05)	287	Kan	0.28-0.51	0.38
			Gen	0.36-0.51	0.48
GENERATION II	Ber-C3 (3.20)	584	Kan	0.30-0.50	0.4
			Gen	0.30-0.50	0.38
	Ber-C4 (3.21)	508	Kan	0.38-0.5	0.44
			Gen	0.38-0.5	0.44
	Ber-C8 (3.22)	250	Kan	0.28-0.5	0.39
			Gen	0.38-0.5	0.4
	Ber-C10 (3.23)	200	Kan	0.17-0.51	0.31
			Gen	0.17-0.51	0.33
	Ber-C12 (3.24)	180	Kan	0.26-0.51	0.36
			Gen	0.26-0.77	0.46
GENERATION III	Ber-pAr (3.25)	400	Kan	0.52-0.57	0.55
			Gen	0.33-0.52	0.43
	Ber-Biphenyl (3.26)	502	Kan	0.5-0.51	0.51
			Gen	0.52	0.52
	Ber-PEG5 (3.27)	545	Kan	0.56	0.56
			Gen	0.48-0.53	0.51
	Ber-PEG8 (3.28)	622	Kan	0.55	0.55
			Gen	0.46-0.53	0.49

Table 6.2. Minimum inhibitory concentration [µg/mL] for MexXY-OprM substrates (kanamycin (KAN), amikacin (AMI), gentamicin (GEN), tobramycin (TOB), tigecycline (TIG), cefepime (CEF), and ciprofloxacin (CIP)) and non-substrate (imipenem (IMI) in *P. aeruginosa* PAO1, clinical pan-aminoglycoside resistant *P. aeruginosa* K2156 and K2161, and respective isogenic *mexXY* knockout strains with select berberine analogs

Strain	**PAO1**						**K2156**					
	WT	**ΔXY**	**WT**				**WT**	**ΔXY**	**WT**			
Ber Analog [64 µg/mL]	**-**	**-**	**BER** (3.01)	**pAr** (3.25)	**C3** (3.20)	**C12** (3.24)	**-**	**-**	**BER** (3.01)	**pAr** (3.25)	**C3** (3.20)	**C12** (3.24)
KAN	64	16	32	16	16	8	256	16	16	16	16	8
AMI	1	0.25	0.5	0.25	0.25	0.125	8	0.5	0.5	0.5	0.5	0.5
GEN	1	0.25	0.5	0.25	0.25	0.125	8	0.5	1	1	0.5	0.5
TOB	0.5	0.25	0.25	0.125	0.25	0.125	2	1	0.5	0.5	0.25	0.5
TIG	4	0.5	4	4	2	2	4	0.5	4	4	2	1
CEF	1	0.5	1	1	0.5	2	2	1	2	2	2	2
CIP	0.125	0.125	0.125	0.25	0.125	0.5	1	1	1	2	1	4
IMI	4	4	4	2	4	2	2	2	2	2	2	2

Strain	**K2161**					
	WT	**ΔXY**	**WT**			
Ber Analog [64 µg/mL]	**-**	**-**	**BER** (3.01)	**pAr** (3.25)	**C3** (3.20)	**C12** (3.24)
KAN	256	64	256	256	128	128
AMI	16	2	8	8	4	8
GEN	16	2	8	8	4	4
TOB	8	2	4	4	2	2
TIG	4	1	4	4	4	2
CEF	0.25	0.125	0.5	1	0.25	1
CIP	0.125	0.06	0.25	0.25	0.25	0.5
IMI	2	2	2	2	2	1

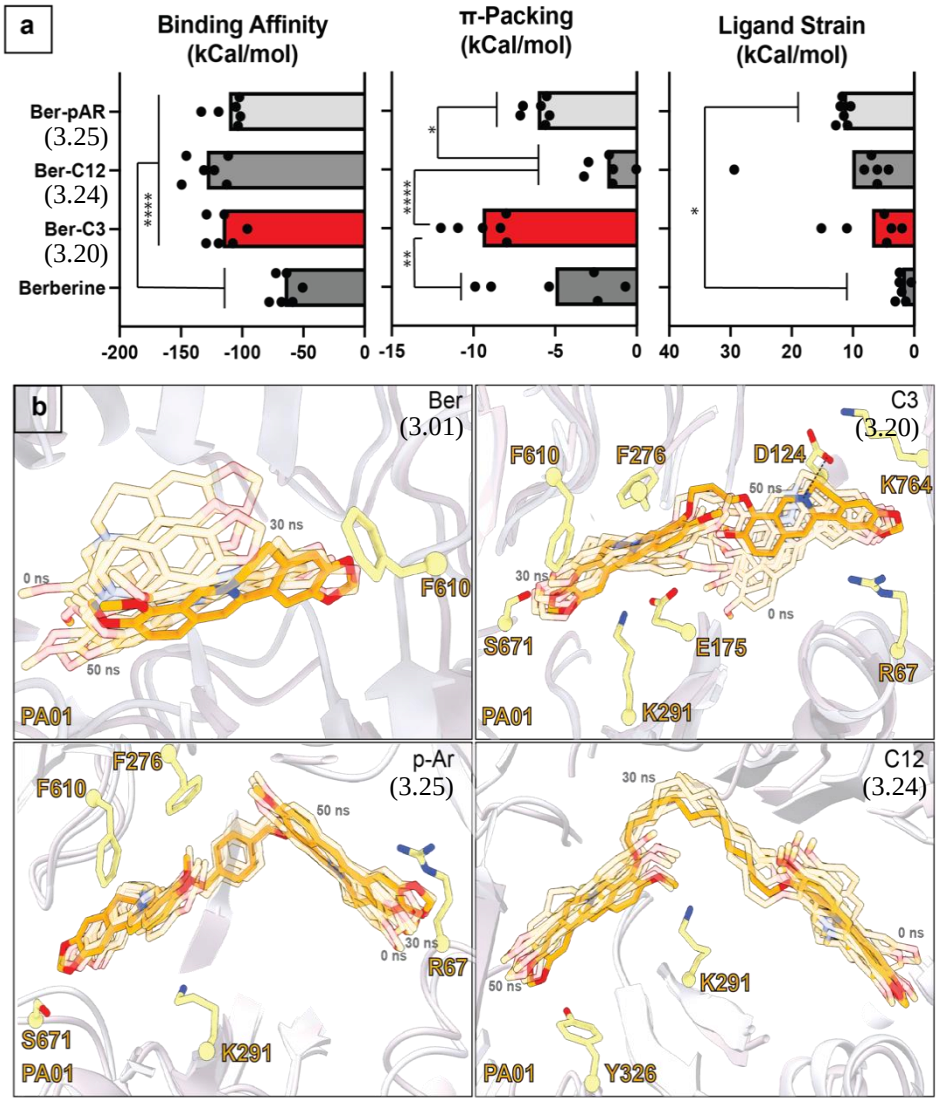

Figure 6.2. A. MMGBSA plots calculated for binding affinity, π-packing, and ligand strain. Data represent individual values for six frames (every 10 ns from 0-50 ns) with the average shown as a bar plot. Statistical analysis was performed using one-way ANOVA on the mean for each compound and statistically significant results are shown (* $p \leq 0.05$, ** $p \leq 0.01$, *** $p \leq 0.001$, and **** $p \leq 0.0001$). **B.** 50 ns molecular dynamics simulations of berberine (3.01, top left) and berberine dimers, Ber-C3 (3.20, top right), Ber-pAr (3.25 bottom left), and Ber-C12 (3.24, bottom right) in the MexY DBP and PBP are shown. Conformations at 0-40ns are shown in transparent gold, with 0 and 30 ns frames marked. Final conformation at 50 ns is shown as opaque gold

6.2 Biological assays

Bacterial Strains and Culture Conditions

P. aeruginosa PA01 and PA14, and *S. aureus* USA300 and SH1000 were gifts from Dr. Buttaro (Temple University). *A. baumannii* ATCC 17978, *E. faecalis* (ATCC 51575), *S. aureus* ATCC 33592 were purchased from American Type Culture Collection (ATCC). *S. mutans* UA159 and *E. coli* MC4100 were also obtained from commercial sources. All bacterial cultures with the exception of UA159 were grown from freezer stocks overnight (16-24 hr) with shaking at 37°C in 5 mL of Tryptic Soy Broth (TSB) or BD™ Mueller Hinton broth (MHB). Bacterial cultures of *S. mutans* UA159 were grown from a freshly streaked Petri dish (grown from a freezer stock) overnight (16 hours) statically at 37 °C in a CO_2 incubator (5% CO_2) in 10 mL media (Tryptic Soy Broth containing 5% sucrose to reflect physiological conditions and promote biofilm formation). Growth curves were obtained for *A. baumanii, E. coli, E. faecalis, S. aureus,* and *S. mutans* strains by previous members of the group to determine the optical density (OD) of each strain in exponential growth; OD readings at a wavelength of 600 nm were taken every 10 minutes for 6 hours in a plate reader at 37°C with shaking and repeated six times. This data was used without alteration for this report.

Pseudomonas aeruginosa PA14 allelic replacement strains were constructed using an unmarked, non-polar deletion strategy.[261-262] Efflux deletion mutants were individually constructed and sequentially constructed to create an efflux null strain missing 8 efflux systems beginning with mexXY followed by mexCD-oprJ, mexJK, opmH, mexEF-oprN, oprD, mexGHI-opmD, and mexAB, respectively. To create each suicide vector, gBlocks containing 500-1000bp upstream and downstream of the genes of interest removing the entire coding region were amplified using primers UP and DN primer sets (Table 6.7). The resultant PCR products were cloned into the suicide vector, pEX100T, via Gibson Assembly (New England BioLabs) recombination according

to the manufacturer's protocols. The resultant plasmid was verified by sequence analysis (ELIM Biopharm) and transformed into the conjugation-competent auxotroph, S17-1 ΔhemA cells supplemented with 50 μg ml−1 5-aminolevulinic acid.[263] The suicide vector was introduced into the strain of interest via conjugation.[262] Single cross-over mutants were selected on LB containing 10 μg ml−1 gentamicin or a lower concentration as efflux mutants were created. Unmarked, double cross-over mutants were selected on LB without NaCl plates containing 10% sucrose and confirmed by PCR and sequence analysis.

Table 6.3. Primers used in generation of the novel PA14 efflux deletion strain

Primers **Name**	**Sequence**
pEX18gm Gibson Assembly universal F	ggtcatagctgtttcctgtgtg
pEX18gm Gibson Assembly Universal R	caacgtcgtgactgggaaaac
mexCD-oprJ KO GA F	ccagtcacgacgttgGCTTCCAGGTAGGACTGC
mexCD-oprJ KO GA R	ggaaacagctatgaccCACCATGGGAGAACTGGC
mexCD-oprJ outside seq F	GATGAACAGTTCGGTGAACACGG
mexCD-oprJ outside seq R	CAGGACCAGCGTCTGCTCAAG
mexCD-oprJ inside seq F	CCATCCTGGTGGTCTTCCTG
mexCD-oprJ inside seq R	GATACGCCGAATGCAGGTTTG
mexEF-OprN KO GA F	ccagtcacgacgttgCGTCGACGAGGAACTGGAG
mexEF-OprN KO GA R	ggaaacagctatgaccCCTTGCAACAGCTCAATCAC
mexEF-OprN outside seq F	CAGCTGACCCTCGACGACTAC
mexEF-OprN outside seq R	CCAACCTGCAAGTCGACCTG
mexEF-OprN inside seq F	GATCGTCGAGTTCGCCAAGG
mexEF-OprN inside seq R	GACCAACTGGTTCAGGGTCG
opmH KO GA F	ccagtcacgacgttgCCTTGCGCGAGTTCGGGA
opmH KO GA R	ggaaacagctatgaccGACCTGCTGATCCTCAACTTTCCG
ompH outside seq F	GAGGGAGATTTCCCGCACC
ompH outside seq R	GATCCCGACTACCTGGTCTAC
ompH inside seq F	CTGGTGACCCTGACCAACC
ompH inside seq R	GCTCGACGTCGGTATTCAC
mexXY KO GA F	ccagtcacgacgttgCTTGAGGTAGAGGATCTCCAG
mexXY KO GA R	ggaaacagctatgaccGTTGTTCCTCACCGATCTG

mexXY outside seq F	CGATTGCAGATAGATGCTGG
mexXY outside seq R	GTGATCGACATCGACGATCC
mexXY inside seq F	GCAGATCGATCCGATCTACG
mexXY inside seq R	GTAGCGTTCTCCGTCACTG
mexGHI - opmD KO GA F	ccagtcacgacgttgCCACATATGGCAAGTCCTGC
mexGHI - opmD KO GA R	ggaaacagctatgaccGAAGGCGAGCAACCTGGC
mexGHI - opmD outside seq F	CTAAGCGGTCATCCGCACTAC
mexGHI - opmD outside seq R	CGAAGACTTCTACAGCTACCTG
mexGHI - opmD inside seq F	CAACCGCTTCGGCATGGAAG
mexGHI - opmD inside seq R	GTTCATCGTCGCGTAGCCCAG
mexJK KO GA F	ccagtcacgacgttgCCATCTCGTCGATCACCTGC
mexJK KO GA R	ggaaacagctatgaccGGACGTGCGCATCGAACTG
mexJK outside seq F	CTTGACCAGCATGAAGAAGTG
mexJK outside seq R	GACGCTGTCATGTTCCGACTC
mexJK inside seq F	GAGCTGCTGCTGGACATCAAG
mexJK inside seq R	CTCGGCAGCAACGACAGGTC
oprD KO GA F	ccagtcacgacgttgCTCGATGGCAACCAACCCTTG
oprD KO GA R	ggaaacagctatgaccGCAGGCAATGAACGCGGC
oprD outside seq F	CAAACGCATTCGCCACAGAC
oprD outside seq R	GGCCATCGATGATGAGGAGTC
oprD inside seq F	GATGCCTTCGGCTACCTCGG
oprD inside seq R	CGCATCCAGAGTGTAGGCTGC
mexAB KO GA F	ccagtcacgacgttgCATCACCGGCAACCTGAC
mexAB KO GA R	ggaaacagctatgaccGGACGAAGAGAAGCTGCTC
mexAB outside seq F	CATCAGGTCGGGATTCACG
mexAB outside seq R	GGAAGAGTTCCTCGACGAC
mexAB inside seq F	CATGTTCGTTCACGCGCAG
mexAB inside seq R	CATCTGCTGCTCGATCACCTG

MIC/IC_{50} Assay

Compounds were serially diluted in sterile DI water from a stock solution (1 mM in 10% DMSO/90% H_2O) to yield twelve test concentrations (or 24 in the case of promysalin analogs). Overnight cultures were diluted 1:100 in 5 mL fresh media and grown with shaking at 37 °C to an OD reflecting exponential growth based on growth curve data. Bacteria were diluted to an optical density of 0.004 using the following equation: (x μL bacterial culture)(OD reading) =

(0.004)(volume needed) and 100 μL was inoculated into each well of a flat-bottom 96-well plate (Corning 3370) containing 100 μL of compound solution. Plates were incubated statically at 37°C for 24 hours, upon which time the OD at 595 nm was measured using a plate reader (for compounds displaying MICs, the MIC values were scored visually). IC_{50} values were calculated by fitting the OD readings vs. concentration with a 4 parameter logistic model. Controls were prepared by serially diluting a 10% DMSO/90% H_2O the same as the compound stock solution. Compounds were tested in triplicate from separate cultures and results were averaged (Table 6.8).

Hemolysis Assay

Compounds were serially diluted in sterile DI water from a stock solution (1 mM in 10% DMSO/90% H2O) to yield twelve test concentrations. Defibrinated sheep's blood (Hemostat, DSB030, 1.5 mL) was centrifuged at 10,000 rpm for ten minutes. The supernatant was removed and the blood was resuspended in 1 mL of phosphate buffered saline (PBS). The centrifugation, supernatant removal, and resuspension was repeated three times until the supernatant was clear. The final cell suspension was diluted 1:20 with PBS and aliquoted into the microcentrifuge tubes containing the serially-diluted compounds. Tubes were then incubated at 37 °C for 1 hour with shaking at 200 rpm. Samples were then centrifuged at 10,000 rpm for ten minutes. The supernatant of each sample was carefully transferred to a flat-bottom 96-well plate (Corning 3370), and absorbance measurements were taken at 540 nm using a plate reader. LC20 values were calculated by taking 20% of the difference between the absorbance values of the positive control (TritonX, 1% by volume, 100% lysis marker) and the negative control (sterile PBS, 0% lysis marker) and using that as a cutoff point. Assay was performed in triplicate to ensure reproducibility.

PA14		
Analogue	IC_{50}	R^2
acrylamide 2 (2.13)	5.58	0.938
nitrile 2 (2.10)	3.67	0.970
acrylamide 1 (2.12)	5.24	0.971
nitrile 1 (2.09)	1.58	0.977
boronic acid (2.11)	21.6	0.962
amide acid (2.06)	>250	N/A
dehydroxy-2.01	0.516	0.974
gentamicin	6.16	0.981

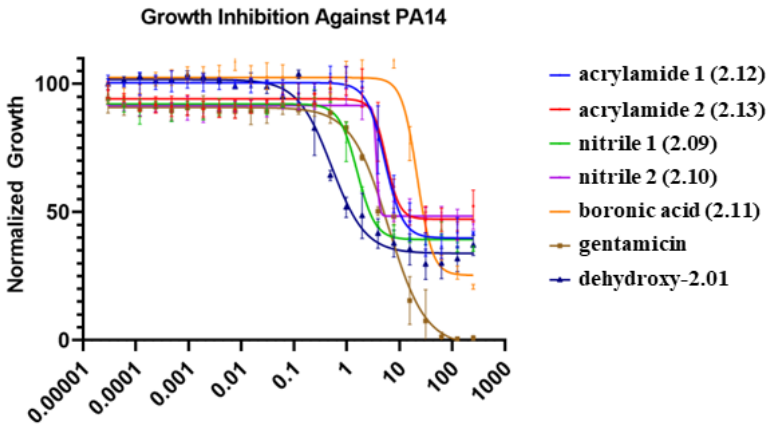

PAO1		
Analogue	IC_{50}	R^2
acrylamide 2 (2.13)	7.69	0.917
nitrile 2 (2.10)	2.56	0.928
acrylamide 1 (2.12)	15.2	0.914
nitrile 1 (2.09)	2.04	0.878
boronic acid (2.11)	42.2	0.670
amide acid (2.06)	>250	N/A
dehydroxy-2.01	3.29	0.920
gentamicin	4.90	0.992

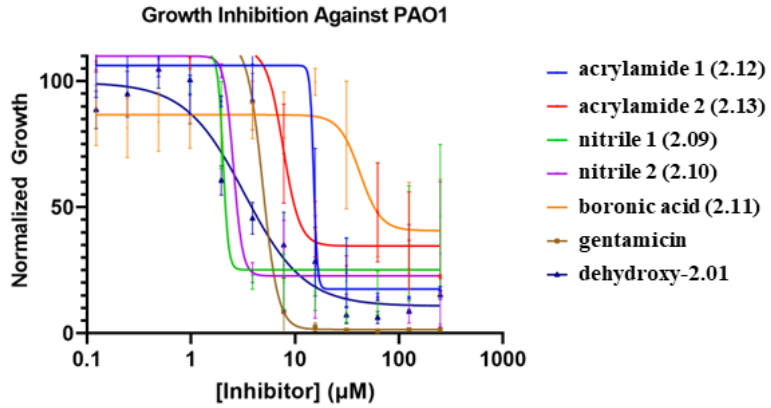

PA14 efflux		
Analogue	IC_{50}	R^2
acrylamide 2 (2.13)	0.388	0.950
nitrile 2 (2.10)	1.28	0.974
acrylamide 1 (2.12)	0.00299	0.920
nitrile 1 (2.09)	0.267	0.977
boronic acid (2.11)	N.T	N/A
amide acid (2.06)	N.T	N/A
dehydroxy-2.01	7.44E-05	0.942
gentamicin	3.50	0.988

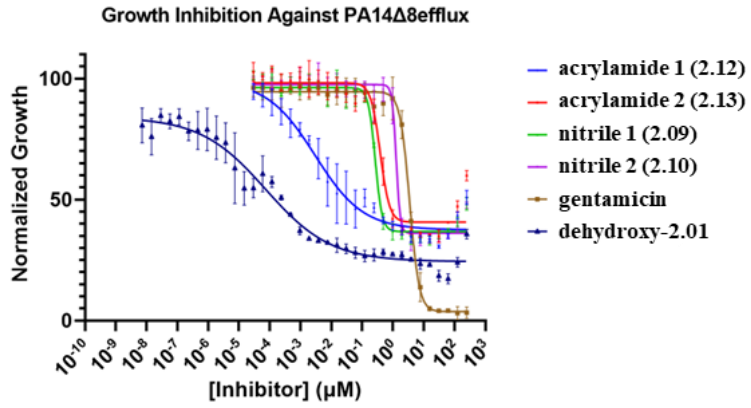

Table 6.4. IC_{50} values (μM) for all active compounds tested

Figure 6.3. IC_{50} curves (μM) for all active compounds tested. Error bars represent ± 1 SEM. Analog dehydroxy-**2.01** was omitted from the curves because its IC_{50} was not below 250 μM

Table 6.5. Hemolysis data for all tricepyridinium compounds tested, with optical densities at LD_{20} highlighted in red for each compound

TRIAL 1	250 µM	125 µM	64 µM	32 µM	16 µM	8 µM	4 µM	2 µM	1 µM	0.5 µM	0.25 µM	0.125 µM
TBS buffer	0.0398	0.0512	0.0487	0.0499	0.0512	0.032	0.0472	0.0486	0.0415	0.0429	0.0443	0.0443
Triton X	0.3677	0.4131	0.7373	0.6971	0.056	0.032	0.0433	0.0437	0.0429	0.0436	0.0446	0.0462
4.09	0.3716	0.1188	0.0549	0.0512	0.05	0.0604	0.0472	0.0468	0.043	0.0414	0.045	0.043
4.10	0.364	0.2074	0.086	0.0683	0.0519	0.0518	0.0504	0.0464	0.0465	0.0432	0.0441	0.044
4.11	0.3261	0.1424	0.0683	0.0514	0.0489	0.0585	0.0458	0.0455	0.0436	0.0399	0.045	0.0438
4.12	0.3862	0.1482	0.0673	0.0537	0.0471	0.0489	0.0443	0.0447	0.0412	0.0343	0.0443	0.0452
4.01	0.3826	0.2132	0.0669	0.0542	0.0492	0.0523	0.0503	0.046	0.0447	0.0391	0.0462	0.0444

TRIAL 2	250 µM	125 µM	64 µM	32 µM	16 µM	8 µM	4 µM	2 µM	1 µM	0.5 µM	0.25 µM	0.125 µM
TBS buffer	0.0405	0.058	0.0444	0.0484	0.0512	0.0483	0.0356	0.0488	0.0531	0.0556	0.0565	0.0516
Triton X	1.0977	1.6338	0.5305	0.0884	0.0466	0.0405	0.0323	0.0467	0.0485	0.0484	0.046	0.0506
4.09	0.4661	0.0744	0.0513	0.05	0.0475	0.0614	0.0547	0.0499	0.0513	0.0501	0.0498	0.0603
4.10	0.5319	0.2851	0.0991	0.0669	0.0489	0.0523	0.0474	0.0489	0.0481	0.0517	0.0514	0.0604
4.11	0.5099	0.1716	0.0626	0.0519	0.0469	0.0524	0.0564	0.0561	0.0542	0.054	0.0552	0.0554
4.12	0.466	0.1924	0.0704	0.0489	0.0463	0.0502	0.0472	0.048	0.0485	0.0499	0.0517	0.0598
4.01	0.5265	0.2732	0.0763	0.0472	0.048	0.0524	0.0544	0.0494	0.0483	0.0508	0.0552	0.0686

TRIAL 3	250 µM	125 µM	64 µM	32 µM	16 µM	8 µM	4 µM	2 µM	1 µM	0.5 µM	0.25 µM	0.125 µM
TBS buffer	0.0437	0.0456	0.0536	0.0706	0.0558	0.0439	0.0529	0.0326	0.0429	0.0454	0.0453	0.0412
Triton X	1.6319	0.98	0.3139	0.0567	0.0488	0.0432	0.0449	0.0481	0.0445	0.0473	0.052	0.0483
4.09	0.5265	0.1268	0.0512	0.0435	0.0446	0.0432	0.0341	0.0498	0.0477	0.0504	0.055	0.046
4.10	0.5469	0.2365	0.1045	0.0686	0.0487	0.0494	0.0528	0.0471	0.0476	0.0486	0.0514	0.0476
4.11	0.4617	0.1601	0.0818	0.0485	0.0485	0.048	0.0494	0.0515	0.0482	0.0516	0.0534	0.0484
4.12	0.5909	0.1718	0.0736	0.0571	0.0495	0.0494	0.0504	0.0472	0.0471	0.0487	0.0492	0.0484
4.01	0.5867	0.2356	0.0842	0.051	0.0491	0.0496	0.051	0.0487	0.0478	0.0495	0.0491	0.0469

6.3 Chemistry

6.3.1 Instrumentation and General Notes

NMR spectra were obtained using the following spectrometers: Varian INOVA 600 (600/150 MHz), Varian INOVA 500 (500/125 MHz) or Varian INOVA 400 (400/100 MHz). Chemical shifts are in ppm relative to TMS and use the indicated solvent as an internal reference. The following abbreviations are used to describe signal multiplicities: s (singlet), d (doublet), t (triplet), q (quartet), m (multiplet), br (broad), dd (doublet of doublets), dt (doublet of triplets), etc. Accurate mass spectra were recorded on a ThermoScientific Exactive Plus Orbitrap MS.

Non-aqueous reactions were performed under an atmosphere of argon, in flame- dried glassware, with HPLC-grade solvents dried by passage through activated alumina. 2,6-lutidine, triethylamine, and diisopropylethylamine were freshly distilled from CaH_2 prior to use. Brine refers to a saturated aqueous solution of sodium chloride, sat. $NaHCO_3$ refers to a saturated aqueous solution of sodium bicarbonate, sat. NH_4Cl refers to a saturated aqueous solution of ammonium chloride, etc. 3Å molecular sieves were activated via storage in a 120 °C oven, and flame-dried under vacuum before use. “Column chromatography” refers to purification in a normal-phase gradient on a Biotage® flash chromatography purification system. Metathesis catalysts were obtained as generous gifts from Materia, Inc. All other chemicals were used as received from Oakwood, TCI America, Sigma-Aldrich, Alfa Aesar, Ambeed, CombiBlocks, or AK Scientific. All synthetic analogs undergoing biological testing were purified to >95% purity by HPLC using a gradient of 5-95% ACN/H_2O.

6.3.2 Promysalin Experimental Procedures and Characterization Data

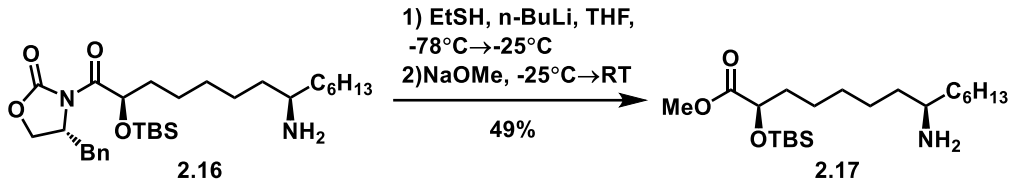

Methyl (2R,8R)-8-amino-2-((tert-butyldimethylsilyl)oxy)tetradecanoate 2.17. A solution of ethanethiol (0.565 mL, 7.630 mmol, 62 eq.) dissolved in tetrahydrofuran (2 mL) was cooled to -78°C and n-BuLi (2M in hexanes, 0.123 mL, 0.246 mmol, 2 eq.) was added dropwise. The solution was stirred for 30 minutes at -78°C, then oxazolidinone **2.16**[95] (65.5 mg, 0.123 mmol, 1 eq.) dissolved in tetrahydrofuran (2 mL) was added dropwise). The solution was warmed to -20°C and stirred for an additional 30 minutes. A freshly-prepared solution of 30% sodium hydroxide in methanol (v/v, 0.390 mL, 3 eq) was added dropwise. The reaction was allowed to warm to room temperature over 3.5 hours, at which point it was concentrated under reduced pressure. Product was purified by silica column chromatography (20-100% EtOAc in hexanes, then 0-100% iPrOH in hexanes) to yield the title compound as a pale yellow oil (23.2 mg, 49% yield).

^{1}H NMR (600 MHz, $CDCl_3$): δ 4.17 (t, J = 5.8 Hz, 1H), 3.70 (s, 3H), 2.12 (br s, 1 H), 1.80-1.54 (m, 7H), 1.54 – 1.03 (m, 22H), 1.03 – 0.63 (m, 15H), 0.05 (d, J = 12.8 Hz, 6H). **^{13}C NMR** (125 MHz, $CDCl_3$): δ 174.2, 77.3, 77.0, 76.8, 72.1, 52.5, 51.7, 35.0, 32.58, 32.51, 31.5, 29.0, 28.9, 25.8, 25.7, 25.21, 25.17, 24.8, 22.6, 22.4, 18.3, 14.0, -5.0, -5.3. **HRMS** Accurate Mass (ES^+): Found 388.32375 (-1.02 ppm), $C_{21}H_{46}O_3N^{28}Si$ ($M + H^+$) requires 388.32415.

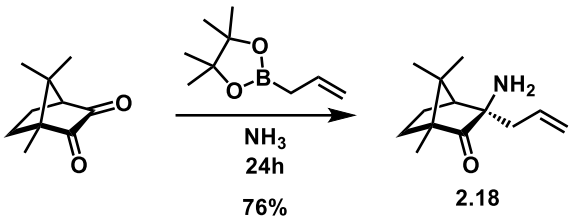

(1S,3R,4S)-3-allyl-3-amino-1,7,7-trimethylbicyclo[2.2.1]heptan-2-one 2.18. To a solution of (R)-camphorquinone (560 mg, 3.37 mmol, 1.0 eq.) in methanolic ammonia (7N, 5 mL) was added allylboronic acid pinacol ester (0.947 mL, 848 mg, 5.05 mmol, 1.5 eq.) dropwise. The reaction stirred at room temperature for 24 hours, turning pale yellow. Reaction solution was acidified to pH 1 with 3M HCl, turning bright yellow. After stirring an additional 30 minutes, the aqueous layer was washed thrice with DCM. Additional 3M HCl was added to the organic layer and this aqueous layer was washed thrice with DCM. Aqueous layers were combined and basified to pH 10 with 6M NaOH. DCM was added and the aqueous layer was extracted 4x. Combined organic layers were dried over anhydrous $MgSO_4$, filtered, and concentrated *in vacuo*. Crude product was purified by silica column chromatography (25% EtOAc/hexanes, isocratic), affording the title compound as a pale yellow oil (528 mg, 76% yield). Spectral data are consistent with literature reports.

^{1}H NMR (400 MHz, $CDCl_3$): δ 5.85 (dddd, *J* = 16.8, 10.3, 7.9, 6.3 Hz, 1H), 5.21 – 5.12 (m, 2H), 2.25 (dd, *J* = 14.5, 6.3 Hz, 1H), 2.10 (dd, *J* = 14.5, 7.9 Hz, 1H), 1.93 – 1.84 (m, 2H), 1.70 – 1.62 (m, 2H), 1.51 – 1.44 (m, 2H), 1.07 (s, 3H), 1.00 (s, 3H), 0.91 (s, 3H).

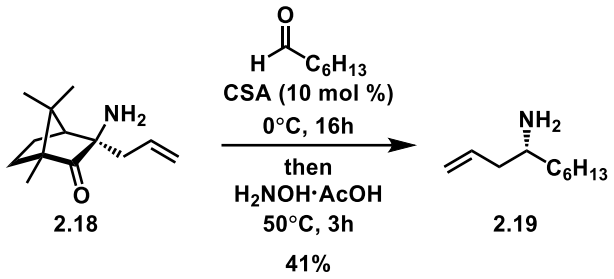

(R)-dec-1-en-4-amine 2.19. A solution of amine **2.18** (104 mg, 0.500 mmol, 1.0 eq.) in DCE (1 mL) was cooled to 0°C. Heptanal (0.07 mL, 57.1 mg, 0.500 mmol, 1.0 eq.) was added, followed by camphorsulfonic acid (19.3 mg, 0.0830 mmol, 0.17 eq.). The reaction temperature was maintained at 0°C as it stirred overnight. Hydroxylamine acetate (2 mL) was added, the reaction was heated to 50°C, and continued to stir 3 hours. The solution pH was brought to 1 using HCl (3M) and the reaction stirred an additional 30 minutes. The aqueous layer was washed thrice with DCM, then was basified to pH 10 using 6M NaOH and extracted thrice with DCM. Combined organic layers were dried over anhydrous $MgSO_4$, filtered, and concentrated *in vacuo*. Crude product was purified via preparative TLC (100% EtOAc, eluted off silica with 7:1 hexanes:triethylamine), yielding the title compound as a low-melting solid (32.0 mg, 41% yield). Spectral data are consistent with literature reports.

^{1}H NMR (400 MHz, $CDCl_3$): δ 5.76 (ddt, *J* = 14.5, 10.5, 7.2 Hz, 1H), 5.12 – 5.03 (m, 2H), 3.26 (dt, *J* = 13.1, 6.9 Hz, 2H), 2.79 (br s, 1H), 2.23 (dt, *J* = 11.2, 5.3 Hz, 1H), 2.01 (dt, *J* = 14.7, 7.9 Hz, 1H), 1.93 (d, *J* = 7.4 Hz, 1H), 1.34 – 1.19 (m, 11H), 0.85 (t, *J* = 6.5 Hz, 3H).

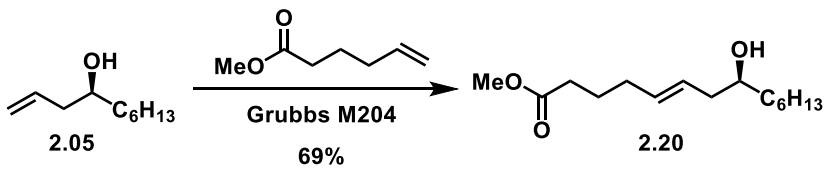

Methyl (S,E)-8-hydroxytetradec-5-enoate 2.20. A 10 mL round-bottom flask was flame-dried and purged thrice with argon. **2.05**[93] (306.9 mg, 1.964 mmol, 1.0 eq.), methyl hex-5-enoate (1.12 mL, 7.856 mmol, 4.0 eq.), and Grubbs II catalyst (M204, 166.9 mg, 0.196 mmol, 0.1 eq.) were sequentially added. The dark red reaction stirred at room temperature overnight. Crude product was purified by silica column chromatography (50-100% DCM/hexanes to remove ester dimer, then 0-10% EtOAc/DCM to elute cross product), yielding the title compound as a brown oil (348.5 mg, 69% yield).

^{1}H NMR (500 MHz, $CDCl_3$): δ 5.56 – 5.38 (m, 2H), 3.66 (s, 3H), 3.61 – 3.54 (m, 1H), 2.31 (t, J = 7.5 Hz, 2H), 2.22 (dq, J = 14.4, 4.4 Hz, 1H), 2.10 – 2.03 (m, 3H), 1.75 – 1.67 (m, 2H), 1.61 (s, 2H), 1.43 (t, J = 5.7 Hz, 3H), 1.33 – 1.22 (m, 8H), 0.89 – 0.85 (m, 3H). **^{13}C NMR** (125 MHz, $CDCl_3$): δ 174.3, 133.1, 127.4, 71.1, 51.7, 40.8, 36.9, 33.5, 32.1, 32.0, 29.5, 25.8, 24.6, 22.8, 14.2. **$[\alpha]^{25}_D$** +0.33 (c 0.60, $CHCl_3$). **HRMS** Accurate Mass (ES^+): Found 257.21101 (-0.43 ppm), $C_{15}H_{29}O_3$ ($M + H^+$) requires 257.21112.

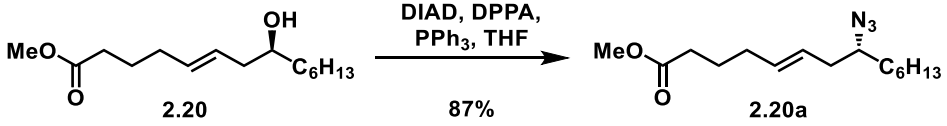

Methyl (R,E)-8-azidotetradec-5-enoate 2.20a. A 10 mL round-bottom flask was flame-dried and purged thrice with argon. Alcohol **2.20** (250 mg, 0.975 mmol, 1.0 eq.) and triphenylphosphine (1.023 g, 3.900 mmol, 4.0 eq.) were added and dissolved in THF (12 mL). The solution was cooled

to 0°C and diisopropyl azodicarboxylate (0.758 mL, 3.900 mmol, 4.0 eq.) and diphenylphosphoryl azide (0.839 mL, 3.900 mmol, 4.0 eq.) were added dropwise. The cloudy white solution was warmed to RT and stirred two hours, then was heated to 45°C and stirred two additional hours, steadily turning more yellow and less cloudy. Crude product was concentrated *in vacuo* and purified by silica column chromatography (10% EtOAc/hexanes, coeluting with DIAD and PPh_3). Product was further purified by preparative TLC (10% EtOAc/hexanes) and triturated with cold pentane. Solution was decanted and concentrated *in vacuo*, affording the title compound as a clear oil (239.2 mg, 87% yield).

^{1}H NMR (600 MHz, $CDCl_3$): δ 5.50 (dq, J = 11.6, 5.9, 5.2 Hz, 1H), 5.43 (dt, J = 15.0, 6.9 Hz, 1H), 3.66 (s, 3H), 3.26 (dt, J = 13.0, 5.8 Hz, 1H), 2.31 (t, J = 7.5 Hz, 2H), 2.24 (dp, J = 14.1, 7.0 Hz, 2H), 2.09 – 2.03 (m, 2H), 1.71 (p, J = 7.5 Hz, 2H), 1.52 – 1.39 (m, 3H), 1.30 (dd, J = 13.9, 8.4 Hz, 7H), 0.88 (t, J = 6.9 Hz, 3H). **^{13}C NMR** (151 MHz, $CDCl_3$): δ 174.2, 133.0, 126.6, 62.9, 51.6, 37.8, 34.0, 33.5, 32.1, 31.8, 29.2, 26.2, 24.6, 22.7, 14.2. **$[\alpha]^{25}_D$** +10.4 (c 0.45, $CHCl_3$). **HRMS** Accurate Mass (ES^+): Found 304.19946 (-0.28 ppm), $C_{15}H_{27}O_2N_3{}^{23}Na$ ($M + Na^+$) requires 304.19955.

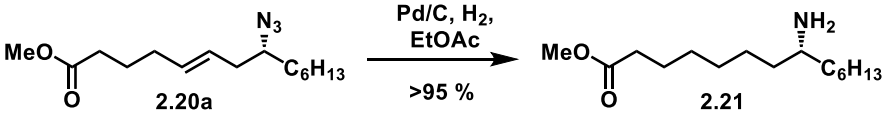

Methyl (R)-8-aminotetradecanoate 2.21. A 20 mL scintillation vial containing azide **2.20a** (77.2 mg, 0.274 mmol, 1.0 eq.) was purged thrice with argon. Palladium on activated carbon (10% Pd, 29.2 mg, 0.274 mmol, 1.0 eq.) was added, followed by ethyl acetate (3 mL). The vial was purged five times with hydrogen and the reaction was left to stir under hydrogen atmosphere (1 atm) for

16 hours. The dark grey suspension was filtered over a pad of celite, eluting with 100% EtOAc, and concentrated *in vacuo*. Product was purified by silica column chromatography (0-10% MeOH/DCM) to yield the title compound as a pale yellow oil (70.1 mg, >95% yield).

^{1}H NMR (500 MHz, $CDCl_3$): δ 3.69-3.57 (m, 5H), 2.74 (br s, 1H), 2.25 (t, J = 7.5 Hz, 2H), 1.61 – 1.53 (m, 2H), 1.45 – 1.38 (m, 2H), 1.37 – 1.18 (m, 17H), 0.83 (t, J = 6.3 Hz, 3H). **^{13}C NMR** (126 MHz, $CDCl_3$): δ 174.3, 51.49, 51.47, 36.5, 36.4, 34.1, 31.8, 29.4, 29.3, 29.1, 25.9, 25.8, 24.9, 22.7, 14.1. **$[\alpha]^{25}_D$** -0.43 (c 0.375, $CHCl_3$). **HRMS** Accurate Mass (ES^+): Found 258.24301 (+ 1.00 ppm), $C_{15}H_{32}O_2N$ ($M + H^+$) requires 258.24276.

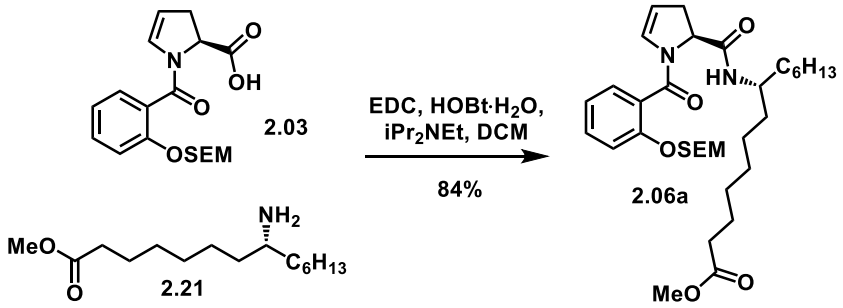

Methyl (R)-8-((S)-1-(2-hydroxybenzoyl)-2,3-dihydro-1H-pyrrole-2-carboxamido)tetradecanoate 2.06a. A 20 mL scintillation vial containing acid **2.03**[93] (48.0 mg, 0.132 mmol, 1.5 eq.) and 3Å molecular sieves was purged 3x with argon. DCM (2.5 mL) was added and the flask was cooled to 0°C. EDC (26.0 mg, 0.132 mmol, 1.5 eq.), HOBt•H_2O (16.0 mg, 0.091 mmol, 1.0 eq.), and diisopropylethylamine (0.040 mL, 0.23 mmol, 2.5 eq.) were added sequentially. Amine **2.21** (22.0 mg, 0.091 mmol, 1.0 eq.) was transferred into the vial dropwise in DCM (2.5 mL). The reaction stirred overnight, allowing it to warm to room temperature. Water was added and the aqueous layer was extracted 5x with DCM, washed once with brine, and back-

extracted twice. Combined organic layers were dried over anhydrous Na_2SO_4, filtered, and concentrated *in vacuo.* Crude product was purified by silica column chromatography (15-35% EtOAc/hex) to yield a yellow oil (43.5 mg, 84% yield).

^{1}H NMR (500 MHz, $CDCl_3$): δ 7.37 (td, J = 8.7, 1.6 Hz, 1H), 7.28 (br s, 1H), 7.23 (d, J = 8.4 Hz, 1H), 7.05 (t, J = 7.4 Hz, 1H), 6.04 (s, 1H), 5.28 – 5.18 (m, 2H), 5.17 – 5.11 (m, 1H), 5.08 – 5.03 (m, 1H), 3.90 (br s, 1H), 3.71 (td, J = 8.6, 3.5 Hz, 2H), 3.63 (s, 3H), 3.03 (d, J = 74.6 Hz, 2H), 2.25 (t, J = 7.5 Hz, 2H), 1.56 (p, J = 7.5 Hz, 2H), 1.51 – 1.43 (m, 2H), 1.37 – 1.18 (m, 17H), 0.96 – 0.90 (m, 2H), 0.82 (t, J = 6.6 Hz, 3H), -0.03 (s, 9H). **^{13}C NMR** (151 MHz, $CDCl_3$): δ 174.3, 169.8, 166.0, 153.6, 131.5, 129.6, 128.5, 125.5, 122.2, 114.8, 111.8, 93.2, 66.9, 59.5, 51.5, 49.4, 35.5, 35.4, 34.1, 31.8, 29.8, 29.32, 29.30, 29.2, 25.8, 25.7, 25.0, 22.7, 18.2, 14.2, -1.3. **$[\alpha]^{25}_D$** -52.132 (c 0.333, $CHCl_3$). **HRMS** Accurate Mass (ES^+): Found 603.38282 (+ 0.71 ppm), $C_{33}H_{55}O_6N_2{}^{28}Si$ (M + H^+) requires 603.38239.

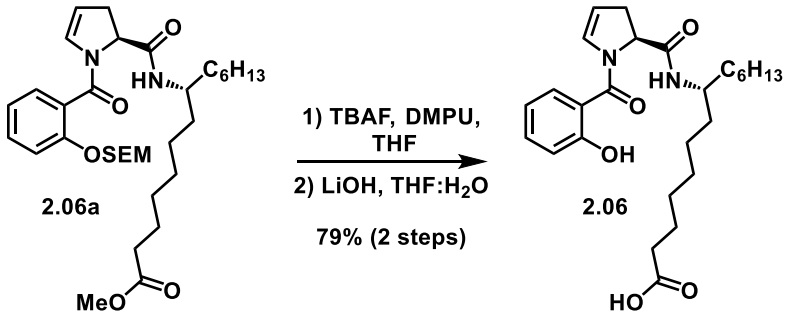

(R)-8-((S)-1-(2-hydroxybenzoyl)-2,3-dihydro-1H-pyrrole-2-carboxamido)tetradecanoic acid 2.06. A 20 mL scintillation vial containing SEM-protected methyl ester **2.06a** (38.3 mg, 0.064 mmol, 1.0 eq.) was purged thrice with argon. DMPU (1.27 mL) was added, followed by TBAF (1M in THF 1.27 mL, 1.27 mmol, 20 eq.), turning the solution a golden color. The reaction stirred

at room temperature for 3 hours, then was quenched with saturated aqueous NH_4Cl (3 mL) and acidified to pH=5. The organic layer was extracted 5x with Et_2O, washed 5x with saturated aqueous NH_4Cl and 5x with brine, and dried over Na_2SO_4, then filtered and concentrated *in vacuo*. Column chromatography (0-75% EtOAc/hexanes) yielded deprotected methyl ester intermediate.

^{1}H NMR (600 MHz, $CDCl_3$): δ 9.67 (s, 1H), 7.40 – 7.34 (m, 2H), 7.00 (d, J = 8.3 Hz, 1H), 6.89 (t, J = 7.6 Hz, 1H), 6.66 (s, 1H), 6.40 (s, 1H), 5.34 (s, 1H), 5.04 (dd, J = 10.4, 3.9 Hz, 1H), 3.89 (qt, J = 8.6, 5.2 Hz, 1H), 3.66 (s, 3H), 3.10 (d, J = 16.1 Hz, 1H), 2.95 (d, J = 11.8 Hz, 1H), 2.23 (t, J = 7.5 Hz, 2H), 1.56 – 1.50 (m, 2H), 1.49 – 1.43 (m, 2H), 1.40 – 1.17 (m, 20H), 0.86 (t, J = 6.9 Hz, 3H).

To this intermediate, THF (4 mL) was added, followed by a solution of LiOH (5.1 mg, 0.212 mmol, 10.0 eq.) in H_2O (0.75 mL). The solution was stirred at room temperature for 4 hours, then was carefully acidified to pH = 4 using HCl (1M) and the aqueous layer was extracted 5x with EtOAc. Combined organic layers were washed twice with brine, back-extracted twice, dried over anhydrous Na_2SO_4, filtered, and concentrated *in vacuo.* Crude product was purified by HPLC to afford the title compound as an off-white solid (7.7 mg, 79% yield).

^{1}H NMR (600 MHz, $CDCl_3$): δ 7.41 – 7.32 (m, 2H), 6.99 (d, J = 8.2 Hz, 1H), 6.89 (t, J = 7.5 Hz, 1H), 6.61 (s, 1H), 6.44 (s, 1H), 5.33 (s, 1H), 5.06 (dd, J = 10.1, 4.3 Hz, 1H), 3.90 (qt, J = 8.2, 5.3 Hz, 1H), 3.03 – 2.95 (m, 2H), 2.26 (h, J = 8.3 Hz, 2H), 1.57 – 1.50 (m, 2H), 1.49 – 1.42 (m, 2H), 1.42 – 1.35 (m, 2H), 1.35 – 1.16 (m, 20H), 0.86 (t, J = 6.9 Hz, 3H). **^{13}C NMR** (151 MHz, $CDCl_3$): δ 178.3, 170.0, 162.4, 157.7, 133.5, 130.2, 128.5, 119.4, 118.0, 117.0, 113.0, 60.9, 52.4, 49.9, 35.3, 35.1, 34.0, 31.9, 29.3, 28.9, 28.8, 26.0, 25.4, 24.5, 22.7, 20.3, 14.2. **$[\alpha]^{25}_D$** -55.35 (c 0.390, $CHCl_3$). **HRMS** Accurate Mass (ES+): Found 459.28528 (- 0.16 ppm), $C_{26}H_{39}O_5N_2$ (M + H+) requires 459.28535.

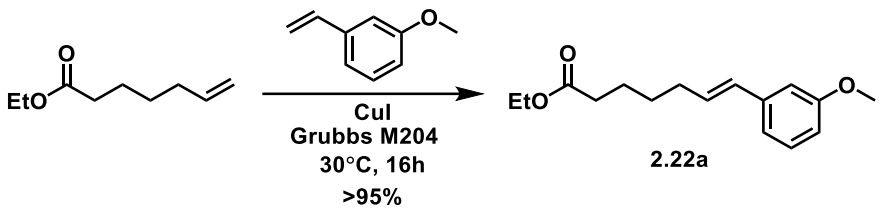

Ethyl (E)-7-(3-methoxyphenyl)hept-6-enoate 2.22a. To a flame-dried sample of copper (I) iodide (14.6 mg, 0.0768 mmol, 0.15 eq.) was sequentially added ethyl hept-6-enoate (80.0 mg, 0.512 mmol, 1.0 eq.), 3-vinylanisole (0.355 mL, 344 mg, 2.56 mmol, 5.0 eq.), Grubbs M204 catalyst (43.5 mg, 0.0512 mmol, 0.10 eq.), and DCM (1 mL). Reaction was warmed to 30 °C and stirred overnight, then was concentrated in vacuo and purified by silica column chromatography (0-4% EtOAc/hexanes), affording product as a colorless oil (153 mg, >95% yield).

^{1}H NMR (600 MHz, $CDCl_3$): δ 7.20 (t, *J* = 7.9 Hz, 1H), 6.93 (d, *J* = 7.6 Hz, 1H), 6.88 (s, 1H), 6.75 (dd, *J* = 8.1, 2.4 Hz, 1H), 6.36 (d, *J* = 15.8 Hz, 1H), 6.20 (dt, *J* = 15.7, 6.9 Hz, 1H), 4.13 (q, *J* = 7.1 Hz, 2H), 3.81 (s, 3H), 2.33 (t, *J* = 7.5 Hz, 2H), 2.23 (q, *J* = 8.0 Hz, 2H), 1.69 (dt, *J* = 15.3, 7.5 Hz, 2H), 1.55 – 1.47 (m, 2H), 1.51 (dt, *J* = 15.3, 7.6 Hz, 2H), 1.26 (t, *J* = 7.1 Hz, 3H). **^{13}C NMR** (151 MHz, $CDCl_3$): δ 173.7, 159.8, 139.2, 130.7, 130.0, 129.4, 118.6, 112.5, 111.3, 60.2, 55.1, 34.2, 32.6, 28.8, 24.5, 14.2.

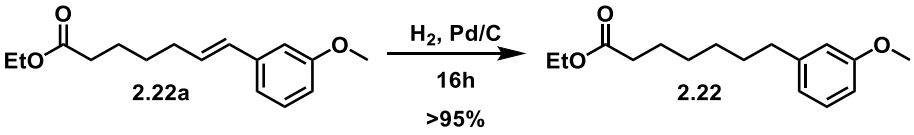

Ethyl 7-(3-methoxyphenyl)heptanoate 2.22. Alkene **2.22a** (153 mg, 0.583 mmol, 1.0 eq.) and palladium on activated carbon (10% Pd, 62 mg, 0.0583 mmol, 0.10 eq.) were combined and dissolved in ethyl acetate (4 mL). The reaction vessel was evacuated and backfilled with hydrogen

gas four times, then the reaction was left to stir under a hydrogen atmosphere (1 atm) for 16 hours. The dark grey suspension was filtered through Celite, eluting with 100% ethyl acetate to afford the title compound as an off-white solid (158.0 mg, >95% yield).

^{1}H NMR (600 MHz, $CDCl_3$): δ 7.21 – 7.16 (m, 1H), 6.76 (d, *J* = 7.5 Hz, 1H), 6.74 – 6.69 (m, 2H), 4.12 (q, *J* = 7.1 Hz, 3H), 3.80 (s, 3H), 2.57 (t, J = 7.8 Hz, 2H), 2.28 (t, *J* = 7.5 Hz, 3H), 1.65 – 1.57 (m, 5H), 1.37 – 1.32 (m, 4H), 1.25 (t, *J* = 7.1 Hz, 3H). **^{13}C NMR** (151 MHz, $CDCl_3$): δ 173.8, 159.6, 144.3, 129.2, 120.8, 114.2, 110.8, 60.1, 55.1, 35.9, 34.3, 31.1, 29.00, 28.9, 24.9, 14.2.

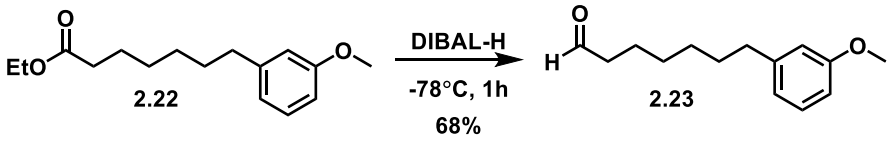

7-(3-methoxyphenyl)heptanal 2.23. A solution of ester **2.22** (414.1 mg, 1.57 mmol, 1.0 eq.) in DCM (10 mL) was cooled to -78 °C. DIBAL-H (1M in DCM, 1.72 mL, 245 mg, 1.72 mmol, 1.1 eq.) was added dropwise over 5 minutes and the reaction stirred at -78 °C for 1 hour. Rochelle's salt (5 mL) was added to quench the reaction, which continued to stir overnight. Solution pH was neutralized and aqueous layer was extracted 6x with DCM and washed once with brine. Combined organic layers were then dried over anhydrous Na_2SO_4, filtered, and concentrated *in vacuo*. Crude product was purified by silica column chromatography (0-8% EtOAc/hexanes), affording the title compound as a colourless oil (233 mg, 68% yield).

^{1}H NMR (500 MHz, $CDCl_3$): δ 9.76 (s, 1H), 7.22 – 7.16 (m, 1H), 6.78 – 6.74 (m, 1H), 6.73 (dt, *J* = 6.8, 1.4 Hz, 2H), 3.80 (s, 3H), 2.61 – 2.53 (m, 2H), 2.42 (td, *J* = 7.3, 1.8 Hz, 2H), 1.69 – 1.55 (m, 5H), 1.35 (t, *J* = 7.4 Hz, 3H). **^{13}C NMR** (126 MHz, $CDCl_3$): δ 202.9, 159.5, 144.3, 129.2, 120.8, 114.2, 110.8, 55.1, 43.8, 35.9, 31.1, 28.98, 28.95, 22.0.

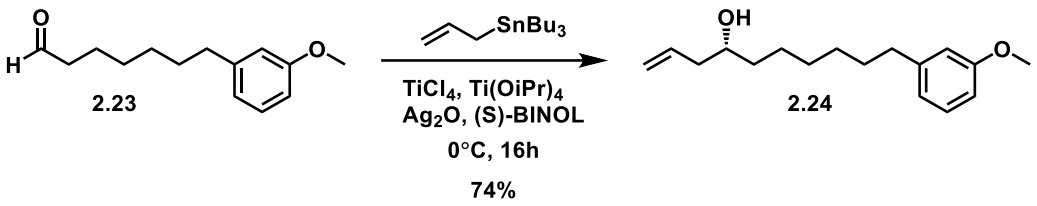

(R)-10-(3-methoxyphenyl)dec-1-en-4-ol 2.24. A solution of $Ti(OiPr)_4$ (0.0358 mL, 33.5 mg, 0.118 mmol, 0.10 eq.) in DCM (1 mL) was cooled to 0 °C. $TiCl_4$ (1M in DCM, 0.059 mL, 11.2 mg, 0.059 mmol, 0.050 eq.) was added and the pale yellow solution was warmed to RT and stirred 1 hour. Silver (I) oxide (27.3 mg, 0.118 mmol, 0.10 eq.) was added and the flask was covered in aluminum foil. Reaction continued to stir at room temperature for 5 hours. The aluminum foil was removed from the flask and (S)-BINOL (67.6 mg, 0.236 mmol, 0.20 eq.) was added, turning the solution orange-brown. Reaction continued to stir 2 hours at room temperature, then was cooled to 0 °C. Aldehyde **2.23** (260 mg, 1.18 mmol, 1.0 eq.) and allyltributylstannane (0.476 mL, 508 mg, 1.53 mmol, 1.3 eq.) were added sequentially, and the reaction temperature was maintained at 0 °C overnight. The reaction was then warmed to room temperature and quenched with 15 mL saturated aqueous NaHCO3 and three scoops of celite, stirring for 1 hour. The aqueous layer was extracted 5x with Et_2O, keeping each organic layer separate. Saturated aqueous KF was added to each organic layer and swirled vigorously. One at a time, each organic layer was added into the separatory funnel and the aqueous layer was removed. Combined organic layers were washed 3x with brine, then dried over anhydrous Na_2SO_4, filtered, and concentrated *in vacuo*. Product was purified by silica column chromatography (0-15% EtOAc/hexanes), yielding the title compound as a colourless oil (230 mg, 74% yield).

^{1}H NMR (600 MHz, $CDCl_3$): δ 7.19 (t, *J* = 8.2 Hz, 1H), 6.77 (d, *J* = 7.5 Hz, 1H), 6.72 (d, *J* = 6.3 Hz, 2H), 5.91 – 5.75 (m, 1H), 5.18 – 5.08 (m, 2H), 3.80 (s, 3H), 3.63 (br s, 1H), 2.61 – 2.54 (m, 2H), 2.33 – 2.25 (m, 1H), 2.13 (dt, *J* = 14.7, 7.9 Hz, 1H), 1.67 – 1.54 (m, 5H), 1.48 – 1.42 (m, 3H),

1.38 – 1.28 (m, 7H). **^{13}C NMR** (101 MHz, $CDCl_3$): δ 159.6, 144.5, 134.9, 129.2, 120.9, 118.2, 114.2, 110.8, 70.6, 55.1, 42.0, 36.8, 36.0, 31.3, 29.5, 29.3, 25.6.

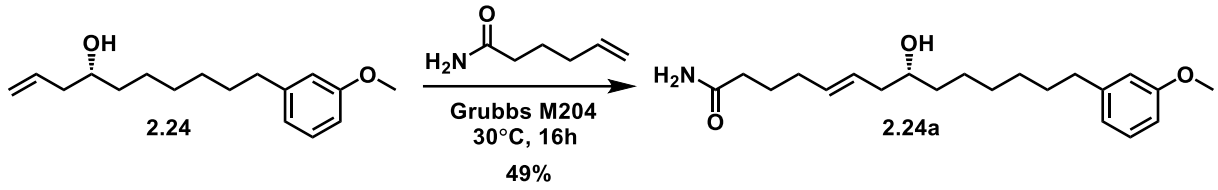

(R,E)-8-hydroxy-14-(3-methoxyphenyl)tetradec-5-enamide 2.24a. To a solution of alcohol **2.24** (211.2 mg, 0.805 mmol, 1.0 eq.) and oct-7-enamide[95] (568.3 mg, 4.03 mmol, 5.0 eq.) in DCM was added Grubbs M204 catalyst(68.4 mg, 0.0805 mmol, 0.10 eq.). Due to insolubility of oct-7-enamide, EtOAc (2 mL) was added as a cosolvent. The cloudy brown solution was heated to 30 °C and stirred overnight. Solvent was evaporated *in vacuo* and crude product was purified by silica column chromatography (0-10% MeOH/DCM), affording the title compound as an off-white solid.

^{1}H NMR (500 MHz, $CDCl_3$): δ 7.21 – 7.14 (m, 1H), 6.76 (d, *J* = 7.5 Hz, 1H), 6.71 (d, *J* = 6.5 Hz, 2H), 5.86 (d, *J* = 32.8 Hz, 2H), 5.56 – 5.35 (m, 2H), 3.78 (s, 3H), 3.56 (br s, 1H), 2.56 (t, *J* = 9.4 Hz, 2H), 2.19 (t, *J* = 7.5 Hz, 4H), 2.14 – 1.99 (m, 3H), 1.75 – 1.55 (m, 5H), 1.47 – 1.38 (m, 3H), 1.35 – 1.27 (m, 5H). **^{13}C NMR** (101 MHz, $CDCl_3$): δ 175.9, 159.5, 144.5, 132.8, 129.2, 127.6, 120.9, 114.2, 110.8, 71.0, 55.1, 40.7, 36.9, 36.0, 35.0, 31.9, 31.3, 29.6, 29.3, 25.7, 24.9.

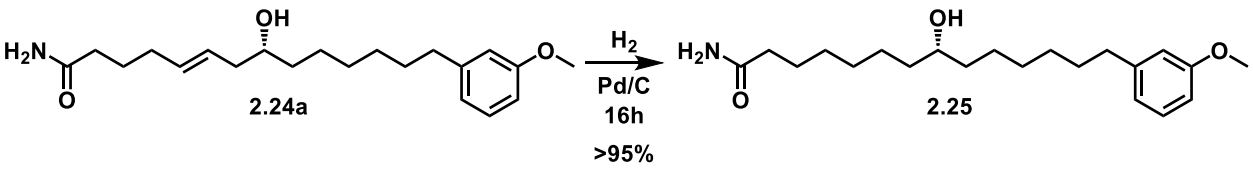

(R)-8-hydroxy-14-(3-methoxyphenyl)tetradecanamide 2.25. Alkene **2.24a** (34.0 mg, 0.0905 mmol, 1.0 eq.) and palladium on activated carbon (10% Pd, 9.6 mg, 0.00905 mmol, 0.10 eq.) were combined and dissolved in ethyl acetate (3 mL). The reaction vessel was evacuated and backfilled with hydrogen gas four times, then the reaction was left to stir under a hydrogen atmosphere (1 atm) for 16 hours. The dark grey suspension was filtered through Celite, eluting with 100% ethyl acetate to afford the title compound as an off-white solid (34.0 mg, >95% yield).

^{1}H NMR (500 MHz, $CDCl_3$): δ 7.22 – 7.12 (m, 1H), 6.76 (d, *J* = 7.4 Hz, 1H), 6.71 (d, *J* = 6.6 Hz, 2H), 5.85 (s, 1H), 5.64 (s, 1H), 3.78 (s, 3H), 3.54 (s, 1H), 2.57 (t, *J* = 9.4 Hz, 2H), 2.19 (t, *J* = 7.6 Hz, 2H), 1.67 – 1.53 (m, 5H), 1.46 – 1.36 (m, 5H), 1.37 – 1.26 (m, 10H). **^{13}C NMR** (126 MHz, $CDCl_3$): δ 176.0, 159.6, 144.6, 129.3, 121.0, 114.3, 110.9, 71.9, 55.2, 37.6, 37.4, 36.1, 36.0, 31.4, 29.7, 29.42, 29.37, 29.2, 25.7, 25.53, 25.50.

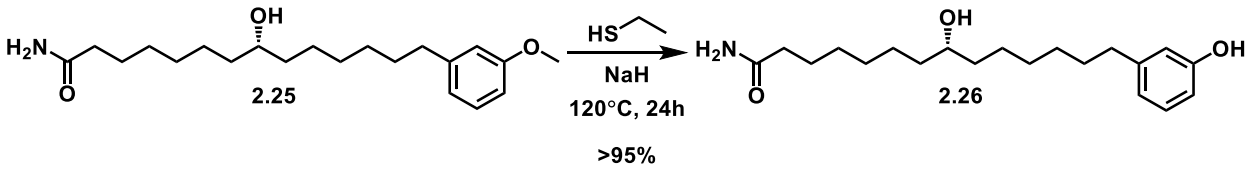

(R)-8-hydroxy-14-(3-hydroxyphenyl)tetradecanamide 2.26. Sodium hydride (60% dispersion, 40.0 mg, 1.0 mmol) was dissolved in DMF (2 mL) and cooled to 0°C. Ethanethiol (93.1 mg, 0.11 mL, 1.5 mmol) was added and the solution was warmed to room temperature and stirred 15 minutes, turning light pink. An aliquot of this ethanethiolate solution (0.5 M, 0.5 mL, 0.25 mmol, 7.2 eq.) was added to anisole **2.25** (12.1 mg, 0.0346 mmol, 1.0 eq.). The solution was heated to

120 °C and stirred for 5 hours, turning yellow. An additional 0.5 mL of ethanethiolate solution was added, and the reaction stirred overnight at 120 °C. The reaction was then cooled to RT and quenched with 2 mL sat. aq. NH_4Cl. Residual ethanethiolate was removed *in vacuo*, and the remaining solution was diluted with DCM and water, then the aqueous layer was extracted 3x with DCM. Combined organic layers were washed once with brine, then dried over anhydrous Na_2SO_4, filtered and concentrated *in vacuo*, yielding crude product as a yellow oil. This product was further purified via preparative TLC (10% MeOH/DCM), affording the title compound as a white solid (11.7 mg, >95% yield).

^{1}H NMR (500 MHz, $CDCl_3$): δ 7.12 (t, J = 7.7 Hz, 1H), 6.77 – 6.62 (m, 3H), 5.61 (br s, 1H), 5.52 (br s, 1H), 3.58 (s, 1H), 2.60 – 2.52 (m, 2H), 2.23 (t, J = 7.5 Hz, 2H), 1.71 – 1.57 (m, 6H), 1.39 – 1.23 (m, 24H), 0.92 – 0.79 (m, 4H).

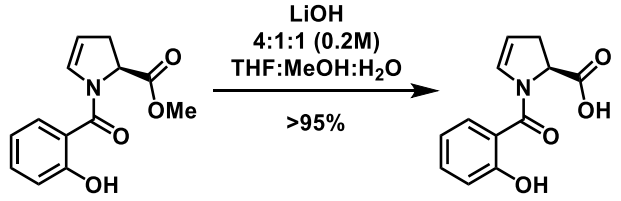

2.03a

(S)-1-(2-hydroxybenzoyl)-2,3-dihydro-1H-pyrrole-2-carboxylic acid 2.03a. To a solution of methyl (S)-1-(2-hydroxybenzoyl)-2,3-dihydro-1H-pyrrole-2-carboxylate[95] (31.2 mg, 0.126 mmol, 1 eq.) dissolved in 4:1 THF:MeOH (2.5 mL) was added a solution of LiOH (52.9 mg, 1.26 mmol, 10 eq.) dissolved in water (0.5 mL) dropwise. The reaction was stirred for 5 hours at room temperature, then was carefully acidified to pH=5 with 1M HCl. The organic layer was extracted 5x with dichloromethane and washed once with brine, then was dried over anhydrous Na_2SO_4,

filtered, and concentrated to afford the title compound as a pale yellow oil that was used in the next step without further purification (30.4 mg, >95% yield).

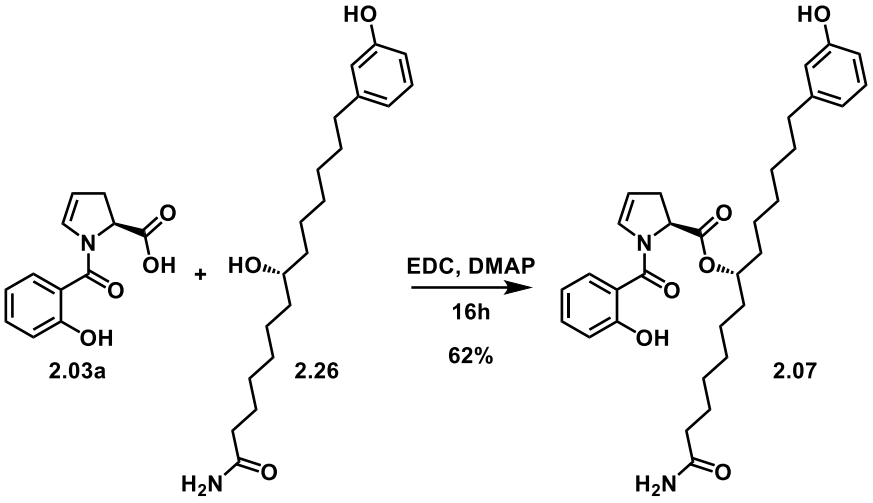

(R)-14-amino-1-(3-hydroxyphenyl)-14-oxotetradecan-7-yl (S)-1-(2-hydroxybenzoyl)-2,3-dihydro-1H-pyrrole-2-carboxylate 2.07. To a solution of acid **2.03a** (20.3 mg, 0.0872 mmol, 2.5 eq.) in DCM (2.5 mL) at 0°C was added EDC (16.7 mg, 0.0872 mmol, 2.5 eq.) and DMAP (10.7 mg, 0.0872 mmol, 2.5 eq.). A solution of alcohol **2.26** (11.7 mg, 0.0349 mmol, 1.0 eq.) in DCM (1.5 mL) was added dropwise. The reaction stirred overnight, allowing it to warm to room temperature. The reaction was added to water, and the organic layer was extracted 4x with DCM. Combined organic layers were washed once with brine, dried over anhydrous Na_2SO_4, filtered, and concentrated *in vacuo*. Product was purified by silica column chromatography (0-10% MeOH/DCM), then HPLC (5-95% MeCN/H_2O), affording the title compound as a white powder (12.0 mg, 62%).

^{1}H NMR (600 MHz, $CDCl_3$): δ 7.42 (d, *J* = 7.5 Hz, 1H), 7.39 – 7.36 (m, 1H), 7.13 (t, *J* = 7.9 Hz, 1H), 7.00 (d, *J* = 8.1 Hz, 1H), 6.90 (t, *J* = 8.2 Hz, 1H), 6.78 (s, 1H), 6.71 (d, *J* = 6.5 Hz, 1H), 6.69

– 6.62 (m, 2H), 5.68 (s, 1H), 5.46 (s, 1H), 5.27 (s, 1H), 5.06 – 4.90 (m, 2H), 3.18 – 3.07 (m, 1H), 2.68 (d, *J* = 14.7 Hz, 1H), 2.53 (t, *J* = 7.5 Hz, 2H), 2.21 (d, *J* = 7.7 Hz, 2H), 1.63 (dt, *J* = 12.9, 6.7 Hz, 2H), 1.61 – 1.53 (m, 5H), 1.35 – 1.22 (m, 24H).

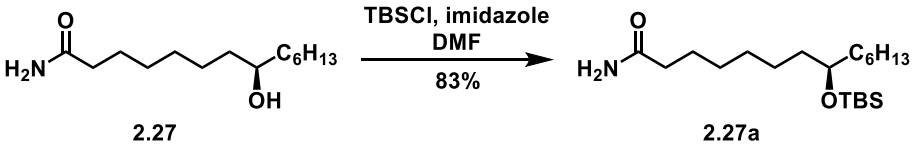

2.27 2.27a

(R)-8-((tert-butyldimethylsilyl)oxy)tetradecanamide 2.27a. To a solution of (R)-8-hydroxytetradecanamide **2.27**[95] (56.3mg, 0.231 mmol, 1 eq) dissolved in dimethylformamide (3 mL) was added tert-butyldimethylsilyl chloride (87.2 mg, 0.578 mmol, 2.5 eq) and imidazole (78.7 mg, 1.157 mmol, 5 eq). The reaction was stirred at room temperature overnight then was added to water. The organic layer was extracted 3x with 1:1 EtOAc: hexanes, washed once with brine, and dried over anhydrous Na_2SO_4, then was filtered and concentrated *in vacuo.* Product was purified by silica column chromatography (25-100% EtOAc in hexanes) to afford the title compound as an off-white solid (68.8 mg, 83% yield).

^{1}H NMR (600 MHz, $CDCl_3$): δ 5.79 (br s, 1H), 5.45 (br s, 1H), 3.63-3.52 (m, 1H), 2.23-2.12 (m, 2H), 1.66-1.54 (m, 2H), 1.41-1.15 (m, 19H), 0.84 (m, 12H), 0.12--0.14 (m, 6H). **^{13}C NMR** (125 MHz, $CDCl_3$): δ 175.8, 72.3, 37.1, 37.0, 36.0, 31.9, 29.6, 29.5, 29.3, 25.9, 25.5, 25.3, 25.2, 22.6, 18.1, 14.1, 4.4. **$[\alpha]^{25}_D$** -1.4 (c 1.03, $CHCl_3$). **HRMS** Accurate Mass (ES^+): Found 356.29909 (+0.16 ppm), $C_{20}H_{42}O_2N^{28}Si$ ($M - H^+$) requires 356.29903.

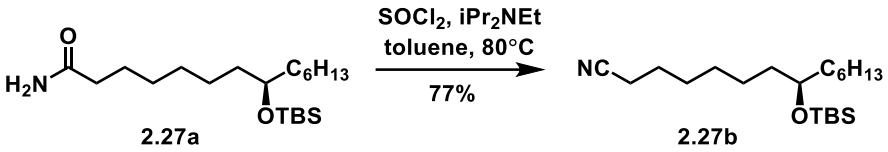

(R)-8-((tert-butyldimethylsilyl)oxy)tetradecanenitrile 2.27b. To a solution of amide **2.27a** (66.6 mg, 0.186 mmol, 1 eq.) dissolved in toluene (3 mL) was added iPr_2NEt (0.194 mL, 1.118 mmol, 6 eq.) and thionyl chloride (0.04 mL, 0.558 mmol, 3 eq.). The solution was heated to 80˚C, resulting in a change in color to a deep red, and was stirred at that temperature overnight. The reaction mixture was then cooled to room temperature and added to water. The organic layer was extracted 4x with hexanes, washed once with brine, and dried over anhydrous Na_2SO_4, then filtered and concentrated *in vacuo.* Product was purified by silica column chromatography (0-20% EtOAc in hexanes) to yield the title compound as a red oil (48.3 mg, 77% yield).

^{1}H NMR (500 MHz, $CDCl_3$): δ 3.61 (p, J = 5.7 Hz, 1H), 2.33 (t, J = 7.1 Hz, 2H), 1.65 (dt, J = 15.0, 7.2 Hz, 2H), 1.50 – 1.19 (m, 20H), 0.95 – 0.80 (m, 12H), 0.03 (d, J = 2.0 Hz, 6H). **^{13}C NMR** (125 MHz, $CDCl_3$): δ 119.8, 77.3, 77.0, 76.8, 72.2, 37.2, 36.9, 31.9, 29.5, 29.0, 28.7, 25.9, 25.34, 25.26, 25.0, 22.6, 18.1, 17.1, 14.1, -4.4. **$[\alpha]^{25}_D$** -2.4 (c 0.25, $CHCl_3$). **HRMS** Accurate Mass (ES^+): Found 340.30165 (-4.02 ppm), $C_{20}H_{42}ON^{28}Si$ ($M + H^+$) requires 340.30302.

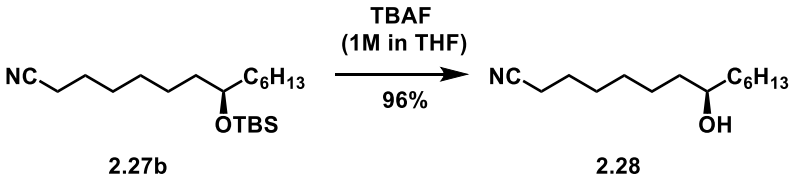

(R)-8-hydroxytetradecanenitrile 2.28. To a flask containing silyl ether **2.27b** (46.3 mg, 0.136 mmol, 1 eq) was added tetrabutylammonium fluoride (1.0 M in THF, 1.36 mL, 1.36 mmol, 10 eq.). The reaction stirred at room temperature for two hours, then was quenched with saturated

aqueous ammonium chloride (4 mL). The organic layer was extracted five times with diethyl ether. The combined organic layers were washed five times with saturated aqueous ammonium chloride and five times with brine, then dried over anhydrous Na_2SO_4, filtered, and concentrated under vacuum to give the title compound as a red oil. (29.5 mg, 96% yield).

^{1}H NMR (600 MHz, $CDCl_3$): δ 3.64-3.49 (m, 1H), 2.33 (t, J = 7.13 Hz, 2 H), 1.66 (q, J = 7.22 Hz, 2H), 1.50-1.22 (m, 20H), 0.88 (t, J = 7.1 Hz, 3H). **^{13}C NMR** (125 MHz, $CDCl_3$): δ 119.8, 71.8, 37.6, 37.2, 31.8, 29.7, 29.3, 28.8, 28.6, 25.6, 25.32, 25.28, 22.6, 17.1, 14.1. **$[\alpha]^{25}_D$** -2.6 (c 0.96, $CHCl_3$). **HRMS** Accurate Mass (ES^+): Found 226.21618 (-1.60 ppm), $C_{14}H_{28}ON$ ($M + H^+$) requires 226.21654.

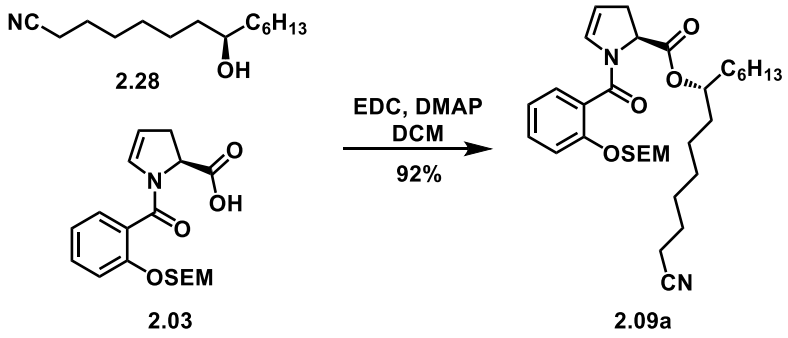

(R)-1-cyanotridecan-7-yl (S)-1-(2-((2-(trimethylsilyl)ethoxy)methoxy)benzoyl)-2,3-dihydro-1H-pyrrole-2-carboxylate 2.09a. A solution of methyl (S)-1-(2-((2-(trimethylsilyl)ethoxy)methoxy)benzoyl)-2,3-dihydro-1H-pyrrole-2-carboxylate **2.03**[1] (67.7 mg, 0.156 mmol, 2 eq.) and alcohol **2.28** (21.0 mg, 0.0932 mmol, 1 eq.) dissolved in dichloromethane (3 mL) was cooled to 0°C and EDC (35.7 mg, 0.186 mmol, 2 eq.) and DMAP (45.5 mg, 0.373 mmol, 4 eq.) were added. The reaction mixture was warmed to room temperature and stirred overnight, then was added to water. The organic layer was extracted 5x with DCM, washed once

with brine, and dried over anhydrous Na_2SO_4, then was filtered and concentrated *in vacuo*. Product was purified by silica column chromatography (0-20% EtOAc in dichloromethane, then 0-10% methanol in dichloromethane) to afford the title compound as a vivid yellow oil (48.9 mg, 92% yield).

^{1}H NMR (500 MHz, $CDCl_3$): δ 7.34 (d, J = 7.3 Hz, 2H), 7.19 (d, J = 8.0 Hz, 1H), 7.04 (td, J = 7.5, 1.0 Hz, 1H), 6.16 (dt, J = 4.3, 2.2 Hz, 1H), 5.28 – 5.18 (m, 3H), 5.02 (dt, J = 4.3, 2.5 Hz, 1H), 4.96 (dd, J = 11.5, 5.0 Hz, 2H), 3.74 (t, J = 8.0 Hz), 3.12 (ddt, J = 16.8, 11.7, 2.4 Hz, 1H), 2.66 (ddt, J = 17.0, 4.8, 2.7 Hz, 1H), 2.30 (t, J = 7.1 Hz, 2H), 1.72 – 1.49 (m, 7H), 1.49 – 1.16 (m, 18H), 0.93 (dd, J = 9.3, 7.2 Hz, 3H), 0.86 (t, J = 8.6 Hz, 3H), -0.02 (s, 9H). **^{13}C NMR** (125 MHz, $CDCl_3$): δ 170.7, 164.9, 153.7, 131.1, 131.0, 128.9, 125.9, 121.9, 119.8, 115.2, 108.1, 93.3, 77.3, 77.0, 76.8, 75.1, 66.5, 58.0, 34.24, 34.16, 34.0, 31.7, 29.7, 29.2, 28.4, 25.24, 25.20, 24.7, 22.6, 18.0, 17.0, 14.0, -1.4. **$[\alpha]^{25}_D$** -46.6 (c 0.86, $CHCl_3$). **HRMS** Accurate Mass (ES^+): Found 571.35500 (-2.07 ppm), $C_{32}H_{51}O_5N_2{}^{28}Si$ ($M + H^+$) requires 571.35618.

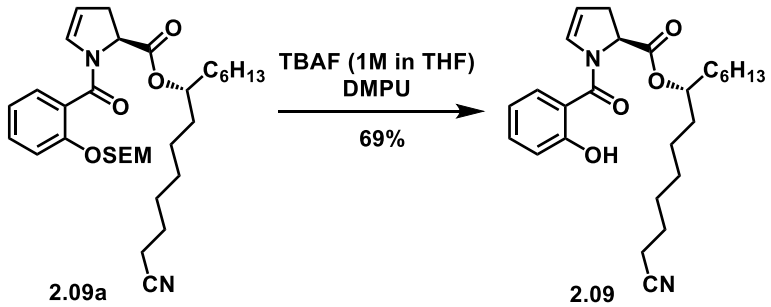

(R)-1-cyanotridecan-7-yl (S)-1-(2-hydroxybenzoyl)-2,3-dihydro-1H-pyrrole-2-carboxylate 2.09. To a solution of silyl ether **2.09a** (23.5 mg, 0.0412 mmol, 1 eq.) dissolved in DMPU (0.823 mL) was added TBAF (1M in THF, 0.823 mL, 0.823 mmol, 20 eq.) dropwise. The reaction was stirred at room temperature for 2 hours, then was quenched with saturated aqueous NH_4Cl (3 mL)

and acidified to pH=5. The organic layer was extracted 5x with Et_2O, washed 5x with saturated aqueous NH_4Cl and 5x with brine, and dried over Na_2SO_4, then filtered and concentrated *in vacuo*. Product was purified by silica column chromatography, followed by HPLC to yield the title compound as a clear oil. (12.6 mg, 69% yield).

^{1}H NMR (500 MHz, $CDCl_3$): δ 9.86 (s, 1H), 7.42 (dd, J = 7.8, 1.7 Hz, 1H), 7.38 (ddt, J = 8.3, 7.3, 2.5, 2.5 Hz, 1H), 7.00 (dd, J = 8.3, 1.1 Hz, 1H), 6.89 (td, J = 7.6, 1.2 Hz, 1H), 6.82 (br s, 1H), 5.27 (dt, J = 4.4, 2.7 Hz, 1H), 5.03-4.89 (m, 2H), 3.12 (ddt, J = 16.5, 11.3, 2.3, 2.3 Hz, 1H), 2.70 (ddd, J = 16.6, 5.3, 2.6 Hz, 1H), 2.32 (t, J = 7.1 Hz, 2H), 1.70-1.48 (m, 7H), 1.48-1.15 (m, 15H), 0.85 (t, J = 7.2 Hz, 3H). **^{13}C NMR** (125 MHz, $CDCl_3$): δ 170.8, 170.7, 159.2, 133.4, 130.9, 128.3, 119.8, 118.8, 118.0, 116.8, 110.5, 75.7, 59.5, 34.1, 34.0, 33.8, 31.7, 29.1, 28.5, 28.4, 25.22, 25.17, 24.7, 22.5, 17.0, 14.0. **$[\alpha]^{25}_D$** -56.0 (c 0.59, $CHCl_3$). **HRMS** Accurate Mass (ES^+): Found 441.27391 (-1.97 ppm), $C_{26}H_{37}O_4N_2$ ($M + H^+$) requires 441.27478.

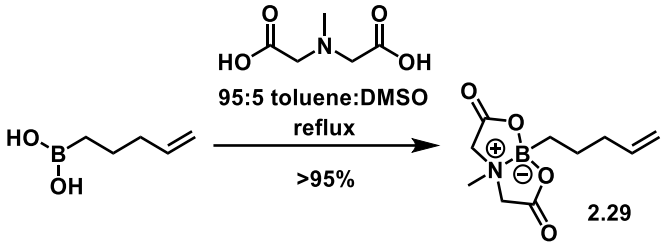

4-methyl-8-(pent-4-en-1-yl)dihydro-4λ^4,8λ^4-[1,3,2]oxazaborolo[2,3-b][1,3,2]oxazaborole-2,6(3H,5H)-dione 2.29. To a solution of pent-4-en-1-ylboronic acid (0.5 M in THF, 8.340 mL, 4.170 mmol) in 95:5 toluene:dimethylsulfoxide (100 mL) was added N-methyliminodiacetic acid (0.6134 g, 4.170 mmol, 1 eq). The flask was fitted with a toluene-filled Dean Stark condenser, heated to reflux, and stirred overnight. The reaction mixture was then cooled to room temperature and concentrated *in vacuo* to a volume of about 5 mL. Acetone (~5 mL) was added, precipitating

a tan solid upon trituration. Ether (~5 mL) was then added to precipitate additional solid. The supernatant was removed to a separate flask and this process was repeated three times. The resulting solids were combined and rinsed one more time with acetone and ether, which was then again removed to give the title compound as an off-white powder (940 mg, >95% yield).

^{1}H NMR (500 MHz, $CDCl_3$): δ 5.78 (ddt, J = 17.0, 10.2, 6.7 Hz, 1H), 4.96 (dd, J = 17.2, 10.2 Hz, 2H), 3.98 (d, J = 16.6 Hz, 2H), 3.69 (d, J = 16.6 Hz, 2H), 2.90 (s, 3H), 2.09 (dt, J = 7.2, 7.1, 2H), 1.45 (dtd, J = 15.1, 9.1, 7.4, 3.9 Hz, 2H), 0.69 – 0.49 (m, 2H). **^{13}C NMR** (125 MHz, $CDCl_3$): δ 167.8, 138.8, 114.7, 61.9, 45.8, 41.0, 36.6, 23.4. **HRMS** Accurate Mass (ES^+): Found 223.11365 (+0.24 ppm), $C_{10}H_{15}O_4N^{10}B$ ($M - H^+$) requires 223.11359.

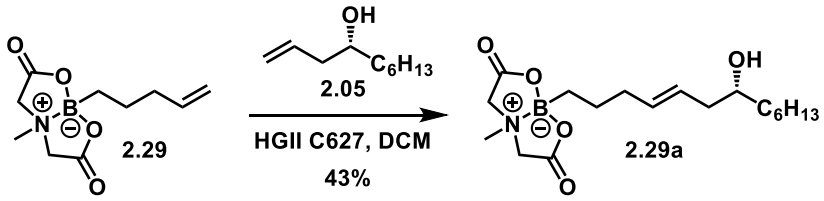

(R)-8-(7-hydroxytridec-4-en-1-yl)-4-methyldihydro-4λ^4,8λ^4-[1,3,2]oxazaborolo[2,3-b][1,3,2]oxazaborole-2,6(3H,5H)-dione 2.29a. Hoveyda-Grubbs C627 catalyst (55.7 mg, 0.089 mmol, 10 mol %) was added to a solution of MIDA boronate **2.29** (200 mg, 0.889 mmol, 1 eq) and **2.05**[1] (416.6 mg, 2.666 mmol, 3 eq) dissolved in dichloromethane (6 mL). The solution stirred at room temperature overnight, then was concentrated under reduced pressure. Product was purified by silica column chromatography (100% Et_2O, then 20-30% acetone in dichloromethane). to give the title compound as a dark brown oil (135.6 mg, 43% yield).

^{1}H NMR (600 MHz, $CDCl_3$): δ 5.57 – 5.47 (m, 1H), 5.45-5.33 (m, 1H), 3.97 (d, J = 16.5 Hz, 2H), 3.70 (d, J = 16.6 Hz, 2H), 3.56 (br s, 1H), 2.90 (s, 3H), 2.27 – 2.15 (m, 1H), 2.13 – 1.95 (m, 3H),

1.88 – 1.56 (m, 2H), 1.46 – 1.38 (m, 4H), 1.35 – 1.16 (m, 8H), 0.91 – 0.67 (t, J = 6.0 Hz, 3H), 0.65 – 0.44 (m, 2H). **^{13}C NMR** (125 MHz, $CDCl_3$): δ 167.8, 134.1, 126.5, 71.0, 61.9, 45.8, 40.7, 36.9, 35.5, 31.8, 29.4, 25.8, 25.7, 23.9, 22.6, 14.1. **$[\alpha]^{25}_D$** +4.8 (c 1.41, DMSO). **HRMS** Accurate Mass (ES^+): Found 354.24393 (-1.99 ppm), $C_{18}H_{33}O_5N^{11}B$ ($M + H^+$) requires 354.24463.

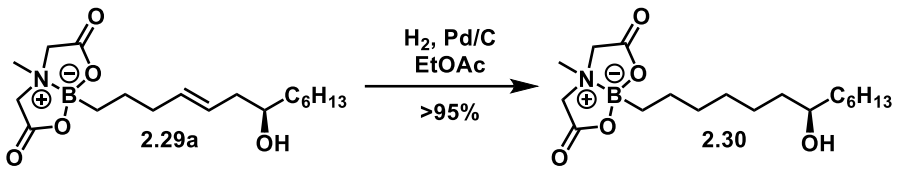

(R)-8-(7-hydroxytridecyl)-4-methyldihydro-4λ^4,8λ^4-[1,3,2]oxazaborolo[2,3-b][1,3,2]oxazaborole-2,6(3H,5H)-dione 2.30. To a solution of **2.29a** (115 mg, 0.326 mmol, 1 eq) dissolved in ethyl acetate (5 mL) was added palladium on carbon (10 wt. %, 32.6 mg). The flask was purged five times with hydrogen and was stirred overnight at room temperature under a hydrogen atmosphere. The following day, the solution was filtered through a pad of Celite and was concentrated under vacuum, yielding the title compound as a white powder (134.9 mg, >95% yield).

^{1}H NMR (400 MHz, $CDCl_3$): δ 3.82 (d, J = 16.3 Hz, 2H), 3.67 (d, J = 16.3 Hz, 2H), 3.58 (br s, 1H), 2.90 (s, 3H), 1.58 (s, 2H) 1.49-1.20 (m, 18H), 0.88 (t, J = 8.0 Hz, 3H), 0.61 (t, J = 7.5 Hz, 2H). **^{13}C NMR** (125 MHz, $CDCl_3$): δ 167.8, 71.9, 61.9, 45.8, 37.6, 37.5, 32.7, 31.8, 29.5, 29.4, 25.7, 25.5, 23.9, 22.6, 14.1. **$[\alpha]^{25}_D$** +0.6 (c 1.05, DMSO). **HRMS** Accurate Mass (ES^+): Found 390.22262 (+0.56 ppm), $C_{18}H_{34}O_5N^{11}B^{35}Cl$ ($M + Cl^-$) requires 390.22240.

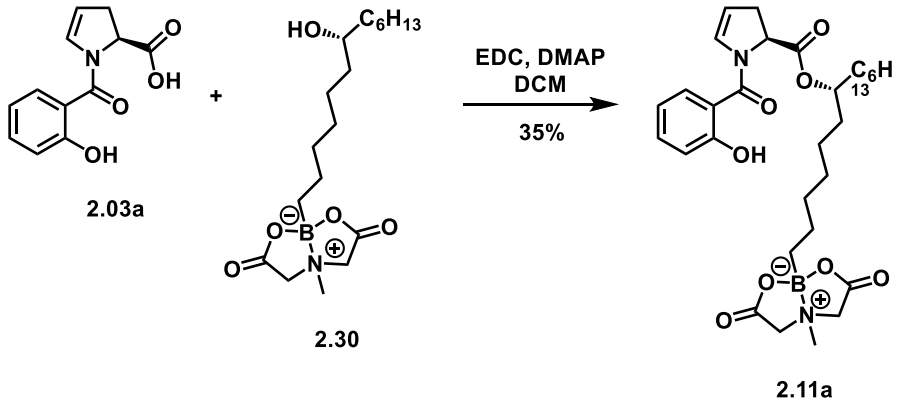

(R)-1-(4-methyl-2,6-dioxotetrahydro-2H-4λ⁴,8λ⁴-[1,3,2]oxazaborolo[2,3-b][1,3,2]oxazaborol-8-yl)tridecan-7-yl (S)-1-(2-hydroxybenzoyl)-2,3-dihydro-1H-pyrrole-2-carboxylate 2.11a. A solution of acid **2.03a** (47.1 mg, 0.202 mmol, 1.5 eq) and alcohol **2.30** (49.9 mg, 0.140 mmol, 1 eq) dissolved in dichloromethane (4 mL) was cooled to 0 °C, and EDC (65.2 mg, 0.420 mmol, 3 eq.) and DMAP (68.4 mg, 0.420 mmol, 4 eq.) were added. The reaction mixture was warmed to room temperature and stirred overnight, then was added to water. The organic layer was extracted 5x with dichloromethane, washed once with brine, and dried over anhydrous Na_2SO_4, then was filtered and concentrated *in vacuo*. Product was then purified by silica column chromatography (0-50% acetone in dichloromethane, then 100% iPrOH) to afford the title compound as a white solid (28.3 mg, 35% yield).

^{1}H NMR (600 MHz, $CDCl_3$): δ 9.73 (s, 1H), 7.41 (dd, J = 7.8, 1.7 Hz, 1H), 7.36 (ddd, J = 8.6, 7.3, 1.7 Hz, 1H), 6.97 (dd, J = 8.3 Hz, 1.1), 6.89 (m, 1H), 6.76 (br s, 1H), 5.34-5.22 (m, 1H), 5.03-4.85 (m, 2H), 3.93-3.84 (m, 2H), 3.71-3.65 (m, 2H), 3.18-3.06 (m, 1H), 2.90-2.83 (m, 3H), 2.74-2.64 (m, 1H), 0.85 (t, J = 7.2 Hz, 3H), 0.60-0.55 (m, 2H). **^{13}C NMR** (125 MHz, $CDCl_3$): δ 170.8, 167.5, 167.4, 159.0, 158.7, 133.4, 130.8, 128.3, 119.0, 117.8, 110.7, 76.0, 72.0, 61.9, 45.7, 37.5, 34.1, 32.5, 31.7, 29.7, 29.1, 28.9, 25.5, 25.2, 24.8, 23.6, 22.5, 14.0. **$[\alpha]^{25}_D$** -25.1 (c 0.342, DMSO).

HRMS Accurate Mass (ES^+): Found 570.3112 (+0.76 ppm), $C_{30}H_{44}O_8N_2{}^{11}B$ ($M + H^+$) requires 571.31852.

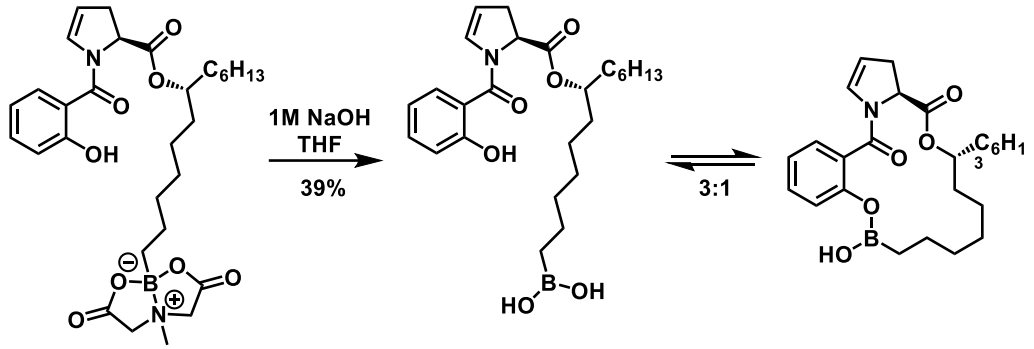

((R)-7-(((S)-1-(2-hydroxybenzoyl)-2,3-dihydro-1H-pyrrole-2-carbonyl)oxy)tridecyl)boronic acid 2.11, 2.11-cyc. To a solution of MIDA boronate **2.11a** (15.4 mg, 0.0270 mmol) dissolved in tetrahydrofuran (1 mL) was added 1 M aqueous sodium hydroxide (0.3 mL) and the reaction stirred at room temperature for ten minutes. The reaction was quenched with phosphate buffer (1M, pH=7, 1 mL) and Et_2O (1 mL) was added. The organic layer was extracted 3x with 1:1 Et_2O:THF, dried over anhydrous $MgSO_4$, filtered, and concentrated under reduced pressure. Product was purified by HPLC to afford the title compounds as a white solid (4.8 mg, 39% yield).

^{1}H NMR (600 MHz, DMSO-d_6, 25°C): δ 10.06 (s, 0.30 H), 9.91 (s, 1H), 7.33 (s, 0.30 H), 7.29 (s, 1H), 7.25 (td, J = 7.8, 7.4, 1.8 Hz, 1H), 7.12 – 7.06 (m, 1H), 7.05-6.99 (m, 0.30 H), 6.99-6.93 (m, 0.30 H), 6.87 (d, J = 8.2 Hz, 1H), 6.83 (td, J = 7.5, 2.8 Hz, 1H), 6.19-6.10 (m, 1H), 5.30-5.20 (m, 0.30 H), 5.11-5.03 (m, 1H), 4.77 (dd, J = 11.5, 5.2 Hz, 3H), 4.50-4.42 (m, 0.30 H), 4.32 (t, J = 5.1 Hz, 1H), 3.79 – 3.59 (m, 1H), 3.39 (qd, J = 6.9, 4.7 Hz, 1H), 3.12 – 3.01 (m, 1H), 2.00-1.88 (m, 0.30 H), 1.45 (s, 7H), 1.37 – 0.91 (m, 36H), 0.88 – 0.67 (m, 7H), 0.52 (dt, J = 15.5, 7.8 Hz, 2H), 0.45-0.30 (m, 0.30 H). **^{13}C NMR** (125 MHz, DMSO-d_6, 25°C): δ 171.4, 157.2, 134.4, 133.4, 130.8,

128.3, 123.0, 119.1, 117.9, 116.6, 88.7, 75.8, 58.3, 53.4, 34.6, 34.3, 31.7, 30.7, 29.7, 29.1, 28.1, 26.5, 25.4, 23.1, 22.6, 14.1. **$[\alpha]^{25}_{D}$** -7.2 (c 0.68, $CHCl_3$). **HRMS** Accurate Mass (ES^+): Found 458.26973 (-2.42 ppm), $C_{25}H_{37}O_6N^{11}B$ ($M - H^+$) requires 458.27084. Found 442.27477 (-2.62 ppm) $C_{25}H_{37}O_5N^{11}B$ ($M + H^+$) requires 442.27593.

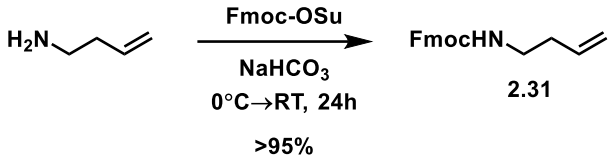

(9H-fluoren-9-yl)methyl but-3-en-1-ylcarbamate 2.31. A solution of but-3-en-1-amine (100 mg, 1.41 mmol, 1.0 eq.) in dioxane (7 mL) was cooled to 0°C. Fmoc-OSu (474 mg, 1.41 mmol, 1.0 eq.) and sodium bicarbonate (2.36g, 2.81 mmol, 2.0 eq.) were added and the solution stirred overnight, allowing it to warm to room temperature. The white suspension was acidified to pH 1 with 3M HCl, then DCM was added and the aqueous layer was extracted 4x with DCM. Combined organic layers were concentrated *in vacuo* and crude product was purified using silica column chromatography (0-7% EtOAc) affording the title compound as a white solid (412 mg, >95% yield).

^{1}H NMR (500 MHz, $CDCl_3$): δ 7.77 (d, *J* = 7.5 Hz, 2H), 7.59 (d, *J* = 7.5 Hz, 2H), 7.40 (t, *J* = 7.5 Hz, 2H), 7.32 (t, *J* = 7.8 Hz, 2H), 5.77 (ddt, *J* = 13.9, 10.1, 6.9 Hz, 1H), 5.23 – 5.03 (m, 2H), 4.80 (s, 1H), 4.40 (d, *J* = 7.0 Hz, 2H), 4.22 (t, *J* = 7.0 Hz, 1H), 3.29 (q, *J* = 6.5 Hz, 2H), 2.28 (q, *J* = 6.6 Hz, 2H).

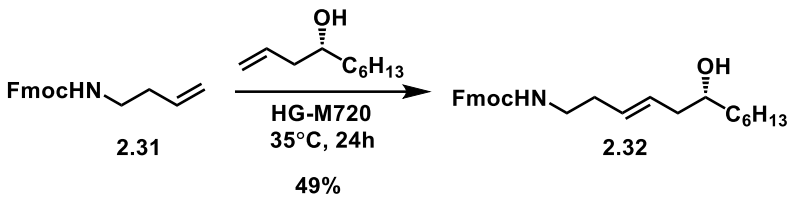

(9H-fluoren-9-yl)methyl (R,E)-(6-hydroxydodec-3-en-1-yl)carbamate 2.32. Protected amine **2.31** (100 mg, 0.341 mmol, 1.0 eq.) and alcohol (242 mg, 1.02 mmol, 3.0 eq.) were dissolved in DCM (1 mL). Hoveyda Grubbs M720 catalyst (32.1 mg, 0.0511 mmol, 0.15 eq.) was then added, followed by more DCM (1 mL). The solution turned rapidly to brown, and was warmed to 35°C and stirred overnight. The solution was concentrated *in vacuo* and the resulting residue was purified by silica column chromatography (0-25% EtOAc/hexanes), affording the title compound as a brown solid (70.0 mg, 49% yield).

^{1}H NMR (600 MHz, $CDCl_3$): δ 7.76 (d, *J* = 7.5 Hz, 2H), 7.59 (d, *J* = 7.4 Hz, 2H), 7.40 (t, *J* = 7.4 Hz, 2H), 7.31 (t, *J* = 7.4 Hz, 2H), 5.63 – 5.37 (m, 2H), 4.47 – 4.36 (m, 2H), 4.21 (t, *J* = 6.6 Hz, 1H), 3.58 (s, 1H), 3.25 (q, *J* = 5.7 Hz, 2H), 2.27 – 2.18 (m, 2H), 2.11 – 2.03 (m, 1H), 1.64 (dt, *J* = 15.4, 7.7 Hz, 1H), 1.48 – 1.38 (m, 4H), 1.37 – 1.23 (m, 10H), 0.90 – 0.85 (m, 3H). **^{13}C NMR** (151 MHz, $CDCl_3$): δ 172.6, 144.1, 141.4, 127.8, 127.2, 127.1, 125.13, 125.06, 120.1, 71.0, 66.7, 47.4, 40.7, 37.0, 31.9, 29.5, 28.0, 25.8, 22.7, 17.7, 14.2.

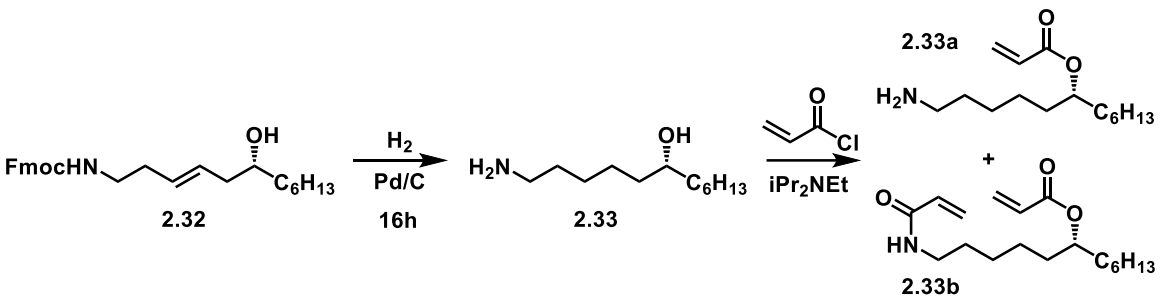

(9H-fluoren-9-yl)methyl (R)-(6-hydroxydodecyl)carbamate 2.33a and 2.33b. Alkene **2.32** (61.2 mg, 0.145 mmol, 1.0 eq.) and palladium on activated carbon (10% Pd, 15.4 mg, 0.0145 mmol, 0.10 eq.) were combined and dissolved in methanol (3 mL) and catalytic MeCN. The reaction vessel was evacuated and backfilled with hydrogen gas four times, then the reaction was left to stir under a hydrogen atmosphere (1 atm) for 16 hours. The dark grey suspension was filtered through Celite, eluting with 100% ethyl acetate to afford crude intermediate **2.33**, which was carried through to the subsequent step without further purification.

^{1}H NMR (400 MHz, $CDCl_3$): δ 3.61 – 3.50 (m, 2H), 2.92 (dt, J = 8.7, 5.0 Hz, 4H), 2.83 – 2.75 (m, 1H), 1.71 – 1.57 (m, 1H), 1.47 – 1.32 (m, 7H), 1.27 – 1.17 (m, 11H), 0.82 (t, J = 6.6 Hz, 2H). **^{13}C NMR** (101 MHz, $CDCl_3$): δ 71.3, 53.0, 51.1, 46.1, 45.5, 37.6, 37.0, 31.9, 29.4, 26.9, 25.7, 25.0, 22.7, 14.1, 9.1.

This intermediate was dissolved in 1 mL THF and cooled to 0 °C. Acryloyl chloride (13.1 mg, 0.011 mL, 0.145 mmol, 1.0 eq.) was added dropwise, followed by dropwise addition of diisopropylethylamine (18.8 mg, 0.025 mL, 0.145 mmol, 1.0 eq.). The reaction stirred for two hours at 0 °C, then was warmed to room temperature and stirred one additional hour. Saturated aqueous NH_4Cl was added to quench the reaction, and the aqueous layer was extracted four times with DCM. Combined organic layers were washed once with saturated aqueous NH_4Cl, dried over anhydrous Na_2SO_4, filtered, and concentrated *in vacuo*. Products were purified by silica column

chromatography (0-40% EtOAc/hexanes), unexpectedly yielding **2.33a** (6.0 mg, 13% yield over two steps) and **2.33b** (15.0 mg, 40% yield over two steps).

2.33a: ^{1}H NMR (600 MHz, $CDCl_3$): δ 6.37 (dd, J = 17.3, 1.3 Hz, 1H), 6.10 (dd, J = 17.3, 10.4 Hz, 1H), 5.80 (dd, J = 10.4, 1.3 Hz, 1H), 4.92 (ddd, J = 12.4, 7.4, 5.2 Hz, 1H), 2.84 (q, J = 7.3 Hz, 3H), 2.69 (t, J = 8.2 Hz, 1H), 1.65 – 1.46 (m, 6H), 1.38 – 1.14 (m, 19H), 0.86 (t, J = 6.9 Hz, 3H).

2.33b: ^{1}H NMR (500 MHz, $CDCl_3$): δ 6.53 (ddd, J = 16.8, 13.9, 10.4 Hz, 1H), 6.42 – 6.30 (m, 2H), 6.10 (ddd, J = 17.3, 10.4, 4.3 Hz, 1H), 5.80 (ddd, J = 10.2, 8.3, 1.6 Hz, 1H), 5.65 (ddd, J = 10.3, 3.3, 2.1 Hz, 1H), 4.98 – 4.89 (m, 1H), 3.42 (q, J = 7.1 Hz, 1H), 3.40 – 3.31 (m, 2H), 3.30 – 3.24 (m, 1H), 1.61 – 1.50 (m, 6H), 1.36 – 1.21 (m, 14H), 1.16 (dt, J = 20.0, 7.1 Hz, 3H), 0.86 (t, J = 6.7 Hz, 3H).

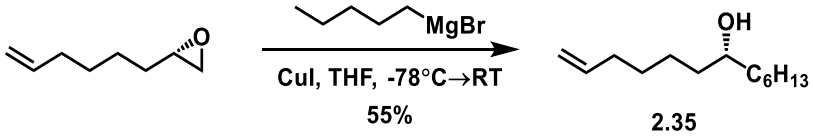

2.35

(R)-tridec-1-en-7-ol 2.35. A 50 mL round-bottom flask was flame-dried and purged thrice with argon. (S)-2-(hex-5-en-1-yl)oxirane[264] (0.589 g, 4.67 mmol, 1.0 eq.) was added and dissolved in THF (7 mL). Flame-dried CuI (0.444 g, 0.5 eq.) was added and the solution was cooled to -78 °C. Pentylmagnesium bromide solution (2.0M in THF, 11.7 mL, 5.0 eq.) was added dropwise and the dark blue reaction stirred 2.5 hours, allowing it to warm to room temperature. A saturated aqueous solution of NH_4Cl (8 mL) was added to quench the reaction, and the aqueous layer was extracted thrice with Et_2O. Combined organic layers were dried over anhydrous Na_2SO_4, filtered, and

concentrated *in vacuo*. Crude product was purified by silica column chromatography (0-8% EtOAc/hexanes), to yield the title compound as a colorless oil (471.0 mg, 51% yield)**.**

^{1}H NMR (500 MHz, $CDCl_3$): δ 5.80 (ddt, J = 16.9, 10.2, 6.7 Hz, 1H), 4.99 (dq, J = 17.1, 2.1 Hz, 1H), 4.93 (ddt, J = 10.2, 2.3, 1.2 Hz, 1H), 3.65 – 3.52 (m, 1H), 2.06 (dt, J = 7.0, 6.9 Hz, 2H), 1.48 – 1.36 (m, 9H), 1.33 – 1.22 (m, 9H), 0.88 (t, J = 7.1 Hz, 3H). **^{13}C NMR** (151 MHz, $CDCl_3$): δ 138.9, 114.3, 71.9, 37.5, 37.3, 33.7, 31.8, 29.4, 29.0, 25.6, 25.1, 22.6, 14.1. **$[\alpha]^{25}_D$** +0.25 (c 0.79, $CHCl_3$). **HRMS** Accurate Mass (ES^+): Found 199.20570 (+ 0.30 ppm), $C_{13}H_{27}O$ ($M + H^+$) requires 199.20564.

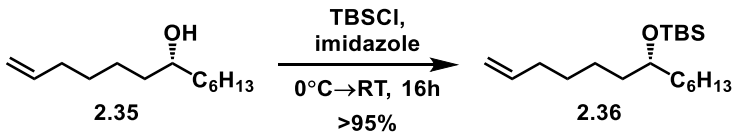

(R)-tert-butyldimethyl(tridec-1-en-7-yloxy)silane 2.36. A solution of alcohol **2.35** (90.0 mg, 0.381 mmol, 1.0 eq.) in DMF (2 mL) was cooled to 0 °C. Imidazole (64.9 mg, 0.953 mmol, 2.5 eq.) and TBSCl (144 mg, 0.953 mmol, 2.5 eq.) were added followed by an additional 2.4 mL DMF, and the reaction was stirred overnight, allowing the reaction to warm to room temperature. Hexanes was added to the reaction and the DMF layer was extracted 4x with hexanes. Combined hexanes layers were washed twice with brine, dried over anhydrous Na_2SO_4, filtered, and concentrated *in vacuo*. Crude product was purified by silica column chromatography (100% hexanes), affording the title compound as a colorless oil (122 mg, >95% yield).

^{1}H NMR (500 MHz, $CDCl_3$): δ 5.81 (ddt, *J* = 16.9, 10.2, 6.7 Hz, 1H), 5.04 – 4.96 (m, 1H), 4.94 (ddt, *J* = 10.2, 2.3, 1.2 Hz, 1H), 3.63 (s, 1H), 2.06 (q, *J* = 7.1 Hz, 2H), 1.46 – 1.35 (m, 7H), 1.35 –

1.19 (m, 10H), 0.92 – 0.86 (m, 15H), 0.04 (s, 6H). **^{13}C NMR** (126 MHz, $CDCl_3$): δ 139.2, 114.4, 72.5, 37.4, 37.2, 34.0, 32.1, 29.7, 29.4, 26.1, 25.9, 25.5, 25.0, 22.8, 18.3, 14.3, -2.8, -4.2.

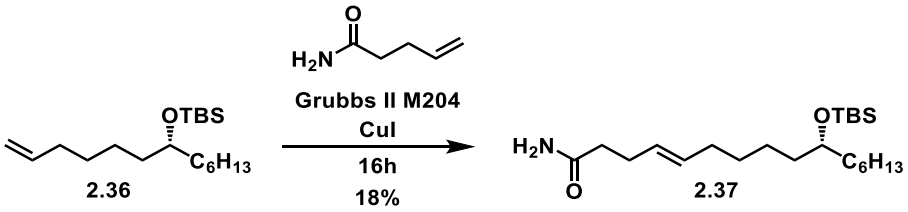

(R,E)-10-((tert-butyldimethylsilyl)oxy)hexadec-4-enamide 2.37. Flame-dried copper (I) iodide (3.2 mg, 0.0168 mmol, 0.10 eq.), silyl ether **2.36** (55 mg, 0.168 mmol, 1.0 eq.) and pent-4-enamide (150 mg, 1.51 mmol, 9.0 eq.) were suspended in DCM (1 mL). Grubbs M204 catalyst (14.0 mg, 0.0168 mmol, 0.10 eq.) was then added, followed by more DCM (1.5 mL). The solution turned rapidly to brown and stirred at room temperature overnight. The solution was concentrated *in vacuo* and the resulting residue was purified by silica column chromatography (0-75% EtOAc/hexanes), affording the title compound as a brown solid (12.0 mg, 18% yield).

^{1}H NMR (600 MHz, $CDCl_3$): δ 5.60 – 5.31 (m, 4H), 3.60 (p, *J* = 5.8 Hz, 1H), 2.34 – 2.24 (m, 5H), 1.98 (q, *J* = 6.5 Hz, 2H), 1.91 (d, *J* = 13.1 Hz, 2H), 1.87 – 1.80 (m, 3H), 1.45 – 1.36 (m, 6H), 1.34 – 1.20 (m, 16H), 0.87 (s, 12H), 0.03 (s, 6H).

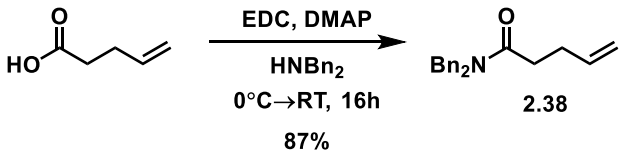

N,N-dibenzylpent-4-enamide 2.38. A solution of pent-4-enoic acid (359 mg, 3.59 mmol, 1.0 eq.) in DCM (25 mL) was cooled to 0 °C. EDC (1.03g, 5.38 mmol, 1.5 eq.) was added and the reaction stirred 15 minutes. DMAP (110 mg, 0.896 mmol, 0.25 eq.) and dibenzylamine (884 mg, 4.48 mmol, 1.25 eq.) were added and the reaction was warmed to room temperature and stirred overnight. Reaction was concentrated *in vacuo* and the crude product was purified by silica column chromatography (0-40% EtOAc/hexanes), yielding the title compound as a colorless oil (868 mg, 87% yield). Spectral data are consistent with literature reports.

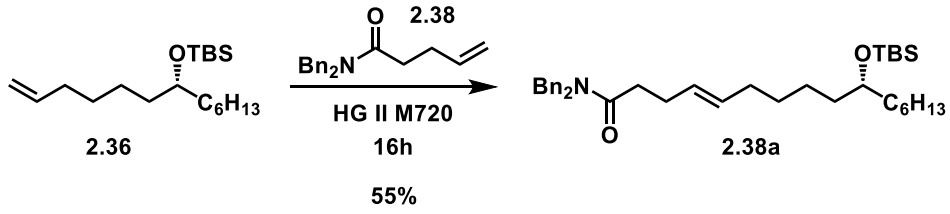

(R,E)-N,N-dibenzyl-10-((tert-butyldimethylsilyl)oxy)hexadec-4-enamide 2.38a. To a sample of silyl ether **2.36** (60.5 mg, 0.194 mmol, 1.0 eq.) was added dibenzylamide **2.38** (216 mg, 0.774 mmol, 4.0 eq.) followed by Hoveyda Grubbs M720 catalyst (12.1 mg, 0.0194 mmol, 0.10 eq.). The green solution was purged once more with argon, then DCM (0.5 mL) was added and the solution stirred at room temperature overnight. Solvent was removed *in vacuo* and the crude reaction mixture was purified by silica column chromatography (0-40% EtOAc/hexanes), yielding a colorless oil (60.2 mg, 55% yield).

^{1}H NMR (500 MHz, $CDCl_3$): δ 7.37 (t, *J* = 7.3 Hz, 2H), 7.34 – 7.25 (m, 5H), 7.24 – 7.21 (m, 2H), 7.16 (d, *J* = 7.2 Hz, 2H), 5.49 – 5.39 (m, 2H), 4.61 (s, 2H), 4.45 (s, 2H), 3.61 (p, *J* = 5.7 Hz, 1H), 2.50 – 2.46 (m, 2H), 2.45 – 2.38 (m, 2H), 1.97 (q, *J* = 5.6, 5.0 Hz, 2H), 1.43 – 1.22 (m, 17H), 0.89

(s, 12H), 0.04 (s, 6H). **^{13}C NMR** (126 MHz, $CDCl_3$): δ 173.2, 137.6, 136.7, 131.7, 129.0, 128.71, 128.68, 128.4, 127.7, 127.5, 126.6, 72.5, 50.0, 48.2, 37.3, 37.1, 33.4, 32.7, 32.0, 29.8, 29.7, 28.6, 26.1, 25.4, 25.1, 22.8, 18.3, 14.2, -4.3.

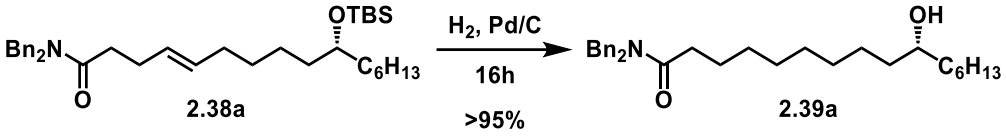

(R)-N,N-dibenzyl-10-((tert-butyldimethylsilyl)oxy)hexadecanamide 2.39a. Alkene **2.38a** (55.0 mg, 0.098 mmol, 1.0 eq.) and palladium on activated carbon (10% Pd, 21.0 mg, 0.00980 mmol, 0.10 eq.) were combined and dissolved in methanol (4 mL). The reaction vessel was evacuated and backfilled with hydrogen gas four times, then the reaction was left to stir under a hydrogen atmosphere (1 atm) for 16 hours. The dark grey suspension was filtered through Celite, eluting with 100% ethyl acetate to afford the title compound, having unexpectedly removed the silyl ether protecting group (44 mg, >95% yield).

^{1}H NMR (600 MHz, $CDCl_3$): δ 7.37 (t, *J* = 7.4 Hz, 2H), 7.31 (t, *J* = 7.2 Hz, 3H), 7.26 (t, *J* = 7.0 Hz, 1H), 7.21 (d, *J* = 7.4 Hz, 2H), 7.15 (d, *J* = 7.5 Hz, 2H), 4.60 (s, 2H), 4.45 (s, 2H), 3.57 (s, 1H), 2.41 (t, *J* = 7.5 Hz, 2H), 1.75 – 1.67 (m, 2H), 1.51 – 1.36 (m, 6H), 1.34 – 1.23 (m, 15H), 0.88 (t, *J* = 6.6 Hz, 3H).

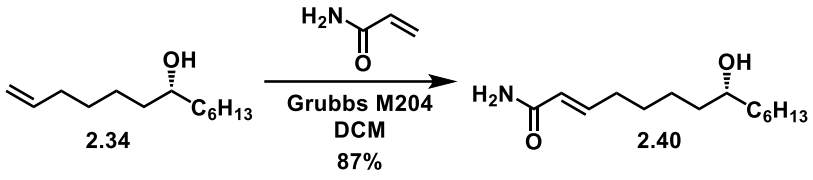

(R,E)-8-hydroxytetradec-2-enamide 2.40. A 10 mL round-bottom flask fitted with reflux condenser was flame-dried and purged 3x with argon. Acrylamide (0.048 mL, 0.76 mmol, 3.0 eq.) was added, followed by Grubbs catalyst (M204, 21.0 mg, 0.025 mmol, 0.10 eq.). Alcohol **2.34** (50.0 mg, 0.25 mmol, 1.0 eq.) was dissolved in DCM (3 mL) and added to the flask in one portion. The reaction was heated to reflux and stirred overnight. Crude product was directly purified by silica column chromatography (0-10 % MeOH/DCM), to yield the title compound as a yellow oil (52.7 mg, 87% yield).

^{1}H NMR (500 MHz, $CDCl_3$): δ 6.79 (dt, J = 14.7, 6.9 Hz, 1H), 6.11 (d, J = 21.3 Hz, 2H), 5.83 (d, J = 15.4 Hz, 1H), 3.60-3.46 (m, 1H), 2.29 (br s, 1H), 2.16 (q, J = 6.3 Hz, 2H), 1.49 – 1.15 (m, 16H), 0.85 (t, J = 6.9 Hz, 3H). **^{13}C NMR** (151 MHz, $CDCl_3$): δ 168.5, 145.9, 123.0, 71.6, 37.5, 37.1, 31.9, 31.8, 29.3, 28.1, 25.6, 25.1, 22.5, 14.0. **$[\alpha]^{25}_D$** -1.6 (c 0.80, $CHCl_3$). **HRMS** Accurate Mass (ES^+): Found 242.21138 (- 0.32 ppm), $C_{14}H_{28}O_2N$ ($M + H^+$) requires 242.21146.

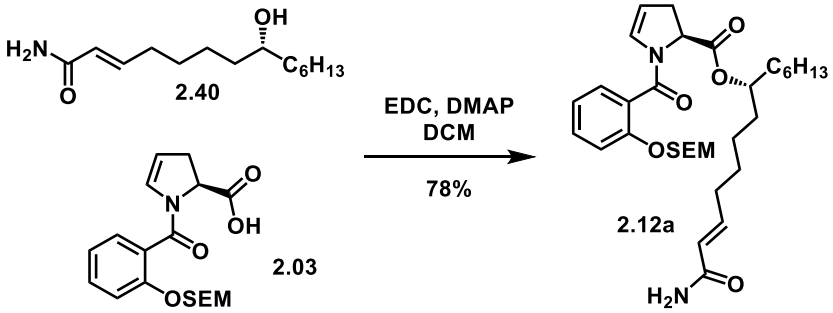

(R,E)-14-amino-14-oxotetradec-12-en-7-yl (S)-1-(2-((2-(trimethylsilyl)ethoxy)methoxy)benzoyl)-2,3-dihydro-1H-pyrrole-2-carboxylate 2.12a. A 20 mL scintillation vial containing acid **2.03** (63.0 mg, 0.173 mmol, 1.0 eq.) was purged thrice with argon. DCM (6 mL) was added and the solution was cooled to 0 °C. EDC (49.8 mg, 0.260 mmol,

1.5 eq.) and DMAP (21.2 mg, 0.173 mmol, 1.0 eq.) were added and the yellow solution strred at 0 °C for 5 minutes. A solution of alcohol **2.40** (83.7 mg, 0.347 mmol, 2.0 eq.) in DCM (3 mL) was added to the vial dropwise. The reaction stirred 16 hours, allowing it to warm to room temperature. The reaction was diluted with water, and the aqueous layer was extracted 5x with DCM. Combined organic layers were washed once with brine, back-extracted once with DCM, dried over anhydrous Na_2SO_4, filtered, and concentrated *in vacuo.* Crude product was purified by silica column chromatography (0-50% EtOAc/hexanes), yielding the title compound as a yellow oil (79.1 mg, 78% yield).

^{1}H NMR (500 MHz, $CDCl_3$): δ 7.37 – 7.31 (m, 2H), 7.18 (d, J = 7.9 Hz, 1H), 7.03 (td, J = 7.5, 0.9 Hz, 1H), 6.78 (dt, J = 15.6, 6.8 Hz, 1H), 6.59 (s, 1H), 6.16 (dt, J = 4.3, 2.1 Hz, 1H), 5.88 (d, J = 15.7 Hz, 1H), 5.27 (d, J = 9.2 Hz, 1H), 5.23 (d, J = 7.1 Hz, 1H), 5.19 (d, J = 7.1 Hz, 1H), 5.05 (dt, J = 4.5, 2.6 Hz, 1H), 4.99 (ddd, J = 12.9, 7.3, 5.4 Hz, 1H), 4.95 (dd, J = 11.7, 4.9 Hz, 1H), 3.72 (dd, J = 9.2, 7.5 Hz, 2H), 3.12 (ddt, J = 16.7, 11.6, 2.4 Hz, 1H), 2.65 (ddt, J = 17.0, 4.8, 2.2 Hz, 1H), 2.18 (q, J = 6.5 Hz, 2H), 1.62 – 1.34 (m, 9H), 1.33 – 1.19 (m, 10H), 0.92 (dd, J = 9.4, 7.3 Hz, 2H), 0.85 (t, J = 7.1 Hz, 3H), -0.03 (s, 9H). **^{13}C NMR** (151 MHz, $CDCl_3$): δ 170.5, 168.6, 165.2, 153.6, 144.5, 131.3, 130.7, 128.7, 125.4, 123.9, 121.9, 115.1, 108.7, 93.1, 75.1, 66.5, 57.9, 34.4, 34.2, 34.1, 31.6, 31.5, 29.1, 27.4, 25.3, 24.2, 22.5, 18.0, 14.0, -1.5. **$[\alpha]^{25}_D$** -23.2 (c 0.97, $CHCl_3$). **HRMS** Accurate Mass (ES+): Found 587.35194 (+ 0.85 ppm), $C_{32}H_{51}O_6N_2{}^{28}Si$ (M + H+) requires 587.35109.

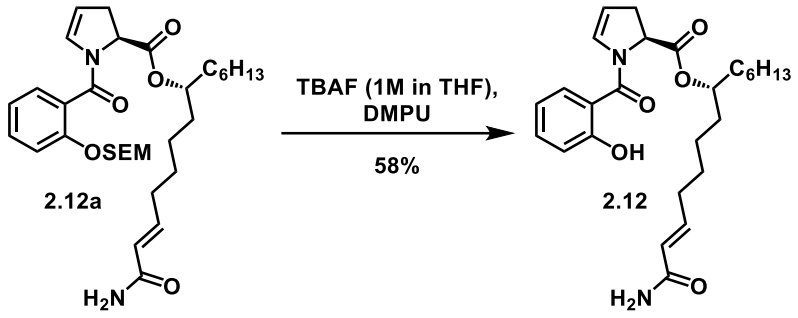

(R,E)-14-amino-14-oxotetradec-12-en-7-yl (S)-1-(2-hydroxybenzoyl)-2,3-dihydro-1H-pyrrole-2-carboxylate 2.12. A 20 mL scintillation vial containing silyl ether **2.12a** (20.0 mg, 0.0341 mmol, 1.0 eq.) was purged thrice with argon. DMPU (0.68 mL) was added, followed by TBAF (1M in THF, 0.68 mL, 0.682 mmol, 20 eq.) dropwise, turning the reaction golden brown. The reaction was stirred at room temperature for 2 hours, then was quenched with saturated aqueous NH_4Cl (6 mL). The aqueous layer was extracted 3x with Et_2O, washed 5x with saturated aqueous NH_4Cl and 5x with brine, and dried over Na_2SO_4, then was filtered and concentrated *in vacuo.* Crude product was purified by silica column chromatography (0-6% MeOH/DCM) followed by HPLC, yielding the title compound as a colorless oil (9.1 mg, 58% yield).

^{1}H NMR (600 MHz, $CDCl_3$): δ 9.69 (s, 1H), 7.41 (d, J = 7.7 Hz, 1H), 7.37 (t, J = 7.7 Hz, 1H), 7.00 (d, J = 8.3 Hz, 1H), 6.90 (t, J = 7.5 Hz, 1H), 6.82 (dt, J = 14.7, 6.9 Hz, 1H), 6.77 (s, 1H), 5.84 (d, J = 15.4 Hz, 1H), 5.75 (s, 1H), 5.48 (s, 1H), 5.27 (d, J = 3.3 Hz, 1H), 5.00 (dd, J = 11.3, 4.6 Hz, 1H), 4.98 (s, 1H), 3.13 (dd, J = 16.4, 11.8 Hz, 1H), 2.69 (d, J = 16.8 Hz, 1H), 2.20 (q, J = 6.7 Hz, 2H), 1.64 – 1.17 (m, 22H), 0.86 (t, J = 7.1 Hz, 3H). **^{13}C NMR** (151 MHz, $CDCl_3$): δ 170.9, 168.3, 167.3, 158.6, 145.9, 133.4, 130.8, 128.2, 123.1, 119.0, 117.9, 117.2, 110.7, 75.8, 59.3, 34.2, 33.9, 33.5, 31.74, 31.66, 29.1, 27.6, 25.3, 24.4, 22.5, 14.0. **$[\alpha]^{25}_D$** -25.1 (c 0.45, $CHCl_3$). **HRMS** Accurate Mass (ES+): Found 457.26983 (+ 0.28 ppm), $C_{26}H_{37}O_5N_2$ (M + H+) requires 457.26970.

(R)-tert-butyldiphenyl(tridec-1-en-7-yloxy)silane 2.34a. A 20 mL scintillation vial was flame-dried and purged thrice with argon. Alcohol **2.34** (100.0 mg, 0.504 mmol, 1.0 eq.), tert-butylchlorodiphenylsilane (0.197 mL, 0.756 mmol, 1.5 eq.), and imidazole (85.8 mg, 1.260 mmol, 2.5 eq.) were added sequentially and dissolved in DMF (5 mL). Solution stirred overnight at room temperature, then was concentrated *in vacuo*. Crude product was purified by silica column chromatography (0-10% EtOAc/hexanes), yielding the title compound as a colorless oil (217.7 mg, >95% yield).

^{1}H NMR (500 MHz, $CDCl_3$): δ 7.72 – 7.69 (m, 4H), 7.45 – 7.41 (m, 2H), 7.40 – 7.36 (m, 4H), 5.77 (ddt, J = 16.9, 10.2, 6.7 Hz, 1H), 4.97 (dq, J = 17.1, 1.6 Hz, 1H), 4.93 (ddt, J = 10.2, 2.3, 1.2 Hz, 1H), 3.73 (p, J = 5.6 Hz, 1H), 1.97 (q, J = 6.9 Hz, 2H), 1.43 (dt, J = 11.7, 5.6 Hz, 4H), 1.31 – 1.19 (m, 9H), 1.20 – 1.12 (m, 4H), 1.08 (s, 9H), 0.88 (t, J = 7.2 Hz, 3H). **^{13}C NMR** (126 MHz, $CDCl_3$): δ 139.1, 136.0, 134.9, 129.4, 127.4, 114.2, 73.2, 36.4, 36.2, 33.7, 31.8, 29.4, 29.0, 27.1, 24.9, 24.4, 22.6, 19.4, 14.1. **$[\alpha]^{25}_{D}$** -0.40 (c 0.443, $CHCl_3$). **HRMS** Accurate Mass (ES+): Found 437.32317 (- 0.25 ppm), $C_{29}H_{45}O^{28}Si$ (M + H+) requires 437.32342.

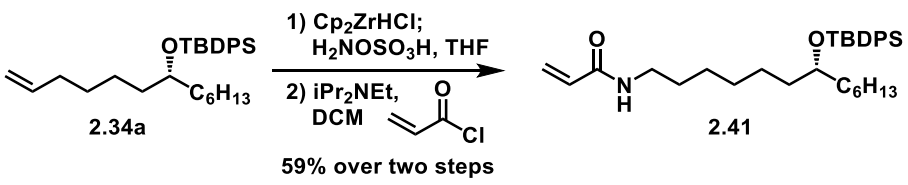

(R)-N-(7-((tert-butyldiphenylsilyl)oxy)tridecyl)acrylamide 2.41.[6] A 5 mL reaction tube containing 3A MS was flame-dried. Schwartz's reagent (Cp_2ZrHCl, 156.0 mg, 0.604 mmol, 1.5

eq.) was added and the reaction tube was purged thrice with argon. Alkene **2.34a** (200.0 mg, 0.403 mmol, 1.0 eq.) was added, followed by THF (1.5 mL). The reaction tube was capped and the cloudy yellow reaction stirred at room temperature until the solution became homogenous (~35 minutes), at which point hydroxylamine-O-sulfonic acid (82.0 mg, 0.725 mmol, 1.8 eq.) was added in one portion. The now-colorless reaction continued to stir at RT for 30 minutes, then NaOH (1M in H_2O, 5 mL) was added followed by H_2O and the aqueous layer was extracted 3x with Et_2O. Combined organic layers were dried over anhydrous Na_2SO_4, filtered, and concentrated in vacuo to yield crude amine, which was purged thrice with argon. DCM (3 mL) was added and the solution was cooled to 0 °C. Diisopropylethylamine (0.175 mL, 1.01 mmol, 2.5 eq.) was added and the solution stirred 5 minutes. Acryloyl chloride (0.050 mL, 0.604 mmol, 1.5 eq.) was added dropwise, the reaction was warmed to room temperature and continued to stir four hours. The reaction was quenched with the addition of water (5 mL) and the aqueous layer was extracted 4x with DCM. Combined organic layers were washed once with brine, back-extracted once with DCM, dried over anhydrous Na_2SO_4, filtered, and concentrated *in vacuo*. Crude product was purified by silica column chromatography (0-40% EtOAc/hexanes), to yield the title compound as a pale yellow oil (119.9 mg, 59% yield over two steps).

^{1}H NMR (500 MHz, $CDCl_3$): δ 7.67 (dt, J = 8.0, 1.2 Hz, 4H), 7.43 – 7.38 (m, 2H), 7.38 – 7.33 (m, 4H), 6.27 (dd, J = 17.0, 1.4 Hz, 1H), 6.07 (dd, J = 17.0, 10.3 Hz, 1H), 5.63 (dd, J = 10.3, 1.4 Hz, 1H), 5.52 (s, 1H), 3.69 (p, J = 5.6 Hz, 1H), 3.28 (q, J = 7.2 Hz, 2H), 1.44 (dt, J = 14.6, 7.2 Hz, 2H), 1.38 (dt, J = 12.2, 6.3 Hz, 4H), 1.26 – 1.08 (m, 17H), 1.04 (s, 9H), 0.85 (t, J = 7.2 Hz, 3H). **^{13}C NMR** (126 MHz, $CDCl_3$): δ 165.6, 136.1, 134.9, 131.1, 129.5, 127.5, 126.3, 73.3, 39.7, 36.5, 36.3, 31.9, 29.6, 29.49, 29.45, 27.2, 27.0, 25.0, 24.9, 22.7, 19.6, 14.2. **$[\alpha]^{25}_D$** -0.97 (c 0.350, $CHCl_3$).

HRMS Accurate Mass (ES+): Found 506.34492 (- 2.10 ppm), $C_{32}H_{48}O_2N^{28}Si$ (M + H+) requires 506.34598.

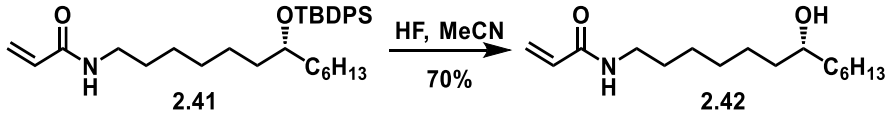

(R)-N-(7-hydroxytridecyl)acrylamide 2.42. A 20 mL scintillation vial containing acrylamide **2.41** (119.9 mg, 0.236 mmol) was purged thrice with argon. Acetonitrile (2 mL) was added and the solution was cooled to 0 °C. Hydrofluoric acid (40% solution in H_2O, 1 mL) was then added and the reaction stirred for 16 hours, allowing it to warm to room temperature. The reaction was poured into a separatory funnel, diluted with water, and carefully neutralized with aqueous sodium bicarbonate. The aqueous layer was then extracted 4x with dichloromethane. Combined organic layers were washed once with brine, back-extracted once, and dried over anhydrous Na_2SO_4 before being filtered and concentrated *in vacuo*. Crude product was purified by silica column chromatography (10-70% EtOAc in hexanes), to yield the title compound as a white solid (44.7 mg, 70% yield)**.**

^{1}H NMR (600 MHz, $CDCl_3$): δ 6.27 (d, J = 17.0 Hz, 1H), 6.07 (ddd, J = 16.9, 10.3, 1.6 Hz, 1H), 5.62 (d, J = 10.3 Hz, 1H), 5.57 (s, 1H), 3.57 (br s, 1H), 3.35 – 3.30 (m, 2H), 1.64 (s, 2H), 1.57 – 1.50 (m, 2H), 1.47 – 1.24 (m, 22H), 0.88 (t, J = 6.2 Hz, 3H). **^{13}C NMR** (151 MHz, $CDCl_3$): δ 165.6, 131.1, 126.4, 72.1, 39.7, 37.7, 37.5, 32.0, 29.6, 29.5, 29.4, 27.0, 25.8, 25.6, 22.8, 14.2. **$[\alpha]^{25}_D$**

-1.8 (c 0.415, $CHCl_3$). **HRMS** Accurate Mass (ES+): Found 268.22815 (- 0.19 ppm), $C_{16}H_{30}O_2N$ (M - H+) requires 268.22820.

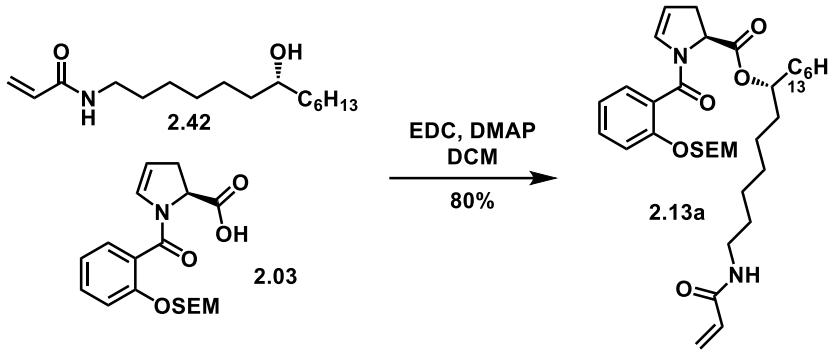

(R)-1-acrylamidotridecan-7-yl (S)-1-(2-((2-(trimethylsilyl)ethoxy)methoxy)benzoyl)-2,3-dihydro-1H-pyrrole-2-carboxylate 2.13a. A 20 mL scintillation vial containing acid **2.03** was purged 3x with argon. DCM (1.5 mL) was added and the solution was cooled to 0 °C. EDC (36.0 mg, 0.19 mmol, 2.5 eq.) and DMAP (36.0 mg, 0.30 mmol, 4 eq.) were added and the reaction stirred 5 minutes at 0 °C. Acrylamide **2.42** was dissolved in DCM (2 mL) and transferred to the reaction vial. The reaction was warmed to RT and stirred 24 hours, then was diluted with water and extracted 5x with DCM. Combined organic layers were washed once with brine, back-extracted once with DCM, dried over anhydrous Na_2SO_4, filtered, and concentrated *in vacuo*. Crude product was purified by silica column chromatography (0-40% EtOAc/hexanes), to yield the title compound as a yellow oil (36.4 mg, 80% yield).

^{1}H NMR (500 MHz, $CDCl_3$): δ 7.37 – 7.29 (m, 2H), 7.19 (d, J = 8.3 Hz, 1H), 7.03 (t, J = 7.5 Hz, 1H), 6.57 (s, 1H), 6.16 (dt, J = 4.1, 2.0 Hz, 1H), 6.12 (dd, J = 17.0, 1.6 Hz, 1H), 5.80 (dd, J = 17.0, 10.3 Hz, 1H), 5.36 (dd, J = 10.3, 1.6 Hz, 1H), 5.24 – 5.18 (m, 2H), 5.05 (dt, J = 4.5, 2.5 Hz, 1H), 5.03 – 4.99 (m, 1H), 4.97 (dd, J = 11.6, 4.7 Hz, 1H), 3.72 (t, J = 8.1 Hz, 2H), 3.25 (ddt, J = 28.3,

13.2, 6.4 Hz, 2H), 3.13 (ddt, J = 16.5, 11.6, 2.3 Hz, 1H), 2.67 (ddt, J = 17.0, 4.7, 2.5 Hz, 1H), 1.99 (s, 1H), 1.62 – 1.46 (m, 6H), 1.42 – 1.18 (m, 16H), 0.92 (dd, J = 9.2, 7.5 Hz, 2H), 0.86 (t, J = 6.9 Hz, 3H), -0.02 (s, 9H). **^{13}C NMR** (126 MHz, $CDCl_3$): δ 170.6, 165.7, 165.3, 153.8, 131.4, 131.3, 131.0, 128.9, 125.8, 125.3, 122.1, 115.3, 108.7, 93.3, 75.2, 66.7, 58.0, 39.3, 34.6, 34.4, 34.1, 31.8, 29.3, 28.6, 28.3, 26.4, 25.5, 24.6, 22.7, 18.2, 14.2, -1.3. **$[\alpha]^{25}_D$** -39.6 (c 0.985, $CHCl_3$). **HRMS** Accurate Mass (ES+): Found 615.38291 (+ 0.84 ppm), $C_{34}H_{55}O_6N_2{}^{28}Si$ (M + H+) requires 615.38239.

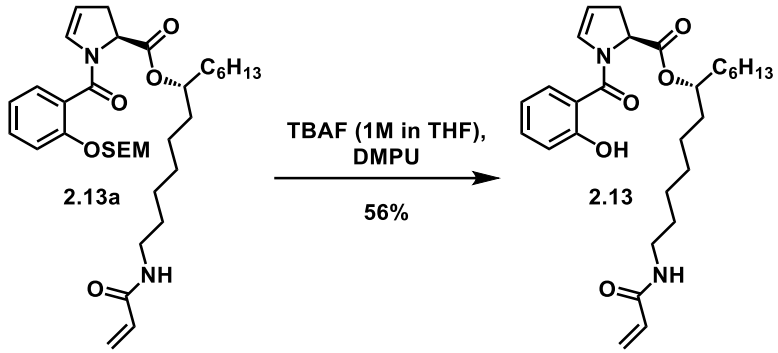

(R)-1-acrylamidotridecan-7-yl (S)-1-(2-hydroxybenzoyl)-2,3-dihydro-1H-pyrrole-2-carboxylate 2.13. A 20 mL scintillation vial containing silyl ether **2.13a** (17.2 mg, 0.0280 mmol, 1.0 eq.) was purged thrice with argon. DMPU (0.56 mL) was added, followed by TBAF (1M in THF, 0.56 mL, 0.559 mmol, 20 eq.) dropwise, turning the reaction golden brown. The reaction was stirred at room temperature for 2 hours, then was quenched with saturated aqueous NH_4Cl (6 mL). The aqueous layer was extracted 3x with Et_2O, washed 5x with saturated aqueous NH_4Cl and 5x with brine, and dried over Na_2SO_4, then was filtered and concentrated *in vacuo*. Crude product was purified by silica column chromatography (10-55% EtOAc/hexanes) followed by HPLC, yielding the title compound as a white solid (7.6 mg, 56% yield).

^{1}H NMR (600 MHz, $CDCl_3$): δ 9.88 (s, 1H), 7.42 (d, J = 7.8 Hz, 1H), 7.37 (t, J = 7.8 Hz, 1H), 6.99 (d, J = 8.3 Hz, 1H), 6.89 (t, J = 7.5 Hz, 1H), 6.80 (s, 1H), 6.24 (d, J = 17.0 Hz, 1H), 6.05 (dd, J = 17.0, 10.3 Hz, 1H), 5.85 (s, 1H), 5.57 (d, J = 11.4 Hz, 1H), 5.28 (d, J = 4.1 Hz, 1H), 5.00 (dd, J = 11.2, 4.9 Hz, 2H), 3.30 (ddq, J = 26.3, 13.3, 6.7 Hz, 2H), 3.12 (dd, J = 16.7, 11.5 Hz, 1H), 2.69 (d, J = 17.1 Hz, 1H), 1.69 (s, 7H), 1.59 – 1.47 (m, 8H), 1.37 – 1.18 (m, 24H), 0.86 (t, J = 7.1 Hz, 4H). **^{13}C NMR** (151 MHz, $CDCl_3$): δ 171.1, 167.5, 165.7, 159.0, 133.6, 131.2, 131.0, 128.4, 126.1, 119.1, 118.1, 117.2, 110.9, 76.0, 59.6, 39.6, 34.4, 34.3, 33.6, 31.8, 29.9, 29.2, 28.9, 26.9, 25.5, 24.9, 22.7, 14.2. **$[\alpha]^{25}_D$** -13.419 (c 0.313, $CHCl_3$). **HRMS** Accurate Mass (ES+): Found 485.30071 (- 0.29 ppm), $C_{28}H_{41}O_5N_2$ (M + H+) requires 485.30100.

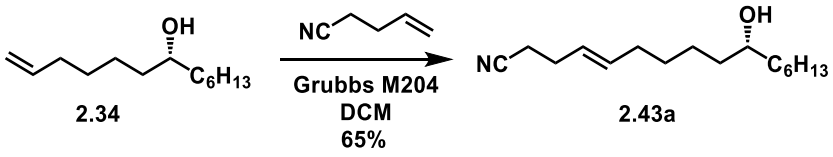

(R,E)-10-hydroxyhexadec-4-enenitrile 2.43a.[111] A 10 mL round-bottom flask fitted with reflux condenser was flame-dried and purged thrice with argon. Homoallyl cyanide (142.2 mg, 1.753 mmol, 3.0 eq.) was added, followed by a solution of alcohol **2.34** (115.9 mg, 0.584 mmol, 1.0 eq.) in DCM (4 mL). Hoveyda-Grubbs catalyst (M720, 55.0 mg, 0.0877 mmol, 0.15 eq.) was added in one portion and the solution was heated to reflux and stirred 2 hours. Product was directly purified by silica column chromatography (0-40% EtOAc/hexanes), yielding title compound as a brown oil (95.3 mg, 65% yield).

^{1}H NMR (500 MHz, $CDCl_3$): δ 5.87 – 5.24 (m, 2H), 3.54 (br s, 1H), 2.38 – 2.34 (m, 1H), 2.34 – 2.26 (m, 1H), 2.08 – 1.95 (m, 2H), 1.60 (s, 1H), 1.47 – 1.33 (m, 8H), 1.32 – 1.20 (m, 8H), 0.86 (t, J = 6.9 Hz, 3H). **^{13}C NMR** (126 MHz, $CDCl_3$): δ 134.2, 125.8, 117.3, 71.9, 37.6, 37.3, 32.4, 31.9,

29.4, 29.3, 28.4, 25.7, 25.1, 22.7, 17.8, 14.2. **[α]$^{25}_{D}$** -2.8 (c 0.638, $CHCl_3$). **HRMS** Accurate Mass (ES+): Found 252.23237 (+ 0.71 ppm), $C_{16}H_{30}ON$ (M + H+) requires 252.23219.

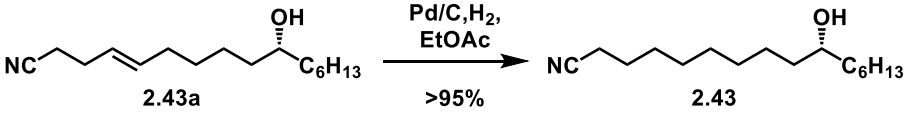

(R)-10-hydroxyhexadecanenitrile 2.43.[265] A 20 mL scintillation vial was flame-dried and purged thrice with argon. Alkene **2.43a** (30.0 mg, 0.119 mmol, 1.0 eq.) and palladium on activated carbon (5% Pd, 8.9 mg, 0.0042 mmol, 0.035 eq.) were added and dissolved in ethyl acetate (2 mL). The vial was evacuated and backfilled with hydrogen gas four times, then the reaction was left to stir under a hydrogen atmosphere (1 atm) for 4 hours. The dark grey suspension was filtered through Celite, eluting with 100% ethyl acetate to afford the title compound as a colorless oil (30.2 mg, >95% yield).

^{1}H NMR (500 MHz, $CDCl_3$): δ 3.56 (dt, J = 8.4, 4.1 Hz, 1H), 2.32 (t, J = 7.1 Hz, 2H), 1.64 (p, J = 7.2 Hz, 2H), 1.49 – 1.34 (m, 10H), 1.34 – 1.21 (m, 14H), 0.87 (t, J = 6.9 Hz, 3H). **^{13}C NMR** (126 MHz, $CDCl_3$): δ 119.9, 72.1, 37.6, 37.5, 32.0, 29.6, 29.5, 29.4, 28.8, 28.7, 25.72, 25.68, 25.5, 22.7, 17.2, 14.2. **[α]$^{25}_{D}$** -1.5 (c 0.881, $CHCl_3$). **HRMS** Accurate Mass (ES+): Found 254.24775 (- 0.35 ppm), $C_{16}H_{32}ON$ (M + H+) requires 254.24784.

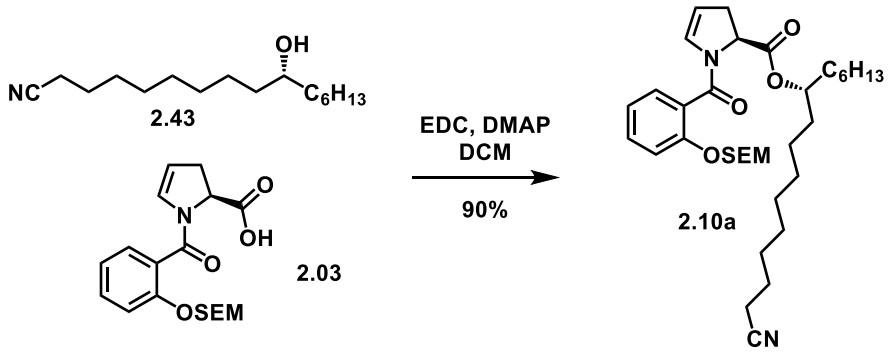

(R)-15-cyanopentadecan-7-yl (S)-1-(2-((2-(trimethylsilyl)ethoxy)methoxy)benzoyl)-2,3-dihydro-1H-pyrrole-2-carboxylate 2.10a. A 20 mL scintillation vial containing acid **2.03** (41.0 mg, 0.113 mmol, 2.0 eq.) was purged thrice with argon. DCM (1.5 mL) was added and the reaction was cooled to 0 °C. EDC (21.6 mg, 0.113 mmol, 2 eq.) and DMAP (27.6 mg, 0.226 mmol, 4.0 eq.) were added and the orange solution stirred 5 minutes at 0 °C. A solution of alcohol **2.43** (14.3 mg, 0.056 mmol, 1.0 eq.) in DCM (2 mL) was added and the reaction stirred overnight, allowing it to warm to room temperature. The reaction was diluted with water and the aqueous phase was extracted 5x with DCM. Combined organic layers were washed once with brine, back-extracted once with DCM, dried over anhydrous Na_2SO_4, filtered, and concentrated *in vacuo*. Product was purified by silica column chromatography (0-25% EtOAc/hexanes), affording the title compound as a yellow oil (30.4 mg, 90% yield).

^{1}H NMR (500 MHz, $CDCl_3$): δ 7.39-7.32 (m, 2H), 7.19 (d, J = 8.0 Hz, 1H), 7.03 (t, J = 7.5 Hz, 1H), 6.16 (s, 1H), 5.25 – 5.19 (m, 2H), 5.02 (dt, J = 4.0, 1.9 Hz, 1H), 4.99 – 4.93 (m, 2H), 3.76 – 3.70 (m, 2H), 3.12 (ddt, J = 16.6, 11.6, 2.3 Hz, 1H), 2.66 (dt, J = 16.8, 2.2 Hz, 1H), 2.30 (t, J = 7.2 Hz, 2H), 1.64 – 1.51 (m, 6H), 1.44 – 1.36 (m, 3H), 1.26 (dd, J = 13.7, 6.9 Hz, 16H), 0.93 (dd, J = 9.4, 7.4 Hz, 2H), 0.86 (t, J = 6.6 Hz, 3H), -0.02 (s, 9H). **^{13}C NMR** (126 MHz, $CDCl_3$): δ 170.8, 165.0, 153.9, 131.2, 131.1, 129.0, 126.0, 122.0, 120.0, 115.3, 108.3, 93.4, 75.5, 66.6, 58.2, 34.4, 34.2, 31.9, 29.4, 29.3, 29.2, 28.7, 28.6, 25.5, 25.3, 25.2, 25.1, 22.7, 18.2, 17.2, 14.2, -1.3. **$[\alpha]^{25}_D$** -

41.4 (c 1.047, $CHCl_3$). **HRMS** Accurate Mass (ES+): Found 599.38769 (+ 0.36 ppm), $C_{34}H_{55}O_5N_2{}^{28}Si$ (M + H+) requires 599.38748.

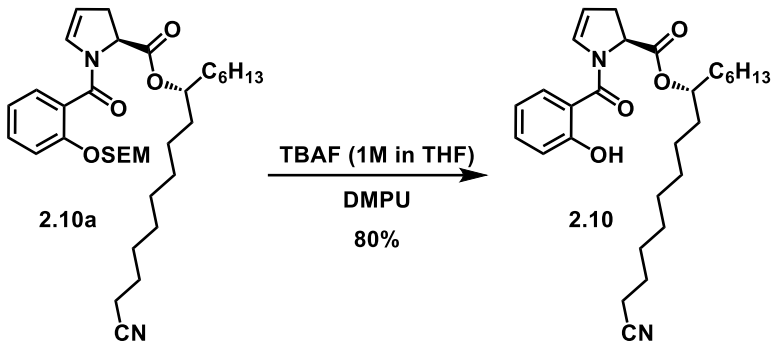

(R)-15-cyanopentadecan-7-yl (S)-1-(2-hydroxybenzoyl)-2,3-dihydro-1H-pyrrole-2-carboxylate 2.10. A 20 mL scintillation vial containing silyl ether **2.10a** (13.6 mg, 0.0227 mmol, 1.0 eq.) was purged thrice with argon. DMPU (0.44 mL) was added, followed by TBAF (1M in THF, 0.44 mL, 0.444 mmol, 20 eq.) dropwise, turning the reaction golden brown. The reaction was stirred at room temperature for 2 hours, then was quenched with saturated aqueous NH_4Cl (6 mL). The aqueous layer was extracted 3x with Et_2O, washed 5x with saturated aqueous NH_4Cl and 5x with brine, and dried over Na_2SO_4, then was filtered and concentrated *in vacuo*. Crude product was purified by silica column chromatography (0-40% EtOAc/hexanes) followed by HPLC, yielding the title compound as a colorless oil (8.5 mg, 80% yield).

^{1}H NMR (600 MHz, $CDCl_3$): δ 9.87 (s, 1H), 7.42 (d, J = 7.9 Hz, 1H), 7.37 (t, J = 8.5 Hz, 1H), 7.00 (d, J = 8.3 Hz, 1H), 6.89 (t, J = 7.5 Hz, 1H), 6.82 (s, 1H), 5.33 – 5.21 (m, 1H), 5.00 (dd, J = 11.2, 5.0 Hz, 1H), 4.96 (br s, 1H), 3.20 – 3.05 (m, 1H), 2.70 (d, J = 16.9 Hz, 1H), 2.31 (t, J = 7.2 Hz, 2H), 1.67 – 1.50 (m, 15H), 1.43 (dt, J = 15.0, 7.4 Hz, 3H), 1.36 – 1.17 (m, 22H), 0.86 (t, J =

7.1 Hz, 3H). **^{13}C NMR** (151 MHz, $CDCl_3$): δ 171.0, 167.6, 159.3, 133.6, 131.1, 128.5, 120.1, 119.0, 118.1, 117.0, 110.7, 76.0, 59.6, 34.2, 33.6, 31.8, 29.9, 29.8, 29.3, 29.2, 28.8, 28.7, 25.5, 25.4, 25.1, 22.7, 17.2, 14.2. **$[\alpha]^{25}_D$** -59.101 (c 0.089, $CHCl_3$). **HRMS** Accurate Mass (ES+): Found 469.30704 (+ 0.96 ppm), $C_{28}H_{41}O_4N_2$ (M + H+) requires 469.30608.

6.3.3 Berberine: Experimental Procedures and Characterization Data

General Procedure 3A: Dimerizations.[142] Berberrubine chloride **3.08** (2.4 eq.) was combined with diiodide (1 eq.) in N,N-dimethylformamide (0.1M). Reaction vessel was sealed and heated to 70°C, and solution was stirred under a static argon atmosphere until TLC analysis showed reaction completion (48-72 hours). Solvent was removed *in vacuo* and product was purified via silica gel column chromatography.

General Procedure 3B: Dimerizations.[142] Berberrubine chloride **3.08** (2.4 eq.) was combined with dibromide (1 eq.) and sodium iodide (2 eq.) in N,N-dimethylformamide (0.1M). Reaction vessel was sealed and heated to 70°C, and solution was stirred under a static argon atmosphere until TLC analysis showed reaction completion (48-72 hours). Solvent was removed *in vacuo* and product was purified via silica gel column chromatography.

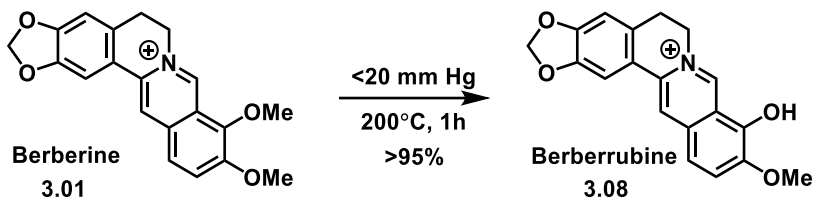

Berberrubine chloride 3.08.[142] Berberine chloride **3.01** (500 mg, 1.34 mmol, 1 eq.) was heated to 200°C under vacuum (<20 mm Hg) for 45 minutes with stirring, causing a color change from yellow to red. Solid was filtered, washing with chloroform. Filtrate was purified by silica column

chromatography (0-10% MeOH in DCM) to yield the title compound as a dark red solid (480 mg, >95% yield).

^{1}H NMR (600 MHz, $CDCl_3$): δ 9.16 (s, 1H), 7.54 (s, 1H), 7.21 (d, *J* = 7.9 Hz, 1H), 7.20 (s, 1H), 6.71 (s, 1H), 6.46 (d, *J* = 7.9 Hz, 1H), 6.02 (s, 2H), 4.36 (s, 2H), 3.87 (s, 3H), 3.08 – 3.02 (m, 2H). **^{13}C NMR** (151 MHz, $CDCl_3$): δ 167.9, 150.8, 149.0, 148.1, 145.6, 132.9, 131.3, 128.1, 122.2, 120.4, 120.0, 117.5, 108.3, 104.5, 102.8, 101.8, 56.0, 53.2, 28.6. **HRMS** Accurate mass (ES+): Found 322.10777 (+1.21 ppm), $C_{19}H_{16}NO_4$ (M^+) requires 322.10738.

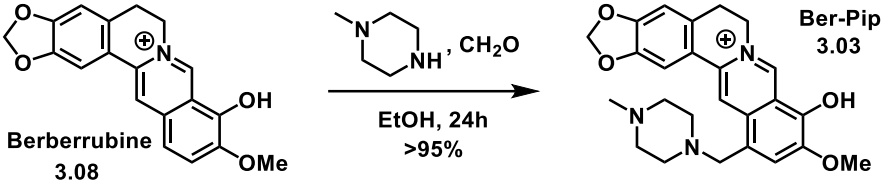

9-hydroxy-10-methoxy-12-((4-methylpiperazin-1-yl)methyl)-5,6-dihydro-[1,3]dioxolo[4,5-g]isoquinolino[3,2-a]isoquinolin-7-ium chloride 3.03.[144] To a solution of berberrubine **3.08** (24 mg, 0.067 mmol, 1 eq.) in anhydrous EtOH (1 mL) was added N-methylpiperazine (0.037 mL, 0.335 mmol, 5 eq.) and formaldehyde (37% aq., 0.035 mL, 0.335 mmol, 5 eq.). The solution stirred at room temperature for 24 hours and was then concentrated *in vacuo* and purified by silica column chromatography (0-5% MeOH/DCM) to afford the title compound as a yellow powder (30.5 mg, >95% yield).

^{1}H NMR (600 MHz, $CDCl_3$): δ 9.21 (s, 1H), 8.03 (s, 1H), 7.21 (s, 1H), 7.18 (s, 1H), 6.70 (s, 1H), 6.02 (s, 2H), 4.38 (t, *J* = 5.9 Hz, 2H), 3.86 (s, 3H), 3.65 (s, 2H), 3.04 (t, *J* = 6.0 Hz, 2H), 2.52 (s, 8H), 2.29 (s, 3H). **^{13}C NMR** (151 MHz, $CDCl_3$): δ 167.2, 149.9, 149.2, 148.2, 145.8, 133.0, 129.7, 128.3, 123.8, 122.6, 120.5, 115.1, 110.0, 108.5, 104.7, 101.9, 64.4, 59.8, 56.3, 55.2, 53.3, 52.7,

45.8, 28.6, 25.5. **HRMS** Accurate mass (ES+): Found 434.20693 (-1.17 ppm), $C_{25}H_{28}N_3O_4$ (M^+) requires 434.20743.

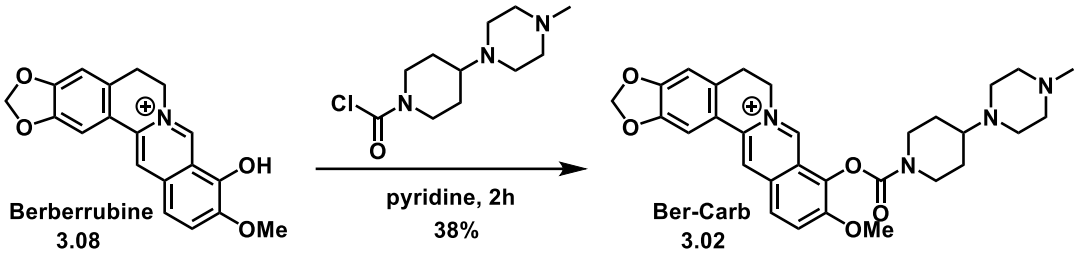

10-methoxy-9-((4-(4-methylpiperazin-1-yl)piperidine-1-carbonyl)oxy)-5,6-dihydro-[1,3]dioxolo[4,5-g]isoquinolino[3,2-a]isoquinolin-7-ium chloride formate 3.02.[143] Berberrubine **3.08** (96.4 mg, 0.300 mmol, 1 eq.) was dissolved in pyridine (1 mL) and added in one portion to 4-(4-methylpiperazin-1-yl)piperidine-1-carbonyl chloride (369 mg, 1.50 mmol, 5 eq.)**.** The solution was stirred at room temperature for 2 hours, then was concentrated *in vacuo* and purified by silica column chromatography (0-5% MeOH/DCM) to yield the title compound as a yellow solid (64.6 mg, 38% yield)**.**

^{1}H NMR (600 MHz, D_2O): δ 9.24 (s, 1H), 8.41 (s, 1H), 8.15 (s, 1H), 7.84 (d, *J* = 19.0 Hz, 2H), 7.14 (s, 1H), 6.80 (s, 1H), 6.00 (s, 2H), 4.65 (s, 2H), 4.40 (s, 1H), 4.11 (d, *J* = 12.9 Hz, 1H), 3.92 (s, 3H), 3.68 – 3.52 (m, 2H), 3.22 – 3.16 (m, 1H), 3.09 – 2.97 (m, 4H), 2.62 (br s, 4H), 2.27 (s, 4H), 2.05 (br s, 2H), 1.56 (d, *J* = 8.5 Hz, 1H), 1.47 (d, *J* = 10.4 Hz, 1H). **^{13}C NMR** (151 MHz, D_2O): δ 171.0, 153.3, 150.5, 150.2, 147.6, 142.7, 138.0, 133.7, 132.9, 130.1, 126.4, 125.3, 121.4, 119.6, 108.3, 105.0, 102.3, 60.6, 56.9, 56.0, 53.5, 47.8, 27.6, 27.2, 26.4. **HRMS** Accurate mass (ES+): Found 531.26012 (-0.14 ppm), $C_{30}H_{35}N_4O_5$ (M^+) requires 531.26020.

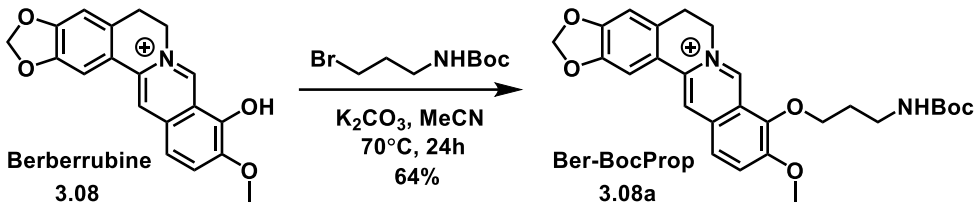

9-(3-((tert-butoxycarbonyl)amino)propoxy)-10-methoxy-5,6-dihydro-[1,3]dioxolo[4,5-g]isoquinolino[3,2-a]isoquinolin-7-ium chloride 3.08a. To a solution of berberrubine **3.08** (50 mg, 0.134 mmol, 1 eq.) and K_2CO_3 (18.6 mg, 0.403 mmol, 3 eq.) in acetonitrile (1 mL) preheated to 70°C was added tert-butyl (3-bromopropyl)carbamate (64 mg, 0.269 mmol, 2 eq.). Additional acetonitrile (0.5 mL) was added, the vessel was sealed, and the reaction continued to stir at 70°C for 24 hours. The crude reaction mixture was cooled to RT and purified by silica column chromatography (0-10% MeOH/DCM), yielding the title compound as a yellow powder (45.9 mg, 64%).

^{1}H NMR (500 MHz, DMSO-d_6): δ 9.83 (s, 1H), 8.93 (s, 1H), 8.19 (d, J = 9.2 Hz, 1H), 7.97 (d, J = 9.0 Hz, 1H), 7.79 (s, 1H), 7.09 (s, 1H), 6.97 (t, J = 5.7 Hz, 1H), 6.16 (s, 2H), 5.00 – 4.89 (m, 2H), 4.28 (t, J = 6.0 Hz, 2H), 4.04 (s, 3H), 3.24 – 3.15 (m, 4H), 1.94 (p, J = 5.9, 5.5 Hz, 2H), 1.34 (s, 9H). **^{13}C NMR** (151 MHz, DMSO-d_6): δ 155.9, 150.3, 149.8, 147.7, 145.4, 142.7, 137.4, 133.0, 130.6, 126.6, 123.3, 121.5, 120.4, 120.2, 108.4, 105.4, 102.1, 77.7, 71.8, 57.1, 55.3, 55.0, 36.7, 30.3, 28.3, 26.3. **HRMS** Accurate mass (ES+): Found 479.21776 (-0.14 ppm), $C_{27}H_{31}N_2O_6$ (M^+) requires 479.21766.

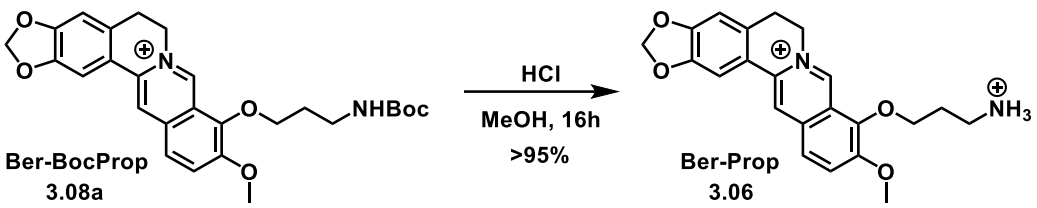

9-(3-ammoniopropoxy)-10-methoxy-5,6-dihydro-[1,3]dioxolo[4,5-g]isoquinolino[3,2-a]isoquinolin-7-ium dichloride 3.06. Carbamate **Ber-BocProp 3.08a** (10 mg, 0.019 mmol, 1 eq.) was dissolved in MeOH (4 mL) and HCl (12M, 2.0 mL, 24 mmol) was added. Reaction was stirred at room temperature for 24 hours, then solvent was removed *in vacuo* to afford the pure HCl salt product as a yellow powder (8.5 mg, >95% yield).

^{1}H NMR (600 MHz, DMSO-d_6): δ 9.98 (s, 1H), 8.94 (s, 1H), 8.24 – 8.17 (m, 4H), 7.98 (d, J = 9.1 Hz, 1H), 7.79 (s, 1H), 7.08 (s, 1H), 6.16 (s, 2H), 5.01 (t, J = 6.2 Hz, 2H), 4.37 (t, J = 5.8 Hz, 2H), 4.07 (s, 3H), 3.22 – 3.17 (m, 2H), 3.10 (q, J = 6.7, 6.3 Hz, 2H), 2.18 (p, J = 6.3 Hz, 2H). **^{13}C NMR** (151 MHz, DMSO-d_6): δ 150.7, 150.3, 148.2, 146.0, 143.1, 138.0, 133.4, 131.2, 127.1, 124.0, 121.9, 120.9, 120.7, 108.9, 105.9, 102.6, 72.0, 57.6, 55.6, 36.6, 28.3, 26.8. **HRMS** Accurate mass (ES-): Found 379.16512 (-0.31 ppm), $C_{22}H_{23}N_2O_4$ (M^{2+} -H^+) requires 379.16523.

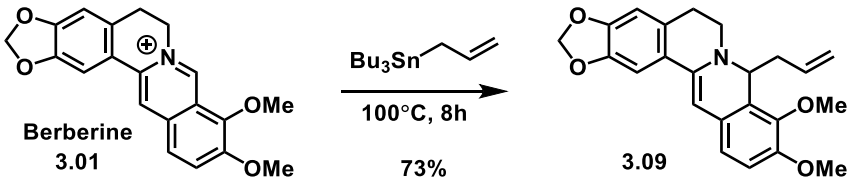

8-allyl-9,10-dimethoxy-5,8-dihydro-6H-[1,3]dioxolo[4,5-g]isoquinolino[3,2-a]isoquinoline 3.09.[147] In a thick-walled pressure tube, berberine chloride **3.01** (0.433g, 1.165 mmol, 1.00 eq.) and allyltributylstannane (1.0 mL, 1.068g, 3.230 mmol, 2.75 eq.) were dissolved in DCM (10 mL). The tube was sealed tightly, placed behind a blast shield, and heated to 100°C, at which

temperature it stirred for 8 hours. Reaction was carefully cooled to room temperature and concentrated *in vacuo*. Crude product was crystallized with methanol at -20°C and filtered, yielding the title compound as yellow crystals (322 mg, 73% yield). Spectral data are consistent with literature reports.

^{1}H NMR (600 MHz, $CDCl_3$): δ 7.13 (s, 1H), 6.74 (q, J = 8.3 Hz, 2H), 6.58 (s, 1H), 5.94 (d, J = 8.7 Hz, 2H), 5.85-5.76 (m, 1H), 5.80 (s, 1H), 4.89 (d, J = 6.7 Hz, 1H), 4.87 (s, 1H), 4.83 (t, J = 5.8 Hz, 1H), 3.89 (s, 3H), 3.84 (s, 3H), 3.50 (td, J = 10.9, 4.1 Hz, 1H), 3.30 (dt, J = 9.6, 4.1 Hz, 1H), 2.83 (tdt, J = 15.0, 7.9, 5.2 Hz, 4H), 2.52 – 2.37 (m, 4H).

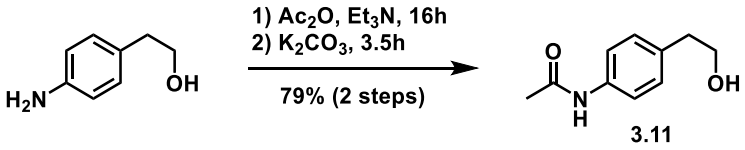

N-(4-(2-hydroxyethyl)phenyl)acetamide 3.11. A solution of 2-(4-aminophenyl)ethanol (1.00g, 7.29 mmol, 1.0 eq.) in DCM (10 mL) was prepared. Freshly distilled triethylamine (2.2 mL, 1.60g, 15.8 mmol, 2.2 eq.) was added, followed by acetic anhydride (2.4 mL, 2.59g, 25.4 mmol, 3.5 eq.). The solution stirred overnight at room temperature and was quenched with sat. aq. $NaHCO_3$. The aqueous layer was extracted 4x with DCM, then combined organic layers were dried over anhydrous Na_2SO_4, filtered, and concentrated *in vacuo*. The product was purified via trituration with hexanes, followed by filtration, yielding diacylated material as tan flakes. These flakes were redissolved in MeOH (30 mL) and excess K_2CO_3 was added. After stirring at room temperature for 3.5 hours, the solvent was evaporated and the crude product was purified by silica column chromatography (dry-loading, 0-10% MeOH/DCM) to yield the title compound as a white powder (1.026g, 79% yield over two steps). Spectral data are consistent with literature reports.

^{1}H NMR (600 MHz, $CDCl_3$): δ 7.43 (d, J = 8.4 Hz, 2H), 7.18 (d, J = 8.3 Hz, 2H), 3.84 (t, J = 6.5 Hz, 2H), 2.83 (t, J = 6.5 Hz, 2H), 2.17 (s, 3H).

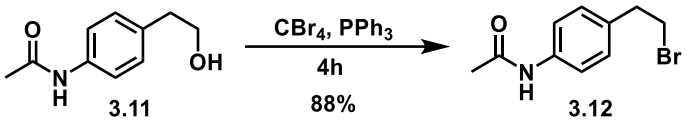

N-(4-(2-bromoethyl)phenyl)acetamide 3.12. Alcohol **3.11** (0.400g, 2.23 mmol, 1.0 eq.) was dissolved in 3:2 DCM : MeCN (4 mL). The solution was cooled to 0°C and carbon tetrabromide (0.925g, 2.79 mmol, 1.3 eq) was added. Triphenylphosphine (0.878g, 3.35 mmol, 1.5 eq.) was then added in three portions over ten minutes and the reaction continued to stir at 0°C. After 15 minutes, the solution was warmed to room temperature and stirred an additional 4 hours, at which point solvent was removed *in vacuo*. Crude product was purified by silica column chromatography (0-40% EtOAc/hexanes), yielding product as a yellow solid (0.476g, 88% yield). Spectral data are consistent with literature reports.

^{1}H NMR (600 MHz, $CDCl_3$): δ 7.45 (d, *J* = 8.3 Hz, 2H), 7.16 (d, *J* = 8.3 Hz, 2H), 3.53 (t, *J* = 7.6 Hz, 2H), 3.12 (t, *J* = 7.6 Hz, 2H), 2.17 (s, 3H). **^{13}C NMR** (151 MHz, $CDCl_3$): δ 168.1, 136.6, 134.8, 129.2, 120.0, 38.7, 32.9, 24.5.

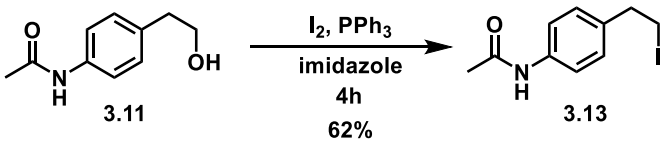

N-(4-(2-iodoethyl)phenyl)acetamide 3.13. Alcohol **3.11** (0.100g, 0.558 mmol, 1.0 eq.), imidazole (0.0760g, 1.12 mmol, 2.0 eq), and triphenylphosphine (0.329g, 1.26 mmol, 2.3 eq.) were dissolved in THF (4 mL). Iodine (0.262g, 1.03 mmol, 1.9 eq.) was then added, causing precipitation of a tan solid. This suspension was vigorously stirred for 4 hours, at which point

solvent was removed *in vacuo*. Crude product was purified by silica column chromatography (0-40% EtOAc/hexanes), yielding product as a yellow solid (0.101g, 62% yield).

^{1}H NMR (600 MHz, $CDCl_3$): δ 7.59 (br s, 1H), 7.44 (d, *J* = 7.9 Hz, 2H), 7.12 (d, *J* = 8.0 Hz, 2H), 3.30 (t, *J* = 7.6 Hz, 2H), 3.12 (t, *J* = 7.7 Hz, 2H), 2.15 (s, 3H).

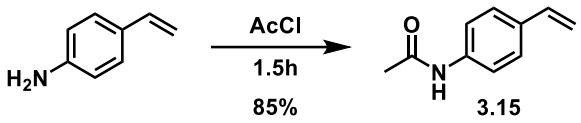

N-(4-vinylphenyl)acetamide 3.15. 4-vinylaniline (500 mg, 4.20 mmol, 1.0 eq.) was dissolved in DCM (5 mL). The solution was cooled to 0°C and acetyl chloride (0.449 mL, 0.493g, 6.29 mmol, 1.5 eq.) was added dropwise. The solution was then warmed to room temperature and stirred for 1.5 hours, then was quenched with sat. aq. $NaHCO_3$. The aqueous layer was extracted 4x with DCM, and the combined organic layers were washed once with brine, dried over anhydrous $NaSO_4$, filtered, and concentrated *in vacuo*. Crude product was purified by silica column chromatography (0-60% EtOAc/hexanes), yielding the title compound as a yellow solid (573 mg, 85% yield). Spectral data are consistent with literature reports.

^{1}H NMR (600 MHz, $CDCl_3$): δ 7.55 (br s, 1H), 7.47 (d, *J* = 8.5 Hz, 2H), 7.35 (d, *J* = 8.5 Hz, 2H), 6.66 (dd, *J* = 17.6, 10.9 Hz, 1H), 5.67 (d, *J* = 17.6 Hz, 1H), 5.19 (d, *J* = 10.9 Hz, 1H), 2.16 (s, 3H).

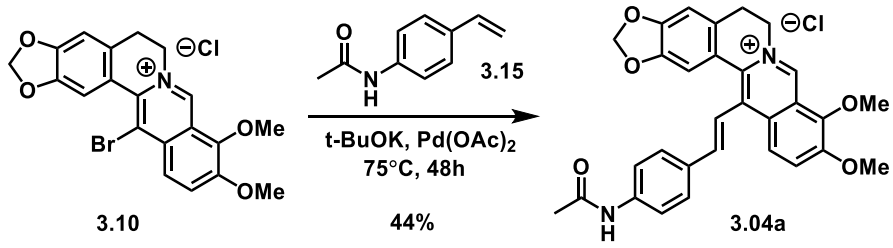

(E)-13-(4-acetamidostyryl)-9,10-dimethoxy-5,6-dihydro-[1,3]dioxolo[4,5-g]isoquinolino[3,2-a]isoquinolin-7-ium chloride 3.04a. Palladium (II) acetate (0.22 mg, 0.00150 mmol, 0.020 eq.),

potassium t-butoxide (20.7 mg, 0.185 mmol, 2.5 eq.), styrene **3.15** (12.0 mg, 0.0744 mmol, 1.0 eq.), and 13-bromoberberine **3.10** (50.0 mg, 0.111 mmol, 1.5 eq.) were sequentially added to a flame-dried vial under argon. Freshly degassed isopropanol (1 mL) was then added. The suspension was heated to 75°C and stirred for 48 hours. Solvent was removed *in vacuo* and the crude product was purified by preparative TLC (15% MeOH/DCM), yielding the title compound as a yellow powder (17.4 mg, 44% yield).

^{1}H NMR (500 MHz, DMSO-d_6): δ 10.17 (s, 1H), 9.89 (s, 1H), 8.94 (s, 1H), 8.39 (s, 1H), 8.19 (s, 1H), 8.11 (d, J = 18.0 Hz, 1H), 7.81 (d, J = 7.7 Hz, 2H), 7.70 (d, J = 6.9 Hz, 2H), 7.56 (d, J = 15.5 Hz, 1H), 7.09 (s, 1H), 6.19 (s, 2H), 4.95 (s, 2H), 4.17 (s, 3H), 4.10 (s, 3H), 3.21 (s, 2H), 2.08 (s, 3H).

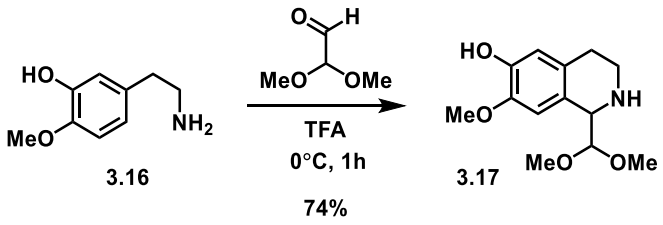

1-(dimethoxymethyl)-7-methoxy-1,2,3,4-tetrahydroisoquinolin-6-ol 3.17.[155] 5-(2-aminoethyl)-2-methoxyphenol **3.16** (0.910 mL, 1.00g, 6.00 mmol, 1.0 eq.) was added to a 50 mL round-bottom flask. 2,2-dimethoxyacetaldehyde (60% in H_2O, 3.11 mL, 3.58g, 18.00 mmol, 3.0 eq.) was extracted 3x with DCM (20 mL total), dried over anhydrous Na_2SO_4, and filtered into the flask. Solution stirred at room temperature for 30 minutes, then was cooled to 0°C. Trifluoroacetic acid (6.86 mL, 10.2g, 90.0 mmol, 15.0 eq.) wa added dropwise and the reaction stirred 1 hour at 0°C. The reaction was neutralized with NaOH (1M) and the aqueous layer was extracted 4x with DCM. Combined organic layers were dried over anhydrous Na_2SO_4, filtered, and concentrated *in vacuo*. Crude product was purified by silica column chromatography (0-15% MeOH/DCM),

yielding product (a golden oil) as a 9:1 mixture of regioisomers which was carried forward without separation (1.122g major isomer, 74% yield, 0.130g minor isomer, 9% yield). Spectral data are consistent with literature reports.

^{1}H NMR (600 MHz, $CDCl_3$): δ 6.92 (s, 1H), 6.64 (s, 1H), 4.45 (d, *J* = 6.2 Hz, 1H), 4.01 (d, *J* = 6.1 Hz, 1H), 3.85 (s, 3H), 3.45 (s, 3H), 3.44 (s, 3H), 3.23 (ddd, *J* = 12.2, 7.2, 5.2 Hz, 1H), 3.01 (dt, *J* = 11.8, 5.6 Hz, 1H), 2.80 – 2.73 (m, 2H). **^{13}C NMR** (151 MHz, $CDCl_3$): δ 144.9, 144.7, 128.6, 124.7, 114.6, 110.7, 107.1, 56.5, 56.4, 56.1, 55.3, 40.7, 28.7.

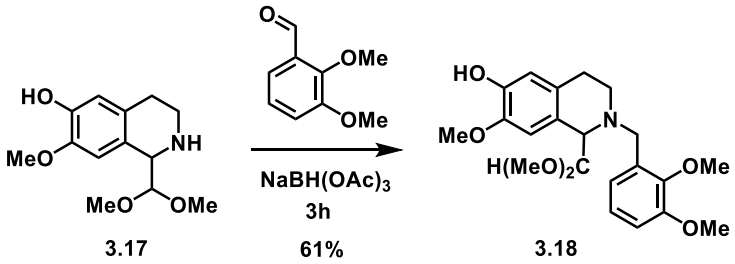

2-(2,3-dimethoxybenzyl)-1-(dimethoxymethyl)-7-methoxy-1,2,3,4-tetrahydroisoquinolin-6-ol 3.18.[155] Amine **3.17** (541 mg, 2.14 mmol, 1.0 eq.) and 2,3-dimethoxyacetaldehyde (686 mg, 4.13 mmol, 1.9 eq.) were dissolved in DCE (9 mL). Sodium triacetoxyborohydride (1.31g, 6.20 mmol, 2.9 eq.) was added and the reaction was stirred at room temperature for 3 hours. The reaction was then quenched with sat. aq. $NaHCO_3$. The aqueous layer was extracted 3x with DCM, then combined organic layers were dried over anhydrous $MgSO_4$, filtered, and concentrated *in vacuo*. Crude product was purified by silica column chromatography (0-5% MeOH/DCM), yielding the title compound as a yellow oil (525 mg, 61% yield). Spectral data are consistent with literature reports.

^{1}H NMR (600 MHz, $CDCl_3$): δ 7.15 (s, 1H), 7.04 (t, *J* = 7.9 Hz, 1H), 6.83 (d, *J* = 8.1 Hz, 1H), 6.80 (s, 1H), 6.66 (s, 1H), 4.43 (s, 1H), 3.90 – 3.87 (m, 1H), 3.86 (s, 3H), 3.85 (s, 3H), 3.76 (d, *J*

= 3.3 Hz, 1H), 3.75 (s, 3H), 3.34 (s, 3H), 3.31 (s, 3H), 3.29 – 3.21 (m, 1H), 2.88 (ddd, *J* = 17.1, 10.6, 5.6 Hz, 2H), 2.58 – 2.45 (m, 1H).

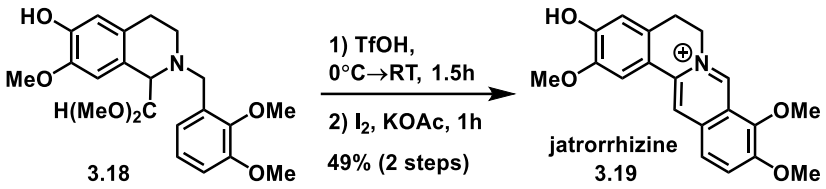

3-hydroxy-2,9,10-trimethoxy-5,6-dihydroisoquinolino[3,2-a]isoquinolin-7-ium iodide 3.19.[155] A solution of acetal **3.18** (637 mg, 1.58 mmol, 1.0 eq.) in DCM (30 mL) was cooled to 0°C and triflic acid (0.42 mL, 0.711g, 4.74 mmol, 3.0 eq.) was added dropwise. The reaction stirred 45 minutes at 0°C, then was warmed to room temperature and stirred an additional 45 minutes. The reaction was then quenched with sat. aq. $NaHCO_3$ and the aqueous layer was extracted 5x with DCM. More $NaHCO_3$ was added and the aqueous layer was extracted an additional 5x with DCM. Combined organic layers were dried over anhydrous Na_2SO_4, filtered, and concentrated *in vacuo*. To this crude product open to the air was added potassium acetate (194 mg, 1.97 mmol, 1.3 eq.) and the mixture was dissolved in EtOH (100%, 40 mL). A solution of iodine (401 mg, 1.58 mmol, 1.0 eq.) in EtOH (10 mL) was added dropwise with vigorous stirring. The reaction stirred open to the air at room temperature for 1 hour, then was filtered through Celite, washing with MeOH. Solvent was removed and product was purified by silica column chromatography (0-15% MeOH/DCM), yielding product as an orange powder (357 mg, 49% yield over two steps). Spectral data are consistent with literature reports.

^{1}H NMR (600 MHz, CD_3OD): δ 9.74 (s, 1H), 8.79 (s, 1H), 8.11 (d, *J* = 9.1 Hz, 1H), 8.01 (d, *J* = 9.0 Hz, 1H), 7.67 (s, 1H), 6.87 (s, 1H), 4.93 – 4.90 (m, 4H), 4.21 (s, 3H), 4.11 (s, 3H), 4.03 (s, 3H), 3.22 – 3.20 (m, 2H).

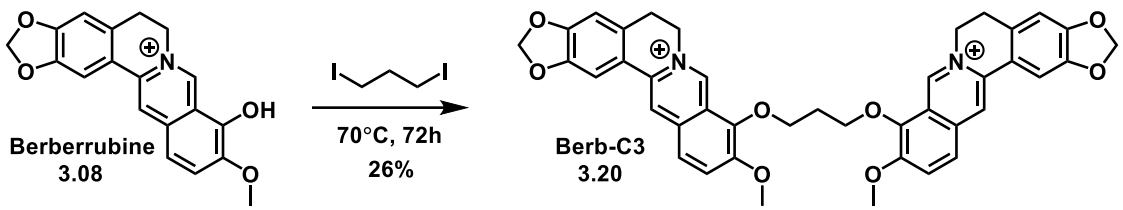

9,9'-(propane-1,4-diylbis(oxy))bis(10-methoxy-5,6-dihydro-[1,3]dioxolo[4,5-g]isoquinolino[3,2-a]isoquinolin-7-ium) dichloride 3.20. Following general procedure A, diiodidopropane (16.6 mg. 0.056 mmol) yielded the title compound as a yellow solid (11.2 mg, 26% yield).

^{1}H NMR (600 MHz, DMSO-d_6): δ 9.85 (s, 2H), 8.97 (s, 2H), 8.22 (d, J = 9.2 Hz, 2H), 8.01 (d, J = 9.1 Hz, 2H), 7.81 (s, 2H), 7.11 (s, 2H), 6.19 (s, 4H), 4.97 – 4.92 (m, 4H), 4.59 (t, J = 6.4 Hz, 4H), 4.04 (s, 6H), 3.24 – 3.19 (m, 4H), 2.57 – 2.52 (m, 2H). **^{13}C NMR** (151 MHz, DMSO-d_6): δ 150.9, 150.4, 148.2, 145.8, 143.2, 138.0, 133.5, 131.2, 127.2, 124.0, 122.1, 120.9, 120.7, 108.9, 105.9, 102.6, 72.2, 57.6, 55.8, 30.9, 26.8. **HRMS** Accurate mass (ES+): Found 342.12269 (-1.01 ppm), $C_{41}H_{36}N_2O_8$ (M^{2+}) requires 342.12303.

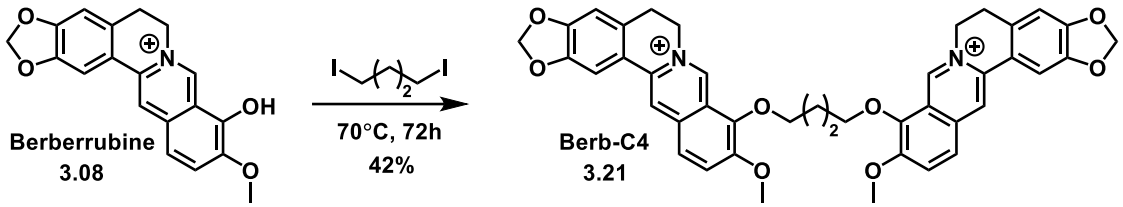

9,9'-(butane-1,4-diylbis(oxy))bis(10-methoxy-5,6-dihydro-[1,3]dioxolo[4,5-g]isoquinolino[3,2-a]isoquinolin-7-ium) dichloride 3.21. Following general procedure A, diiodobutane (17.4 mg. 0.056 mmol) yielded the title compound as a yellow solid (18.3 mg, 42% yield).

^{1}H NMR (500 MHz, DMSO-d_6): δ 9.82 (s, 2H), 8.96 (s, 2H), 8.21 (d, J = 7.9 Hz, 2H), 8.00 (d, J = 7.9 Hz, 2H), 7.81 (s, 2H), 7.10 (s, 2H), 6.18 (s, 4H), 4.96 (s, 4H), 4.41 (s, 4H), 4.05 (s, 6H), 3.20

(s, 4H), 2.14 (s, 4H). **^{13}C NMR** (151 MHz, DMSO-d_6): δ 150.9, 150.3, 148.2, 145.8, 143.2, 138.0, 133.5, 131.2, 127.1, 123.9, 122.1, 120.9, 120.7, 108.9, 105.9, 102.6, 77.0, 74.4, 57.5, 55.8, 26.6. **HRMS** Accurate mass (ES+): Found 349.13082 (-0.11 ppm), $C_{42}H_{38}N_2O_8$ (M^{2+}) requires 349.13086.

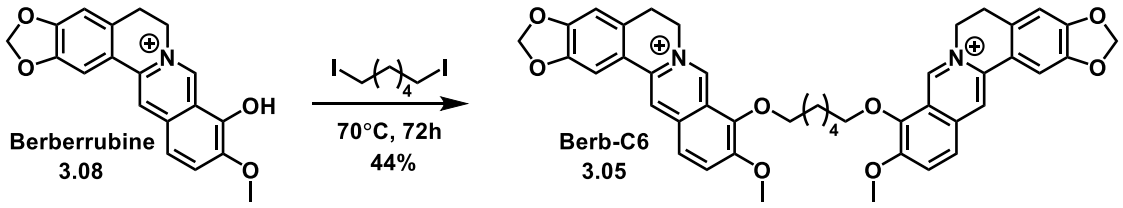

9,9'-(hexane-1,4-diylbis(oxy))bis(10-methoxy-5,6-dihydro-[1,3]dioxolo[4,5-g]isoquinolino[3,2-a]isoquinolin-7-ium) dichloride 3.05. Following general procedure A, diiodohexane (38.0 mg. 0.112 mmol) yielded the title compound as a yellow solid (39.3 mg, 44% yield).

^{1}H NMR (600 MHz, DMSO-d_6): δ 9.75 (s, 2H), 8.93 (s, 2H), 8.20 (d, J = 9.2 Hz, 2H), 7.99 (d, J = 9.1 Hz, 2H), 7.78 (s, 2H), 7.09 (s, 2H), 6.17 (s, 4H), 4.94 (t, J = 6.1 Hz, 4H), 4.31 (t, J = 6.7 Hz, 4H), 4.04 (s, 6H), 3.19 (t, J = 6.1 Hz, 4H), 1.94 (p, J = 6.2 Hz, 4H), 1.60 (p, J = 4.0 Hz, 4H). **^{13}C NMR** (151 MHz, DMSO-d_6): δ 150.4, 149.8, 147.7, 145.2, 142.8, 137.5, 133.0, 130.6, 126.7, 123.3, 121.7, 120.4, 120.2, 108.4, 105.4, 102.1, 74.2, 57.0, 55.3, 29.5, 26.3, 25.1. **HRMS** Accurate mass (ES+): Found 363.14631 (-0.55 ppm), $C_{44}H_{42}N_2O_8$ (M^{2+}) requires 363.14651.

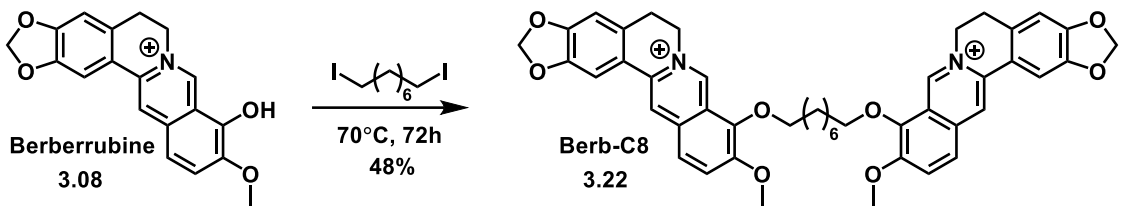

9,9'-(octane-1,8-diylbis(oxy))bis(10-methoxy-5,6-dihydro-[1,3]dioxolo[4,5-g]isoquinolino[3,2-a]isoquinolin-7-ium) dichloride 3.22. Following general procedure A, diiodooctane (20.5 mg. 0.056 mmol) yielded the title compound as a yellow solid (22.2 mg, 48% yield).

^{1}H NMR (600 MHz, DMSO-d_6): δ 9.75 (s, 2H), 8.94 (s, 2H), 8.20 (d, J = 9.2 Hz, 2H), 8.00 (d, J = 9.1 Hz, 2H), 7.79 (s, 2H), 7.09 (s, 2H), 6.18 (s, 4H), 4.98 – 4.93 (m, 4H), 4.30 (t, J = 6.6 Hz, 4H), 4.04 (s, 6H), 3.23 – 3.18 (m, 4H), 1.91 (dt, J = 14.3, 6.9 Hz, 4H), 1.55 – 1.49 (m, 4H), 1.44 (s, 4H). **^{13}C NMR** (151 MHz, DMSO-d_6): δ 150.9, 150.3, 148.2, 145.7, 143.3, 137.9, 133.5, 131.1, 127.2, 123.8, 122.1, 120.9, 120.7, 108.9, 105.9, 102.6, 74.8, 57.5, 55.8, 30.0, 29.3, 26.8, 25.8. **HRMS** Accurate mass (ES+): Found 377.16182 (-0.90 ppm), $C_{46}H_{46}N_2O_8$ (M^{2+}) requires 377.16216.

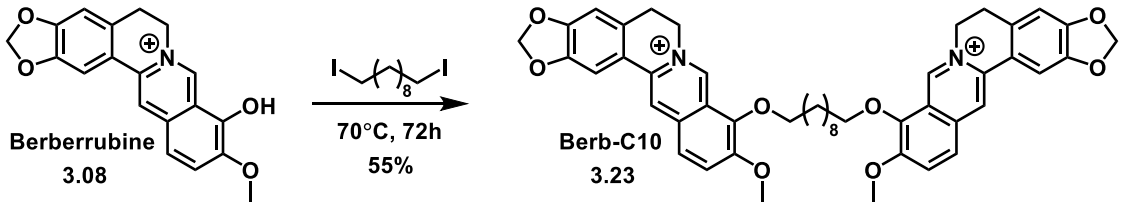

9,9'-(decane-1,4-diylbis(oxy))bis(10-methoxy-5,6-dihydro-[1,3]dioxolo[4,5-g]isoquinolino[3,2-a]isoquinolin-7-ium) dichloride 3.23. Following general procedure A, diiododecane (23.0 mg. 0.058 mmol) yielded the title compound as a yellow solid (27.3 mg, 55% yield).

^{1}H NMR (600 MHz, DMSO-d_6): δ 9.75 (s, 2H), 8.95 (s, 2H), 8.20 (d, *J* = 9.1 Hz, 2H), 8.00 (d, *J* = 9.0 Hz, 2H), 7.80 (s, 2H), 7.09 (s, 2H), 6.18 (s, 4H), 4.98 – 4.93 (m, 4H), 4.29 (t, *J* = 6.7 Hz, 4H), 4.05 (s, 6H), 3.21 (d, *J* = 11.3 Hz, 4H), 1.89 (dt, *J* = 14.4, 6.9 Hz, 4H), 1.51 – 1.46 (m, 4H), 1.41 – 1.22 (m, 22H). **^{13}C NMR** (151 MHz, DMSO-d_6): δ 150.9, 150.3, 148.2, 145.7, 143.4, 137.9, 133.5, 131.2, 127.2, 123.8, 122.1, 120.9, 120.7, 108.9, 105.9, 102.6, 74.7, 57.5, 55.8, 30.0, 29.5, 29.4, 26.8, 25.8. **HRMS** Accurate mass (ES+): Found 391.1773 (-1.31 ppm), $C_{48}H_{90}N_2O_8$ (M^{2+}) requires 391.17781.

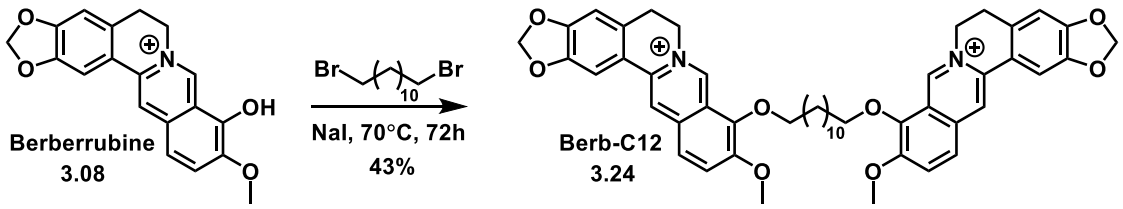

9,9'-(dodecane-1,4-diylbis(oxy))bis(10-methoxy-5,6-dihydro-[1,3]dioxolo[4,5-g]isoquinolino[3,2-a]isoquinolin-7-ium) dichloride 3.24. Following general procedure B, dibromododecane (15.3 mg. 0.047 mmol) yielded the title compound as a yellow solid (17.8 mg, 43% yield).

^{1}H NMR (600 MHz, DMSO-d_6): δ 9.75 (s, 2H), 8.94 (s, 2H), 8.20 (d, *J* = 9.1 Hz, 2H), 7.99 (d, *J* = 9.0 Hz, 2H), 7.80 (s, 2H), 7.09 (s, 2H), 6.18 (s, 4H), 4.99 – 4.91 (m, 4H), 4.28 (t, *J* = 6.5 Hz, 4H), 4.05 (s, 6H), 3.23 – 3.18 (m, 4H), 1.93 – 1.82 (m, 4H), 1.52 – 1.43 (m, 4H), 1.40 – 1.21 (m, 22H). **^{13}C NMR** (151 MHz, DMSO-d_6): δ 150.9, 150.3, 148.2, 145.8, 143.4, 137.9, 133.5, 131.2, 127.2, 123.8, 122.2, 120.9, 120.7, 108.9, 105.9, 102.6, 74.7, 57.5, 55.8, 30.0, 29.6, 29.5, 29.4, 26.8, 25.8. **HRMS** Accurate mass (ES+): Found 405.19332 (-0.33 ppm), $C_{50}H_{54}N_2O_8$ (M^{2+}) requires 405.19346.

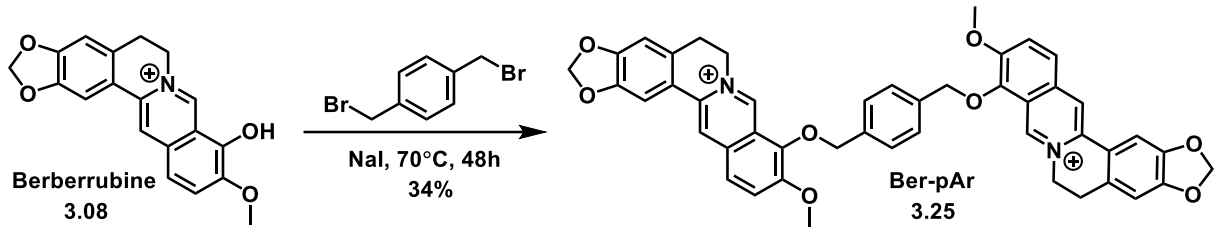

9,9'-((1,4-phenylenebis(methylene))bis(oxy))bis(10-methoxy-5,6-dihydro-[1,3]dioxolo[4,5-g]isoquinolino[3,2-a]isoquinolin-7-ium) dichloride 3.25. Following general procedure B, 1,4-bis(bromomethyl)benzene (29.2 mg. 0.111 mmol) yielded the title compound as a yellow solid (34.0 mg, 34% yield).

^{1}H NMR (600 MHz, DMSO-d_6): δ 9.70 (s, 2H), 8.91 (s, 2H), 8.21 (d, J = 9.2 Hz, 2H), 8.00 (d, J = 9.0 Hz, 2H), 7.75 (s, 2H), 7.60 (s, 4H), 7.05 (s, 2H), 6.16 (s, 4H), 5.34 (s, 4H), 4.91 (t, J = 6.2 Hz, 4H), 4.07 (s, 6H), 3.22 – 3.14 (t, J = 6.2 Hz, 4H). **^{13}C NMR** (151 MHz, DMSO-d_6): δ 150.7, 149.8, 147.7, 145.2, 141.8, 137.4, 136.6, 132.9, 130.6, 128.9, 126.5, 123.8, 121.8, 120.3, 120.2, 108.4, 105.4, 102.1, 75.0, 57.0, 55.3, 26.3. **HRMS** Accurate mass (ES+): Found 373.13073 (-0.35 ppm), $C_{46}H_{38}N_2O_8$ (M^{2+}) requires 373.13086.

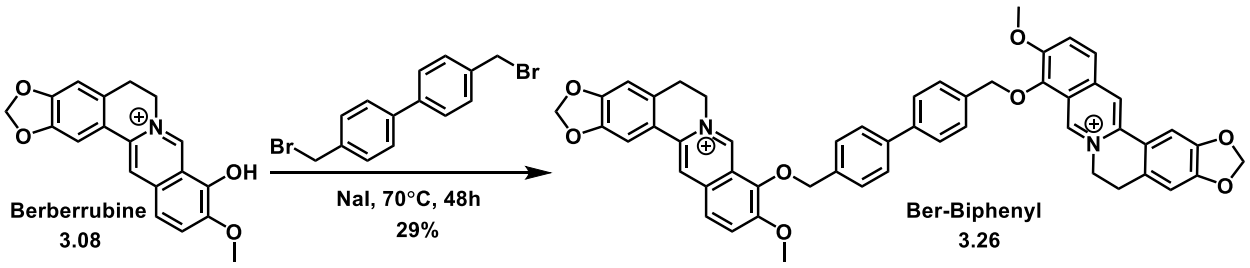

9,9'-(([1,1'-biphenyl]-4,4'-diylbis(methylene))bis(oxy))bis(10-methoxy-5,6-dihydro-[1,3]dioxolo[4,5-g]isoquinolino[3,2-a]isoquinolin-7-ium) dichloride 3.26. Following general procedure B, 4,4'-bis(bromomethyl)-1,1'-biphenyl (38.2 mg, 0.112 mmol) yielded the title compound as a yellow solid (28.5 mg, 29% yield).

^{1}H NMR (600 MHz, DMSO-d_6): δ 9.80 (s, 2H), 8.95 (s, 2H), 8.24 (d, J = 9.2 Hz, 2H), 8.02 (d, J = 9.1 Hz, 2H), 7.80 (s, 2H), 7.74 (d, J = 8.3 Hz, 4H), 7.70 (d, J = 8.4 Hz, 4H), 7.10 (s, 2H), 6.18 (s, 4H), 5.41 (s, 4H), 4.94 (t, J = 6.4 Hz, 4H), 4.11 (s, 6H), 3.20 (t, J = 6.4, 4H). **^{13}C NMR** (151 MHz, DMSO-d_6): δ 150.69, 149.88, 147.72, 145.35, 142.06, 139.62, 137.48, 135.91, 132.97, 130.68, 129.65, 129.38, 126.63, 123.79, 121.80, 120.42, 120.28, 108.44, 105.44, 102.12, 75.05, 57.09, 55.34, 26.35. **HRMS** Accurate mass (ES+): Found 411.14652 (+0.02 ppm), $C_{52}H_{42}N_2O_8$ (M^{2+}) requires 411.14651.

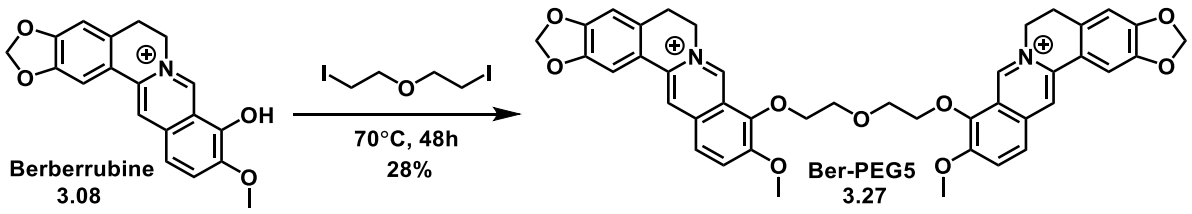

9,9'-((oxybis(ethane-2,1-diyl))bis(oxy))bis(10-methoxy-5,6-dihydro-[1,3]dioxolo[4,5-g]isoquinolino[3,2-a]isoquinolin-7-ium) dichloride 3.27. Following general procedure A, 1-iodo-2-(2-iodoethoxy)ethane (15.0 mg. 0.046 mmol) yielded the title compound as a yellow solid (12.3 mg, 28% yield).

^{1}H NMR (600 MHz, DMSO-d_6): δ 9.54 (s, 2H), 8.75 (s, 2H), 8.09 (d, *J* = 9.2 Hz, 2H), 7.93 – 7.85 (m, 2H), 7.39 (s, 2H), 7.04 (s, 2H), 6.13 (s, 4H), 4.88 (t, *J* = 5.7 Hz, 4H), 4.30 – 4.23 (m, 4H), 3.92 (s, 6H), 3.88 – 3.84 (m, 4H), 3.18 – 3.11 (m, 4H). **^{13}C NMR** (151 MHz, DMSO-d_6): δ 150.1, 149.7, 147.5, 145.1, 142.6, 137.0, 132.8, 130.2, 126.1, 123.6, 121.8, 120.1, 120.0, 108.2, 105.0, 102.1, 72.8, 69.5, 56.8, 55.1, 26.2. **HRMS** Accurate mass (ES+): Found 357.12815 (-0.47 ppm), $C_{42}H_{38}N_2O_9$ (M^{2+}) requires 357.12832.

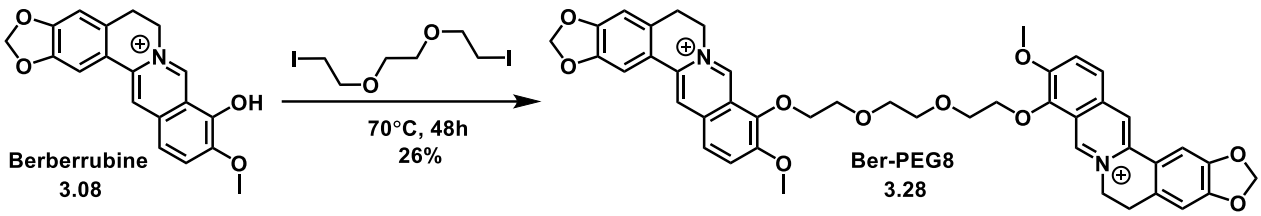

9,9'-(((ethane-1,2-diylbis(oxy))bis(ethane-2,1-diyl))bis(oxy))bis(10-methoxy-5,6-dihydro-[1,3]dioxolo[4,5-g]isoquinolino[3,2-a]isoquinolin-7-ium) dichloride 3.28. Following general procedure A, 1,2-bis(2-iodoethoxy)ethane (17.0 mg. 0.047 mmol) yielded the title compound as a yellow solid (12.1 mg, 26% yield).

^{1}H NMR (600 MHz, DMSO-d_6): δ 9.69 (s, 2H), 8.86 (s, 2H), 8.11 (d, J = 9.2 Hz, 2H), 7.92 (d, J = 9.1 Hz, 2H), 7.68 (s, 2H), 7.05 (s, 2H), 6.15 (s, 4H), 4.92 (t, J = 6.1 Hz, 4H), 4.35 – 4.31 (m, 4H), 3.95 (s, 6H), 3.83 – 3.79 (m, 4H), 3.67 (s, 4H), 3.22 – 3.17 (m, 4H). **^{13}C NMR** (151 MHz, DMSO-d_6): δ 150.8, 150.2, 148.1, 145.7, 142.8, 137.8, 133.3, 131.0, 126.8, 124.0, 122.1, 120.8, 120.6, 108.8, 105.7, 102.6, 73.7, 70.1, 69.9, 57.3, 55.9, 26.8. **HRMS** Accurate mass (ES+): Found 379.1414 (-0.07 ppm), $C_{44}H_{42}N_2O_{10}$ (M^{2+}) requires 379.14142.

6.3.4 Tricepyridinium: Experimental Procedures and Characterization Data

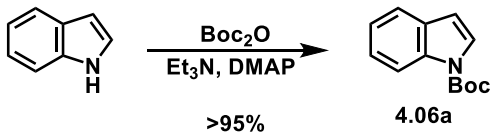

Tert-butyl 1H-indole-1-carboxylate 4.06a. Indole (1.17 g, 9.99 mmol, 1.00 eq.), freshly distilled triethylamine (3.03 g, 4.17 mL, 29.9 mmol, 3.00 eq.), and DMAP (0.244 g, 2.00 mmol, 0.20 eq.) were dissolved in DCM (20 mL). A solution of Boc_2O (2.42 g, 2.55 mL, 11.1 mmol, 1.11 eq.) in DCM (5 mL) was added dropwise. The reaction was stirred at room temperature for 2 hours, then was poured into water and the aqueous layer was extracted thrice with DCM. Combined organic layers were dried over anhydrous $MgSO_4$, filtered, and concentrated *in vacuo*. Crude product was

purified by silica column chromatography (0-20% EtOAc/hexanes), yielding the title compound as a colorless oil (2.087 g, >95% yield). Spectral data are consistent with literature reports.

^{1}H NMR (400 MHz, $CDCl_3$): δ 8.14 (d, *J* = 7.1 Hz, 1H), 7.59 (d, *J* = 3.3 Hz, 1H), 7.55 (ddd, *J* = 7.7, 1.3, 0.8 Hz, 1H), 7.30 (ddd, *J* = 8.4, 7.2, 1.4 Hz, 1H), 7.22 (ddd, *J* = 7.7, 7.3, 1.1 Hz, 1H), 6.63 – 6.53 (m, 1H), 6.56 (dd, *J* = 3.8, 0.9 Hz, 1H), 1.67 (s, 9H).

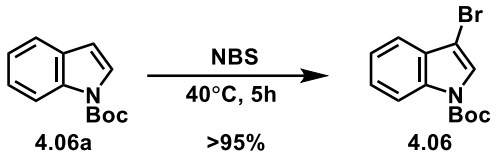

4.06a >95% 4.06

***Tert*-butyl 3-bromo-1H-indole-1-carboxylate 4.06.** To a sample of N-bromosuccinimide (0.497 g, 2.29 mmol, 1.00 eq.) was added a solution of protected indole **4.06a** (0.611 g, 3.43 mmol, 1.5 eq.) in DCM (20 mL). The reaction was heated to reflux and was stirred 5 hours. It was then returned to room temperature and quenched with water. The aqueous layer was extracted thrice with DCM. Combined organic layers were washed once with 10% aq. KOH, dried over anhydrous Na_2SO_4, filtered, and concentrated *in vacuo*. Crude product was purified by silica column chromatography (0-10% EtOAc/hexanes), yielding the title compound as a yellow powder (0.656 g, >95% yield). Spectral data are consistent with literature reports.

^{1}H NMR (400 MHz, $CDCl_3$): δ 8.16 (d, *J* = 7.0 Hz, 1H), 7.65 (s, 1H), 7.53 (ddd, *J* = 7.6, 1.3, 0.7 Hz, 1H), 7.44 – 7.28 (m, 3H), 1.67 (s, 13H).

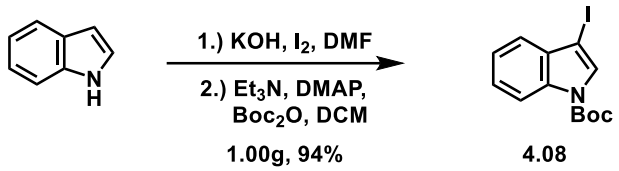

***Tert*-butyl 3-iodo-1H-indole-1-carboxylate 4.08.**[266] Indole (1.00 g, 8.54 mmol, 1.00 eq.) and potassium hydroxide (1.92 g, 34.2 mmol, 4.00 eq) were dissolved in dimethylformamide (15 mL). The solution was stirred for 20 minutes, then was cooled to 0°C. A solution of iodine (2.28 g, 8.97 mmol, 1.05 eq.) in dimethylformamide (15 mL) was then added dropwise to the reaction. The reaction was stirred for 15 minutes at 0°C then was warmed to room temperature and stirred for an additional 1 hour. Water was added and the organic layer was extracted 3 times with dichloromethane. The combined organic layers were washed once with brine and then dried over anhydrous sodium sulfate; then were filtered and concentrated *in vacuo*. The crude product was then redissolved in dichloromethane (30 mL), and 4-dimethylaminopyridine (0.104 g, 0.854 mmol, 0.100 eq.) and freshly-distilled triethylamine (3.57 mL, 25.6 mmol, 3.00 eq.) were added to the solution followed by di-*tert*-butyl dicarbonate (2.05 g, 9.39 mmol, 1.10 eq). The reaction stirred at room temperature for two hours, then water was added. The organic layer was extracted 3 times with dichloromethane. The organic layers were combined and washed once with brine and then dried over anhydrous sodium sulfate, filtered, and concentrated *in vacuo*. Product was then purified using silica column chromatography (0-10% ethyl acetate in hexanes) yielding the title compound as a colorless, light-sensitive oil (2.77 g, 94% yield).

^{1}H NMR (600 MHz, $CDCl_3$): δ 8.14 (m, 1H), 7.74 (br s, 1H), 7.41 (d, J = 7.7 Hz, 1H), 7.38 (t, J = 7.7 Hz, 1H), 7.32 (t, J = 7.5 Hz, 1H), 1.68 (s, 12H). **^{13}C NMR** (126 MHz, $CDCl_3$): δ 148.8, 134.9, 132.2, 130.2, 125.4, 123.4, 121.6, 115.2, 84.4, 65.6, 28.3. **HRMS** Accurate Mass (ES^+): Found 343.00617 (-0.59 ppm), $C_{13}H_{14}O_2N^{127}I$ (M) requires 343.00637.

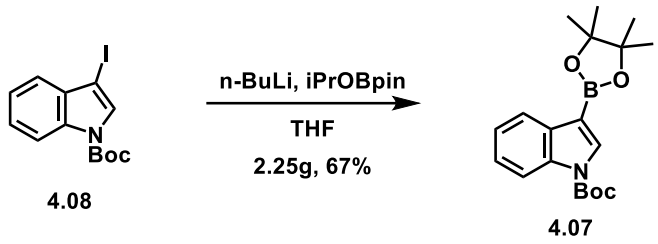

4.08 4.07

***Tert*-butyl 3-(4,4,5,5-tetramethyl-1,3,2-dioxaborolan-2-yl)-1H-indole-1-carboxylate 4.07.**[199] Boc-protected iodoindole **4.08** (2.25 g, 6.56 mmol, 1.00 eq.) was dissolved in anhydrous tetrahydrofuran (30 mL) and cooled to -78° C. A solution of n-butyllithium (approx. 2 M in THF, 3.61 mL, 7.21 mmol, 1.10 eq.) was added to the solution dropwise. The reaction was stirred for 30 minutes at -78° C. 2-Isopropoxy-4,4,5,5-tetramethyl-1,3,2-dioxaborolane (1.47 mL, 7.21 mmol, 1.10 eq.) was then added dropwise to the reaction. The reaction stirred for 1 hour at -78° C, then at room temperature for an additional 30 minutes. 15 mL of saturated monopotassium phosphate solution was then added to the reaction flask. The organic layer was extracted with diethyl ether and water 3 times. The organic layers were combined and washed once with brine. The product was then dried over anhydrous sodium sulfate, filtered, and concentrated under vacuum. The product was purified using silica column chromatography (0-5% ethyl acetate in hexanes) yielding the title compound as a white solid (1.50 g, 67% yield).

^{1}H NMR (600 MHz, $CDCl_3$): δ 8.16 (d, J = 8.1 Hz, 1H), 8.01 (s, 1H), 7.98 (ddd, J = 7.7, 1.3, 0.7 Hz, 1H), 7.30 (ddd, J = 8.4, 7.3, 1.3 Hz, 1H), 7.28 – 7.24 (m, 3H), 1.66 (s, 9H), 1.38 (s, 12H). **^{13}C NMR** (150 MHz, $CDCl_3$): δ 149.6, 136.3, 135.3, 133.6, 124.3, 123.1, 122.8, 115.0, 84.0, 83.5, 28.3, 25.1. **HRMS** Accurate Mass (ES^+): Found 343.20610 (-0.87 ppm), $C_{19}H_{27}O_4N^{10}B$ ($M + H^+$) requires 343.20640.

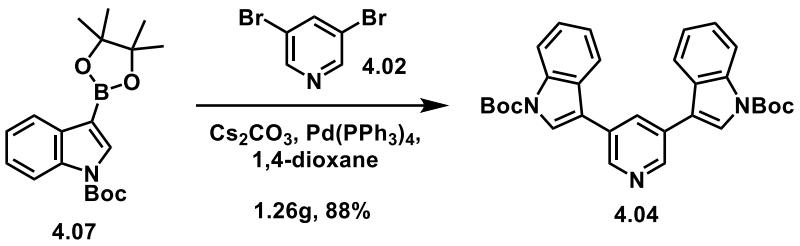

Di-*tert*-butyl 3,3'-(pyridine-3,5-diyl)bis(1H-indole-1-carboxylate) 4.04.

Tetrakis(triphenylphosphine)palladium(0) (0.141 g, 0.122 mmol, 0.100 eq.) was dissolved in 1,4 dioxane (12.5 mL) and left to stir at room temperature for 20 minutes, resulting in a black solution. Cesium carbonate (1.99 g, 6.11 mmol, 5.00 eq.), **4.07** (1.26 g, 5.32 mmol, 4.00 eq.) dissolved in 1,4 dioxane (12.5 mL), and 3,5 dibromopyridine **4.02** (0.298 g, 1.26 mmol, 1.00 eq) were sequentially added to the solution. The reaction was heated to reflux and stirred for 18 hours. Water was then added and the organic layer was extracted 3 times using dichloromethane. The organic layers were combined and washed once with water and once with brine, then dried over anhydrous sodium sulfate, filtered, and concentrated *in vacuo*. The product was purified using silica column chromatography (0-40% ethyl acetate in hexanes) to afford the title compound as a light brown solid (549.1 mg, 88% yield).

^{1}H NMR (500 MHz, $CDCl_3$): δ 8.92 (d, J = 2.1 Hz, 2H), 8.31 – 8.27 (m, 2H), 8.26 (br s, 1H), 7.87 (s, 2H), 7.82 (dt, J = 7.9, 0.9 Hz, 2H), 7.43 (ddd, J = 8.4, 7.2, 1.2 Hz, 2H), 7.35 (ddd, J = 8.1, 7.3, 1.1 Hz, 2H), 1.72 (s, 18H). **^{13}C NMR** (151 MHz, $CDCl_3$): δ 149.7, 147.5, 136.1, 134.2, 130.1, 128.7, 125.2, 123.8, 123.5, 119.6, 118.7, 115.8, 84.5, 28.4. **HRMS** Accurate Mass (ES^+): Found 510.23806 (-1.32 ppm), $C_{31}H_{32}O_4N_3$ ($M + H^+$) requires 510.23873.

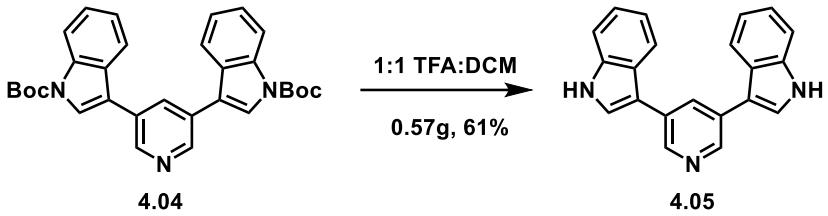

4.04 4.05

3,5-di(1H-indol-3-yl)pyridine 4.05. Protected diindolepyridine **4.04** (0.570 g, 1.120 mmol, 1 eq.) was dissolved in dichloromethane (2 mL) and cooled to 0°C. Trifluoroacetic acid (2 mL) was added dropwise into the solution, and the reaction stirred at room temperature for 4 hours. The reaction was brought to pH 7 with 2M potassium hydroxide. The organic layer was extracted 4 times with ethyl acetate and washed once with brine. A buoyant white precipitate formed upon standing of the aqueous layer; this was collected via gravity filtration and combined with the organic layers. Combined organic layers were then dried over anhydrous sodium sulfate, filtered, and concentrated *in vacuo*. Crude product was dry-loaded onto a silica column and purified using silica column chromatography (50-100% ethyl acetate in hexanes, then 0-15% methanol in dichloromethane) affording a tan powder with low solubility in organic solvents, with the exception of pyridine (210 mg, 65% yield).

^{1}H NMR (600 MHz, DMSO-d_6): δ 11.55 (s, 2H), 8.81 (s, 2H), 8.29 (t, J = 1.9 Hz, 1H), 7.99 – 7.89 (m, 4H), 7.51 (d, J = 8.0 Hz, 2H), 7.20 (t, J = 7.3 Hz, 2H), 7.15 (t, J = 7.3 Hz, 2H). **^{13}C NMR** (151 MHz, DMSO-d_6): δ 144.2, 137.0, 131.7, 130.6, 124.9, 124.4, 121.7, 120.0, 118.8, 112.4, 112.1. **HRMS** Accurate Mass (ES^+): Found 510.23806 (-1.32 ppm), $C_{31}H_{32}O_4N_3$ requires 510.23873.

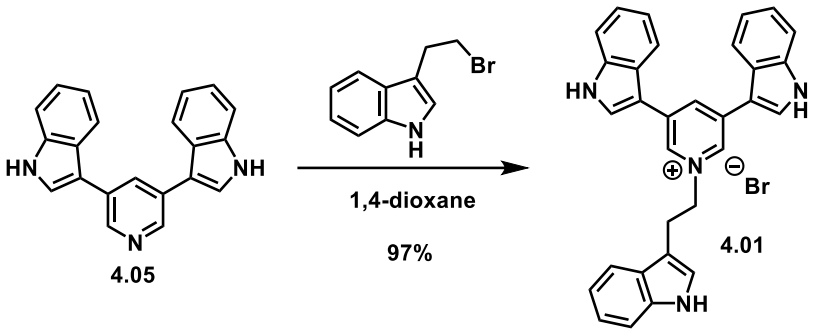

1-(2-(1H-indol-3-yl)ethyl)-3,5-di(1H-indol-3-yl)pyridin-1-ium bromide 4.01.[191] Disubstituted pyridine **4.05** (30 mg, 0.097 mmol, 1 eq.) was dissolved in 1,4-dioxane (1 mL) and 3-(2-bromoethyl)indole (32.6 mg, 0.145 mmol, 1.5 eq.) was added. The reaction mixture was heated to reflux and stirred for 72 hours. The reaction mixture was then cooled to room temperature and loaded directly onto a short silica column, which was flushed first with 100% ethyl acetate to elute trace starting materials, followed by 100% methanol. The ethyl acetate fraction was concentrated *in vacuo*, then reloaded onto the column and flushed again with 100% ethyl acetate, then 100% methanol. The methanol fractions were combined and concentrated *in vacuo* to furnish the title compound as a yellow powder (50 mg, 97% yield).

^{1}H NMR (600 MHz, CD_3OD): δ 8.65 (t, J = 1.6 Hz, 1H), 8.37 (d, J = 1.7 Hz, 2H), 7.68 (s, 2H), 7.50 (d, J = 7.9 Hz, 1H), 7.46 (d, J = 8.2 Hz, 2H), 7.36 (d, J = 8.0 Hz, 3H), 7.20 (ddd, J = 8.1, 7.1, 1.0 Hz, 2H), 7.16-7.10 (m, 3H), 7.04 (ddd, J = 8.0, 7.1, 0.9 Hz, 1H), 6.99 (s, 1H), 4.91 (t, J = 6.1 Hz, 2H), 3.52 (t, J = 6.1 Hz, 2H). **^{13}C NMR** (151 MHz, CD_3OD): δ 138.8, 138.4, 138.3, 137.4, 137.0, 128.0, 127.4, 125.4, 125.3, 123.8, 123.2, 122.4, 120.6, 119.3, 118.7, 113.3, 113.0, 110.6, 109.7, 63.8, 28.7. **HRMS** Accurate Mass (ES): Found 453.20631 (-2.34 ppm), $C_{31}H_{25}N_4^+$ (M) requires 453.20737.

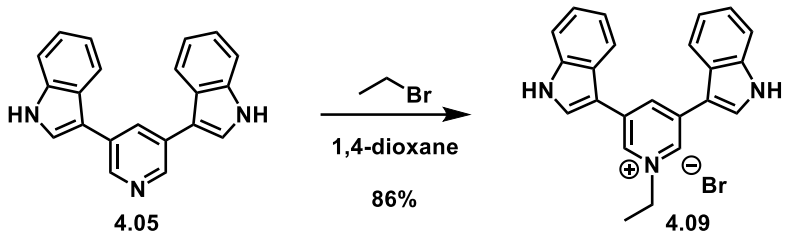

1-ethyl-3,5-di(1H-indol-3-yl)pyridin-1-ium 4.09.[191] Disubstituted pyridine **4.05** (20 mg, 0.0646 mmol, 1 eq.) was dissolved in 1,4-dioxane (1 mL) and 1-bromoethane (7.2 µL, 0.0970 mmol, 1.5 eq.) was added. The reaction mixture was covered with aluminum foil, heated to reflux, and stirred for 48 hours. Additional 1-bromoethane (7.2 µL, 0.0970 mmol, 1.5 eq.) was added and the reaction continued to stir at reflux for an additional 24 hours. The reaction mixture was then cooled to room temperature and loaded directly onto a short silica column, which was flushed first with 100% ethyl acetate to elute trace starting materials, followed by 100% methanol containing 1% acetic acid. The ethyl acetate fraction was concentrated *in vacuo*, then reloaded onto the column and flushed again with 100% ethyl acetate, then 100% methanol containing 1% acetic acid. The methanol fractions were combined and concentrated *in vacuo* to furnish the title compound as a yellow powder (23.2 mg, 86% yield).

^{1}H NMR (600 MHz, CD_3OD): δ 9.03 – 8.98 (m, 2H), 8.95 (s, 1H), 8.03 (s, 2H), 8.00 (dd, J = 6.4, 2.1 Hz, 2H), 7.55 (dd, J = 6.5, 2.0 Hz, 2H), 7.31 – 7.24 (m, 4H), 4.78 (q, J = 7.3 Hz, 2H), 1.78 (t, J = 7.3 Hz, 3H). **^{13}C NMR** (151 MHz, CD_3OD): δ 139.2, 139.0, 137.54, 137.47, 127.6, 125.8, 124.0, 122.4, 119.4, 113.6, 110.8, 58.7, 24.2. **HRMS** Accurate Mass (ES): Found 338.1645 (-1.99 ppm), $C_{23}H_{20}N_3^+$ (M) requires 338.16517.

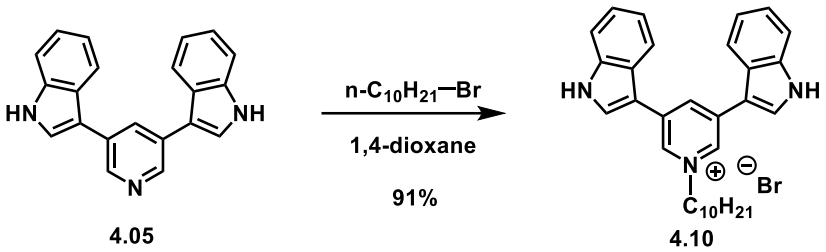

1-decyl-3,5-di(1H-indol-3-yl)pyridin-1-ium 4.10. Disubstituted pyridine **4.05** (30 mg, 0.097 mmol, 1 eq.) was dissolved in 1,4-dioxane (1 mL) and 1-bromodecane (30 µL, 0.145 mmol, 1.5 eq.) was added. The reaction mixture was heated to reflux and stirred for 72 hours. The reaction mixture was then cooled to room temperature and loaded directly onto a short silica column, which was flushed first with 100% ethyl acetate to elute trace starting materials, followed by 100% methanol. The ethyl acetate fraction was concentrated *in vacuo*, then reloaded onto the column and flushed again with 100% ethyl acetate, then 100% methanol. The methanol fractions were combined and concentrated *in vacuo* to furnish the title compound as a yellow powder (46.7 mg, 91% yield).

^{1}H NMR (600 MHz, CD_3OD): δ 8.80 (s, 2H), 8.64 (s, 1H), 7.95 (s, 2H), 7.86 (dd, J = 6.8, 1.7 Hz, 2H), 7.47 (d, J = 7.5 Hz, 2H), 7.23-7.15 (m, 4H), 4.59 (t, J = 7.5 Hz, 2H), 2.03 (p, J = 7.3 Hz, 2H), 1.44 (p, J = 7.5, 7.1 Hz, 2H), 1.38 (p, J = 6.5 Hz, 2H), 1.27-1.19 (m, 10H), 0.83 (t, J = 7.1 Hz, 3H). **^{13}C NMR** (151 MHz, CD_3OD): δ 138.8, 138.7, 137.2, 136.5, 127.8, 125.6, 123.9, 122.4, 119.4, 113.6, 110.6, 63.1, 33.0, 32.8, 30.7, 30.5, 30.4, 30.1, 27.3, 23.7, 14.4. **HRMS** Accurate Mass (ES): Found 450.28929 (-2.41 ppm), $C_{31}H_{36}N_3^+$ (M) requires 450.29037.

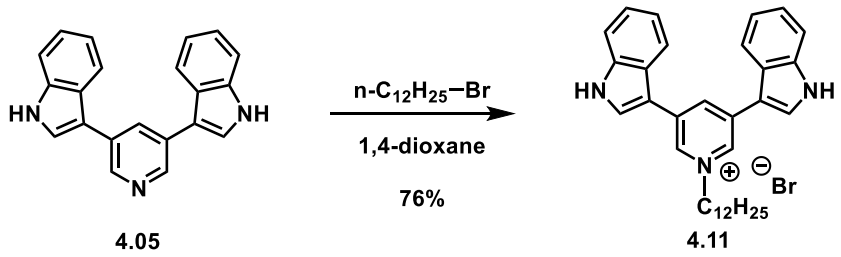

4.05 4.11

1-dodecyl-3,5-di(1H-indol-3-yl)pyridin-1-ium 4.11. Disubstituted pyridine **4.05** (20 mg, 0.0646 mmol, 1 eq.) was dissolved in 1,4-dioxane (1 mL) and 1-bromododecane (23.3 µL, 0.0970 mmol, 1.5 eq.) was added. The reaction mixture was heated to reflux and stirred for 72 hours. The reaction mixture was then cooled to room temperature and loaded directly onto a short silica column, which was flushed first with 100% ethyl acetate to elute trace starting materials, followed by 100% methanol. The ethyl acetate fraction was concentrated *in vacuo*, then reloaded onto the column and flushed again with 100% ethyl acetate, then 100% methanol. The methanol fractions were combined and concentrated *in vacuo* to furnish the title compound as a yellow powder (27.2 mg, 76% yield).

^{1}H NMR (600 MHz, CD_3OD): δ 8.98 (s, 2H), 8.93 (s, 1H), 8.03 (s, 2H), 7.99 (dd, J = 6.6, 1.7 Hz, 2H), 7.54 (dd, J = 6.7, 1.8 Hz, 2H), 7.31 – 7.24 (m, 4H), 4.72 (t, J = 7.5 Hz, 2H), 2.15 (p, 7.6 Hz, 2H), 1.51 (p, J = 7.0 Hz, 2H), 1.44 (p, 6.7 Hz, 2H), 1.38-1.19 (m, 16H), 0.87 (t, J = 7.1 Hz, 3H). **^{13}C NMR** (151 MHz, CD_3OD): δ 139.04, 138.99, 137.7, 137.5, 127.6, 125.8, 124.0, 122.4, 119.4, 113.6, 110.8, 63.2, 33.0, 32.8, 30.7, 30.6, 30.5, 30.4, 30.1, 27.3, 24.1, 23.7, 14.4. **HRMS** Accurate Mass (ES): Found 478.32117 (-1.06 ppm), $C_{33}H_{40}N_3^+$ (M) requires 478.32167.

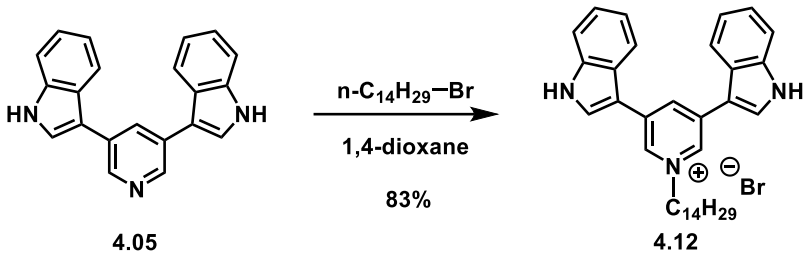

4.05 4.12

3,5-di(1H-indol-3-yl)-1-tetradecylpyridin-1-ium 4.12. Disubstituted pyridine **4.05** (20 mg, 0.0676 mmol, 1 eq.) was dissolved in 1,4-dioxane (1 mL) and 1-bromotetradecane (28.8 µL, 0.0970 mmol, 1.5 eq.) was added. The reaction mixture was heated to reflux and stirred for 72 hours. The reaction mixture was then cooled to room temperature and loaded directly onto a short silica column, which was flushed first with 100% ethyl acetate to elute trace starting materials, followed by 100% methanol. The ethyl acetate fraction was concentrated *in vacuo*, then reloaded onto the column and flushed again with 100% ethyl acetate, then 100% methanol. The methanol fractions were combined and concentrated *in vacuo* to furnish the title compound as a yellow powder (31.2 mg, 83% yield).

^{1}H NMR (600 MHz, CD_3OD): δ 8.91 (s, 2H), 8.82 (s, 1H), 8.00 (s, 2H), 7.94 (dd, J = 6.6, 1.8 Hz, 2H), 7.52 (dd, J = 6.7, 1.8 Hz, 2H), 7.28 – 7.20 (m, 4H), 4.67 (t, J = 7.5 Hz, 2H), 2.10 (p, J = 7.6 Hz, 2H), 1.48 (p, 7.0 Hz, 2H), 1.42 (p, 6.8 Hz, 2H), 1.36 – 1.18 (m, 23H), 0.87 (t, J = 7.1 Hz, 4H). **^{13}C NMR** (151 MHz, CD_3OD): δ 139.0, 138.9, 137.5, 137.1, 127.7, 125.7, 124.0, 122.4, 119.4, 113.6, 110.7, 63.2, 33.0, 32.8, 30.73, 30.70, 30.68, 30.6, 30.5, 30.4, 30.1, 27.3, 24.2, 23.7, 14.4. **HRMS** Accurate Mass (ES): Found 506.35261 (-0.73 ppm), $C_{35}H_{44}N_3^+$ (M) requires 506.35297.

6.3.5 Lumazines: Experimental Procedures and Characterization Data

General Procedure 5A: Amino Acid-Anthranilate HATU Coupling.

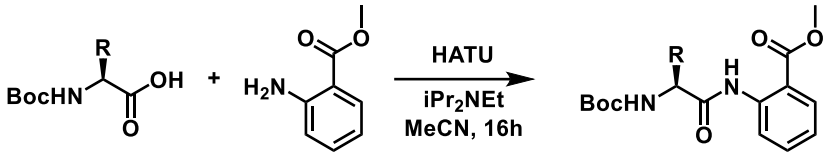

A solution of protected amino acid (1.00 eq.) dissolved in MeCN (0.5 M) was prepared and cooled to 0°C. Diisopropylethylamine (2.50 eq.) and HATU (1.50 eq.) were added and the solution was stirred at 0°C for 5 minutes. A solution of methyl 2-aminobenzoate (2.00 eq.) in MeCN (1 M) was then added. The reaction was allowed to warm to room temperature as it stirred for 16 hours. The reaction was quenched with saturated aqueous NH_4Cl and extracted 4x with Et_2O. Combined organic layers were washed once with brine, dried over anhydrous Na_2SO_4, filtered, and concentrated *in vacuo*. Crude product was purified by silica column chromatography (0-45% EtOAc/hexanes), yielding pure product.

General Procedure 5B: Amino Acid-Anthranilate Boc Deprotection.

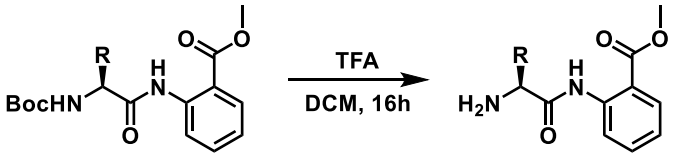

Protected amino acid-anthranilate substrate (1.00 eq.) was dissolved in DCM (0.5M). TFA (10 eq.) was added dropwise, and the solution stirred for 16 hours at room temperature. Reaction was neutralized with saturated aqueous $NaHCO_3$, and the aqueous phase was extracted 4x with DCM. Combined organic layers were washed once with saturated aqueous $NaHCO_3$ and once with brine, dried over anhydrous Na_2SO_4, filtered, and concentrated *in vacuo* to yield product of sufficient purity for the following step.

General Procedure 5C: Lumazine-Amino Acid-Anthranilate HATU Coupling.

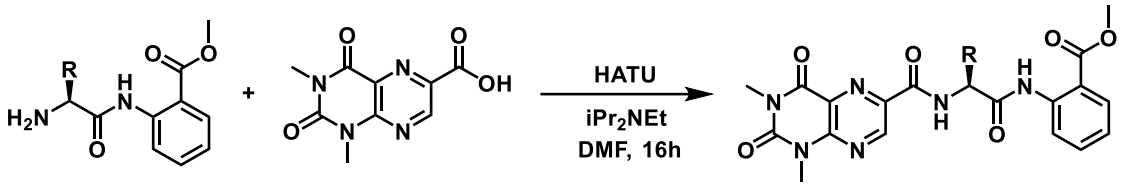

A solution of lumazine-6-carboxylic acid (1.00 eq.) dissolved in DMF (0.1 M) was prepared and cooled to 0°C. Diisopropylethylamine (2.50 eq.) and HATU (1.50 eq.) were added and the solution was stirred at 0°C for 5 minutes. Amine substrate (1.1 eq.) was then added in one portion. The reaction was allowed to warm to room temperature as it stirred for 16 hours. The reaction was quenched with saturated aqueous NH_4Cl and extracted 4x with DCM. Combined organic layers were washed once with brine, dried over anhydrous Na_2SO_4, filtered, and concentrated *in vacuo*. Crude product was purified by silica column chromatography (0-65% EtOAc/hexanes), yielding pure product.

General Procedure 5D: Lumazine-Amino Acid-Anthranilate Saponification.[248]

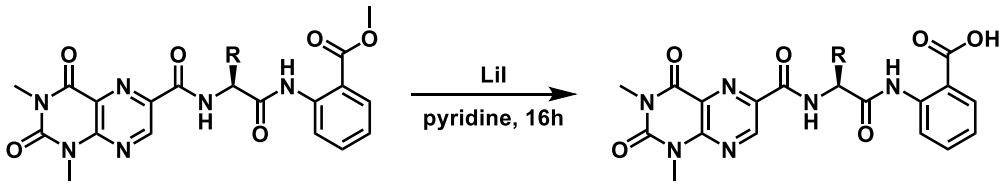

Methyl ester substrate (1.00 eq.) and lithium iodide (10.0 eq.) were dissolved in pyridine (0.1M). The vessel was sealed and heated to 135°C for 6 hours. Ethyl acetate and 5% aq. KOH were added and the aqueous layer was washed twice with ethyl acetate. The aqueous layer was acidified to pH 2 using 1M HCl and was extracted thrice with EtOAc. Combined organic layers were dried over anhydrous Na_2SO_4, filtered, and concentrated in vacuo, which was purified by preparative HPLC (35-95% MeCN/water) to yield product.

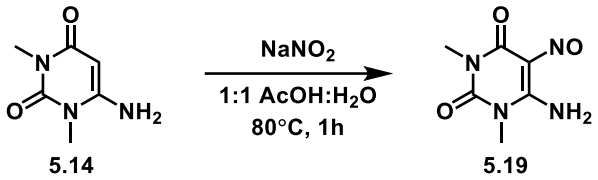

6-amino-1,3-dimethyl-5-nitrosopyrimidine-2,4(1H,3H)-dione 5.19.[241] Commercial uracil derivative **5.14** (5.00 g, 32.2 mmol, 1.0 eq.) was dissolved in 1:1 water : acetic acid (160 mL). A solution of sodium nitrite (4.45 g, 64.4 mmol, 2.0 eq.) in water (10 mL) was carefully added dropwise, turning the solution a vibrant pink. The solution was heated to 80°C and stirred 1.5 hours. The reaction was cooled to 0°C and left to stand for 30 minutes, precipitating a large amount of pink solid. This solid was filtered, washing with cold water to afford the title compound as a bright pink solid (5.54 g, 90%). Spectral data are consistent with literature reports.

^{1}H NMR (400 MHz, CD_3OD): δ 3.42 (s, 3H), 3.39 (s, 3H).

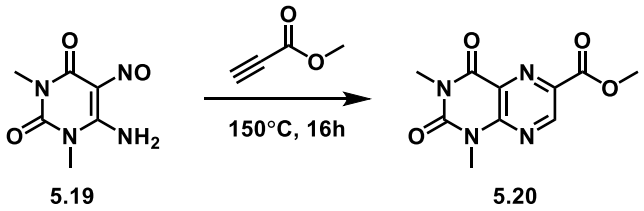

Methyl 1,3-dimethyl-2,4-dioxo-1,2,3,4-tetrahydropteridine-6-carboxylate 5.20. Nitroso compound **5.19** (1.80 g, 9.78 mmol, 3.5 eq.) was dissolved in DMF (13 mL), causing a color change to a royal purple. Methyl propiolate (235 mg, 0.25 mL, 2.80 mmol, 1.0 eq.) was added and the reaction was heated to reflux and stirred 16 hours, causing further darkening of the solution to nearly black. Solvent was removed *in vacuo* and the crude material was directly subjected to silica column chromatography (20-80% EtOAc/hexanes) to afford pure product as a

yellow powder. Alternatively, after removal of DMF, recrystallization from boiling ethanol instead of chromatographic separation also led to successful purification of the title compound (390 mg, 56% yield). Spectral data are consistent with literature reports.

^{1}H NMR (600 MHz, $CDCl_3$): δ 9.34 (s, 1H), 4.05 (s, 3H), 3.76 (s, 3H), 3.56 (s, 3H). **^{13}C NMR** (151 MHz, $CDCl_3$): δ 163.8, 159.1, 150.5, 149.7, 149.4, 138.8, 126.9, 53.3, 30.0, 29.4.

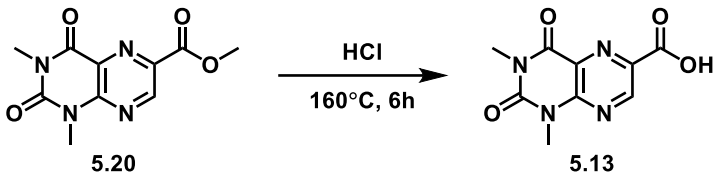

5.20 5.13

1,3-dimethyl-2,4-dioxo-1,2,3,4-tetrahydropteridine-6-carboxylic acid 5.13. In a thick-walled reaction tube, methyl ester **5.20** (160 mg, 0.639 mmol, 1.0 eq.) was dissolved in concentrated HCl (4 mL). The yellow solution was heated to 160°C for 6 hours. Product was obtained in sufficient purity for subsequent reactions after removal of HCl *in vacuo*, but if desired can be recrystallized from boiling methanol to afford the title compound as yellow needles (151 mg, >95% yield). Spectral data are consistent with literature reports.

^{1}H NMR (600 MHz, TFA-*d*): δ 9.12 (s, 1H), 3.59 (s, 3H), 3.37 (s, 3H). **^{13}C NMR** (151 MHz, TFA-*d*): δ 169.7, 162.0, 151.9, 149.0, 148.4, 144.1, 126.2, 29.5, 28.8.

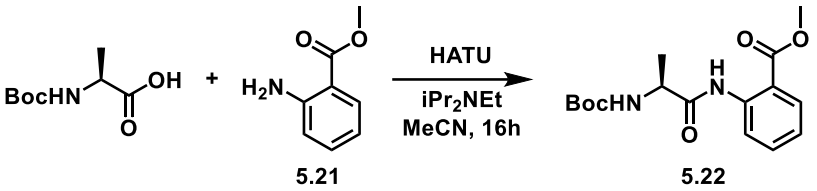

Methyl (S)-2-(2-((tert-butoxycarbonyl)amino)propanamido)benzoate 5.22. Following General Procedure 5A, (tert-butoxycarbonyl)-L-alanine (200 mg, 1.06 mmol, 1.00 eq.) was coupled to methyl anthranilate **5.21**, yielding the title compound as a white solid (279 mg, 82% yield).

^{1}H NMR (600 MHz, $CDCl_3$): δ 11.53 (s, 1H), 8.69 (d, J = 8.5 Hz, 1H), 7.99 (d, J = 8.0 Hz, 1H), 7.51 (t, J = 7.8 Hz, 1H), 7.06 (t, J = 7.6 Hz, 1H), 5.23 (s, 1H), 4.41 – 4.25 (m, 1H), 3.88 (s, 3H), 1.50-1.44 (m, 12H). **^{13}C NMR** (151 MHz, $CDCl_3$): δ 172.0, 168.6, 155.4, 141.3, 134.8, 131.0, 122.9, 120.5, 115.5, 80.2, 52.5, 51.8, 28.5, 19.1. **$[\alpha]^{25}_D$** -25 (c 0.35, DMSO). **HRMS** Accurate Mass (ES-): Found 321.14523 (-1.15 ppm), $C_{16}H_{21}O_5N_2$ ($M - H^+$) requires 321.1456.

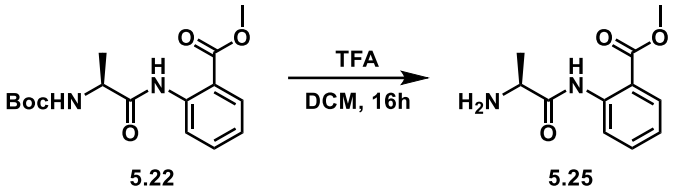

Methyl (S)-2-(2-aminopropanamido)benzoate 5.25. Following General Procedure 5B, protected alanine-anthranilate **5.22** (273 mg, 0.847 mmol, 1.0 eq.) was deprotected to yield the title compound as a white solid (186 mg, >95% yield).

^{1}H NMR (600 MHz, $CDCl_3$): δ 11.95 (s, 1H), 8.72 (d, *J* = 8.5 Hz, 1H), 7.96 (d, *J* = 8.0 Hz, 1H), 7.46 (t, *J* = 7.8 Hz, 1H), 7.01 (t, *J* = 7.6 Hz, 1H), 3.86 (s, 3H), 3.61 (q, *J* = 6.9 Hz, 1H), 1.69 (s, 2H), 1.39 (d, *J* = 7.0 Hz, 3H). **^{13}C NMR** (151 MHz, $CDCl_3$): δ 175.2, 168.1, 141.0, 134.4, 130.9,

122.5, 120.3, 115.6, 52.3, 52.1, 21.8. **[α]$^{25}_{D}$** +8.7 (c 0.41, DMSO). **HRMS** Accurate Mass (ES+): Found 223.10701 (-3.18 ppm), $C_{11}H_{15}O_3N_2$ (M + H^+) requires 223.10772.

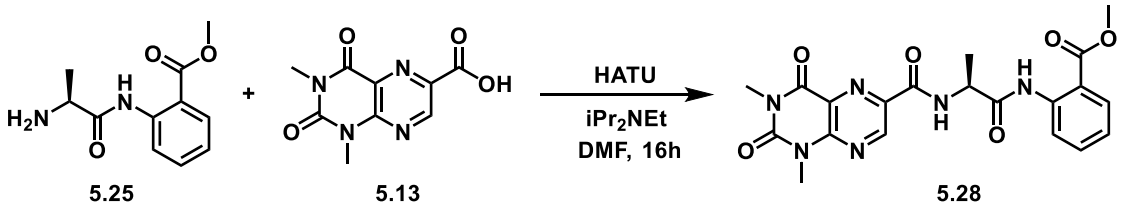

5.25 5.13 5.28

Methyl (S)-2-(2-(1,3-dimethyl-2,4-dioxo-1,2,3,4-tetrahydropteridine-6-carboxamido)propanamido)benzoate 5.28. Following General Procedure 5C, deprotected alanine-anthranilate **5.25** (45.0 mg, 0.191 mmol, 1.0 eq.) was coupled to lumazine-6-carboxylic acid **5.13** to afford the title compound as a light yellow powder (80 mg, 95% yield).

^{1}H NMR (600 MHz, DMSO-d_6): δ 11.00 (s, 1H), 9.29 (s, 1H), 9.07 (d, J = 7.6 Hz, 1H), 8.34 (dd, J = 8.4, 0.9 Hz, 1H), 7.90 (dd, J = 7.9, 1.5 Hz, 1H), 7.63 (ddd, J = 8.7, 7.4, 1.6 Hz, 1H), 7.21 (td, J = 8.7, 7.5, 1.2 Hz, 1H), 4.74 (p, J = 7.1 Hz, 1H), 3.69 (s, 3H), 3.60 (s, 3H), 3.37 (s, 3H), 1.55 (d, J = 7.1 Hz, 3H). **^{13}C NMR** (151 MHz, DMSO-d_6): δ 170.7, 167.3, 162.5, 159.2, 150.4, 149.5, 146.7, 139.4, 139.2, 134.1, 130.6, 126.3, 123.5, 121.0, 117.7, 52.4, 50.0, 29.4, 28.6, 17.3. **[α]$^{25}_{D}$** +36 (c 0.31, DMSO). **HRMS** Accurate Mass (ES+): Found 441.15261 (+2.03 ppm), $C_{20}H_{21}O_6N_6$ (M + H^+) requires 441.15171.

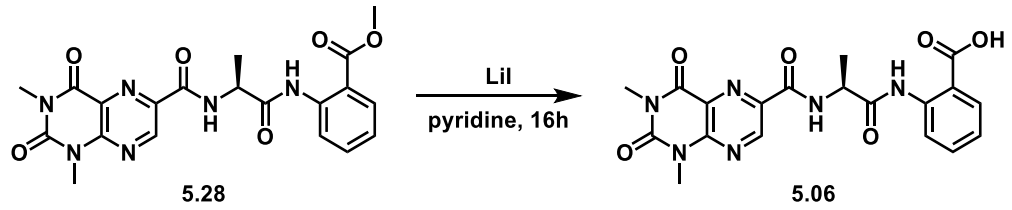

5.28 5.06

(S)-2-(2-(1,3-dimethyl-2,4-dioxo-1,2,3,4-tetrahydropteridine-6-carboxamido)propanamido)benzoic acid 5.06. Following General Procedure 5D, methyl ester **5.28** (20.0 mg, 0.0454 mmol, 1.0 eq.) was saponified to afford the title compound as a tan powder (8.7 mg, 45% yield).

^{1}H NMR (600 MHz, DMSO-d_6): δ 12.21 (s, 1H), 9.30 (s, 1H), 9.17 – 9.07 (m, 1H), 8.56 (d, J = 8.4 Hz, 1H), 7.94 (d, J = 7.9 Hz, 1H), 7.54 (t, J = 7.6 Hz, 1H), 7.11 (t, J = 7.5 Hz, 1H), 4.71 (p, J = 7.5 Hz, 1H), 3.58 (s, 3H), 3.36 (s, 3H), 1.54 (d, J = 7.1 Hz, 3H). **^{13}C NMR** (151 MHz, DMSO-d_6): δ 170.5, 169.2, 163.1, 162.4, 159.2, 150.4, 149.4, 146.7, 140.4, 139.5, 133.2, 131.2, 126.2, 122.5, 119.4, 50.1, 29.4, 28.6, 17.3. **$[\alpha]^{25}_{D}$** +65 (c 0.45, DMSO). **HRMS** Accurate Mass (ES+): Found 427.13681 (+1.76 ppm), $C_{19}H_{19}O_6N_6$ ($M + H^+$) requires 427.13606.

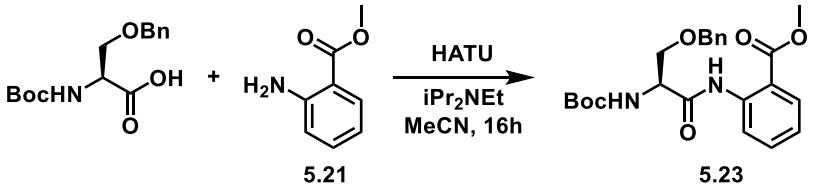

5.21 5.23

Methyl (S)-2-(3-(benzyloxy)-2-((tert-butoxycarbonyl)amino)propanamido)benzoate 5.23. Following General Procedure 5A, (tert-butoxycarbonyl)-L-serine (200 mg, 0.677 mmol, 1.0 eq.) was coupled to methyl anthranilate **5.21**, yielding the title compound as a white solid (240 mg, 83% yield).

^{1}H NMR (600 MHz, $CDCl_3$): δ 11.76 (s, 1H), 8.78 (d, J = 8.4 Hz, 1H), 8.04 (d, J = 9.1 Hz, 1H), 7.63 – 7.51 (m, 1H), 7.31 – 7.24 (m, 5H), 7.11 (t, J = 6.4 Hz, 1H), 5.60 (d, J = 6.5 Hz, 1H), 4.55 (ABq, J = 12.0 Hz, 2H), 4.48 (s, 1H), 4.14 – 4.07 (m, 1H), 3.89 (s, 3H), 3.74 (dd, J = 9.5, 4.3 Hz, 1H), 1.51 (s, 9H). **^{13}C NMR** (151 MHz, $CDCl_3$): δ 169.8, 168.3, 155.7, 141.1, 137.7, 134.7, 130.9, 128.5, 127.9, 127.8, 122.9, 120.5, 115.6, 80.4, 73.5, 69.9, 56.0, 52.3, 28.5. **$[\alpha]^{25}_D$** -0.41 (c 0.97, DMSO). **HRMS** Accurate Mass (ES-): Found 429.20087 (-2.67 ppm), $C_{23}H_{29}O_6N_2$ ($M + H^+$) requires 429.20201.

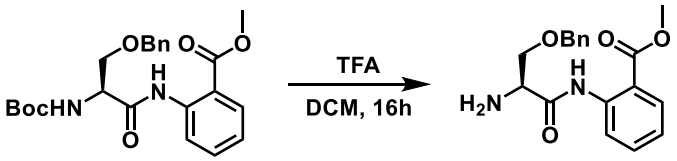

5.23 **5.26**

Methyl (S)-2-(2-amino-3-(benzyloxy)propanamido)benzoate 5.26. Following General Procedure 5B, protected serine-anthranilate **5.23** (211 mg, 0.493 mmol, 1.0 eq.) was N-deprotected to yield the title compound as a white solid (158 mg, >95% yield).

^{1}H NMR (600 MHz, $CDCl_3$): δ 11.55 (s, 1H), 8.48 (d, *J* = 8.3 Hz, 1H), 8.01 (dd, *J* = 8.0, 1.4 Hz, 1H), 7.49 (t, *J* = 7.9 Hz, 1H), 7.22 – 7.10 (m, 6H), 4.61 (d, *J* = 12.1 Hz, 1H), 4.47 (d, *J* = 12.1 Hz, 1H), 4.40 (s, 1H), 4.04 – 3.93 (m, 2H), 3.84 (s, 3H). **^{13}C NMR** (151 MHz, $CDCl_3$): δ 168.6, 165.0, 139.8, 136.5, 135.0, 131.0, 128.5, 128.2, 124.1, 120.9, 115.8, 73.6, 66.9, 54.8, 52.7. **$[\alpha]^{25}_D$** -0.88 (c 0.66, DMSO). **HRMS** Accurate Mass (ES-): Found 329.14937 (-0.65 ppm), $C_{18}H_{21}O_4N_2$ ($M + H^+$) requires 329.14958.

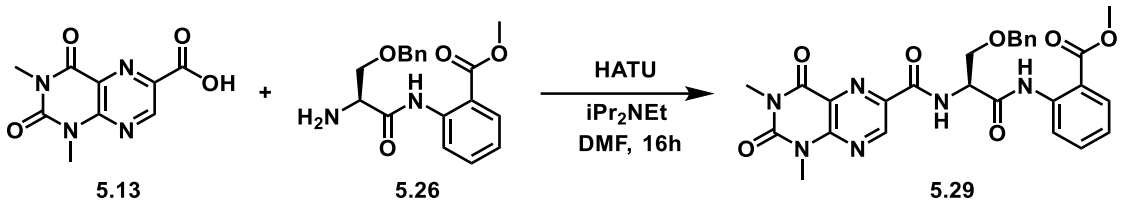

5.13 5.26 5.29

Methyl (S)-2-(3-(benzyloxy)-2-(1,3-dimethyl-2,4-dioxo-1,2,3,4-tetrahydropteridine-6-carboxamido)propanamido)benzoate 5.29. Following General Procedure 5C, N-deprotected serine-anthranilate **5.26** (70.0 mg, 0.296 mmol, 1.0 eq.) was coupled to lumazine-6-carboxylic acid **5.13** to afford the title compound as a light yellow powder (137 mg, 85% yield).

^{1}H NMR (600 MHz, DMSO-d_6): δ 11.13 (s, 1H), 9.32 (s, 1H), 8.89 (d, J = 7.9 Hz, 1H), 8.38 (d, J = 9.3 Hz, 1H), 7.91 (dd, J = 7.9, 1.6 Hz, 1H), 7.64 (ddd, J = 8.7, 7.5, 1.6 Hz, 1H), 7.35 (d, J = 7.0 Hz, 2H), 7.30 (t, J = 7.3 Hz, 2H), 7.25 (t, J = 7.2 Hz, 1H), 7.21 (td, J = 8.0, 1.1 Hz, 1H), 4.93 (dt, J = 7.9, 5.0 Hz, 1H), 4.59 (ABq, J = 12.0 Hz, 2H), 4.05 (dd, J = 10.0, 5.4 Hz, 1H), 3.94 (dd, J = 10.0, 4.5 Hz, 1H), 3.66 (s, 3H), 3.61 (s, 3H), 3.38 (s, 3H). **^{13}C NMR** (151 MHz, DMSO-d_6): δ 168.2, 167.3, 162.6, 159.1, 150.4, 149.7, 146.5, 139.1, 138.8, 137.8, 134.2, 130.7, 128.3, 127.5, 126.3, 123.6, 120.8, 117.3, 72.1, 68.8, 54.2, 52.4, 29.4, 28.6. **$[\alpha]^{25}_D$** -0.21 (c 0.97, DMSO). **HRMS** Accurate Mass (ES+): Found 547.19468 (+2.02 ppm), $C_{27}H_{27}O_7N_6$ ($M + H^+$) requires 547.19357.

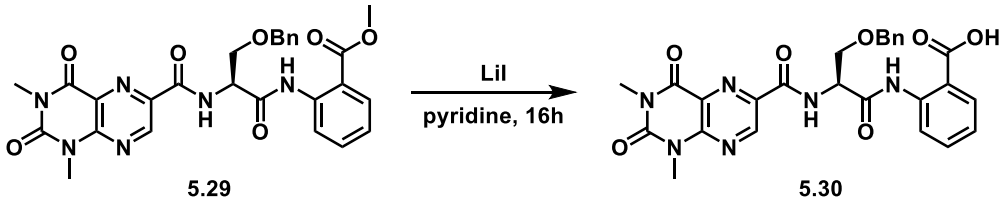

5.29 5.30

(S)-2-(3-(benzyloxy)-2-(1,3-dimethyl-2,4-dioxo-1,2,3,4-tetrahydropteridine-6-carboxamido)propanamido)benzoic acid 5.30. Following General Procedure 5D, methyl ester

5.29 (63.8 mg, 0.117 mmol, 1.0 eq.) was saponified to afford the title compound as an orange solid (14.3 mg, 23% yield).

^{1}H NMR (600 MHz, DMSO-d_6): δ 13.57 (s, 1H), 12.41 (s, 1H), 9.30 (s, 1H), 8.87 (d, J = 7.7 Hz, 1H), 8.57 (d, J = 8.4 Hz, 1H), 7.95 (dd, J = 7.8, 1.3 Hz, 1H), 7.54 (t, J = 7.5 Hz, 1H), 7.34 (d, J = 7.3 Hz, 2H), 7.29 (t, J = 7.4 Hz, 2H), 7.24 (t, J = 7.2 Hz, 1H), 7.12 (t, J = 7.4 Hz, 1H), 4.87 (dt, J = 8.0, 4.9 Hz, 1H), 4.57 (s, 2H), 4.08 (dd, J = 9.9, 5.4 Hz, 1H), 3.92 (dd, J = 9.9, 4.1 Hz, 1H), 3.57 (s, 3H), 3.37 (s, 3H). **^{13}C NMR** (151 MHz, DMSO-d_6): δ 169.6, 168.0, 163.2, 162.5, 159.1, 150.3, 149.6, 146.6, 140.2, 138.8, 137.9, 133.1, 131.2, 128.3, 127.6, 127.5, 126.2, 122.7, 119.2, 72.1, 68.9, 54.3, 29.4, 28.6. **$[\alpha]^{25}_D$** +0.26 (c 0.92, DMSO). **HRMS** Accurate Mass (ES+): Found 533.17899 (+2.00 ppm), $C_{26}H_{25}O_7N_6$ ($M + H^+$) requires 533.17792.

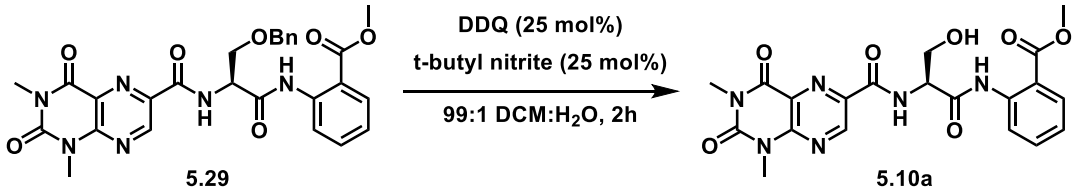

Methyl (S)-2-(2-(1,3-dimethyl-2,4-dioxo-1,2,3,4-tetrahydropteridine-6-carboxamido)-3-hydroxypropanamido)benzoate 5.10a.[250] In a reaction tube, DDQ (2.8 mg, 0.0124 mmol, 0.25 eq.) was added, followed by a solution of benzyl ether **5.29** (26.5 mg, 0.0498 mmol, 1 eq.) in 99:1 DCM : water (5 mL), turning the reaction dark brown. A drop of tert-butyl nitrite was then added and the solution was irradiated under blue LED (Hydrofarm® PPB1002 PowerPAR LED Bulb-Blue 15W/E27) for 2 hours. Solvent was removed *in vacuo* and reaction mixture was purified by preparative HPLC, yielding the title compound as a light yellow powder (6.2 mg, 28%).

^{1}H NMR (600 MHz, DMSO-d_6): δ 11.12 (s, 1H), 9.32 (s, 1H), 8.78 (d, J = 7.5 Hz, 1H), 8.44 (d, J = 8.4 Hz, 1H), 7.92 (dd, J = 7.9, 1.5 Hz, 1H), 7.67 – 7.61 (m, 1H), 7.25 – 7.16 (m, 1H), 5.45 (br s, 1H), 4.67 (dt, J = 7.4, 4.6 Hz, 1H), 4.02 (dd, J = 11.1, 4.8 Hz, 1H), 3.90 (dd, J = 11.1, 4.5 Hz, 1H), 3.69 (s, 3H), 3.61 (s, 3H), 3.37 (s, 3H). **^{13}C NMR** (151 MHz, DMSO-d_6): δ 168.8, 167.4, 162.6, 159.2, 150.4, 149.7, 146.6, 139.4, 139.0, 134.2, 130.7, 126.2, 123.4, 120.7, 117.0, 61.0, 56.7, 52.4, 29.4, 28.6. **[α]$^{25}_D$** -1.36 (c 0.41, DMSO). **HRMS** Accurate Mass (ES+): Found 457.14725 (+1.37 ppm), $C_{20}H_{21}O_7N_6$ ($M + H^+$) requires 457.14662.

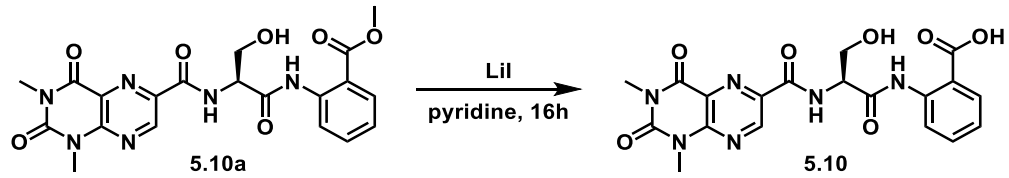

5.10a 5.10

(S)-2-(2-(1,3-dimethyl-2,4-dioxo-1,2,3,4-tetrahydropteridine-6-carboxamido)-3-hydroxypropanamido)benzoic acid 5.10. Following General Procedure 5D, methyl ester **5.10a** (10.0 mg, 0.0220 mmol, 1.0 eq.) was saponified to afford the title compound as a light yellow solid (3.3 mg, 34% yield).

^{1}H NMR (600 MHz, DMSO-d_6): δ 13.64 (s, 1H), 12.20 (s, 1H), 9.32 (s, 1H), 8.77 (d, J = 7.0 Hz, 1H), 8.59 (d, J = 8.4 Hz, 1H), 7.94 (d, J = 8.2 Hz, 1H), 7.54 (t, J = 7.5 Hz, 1H), 7.11 (t, J = 7.4 Hz, 1H), 5.41 (s, 1H), 4.62 (dt, J = 8.4, 4.4 Hz, 1H), 4.04 (d, J = 7.6 Hz, 1H), 3.89 (d, J = 9.8 Hz, 1H), 3.60 (s, 3H), 3.37 (s, 3H). **^{13}C NMR** (151 MHz, DMSO-d_6): δ 169.2, 168.6, 163.1, 162.6, 159.1, 150.4, 149.6, 146.6, 140.3, 139.0, 136.1, 131.2, 126.2, 122.7, 119.4, 61.0, 56.9, 29.4, 28.7. **[α]$^{25}_D$** +1.7 (c 0.23, DMSO). **HRMS** Accurate Mass (ES+): Found 441.11514 (-2.89 ppm), $C_{19}H_{17}O_7N_6$ ($M - H^+$) requires 441.11642.

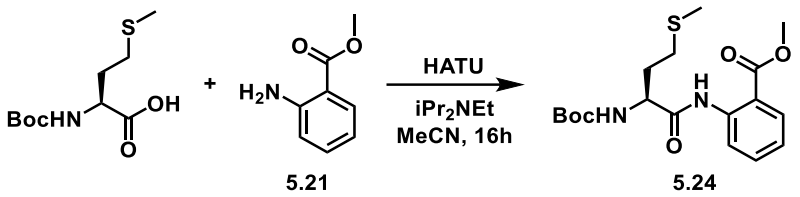

Methyl (S)-2-(2-((tert-butoxycarbonyl)amino)-4-(methylthio)butanamido)benzoate 5.24. Following General Procedure 5A, (tert-butoxycarbonyl)-L-methionine (200 mg, 0.802 mmol, 1.00 eq.) was coupled to methyl anthranilate **5.21**, yielding the title compound as a white solid (248 mg, 81% yield).

^{1}H NMR (600 MHz, $CDCl_3$): δ 11.57 (s, 1H), 8.70 (d, J = 9.4 Hz, 1H), 8.04 (d, J = 9.2 Hz, 1H), 7.55 (t, J = 8.4 Hz, 1H), 7.11 (t, J = 7.5 Hz, 1H), 5.30 (br s, 1H), 4.48 (s, 1H), 3.93 (s, 3H), 2.61 (t, J = 7.5 Hz, 2H), 2.29 (dq, J = 11.9, 7.2 Hz, 1H), 2.12 (s, 3H), 2.02 (dq, J = 13.5, 7.1, 5.9 Hz, 1H), 1.48 (s, 9H). **^{13}C NMR** (151 MHz, $CDCl_3$): δ 170.9, 168.6, 155.6, 141.1, 134.8, 131.0, 123.1, 120.5, 115.6, 80.4, 55.4, 52.5, 32.4, 30.4, 28.5, 15.6. **$[\alpha]^{25}_{D}$** -10.3 (c 0.19, DMSO). **HRMS** Accurate Mass (ES-): Found 381.14844 (-1.37 ppm), $C_{18}H_{25}O_5N_2{}^{32}S$ ($M - H^+$) requires 381.14897.

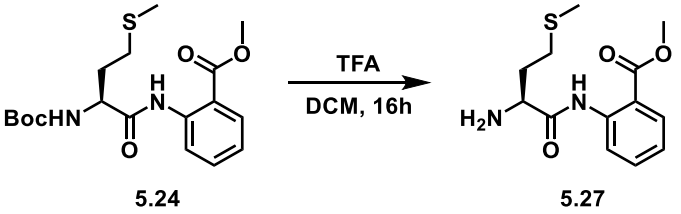

Methyl (S)-2-(2-amino-4-(methylthio)butanamido)benzoate 5.27. Following General Procedure 5B, protected methionine-anthranilate **5.24** (248 mg, 0.650 mmol, 1.0 eq.) was deprotected to yield the title compound as a white solid (183 mg, >95% yield).

^{1}H NMR (600 MHz, $CDCl_3$): δ 11.49 (s, 1H), 8.52 (d, *J* = 8.4 Hz, 1H), 8.01 (d, *J* = 8.8 Hz, 1H), 7.53 (t, *J* = 7.9 Hz, 1H), 7.13 (t, *J* = 7.7 Hz, 1H), 4.37 (t, *J* = 6.2 Hz, 1H), 3.92 (s, 3H), 2.69 (ddt, *J* = 36.2, 13.8, 7.0 Hz, 2H), 2.35 (d, *J* = 6.5 Hz, 2H), 2.09 (s, 3H). **^{13}C NMR** (151 MHz, $CDCl_3$): δ 168.8, 167.2, 139.8, 134.9, 131.1, 124.1, 121.1, 116.0, 54.1, 52.8, 30.4, 29.3, 14.9. **$[\alpha]^{25}_D$** -4.5 (c 0.69, DMSO). **HRMS** Accurate Mass (ES+): Found 283.11062 (-1.67 ppm), $C_{13}H_{19}O_3N_2{}^{32}S$ ($M + H^+$) requires 283.11109.

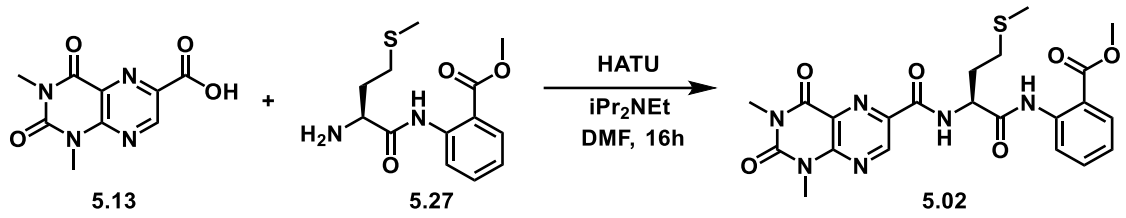

5.13 5.27 5.02

Methyl (S)-2-(2-(1,3-dimethyl-2,4-dioxo-1,2,3,4-tetrahydropteridine-6-carboxamido)-4-(methylthio)butanamido)benzoate 5.02. Following General Procedure 5C, deprotected methionine-anthranilate **5.27** (47.2 mg, 0.200 mmol, 1.0 eq.) was coupled to lumazine-6-carboxylic acid **5.13** to afford the title compound as an off-white solid (37 mg, 37% yield).

^{1}H NMR (600 MHz, DMSO-d_6): δ 11.05 (s, 1H), 9.30 (s, 1H), 9.18 (d, J = 8.1 Hz, 1H), 8.34 (dd, J = 8.4, 1.0 Hz, 1H), 7.90 (dd, J = 7.9, 1.6 Hz, 1H), 7.63 (ddd, J = 8.6, 7.5, 1.6 Hz, 1H), 7.24 – 7.18 (m, 1H), 4.82 (td, J = 9.2, 4.6 Hz, 1H), 3.67 (s, 3H), 3.60 (s, 3H), 3.36 (s, 3H), 2.68 – 2.58 (m, 1H), 2.57 – 2.54 (m, 1H), 2.35 – 2.28 (m, 1H), 2.28 – 2.20 (m, 1H), 2.08 (s, 3H). **^{13}C NMR** (151 MHz, DMSO-d_6): δ 169.9, 167.3, 163.1, 159.2, 150.4, 149.5, 146.8, 139.5, 139.1, 134.1, 130.6, 126.3, 123.5, 121.0, 117.7, 53.4, 52.4, 30.3, 30.0, 29.4, 28.6, 14.6. **$[\alpha]^{25}_D$** +8.74 (c 0.17, DMSO). **HRMS** Accurate Mass (ES+): Found 501.15603 (+1.90 ppm), $C_{22}H_{25}O_6N_6{}^{32}S$ ($M + H^+$) requires 501.15508.

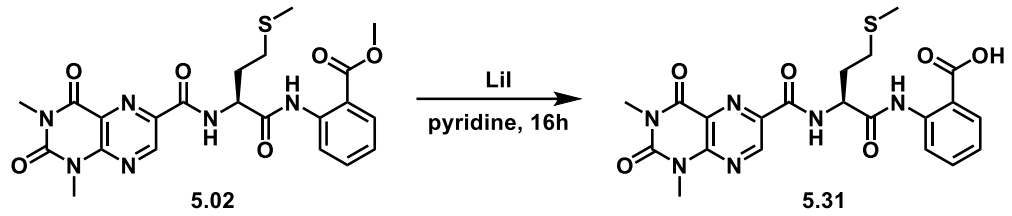

(S)-2-(2-(1,3-dimethyl-2,4-dioxo-1,2,3,4-tetrahydropteridine-6-carboxamido)-4-(methylthio)butanamido)benzoic acid 5.31. Following General Procedure 5D, methyl ester **5.02** (28.0 mg, 0.0560 mmol, 1.0 eq.) was saponified to afford the title compound as a tan powder (6.5 mg, 24% yield).

^{1}H NMR (600 MHz, DMSO-d_6): δ 13.55 (s, 1H), 11.79 (s, 1H), 9.31 (s, 1H), 9.22 (d, J = 8.0 Hz, 1H), 8.57 (d, J = 8.3 Hz, 1H), 7.95 (dd, J = 7.9, 1.5 Hz, 1H), 7.59 (t, J = 7.7 Hz, 1H), 7.14 (t, J = 7.3 Hz, 1H), 4.82 (td, J = 9.3, 4.3 Hz, 1H), 3.60 (s, 3H), 3.37 (s, 3H), 2.59 (ddd, J = 13.4, 8.4, 5.1 Hz, 1H), 2.54 – 2.52 (m, 1H), 2.37 – 2.30 (m, 1H), 2.31 – 2.17 (m, 1H), 2.07 (s, 3H). **^{13}C NMR** (151 MHz, DMSO-d_6): δ 174.5, 169.9, 169.4, 163.0, 159.2, 150.4, 149.5, 146.8, 140.4, 139.5, 133.9, 131.2, 126.3, 122.8, 119.7, 53.4, 30.7, 30.1, 29.4, 28.7, 14.6. **$[\alpha]^{25}_{D}$** -0.88 (c 0.94, DMSO). **HRMS** Accurate Mass (ES+): Found 487.14022 (+1.62 ppm), $C_{21}H_{23}O_6N_6{}^{32}S$ ($M + H^+$) requires 487.13943.

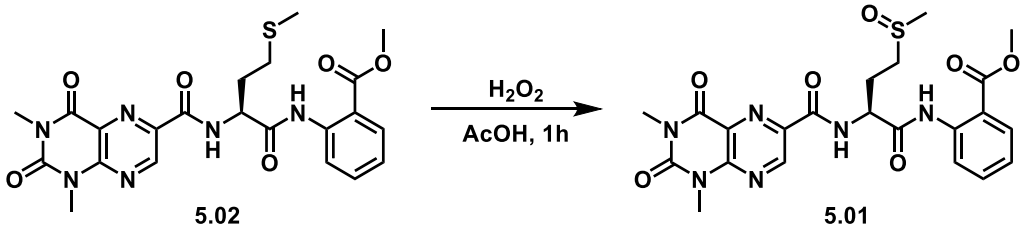

Methyl 2-((2S)-2-(1,3-dimethyl-2,4-dioxo-1,2,3,4-tetrahydropteridine-6-carboxamido)-4-(methylsulfinyl)butanamido)benzoate 5.01. Methionine peptide **5.02** (14.0 mg, 0.0280 mmol,

1.0 eq.) was dissolved in acetic acid (1 mL) and the solution was cooled to 0°C. Hydrogen peroxide (30% aqueous solution, 6.3 mg, 5.7 µL, 0.0559 mmol, 2 eq.) was added to the solution and the reaction was warmed to room temperature and stirred 1 hour. Reaction was diluted with DCM and water, then quenched with $Na_2S_2O_3$. The aqueous layer was extracted 4x with DCM, then combined organic layers were washed once with brine, dried over anhydrous Na_2SO_4, filtered, and concentrated *in vacuo* to afford crude product. This product was purified via preparative HPLC to afford the title compound as an off-white powder (14 mg, >95% yield).

Note: Due to the 1:1 mixture of stereoisomers about the chiral S=O bond, many ^{1}H signals have unexpected splitting patterns (for example, the methyl signals at 3.67 and 2.55 ppm appear as doublets) and are reported as observed. Similarly, many of the ^{13}C NMR peaks near this chiral center appear doubled.

^{1}H NMR (600 MHz, DMSO-d_6): δ 11.03 (d, J = 10.8 Hz, 1H), 9.31 (s, 1H), 9.25 (dd, J = 15.6, 8.2 Hz, 1H), 8.32 (ddd, J = 12.2, 8.4, 0.9 Hz, 1H), 7.89 (dt, J = 7.9, 1.6 Hz, 1H), 7.67 – 7.60 (m, 1H), 7.24 – 7.19 (m, 1H), 4.84 (qd, J = 8.0, 4.8 Hz, 1H), 3.67 (d, J = 3.0 Hz, 3H), 3.60 (s, 3H), 3.36 (s, 3H), 2.94 – 2.85 (m, 1H), 2.82 – 2.71 (m, 1H), 2.55 (d, J = 5.1 Hz, 3H), 2.50 – 2.41 (m, 4H), 2.38 – 2.24 (m, 1H). **^{13}C NMR** (151 MHz, DMSO-d_6): δ 169.43, 169.41, 167.28, 167.27, 163.03, 162.97, 159.17, 159.16, 150.4, 149.5, 146.81, 146.78, 139.39, 139.35, 139.0, 138.9, 134.1, 134.0, 130.59, 130.58, 126.26, 123.7, 123.6, 121.3, 121.2, 118.1, 117.9, 53.6, 53.3, 52.4, 50.0, 49.8, 38.1, 38.0, 29.4, 28.6, 24.2, 23.9. **$[\alpha]^{25}_{D}$** +2.5 (c 0.47, DMSO). **HRMS** Accurate Mass (ES+): Found 517.15119 (+2.31 ppm), $C_{22}H_{25}O_7N_6{}^{32}S$ ($M + H^+$) requires 517.14999.

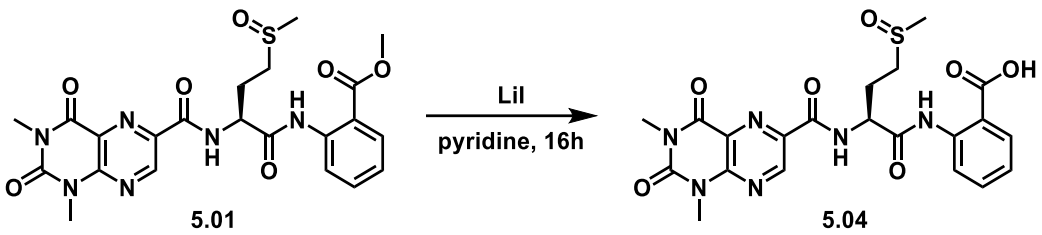

2-((2S)-2-(1,3-dimethyl-2,4-dioxo-1,2,3,4-tetrahydropteridine-6-carboxamido)-4-(methylsulfinyl)butanamido)benzoic acid 5.04. Following General Procedure 5D, methyl ester **5.01** (14.0 mg, 0.0271 mmol, 1.0 eq.) was saponified to afford the title compound as a yellow powder (7.0 mg, 51% yield).

Note: Due to the 1:1 mixture of stereoisomers about the chiral S=O bond, many ^{1}H signals have unexpected splitting patterns and are reported as observed. Similarly, many of the ^{13}C NMR peaks near this chiral center appear doubled.

^{1}H NMR (600 MHz, DMSO-d_6): δ 13.75 (s, 1H), 12.87 (s, 1H), 9.32 (s, 1H), 9.24 (dd, J = 16.4, 8.1 Hz, 1H), 8.54 (td, J = 7.9, 6.3, 1.0 Hz, 1H), 7.93 (dd, J = 7.8, 1.6 Hz, 1H), 7.48 (t, J = 7.5 Hz, 1H), 7.08 (t, J = 7.5 Hz, 1H), 4.78 (qd, J = 8.8, 4.7 Hz, 1H), 3.58 (s, 3H), 3.36 (s, 3H), 2.93-2.81 (m, 1H), 2.80-2.68 (m, 1H), 2.54 (s, 3H), 2.49 – 2.41 (m, 1H), 2.35-2.23 (m, 1H). **^{13}C NMR** (151 MHz, DMSO-d_6): δ 169.2, 169.12, 169.07, 163.1, 162.92, 162.85, 159.2, 150.4, 149.41, 149.40, 146.89, 146.87, 140.29, 140.27, 139.6, 139.5, 131.1, 126.2, 122.4, 119.2, 53.7, 53.5, 50.1, 50.0, 38.1, 37.9, 30.7, 29.4, 28.6, 24.3, 23.9. **$[\alpha]^{25}_{D}$** +1.8 (c 0.35, DMSO). **HRMS** Accurate Mass (ES+): Found 503.13453 (+0.37 ppm), $C_{21}H_{23}O_7N_6{}^{32}S$ ($M + H^+$) requires 503.13434.

6.4 Chapter 6 References

(261) Schweizer, H. P.; Hoang, T. T. An Improved System for Gene Replacement and XylE Fusion Analysis in Pseudomonas Aeruginosa. *Gene* **1995**, *158* (1), 15–22. https://doi.org/10.1016/0378-1119(95)00055-b.

(262) Hmelo, L. R.; Borlee, B. R.; Almblad, H.; Love, M. E.; Randall, T. E.; Tseng, B. S.; Lin, C.; Irie, Y.; Storek, K. M.; Yang, J. J.; Siehnel, R. J.; Howell, P. L.; Singh, P. K.; Tolker-Nielsen, T.; Parsek, M. R.; Schweizer, H. P.; Harrison, J. J. Precision-Engineering the Pseudomonas Aeruginosa Genome with Two-Step Allelic Exchange. *Nat Protoc* **2015**, *10* (11), 1820–1841. https://doi.org/10.1038/nprot.2015.115.

(263) Avissar, Y. J.; Beale, S. I. Identification of the Enzymatic Basis for Delta-Aminolevulinic Acid Auxotrophy in a HemA Mutant of Escherichia Coli. *J Bacteriol* **1989**, *171* (6), 2919–2924. https://doi.org/10.1128/jb.171.6.2919-2924.1989.

(264) Kubizna, P.; Špánik, I.; Kožíšek, J.; Szolcsányi, P. Synthesis of 2,6-Disubstituted Piperidine Alkaloids from Ladybird Beetles Calvia 10-Guttata and Calvia 14-Guttata. *Tetrahedron* **2010**, *66* (13), 2351–2355. https://doi.org/10.1016/j.tet.2010.01.106.

(265) Montes Vidal, D.; von Rymon-Lipinski, A.-L.; Ravella, S.; Groenhagen, U.; Herrmann, J.; Zaburannyi, N.; Zarbin, P. H. G.; Varadarajan, A. R.; Ahrens, C. H.; Weisskopf, L.; Müller, R.; Schulz, S. Long-Chain Alkyl Cyanides: Unprecedented Volatile Compounds Released by Pseudomonas and Micromonospora Bacteria. *Angewandte Chemie International Edition* **2017**, *56* (15), 4342–4346. https://doi.org/10.1002/anie.201611940.

(266) Abe, M.; Jean, A.; Blanchet, J.; Rouden, J.; Maddaluno, J.; De Paolis, M. H-Bonding vs Protonation of Alkynes in Regioselective Hydroamination Reactions: A Glimpse into the Reactivity of Arylogous Ynolethers and Ynamines. *J. Org. Chem.* **2019**, *84* (23), 15448–15475. https://doi.org/10.1021/acs.joc.9b02471.

Chapter 7 - Appendix

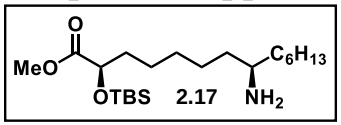

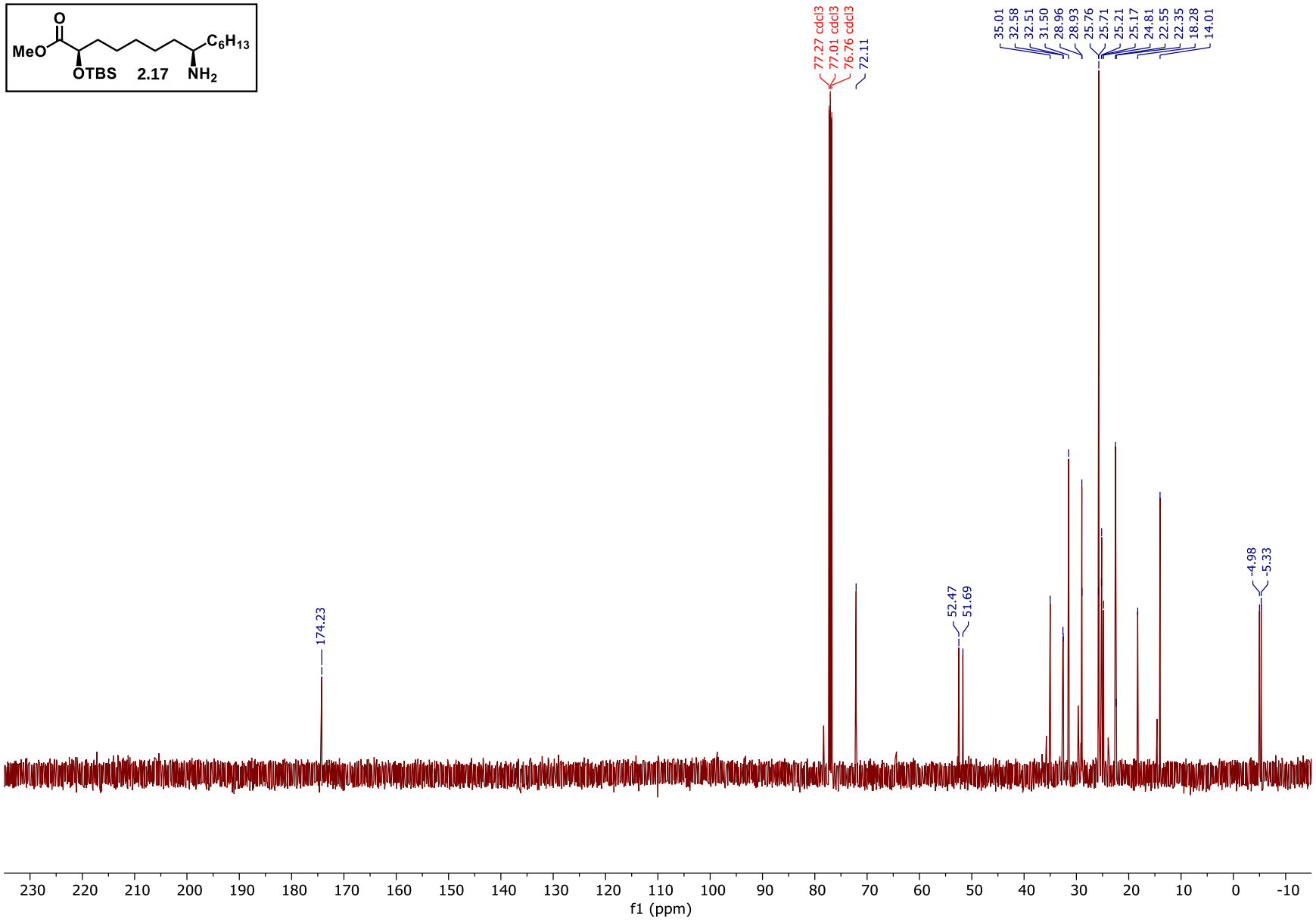
MeO
O
OTBS
2.17
NH2
C6H13
77.27 cdcl3
77.01 cdcl3
76.76 cdcl3
72.11
35.01
32.58
32.51
31.50
28.96
28.93
25.76
25.71
25.21
25.17
24.81
22.55
22.35
18.28
14.01
174.23
52.47
51.69
-4.98
-5.33
230 220 210 200 190 180 170 160 150 140 130 120 110 100 90 80 70 60 50 40 30 20 10 0 -10
f1 (ppm)

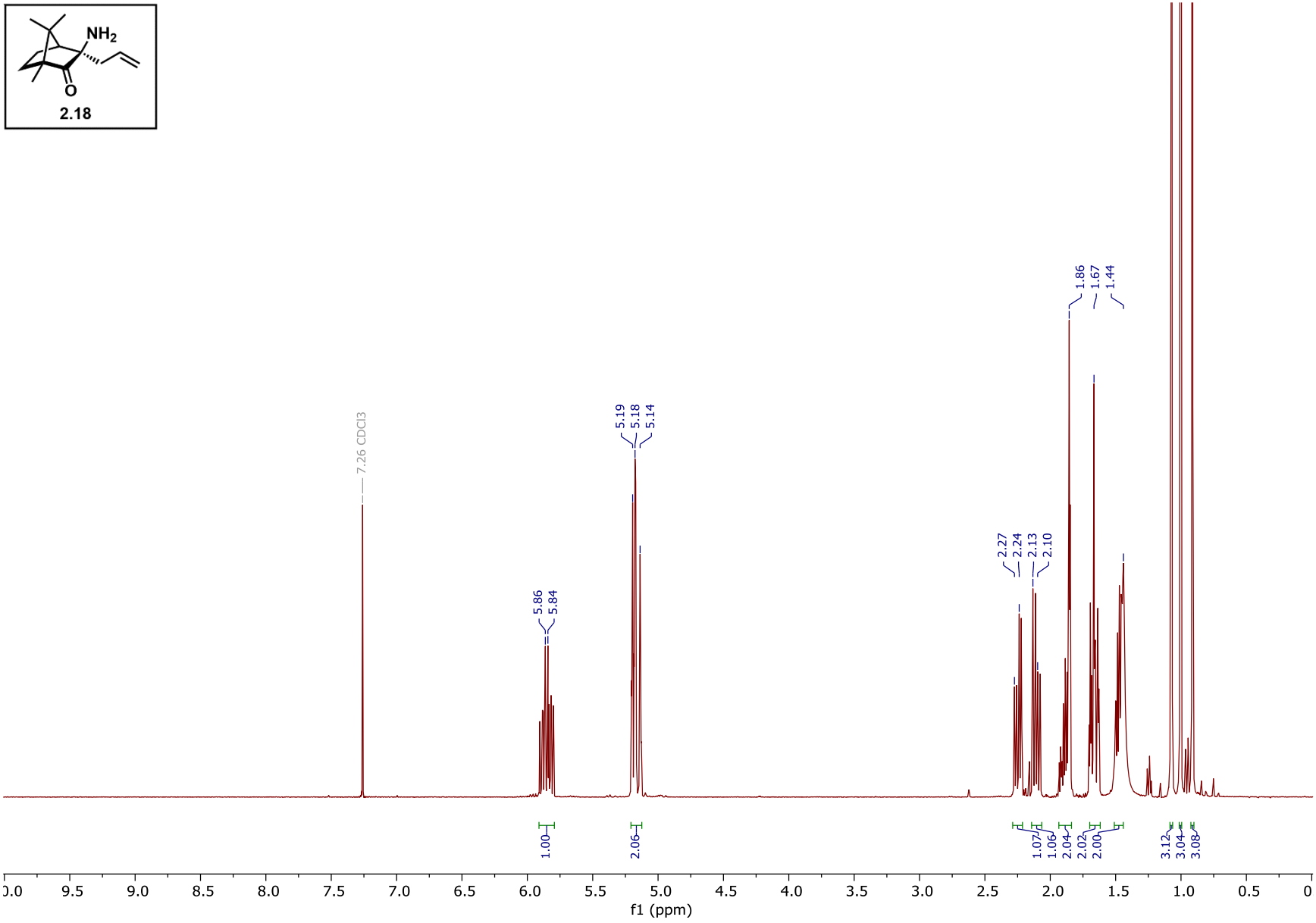
NH2
O
2.18
7.26 CDCl3
5.86
5.84
5.19
5.18
5.14
2.27
2.24
2.13
2.10
1.86
1.67
1.44
1.00
2.06
1.07
1.06
2.04
2.02
2.00
3.12
3.04
3.08
f1 (ppm)

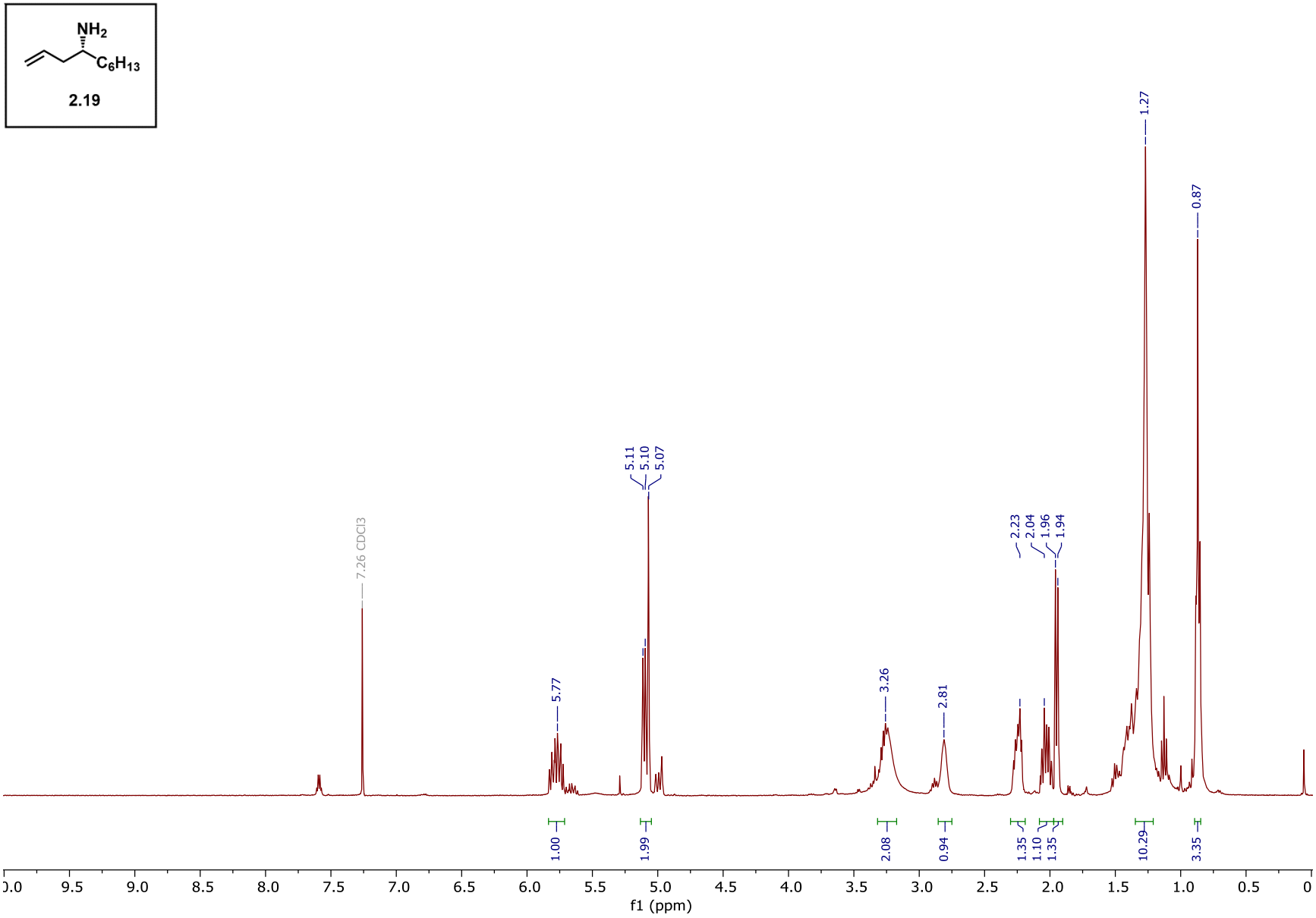
NH2
C6H13
2.19
7.26 CDCl3
5.77
5.11
5.10
5.07
3.26
2.81
2.23
2.04
1.96
1.94
1.27
0.87
1.00
1.99
2.08
0.94
1.35
1.10
1.35
10.29
3.35
f1 (ppm)

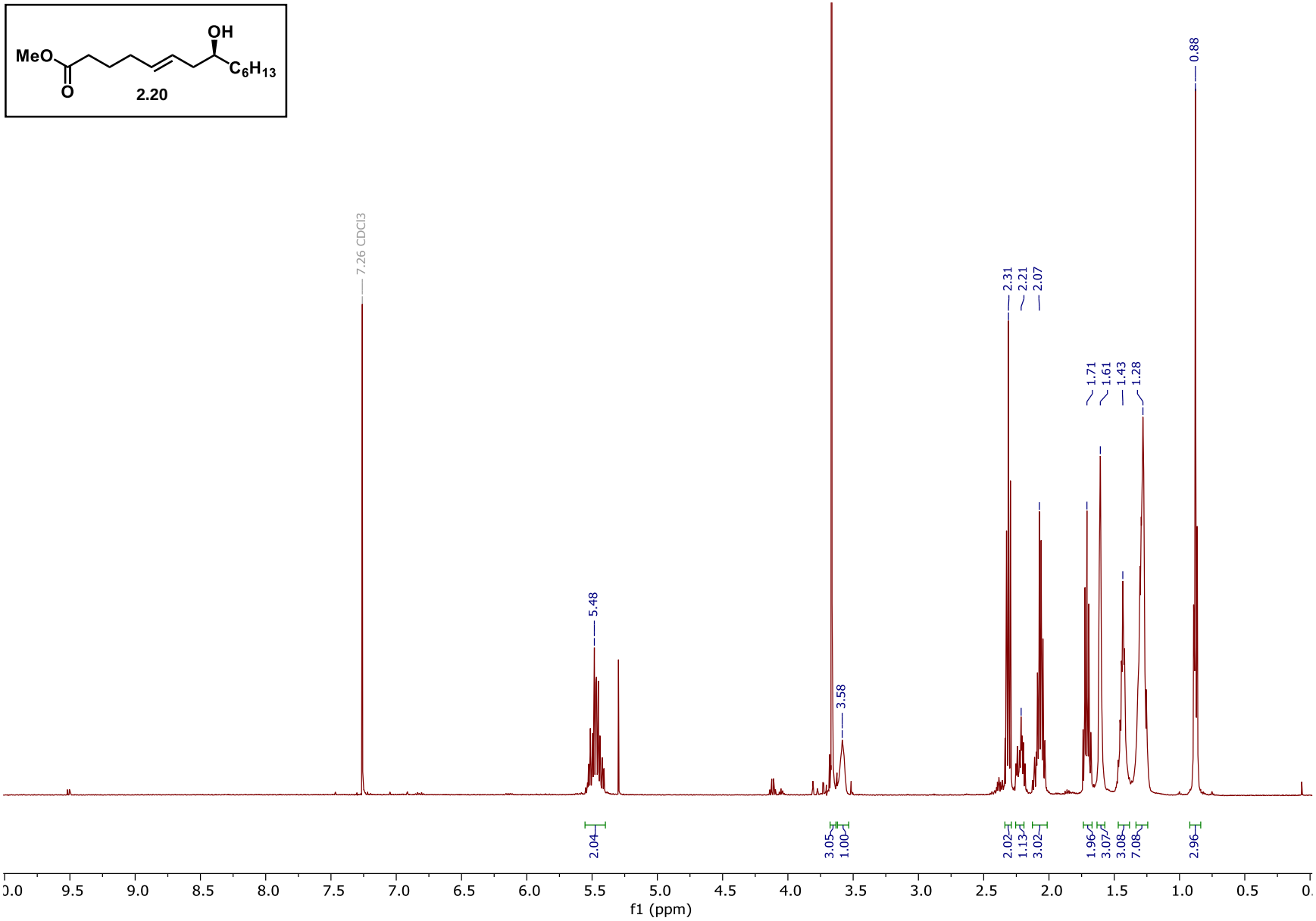
MeO
O
OH
C_6H_{13}
2.20
7.26 CDCl3
5.48
3.58
2.31
2.21
2.07
1.71
1.61
1.43
1.28
0.88
2.04
3.05
1.00
2.02
1.13
3.02
1.96
3.07
3.08
7.08
2.96
f1 (ppm)

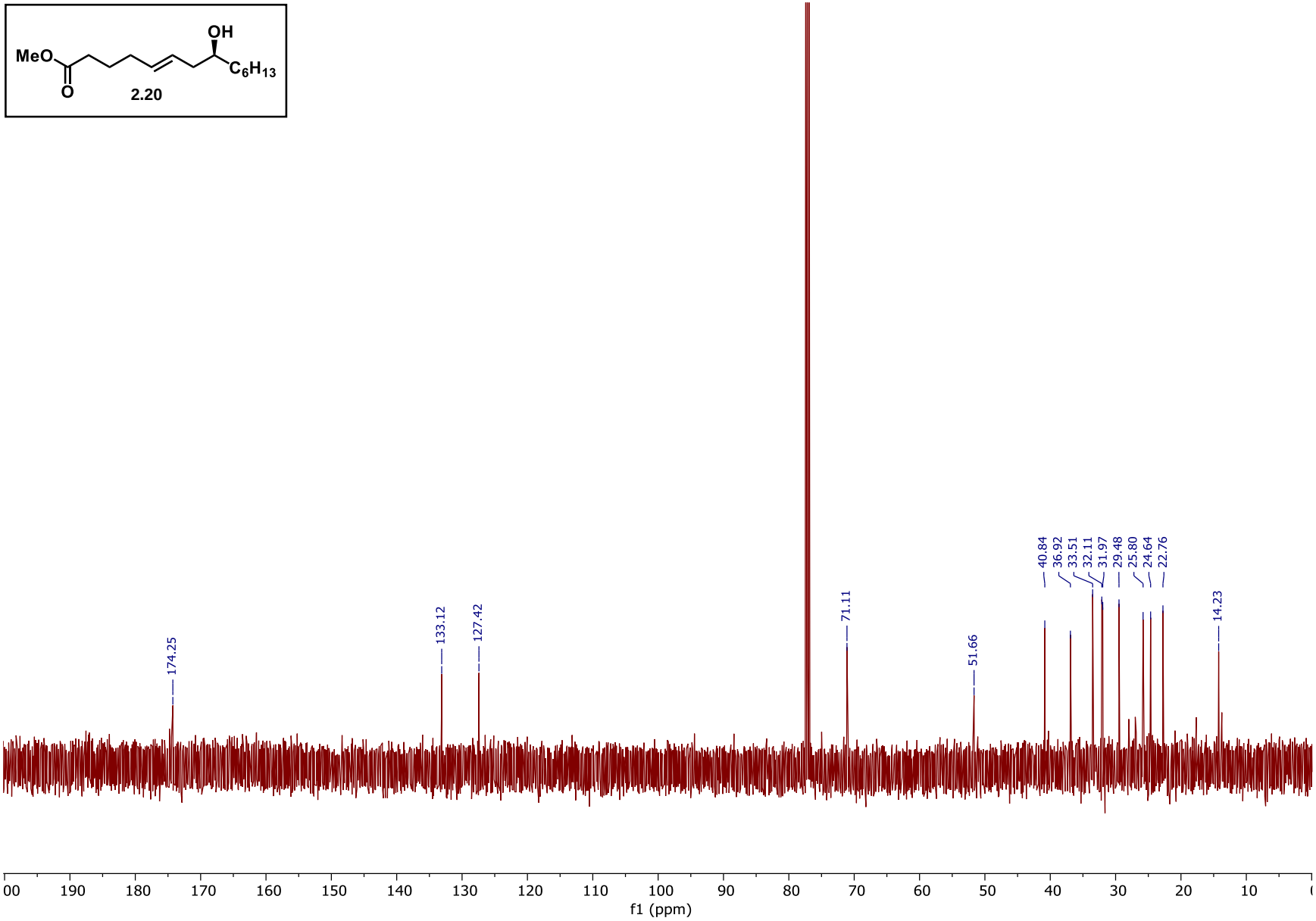
MeO
O
OH
C6H13
2.20
174.25
133.12
127.42
71.11
51.66
40.84
36.92
33.51
32.11
31.97
29.48
25.80
24.64
22.76
14.23
f1 (ppm)

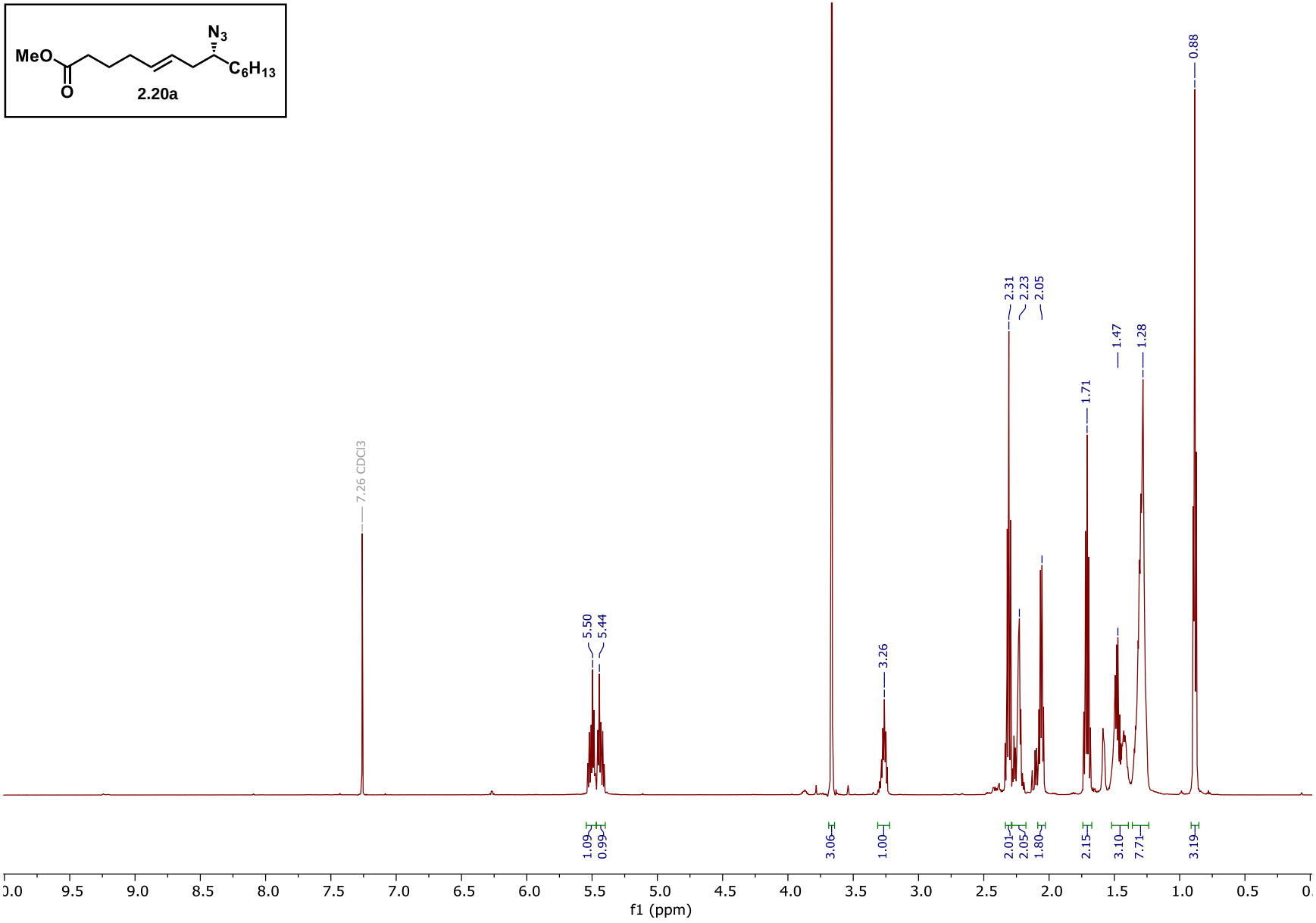
MeO
O
N3
C6H13
2.20a
7.26 CDCl3
5.50
5.44
3.26
2.31
2.23
2.05
1.71
1.47
1.28
0.88
1.09
0.99
3.06
1.00
2.01
2.05
1.80
2.15
3.10
7.71
3.19
f1 (ppm)

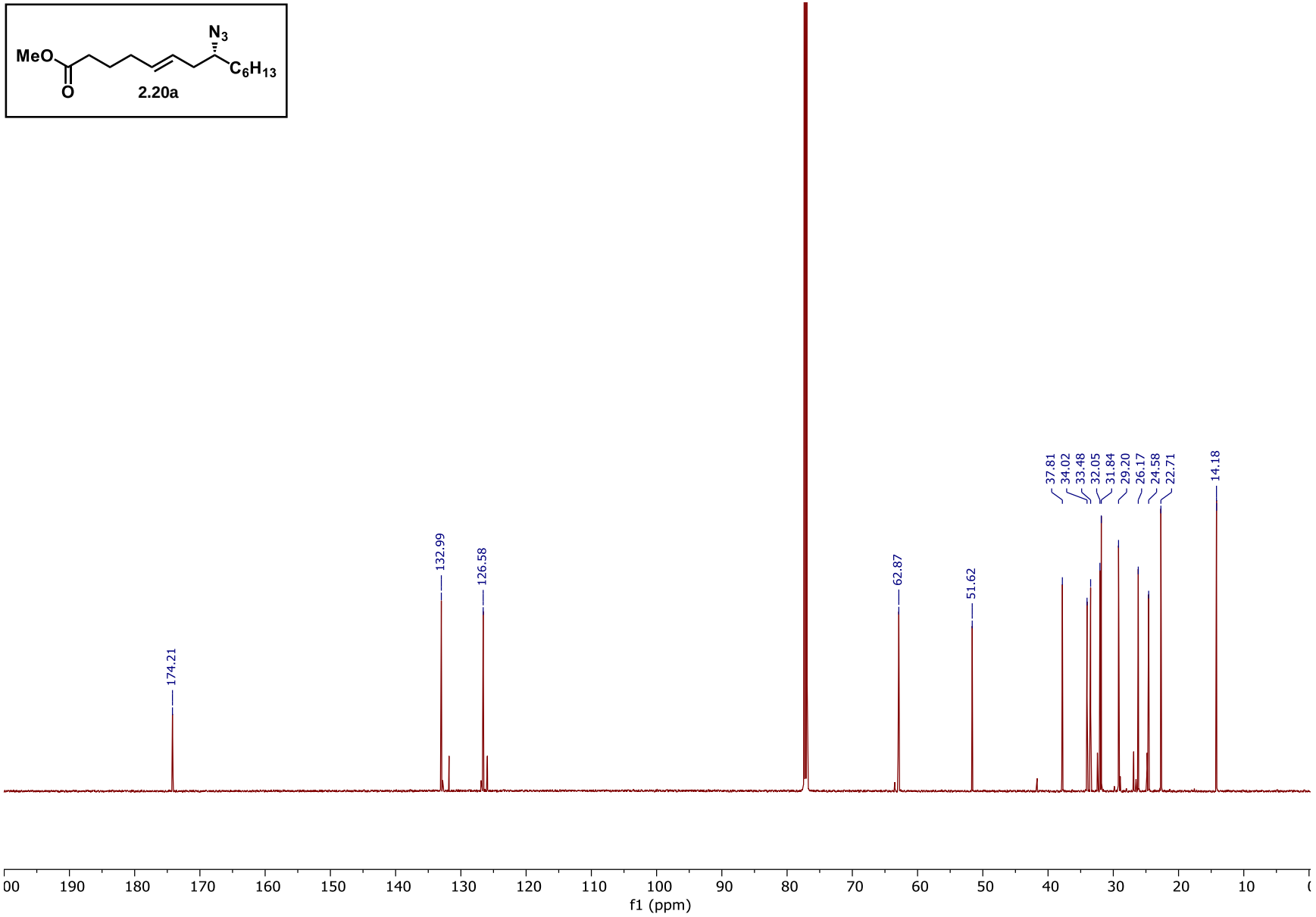
MeO
O
N3
C6H13
2.20a
174.21
132.99
126.58
62.87
51.62
37.81
34.02
33.48
32.05
31.84
29.20
26.17
24.58
22.71
14.18
f1 (ppm)

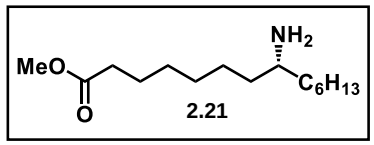
NH2
MeO
C6H13
O
2.21

3.61
1.57
1.41
1.40
1.33
1.27
1.23
0.83
2.25
2.74
7.26 CDCl3
5.16
1.00
2.04
2.08
2.05
16.97
2.98
f1 (ppm)

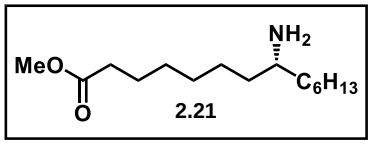
NH2
MeO
C6H13
O
2.21

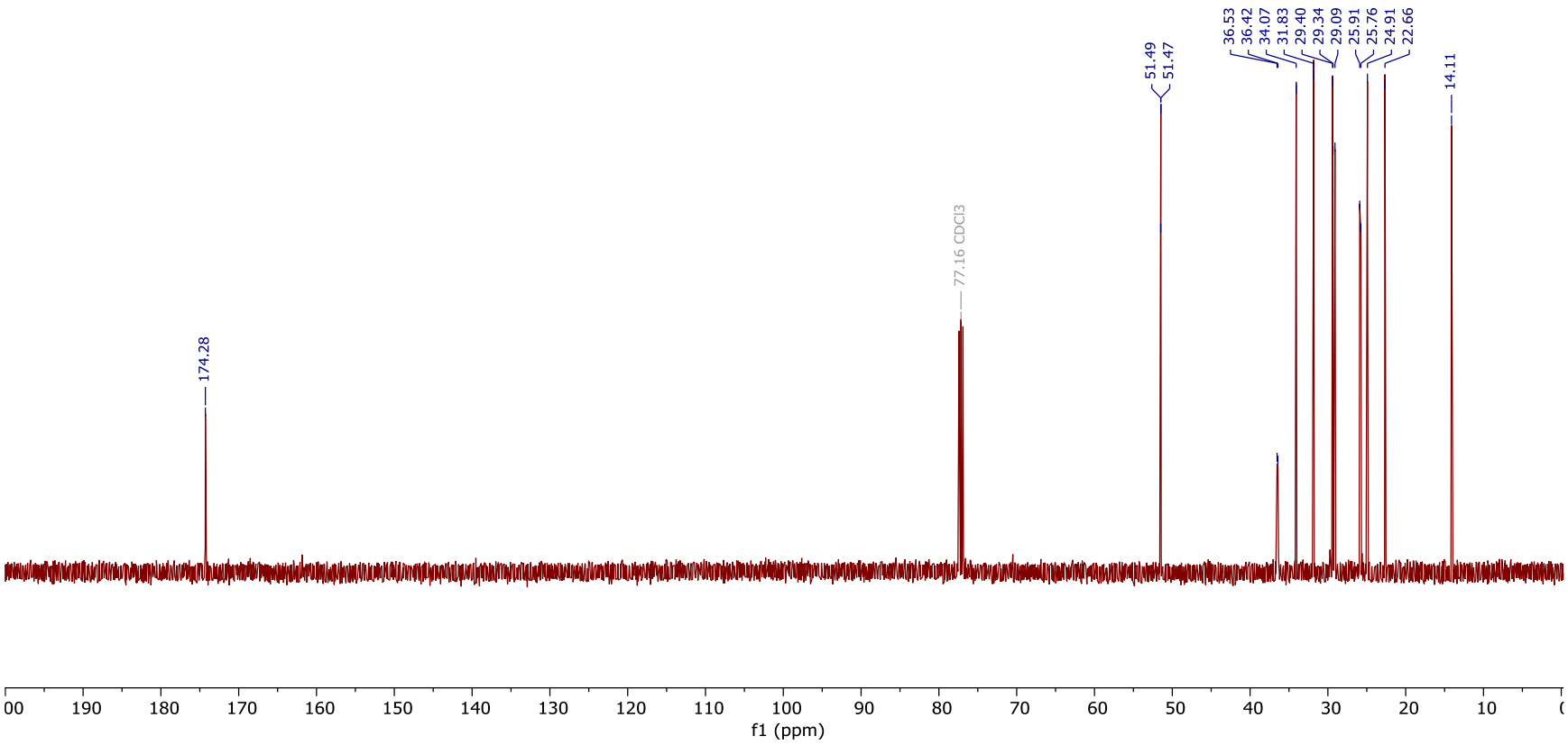
174.28
77.16 CDCl3
51.49
51.47
36.53
36.42
34.07
31.83
29.40
29.34
29.09
25.91
25.76
24.91
22.66
14.11
f1 (ppm)

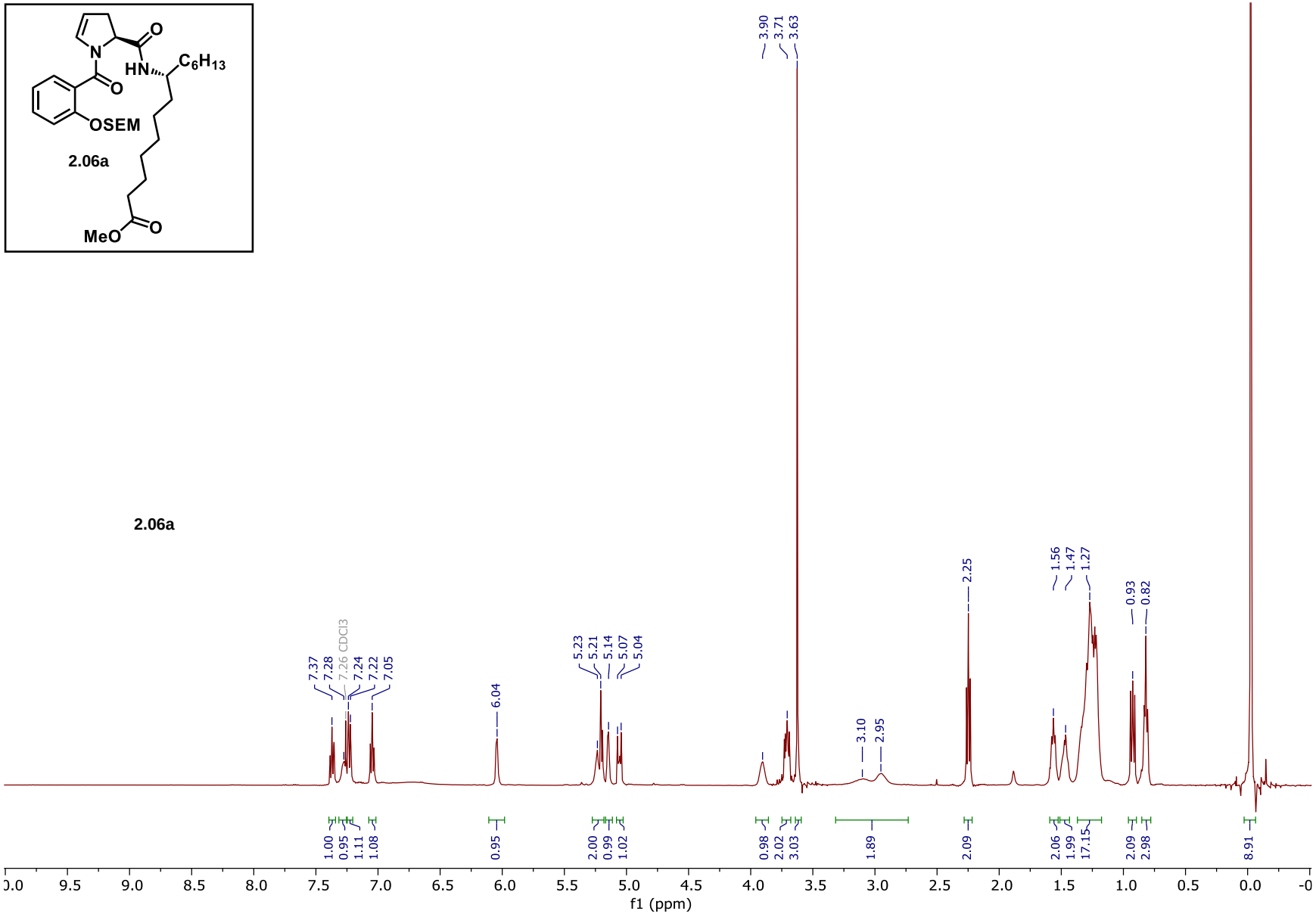
2.06a
2.06a
3.90
3.71
3.63
7.37
7.28
7.26 CDCl3
7.24
7.22
7.05
6.04
5.23
5.21
5.14
5.07
5.04
3.10
2.95
2.25
1.56
1.47
1.27
0.93
0.82
1.00
0.95
1.11
1.08
0.95
2.00
0.99
1.02
0.98
2.02
3.03
1.89
2.09
2.06
1.99
17.15
2.09
2.98
8.91
f1 (ppm)

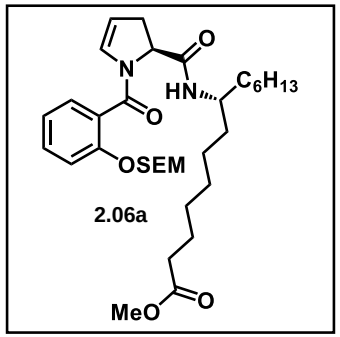
O
N
HN
C_6H_{13}
O
OSEM
2.06a
MeO
O

-1.30
35.53
35.35
34.13
31.83
29.79
29.32
29.30
29.21
25.84
25.68
24.97
22.70
18.19
14.17
59.46
51.52
49.37
93.24
66.92
131.54
129.55
128.54
125.51
122.20
114.79
111.83
153.55
174.26
169.78
166.04
00
190
180
170
160
150
140
130
120
110
100
90
80
70
60
50
40
30
20
10
0
-1
f1 (ppm)

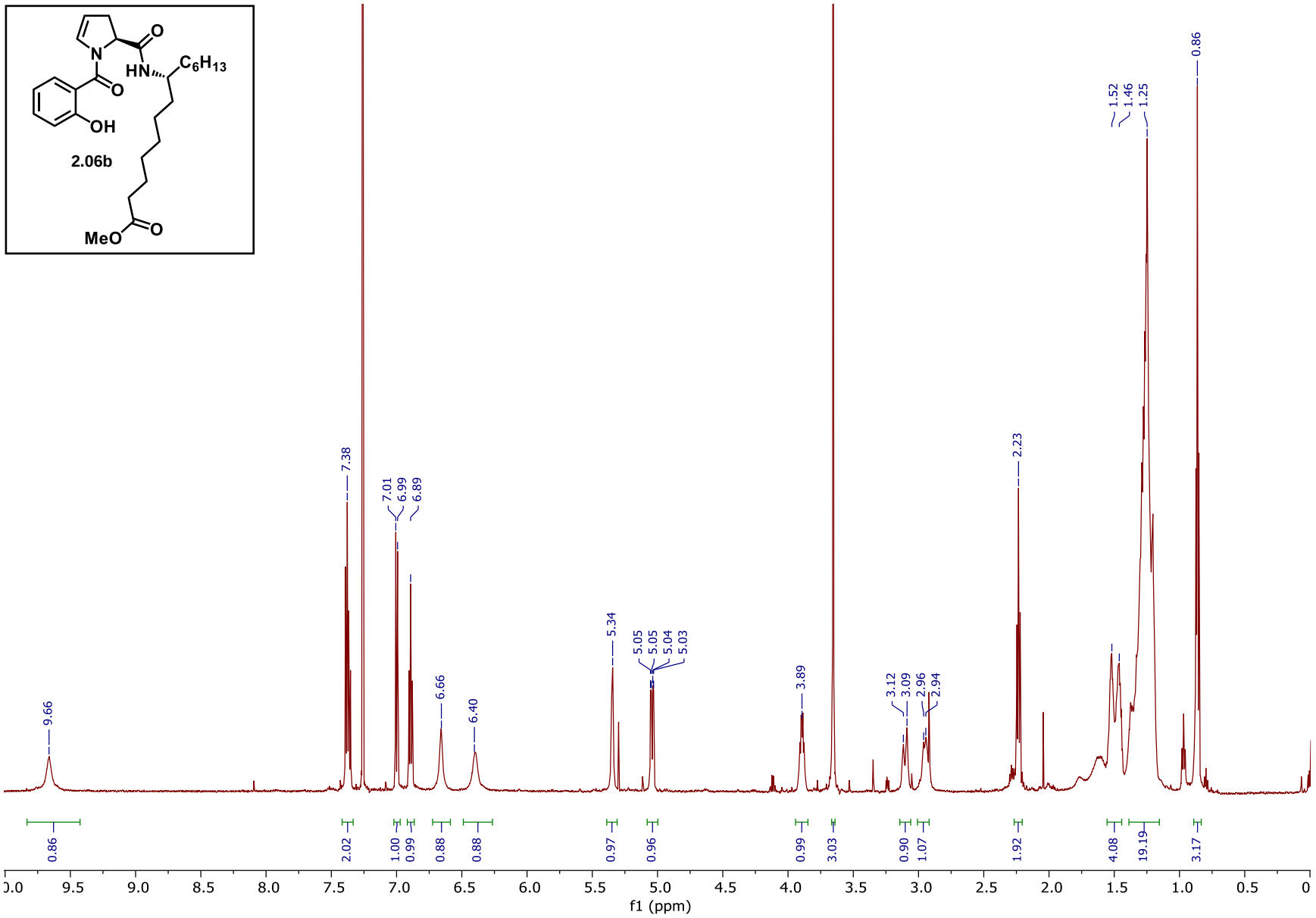
2.06b
9.66
7.38
7.01
6.99
6.89
6.66
6.40
5.34
5.05
5.05
5.04
5.03
3.89
3.12
3.09
2.96
2.94
2.23
1.52
1.46
1.25
0.86
0.86
2.02
1.00
0.99
0.88
0.88
0.97
0.96
0.99
3.03
0.90
1.07
1.92
4.08
19.19
3.17
f1 (ppm)

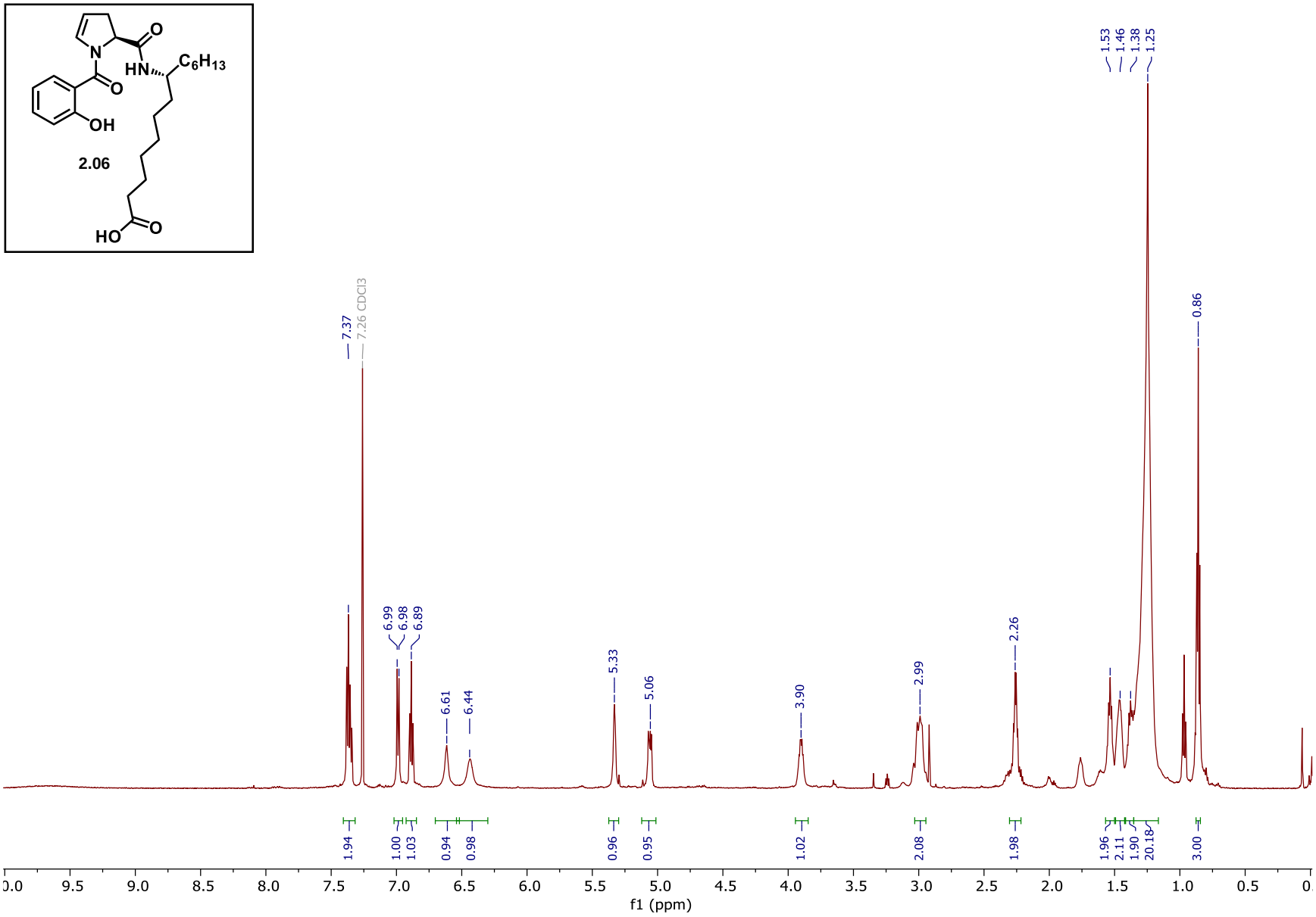
O
N
HN
C6H13
O
OH
2.06
HO
O
7.37
7.26 CDCl3
6.99
6.98
6.89
6.61
6.44
5.33
5.06
3.90
2.99
2.26
1.53
1.46
1.38
1.25
0.86
1.94
1.00
1.03
0.94
0.98
0.96
0.95
1.02
2.08
1.98
1.96
2.11
1.90
20.18
3.00
f1 (ppm)

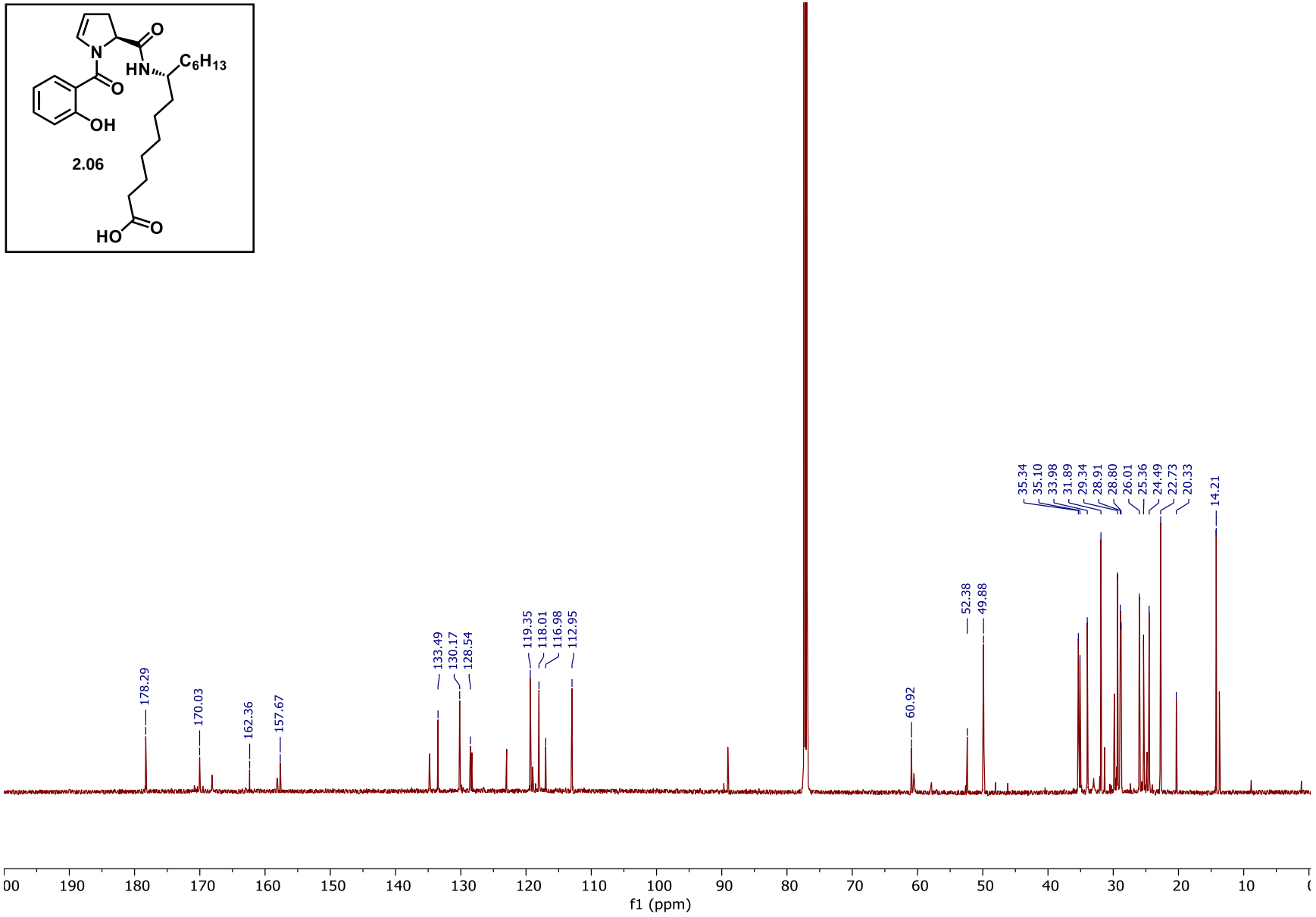
N
O
HN
C_6H_{13}
O
OH
2.06
HO
O
178.29
170.03
162.36
157.67
133.49
130.17
128.54
119.35
118.01
116.98
112.95
60.92
52.38
49.88
35.34
35.10
33.98
31.89
29.34
28.91
28.80
26.01
25.36
24.49
22.73
20.33
14.21
f1 (ppm)

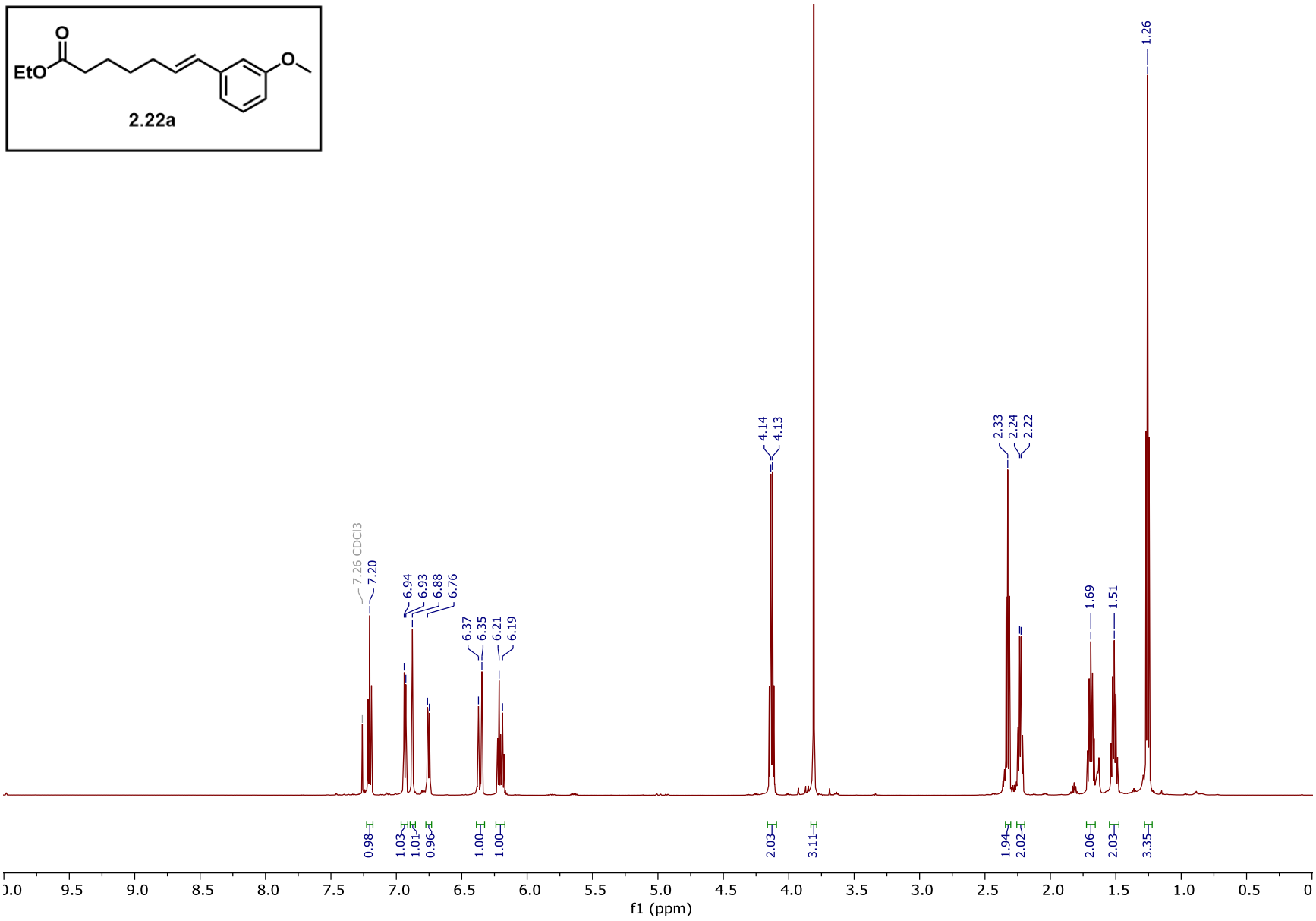
EtO
O
O
2.22a
7.26 CDCl3
7.20
6.94
6.93
6.88
6.76
6.37
6.35
6.21
6.19
4.14
4.13
2.33
2.24
2.22
1.69
1.51
1.26
0.98
1.03
1.01
0.96
1.00
1.00
2.03
3.11
1.94
2.02
2.06
2.03
3.35
f1 (ppm)

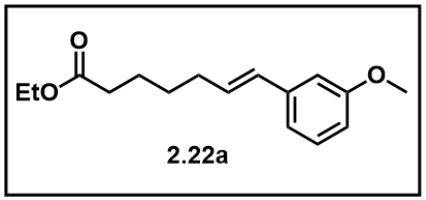
O
EtO
O

2.22a

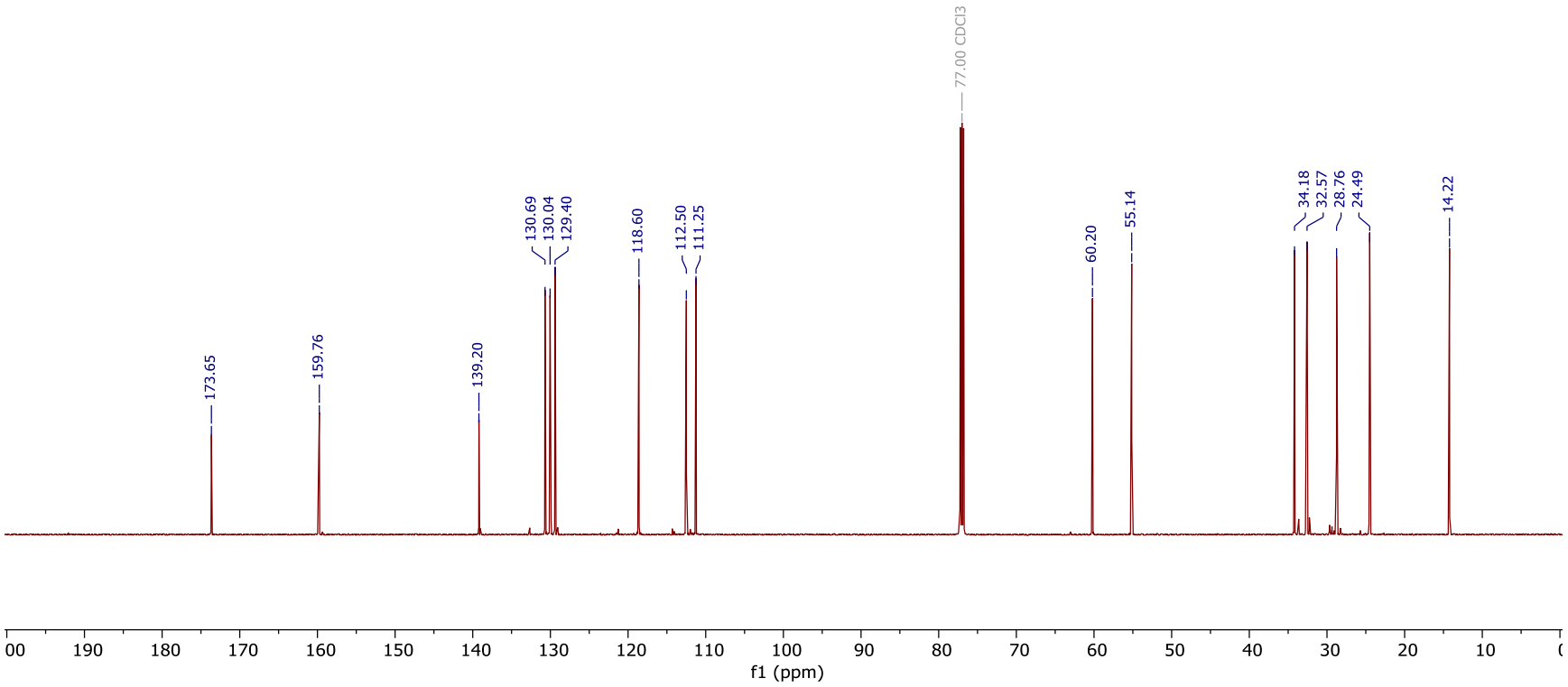
173.65
159.76
139.20
130.69
130.04
129.40
118.60
112.50
111.25
77.00 CDCl3
60.20
55.14
34.18
32.57
28.76
24.49
14.22
f1 (ppm)

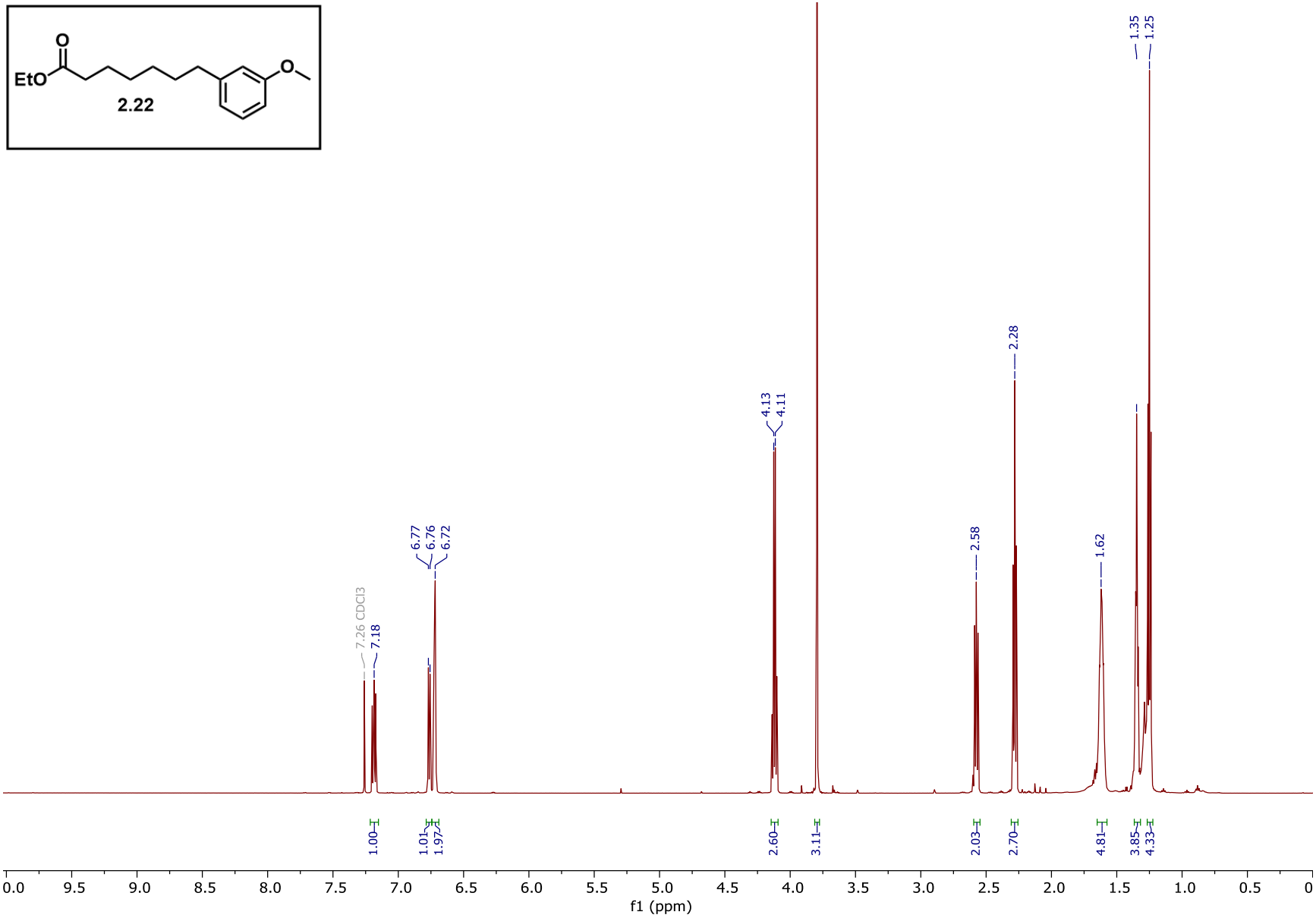
EtO
O
O
2.22
7.26 CDCl3
7.18
6.77
6.76
6.72
4.13
4.11
2.58
2.28
1.62
1.35
1.25
1.00
1.01
1.97
2.60
3.11
2.03
2.70
4.81
3.85
4.33
0.0
9.5
9.0
8.5
8.0
7.5
7.0
6.5
6.0
5.5
5.0
4.5
4.0
3.5
3.0
2.5
2.0
1.5
1.0
0.5
0
f1 (ppm)

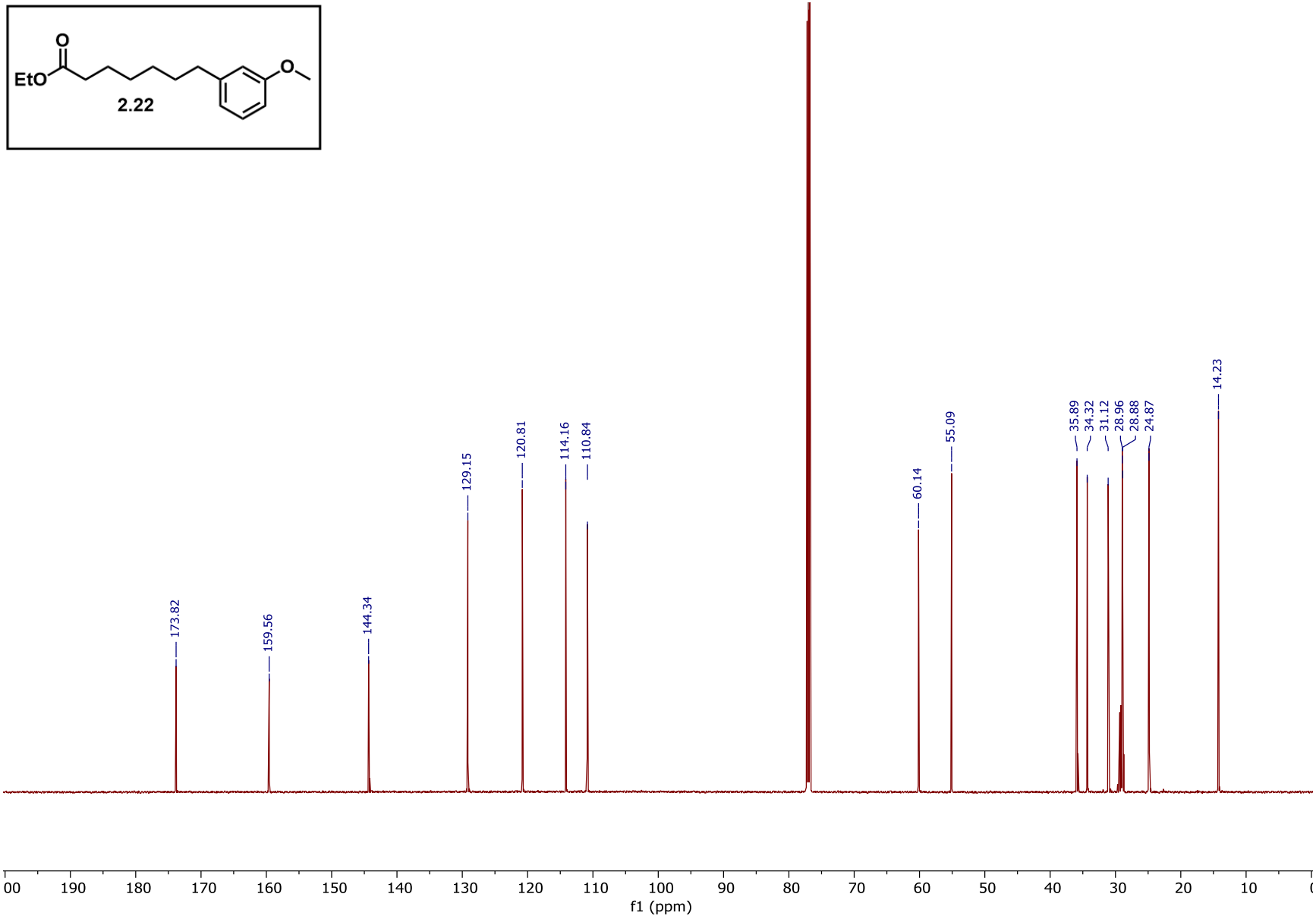
O
EtO
O
2.22
173.82
159.56
144.34
129.15
120.81
114.16
110.84
60.14
55.09
35.89
34.32
31.12
28.96
28.88
24.87
14.23
f1 (ppm)

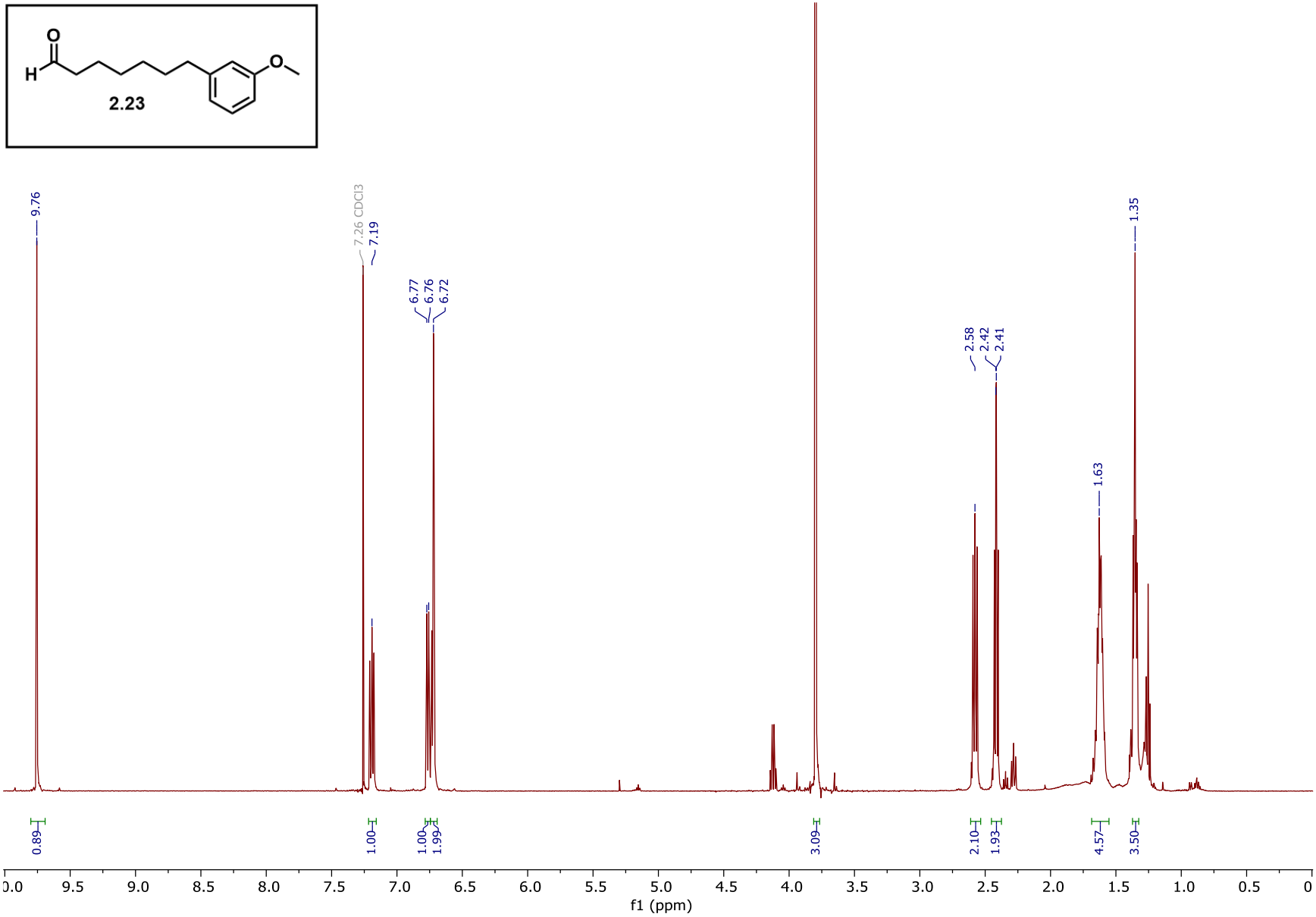
O
H
O
2.23
9.76
7.26 CDCl3
7.19
6.77
6.76
6.72
2.58
2.42
2.41
1.63
1.35
0.89
1.00
1.00
1.99
3.09
2.10
1.93
4.57
3.50
f1 (ppm)

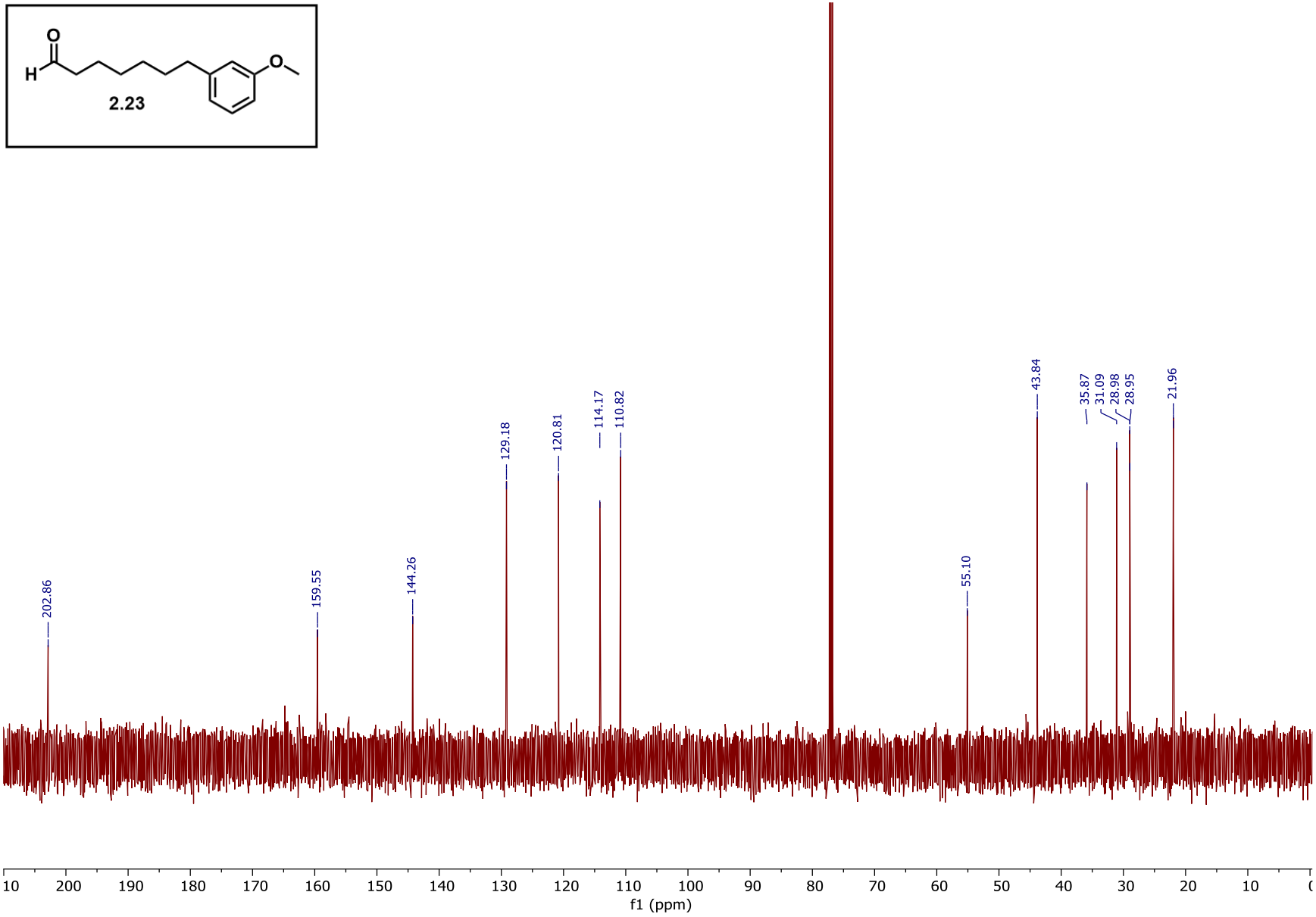
O
H
O
2.23
202.86
159.55
144.26
129.18
120.81
114.17
110.82
55.10
43.84
35.87
31.09
28.98
28.95
21.96
10
200
190
180
170
160
150
140
130
120
110
100
90
80
70
60
50
40
30
20
10
f1 (ppm)

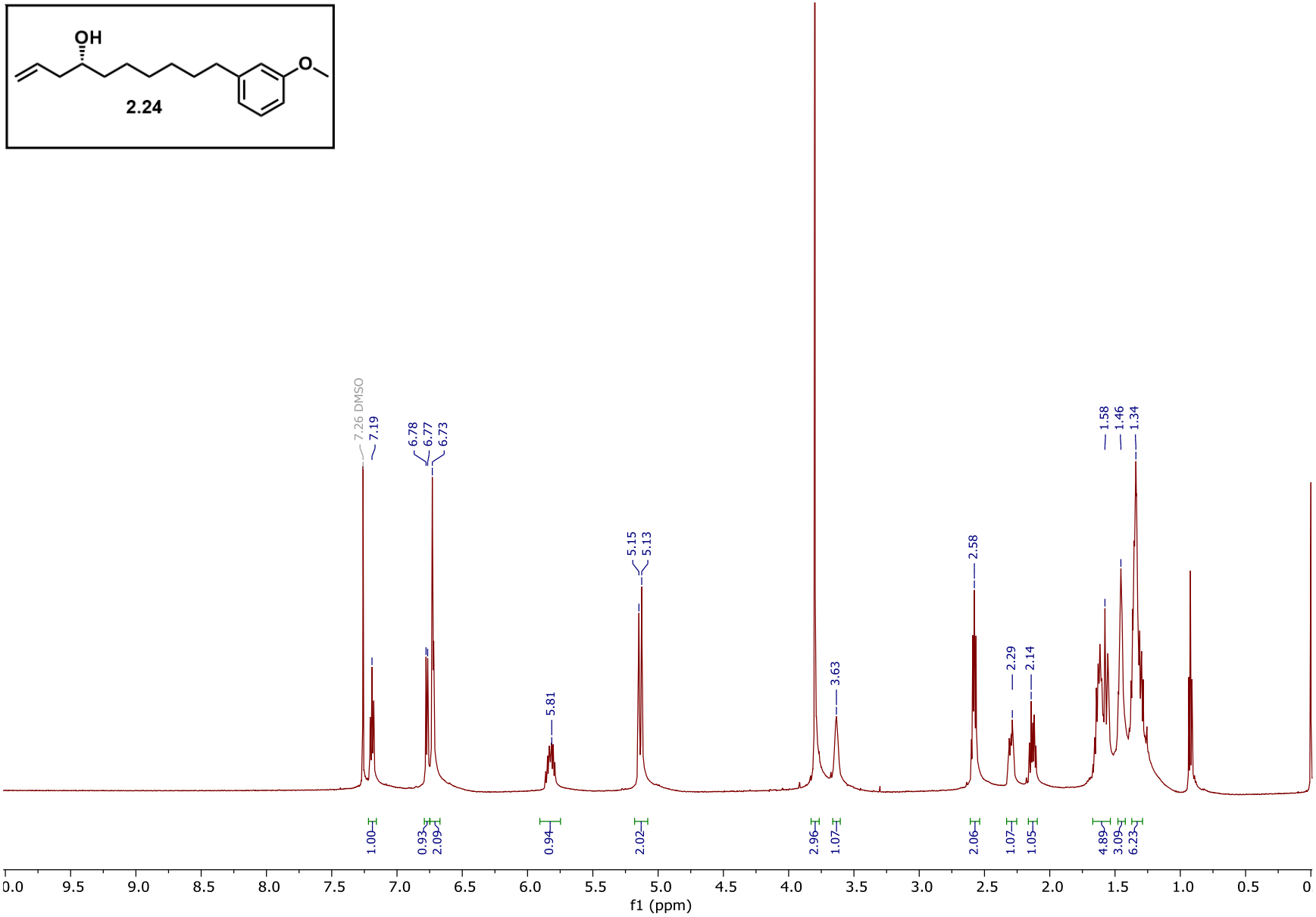
OH
O
2.24
7.26 DMSO
7.19
6.78
6.77
6.73
5.15
5.13
5.81
3.63
2.58
2.29
2.14
1.58
1.46
1.34
1.00
0.93
2.09
0.94
2.02
2.96
1.07
2.06
1.07
1.05
4.89
3.09
6.23
f1 (ppm)

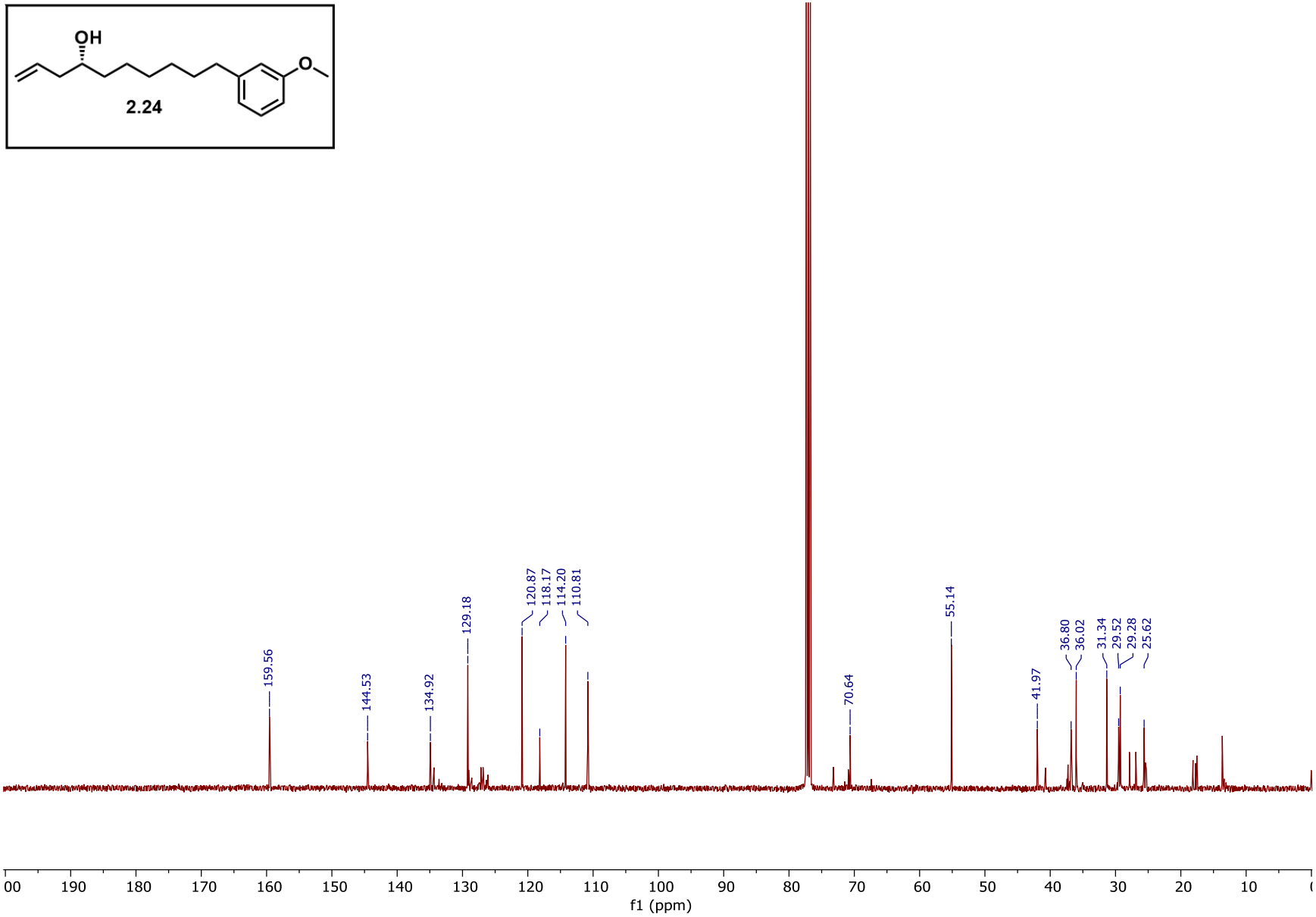
OH
O
2.24
159.56
144.53
134.92
129.18
120.87
118.17
114.20
110.81
70.64
55.14
41.97
36.80
36.02
31.34
29.52
29.28
25.62
f1 (ppm)

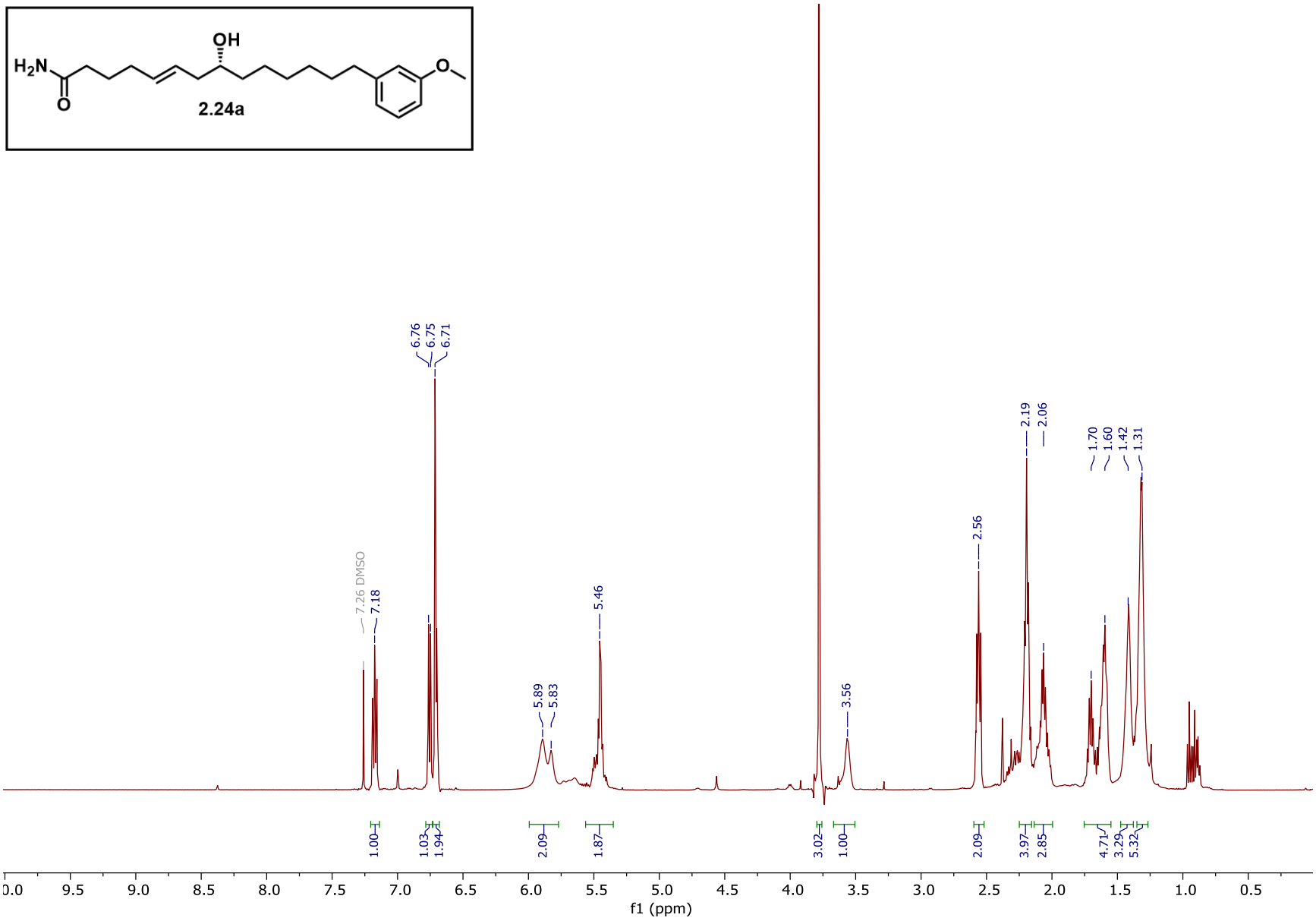
OH
H2N
O
O
2.24a
7.26 DMSO
7.18
6.76
6.75
6.71
5.89
5.83
5.46
3.56
2.56
2.19
2.06
1.70
1.60
1.42
1.31
1.00
1.03
1.94
2.09
1.87
3.02
1.00
2.09
3.97
2.85
4.71
3.29
5.32
f1 (ppm)

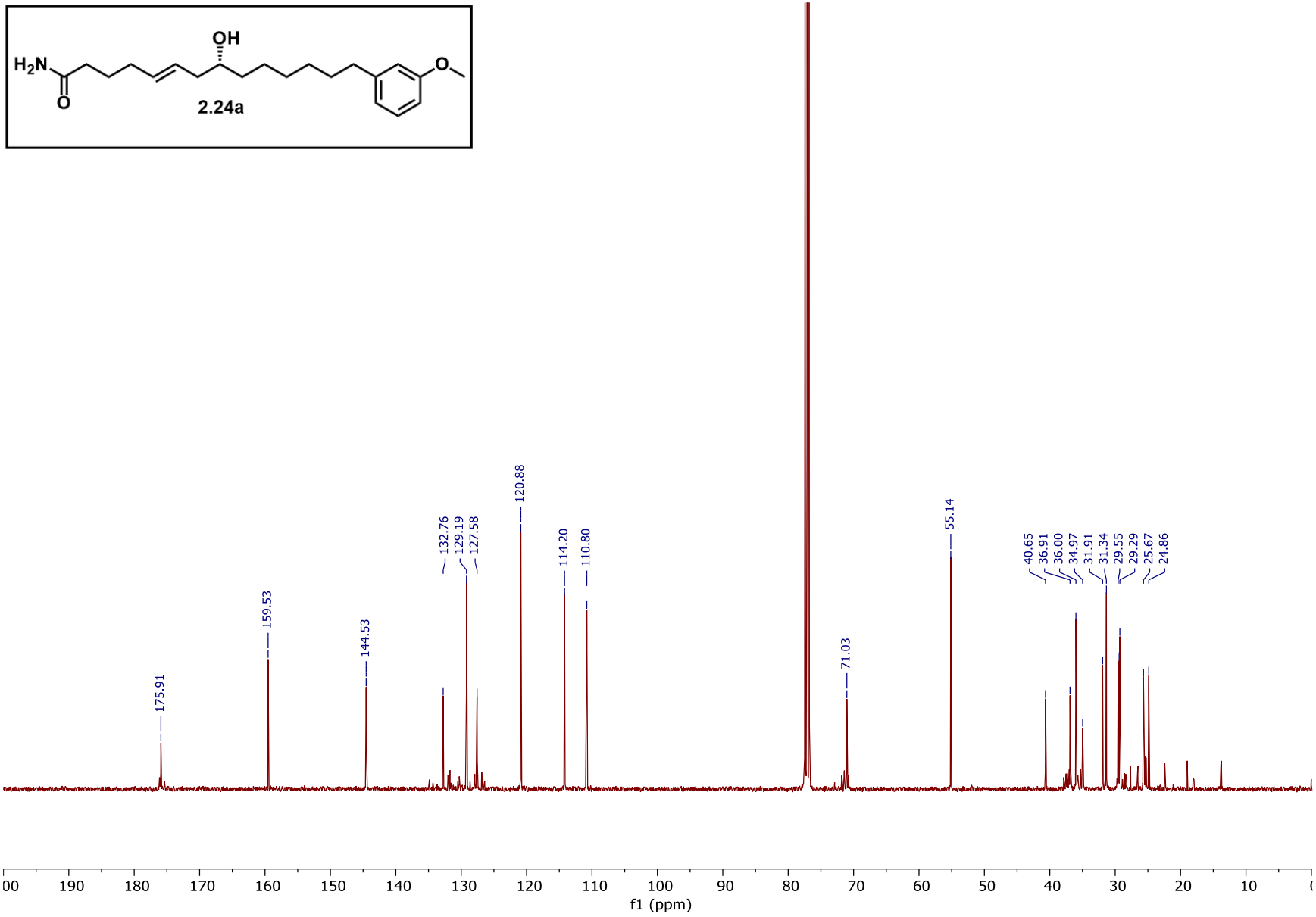
OH
H2N
O
O
2.24a
175.91
159.53
144.53
132.76
129.19
127.58
120.88
114.20
110.80
71.03
55.14
40.65
36.91
36.00
34.97
31.91
31.34
29.55
29.29
25.67
24.86
f1 (ppm)

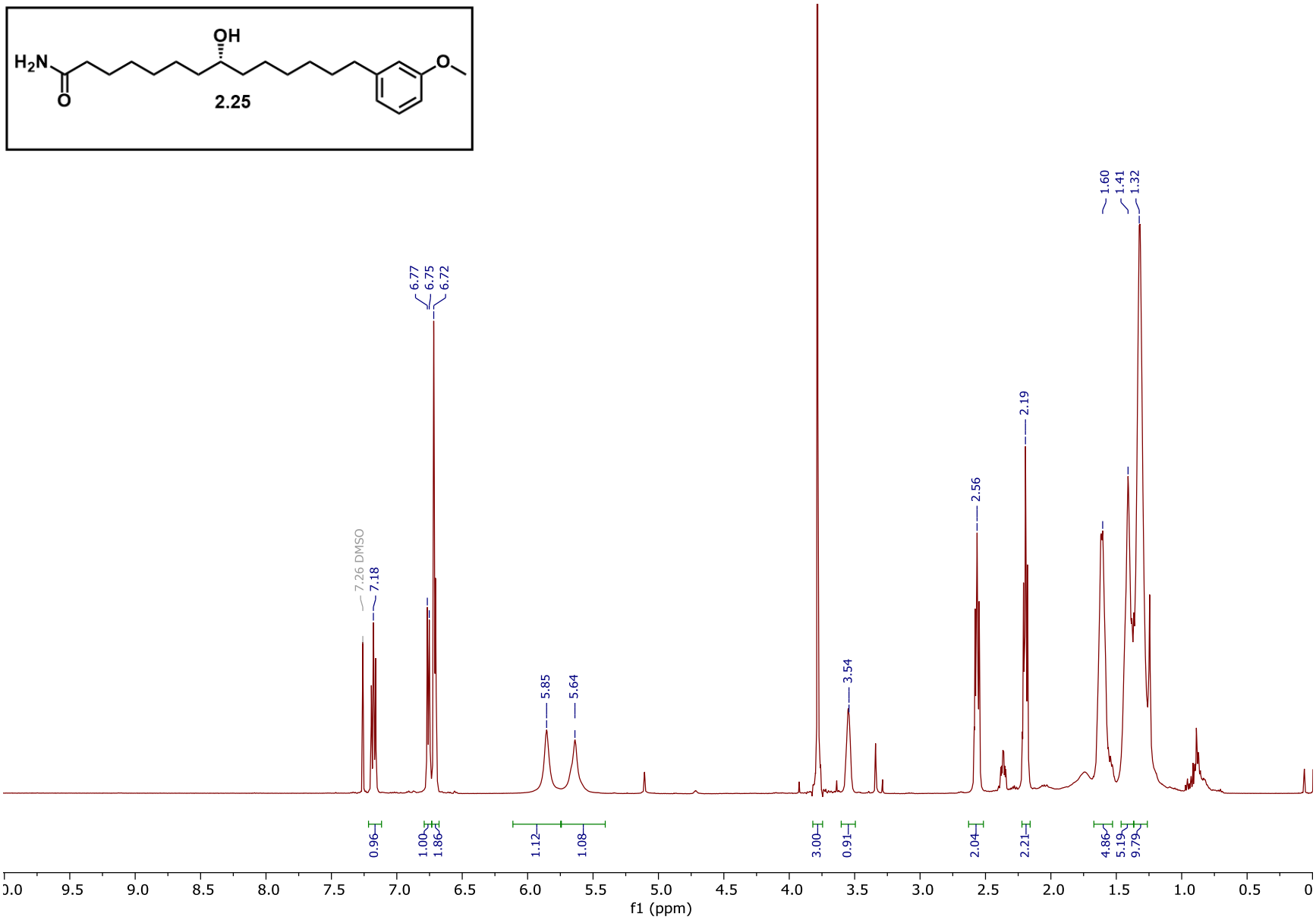
OH
H2N
O
O
2.25
7.26 DMSO
7.18
6.77
6.75
6.72
5.85
5.64
3.54
2.56
2.19
1.60
1.41
1.32
0.96
1.00
1.86
1.12
1.08
3.00
0.91
2.04
2.21
4.86
5.19
9.79
f1 (ppm)

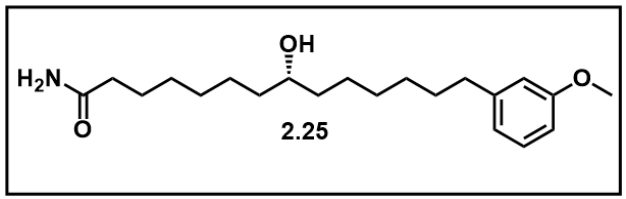
OH
H2N
O
O
2.25

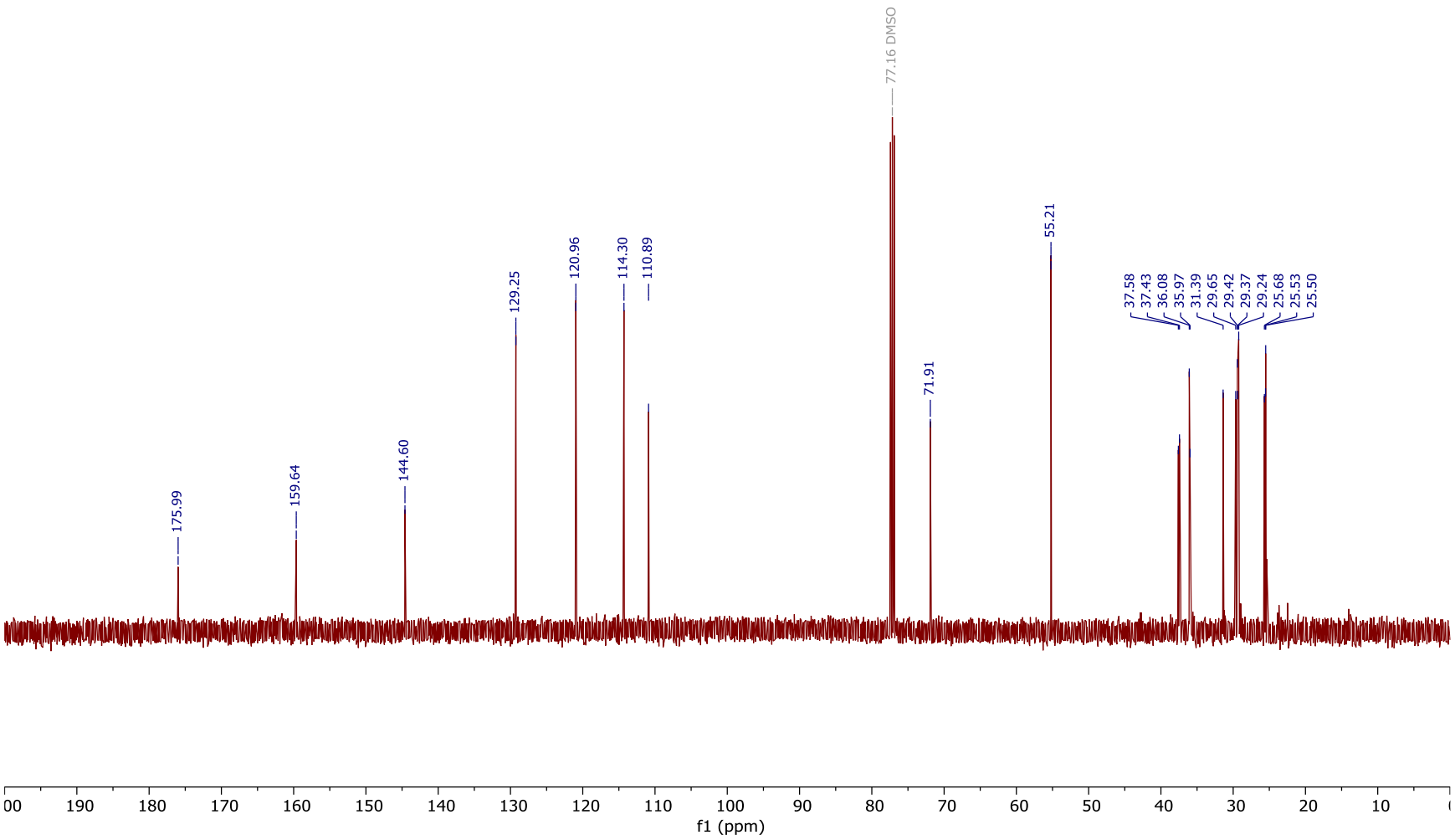
175.99
159.64
144.60
129.25
120.96
114.30
110.89
77.16 DMSO
71.91
55.21
37.58
37.43
36.08
35.97
31.39
29.65
29.42
29.37
29.24
25.68
25.53
25.50
00
190
180
170
160
150
140
130
120
110
100
90
80
70
60
50
40
30
20
10
f1 (ppm)

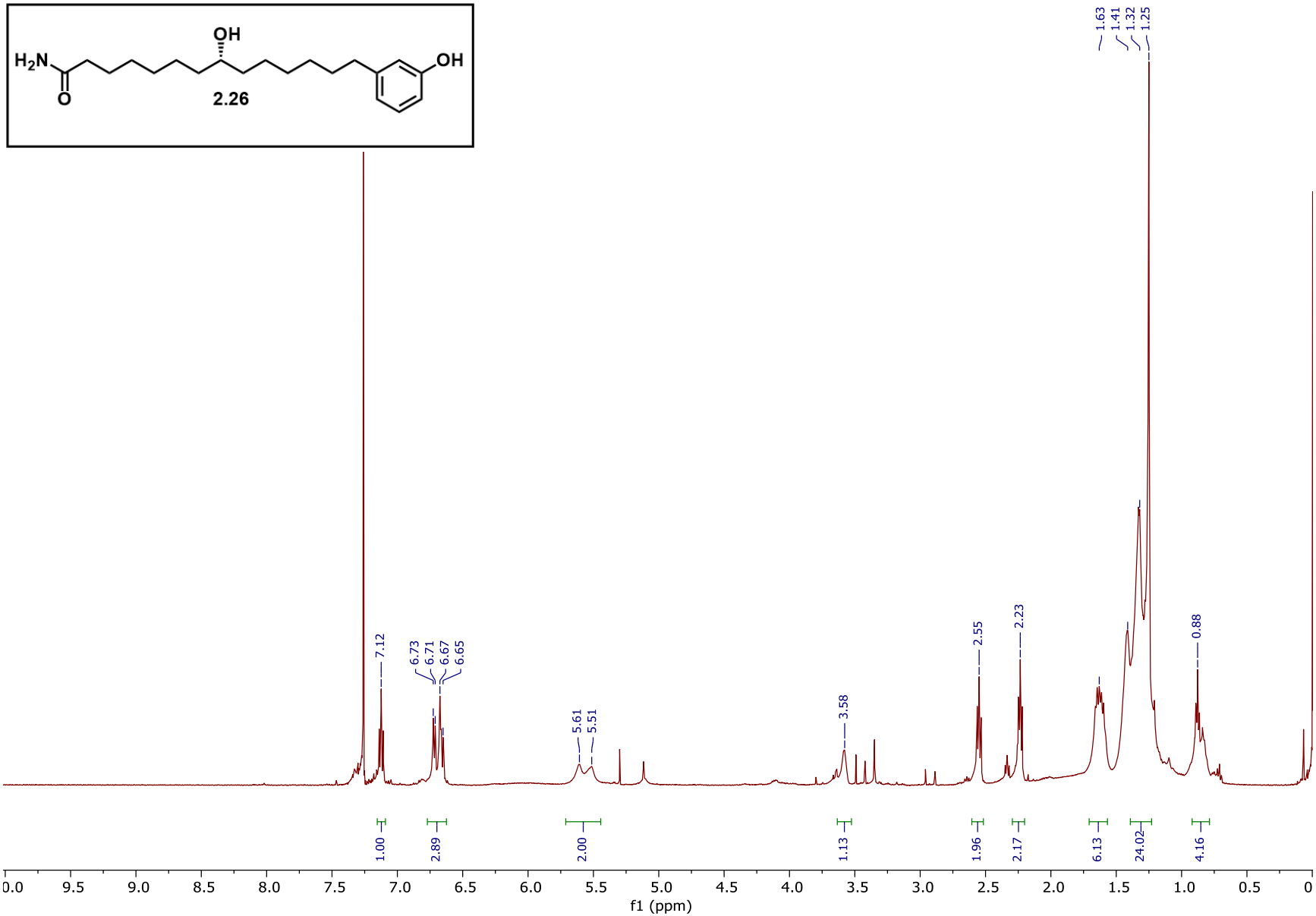
OH
H2N
O
OH
2.26
1.63
1.41
1.32
1.25
7.12
6.73
6.71
6.67
6.65
5.61
5.51
3.58
2.55
2.23
0.88
1.00
2.89
2.00
1.13
1.96
2.17
6.13
24.02
4.16
f1 (ppm)

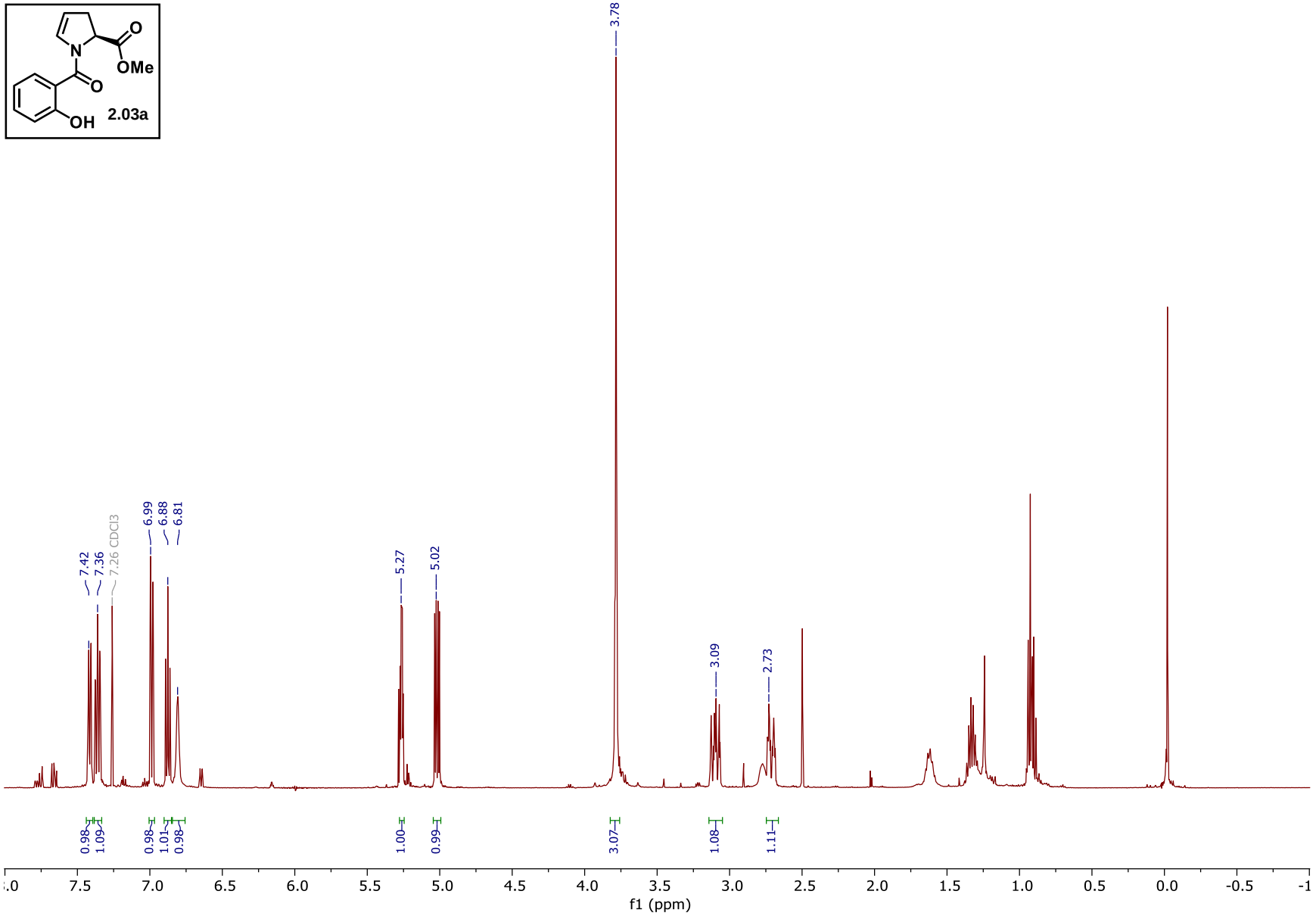
O
N
OMe
O
OH
2.03a
3.78
7.42
7.36
7.26 CDCl3
6.99
6.88
6.81
5.27
5.02
3.09
2.73
0.98
1.09
0.98
1.01
0.98
1.00
0.99
3.07
1.08
1.11
7.5
7.0
6.5
6.0
5.5
5.0
4.5
4.0
3.5
3.0
2.5
2.0
1.5
1.0
0.5
0.0
-0.5
f1 (ppm)

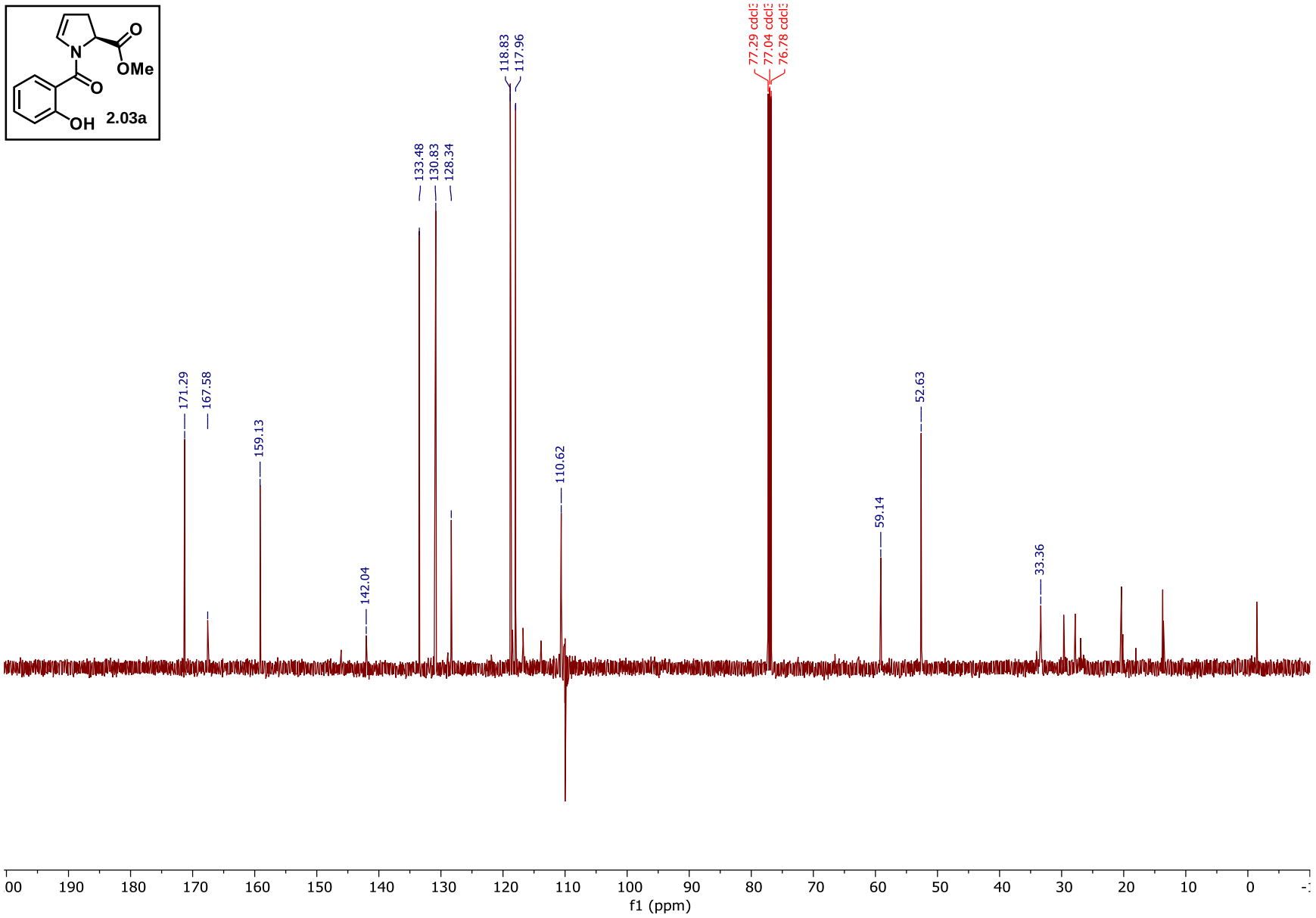
2.03a
171.29
167.58
159.13
142.04
133.48
130.83
128.34
118.83
117.96
110.62
77.29 cdcl3
77.04 cdcl3
76.78 cdcl3
59.14
52.63
33.36
f1 (ppm)

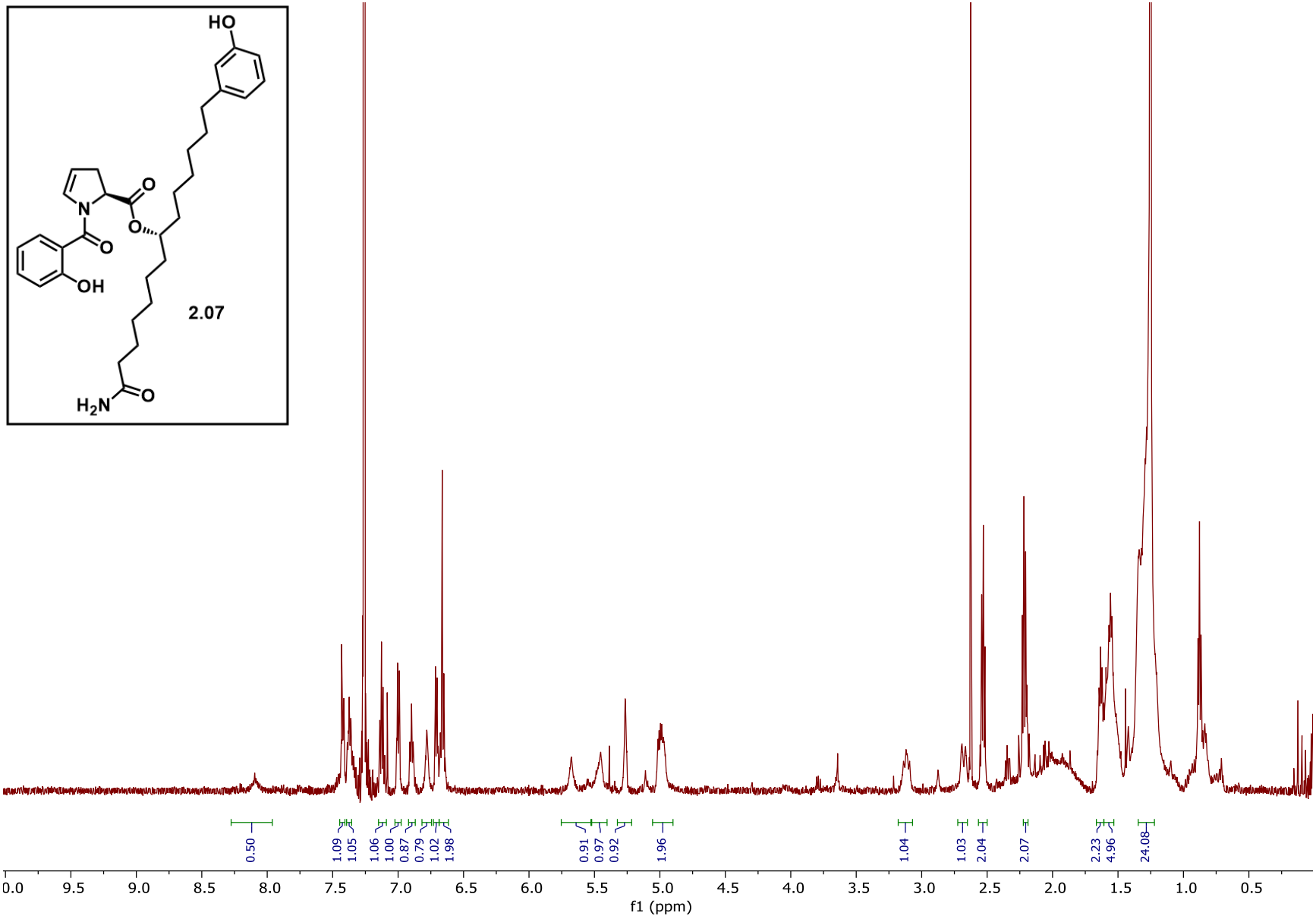
HO
O
N
O
O
O
OH
2.07
H2N
O
0.50
1.09
1.05
1.06
1.00
0.87
0.79
1.02
1.98
0.91
0.97
0.92
1.96
1.04
1.03
2.04
2.07
2.23
4.96
24.08
0.0
9.5
9.0
8.5
8.0
7.5
7.0
6.5
6.0
5.5
5.0
4.5
4.0
3.5
3.0
2.5
2.0
1.5
1.0
0.5
f1 (ppm)

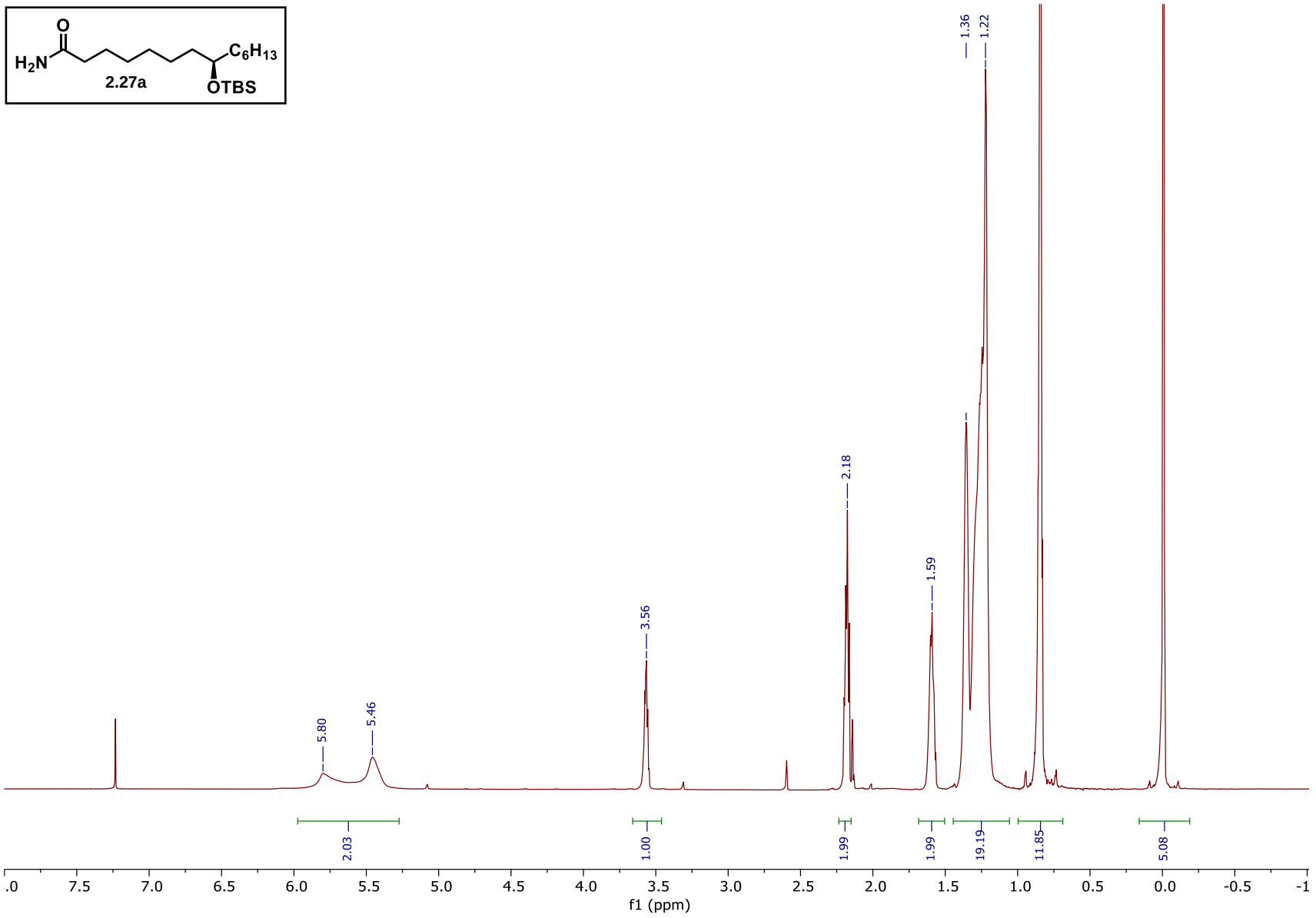
O
H2N
C6H13
OTBS
2.27a
1.36
1.22
2.18
1.59
3.56
5.80
5.46
2.03
1.00
1.99
1.99
19.19
11.85
5.08
f1 (ppm)

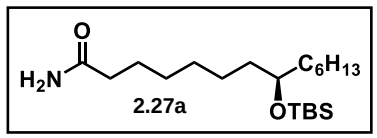
O
H2N
C6H13
2.27a
OTBS

37.14
37.05
35.94
31.87
29.55
29.52
29.28
25.94
25.51
25.27
25.18
22.61
18.14
14.07
77.27 cdcl3
77.01 cdcl3
76.76 cdcl3
72.31
-4.42
175.81
00
190
180
170
160
150
140
130
120
110
100
90
80
70
60
50
40
30
20
10
0
-1
f1 (ppm)

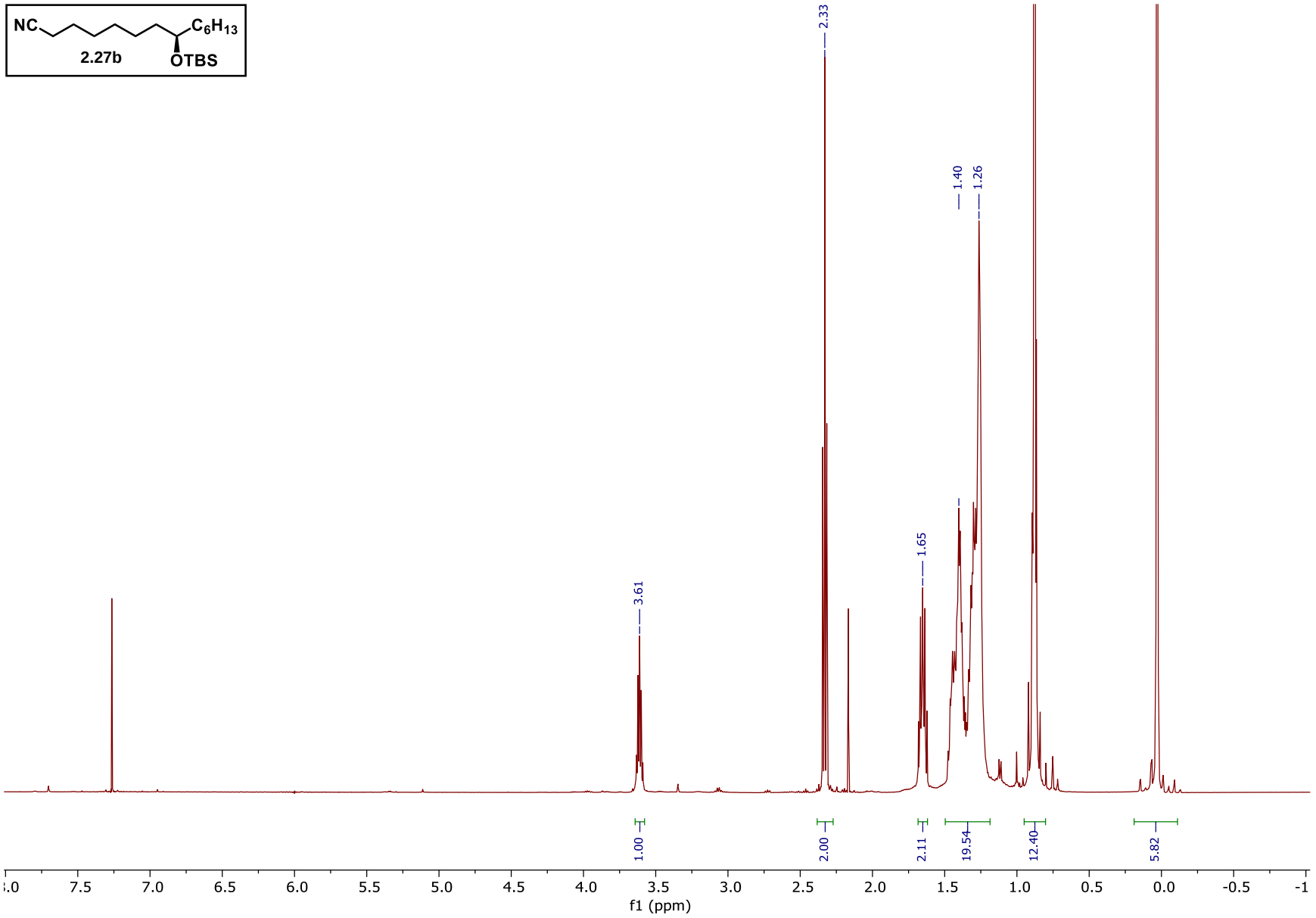
NC
C6H13
OTBS
2.27b
2.33
1.40
1.26
1.65
3.61
1.00
2.00
2.11
19.54
12.40
5.82
f1 (ppm)

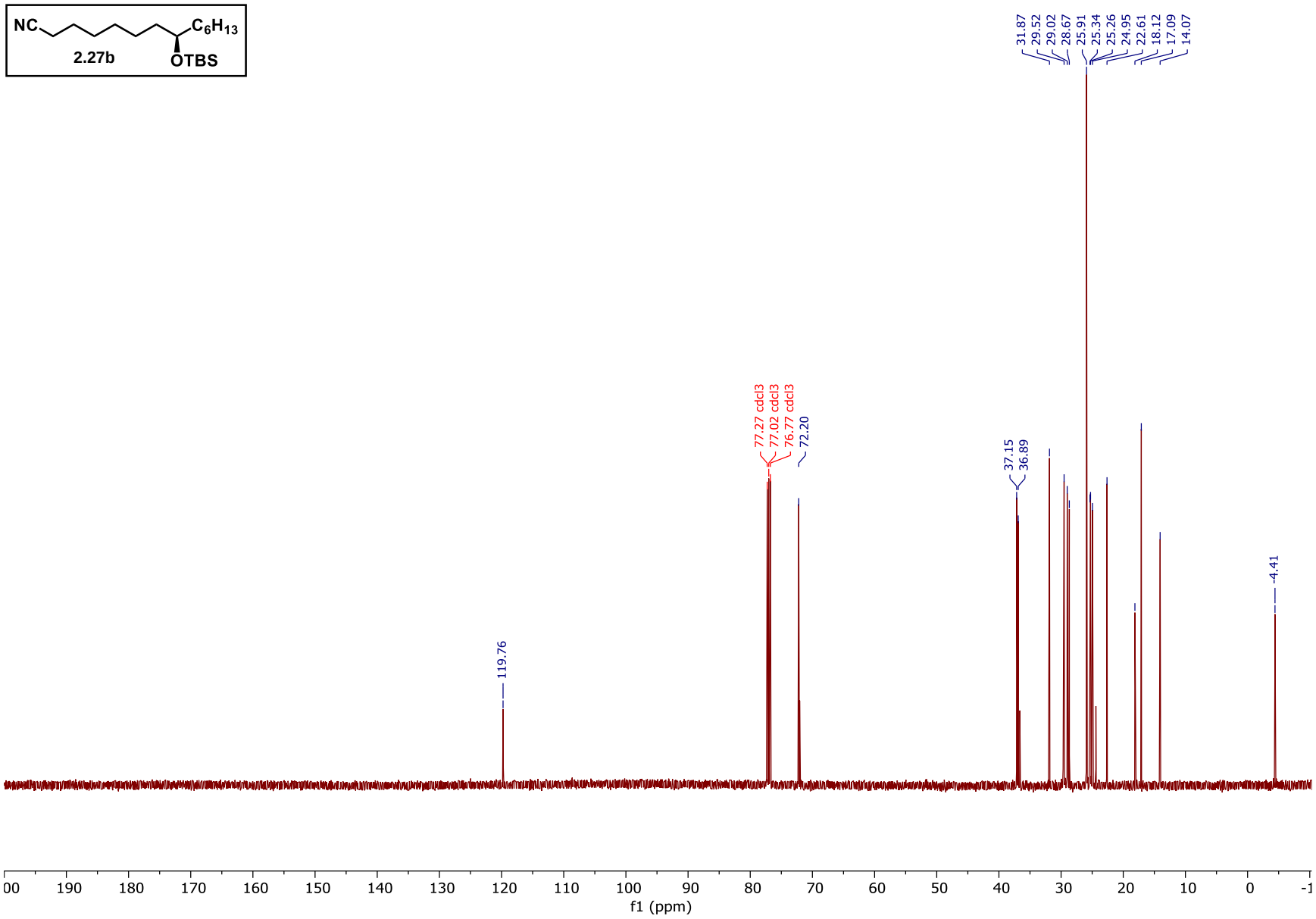
NC
C6H13
OTBS
2.27b
31.87
29.52
29.02
28.67
25.91
25.34
25.26
24.95
22.61
18.12
17.09
14.07
77.27 cdcl3
77.02 cdcl3
76.77 cdcl3
72.20
37.15
36.89
119.76
-4.41
f1 (ppm)

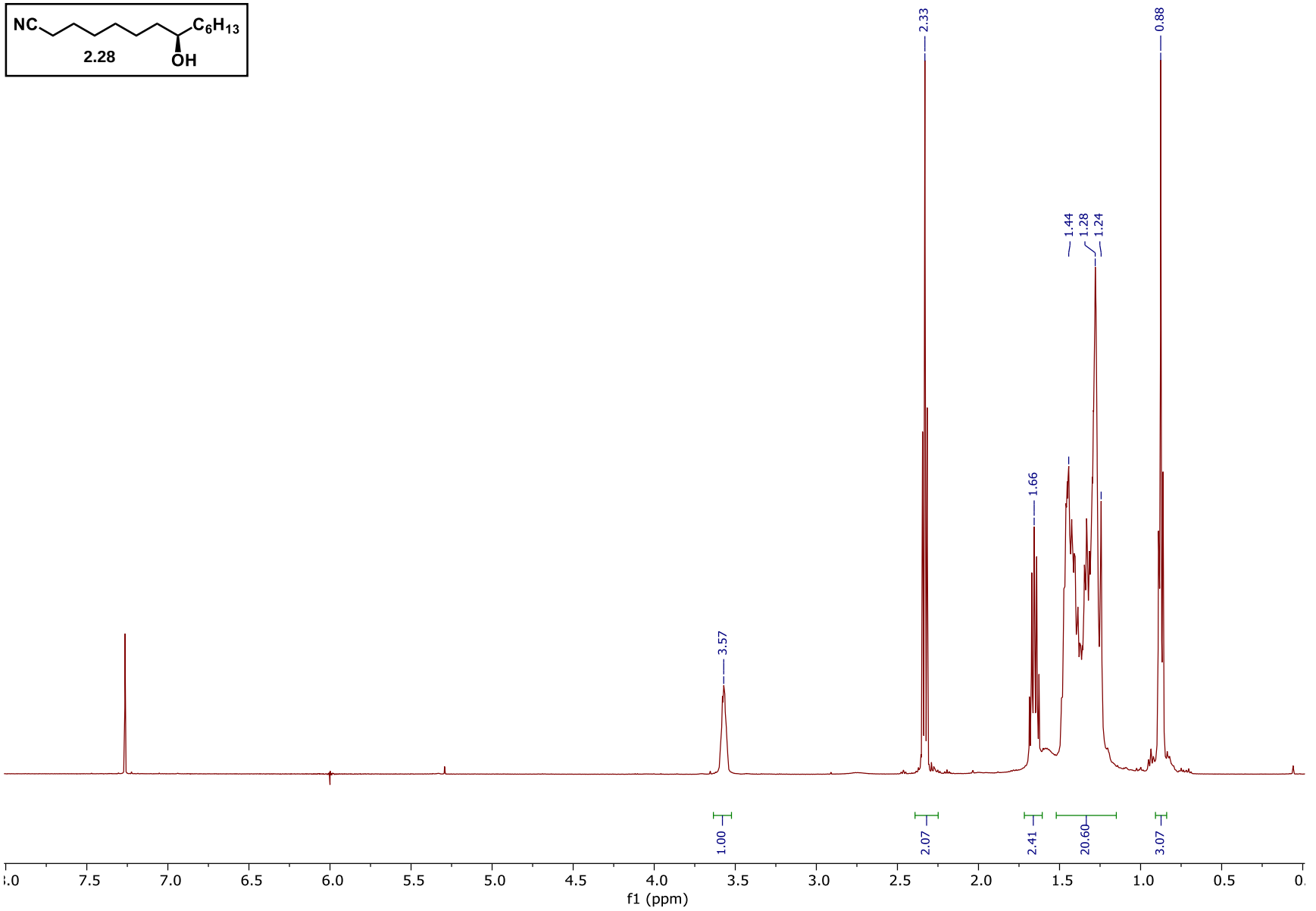
NC
C6H13
2.28
OH
2.33
0.88
1.44
1.28
1.24
1.66
3.57
1.00
2.07
2.41
20.60
3.07
7.5
7.0
6.5
6.0
5.5
5.0
4.5
4.0
3.5
3.0
2.5
2.0
1.5
1.0
0.5
f1 (ppm)

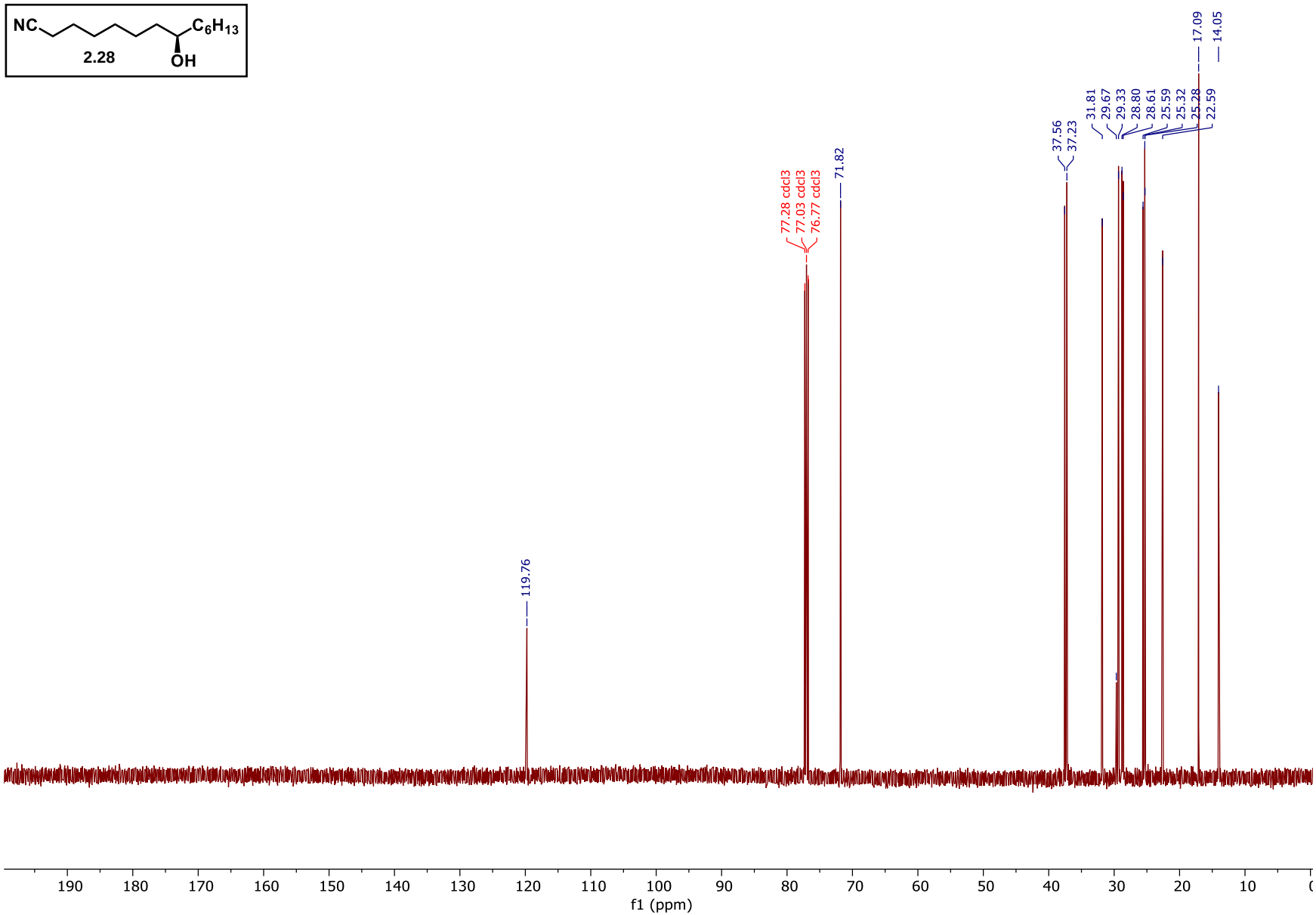
NC
C6H13
2.28
OH
17.09
14.05
31.81
29.67
29.33
28.80
28.61
25.59
25.32
25.28
22.59
37.56
37.23
71.82
77.28 cdcl3
77.03 cdcl3
76.77 cdcl3
119.76
190
180
170
160
150
140
130
120
110
100
90
80
70
60
50
40
30
20
10
f1 (ppm)

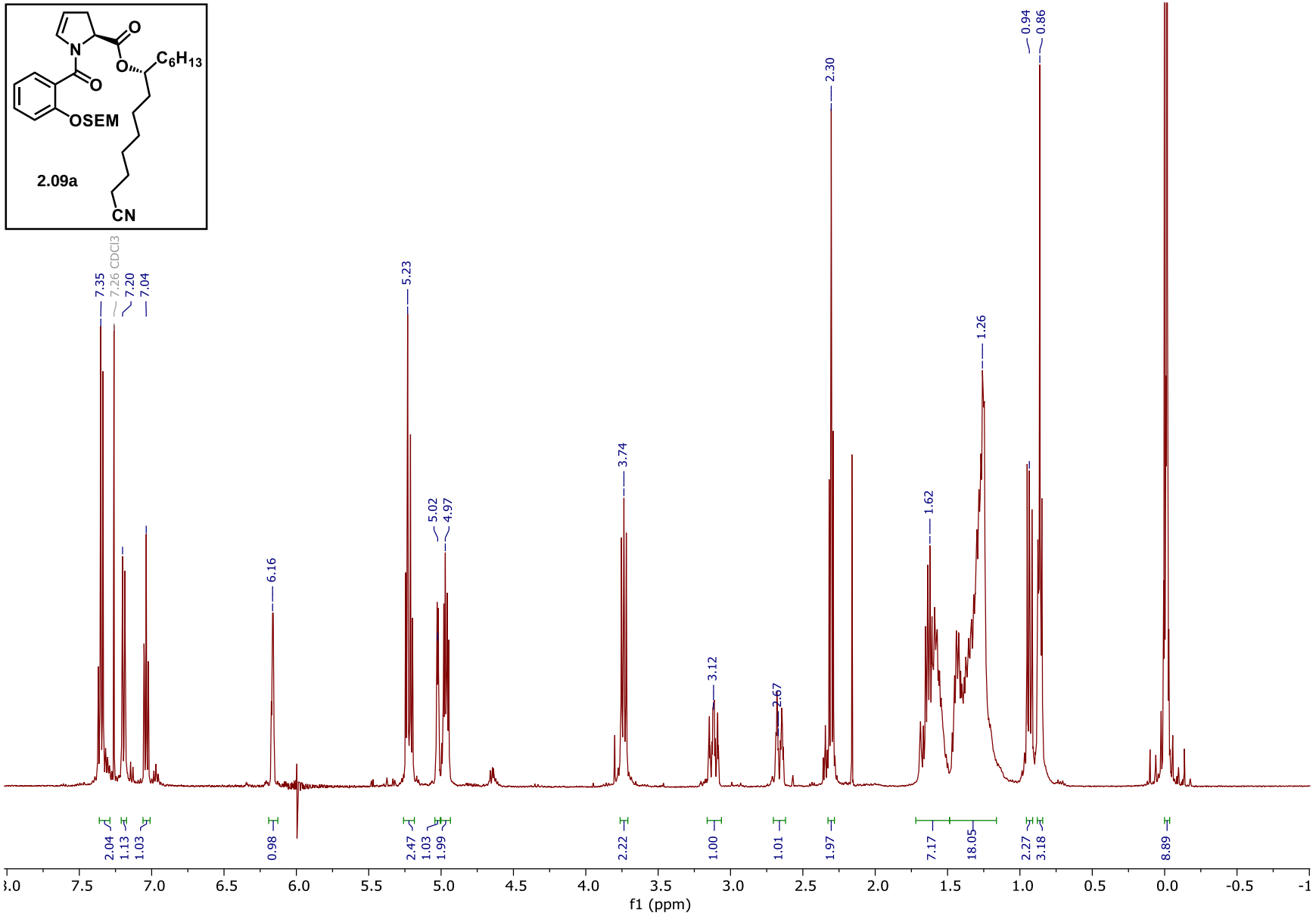
OSEM
2.09a
CN
7.35
7.26 CDCl3
7.20
7.04
6.16
5.23
5.02
4.97
3.74
3.12
2.67
2.30
1.62
1.26
0.94
0.86
2.04
1.13
1.03
0.98
2.47
1.03
1.99
2.22
1.00
1.01
1.97
7.17
18.05
2.27
3.18
8.89
f1 (ppm)

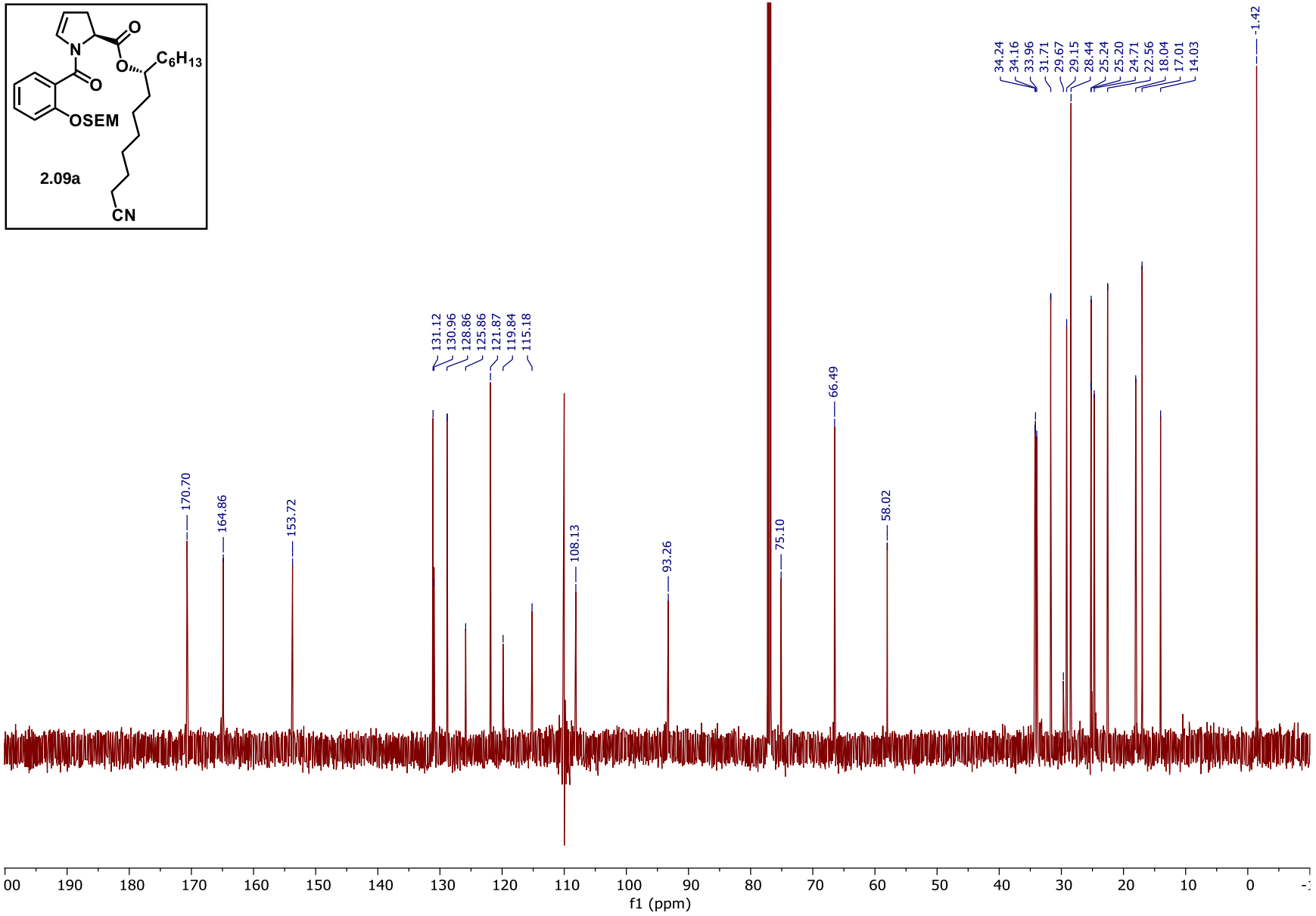
O
N
O
O
C_6H_{13}
OSEM
2.09a
CN
170.70
164.86
153.72
131.12
130.96
128.86
125.86
121.87
119.84
115.18
108.13
93.26
75.10
66.49
58.02
34.24
34.16
33.96
31.71
29.67
29.15
28.44
25.24
25.20
24.71
22.56
18.04
17.01
14.03
-1.42
f1 (ppm)

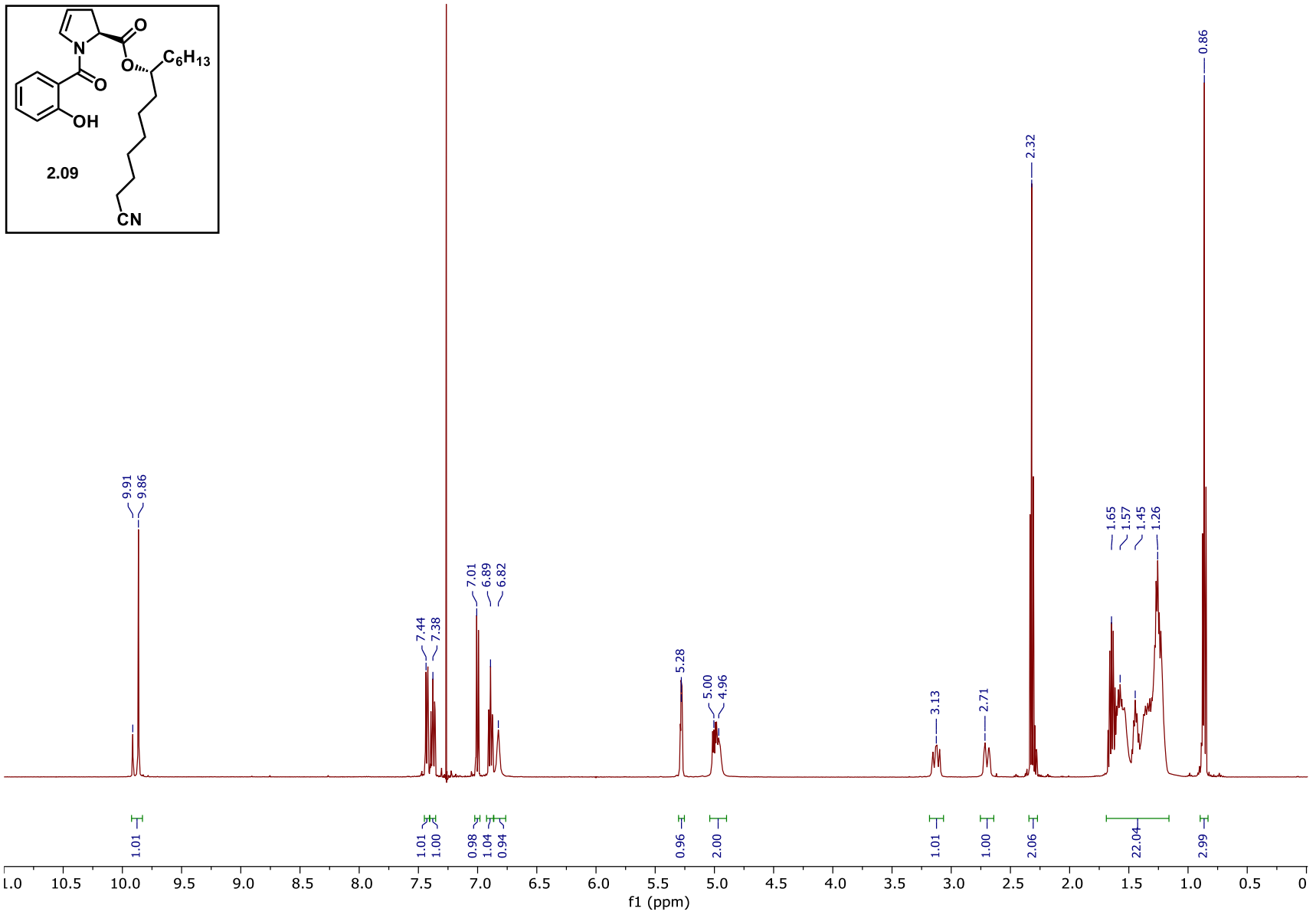
2.09
CN
OH
9.91
9.86
7.44
7.38
7.01
6.89
6.82
5.28
5.00
4.96
3.13
2.71
2.32
1.65
1.57
1.45
1.26
0.86
1.01
1.01
1.00
0.98
1.04
0.94
0.96
2.00
1.01
1.00
2.06
22.04
2.99
f1 (ppm)

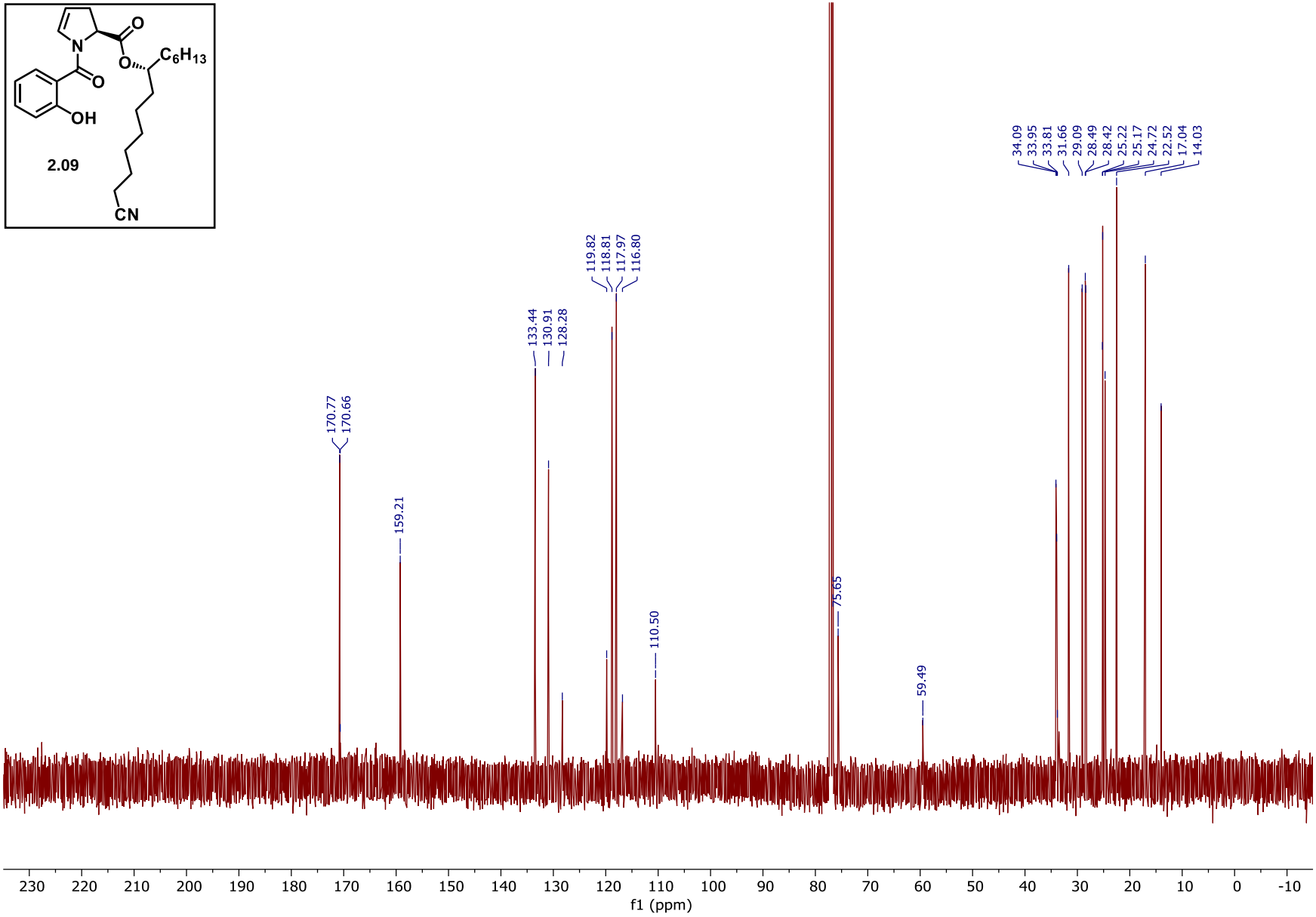
2.09
OH
CN
170.77
170.66
159.21
133.44
130.91
128.28
119.82
118.81
117.97
116.80
110.50
75.65
59.49
34.09
33.95
33.81
31.66
29.09
28.49
28.42
25.22
25.17
24.72
22.52
17.04
14.03
f1 (ppm)

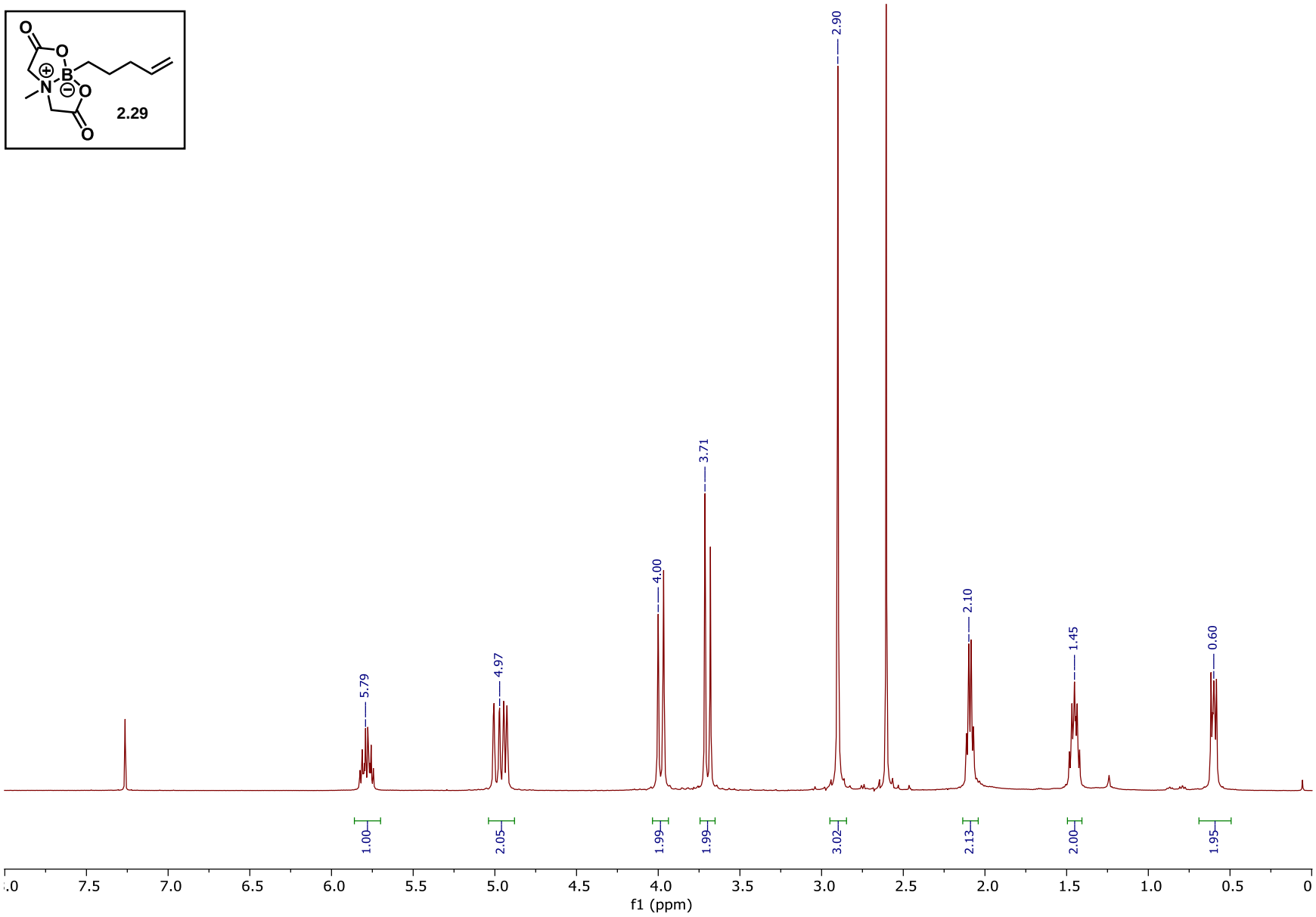
2.29
5.79
4.97
4.00
3.71
2.90
2.10
1.45
0.60
1.00
2.05
1.99
1.99
3.02
2.13
2.00
1.95
7.5
7.0
6.5
6.0
5.5
5.0
4.5
4.0
3.5
3.0
2.5
2.0
1.5
1.0
0.5
0
f1 (ppm)

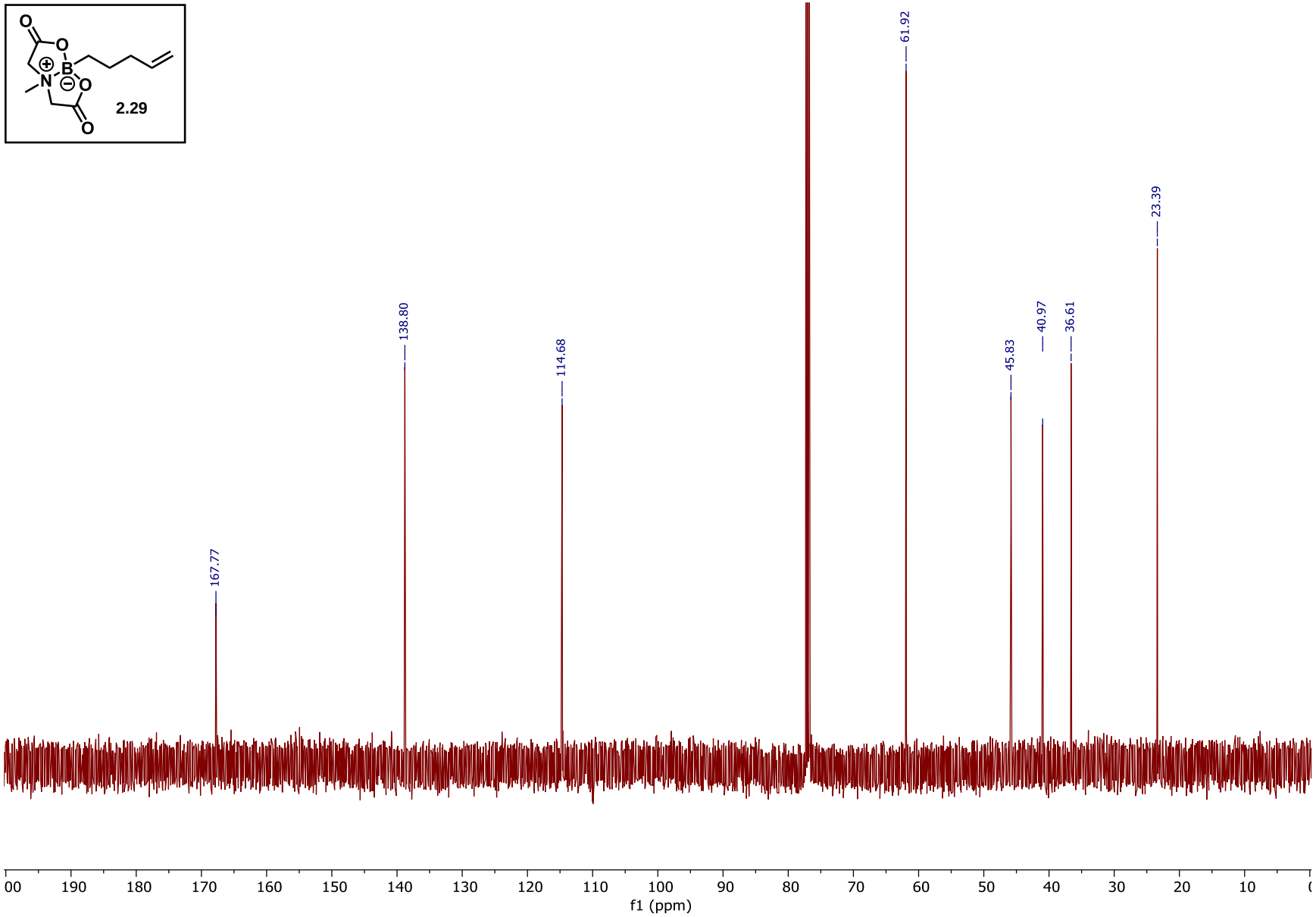
2.29
167.77
138.80
114.68
61.92
45.83
40.97
36.61
23.39
f1 (ppm)

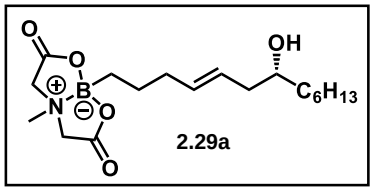
O
O
B
N
O
O
OH
C_6H_{13}
2.29a

7.26 CDCl3
5.51
5.41
3.98
3.71
2.90
2.21
2.05
1.80
1.42
1.27
0.87
0.59
0.90
0.99
2.04
2.00
1.05
3.06
1.09
2.97
1.82
4.09
7.99
2.97
1.99
f1 (ppm)

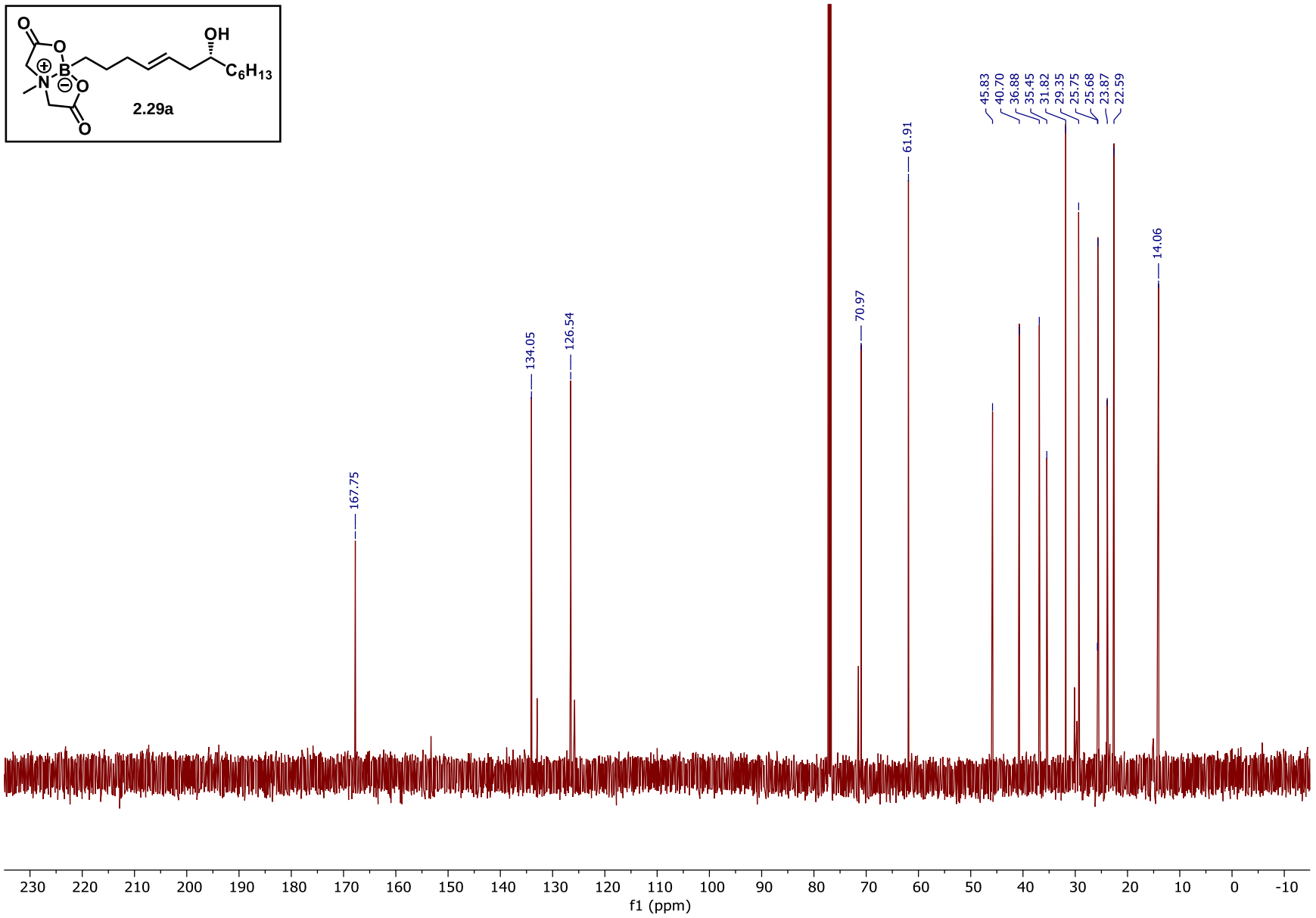
2.29a
167.75
134.05
126.54
70.97
61.91
45.83
40.70
36.88
35.45
31.82
29.35
25.75
25.68
23.87
22.59
14.06
f1 (ppm)

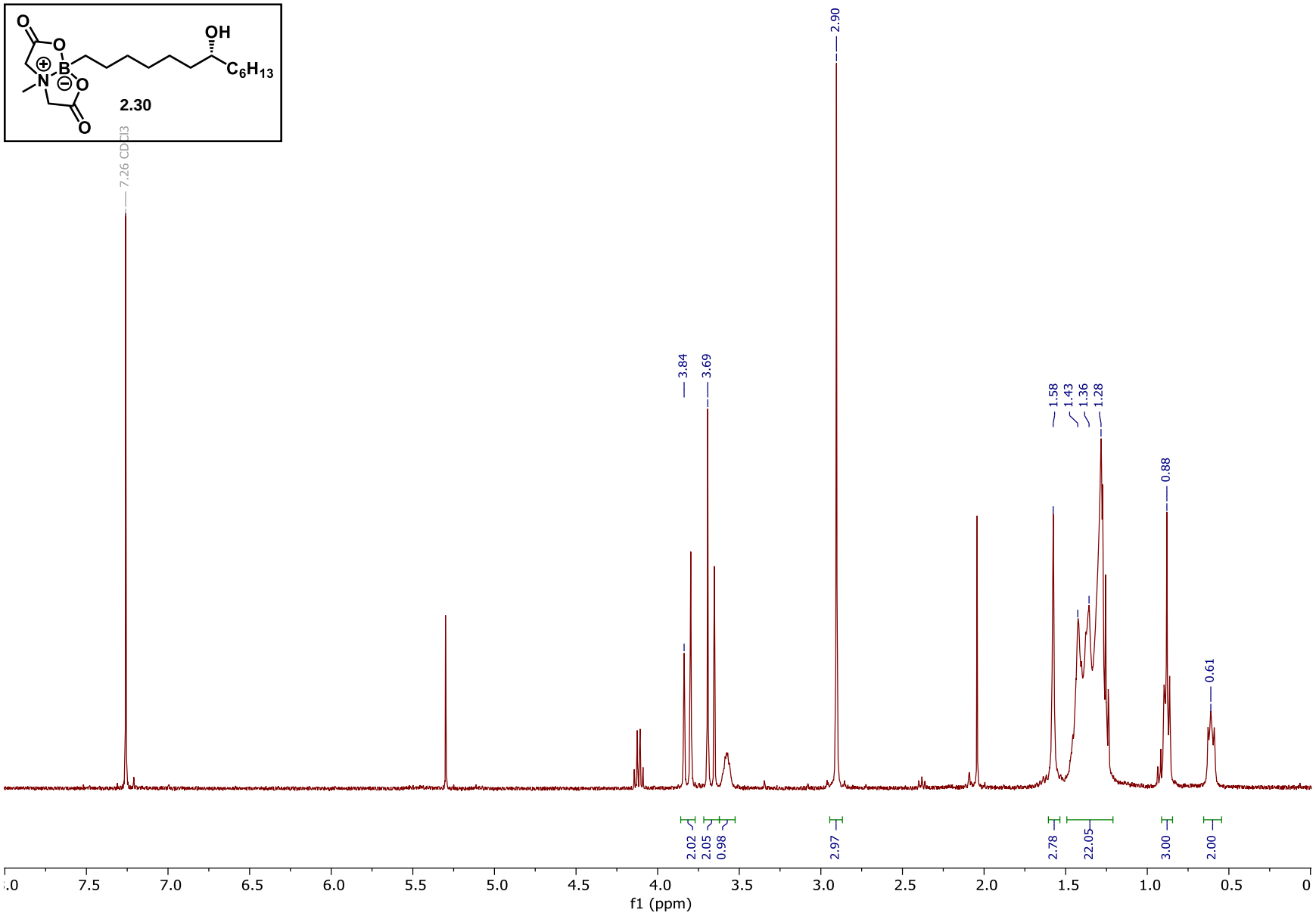
2.30
7.26 CDCl3
3.84
3.69
2.90
1.58
1.43
1.36
1.28
0.88
0.61
2.02
2.05
0.98
2.97
2.78
22.05
3.00
2.00
f1 (ppm)

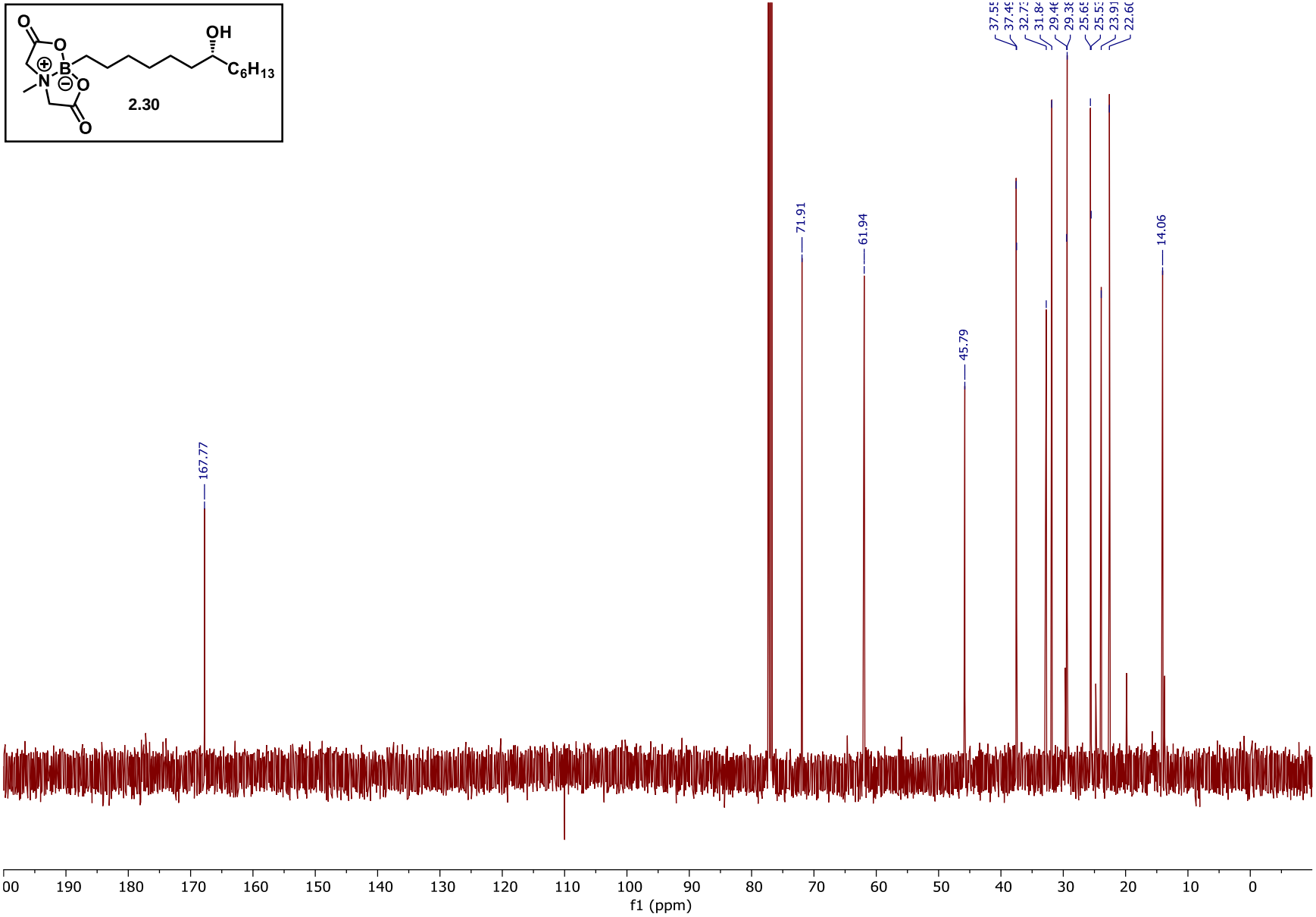
OH
C_6H_{13}
2.30
167.77
71.91
61.94
45.79
14.06
f1 (ppm)

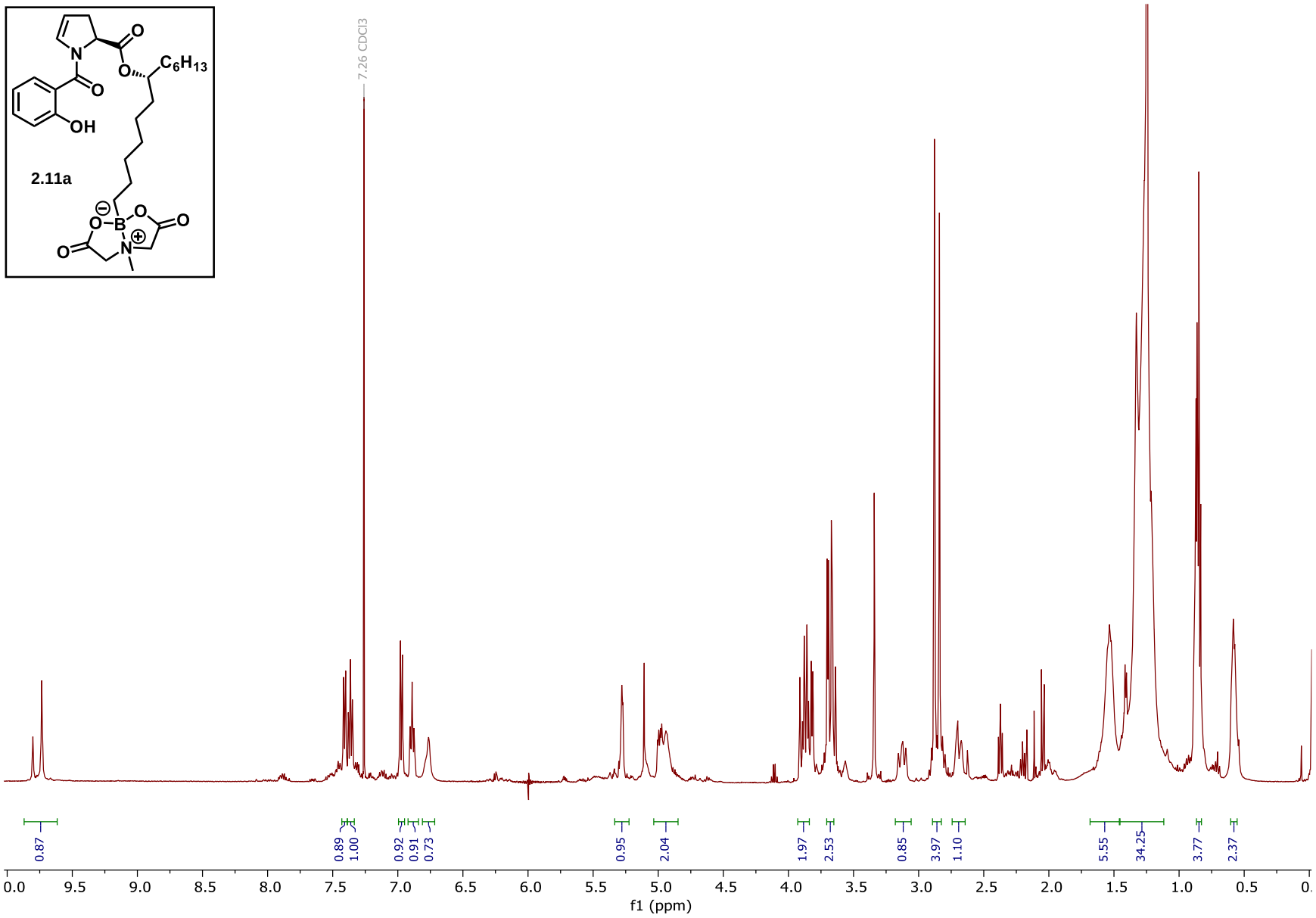
2.11a
7.26 CDCl3
0.87
0.89
1.00
0.92
0.91
0.73
0.95
2.04
1.97
2.53
0.85
3.97
1.10
5.55
34.25
3.77
2.37
f1 (ppm)

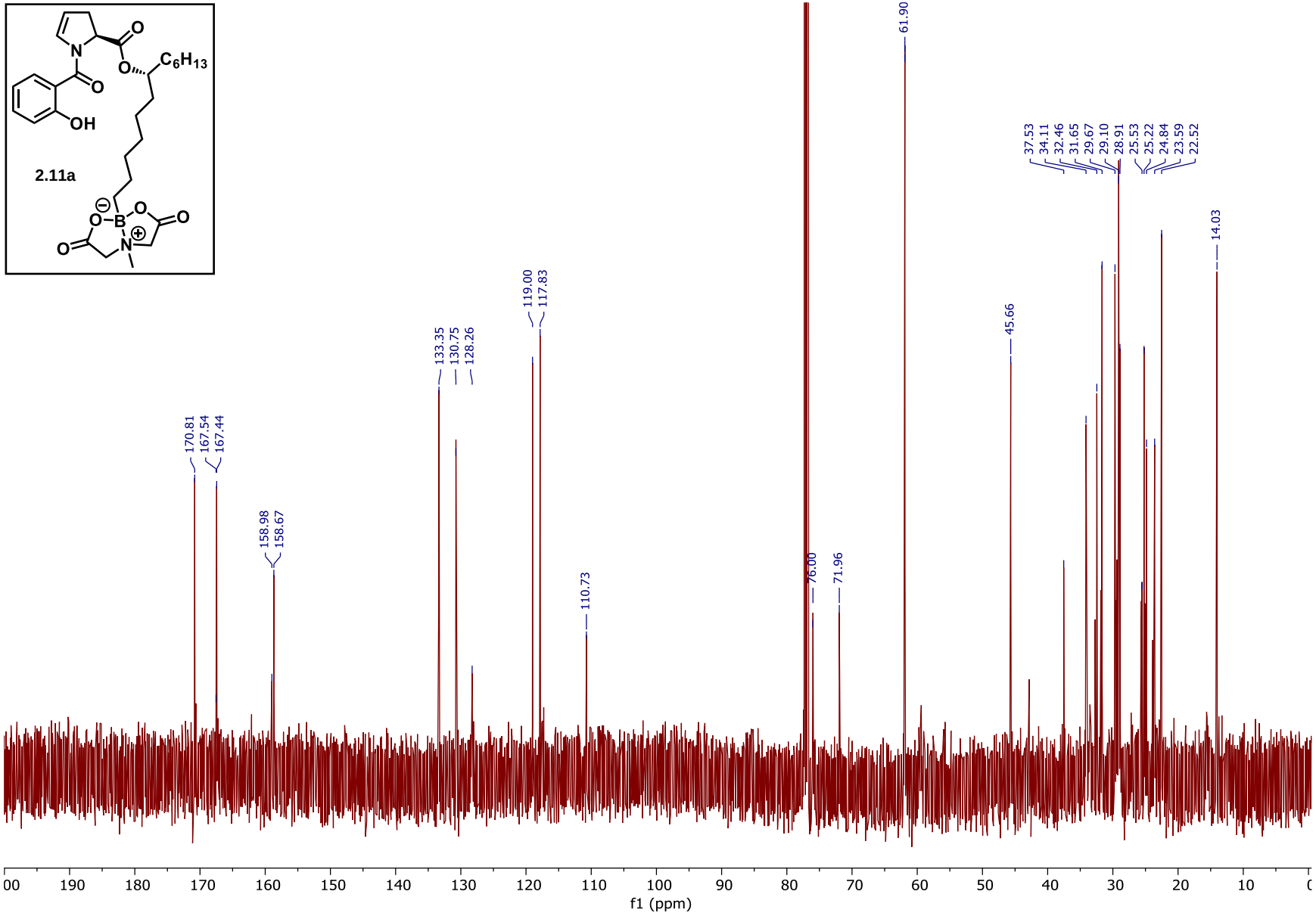
2.11a
170.81
167.54
167.44
158.98
158.67
133.35
130.75
128.26
119.00
117.83
110.73
76.00
71.96
61.90
45.66
37.53
34.11
32.46
31.65
29.67
29.10
28.91
25.53
25.22
24.84
23.59
22.52
14.03
f1 (ppm)

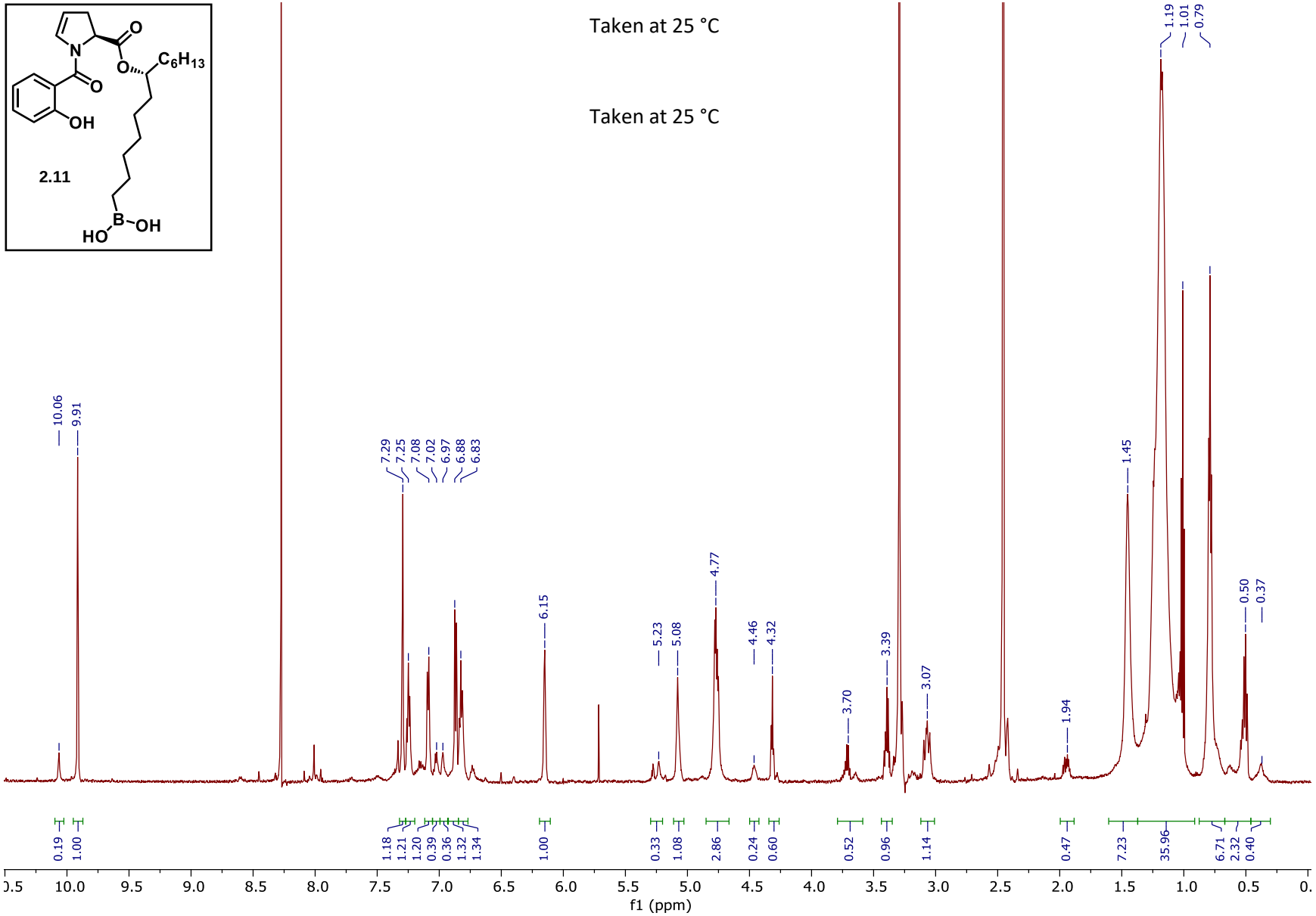
Taken at 25 °C
Taken at 25 °C
2.11
OH
HO
B
OH
O
N
O
O
C6H13
10.06
9.91
7.29
7.25
7.08
7.02
6.97
6.88
6.83
6.15
5.23
5.08
4.77
4.46
4.32
3.70
3.39
3.07
1.94
1.45
1.19
1.01
0.79
0.50
0.37
0.19
1.00
1.18
1.21
1.20
0.39
0.36
1.32
1.34
1.00
0.33
1.08
2.86
0.24
0.60
0.52
0.96
1.14
0.47
7.23
35.96
6.71
2.32
0.40
f1 (ppm)

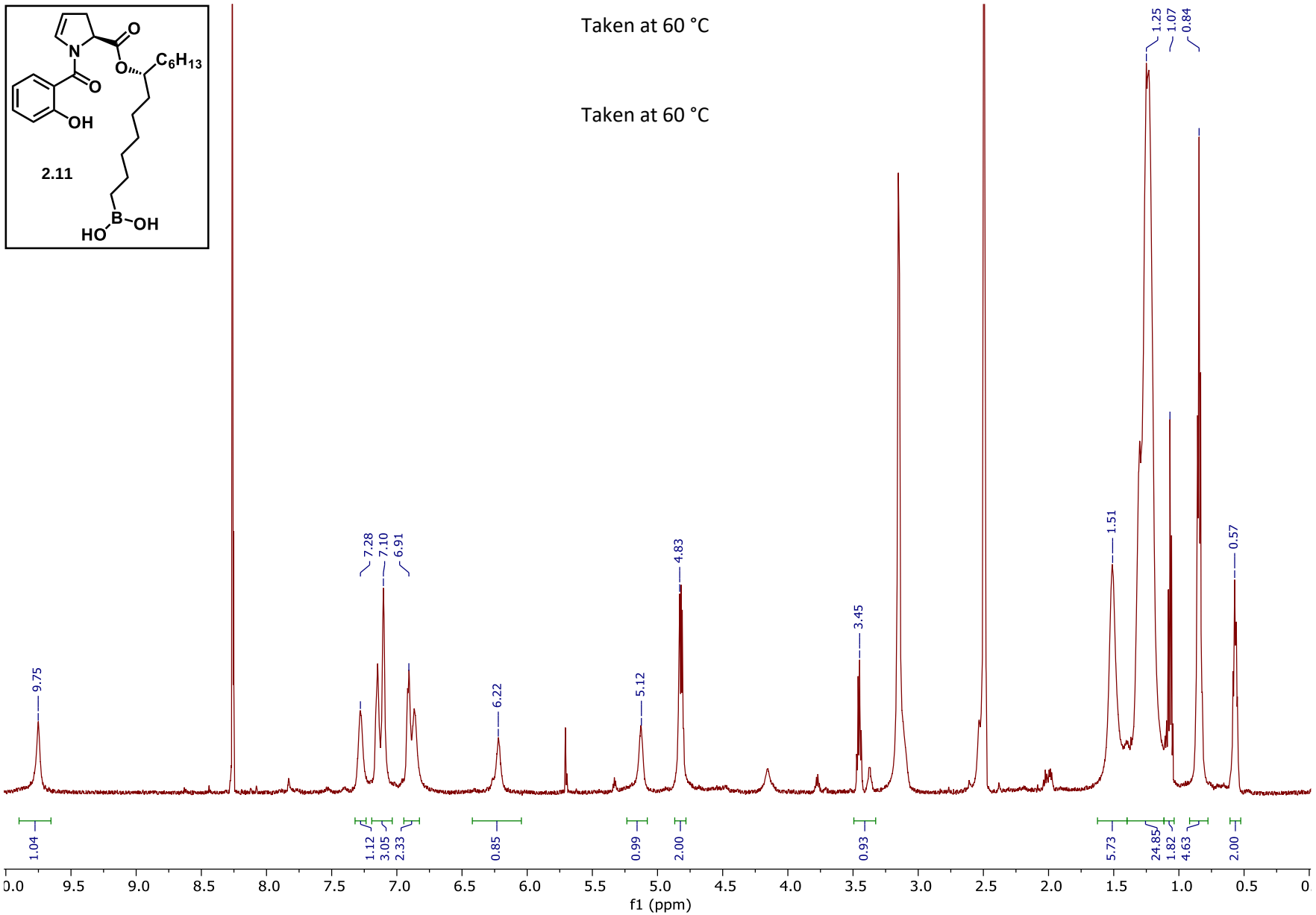
Taken at 60 °C
Taken at 60 °C
2.11
9.75
7.28
7.10
6.91
6.22
5.12
4.83
3.45
1.51
1.25
1.07
0.84
0.57
1.04
1.12
3.05
2.33
0.85
0.99
2.00
0.93
5.73
24.85
1.82
4.63
2.00
f1 (ppm)

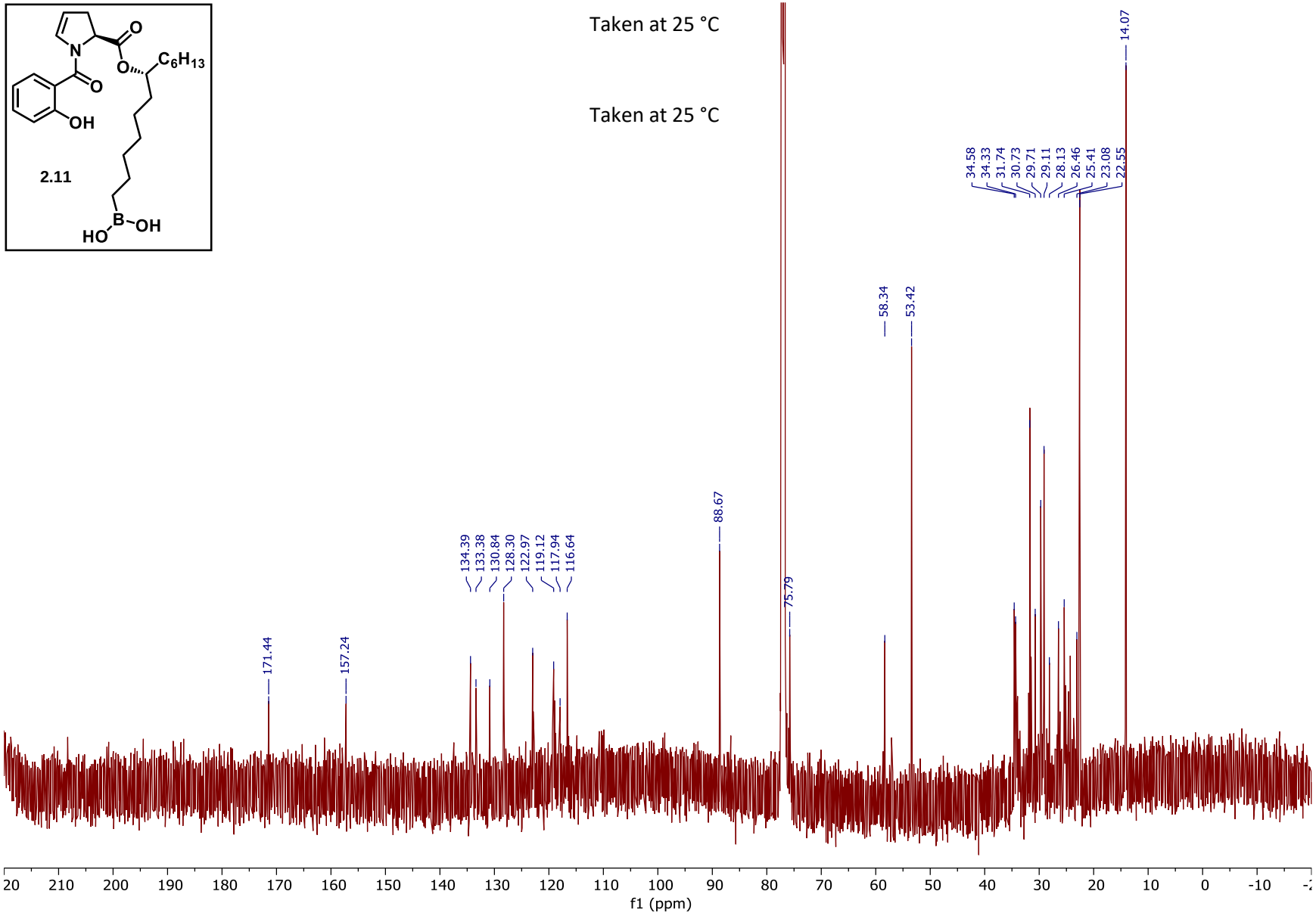
Taken at 25 °C
Taken at 25 °C
2.11
OH
HO
B
OH
O
N
O
O
C_6H_{13}
14.07
34.58
34.33
31.74
30.73
29.71
29.11
28.13
26.46
25.41
23.08
22.55
58.34
53.42
88.67
75.79
134.39
133.38
130.84
128.30
122.97
119.12
117.94
116.64
171.44
157.24
f1 (ppm)

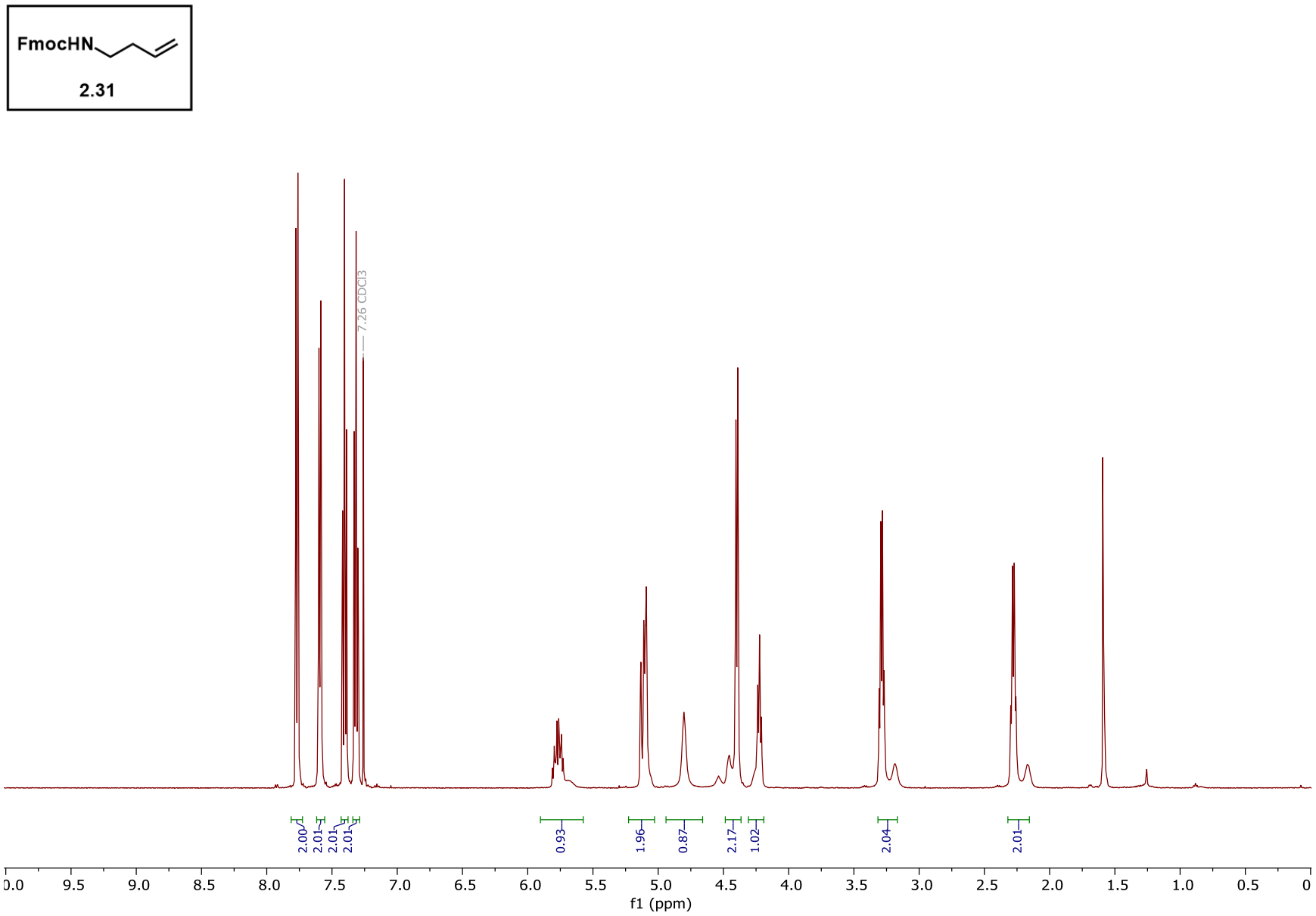
FmocHN
2.31
7.26 CDCl3
2.00
2.01
2.01
2.01
0.93
1.96
0.87
2.17
1.02
2.04
2.01
f1 (ppm)

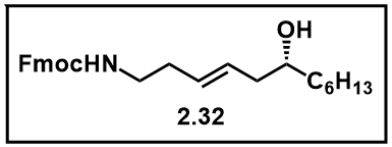
OH
FmocHN
C_6H_{13}

2.32

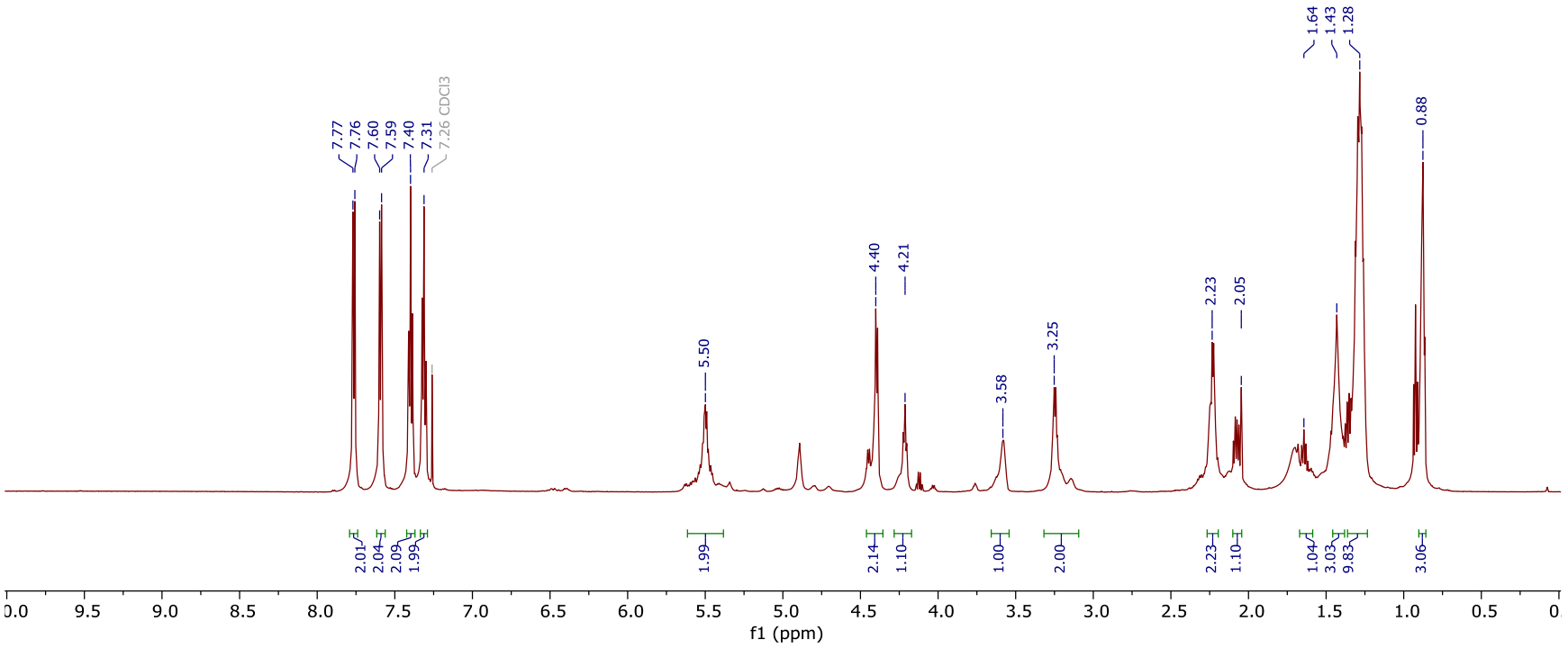
7.77
7.76
7.60
7.59
7.40
7.31
7.26 CDCl3
5.50
4.40
4.21
3.58
3.25
2.23
2.05
1.64
1.43
1.28
0.88
2.01
2.04
2.09
1.99
1.99
2.14
1.10
1.00
2.00
2.23
1.10
1.04
3.03
9.83
3.06
f1 (ppm)

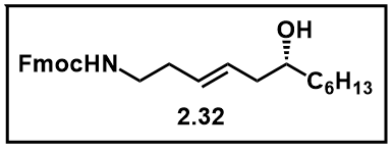
FmocHN
OH
C_6H_{13}

2.32

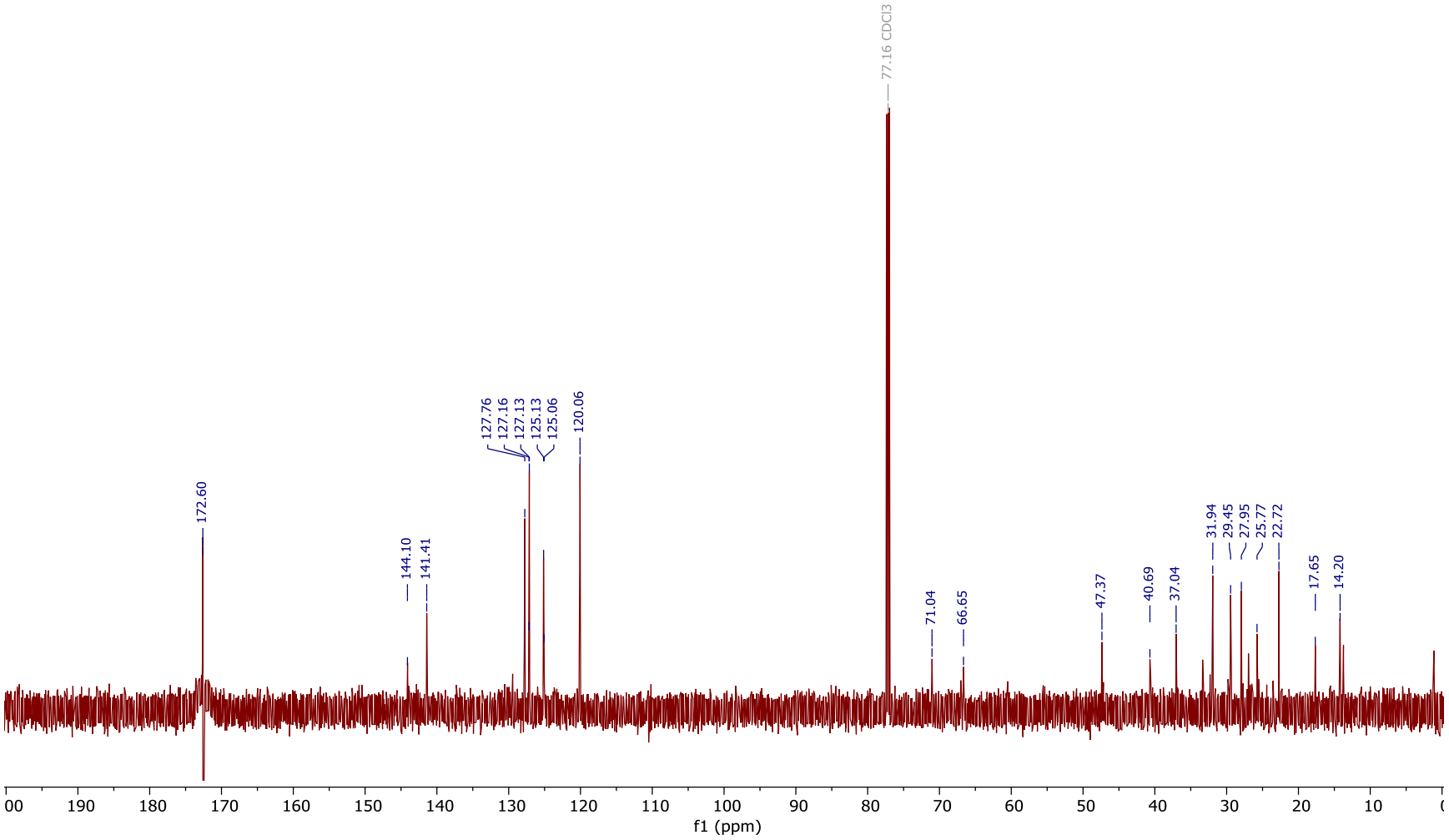
77.16 CDCl3
172.60
144.10
141.41
127.76
127.16
127.13
125.13
125.06
120.06
71.04
66.65
47.37
40.69
37.04
31.94
29.45
27.95
25.77
22.72
17.65
14.20
f1 (ppm)

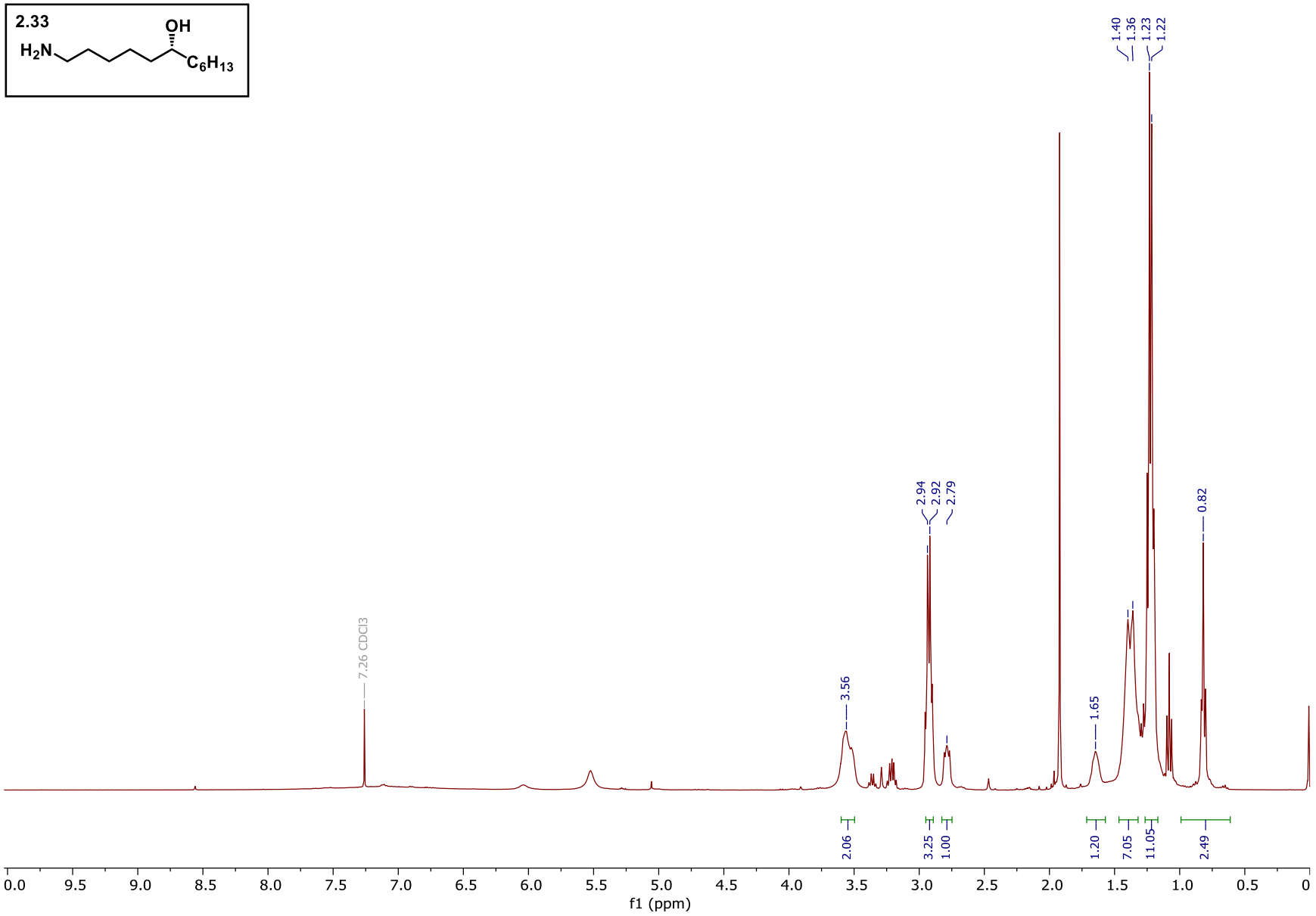
2.33
OH
H2N
C6H13
1.40
1.36
1.23
1.22
2.94
2.92
2.79
0.82
7.26 CDCl3
3.56
1.65
2.06
3.25
1.00
1.20
7.05
11.05
2.49
0.0
9.5
9.0
8.5
8.0
7.5
7.0
6.5
6.0
5.5
5.0
4.5
4.0
3.5
3.0
2.5
2.0
1.5
1.0
0.5
0
f1 (ppm)

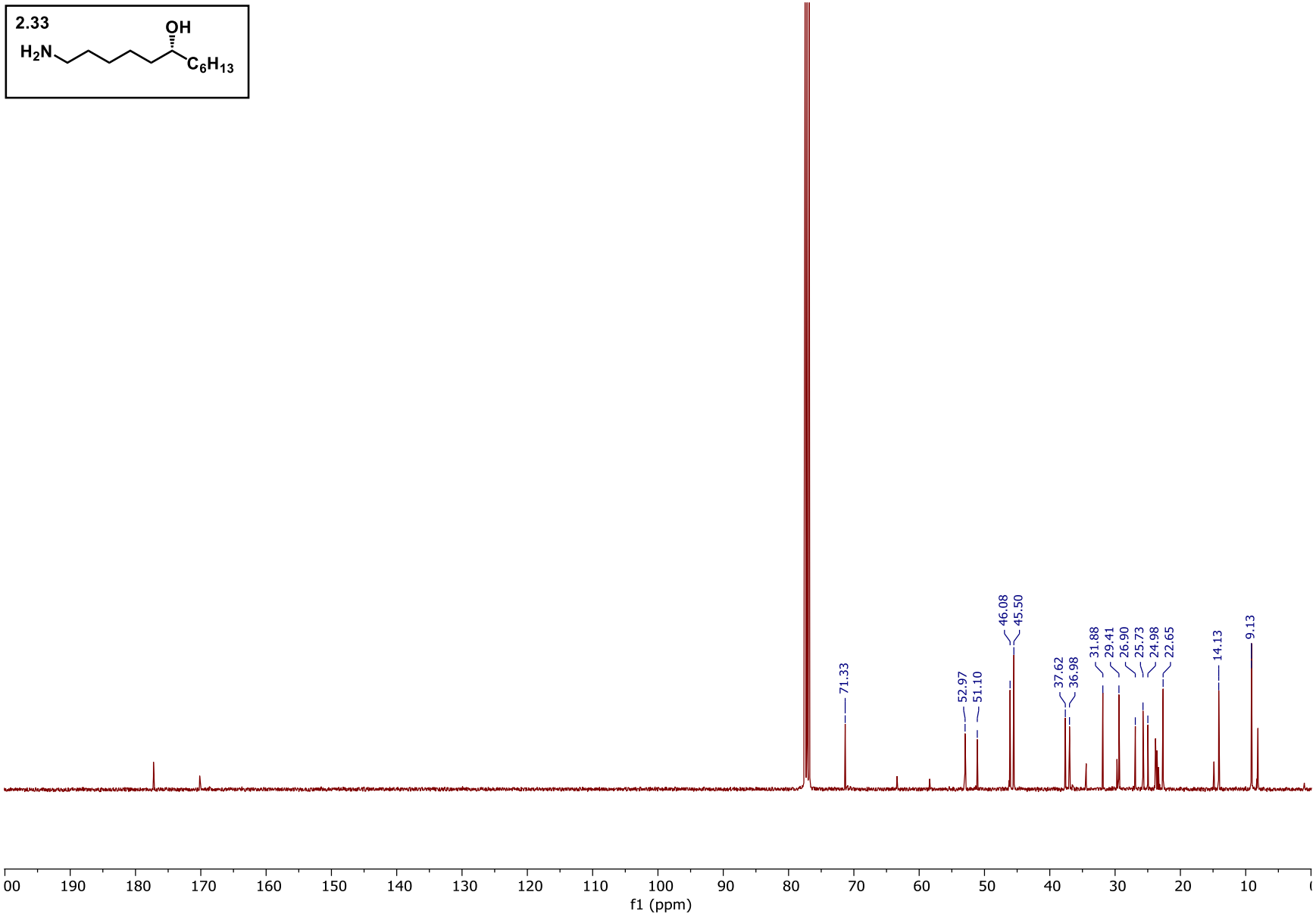
2.33
OH
H2N
C6H13
71.33
52.97
51.10
46.08
45.50
37.62
36.98
31.88
29.41
26.90
25.73
24.98
22.65
14.13
9.13
f1 (ppm)

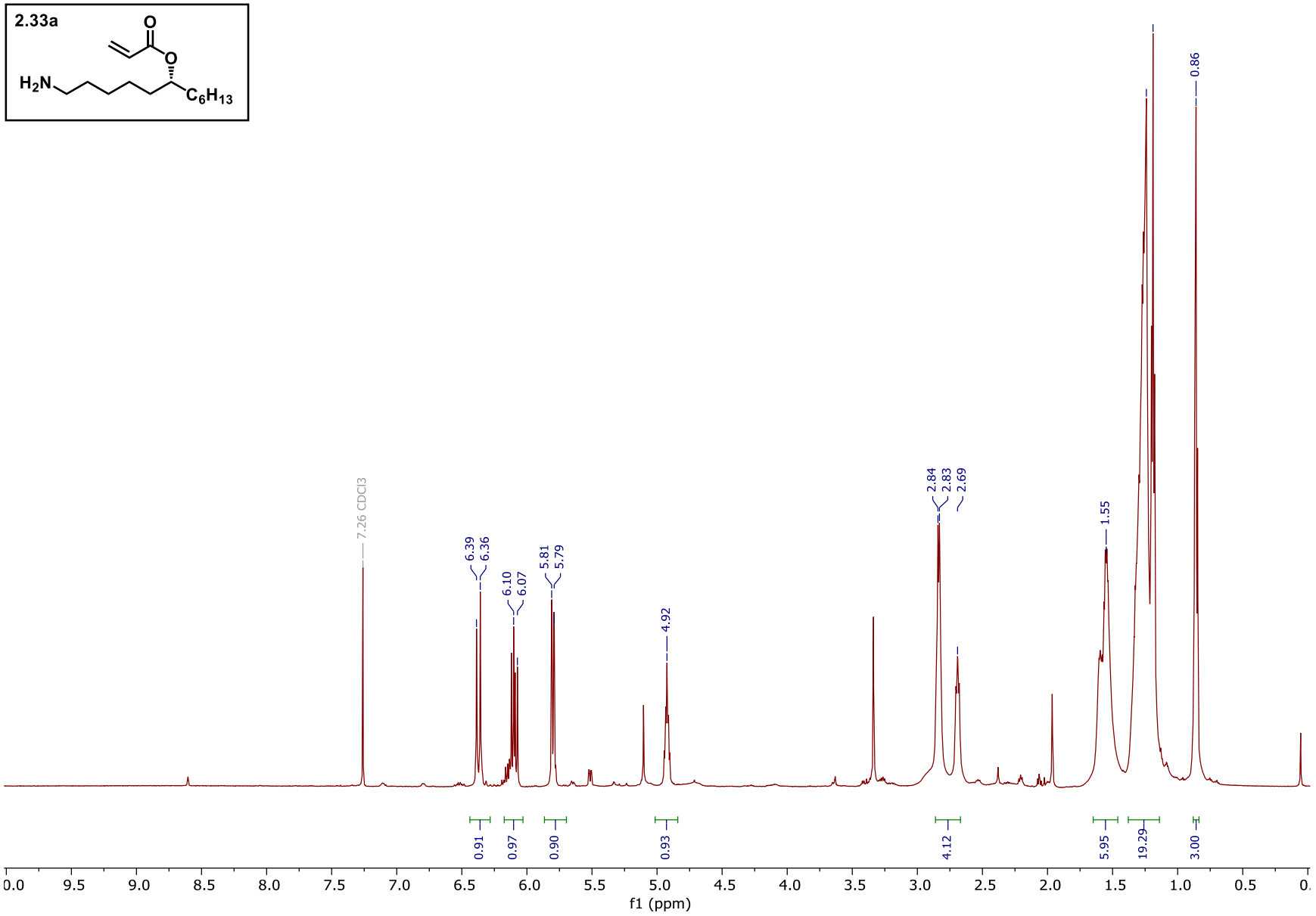
2.33a
O
O
H2N
C6H13
7.26 CDCl3
6.39
6.36
6.10
6.07
5.81
5.79
4.92
2.84
2.83
2.69
1.55
0.86
0.91
0.97
0.90
0.93
4.12
5.95
19.29
3.00
f1 (ppm)

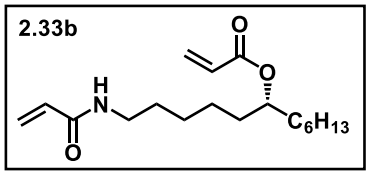
2.33b
O
O
H
N
O
C_6H_{13}

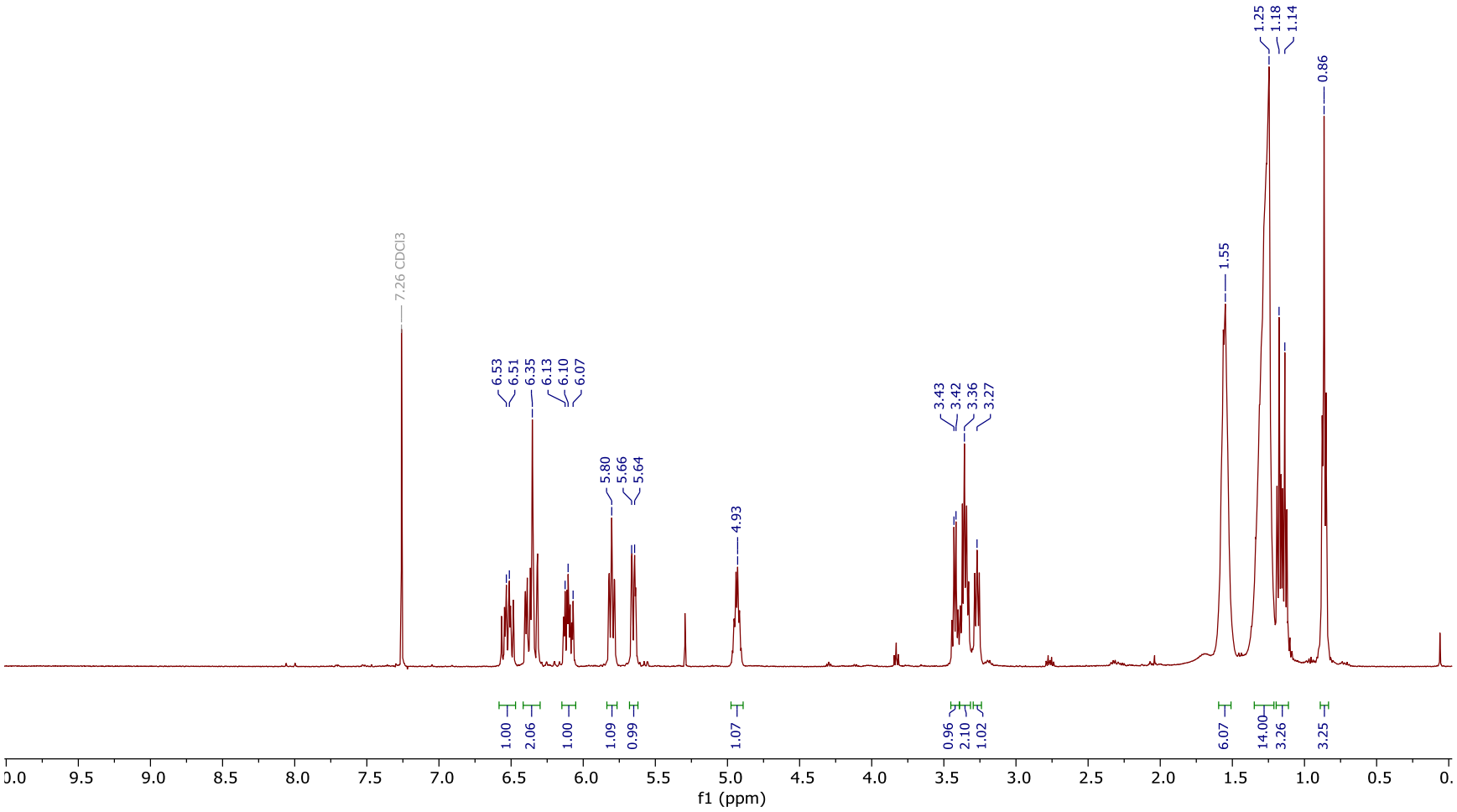
7.26 CDCl3
6.53
6.51
6.35
6.13
6.10
6.07
5.80
5.66
5.64
4.93
3.43
3.42
3.36
3.27
1.55
1.25
1.18
1.14
0.86
1.00
2.06
1.00
1.09
0.99
1.07
0.96
2.10
1.02
6.07
14.00
3.26
3.25
f1 (ppm)

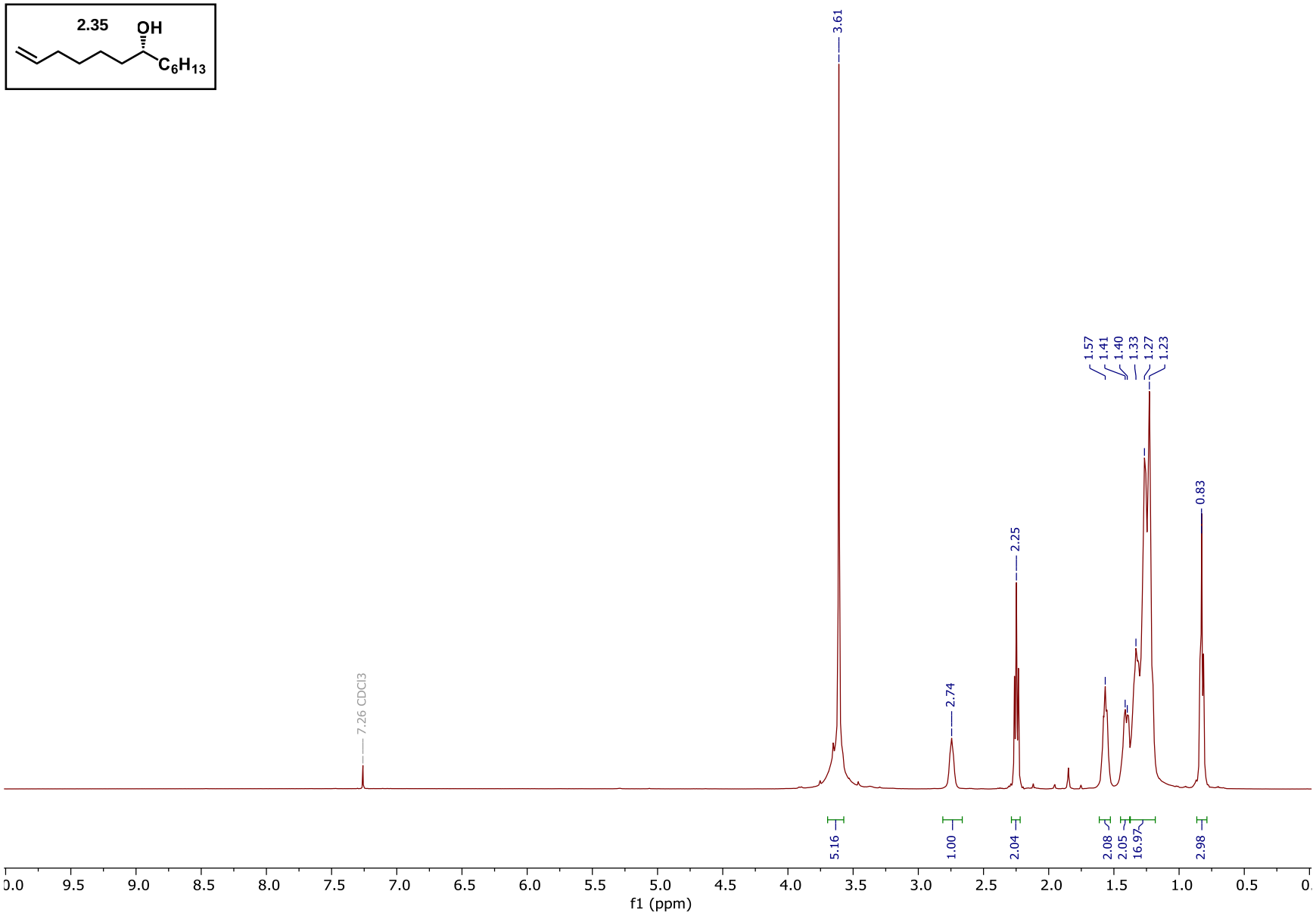
2.35
OH
C6H13
3.61
7.26 CDCl3
2.74
2.25
1.57
1.41
1.40
1.33
1.27
1.23
0.83
5.16
1.00
2.04
2.08
2.05
16.97
2.98
f1 (ppm)

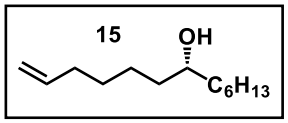
15
OH
C6H13

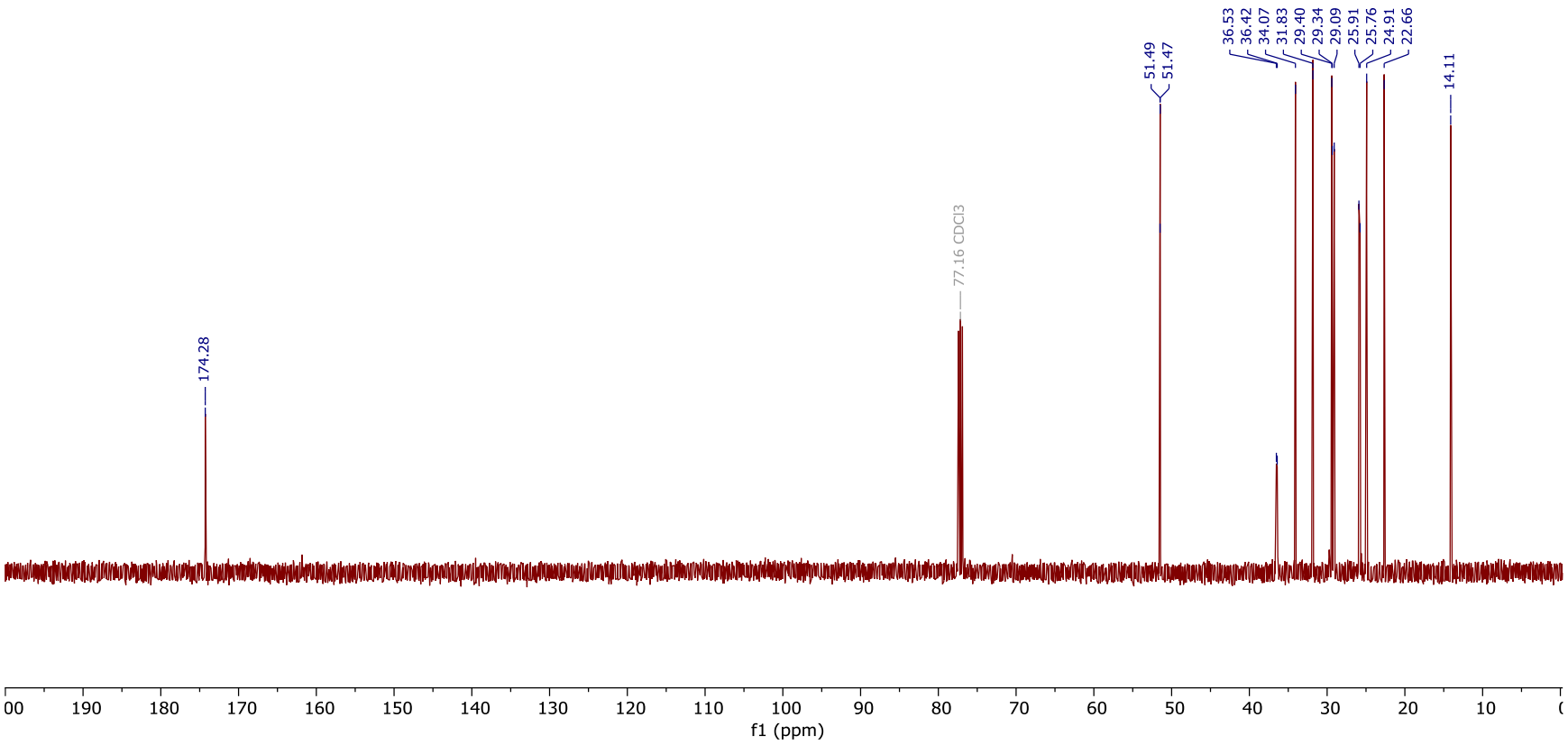
174.28
77.16 CDCl3
51.49
51.47
36.53
36.42
34.07
31.83
29.40
29.34
29.09
25.91
25.76
24.91
22.66
14.11
f1 (ppm)

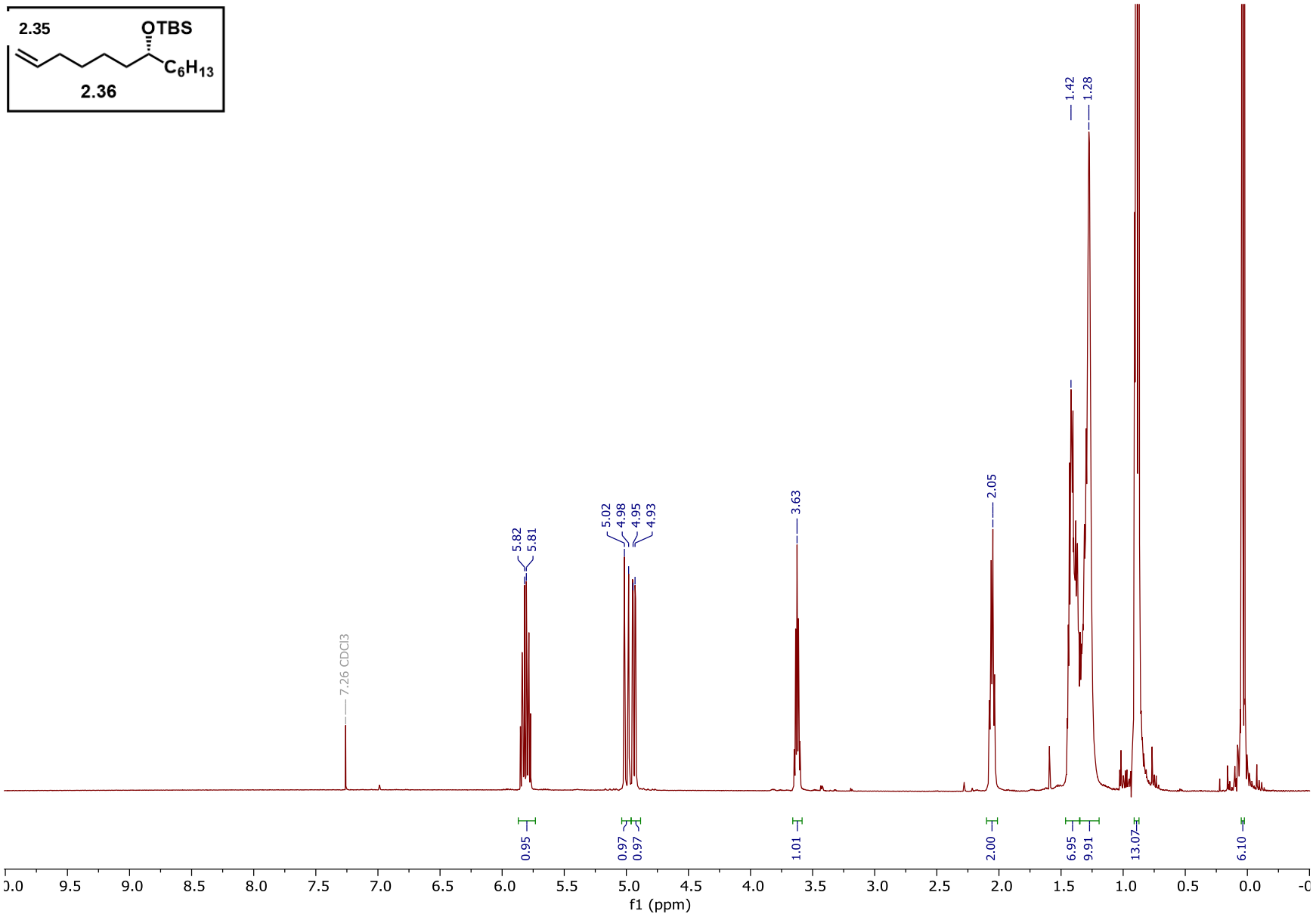
2.35
OTBS
C6H13
2.36
7.26 CDCl3
5.82
5.81
5.02
4.98
4.95
4.93
3.63
2.05
1.42
1.28
0.95
0.97
0.97
1.01
2.00
6.95
9.91
13.07
6.10
f1 (ppm)

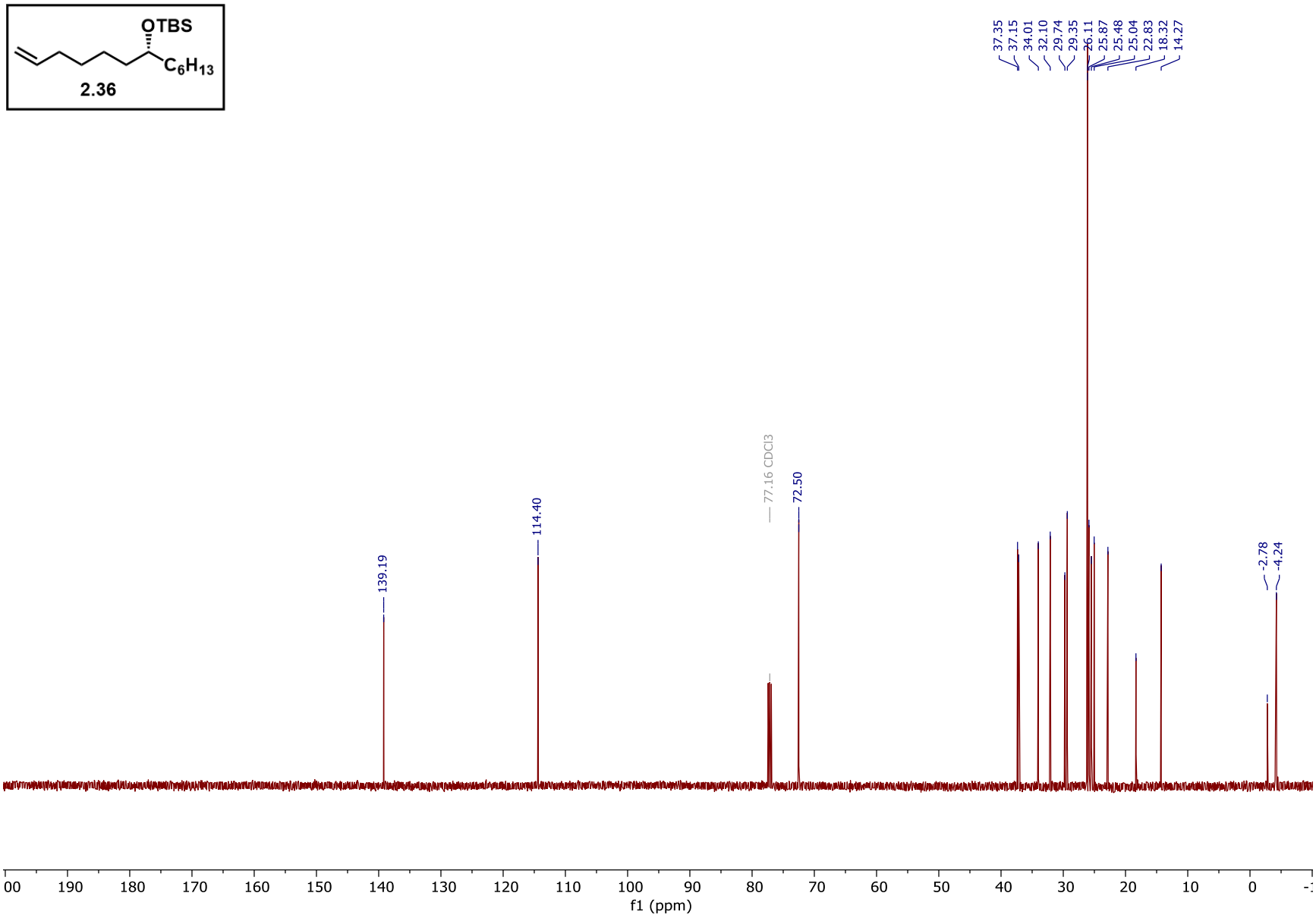
OTBS
C_6H_{13}
2.36
37.35
37.15
34.01
32.10
29.74
29.35
26.11
25.87
25.48
25.04
22.83
18.32
14.27
77.16 CDCl3
72.50
114.40
139.19
-2.78
-4.24
f1 (ppm)

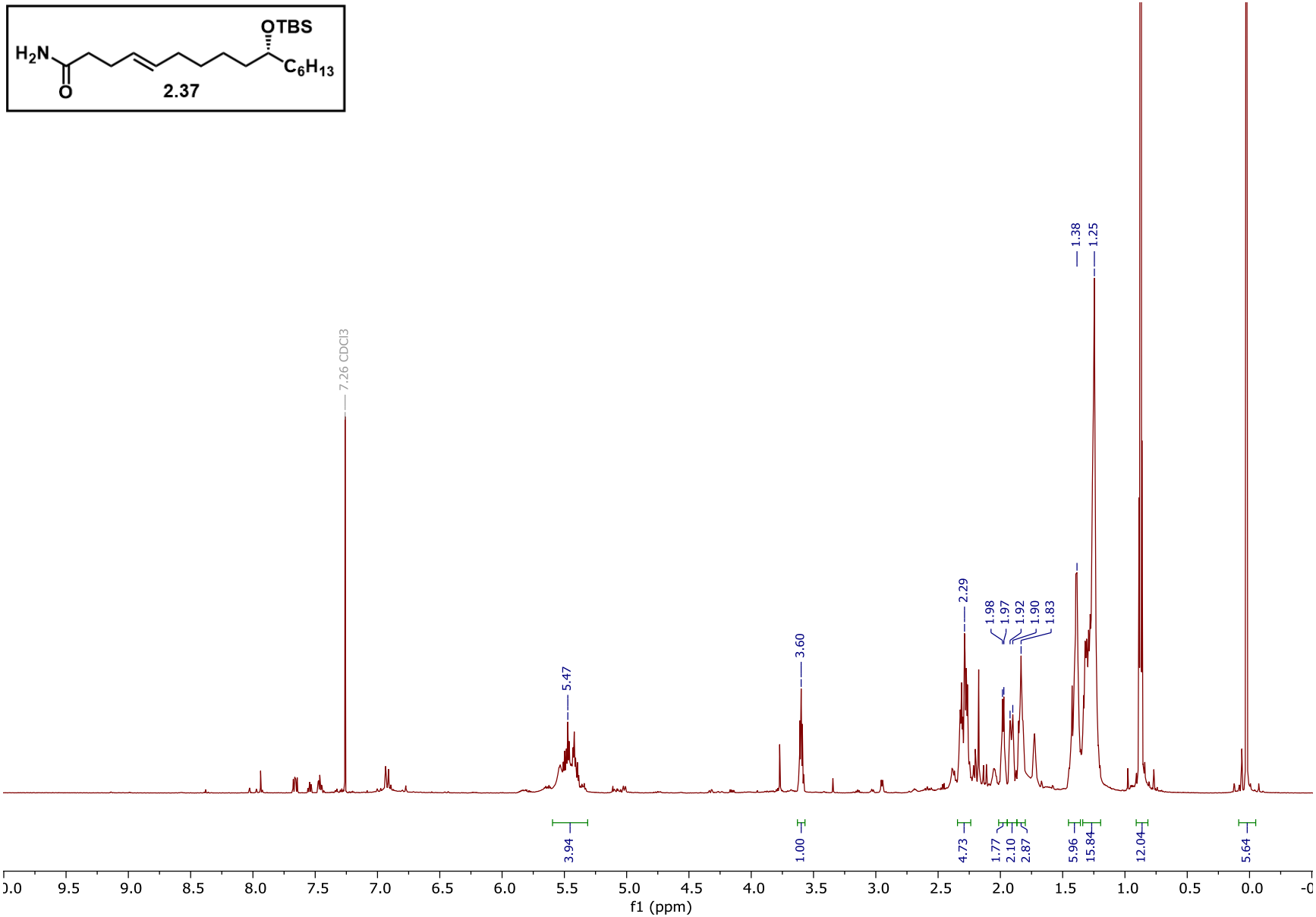
OTBS
H2N
O
C6H13
2.37
7.26 CDCl3
5.47
3.60
2.29
1.98
1.97
1.92
1.90
1.83
1.38
1.25
3.94
1.00
4.73
1.77
2.10
2.87
5.96
15.84
12.04
5.64
f1 (ppm)

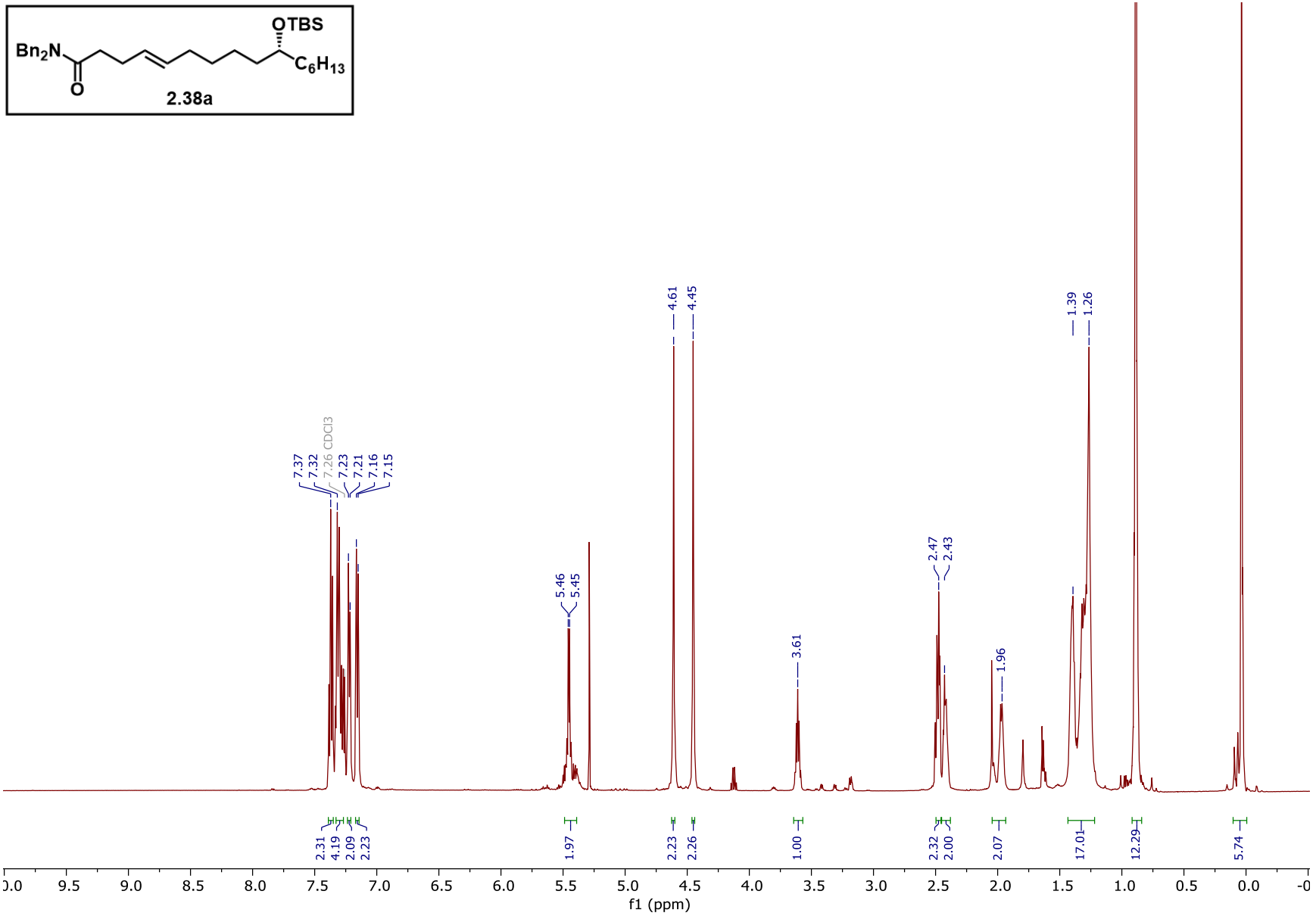
OTBS
Bn2N
C6H13
O
2.38a
7.37
7.32
7.26 CDCl3
7.23
7.21
7.16
7.15
5.46
5.45
4.61
4.45
3.61
2.47
2.43
1.96
1.39
1.26
2.31
4.19
2.09
2.23
1.97
2.23
2.26
1.00
2.32
2.00
2.07
17.01
12.29
5.74
f1 (ppm)

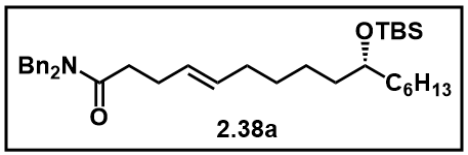
OTBS
Bn2N
C6H13
O

2.38a

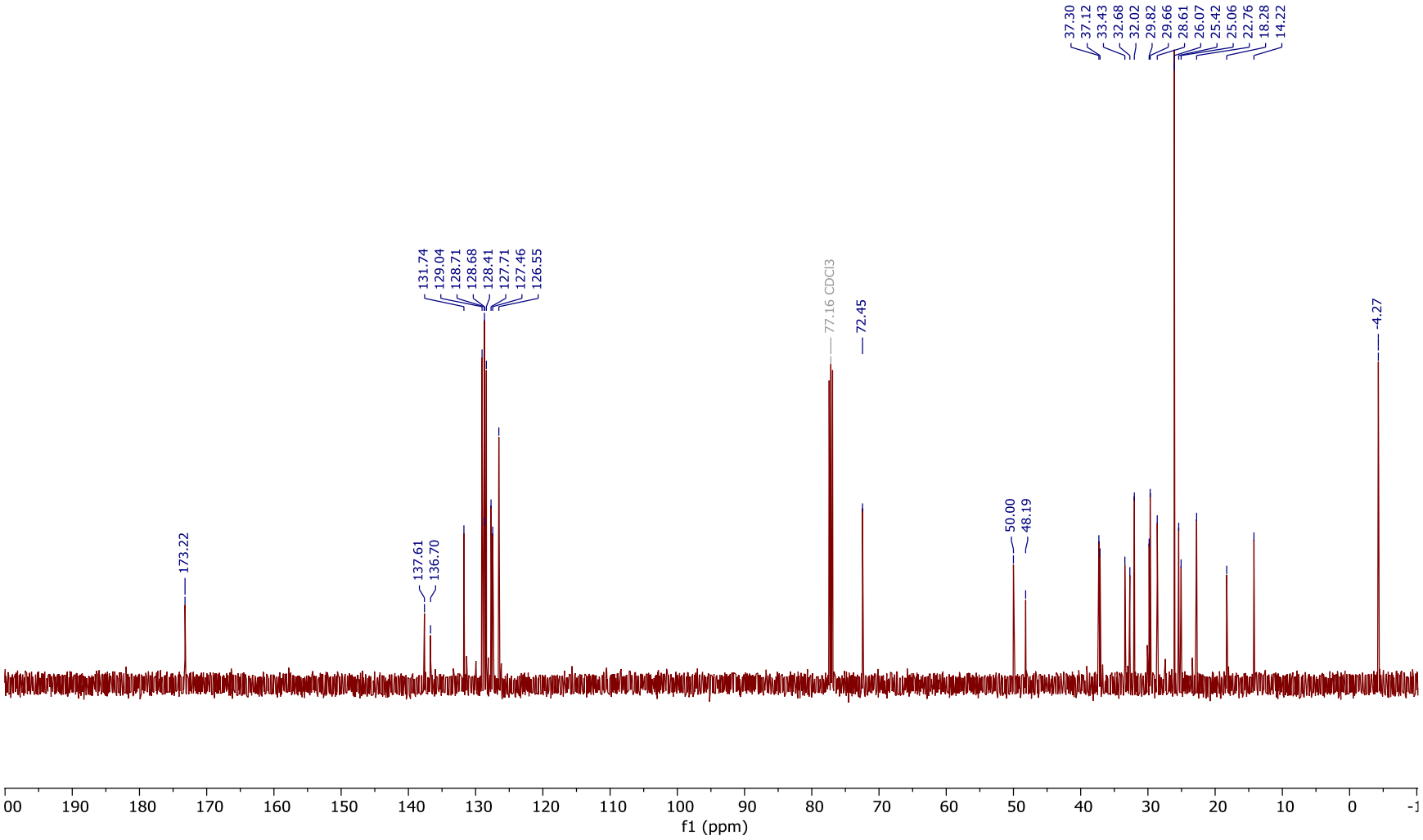
37.30
37.12
33.43
32.68
32.02
29.82
29.66
28.61
26.07
25.42
25.06
22.76
18.28
14.22
131.74
129.04
128.71
128.68
128.41
127.71
127.46
126.55
77.16 CDCl3
72.45
-4.27
173.22
137.61
136.70
50.00
48.19
f1 (ppm)

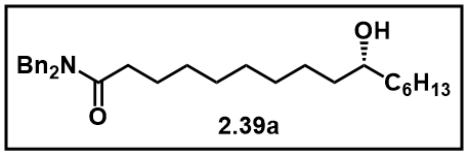
OH
Bn2N
C6H13
O

2.39a

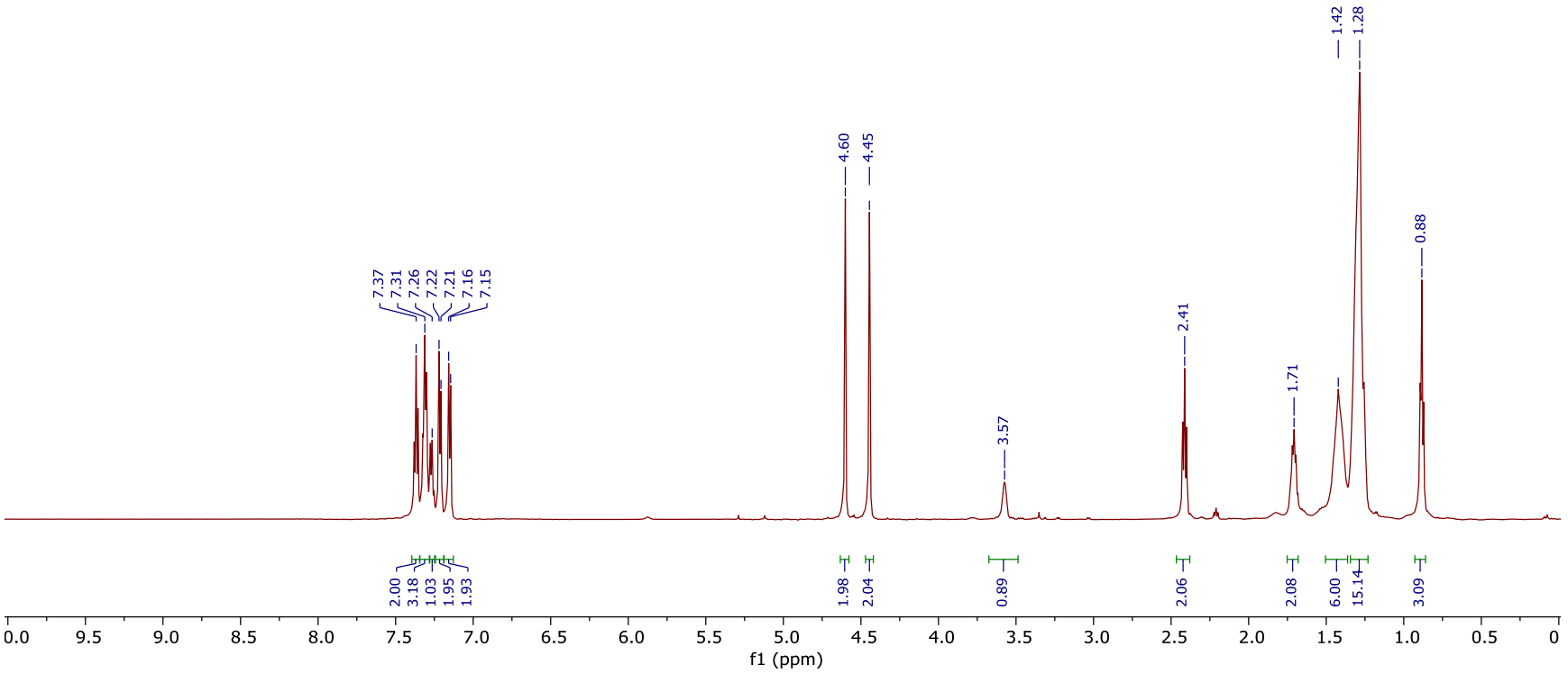
7.37
7.31
7.26
7.22
7.21
7.16
7.15
4.60
4.45
3.57
2.41
1.71
1.42
1.28
0.88
2.00
3.18
1.03
1.95
1.93
1.98
2.04
0.89
2.06
2.08
6.00
15.14
3.09
0.0
9.5
9.0
8.5
8.0
7.5
7.0
6.5
6.0
5.5
5.0
4.5
4.0
3.5
3.0
2.5
2.0
1.5
1.0
0.5
0
f1 (ppm)

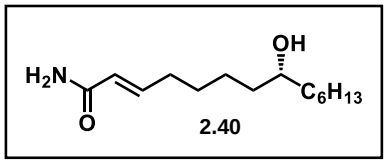
OH
H2N
C6H13
O

2.40

7.26 CDCl3
6.79
6.13
6.09
5.84
5.81
3.53
2.29
2.17
2.15
1.42
1.39
1.24
0.85
1.00
2.04
1.00
1.01
1.06
2.10
16.44
3.04
f1 (ppm)

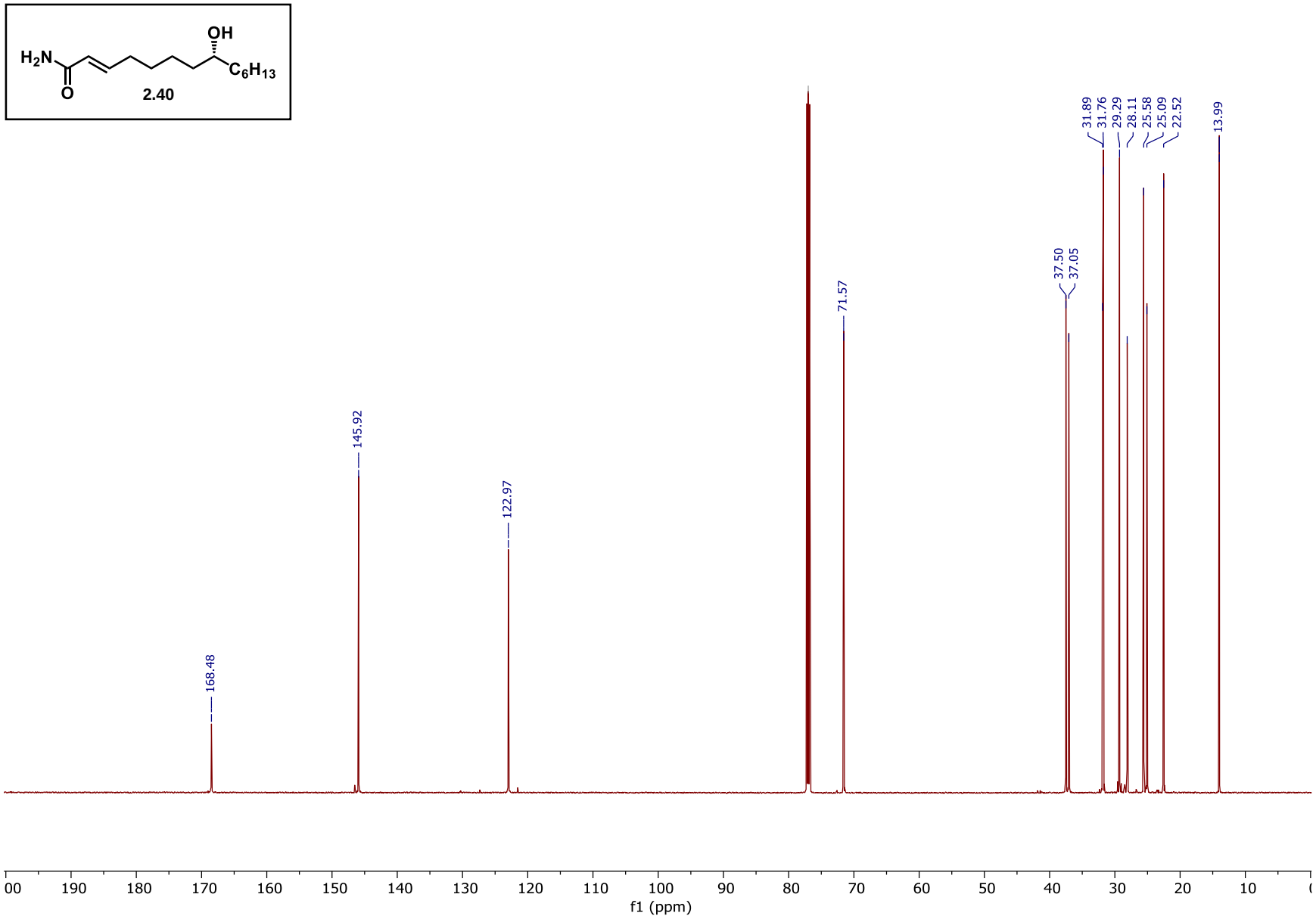
OH
H2N
C6H13
O
2.40
168.48
145.92
122.97
71.57
37.50
37.05
31.89
31.76
29.29
28.11
25.58
25.09
22.52
13.99
f1 (ppm)

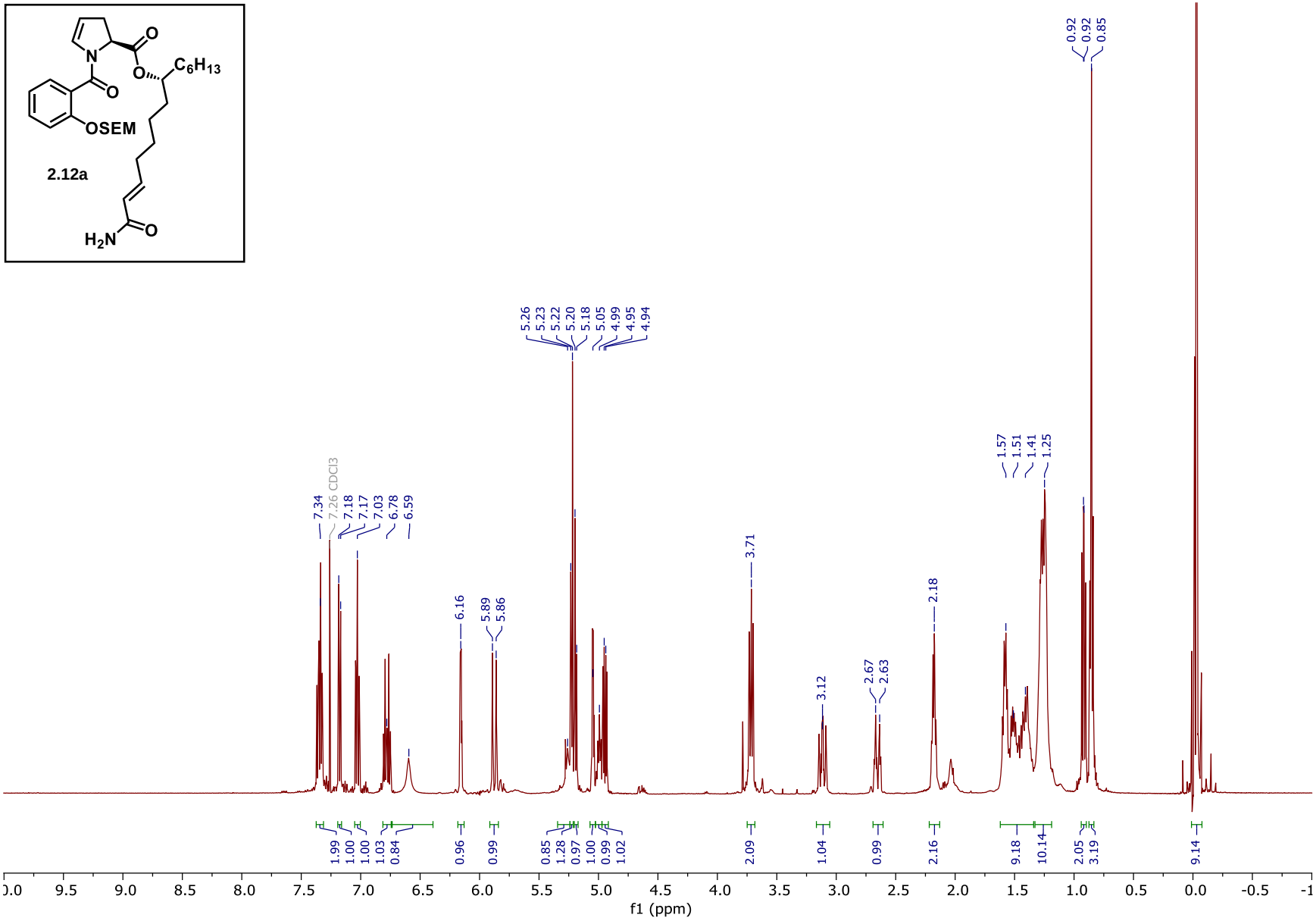
OSEM
2.12a
C_6H_{13}
H_2N
7.34
7.26 CDCl3
7.18
7.17
7.03
6.78
6.59
6.16
5.89
5.86
5.26
5.23
5.22
5.20
5.18
5.05
4.99
4.95
4.94
3.71
3.12
2.67
2.63
2.18
1.57
1.51
1.41
1.25
0.92
0.92
0.85
1.99
1.00
1.00
1.03
0.84
0.96
0.99
0.85
1.28
0.97
1.00
0.99
1.02
2.09
1.04
0.99
2.16
9.18
10.14
2.05
3.19
9.14
f1 (ppm)

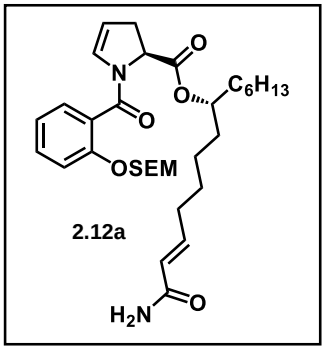
O
N
O
O
C6H13
OSEM
2.12a
H2N
O

170.47
168.63
165.19
153.55
144.48
131.27
130.73
128.68
125.41
123.86
121.85
115.11
108.69
93.13
75.07
66.54
57.85
34.39
34.17
34.07
31.64
31.51
29.05
27.40
25.30
24.16
22.48
17.95
13.98
-1.48
210 200 190 180 170 160 150 140 130 120 110 100 90 80 70 60 50 40 30 20 10 0 -10
f1 (ppm)

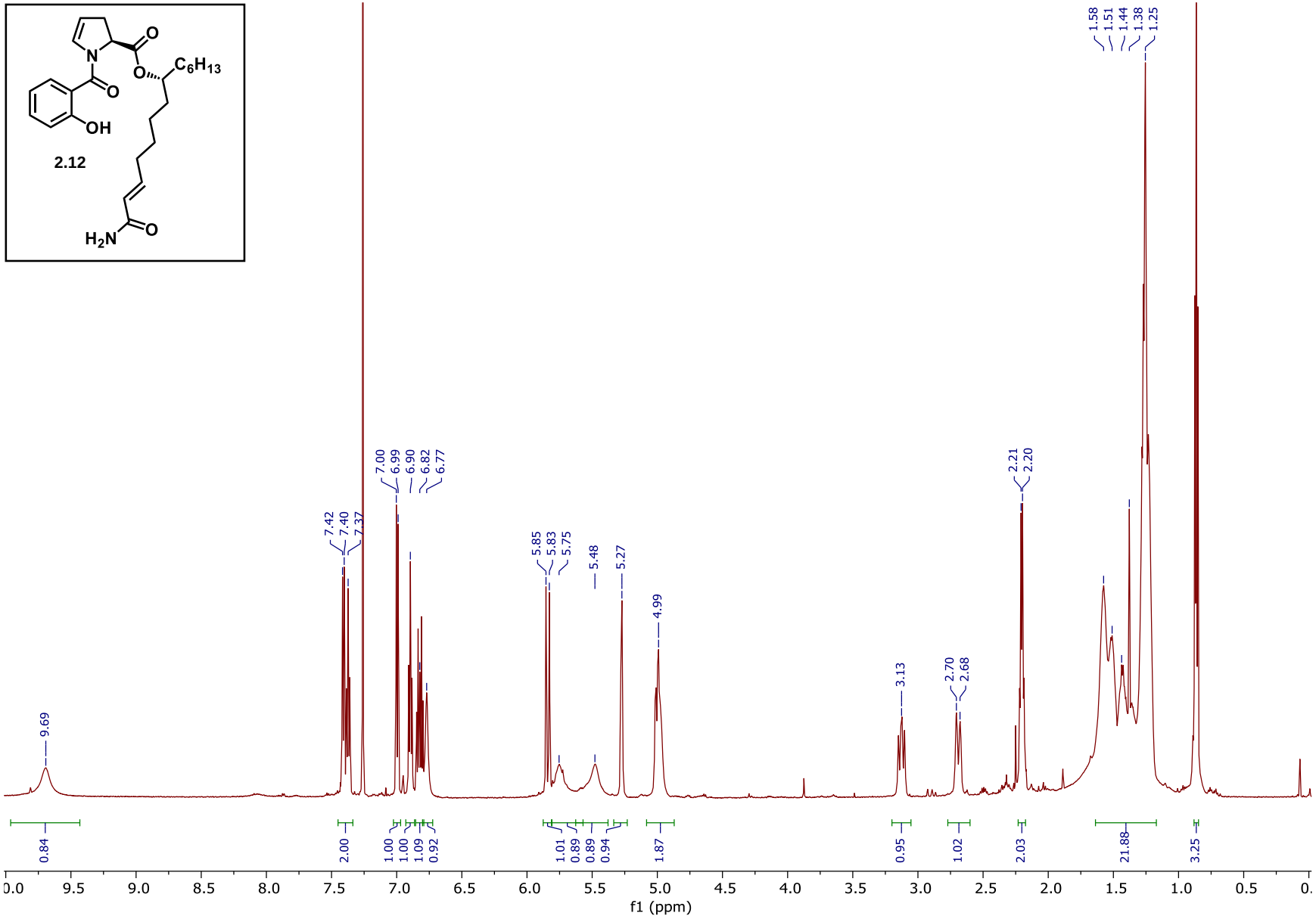
2.12
f1 (ppm)

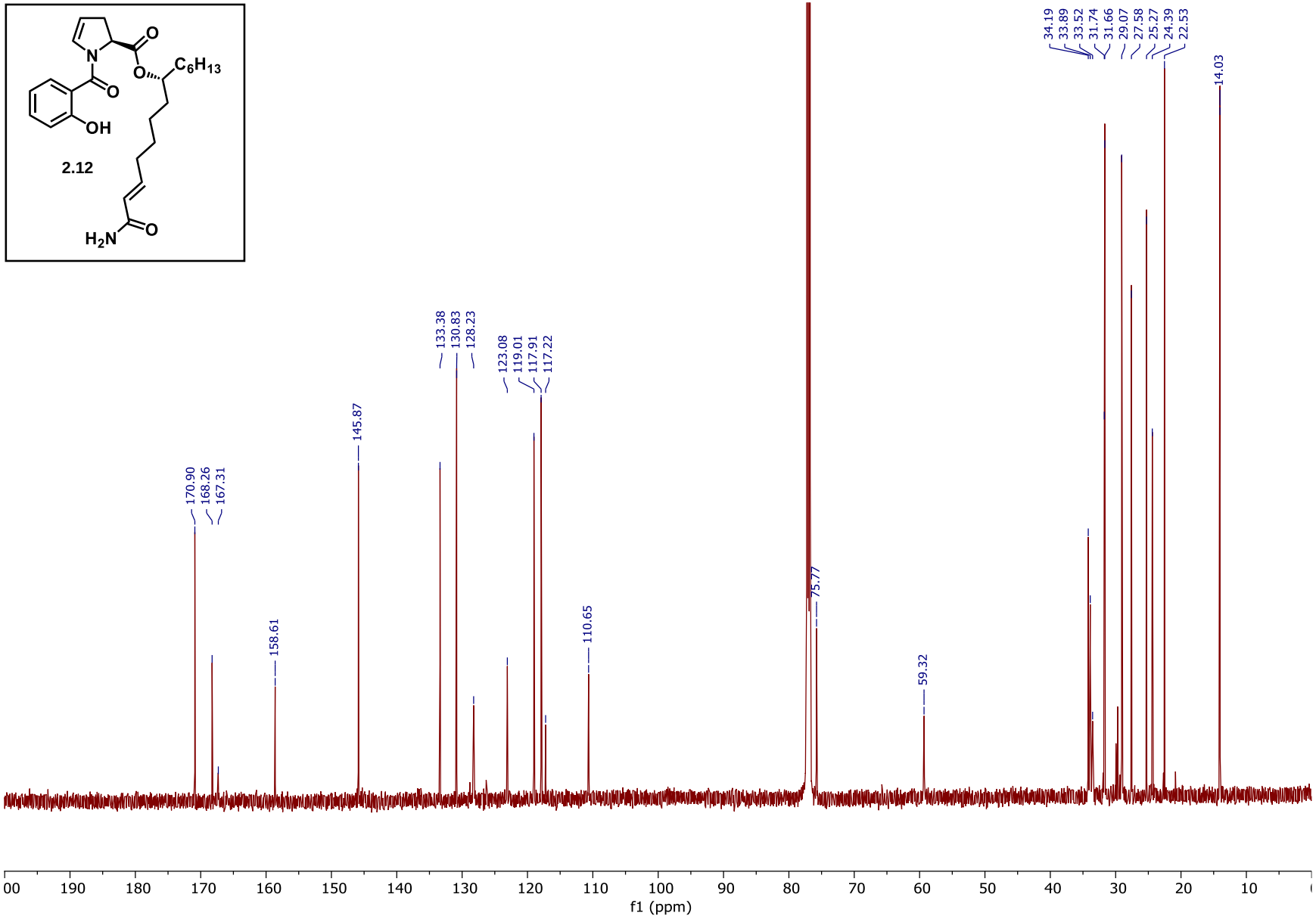
2.12
34.19
33.89
33.52
31.74
31.66
29.07
27.58
25.27
24.39
22.53
14.03
170.90
168.26
167.31
158.61
145.87
133.38
130.83
128.23
123.08
119.01
117.91
117.22
110.65
75.77
59.32
f1 (ppm)

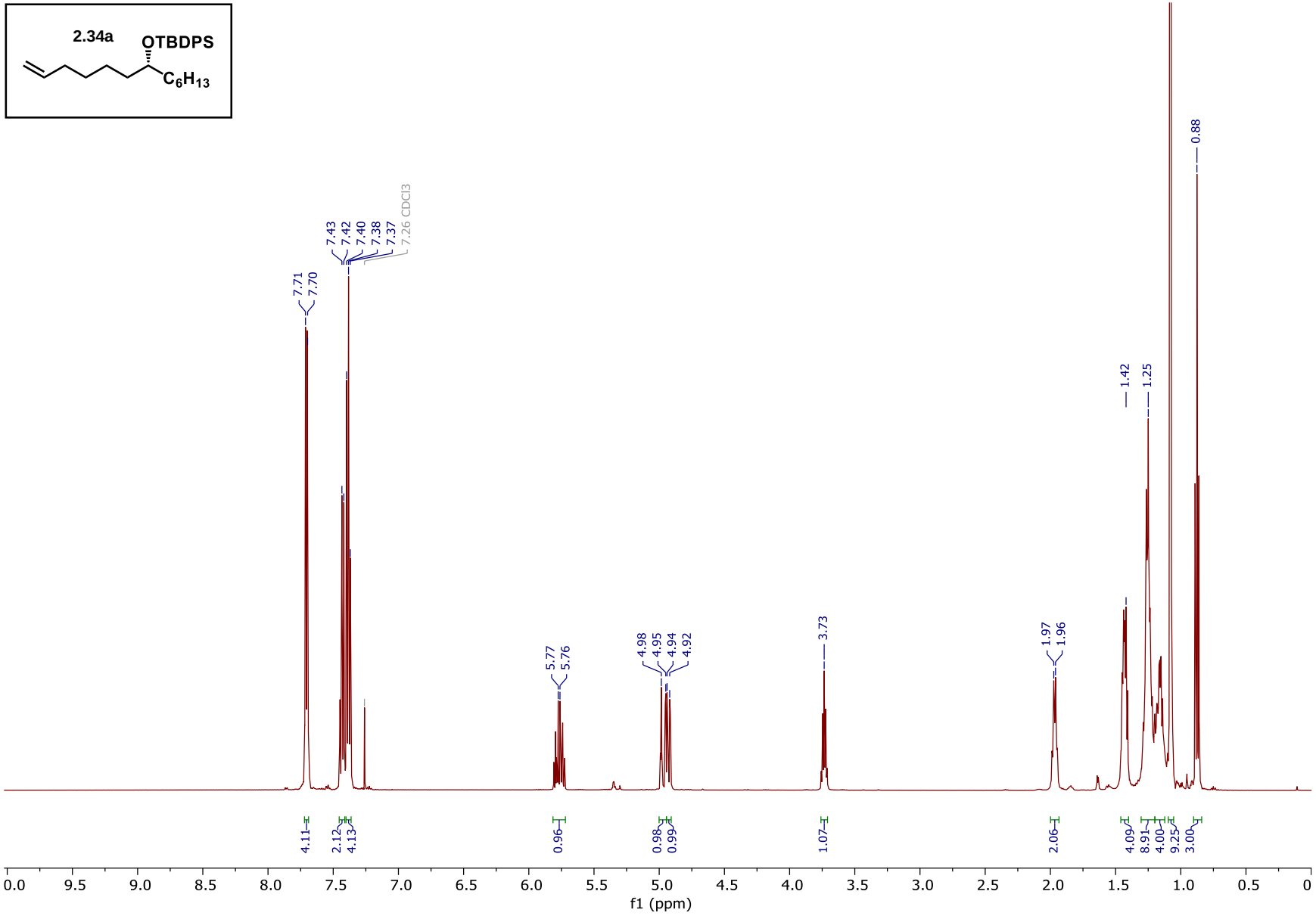
2.34a
OTBDPS
C6H13
7.71
7.70
7.43
7.42
7.40
7.38
7.37
7.26 CDCl3
5.77
5.76
4.98
4.95
4.94
4.92
3.73
1.97
1.96
1.42
1.25
0.88
4.11
2.12
4.13
0.96
0.98
0.99
1.07
2.06
4.09
8.91
4.00
9.25
3.00
f1 (ppm)

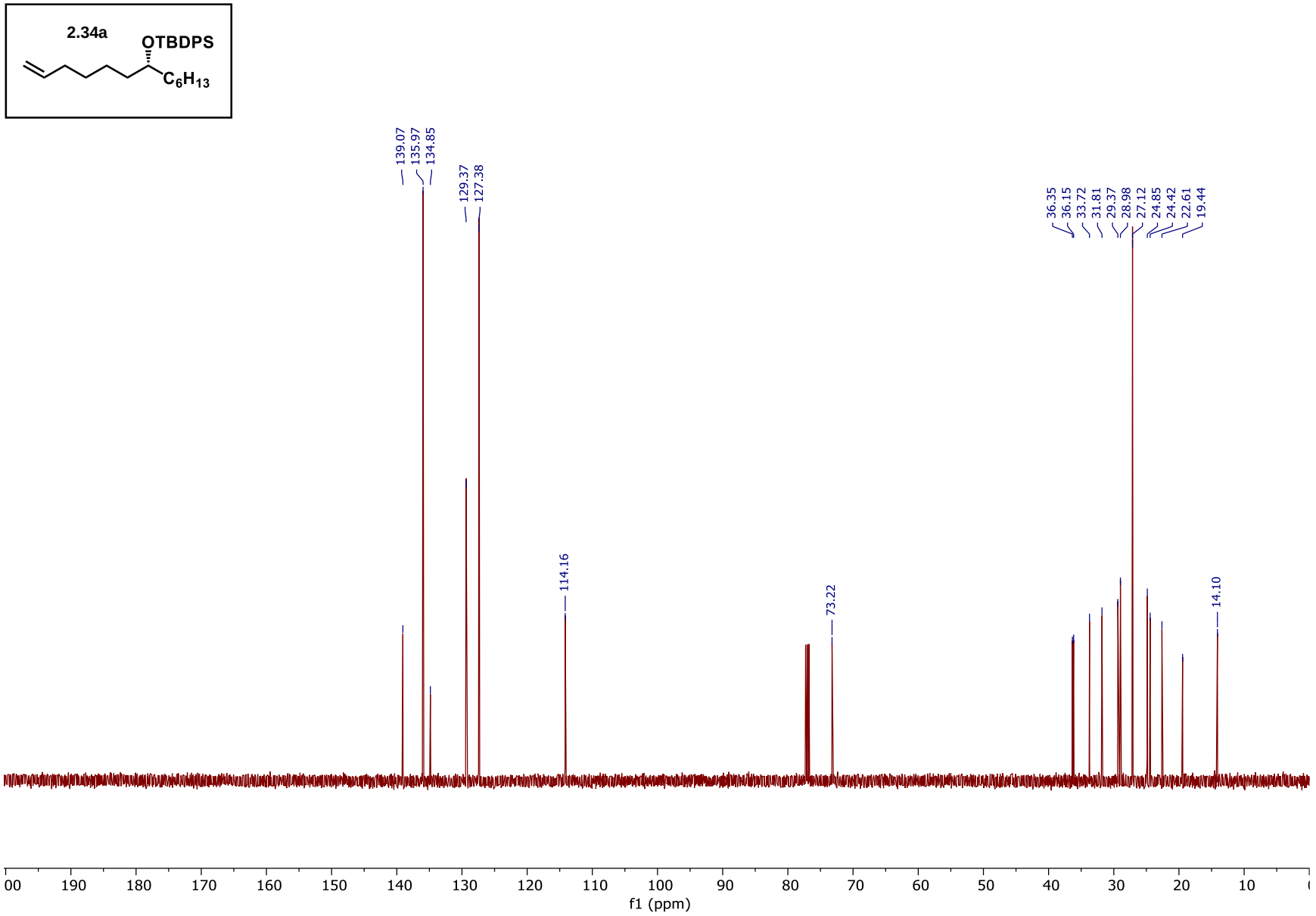
2.34a
OTBDPS
C6H13
139.07
135.97
134.85
129.37
127.38
114.16
73.22
36.35
36.15
33.72
31.81
29.37
28.98
27.12
24.85
24.42
22.61
19.44
14.10
f1 (ppm)

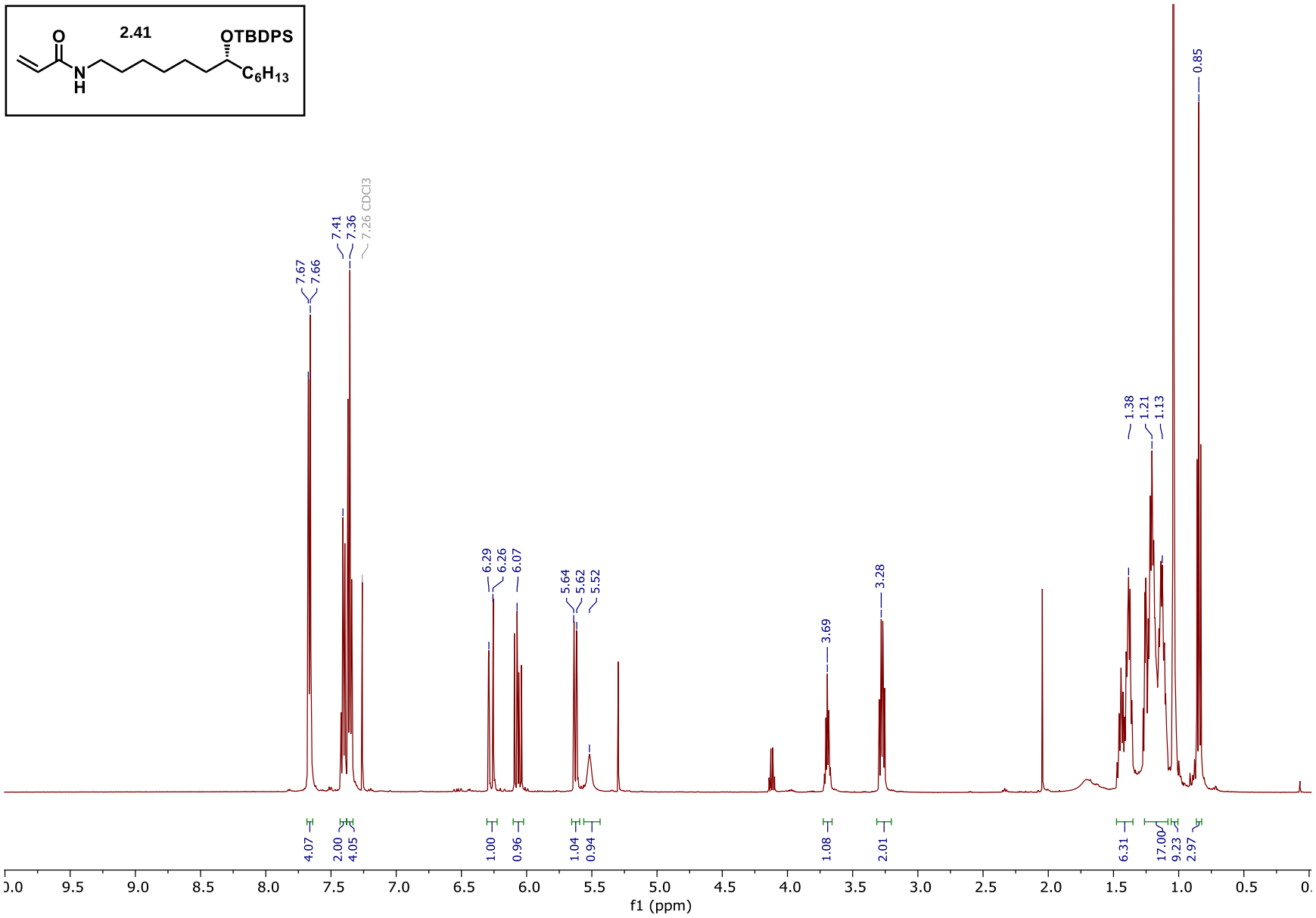
2.41
O
N
H
OTBDPS
C6H13
7.67
7.66
7.41
7.36
7.26 CDCl3
6.29
6.26
6.07
5.64
5.62
5.52
3.69
3.28
1.38
1.21
1.13
0.85
4.07
2.00
4.05
1.00
0.96
1.04
0.94
1.08
2.01
6.31
17.00
9.23
2.97
f1 (ppm)

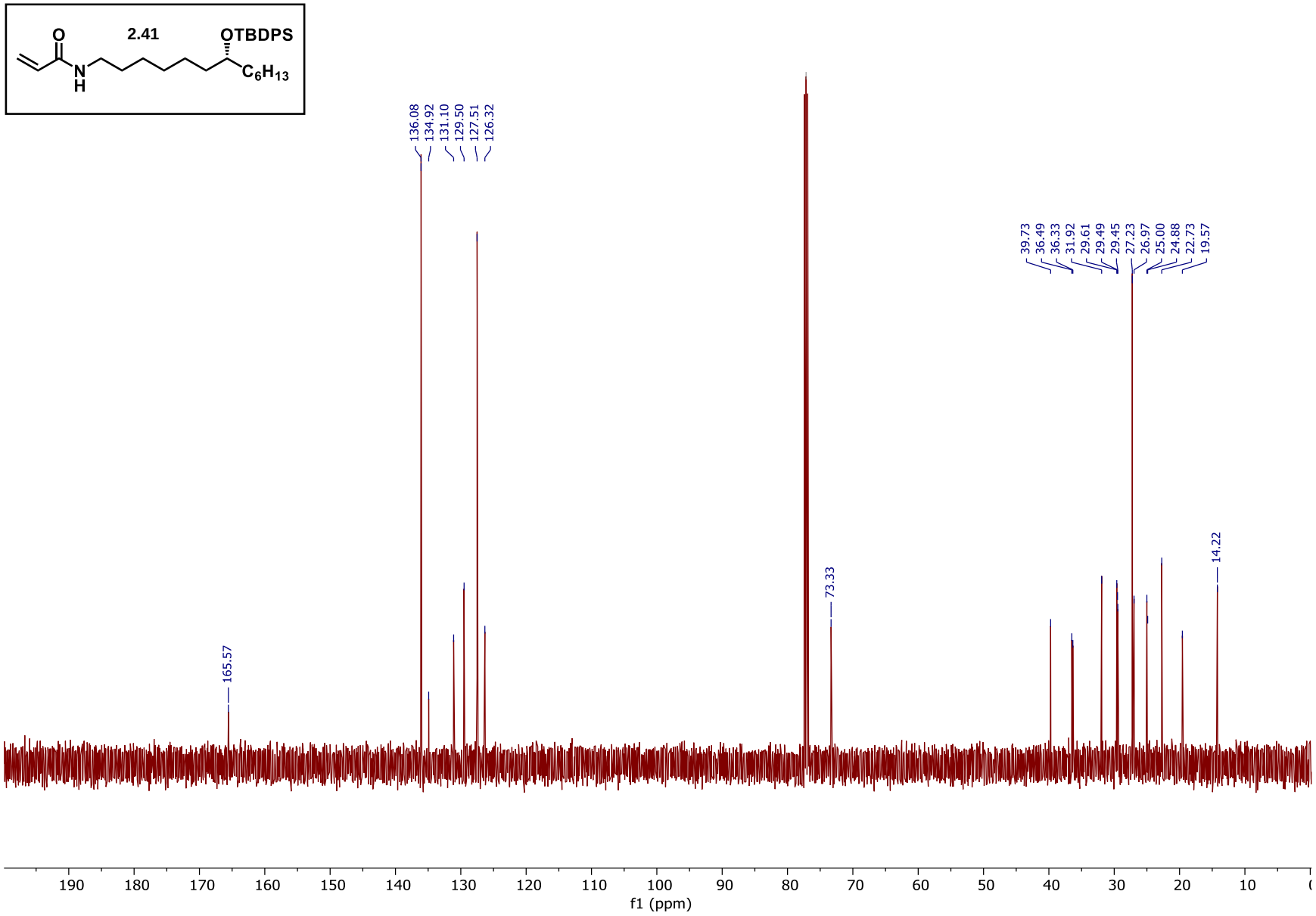
O
2.41
OTBDPS
N
H
C_6H_{13}
136.08
134.92
131.10
129.50
127.51
126.32
165.57
73.33
39.73
36.49
36.33
31.92
29.61
29.49
29.45
27.23
26.97
25.00
24.88
22.73
19.57
14.22
190
180
170
160
150
140
130
120
110
100
90
80
70
60
50
40
30
20
10
f1 (ppm)

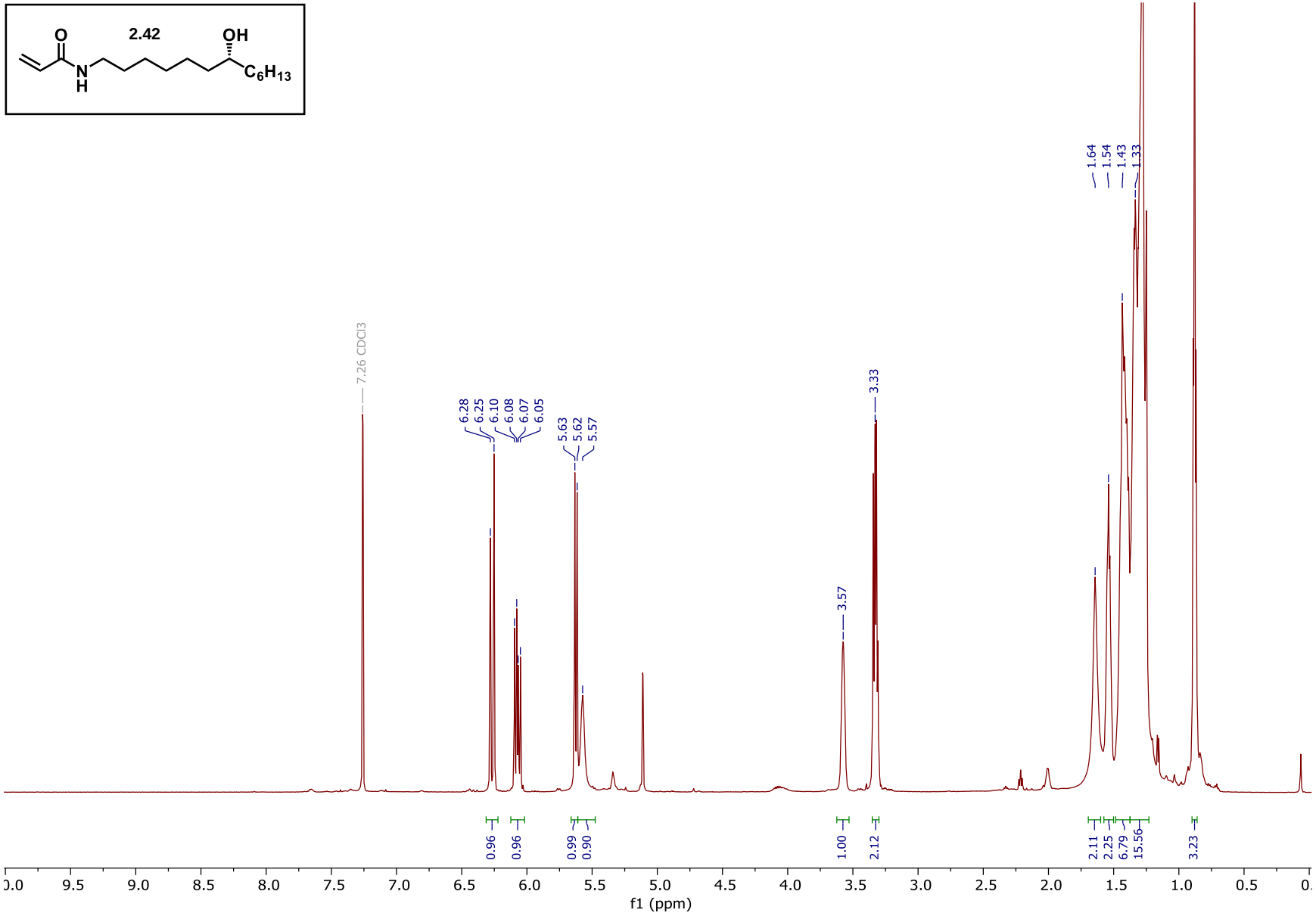
O
2.42
OH
N
H
C6H13
7.26 CDCl3
6.28
6.25
6.10
6.08
6.07
6.05
5.63
5.62
5.57
3.57
3.33
1.64
1.54
1.43
1.33
0.96
0.96
0.99
0.90
1.00
2.12
2.11
2.25
6.79
15.56
3.23
f1 (ppm)

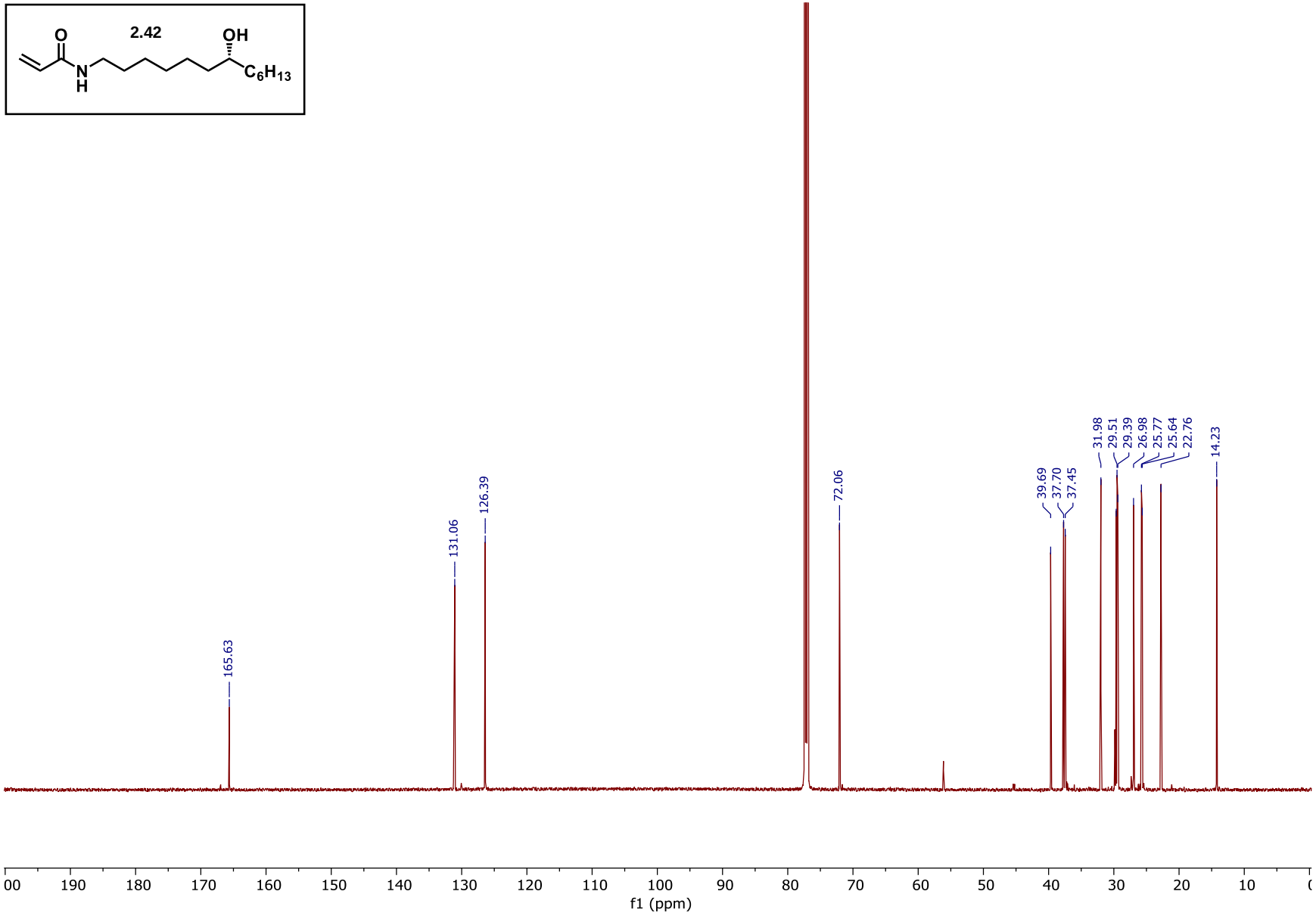
2.42
O
OH
N
H
C6H13
165.63
131.06
126.39
72.06
39.69
37.70
37.45
31.98
29.51
29.39
26.98
25.77
25.64
22.76
14.23
f1 (ppm)

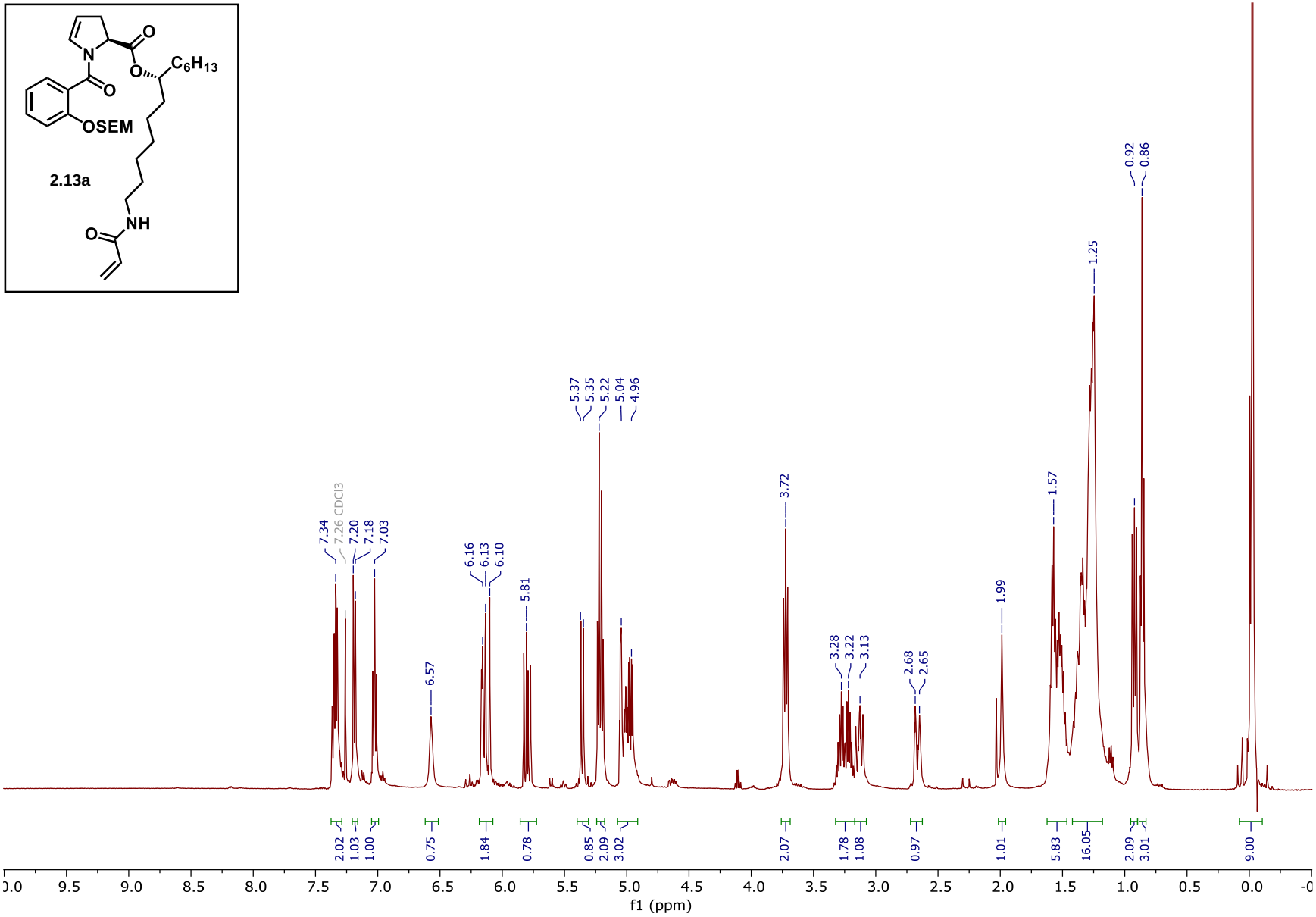
2.13a
OSEM
NH
7.34
7.26 CDCl3
7.20
7.18
7.03
6.57
6.16
6.13
6.10
5.81
5.37
5.35
5.22
5.04
4.96
3.72
3.28
3.22
3.13
2.68
2.65
1.99
1.57
1.25
0.92
0.86
2.02
1.03
1.00
0.75
1.84
0.78
0.85
2.09
3.02
2.07
1.78
1.08
0.97
1.01
5.83
16.05
2.09
3.01
9.00
f1 (ppm)

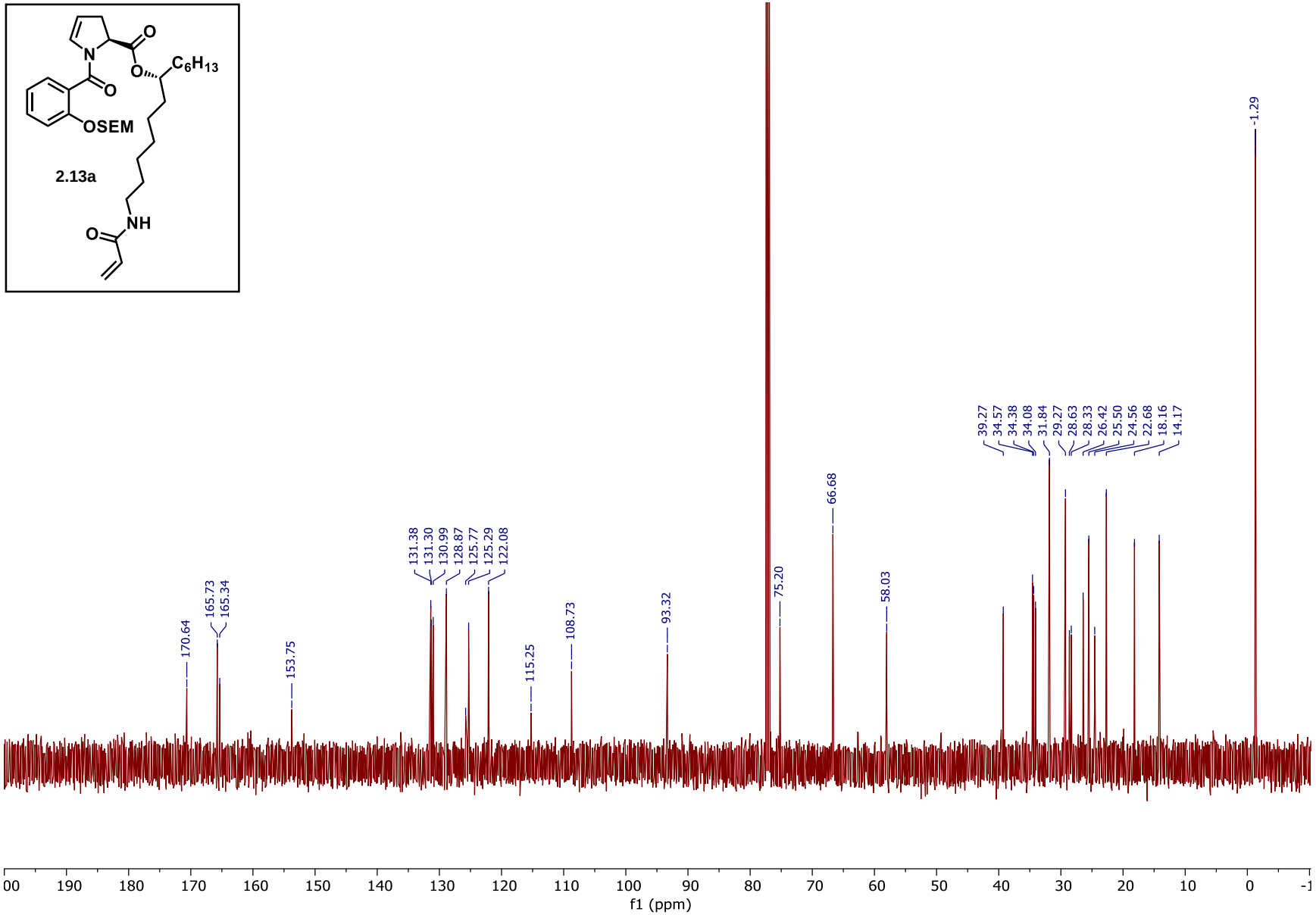
O
N
O
C6H13
O
O
OSEM
2.13a
NH
O
170.64
165.73
165.34
153.75
131.38
131.30
130.99
128.87
125.77
125.29
122.08
115.25
108.73
93.32
75.20
66.68
58.03
39.27
34.57
34.38
34.08
31.84
29.27
28.63
28.33
26.42
25.50
24.56
22.68
18.16
14.17
-1.29
f1 (ppm)

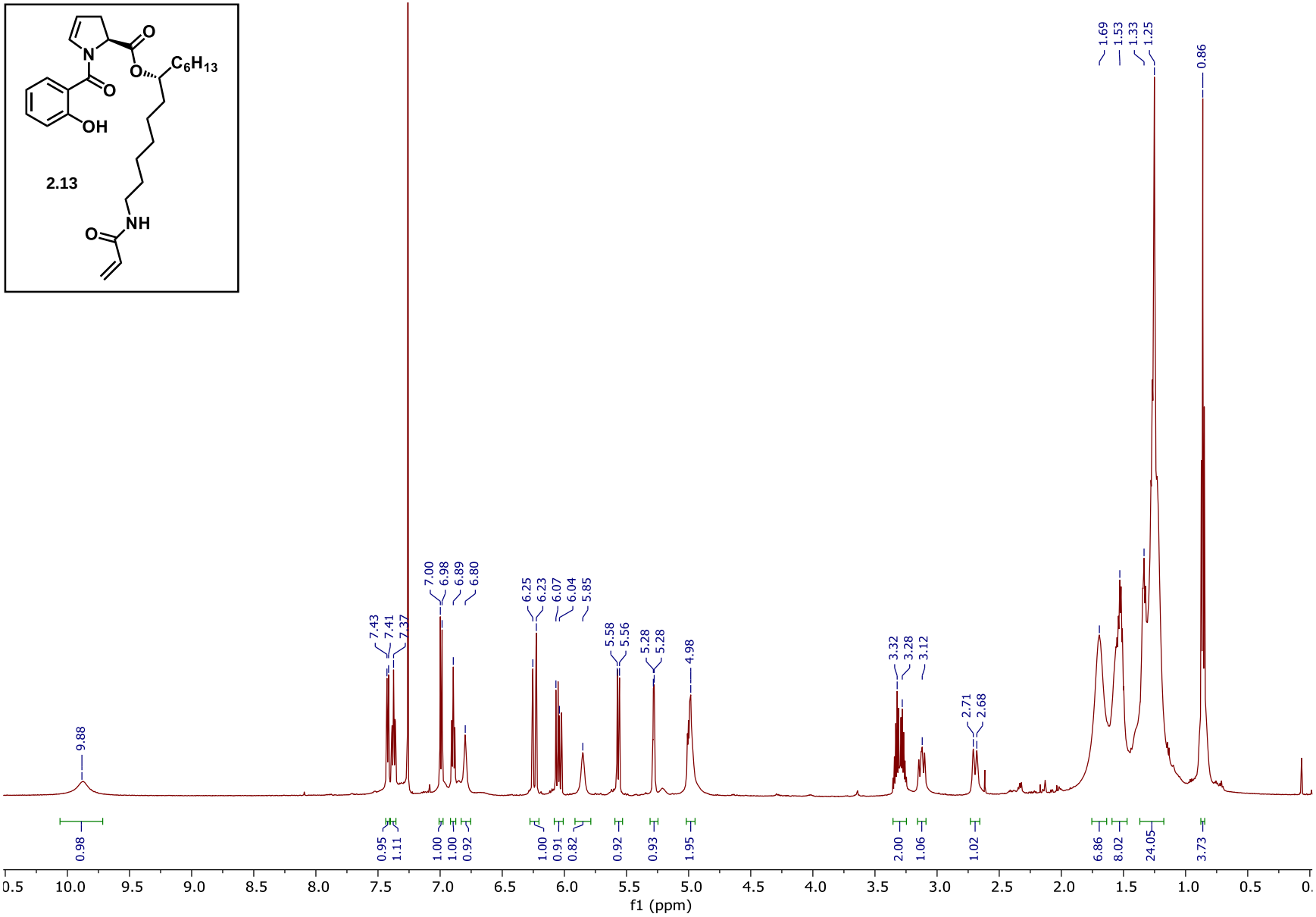
2.13
OH
NH
9.88
7.43
7.41
7.37
7.00
6.98
6.89
6.80
6.25
6.23
6.07
6.04
5.85
5.58
5.56
5.28
5.28
4.98
3.32
3.28
3.12
2.71
2.68
1.69
1.53
1.33
1.25
0.86
0.98
0.95
1.11
1.00
1.00
0.92
1.00
0.91
0.82
0.92
0.93
1.95
2.00
1.06
1.02
6.86
8.02
24.05
3.73
f1 (ppm)

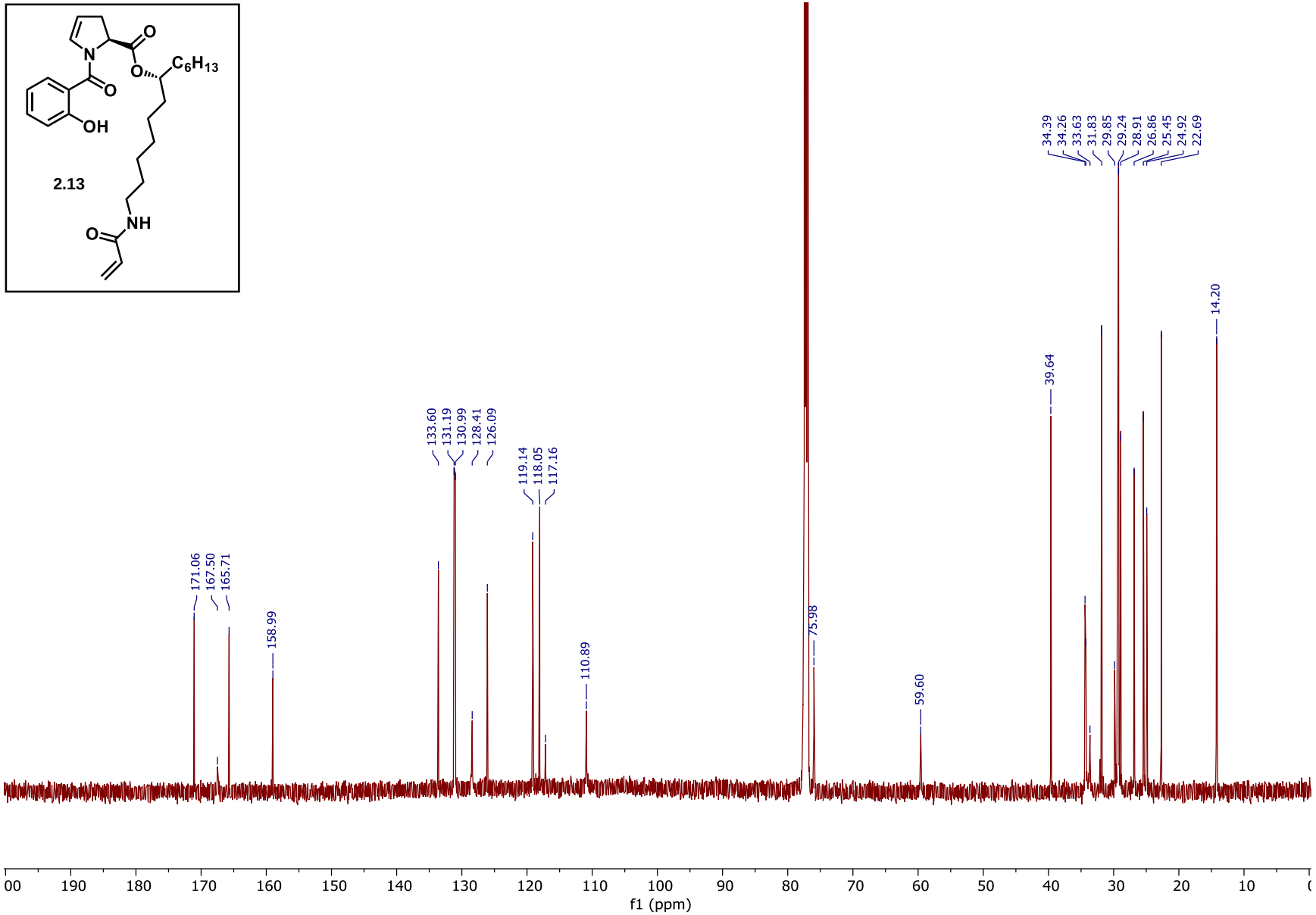
2.13
OH
NH
171.06
167.50
165.71
158.99
133.60
131.19
130.99
128.41
126.09
119.14
118.05
117.16
110.89
75.98
59.60
39.64
34.39
34.26
33.63
31.83
29.85
29.24
28.91
26.86
25.45
24.92
22.69
14.20
f1 (ppm)

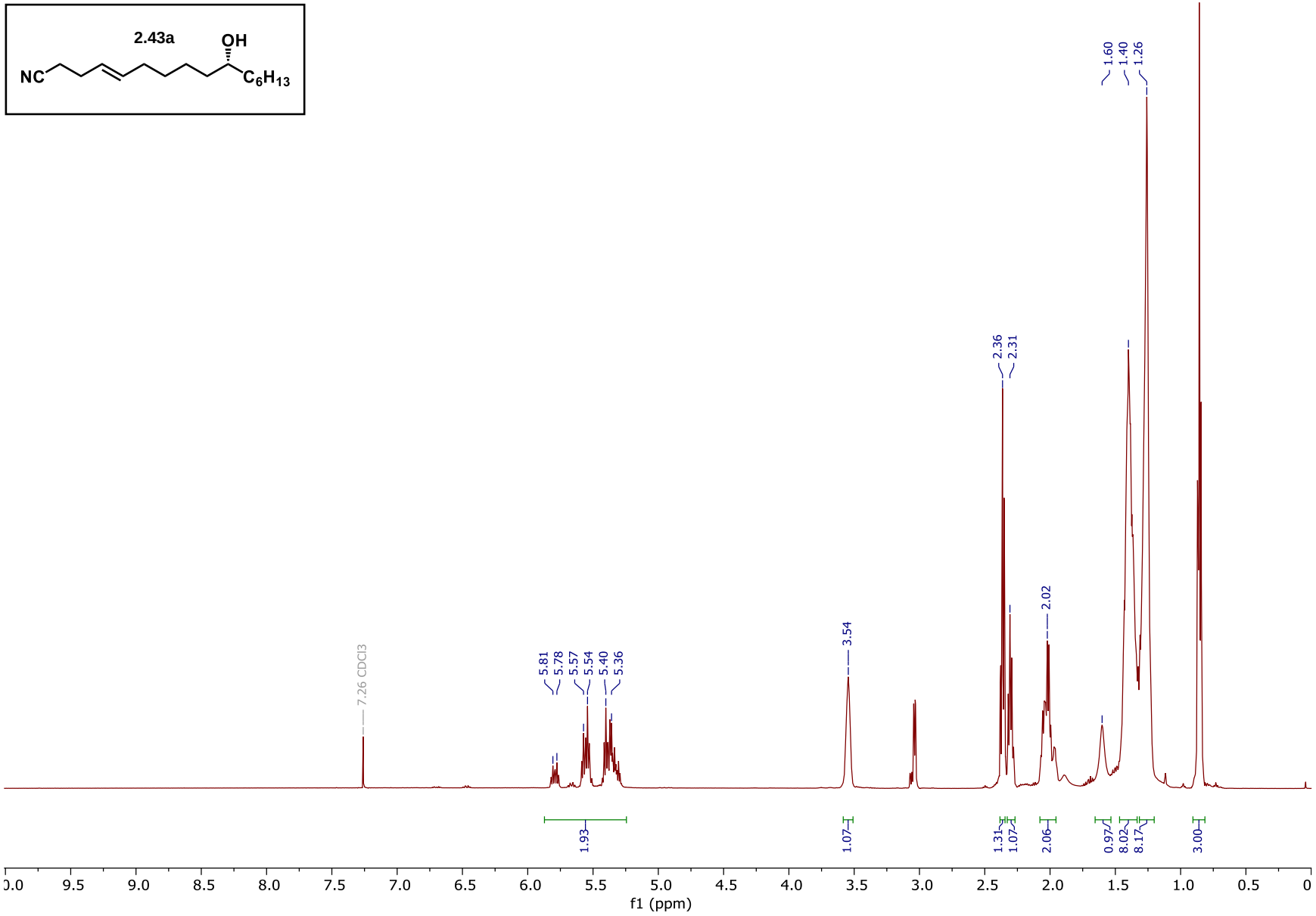
2.43a
OH
NC
C6H13
7.26 CDCl3
5.81
5.78
5.57
5.54
5.40
5.36
3.54
2.36
2.31
2.02
1.60
1.40
1.26
1.93
1.07
1.31
1.07
2.06
0.97
8.02
8.17
3.00
f1 (ppm)

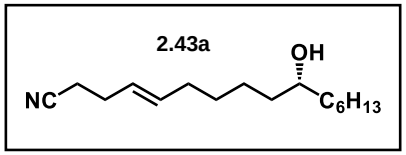
2.43a
OH
NC
C_6H_{13}

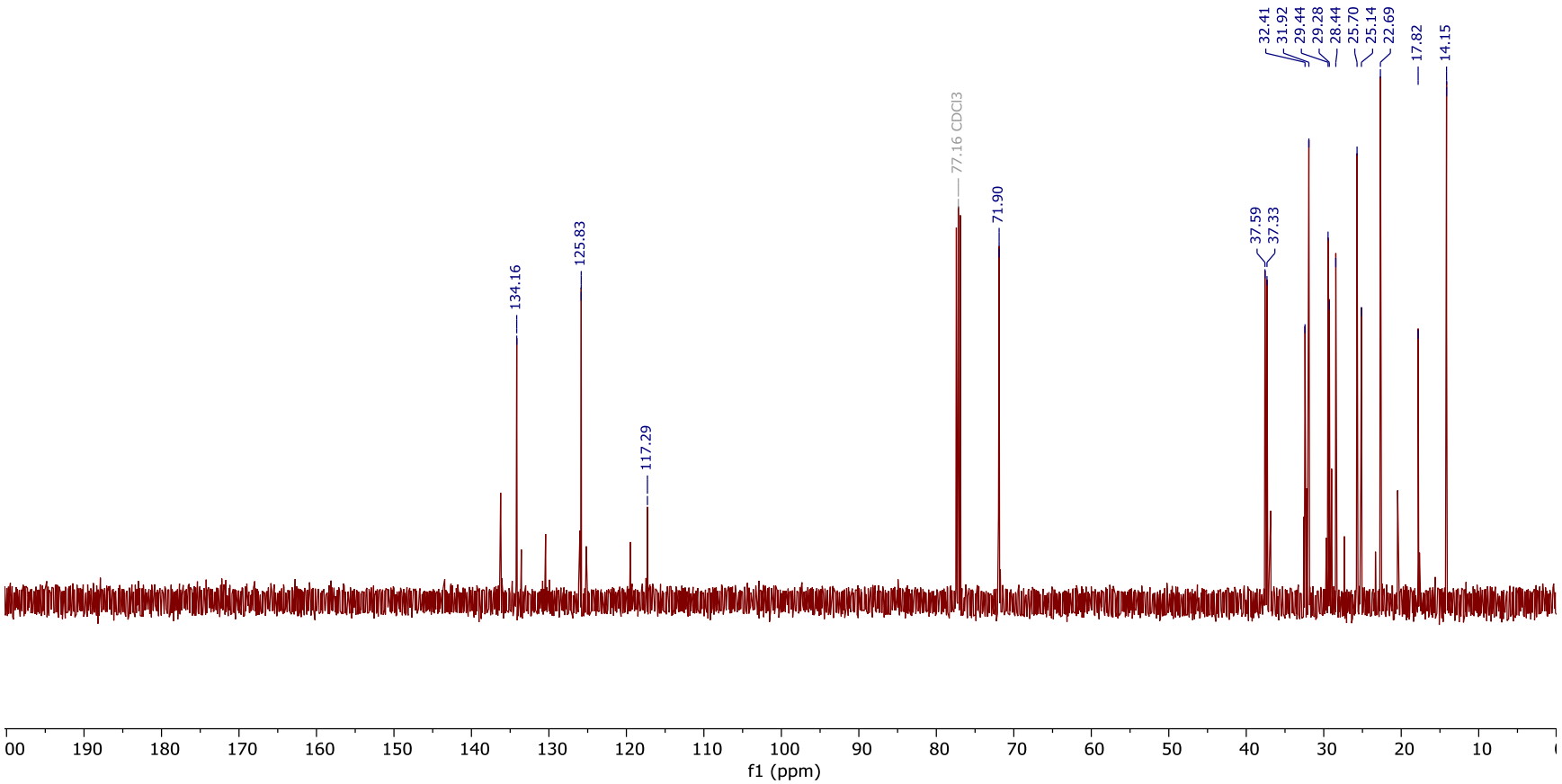
32.41
31.92
29.44
29.28
28.44
25.70
25.14
22.69
17.82
14.15
77.16 CDCl3
71.90
37.59
37.33
134.16
125.83
117.29
00
190
180
170
160
150
140
130
120
110
100
90
80
70
60
50
40
30
20
10
f1 (ppm)

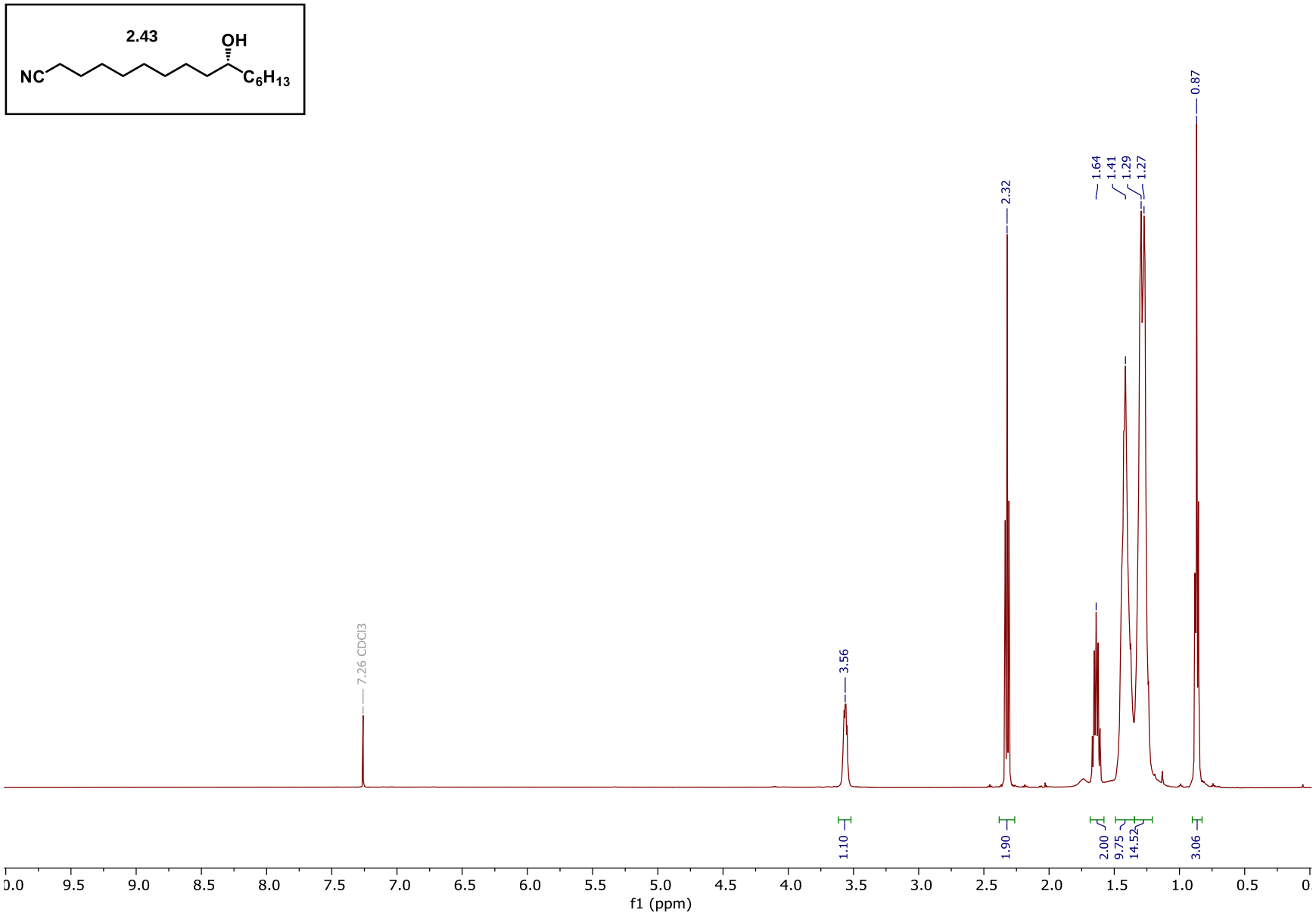
2.43
OH
NC
C6H13
7.26 CDCl3
3.56
2.32
1.64
1.41
1.29
1.27
0.87
1.10
1.90
2.00
9.75
14.52
3.06
f1 (ppm)

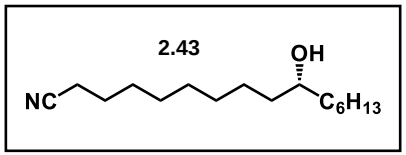
2.43
OH
NC
C6H13

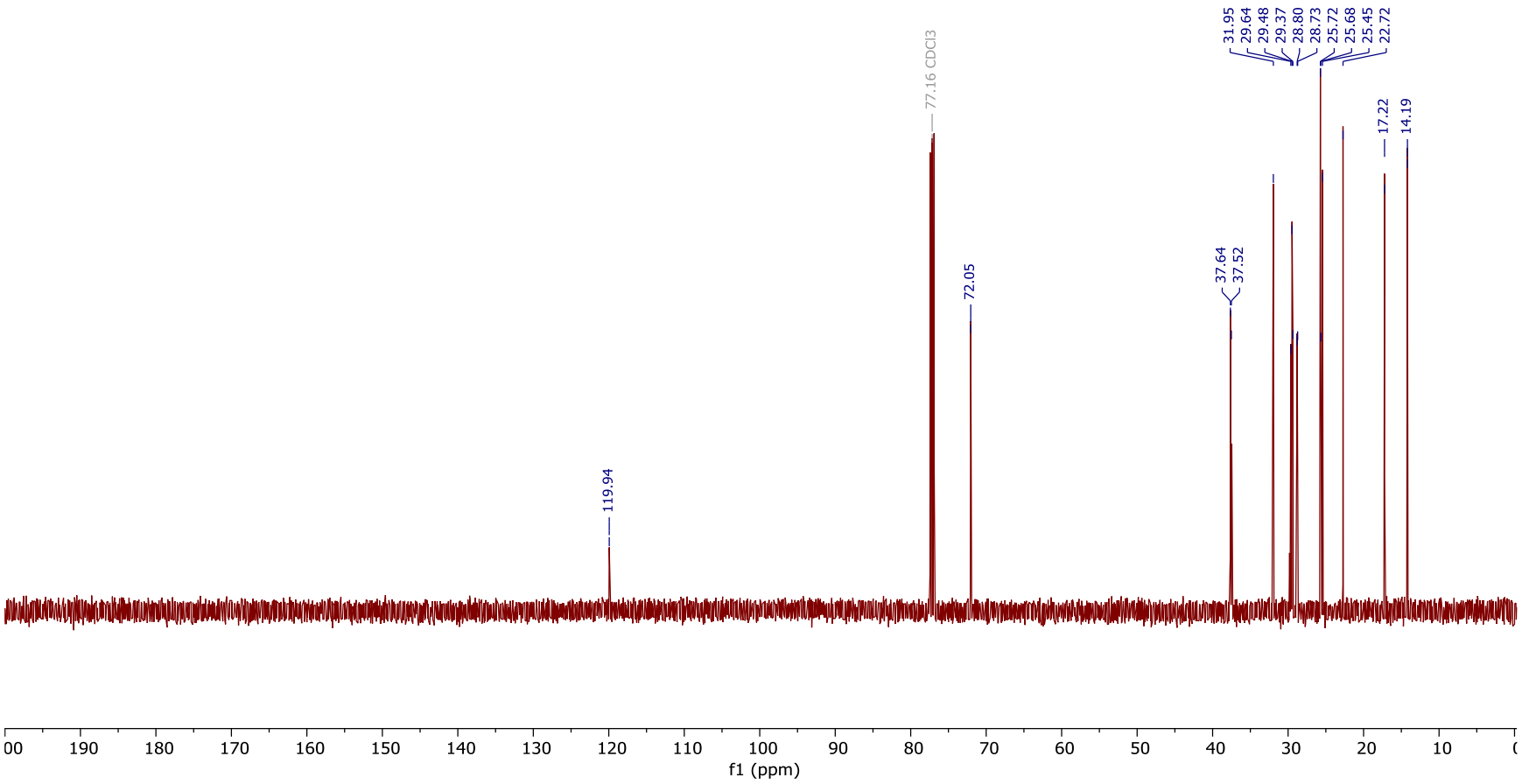
31.95
29.64
29.48
29.37
28.80
28.73
25.72
25.68
25.45
22.72
77.16 CDCl3
17.22
14.19
72.05
37.64
37.52
119.94
00
190
180
170
160
150
140
130
120
110
100
90
80
70
60
50
40
30
20
10
f1 (ppm)

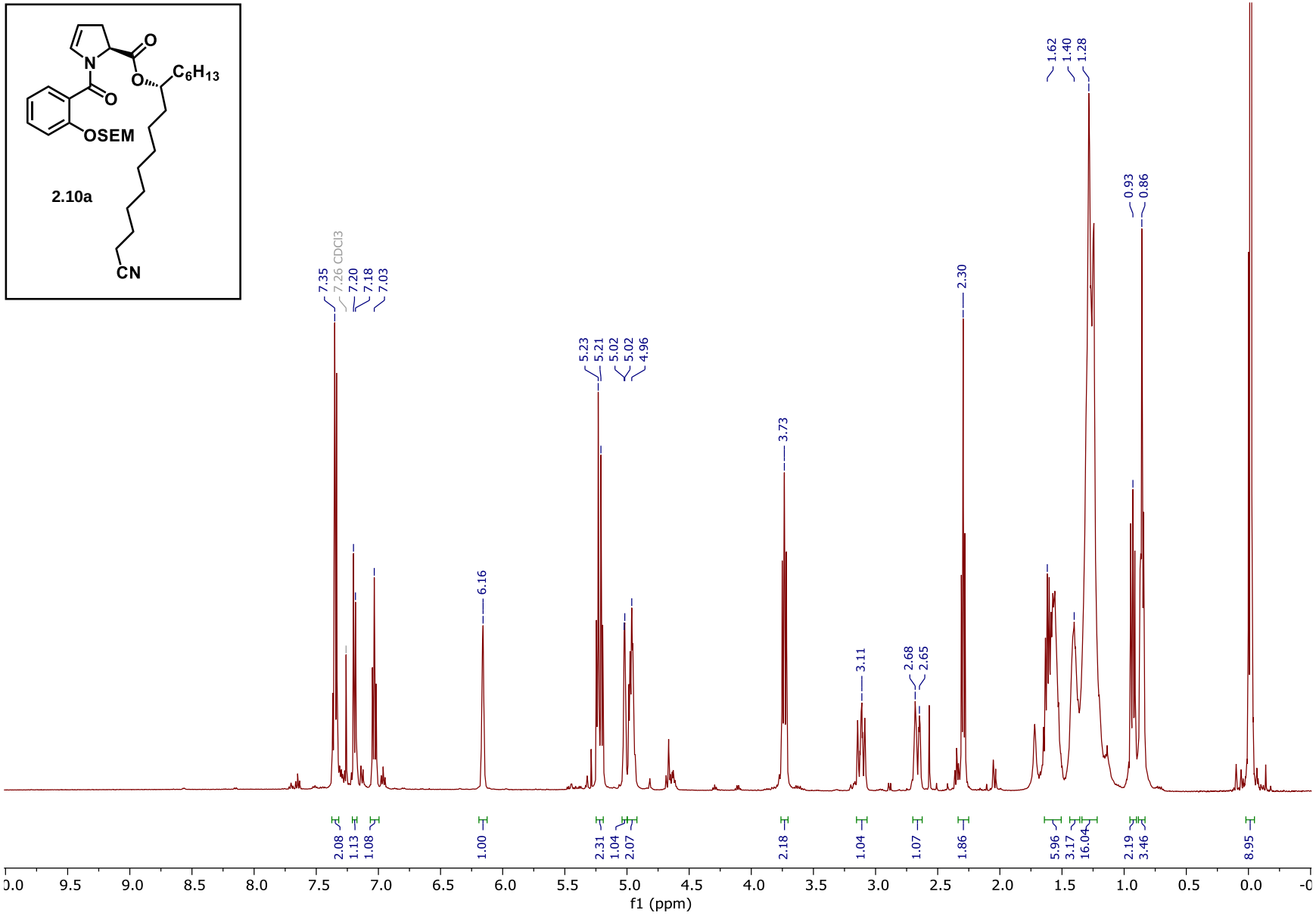
O
N
O
O
C_6H_{13}
O
OSEM
2.10a
CN
7.35
7.26 CDCl3
7.20
7.18
7.03
6.16
5.23
5.21
5.02
5.02
4.96
3.73
3.11
2.68
2.65
2.30
1.62
1.40
1.28
0.93
0.86
2.08
1.13
1.08
1.00
2.31
1.04
2.07
2.18
1.04
1.07
1.86
5.96
3.17
16.04
2.19
3.46
8.95
f1 (ppm)

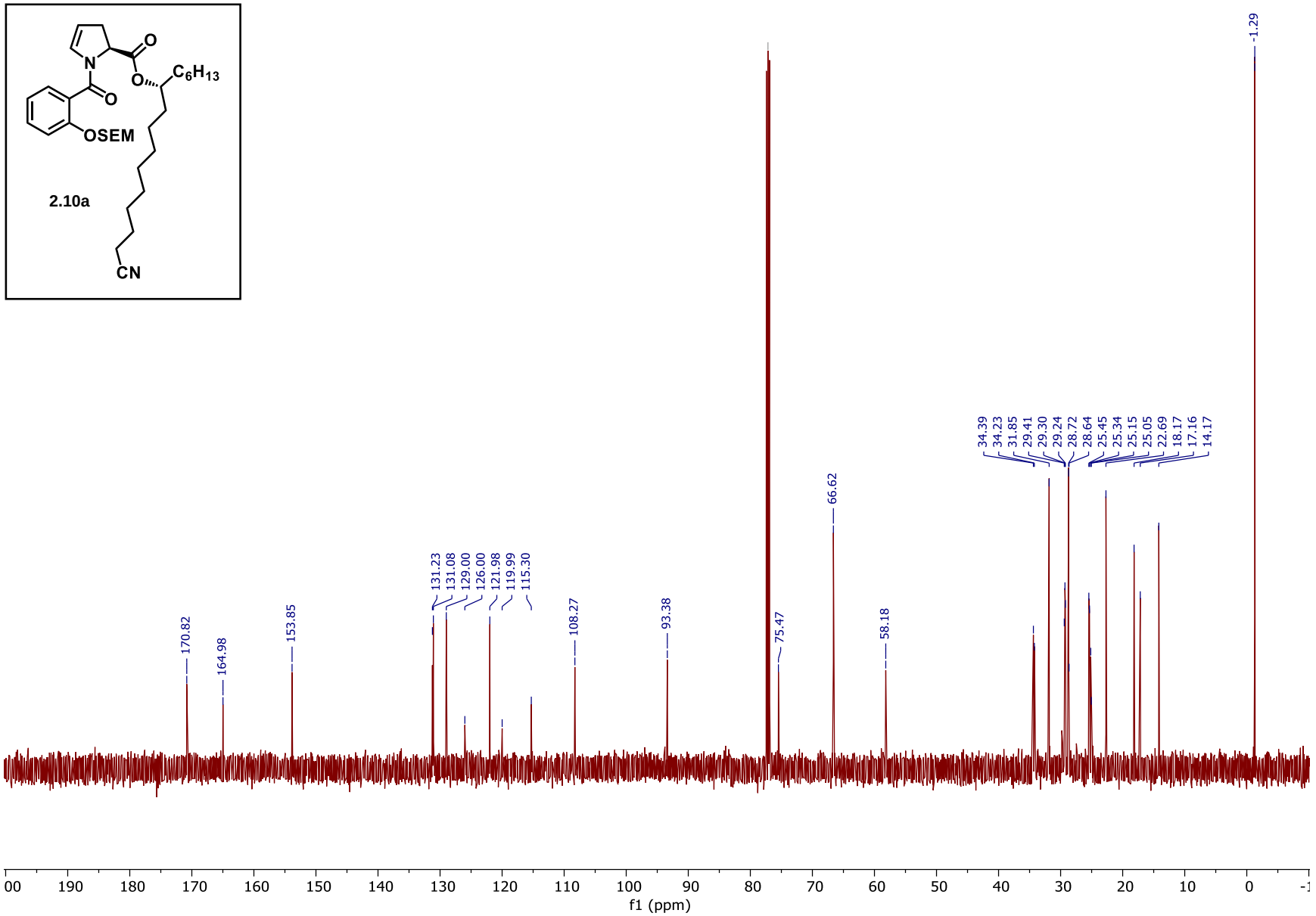
O
N
O
O
C_6H_{13}
OSEM
2.10a
CN
-1.29
34.39
34.23
31.85
29.41
29.30
29.24
28.72
28.64
25.45
25.34
25.15
25.05
22.69
18.17
17.16
14.17
66.62
131.23
131.08
129.00
126.00
121.98
119.99
115.30
170.82
164.98
153.85
108.27
93.38
75.47
58.18
f1 (ppm)

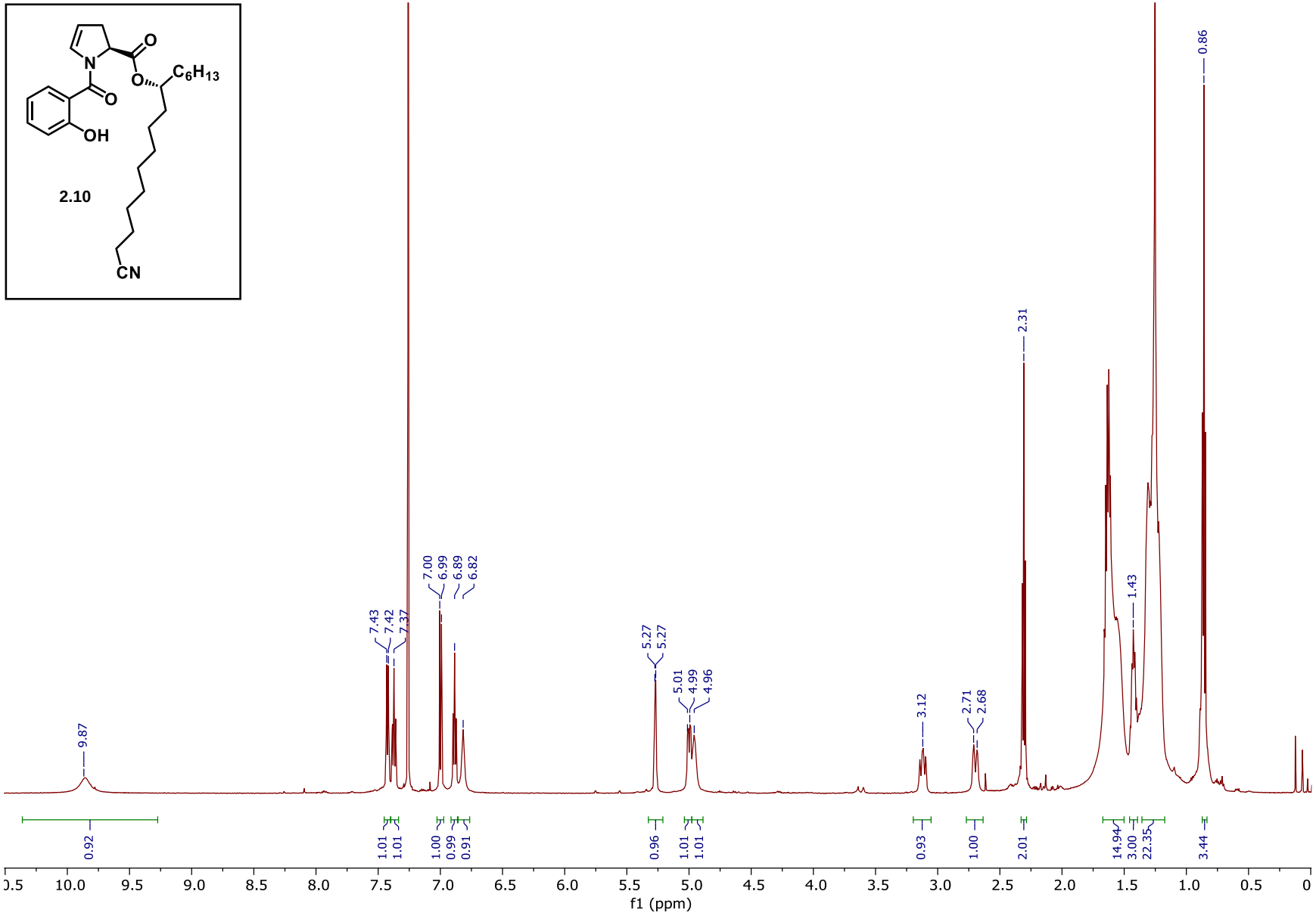
2.10
CN
9.87
7.43
7.42
7.37
7.00
6.99
6.89
6.82
5.27
5.27
5.01
4.99
4.96
3.12
2.71
2.68
2.31
1.43
0.86
0.92
1.01
1.01
1.00
0.99
0.91
0.96
1.01
1.01
0.93
1.00
2.01
14.94
3.00
22.35
3.44
f1 (ppm)

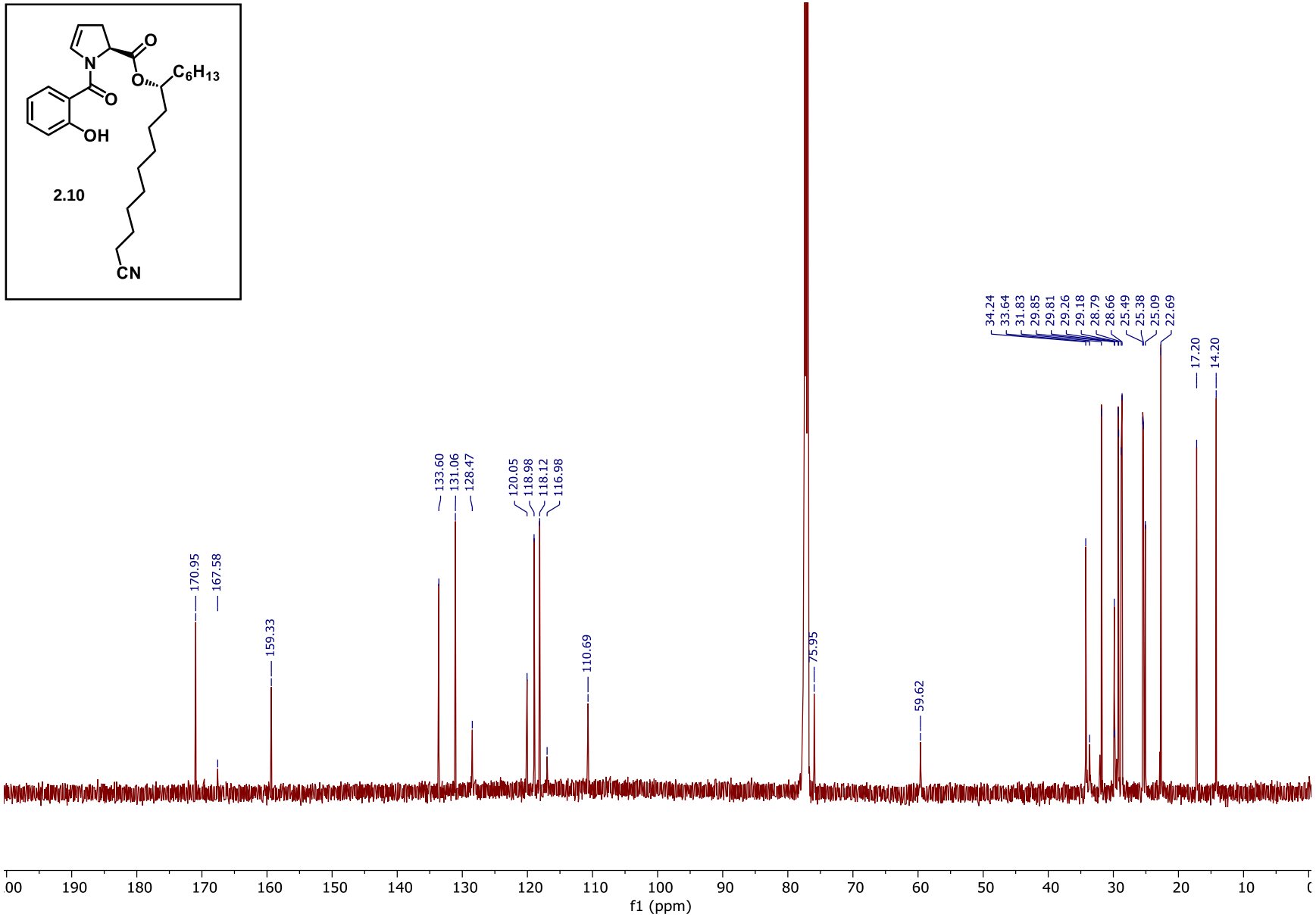
O
N
O
O
C_6H_{13}
OH
2.10
CN
34.24
33.64
31.83
29.85
29.81
29.26
29.18
28.79
28.66
25.49
25.38
25.09
22.69
17.20
14.20
133.60
131.06
128.47
120.05
118.98
118.12
116.98
170.95
167.58
159.33
110.69
75.95
59.62
f1 (ppm)

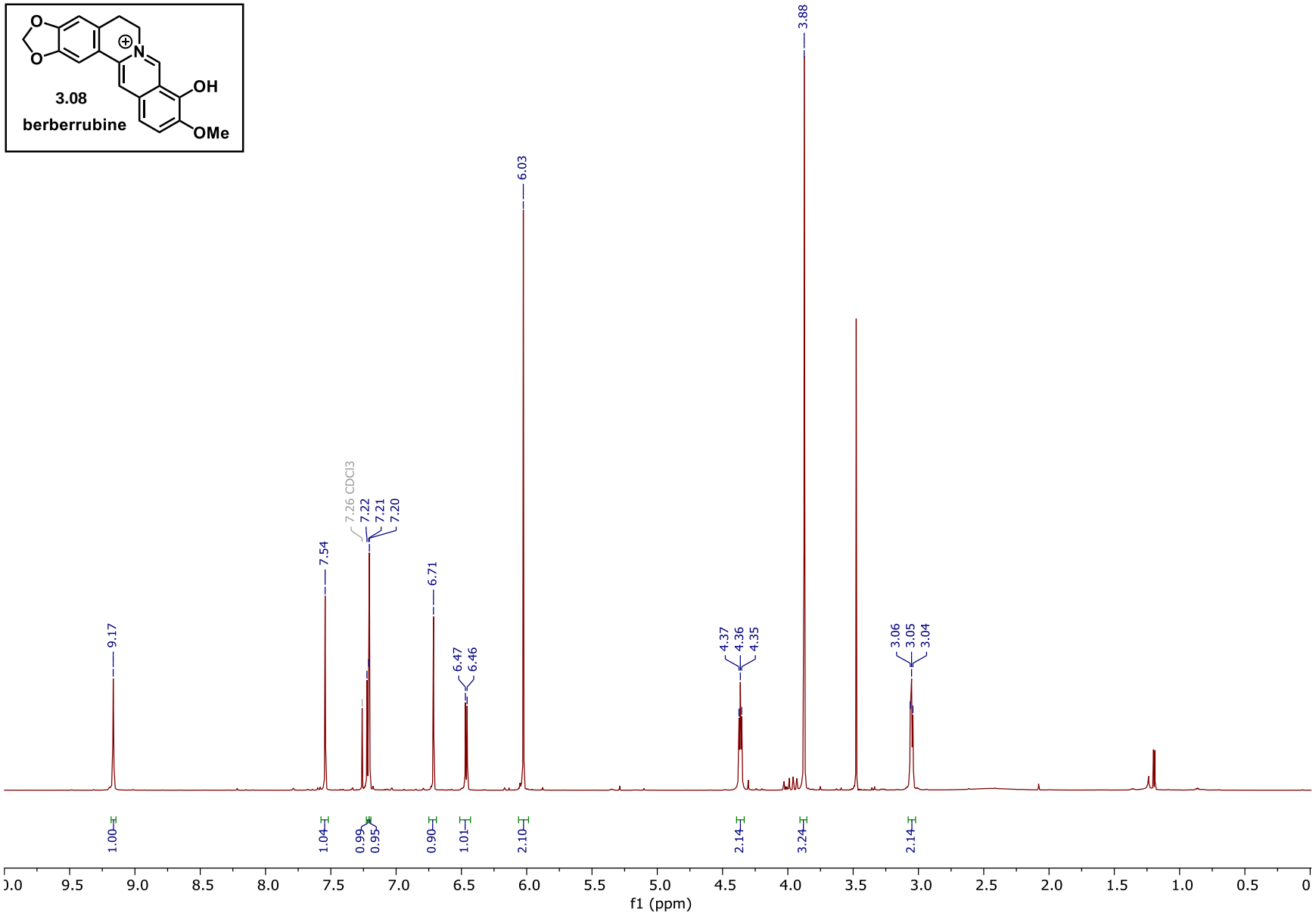
3.08
berberrubine
OH
OMe
9.17
7.54
7.26 CDCl3
7.22
7.21
7.20
6.71
6.47
6.46
6.03
4.37
4.36
4.35
3.88
3.06
3.05
3.04
1.00
1.04
0.99
0.95
0.90
1.01
2.10
2.14
3.24
2.14
f1 (ppm)

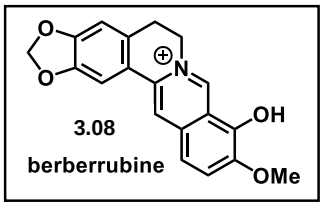

3.08
berberrubine

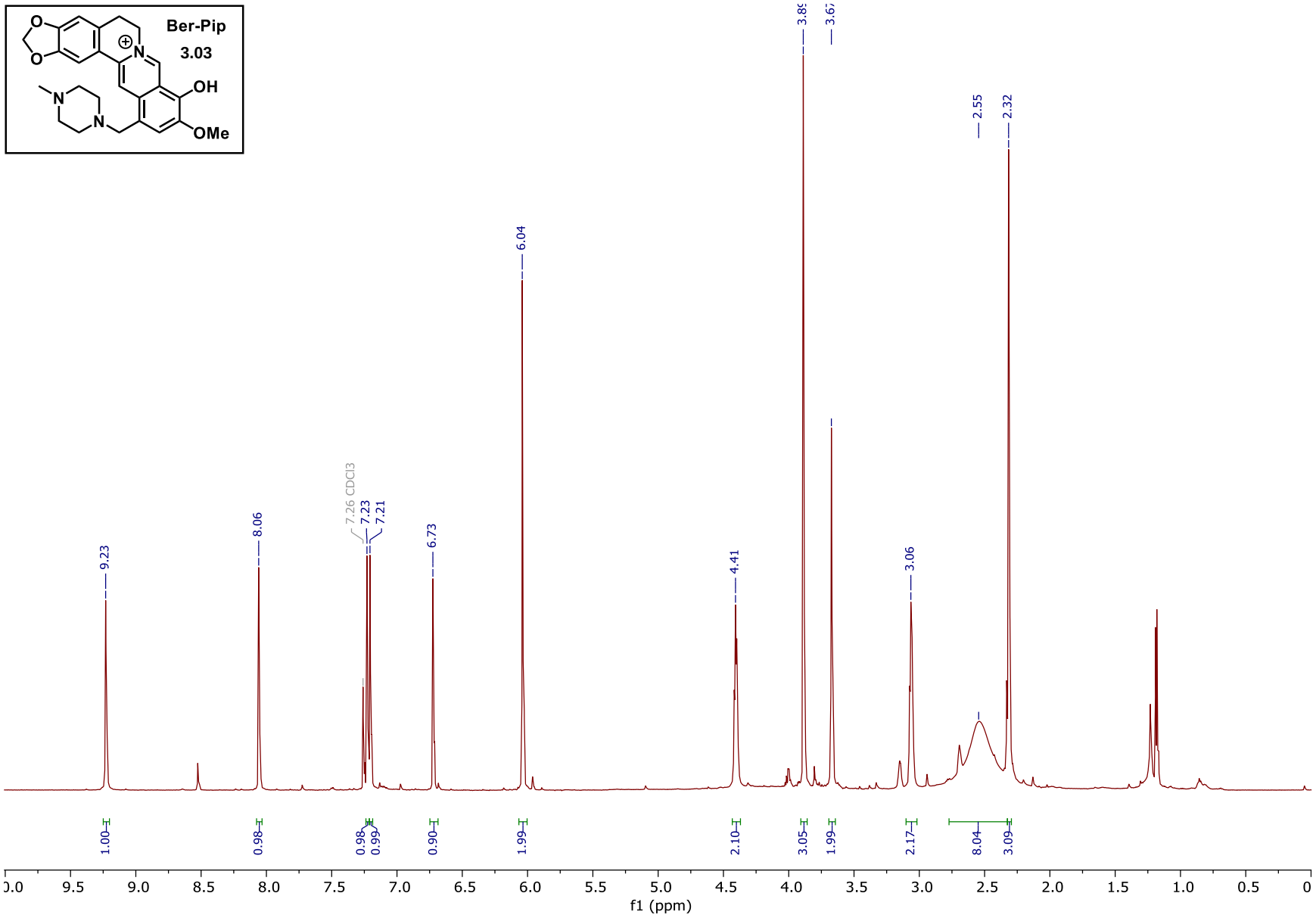
Ber-Pip
3.03
OH
OMe
9.23
8.06
7.26 CDCl3
7.23
7.21
6.73
6.04
4.41
3.85
3.67
3.06
2.55
2.32
1.00
0.98
0.98
0.99
0.90
1.99
2.10
3.05
1.99
2.17
8.04
3.09
f1 (ppm)

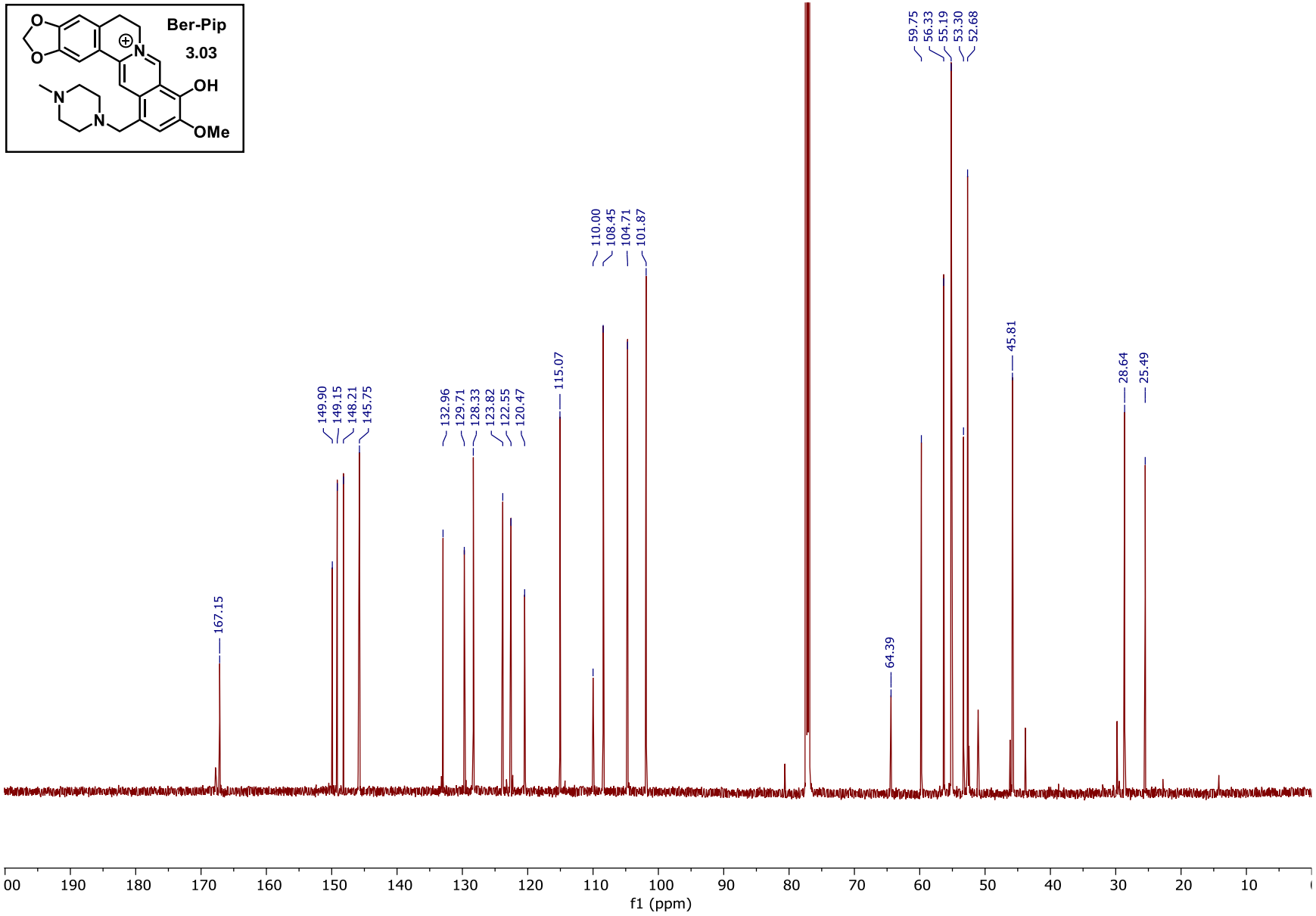
Ber-Pip
3.03
OH
OMe
167.15
149.90
149.15
148.21
145.75
132.96
129.71
128.33
123.82
122.55
120.47
115.07
110.00
108.45
104.71
101.87
64.39
59.75
56.33
55.19
53.30
52.68
45.81
28.64
25.49
f1 (ppm)

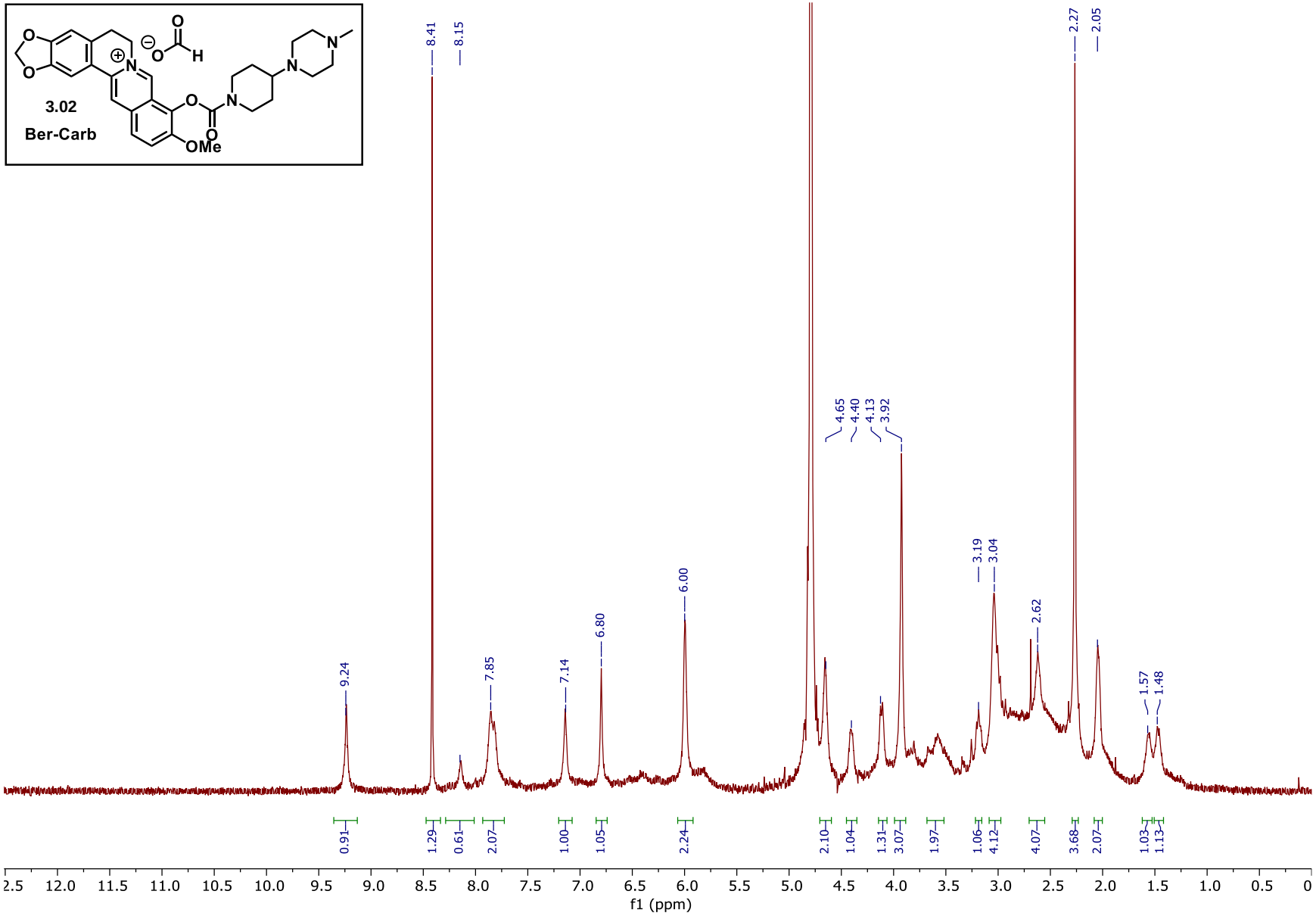
3.02
Ber-Carb
OMe
8.41
8.15
2.27
2.05
4.65
4.40
4.13
3.92
3.19
3.04
6.00
6.80
2.62
9.24
7.85
7.14
1.57
1.48
0.91
1.29
0.61
2.07
1.00
1.05
2.24
2.10
1.04
1.31
3.07
1.97
1.06
4.12
4.07
3.68
2.07
1.03
1.13
f1 (ppm)

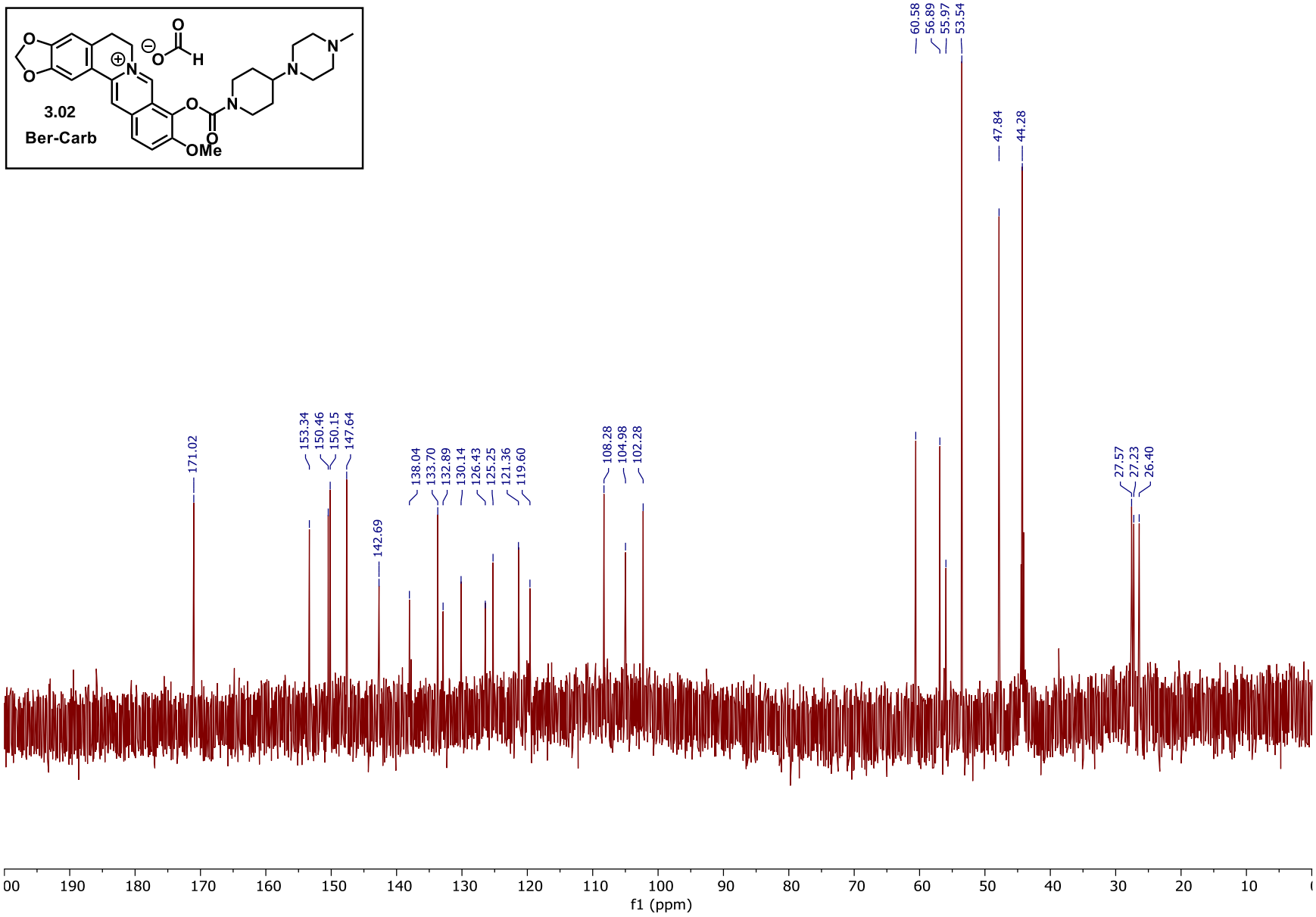
3.02
Ber-Carb
OMe
60.58
56.89
55.97
53.54
47.84
44.28
171.02
153.34
150.46
150.15
147.64
142.69
138.04
133.70
132.89
130.14
126.43
125.25
121.36
119.60
108.28
104.98
102.28
27.57
27.23
26.40
f1 (ppm)

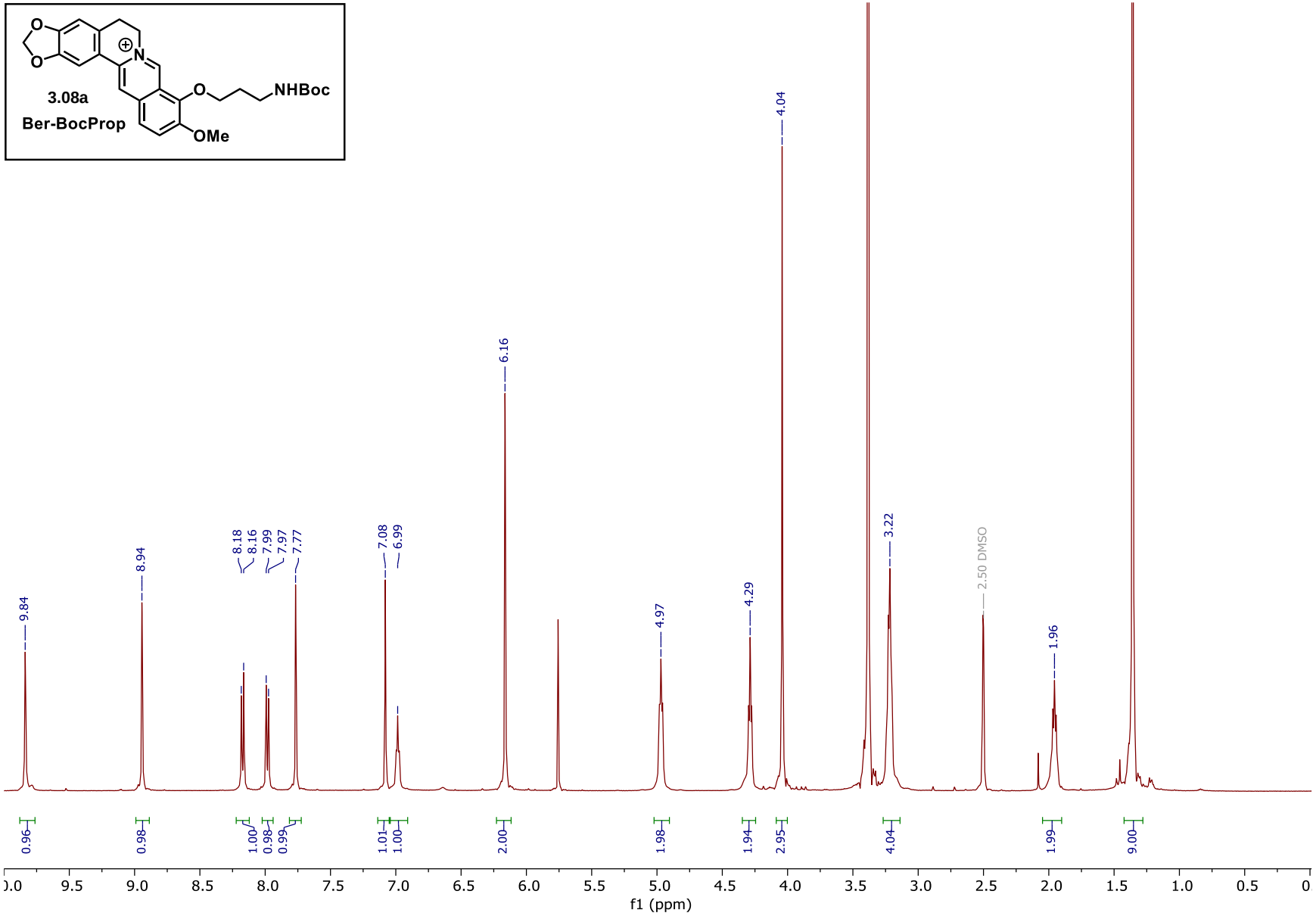
3.08a
Ber-BocProp
NHBoc
OMe
9.84
8.94
8.18
8.16
7.99
7.97
7.77
7.08
6.99
6.16
4.97
4.29
4.04
3.22
2.50 DMSO
1.96
0.96
0.98
1.00
0.98
0.99
1.01
1.00
2.00
1.98
1.94
2.95
4.04
1.99
9.00
f1 (ppm)

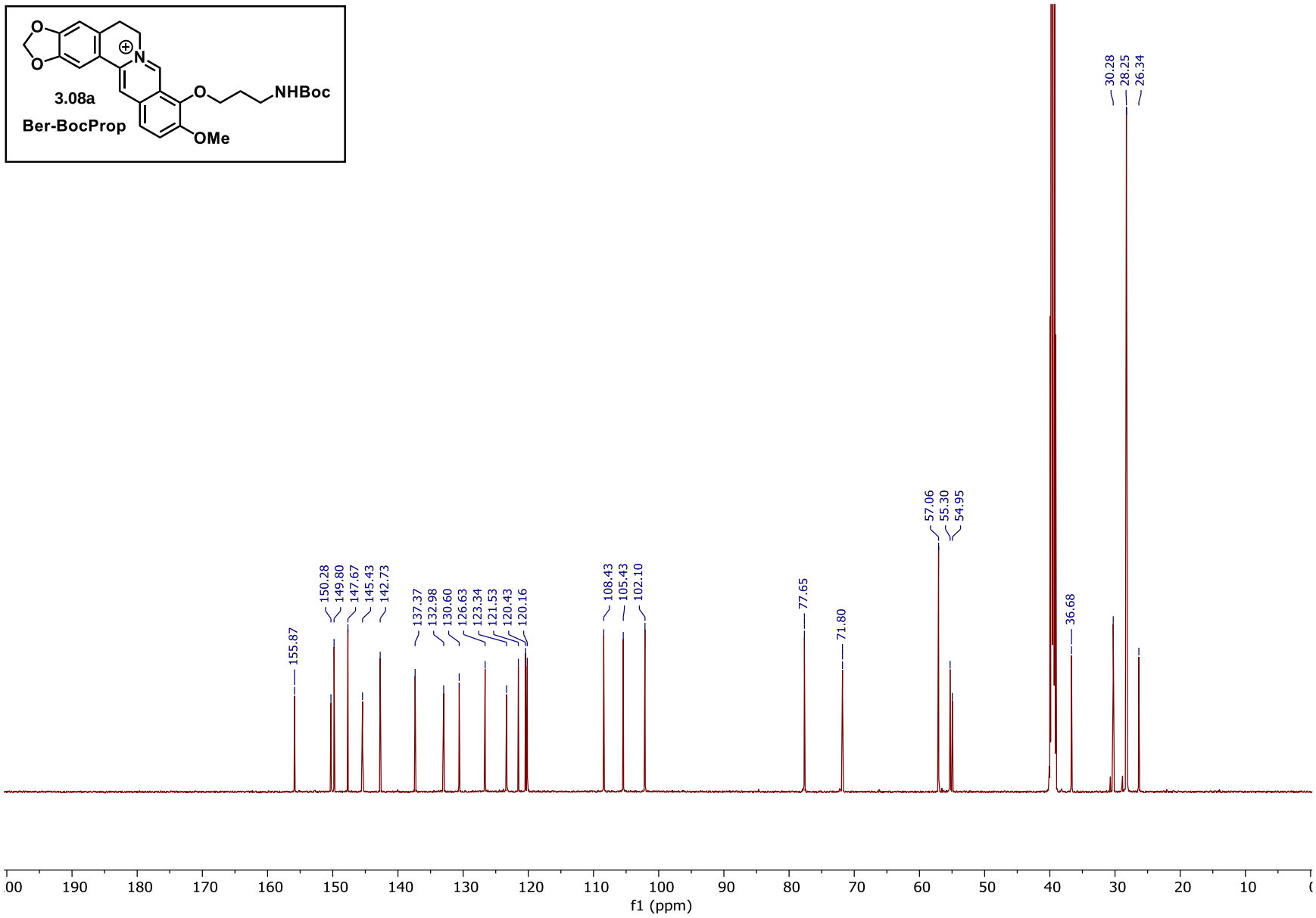
3.08a
Ber-BocProp
NHBoc
OMe
155.87
150.28
149.80
147.67
145.43
142.73
137.37
132.98
130.60
126.63
123.34
121.53
120.43
120.16
108.43
105.43
102.10
77.65
71.80
57.06
55.30
54.95
36.68
30.28
28.25
26.34
f1 (ppm)

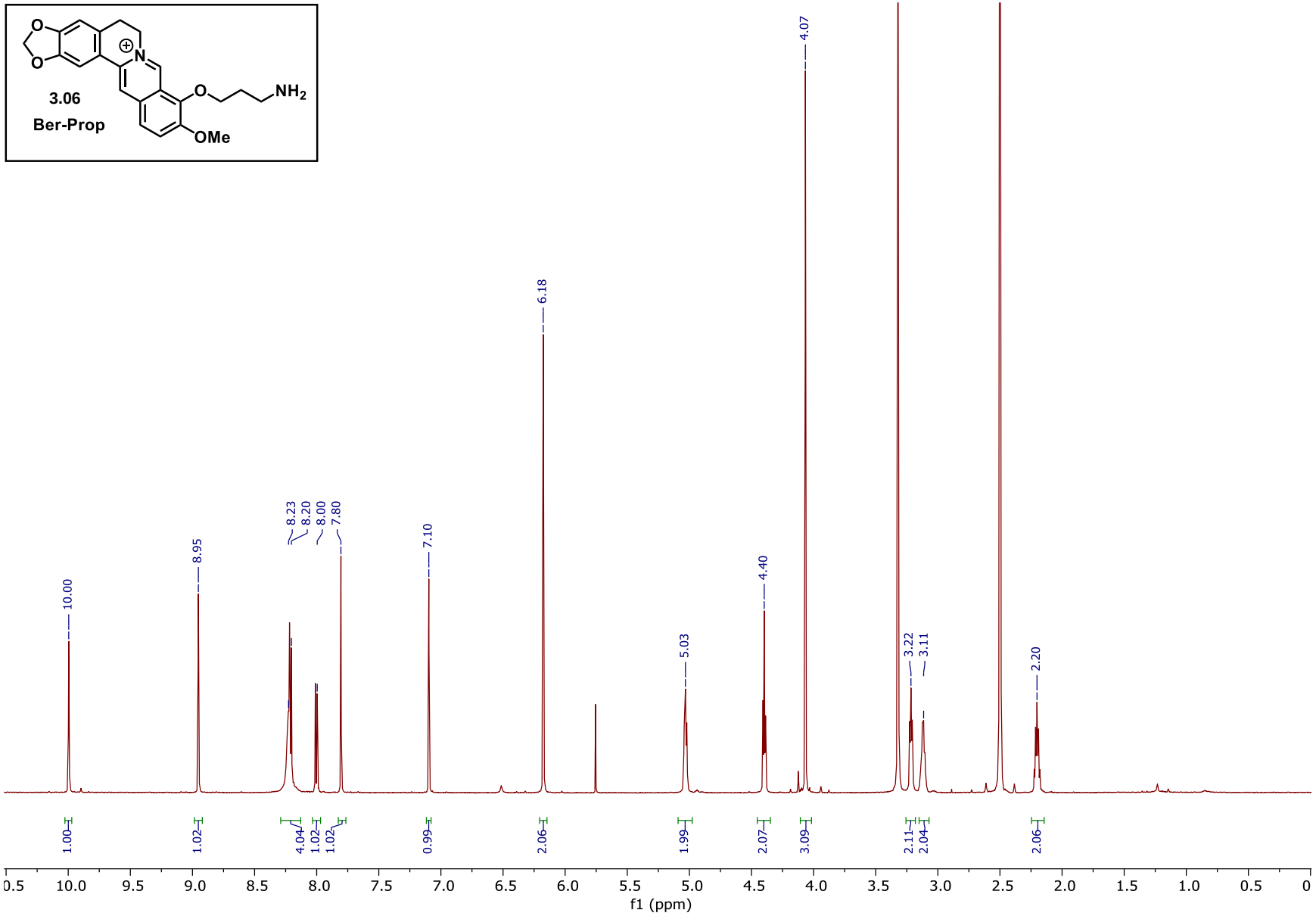
3.06
Ber-Prop
OMe
NH2
10.00
8.95
8.23
8.20
8.00
7.80
7.10
6.18
5.03
4.40
4.07
3.22
3.11
2.20
1.00
1.02
4.04
1.02
1.02
0.99
2.06
1.99
2.07
3.09
2.11
2.04
2.06
f1 (ppm)

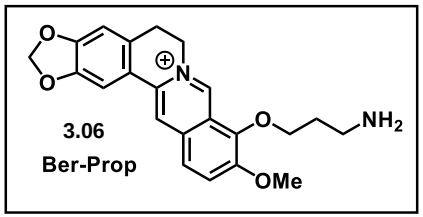
O
O
N
O
NH2
OMe

3.06
Ber-Prop

150.17
149.83
147.69
145.47
142.65
137.48
132.95
130.72
126.62
123.48
121.44
120.44
120.18
108.44
105.42
102.09
71.55
57.11
55.11
36.15
27.81
26.31
00
190
180
170
160
150
140
130
120
110
100
90
80
70
60
50
40
30
20
10
f1 (ppm)

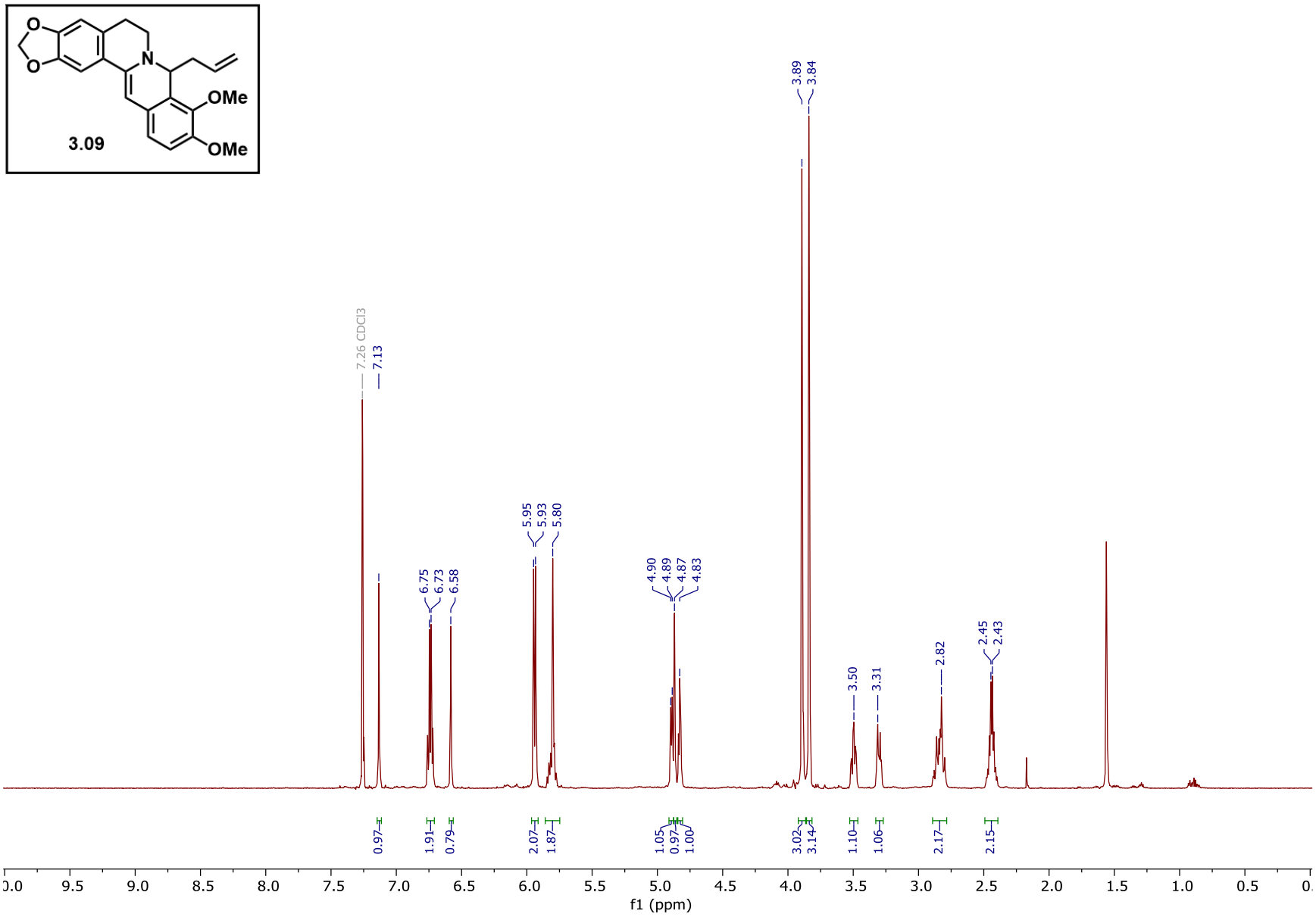
O
O
N
OMe
OMe
3.09
7.26 CDCl3
7.13
6.75
6.73
6.58
5.95
5.93
5.80
4.90
4.89
4.87
4.83
3.89
3.84
3.50
3.31
2.82
2.45
2.43
0.97
1.91
0.79
2.07
1.87
1.05
0.97
1.00
3.02
3.14
1.10
1.06
2.17
2.15
f1 (ppm)

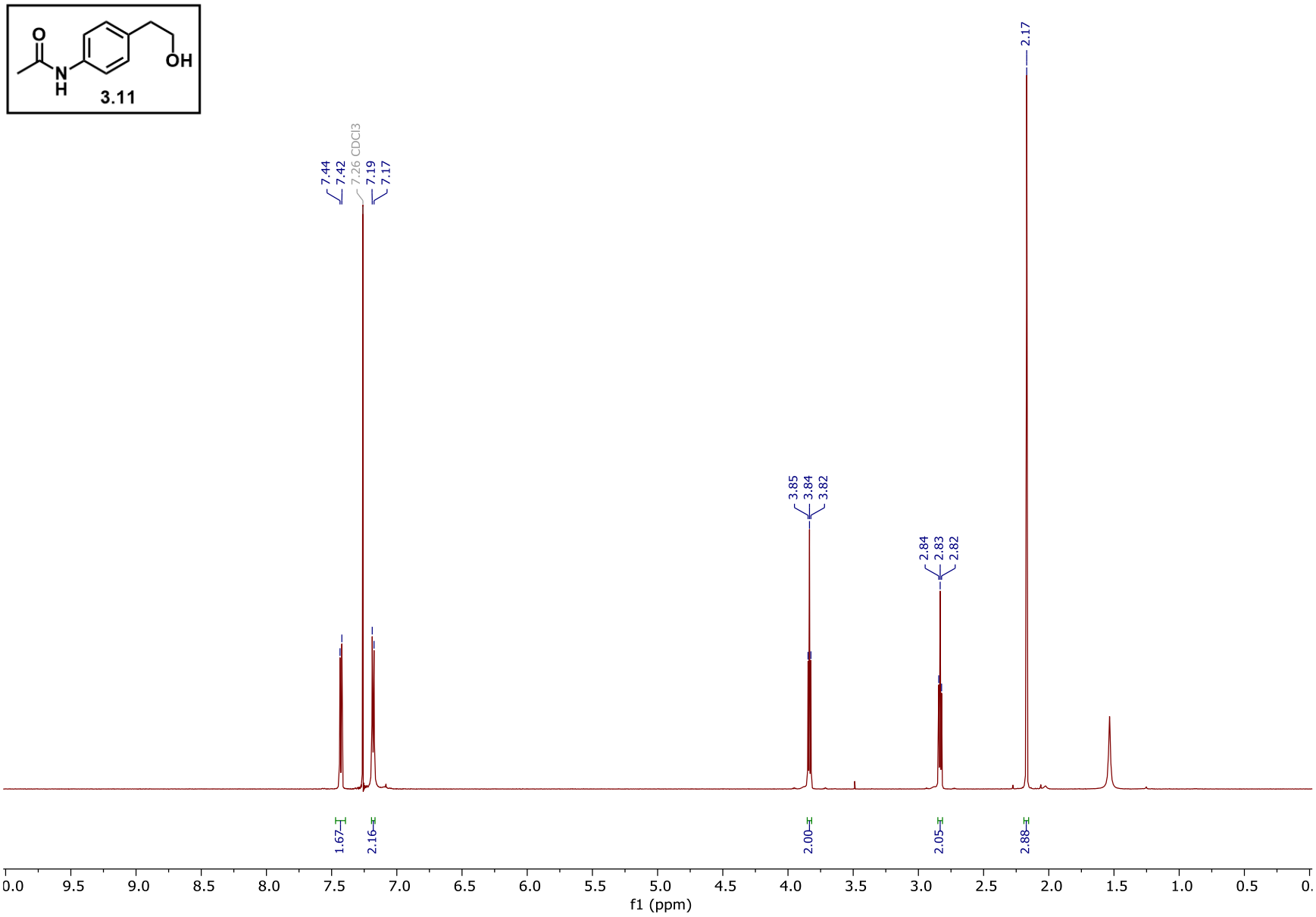
O
N
H
OH
3.11
7.44
7.42
7.26 CDCl3
7.19
7.17
3.85
3.84
3.82
2.84
2.83
2.82
2.17
1.67
2.16
2.00
2.05
2.88
f1 (ppm)

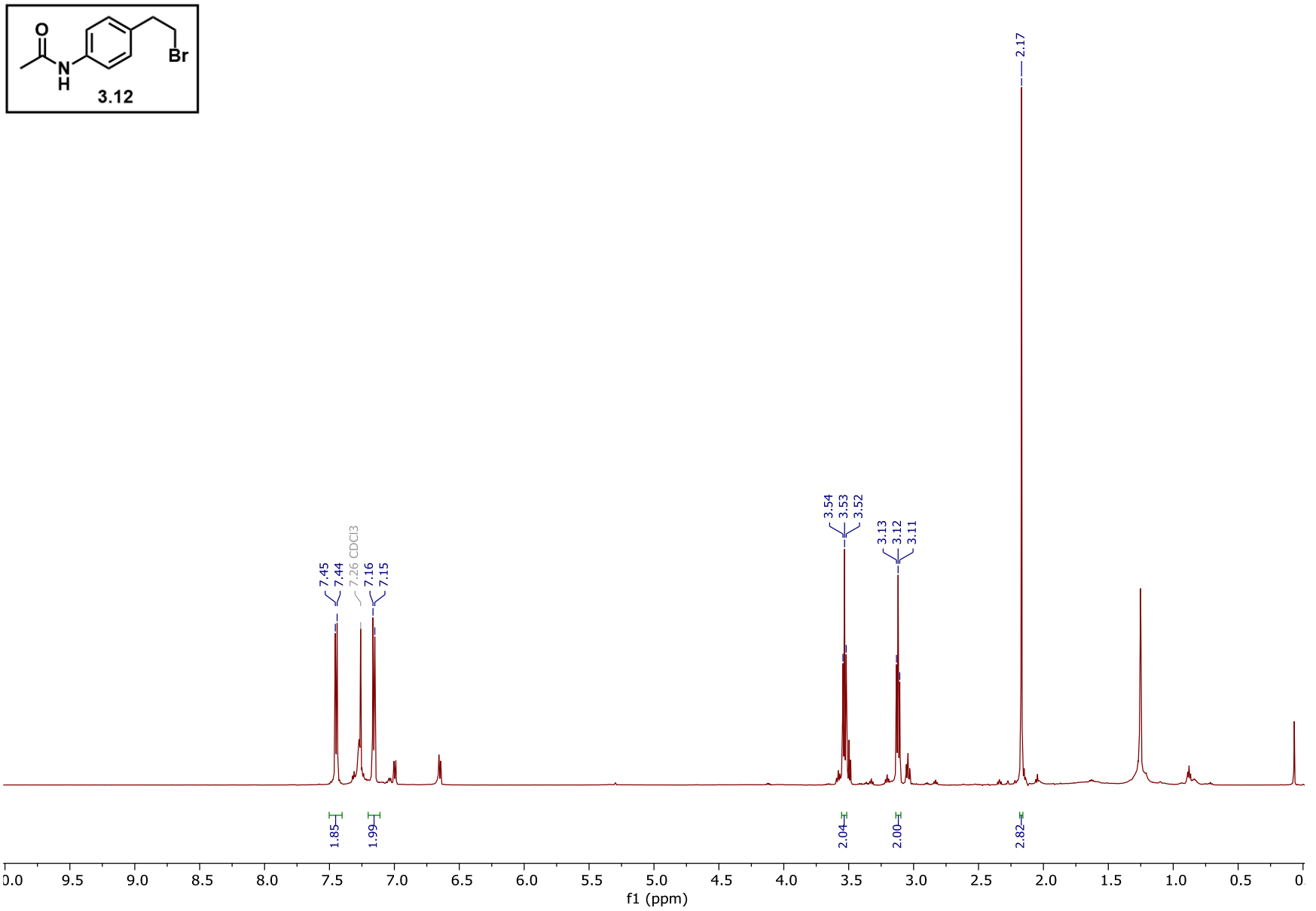
O
N
H
Br
3.12
2.17
3.54
3.53
3.52
3.13
3.12
3.11
7.45
7.44
7.26 CDCl3
7.16
7.15
1.85
1.99
2.04
2.00
2.82
f1 (ppm)

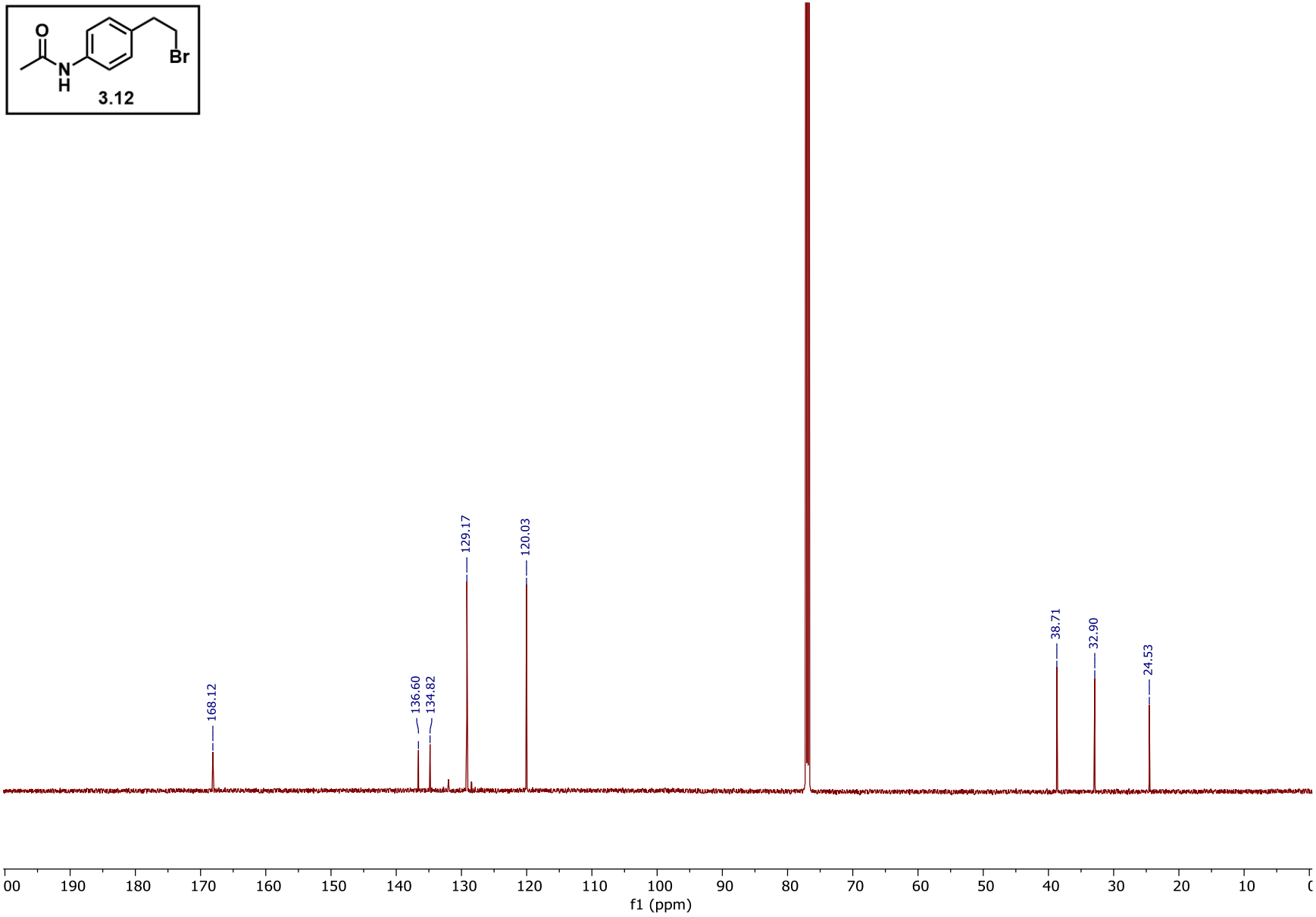
O
N
H
Br
3.12
168.12
136.60
134.82
129.17
120.03
38.71
32.90
24.53
f1 (ppm)

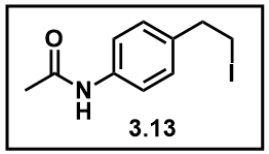
O
N
H
I
3.13

7.59
7.45
7.44
7.26 CDCl3
7.13
7.11
3.32
3.30
3.29
3.13
3.12
3.11
1.01
1.93
2.00
2.07
2.09
3.04
f1 (ppm)

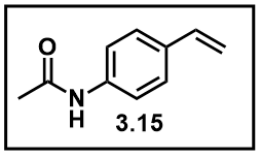
O
N
H
3.15

2.16
7.55
7.48
7.46
7.36
7.34
7.26 CDCl3
6.69
6.67
6.66
6.64
5.69
5.66
5.20
5.18
0.96
1.94
2.00
0.93
1.13
1.06
3.00
f1 (ppm)

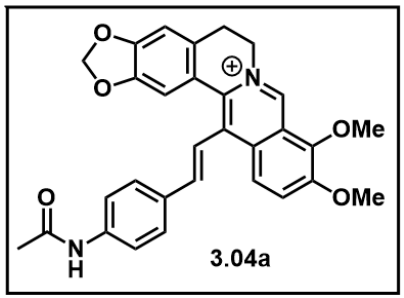
O
O
N
OMe
OMe
O
N
H
3.04a

10.17
9.89
8.94
8.39
8.19
8.13
8.09
7.82
7.80
7.71
7.69
7.57
7.09
6.19
4.95
4.17
4.10
3.21
2.50 DMSO
2.08
1.00
1.01
1.08
1.01
1.13
1.01
2.32
2.02
1.07
1.21
2.17
2.09
3.00
3.03
2.30
3.08
1.0
10.5
10.0
9.5
9.0
8.5
8.0
7.5
7.0
6.5
6.0
5.5
5.0
4.5
4.0
3.5
3.0
2.5
2.0
1.5
1.
f1 (ppm)

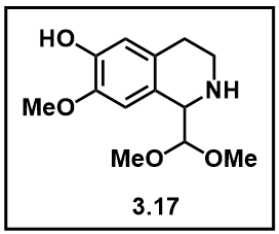
HO
MeO
NH
MeO
OMe

3.17

7.26 CDCl3
6.92
6.64
4.45
4.44
4.02
4.00
3.23
3.01
2.75
1.00
0.91
0.10
1.06
1.05
3.25
3.02
2.94
1.15
1.12
2.03
f1 (ppm)

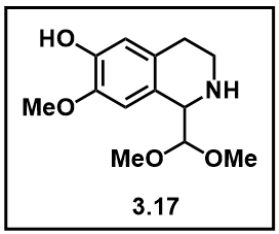
HO
MeO
NH
MeO
OMe

3.17

144.92
144.68
128.59
124.65
114.62
110.66
107.07
56.48
56.38
56.14
55.31
40.73
28.72
20
210
200
190
180
170
160
150
140
130
120
110
100
90
80
70
60
50
40
30
20
10
0
-10
f1 (ppm)

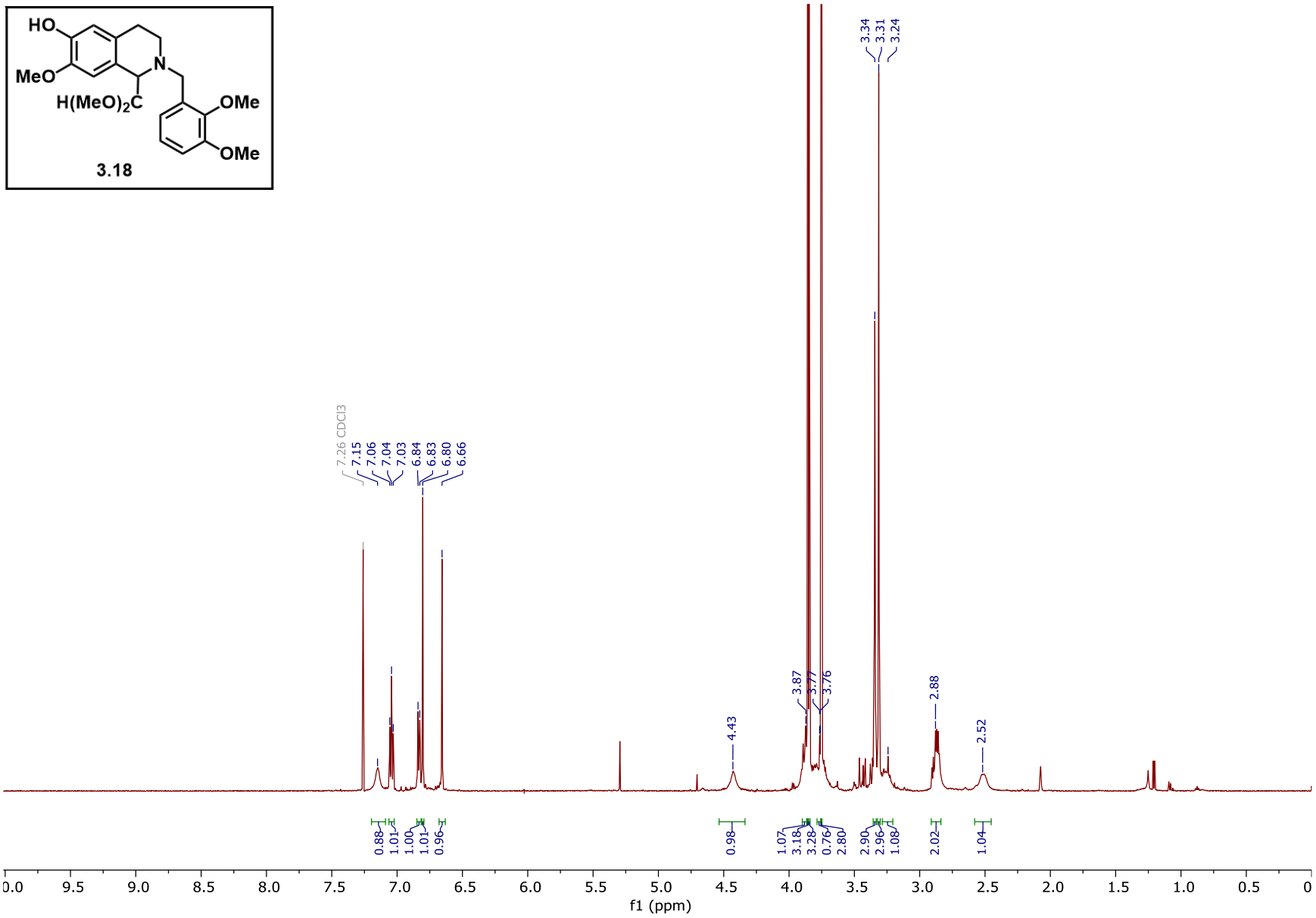
HO
MeO
H(MeO)2C
N
OMe
OMe
3.18
7.26 CDCl3
7.15
7.06
7.04
7.03
6.84
6.83
6.80
6.66
3.34
3.31
3.24
4.43
3.87
3.77
3.76
2.88
2.52
0.88
1.01
1.00
1.01
0.96
0.98
1.07
3.18
3.28
0.76
2.80
2.90
2.96
1.08
2.02
1.04
f1 (ppm)

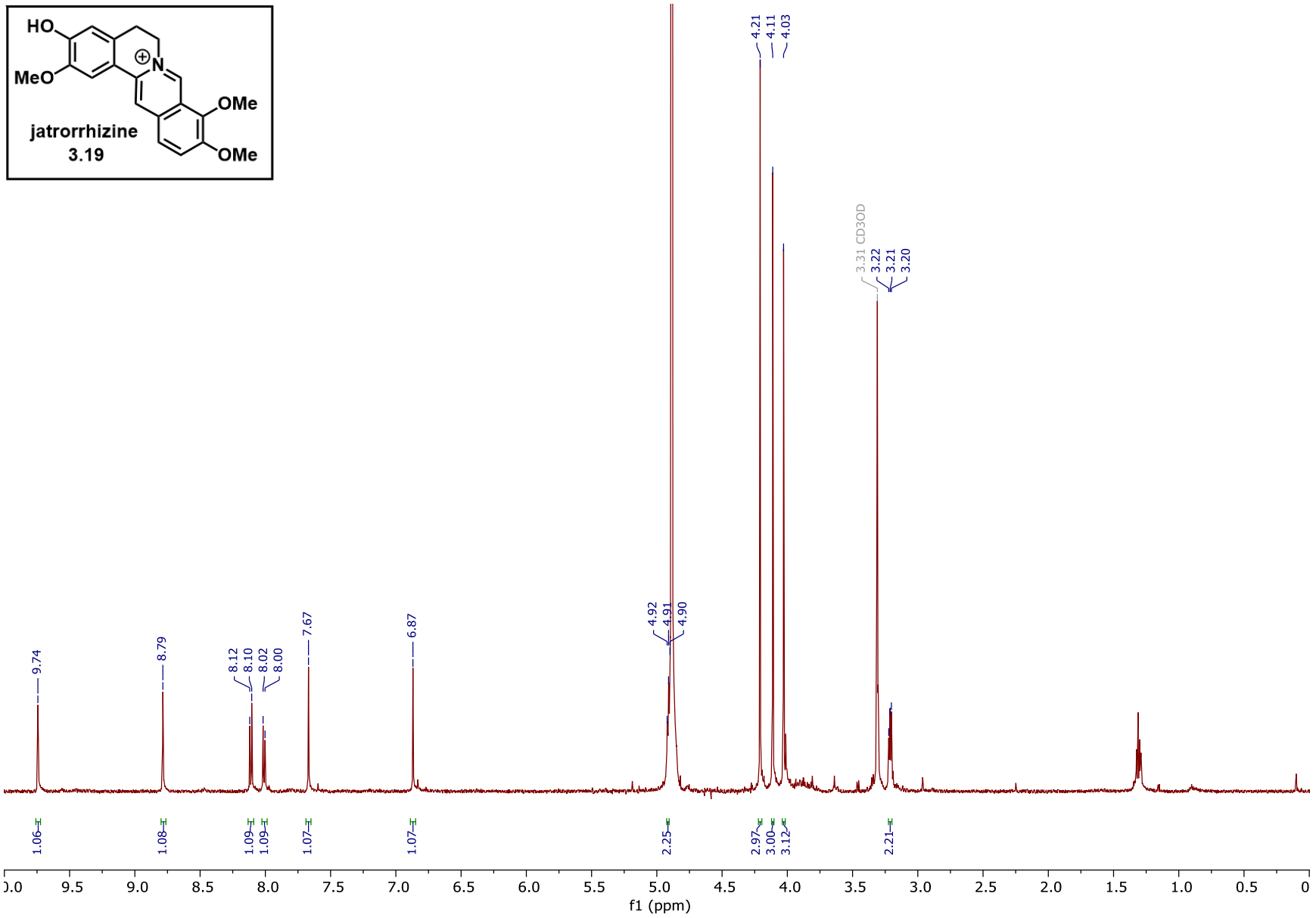
HO
MeO
N
OMe
OMe
jatrorrhizine
3.19
4.21
4.11
4.03
3.31 CD3OD
3.22
3.21
3.20
9.74
8.79
8.12
8.10
8.02
8.00
7.67
6.87
4.92
4.91
4.90
1.06
1.08
1.09
1.09
1.07
1.07
2.25
2.97
3.00
3.12
2.21
f1 (ppm)

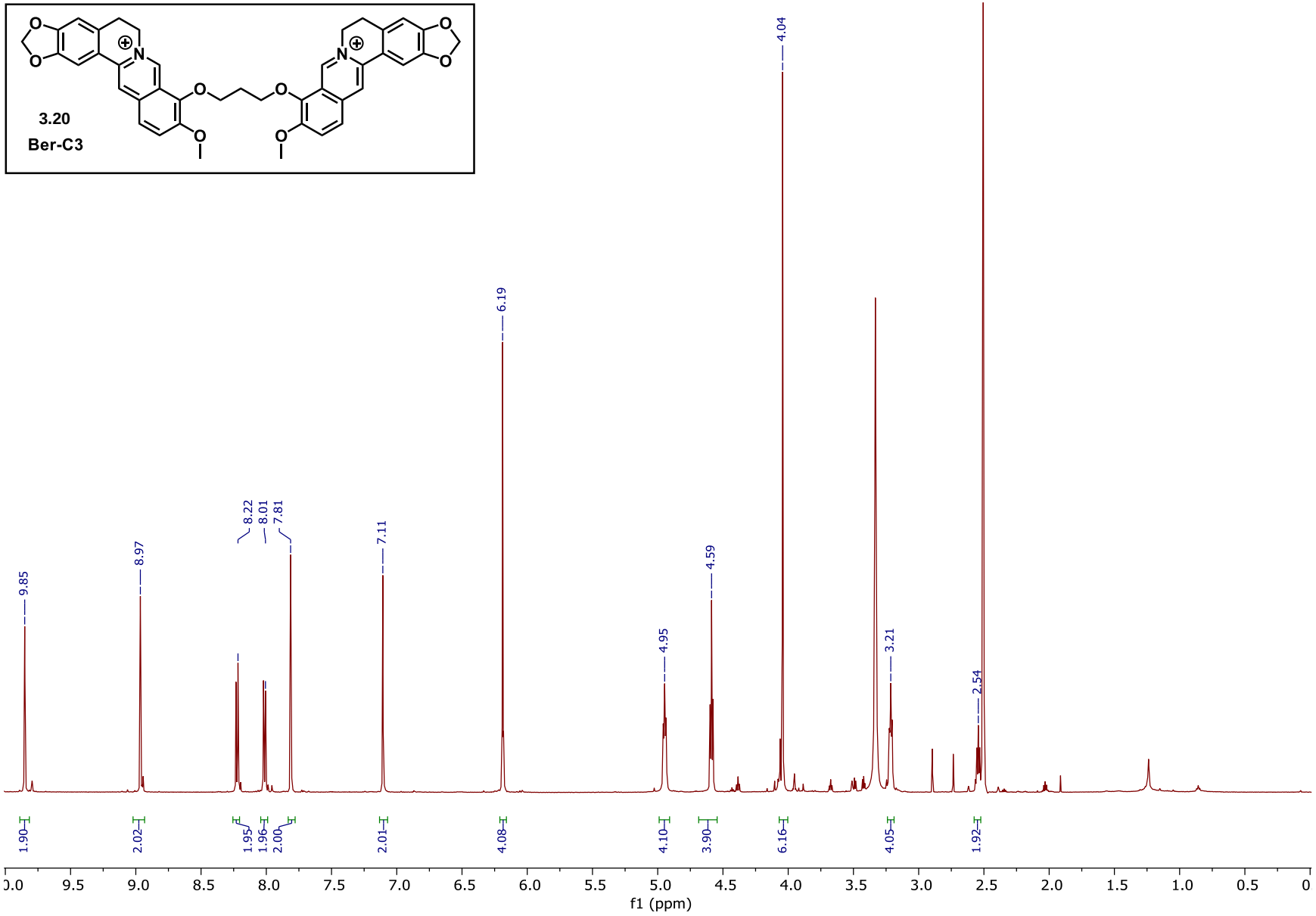
3.20
Ber-C3
9.85
8.97
8.22
8.01
7.81
7.11
6.19
4.95
4.59
4.04
3.21
2.54
1.90
2.02
1.95
1.96
2.00
2.01
4.08
4.10
3.90
6.16
4.05
1.92
f1 (ppm)

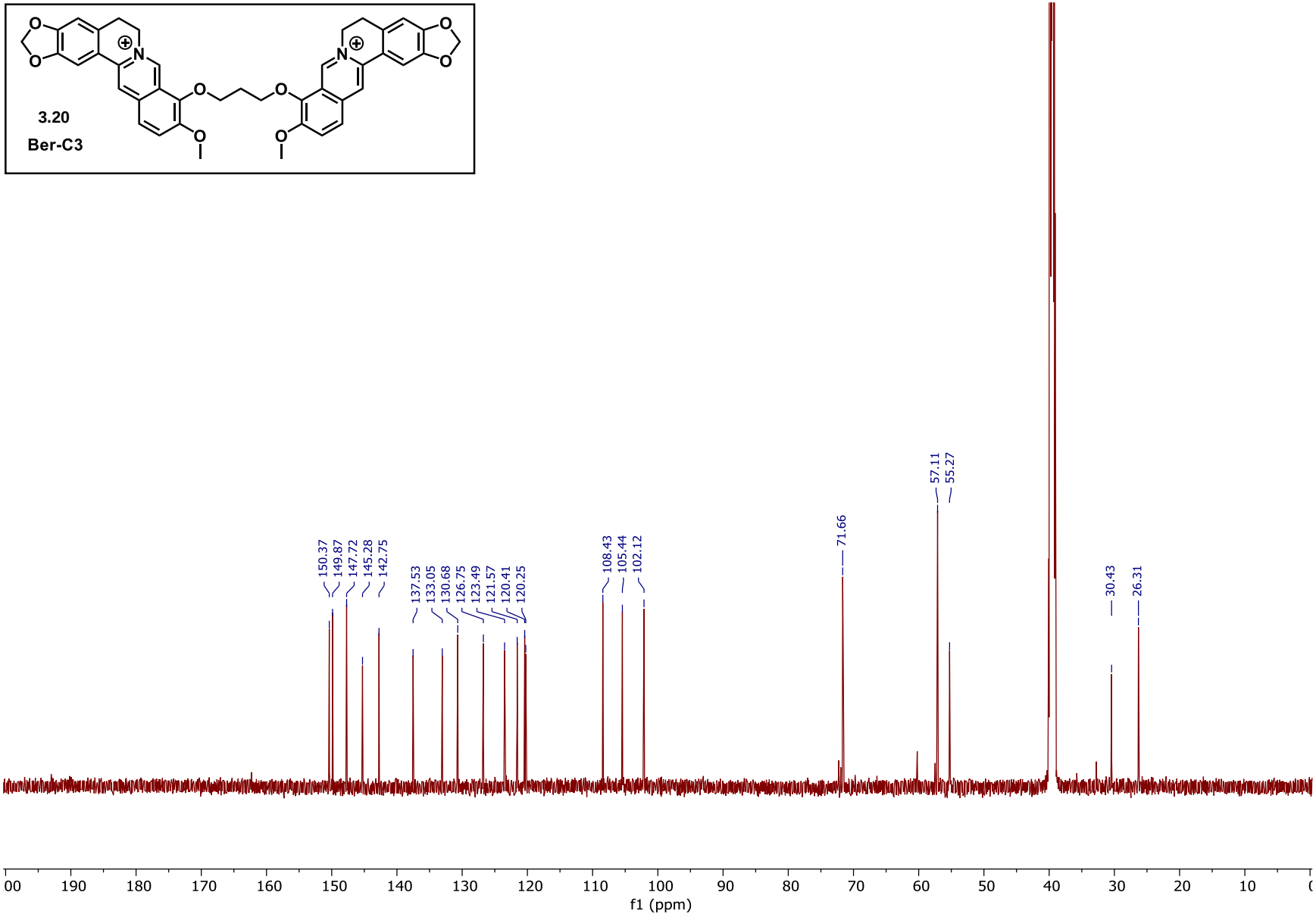
3.20
Ber-C3
150.37
149.87
147.72
145.28
142.75
137.53
133.05
130.68
126.75
123.49
121.57
120.41
120.25
108.43
105.44
102.12
71.66
57.11
55.27
30.43
26.31
f1 (ppm)

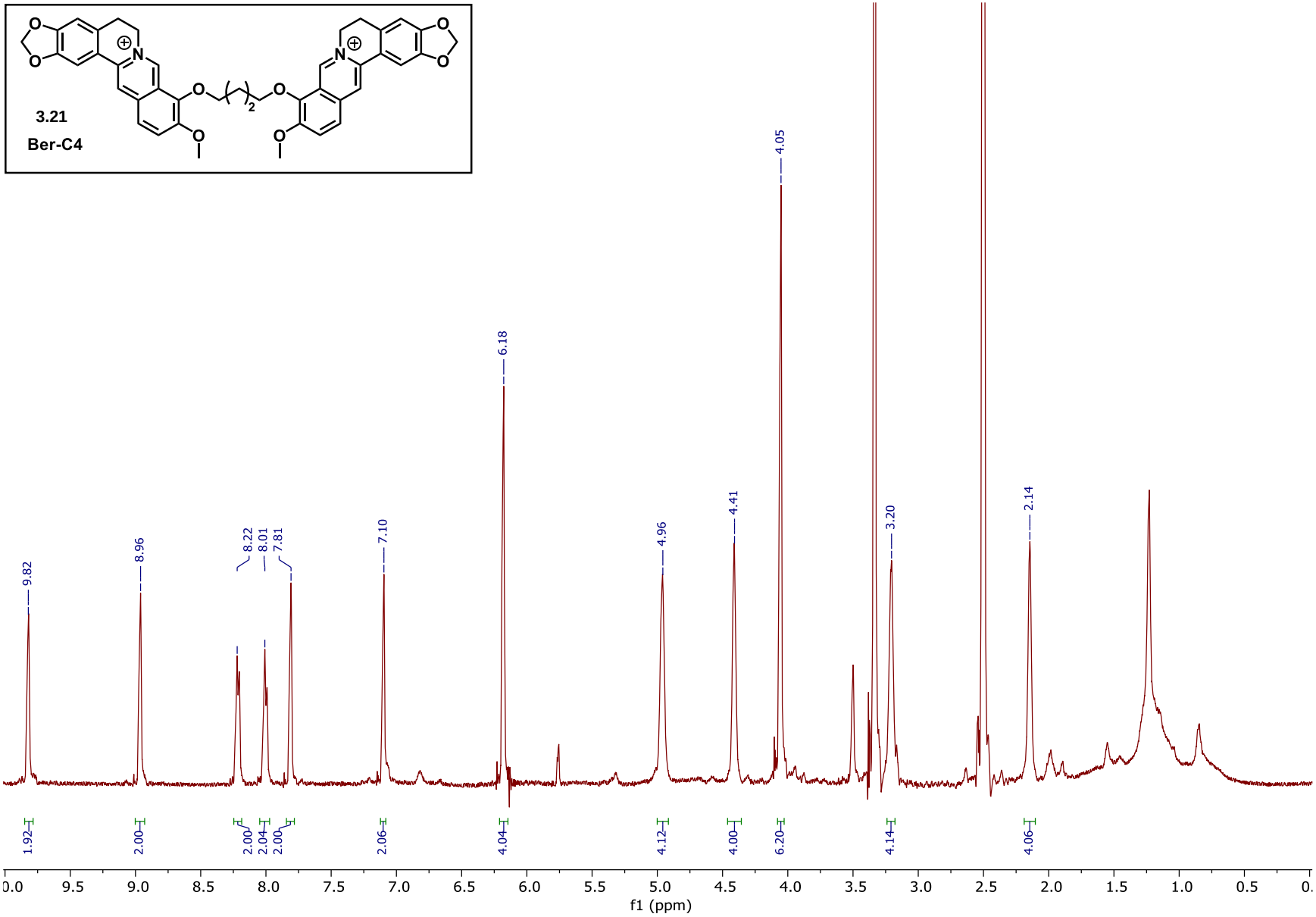
3.21
Ber-C4
9.82
8.96
8.22
8.01
7.81
7.10
6.18
4.96
4.41
4.05
3.20
2.14
1.92
2.00
2.00
2.04
2.00
2.06
4.04
4.12
4.00
6.20
4.14
4.06
f1 (ppm)

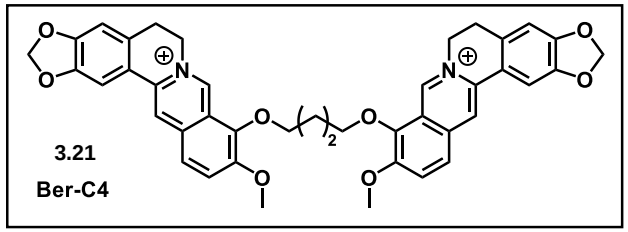
3.21
Ber-C4

150.90
150.32
148.18
145.76
143.17
137.97
133.47
131.16
127.10
123.92
122.11
120.91
120.73
108.92
105.90
102.61
76.98
74.41
57.51
55.78
26.58
f1 (ppm)

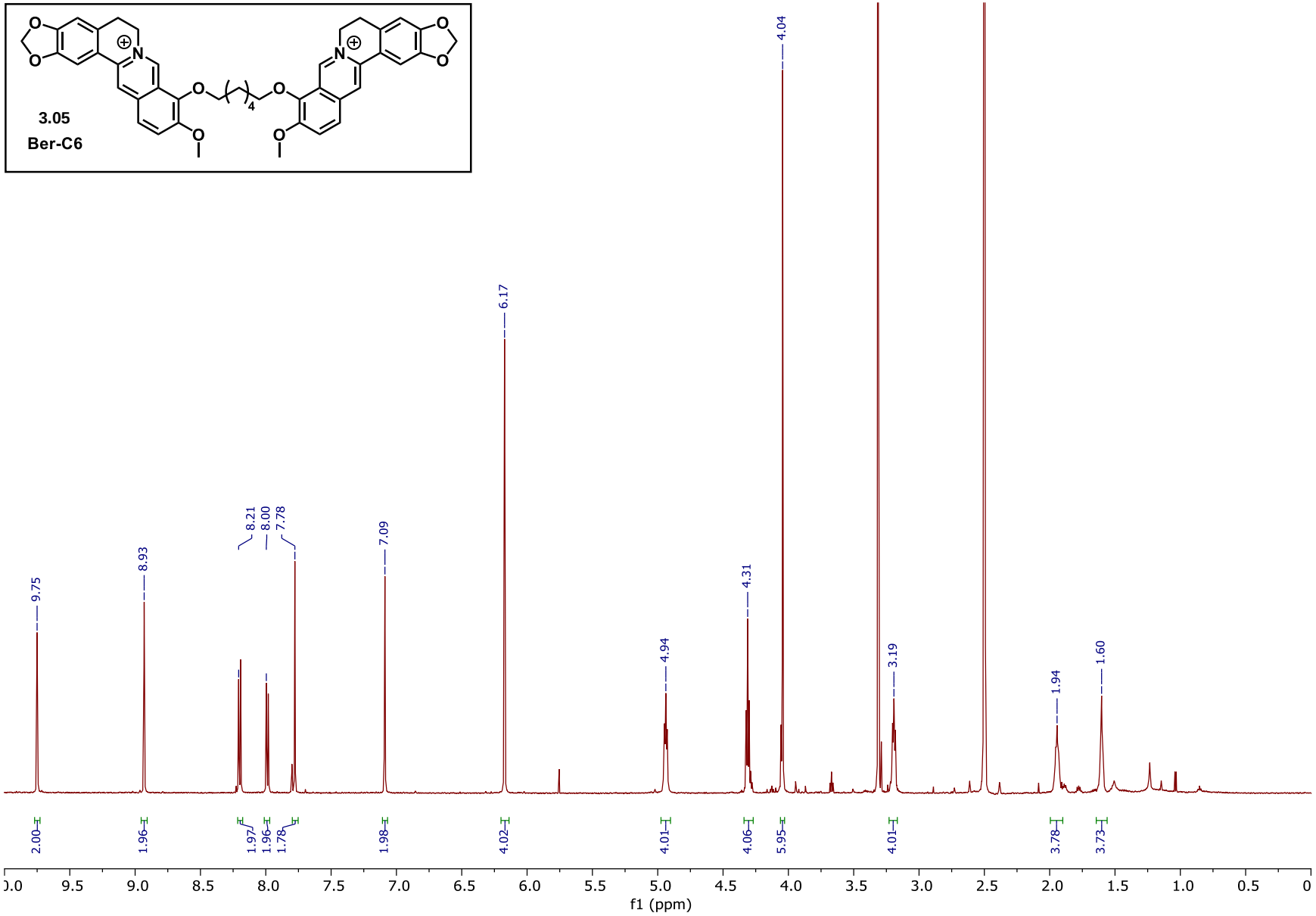
3.05
Ber-C6
9.75
8.93
8.21
8.00
7.78
7.09
6.17
4.94
4.31
4.04
3.19
1.94
1.60
2.00
1.96
1.97
1.96
1.78
1.98
4.02
4.01
4.06
5.95
4.01
3.78
3.73
f1 (ppm)

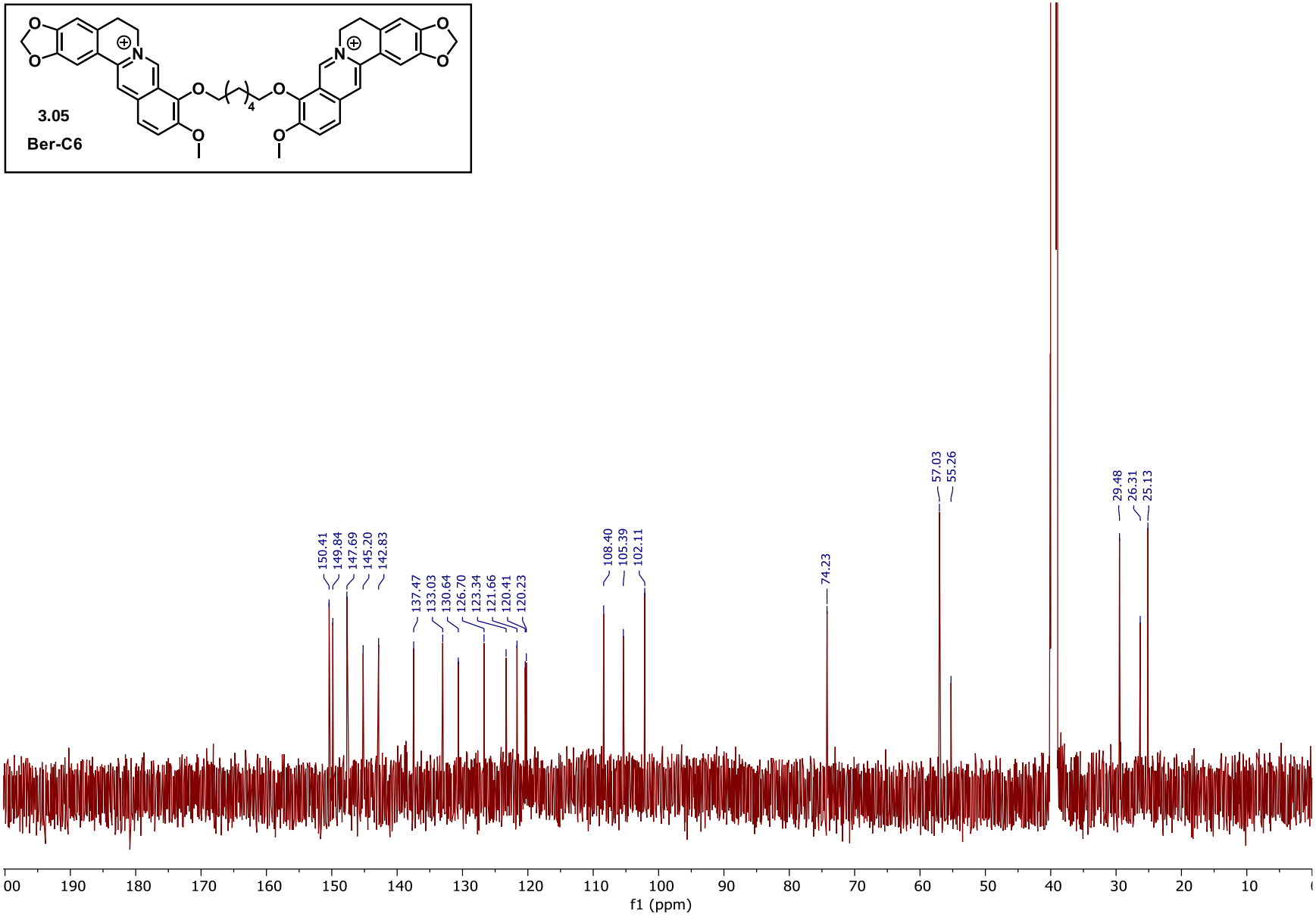
3.05
Ber-C6
150.41
149.84
147.69
145.20
142.83
137.47
133.03
130.64
126.70
123.34
121.66
120.41
120.23
108.40
105.39
102.11
74.23
57.03
55.26
29.48
26.31
25.13
f1 (ppm)

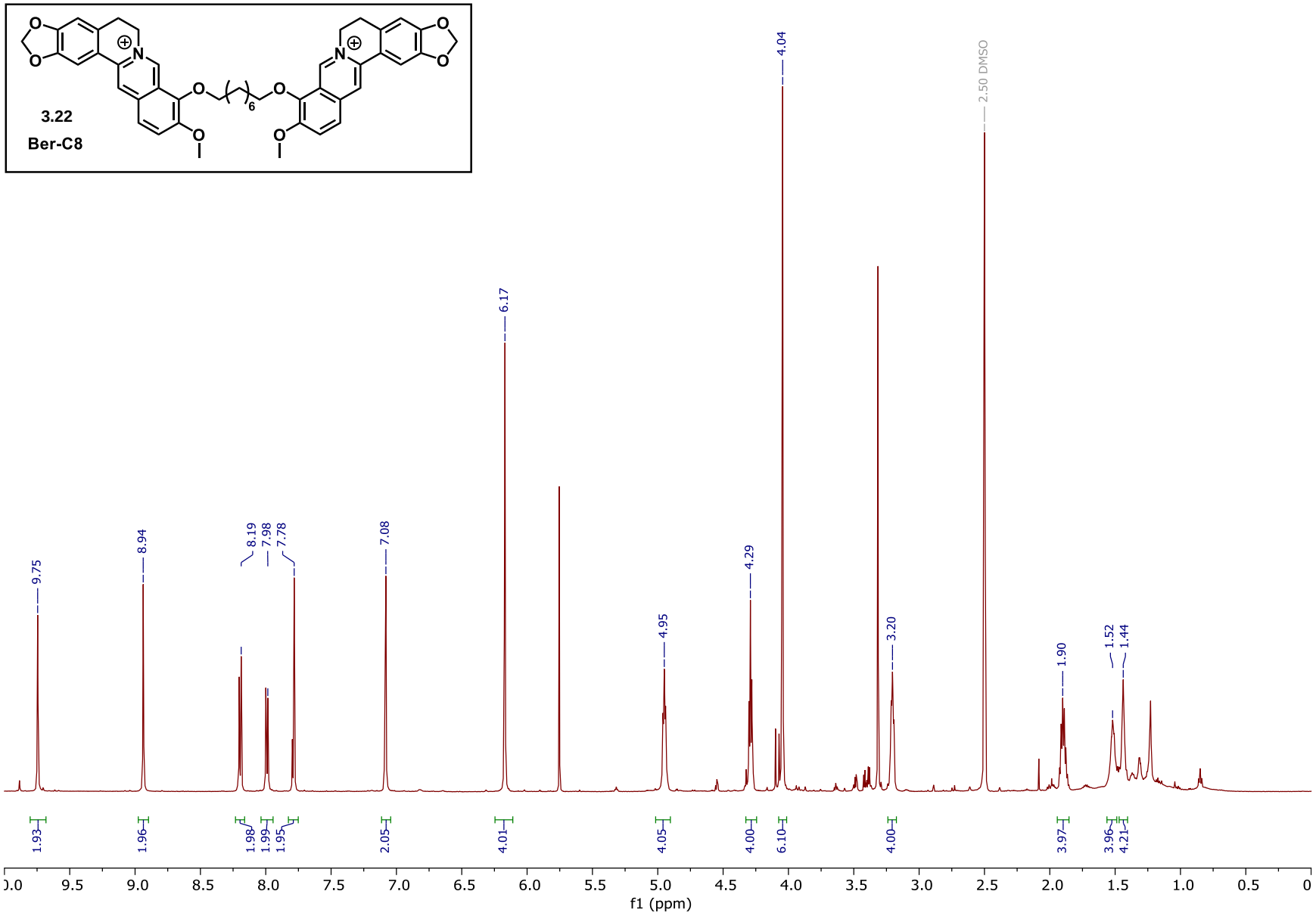
3.22
Ber-C8
9.75
8.94
8.19
7.98
7.78
7.08
6.17
4.95
4.29
4.04
3.20
2.50 DMSO
1.90
1.52
1.44
1.93
1.96
1.98
1.99
1.95
2.05
4.01
4.05
4.00
6.10
4.00
3.97
3.96
4.21
f1 (ppm)

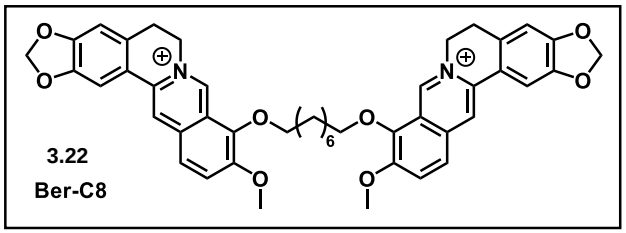
3.22
Ber-C8

150.39
149.81
147.66
145.22
142.85
137.44
133.02
130.64
126.69
123.29
121.64
120.42
120.21
108.38
105.39
102.09
74.26
57.04
55.29
29.50
28.83
26.31
25.26
00
190
180
170
160
150
140
130
120
110
100
90
80
70
60
50
40
30
20
10
f1 (ppm)

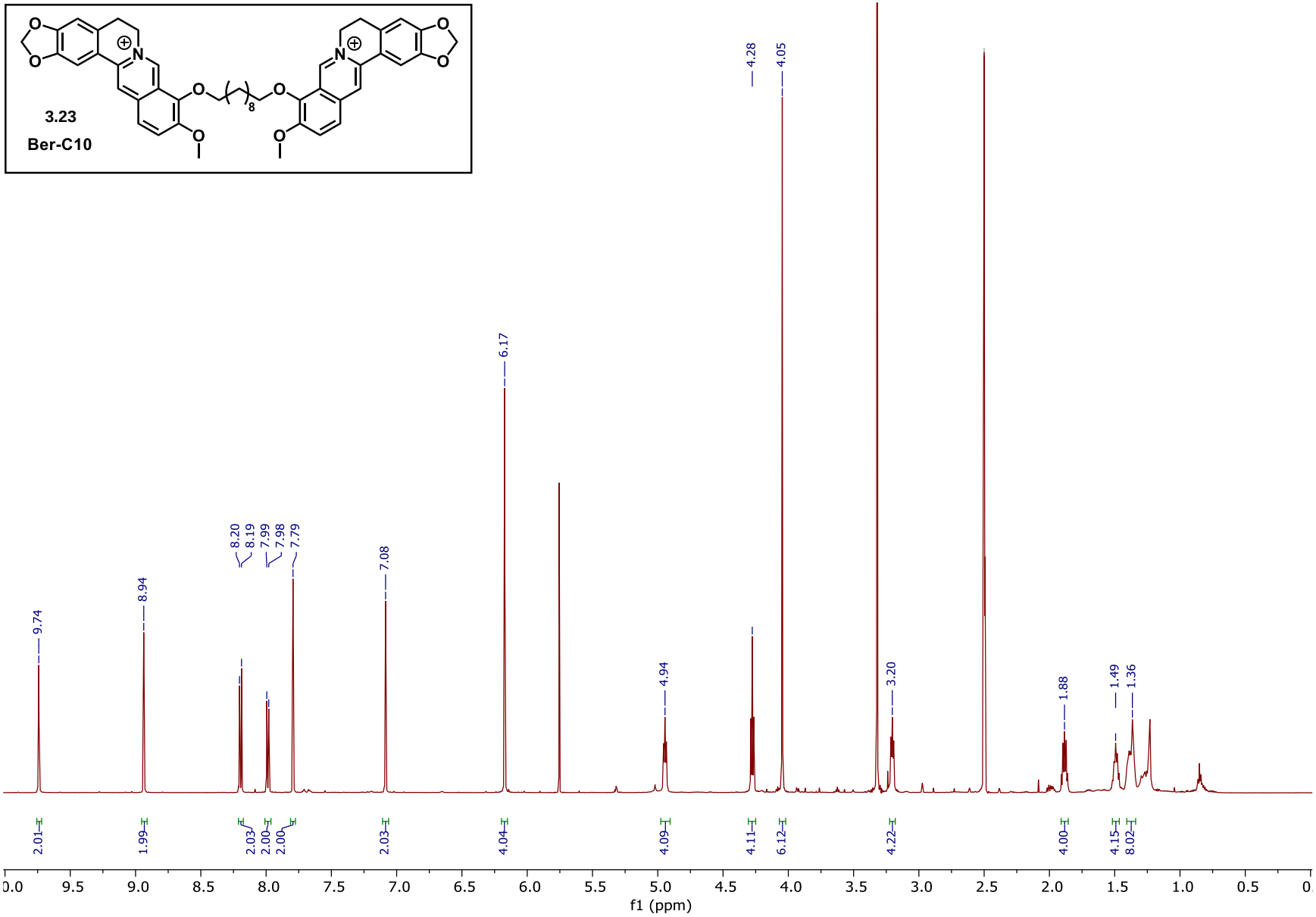
3.23
Ber-C10
9.74
8.94
8.20
8.19
7.99
7.98
7.79
7.08
6.17
4.94
4.28
4.05
3.20
1.88
1.49
1.36
2.01
1.99
2.03
2.00
2.00
2.03
4.04
4.09
4.11
6.12
4.22
4.00
4.15
8.02
f1 (ppm)

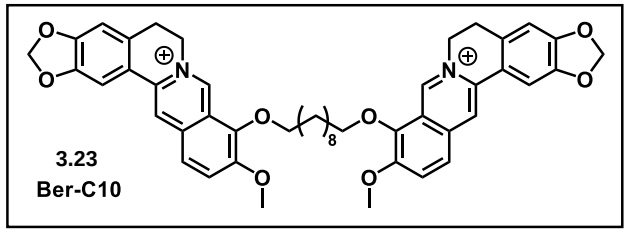
3.23
Ber-C10

150.42
149.83
147.69
145.26
142.85
137.47
133.02
130.68
126.69
123.31
121.66
120.44
120.23
108.42
105.42
102.11
74.26
57.04
55.30
29.51
29.07
28.89
26.33
25.30
f1 (ppm)

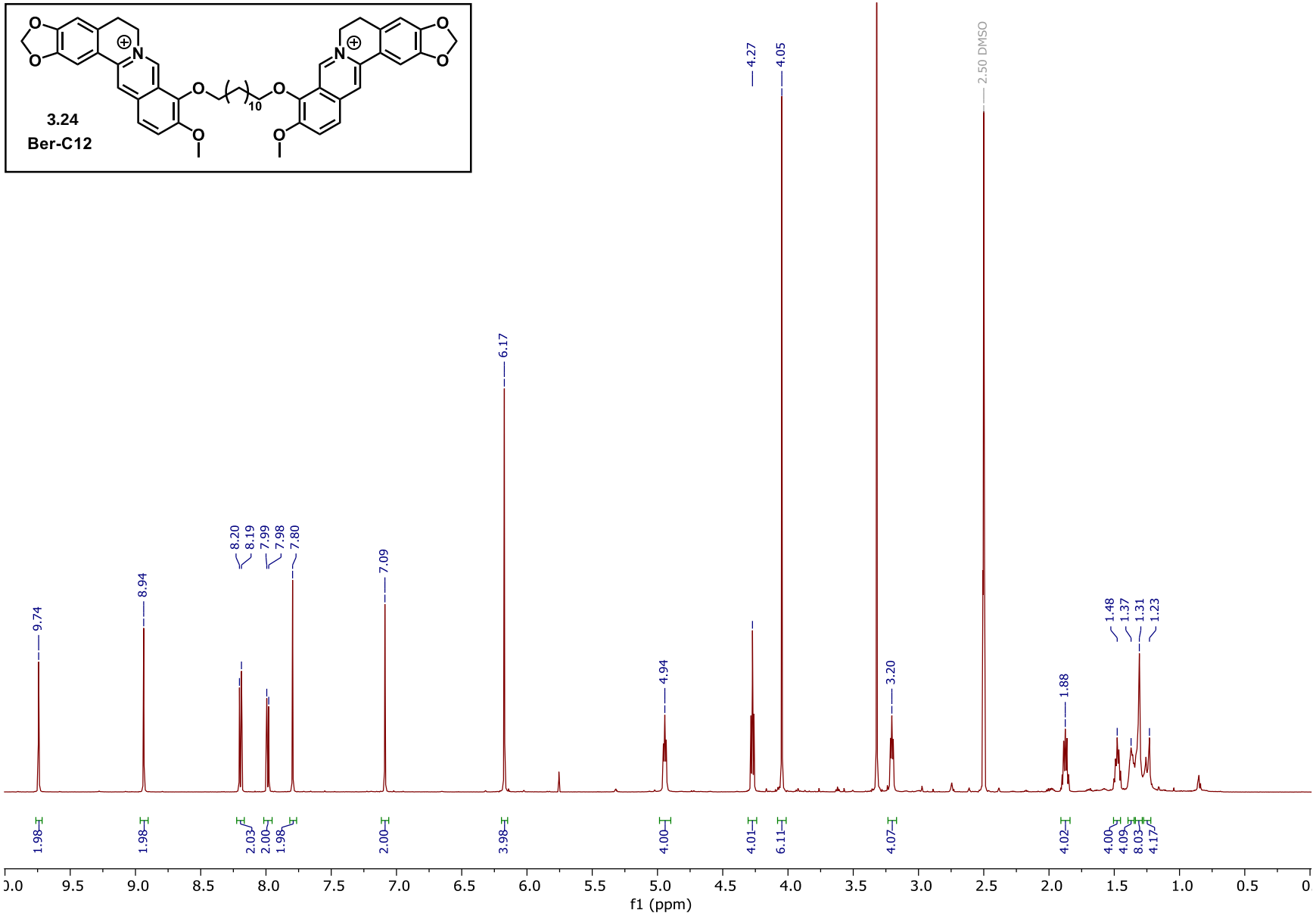
3.24
Ber-C12
9.74
8.94
8.20
8.19
7.99
7.98
7.80
7.09
6.17
4.94
4.27
4.05
3.20
2.50 DMSO
1.88
1.48
1.37
1.31
1.23
1.98
1.98
2.03
2.00
1.98
2.00
3.98
4.00
4.01
6.11
4.07
4.02
4.00
4.09
8.03
4.17
f1 (ppm)

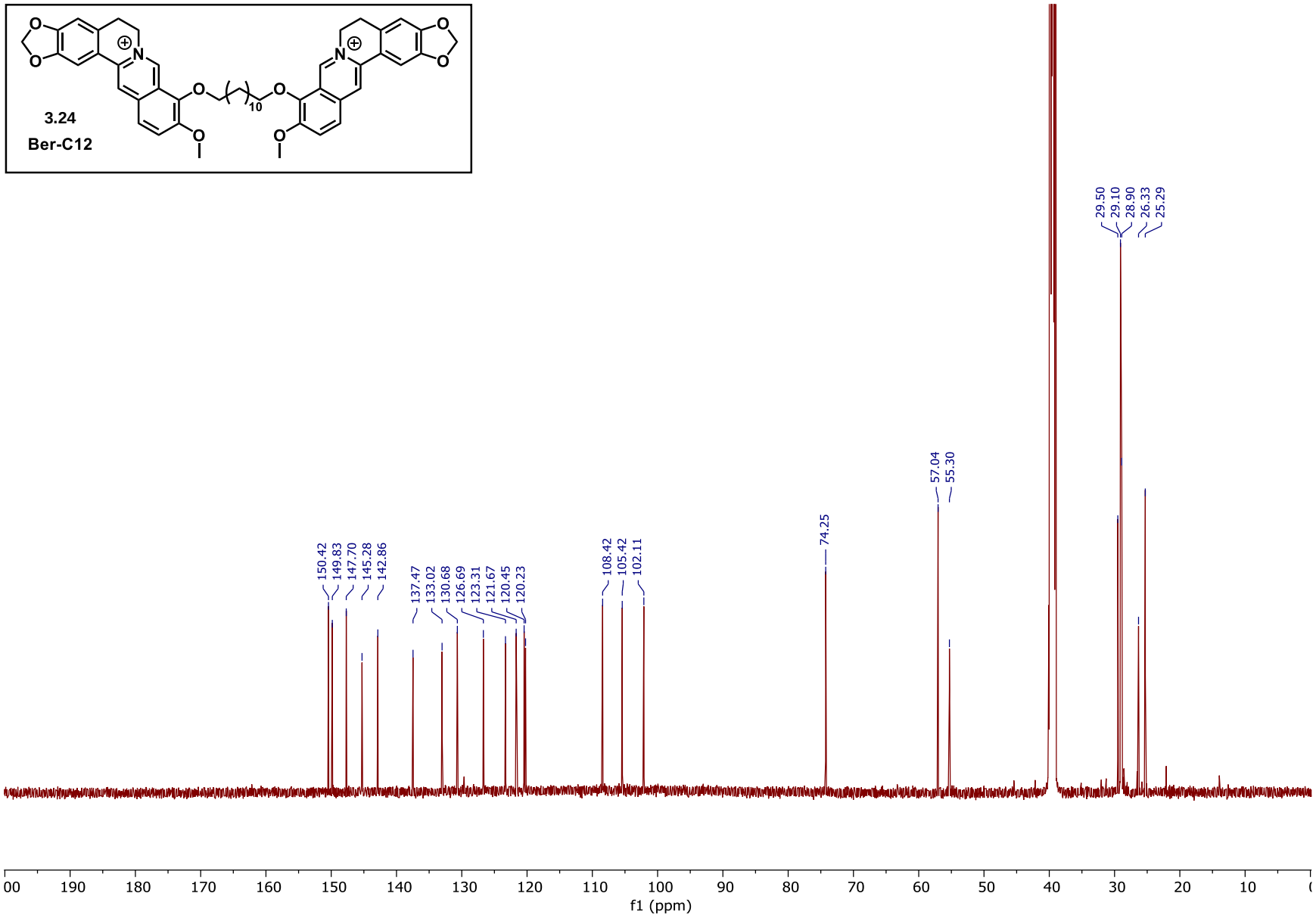
3.24
Ber-C12
150.42
149.83
147.70
145.28
142.86
137.47
133.02
130.68
126.69
123.31
121.67
120.45
120.23
108.42
105.42
102.11
74.25
57.04
55.30
29.50
29.10
28.90
26.33
25.29
f1 (ppm)

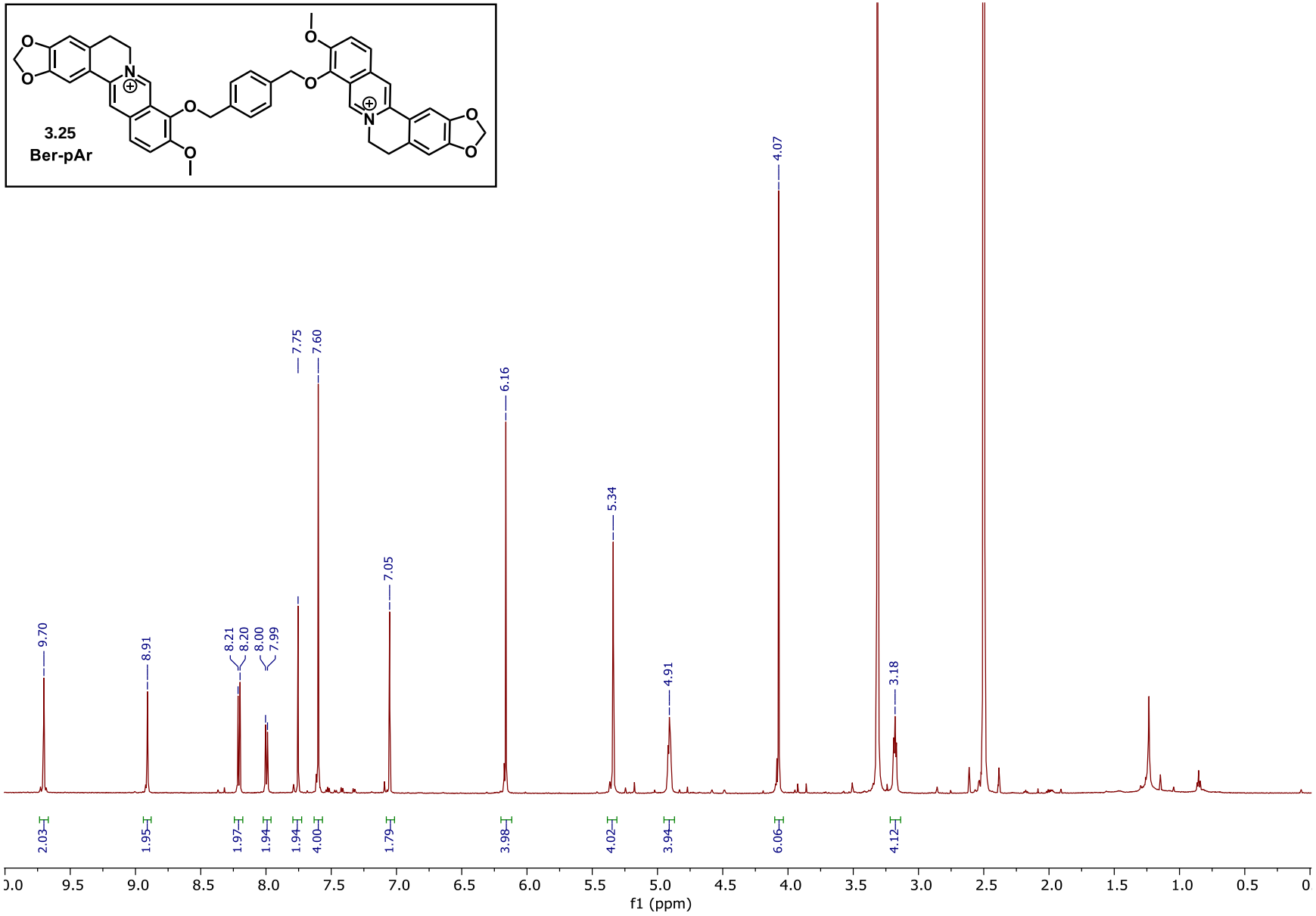
3.25
Ber-pAr
9.70
8.91
8.21
8.20
8.00
7.99
7.75
7.60
7.05
6.16
5.34
4.91
4.07
3.18
2.03
1.95
1.97
1.94
1.94
4.00
1.79
3.98
4.02
3.94
6.06
4.12
f1 (ppm)

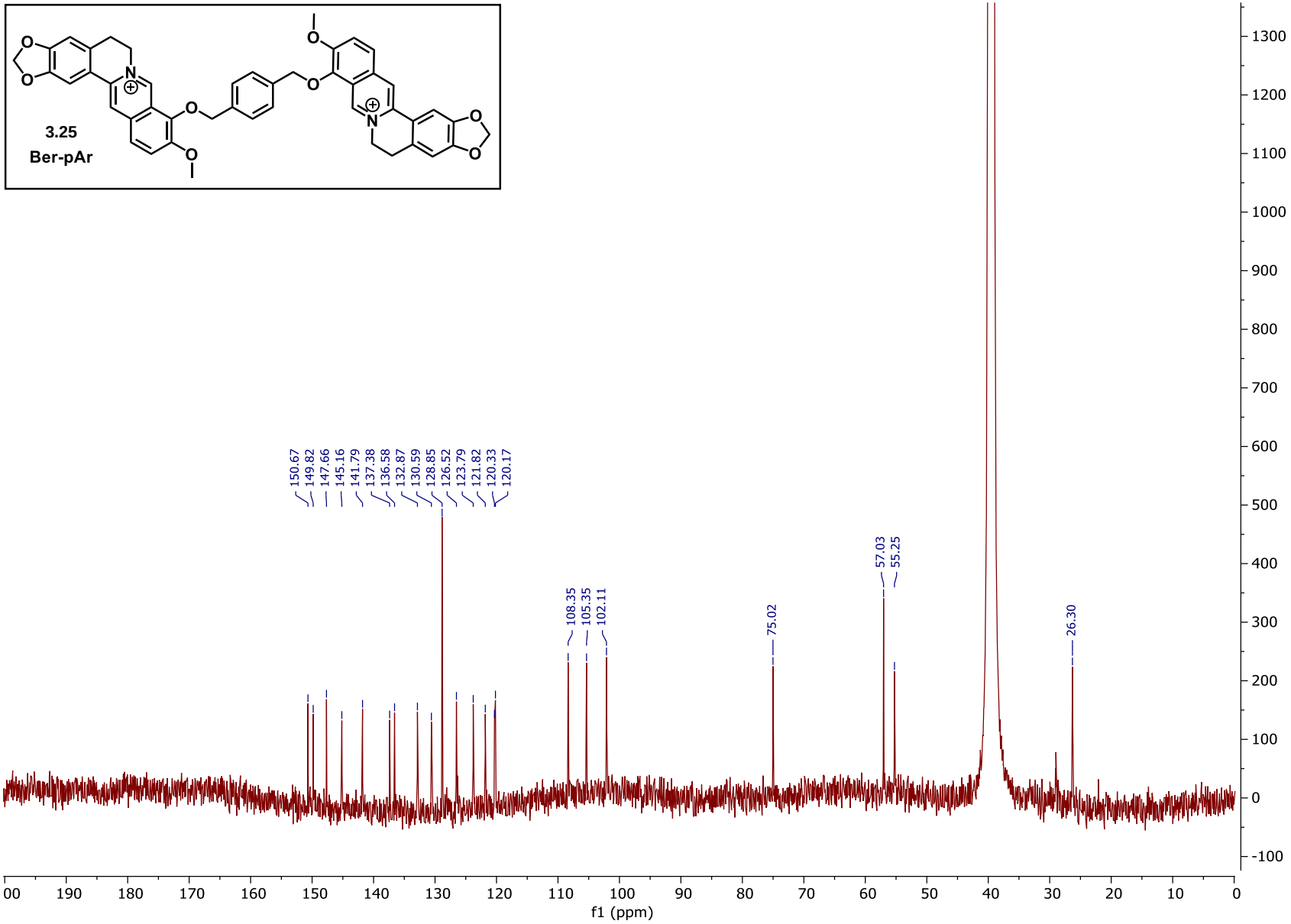
3.25
Ber-pAr
150.67
149.82
147.66
145.16
141.79
137.38
136.58
132.87
130.59
128.85
126.52
123.79
121.82
120.33
120.17
108.35
105.35
102.11
75.02
57.03
55.25
26.30
f1 (ppm)

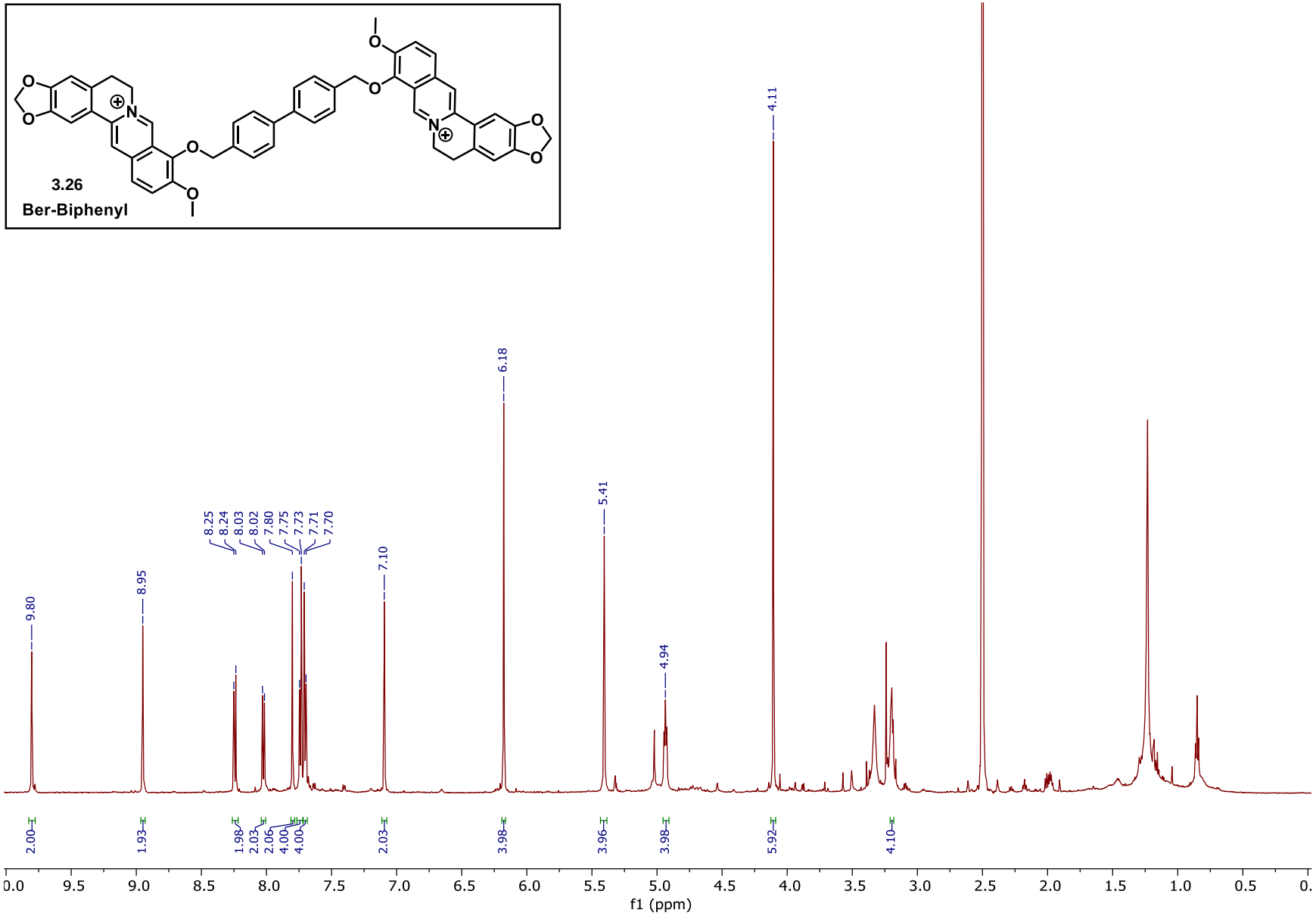
3.26
Ber-Biphenyl
9.80
8.95
8.25
8.24
8.03
8.02
7.80
7.75
7.73
7.71
7.70
7.10
6.18
5.41
4.94
4.11
2.00
1.93
1.98
2.03
2.06
4.00
4.00
2.03
3.98
3.96
3.98
5.92
4.10
f1 (ppm)

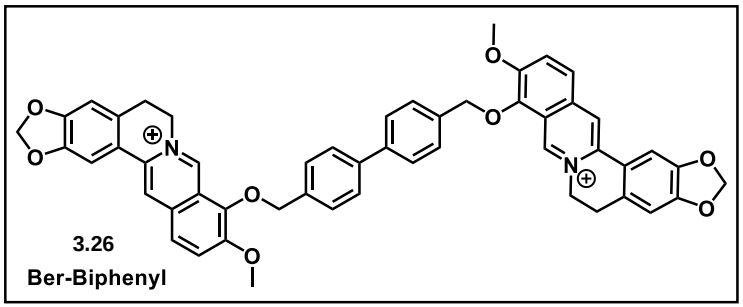
3.26
Ber-Biphenyl

150.69
149.88
147.72
145.35
142.06
139.62
137.48
135.91
132.97
130.68
129.65
129.38
126.63
123.79
121.80
120.42
120.28
108.44
105.44
102.12
75.05
57.09
55.34
26.35
f1 (ppm)

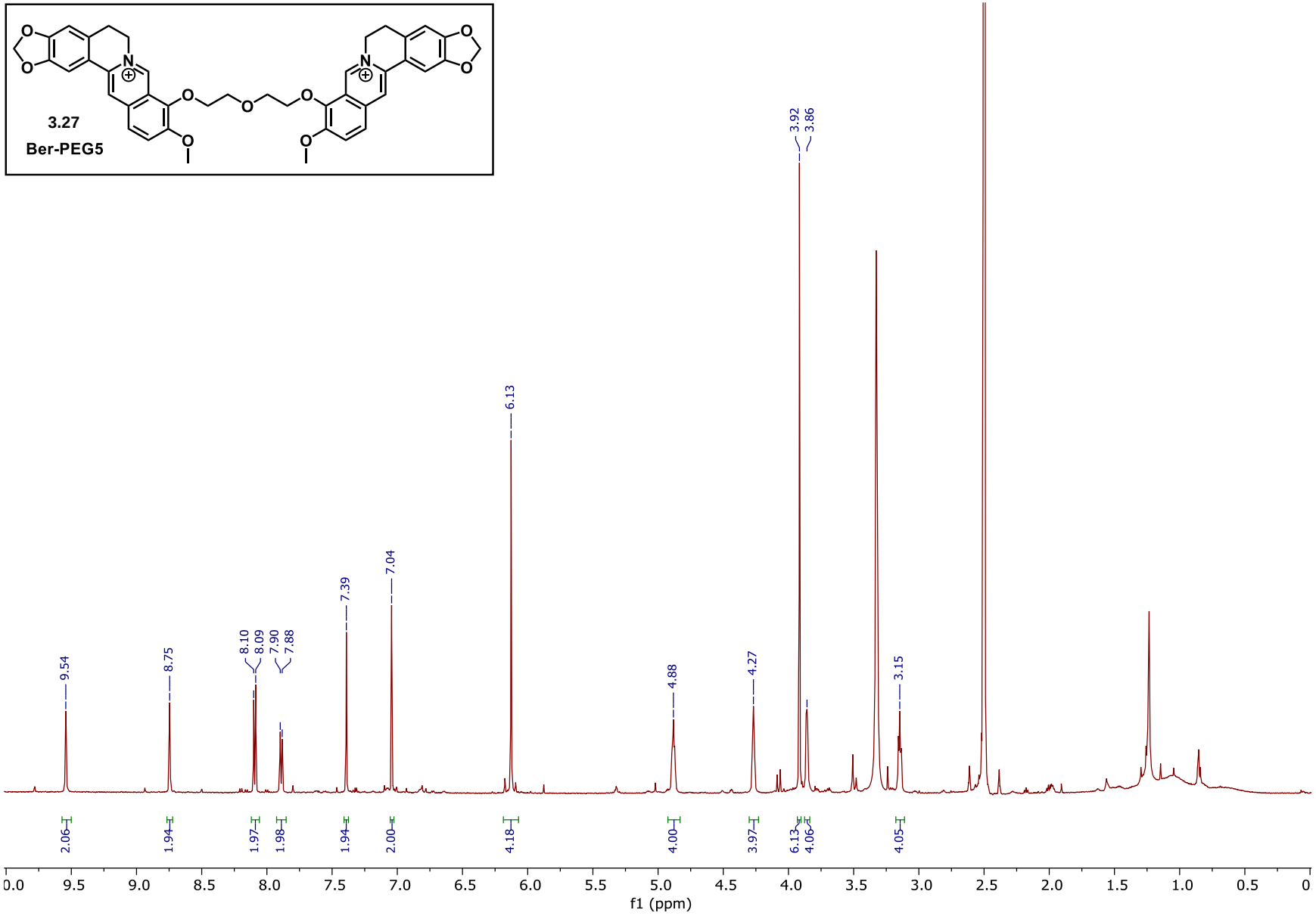
3.27
Ber-PEG5
9.54
8.75
8.10
8.09
7.90
7.88
7.39
7.04
6.13
4.88
4.27
3.92
3.86
3.15
2.06
1.94
1.97
1.98
1.94
2.00
4.18
4.00
3.97
6.13
4.06
4.05
f1 (ppm)

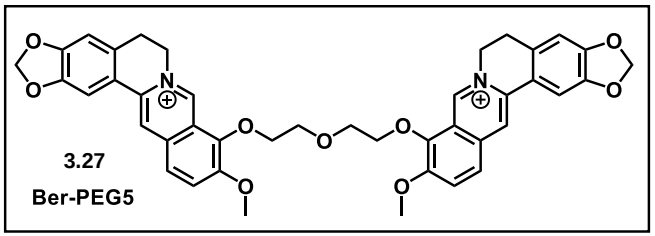
3.27
Ber-PEG5

150.14
149.70
147.50
145.08
142.58
137.04
132.77
130.19
126.10
123.56
121.82
120.11
119.95
108.22
105.04
102.14
72.83
69.48
56.79
55.06
26.16
f1 (ppm)

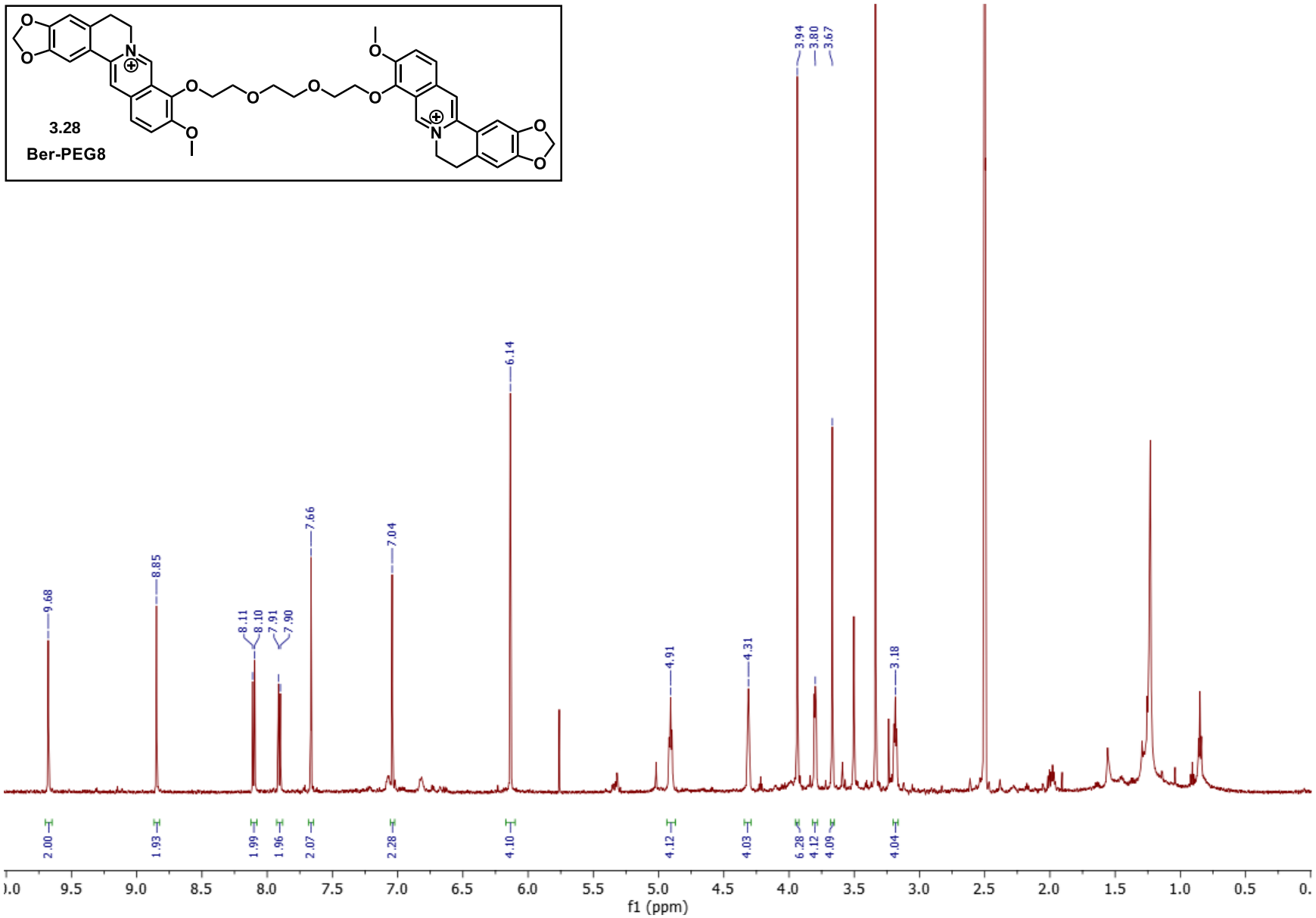
3.28
Ber-PEG8
9.68
8.85
8.11
8.10
7.91
7.90
7.66
7.04
6.14
4.91
4.31
3.94
3.80
3.67
3.18
2.00
1.93
1.99
1.96
2.07
2.28
4.10
4.12
4.03
6.28
4.12
4.09
4.04
f1 (ppm)

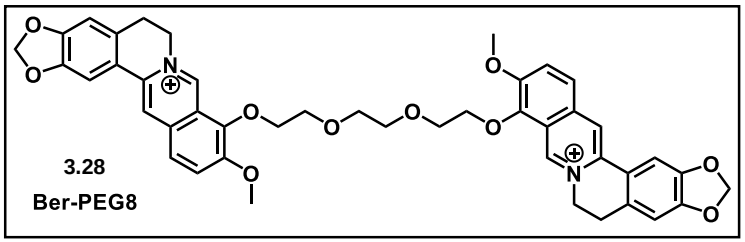
3.28
Ber-PEG8

150.28
149.75
147.59
145.21
142.31
137.30
132.79
130.47
126.29
123.49
121.61
120.29
120.06
108.29
105.24
102.11
73.17
69.64
69.41
56.85
55.40
26.29
f1 (ppm)

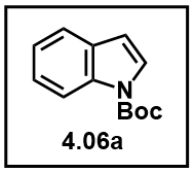
N
Boc

4.06a

8.15
8.13
7.59
7.59
7.56
7.55
7.30
7.22
6.57
6.56
1.00
0.97
1.03
1.03
1.03
1.02
9.04
0.0
9.5
9.0
8.5
8.0
7.5
7.0
6.5
6.0
5.5
5.0
4.5
4.0
3.5
3.0
2.5
2.0
1.5
1.0
0.5
f1 (ppm)

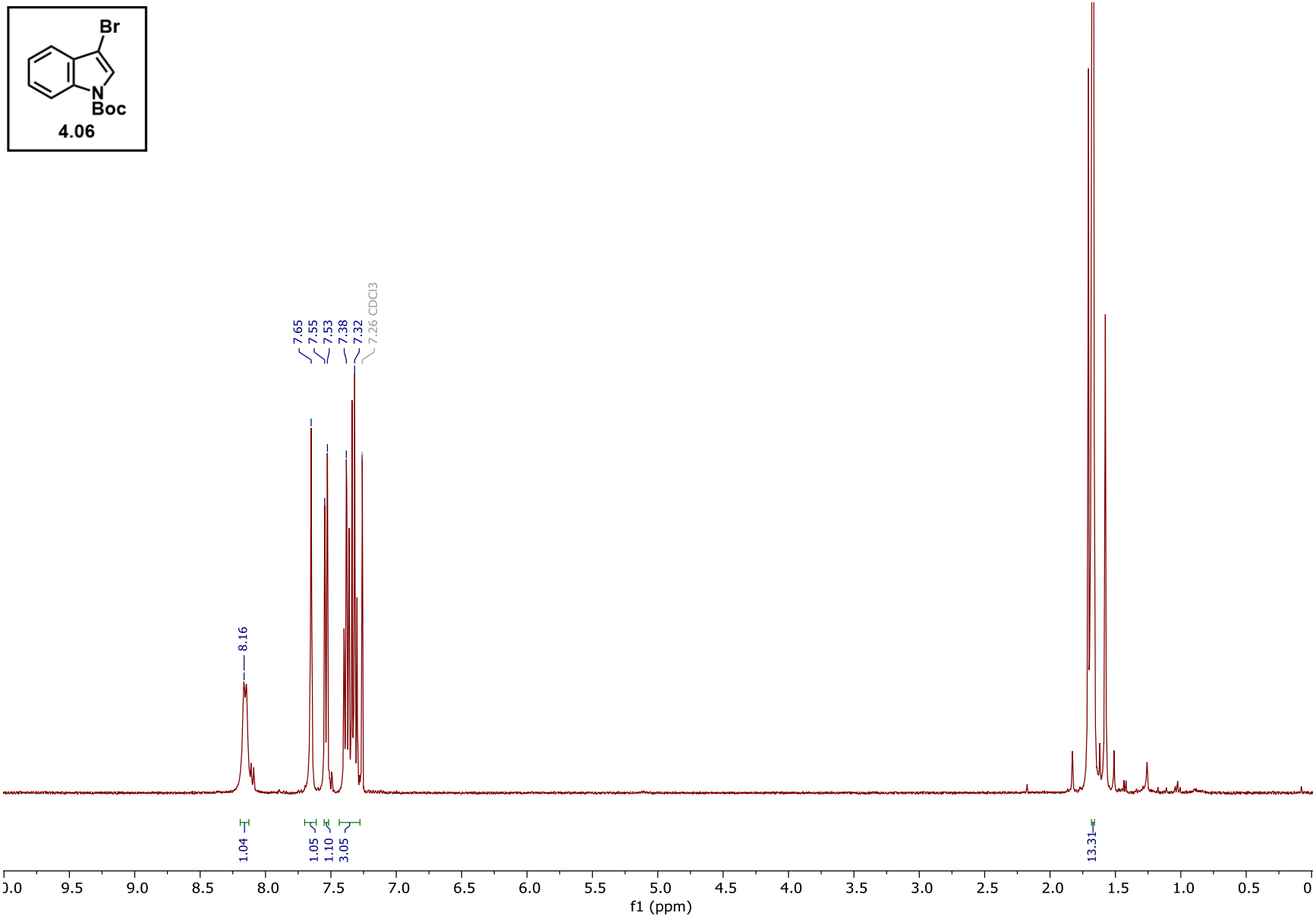
Br
N
Boc
4.06
7.65
7.55
7.53
7.38
7.32
7.26 CDCl3
8.16
1.04
1.05
1.10
3.05
13.31
f1 (ppm)

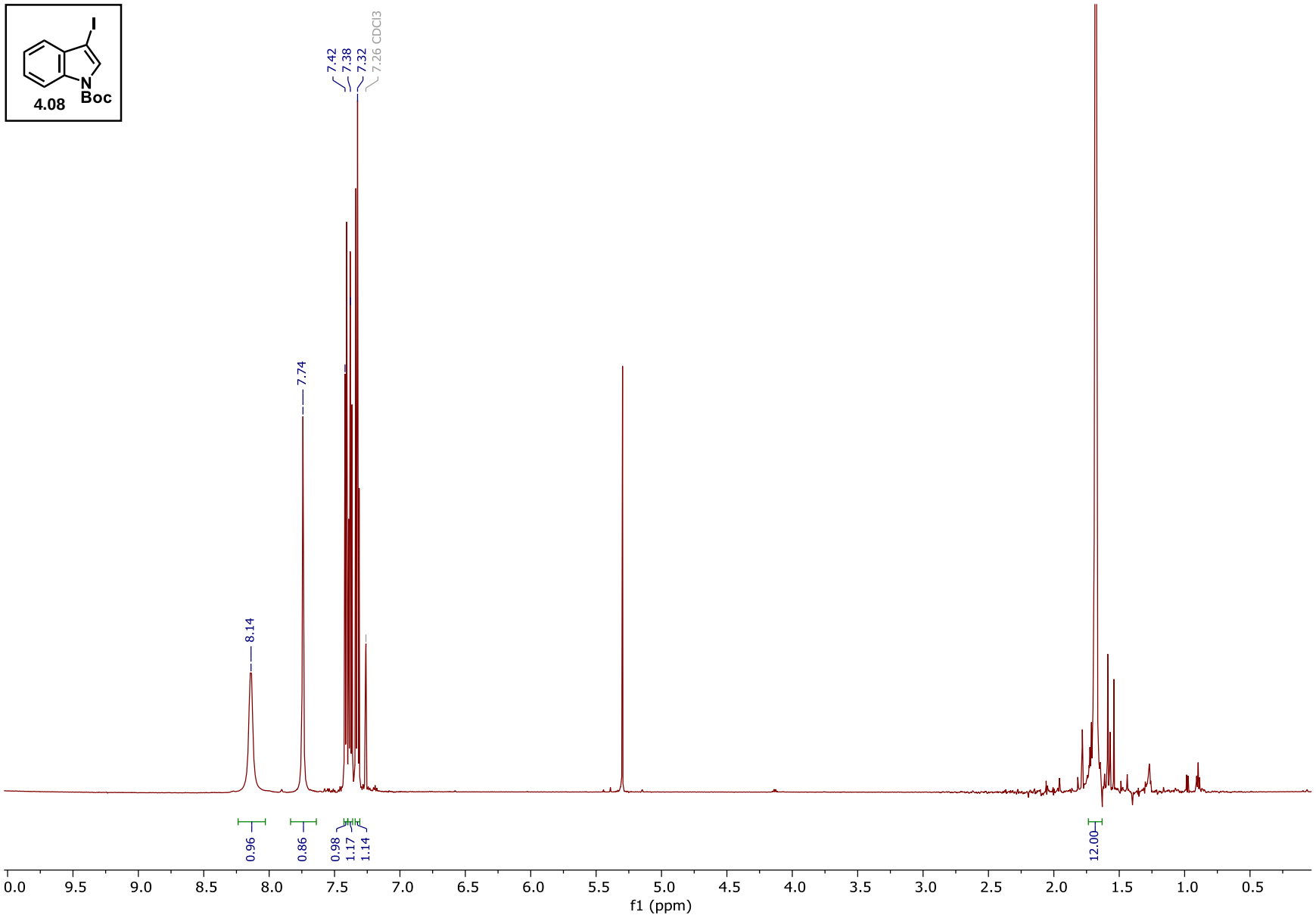
I
N
Boc
4.08
7.42
7.38
7.32
7.26 CDCl3
7.74
8.14
0.96
0.86
0.98
1.17
1.14
12.00
0.0
9.5
9.0
8.5
8.0
7.5
7.0
6.5
6.0
5.5
5.0
4.5
4.0
3.5
3.0
2.5
2.0
1.5
1.0
0.5
f1 (ppm)

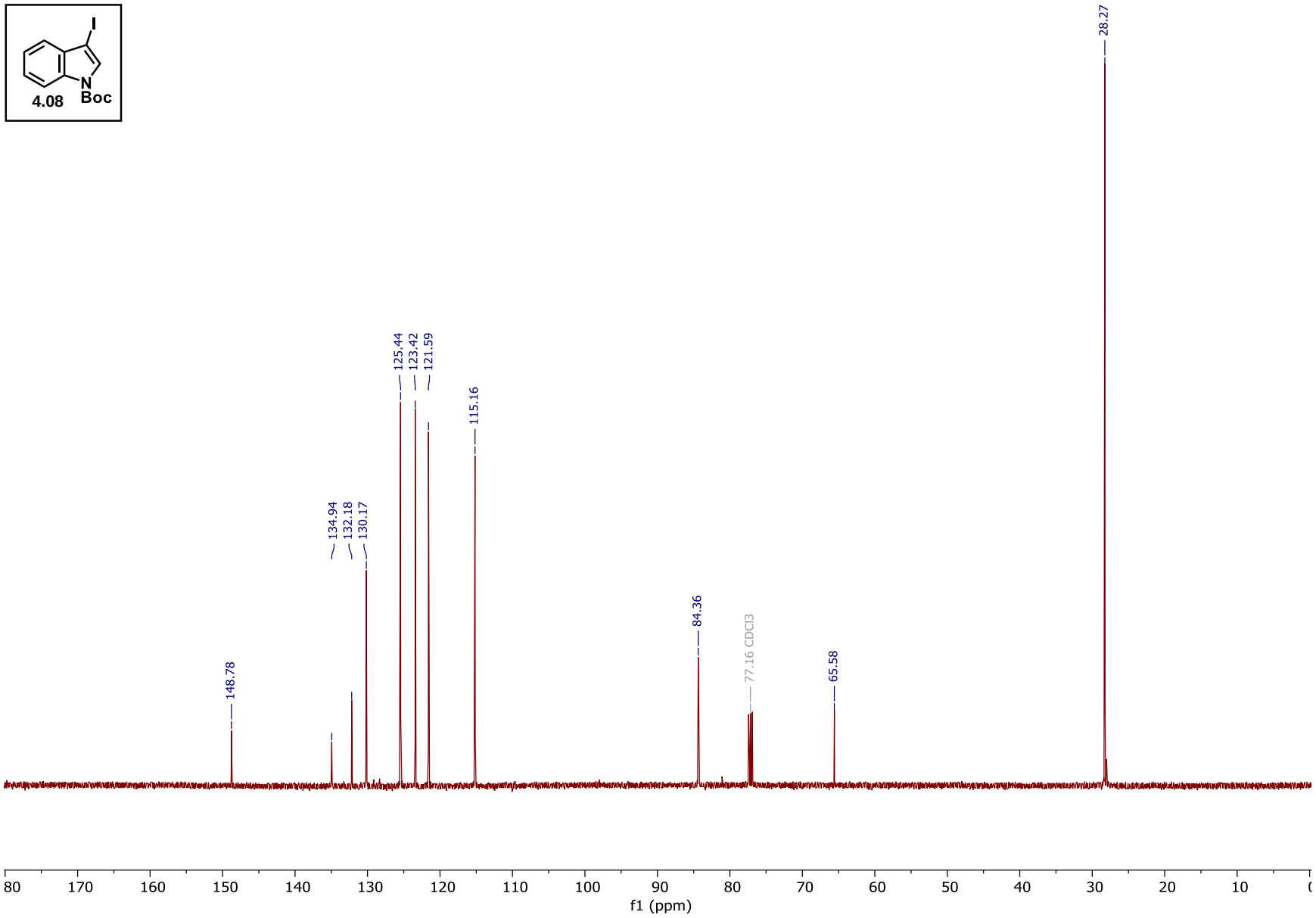
I
N
Boc
4.08
28.27
125.44
123.42
121.59
115.16
134.94
132.18
130.17
84.36
77.16 CDCl3
65.58
148.78
80
170
160
150
140
130
120
110
100
90
80
70
60
50
40
30
20
10
f1 (ppm)

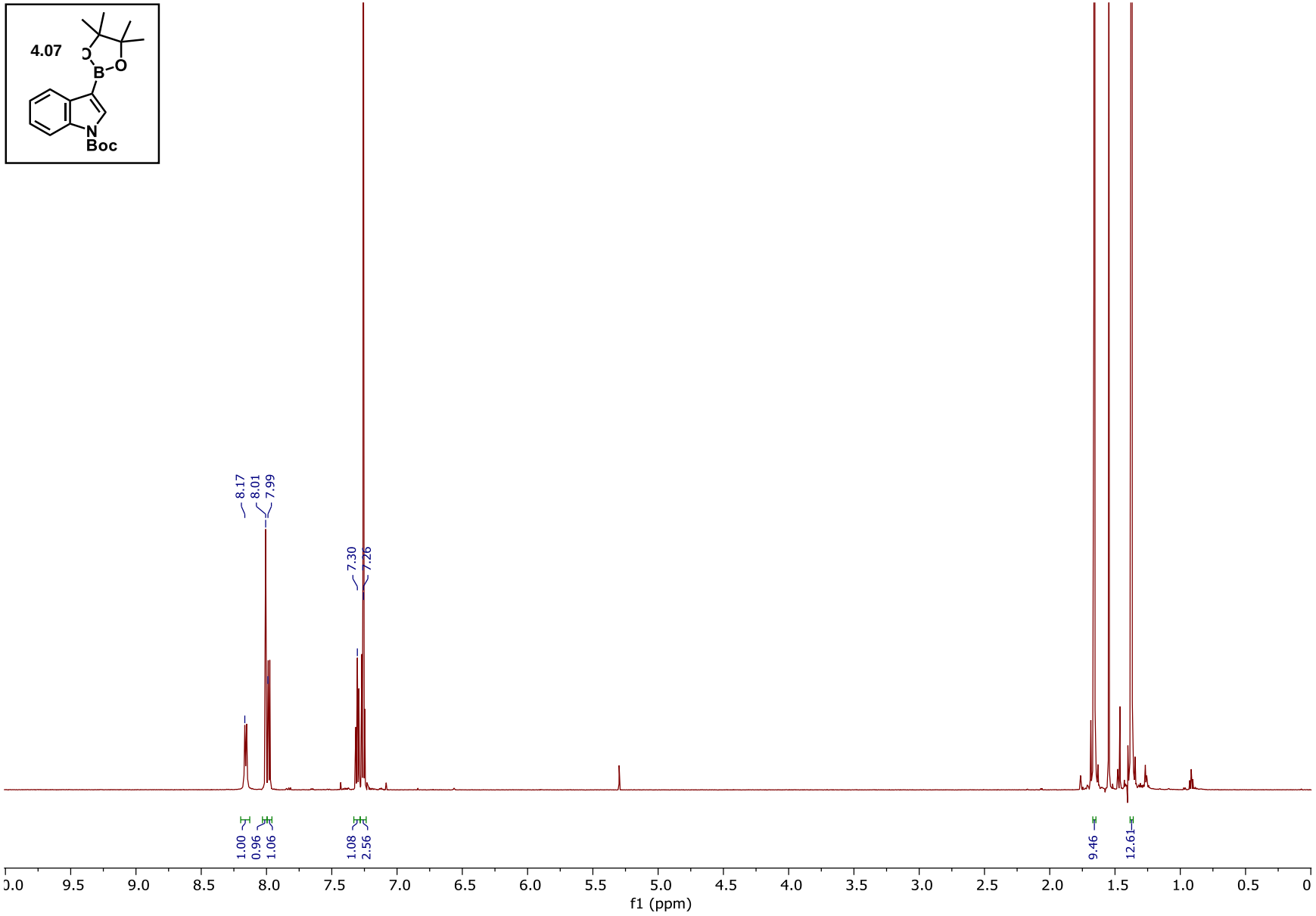
4.07
B
O
N
Boc
8.17
8.01
7.99
7.30
7.26
1.00
0.96
1.06
1.08
2.56
9.46
12.61
f1 (ppm)

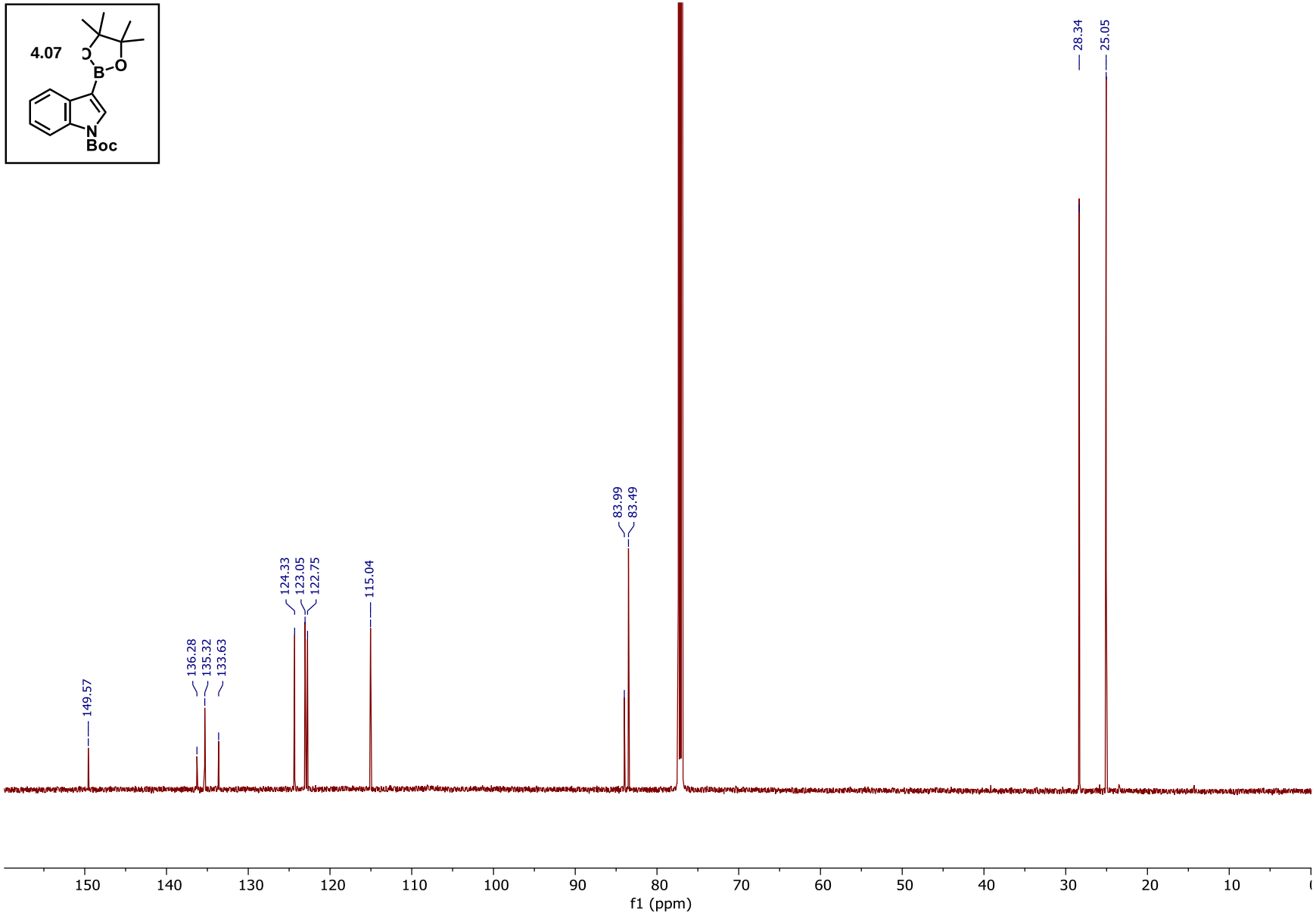
4.07
B
O
N
Boc
28.34
25.05
83.99
83.49
124.33
123.05
122.75
115.04
136.28
135.32
133.63
149.57
150
140
130
120
110
100
90
80
70
60
50
40
30
20
10
f1 (ppm)

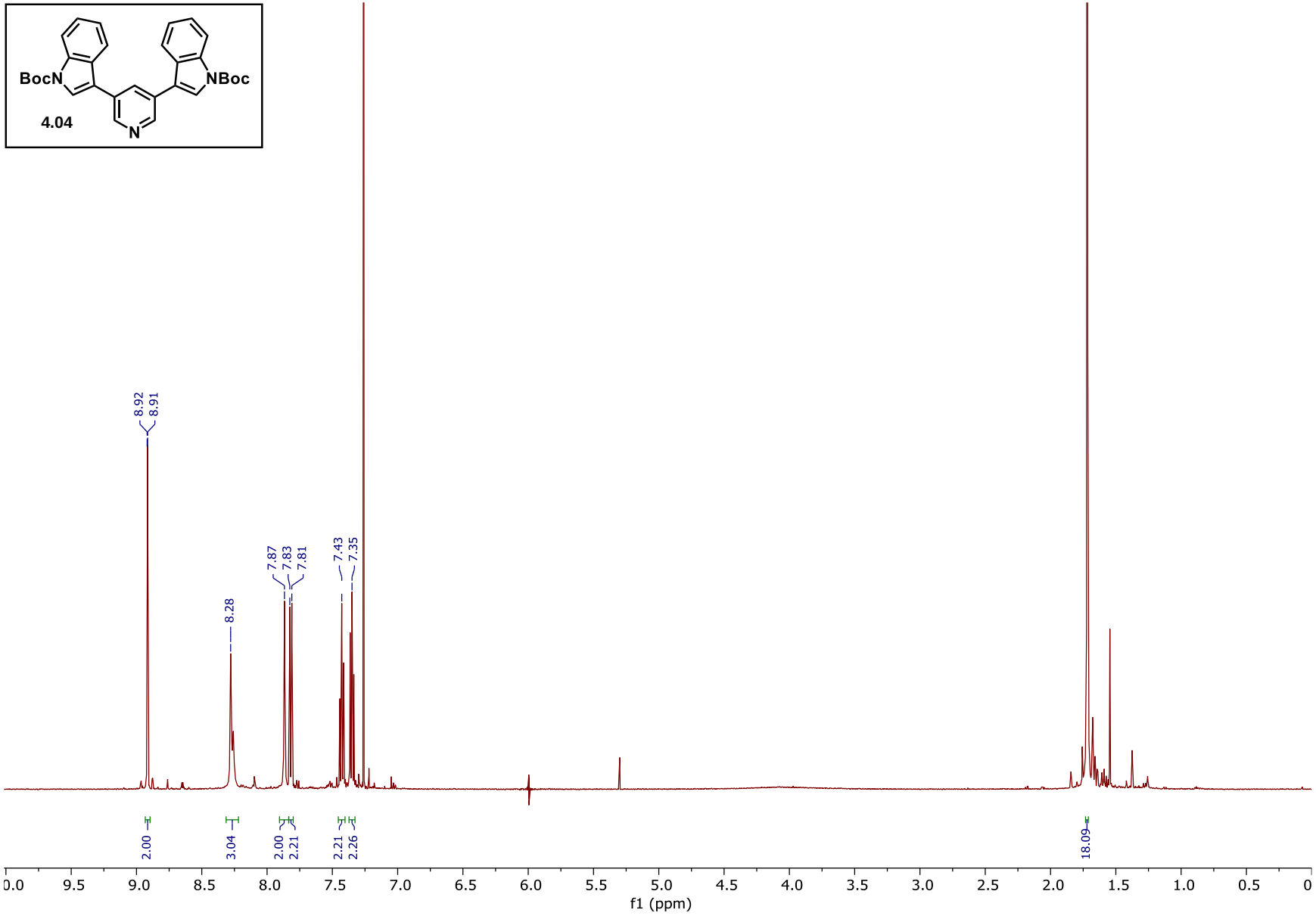
BocN
NBoc
N
4.04
8.92
8.91
8.28
7.87
7.83
7.81
7.43
7.35
2.00
3.04
2.00
2.21
2.21
2.26
18.09
f1 (ppm)

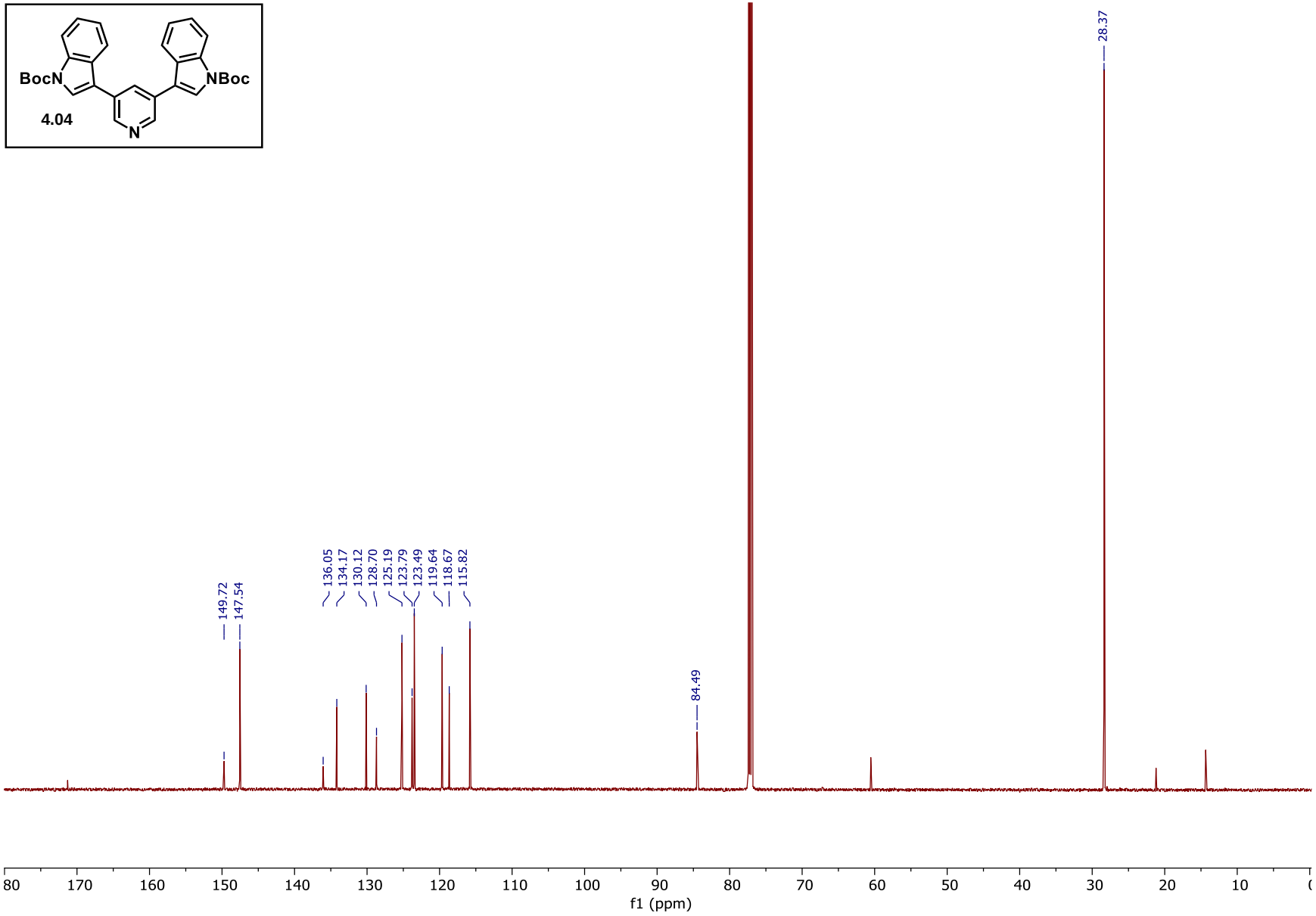
BocN
NBoc
N
4.04
28.37
149.72
147.54
136.05
134.17
130.12
128.70
125.19
123.79
123.49
119.64
118.67
115.82
84.49
80
170
160
150
140
130
120
110
100
90
80
70
60
50
40
30
20
10
f1 (ppm)

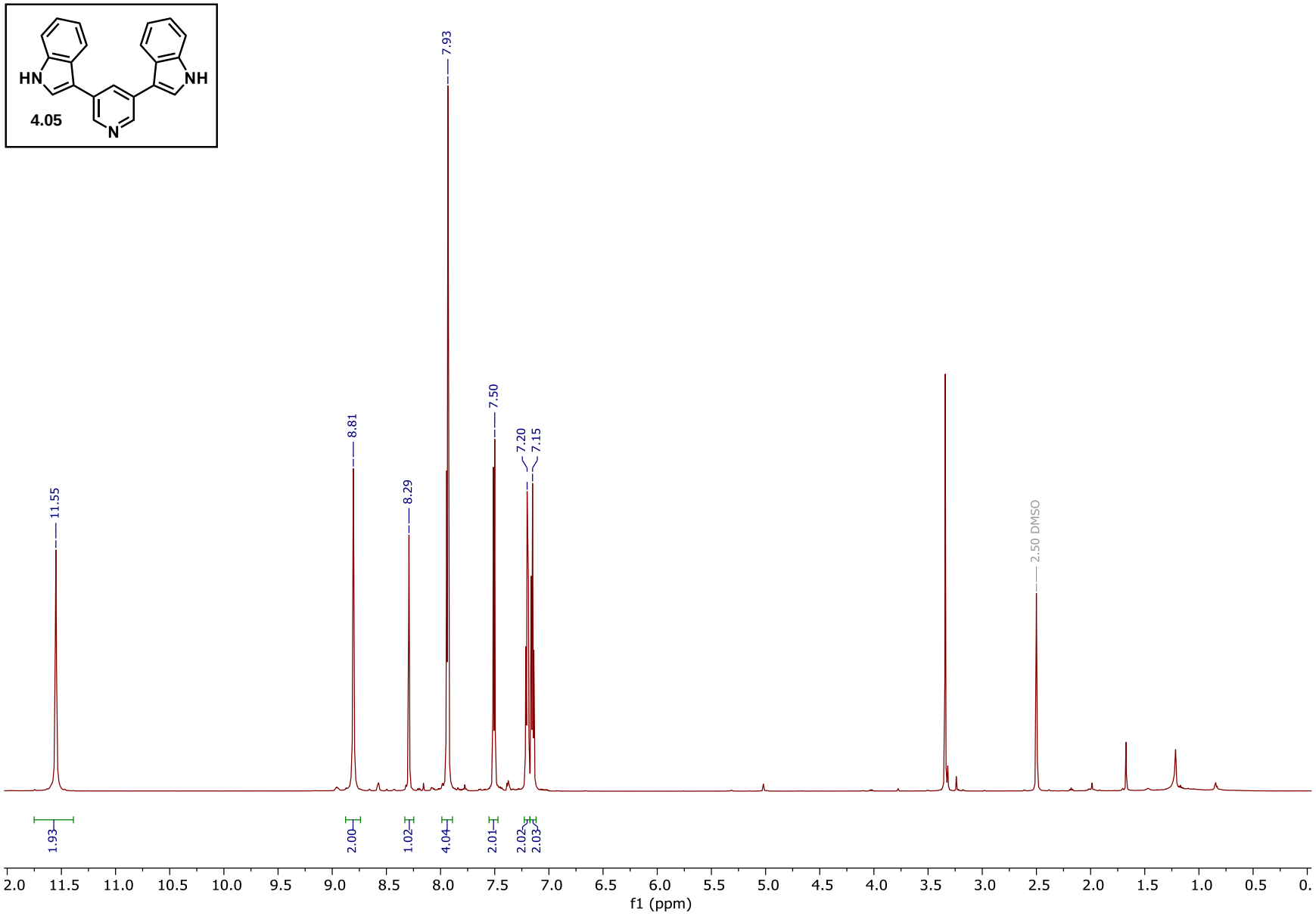
HN
NH
N
4.05
11.55
8.81
8.29
7.93
7.50
7.20
7.15
2.50 DMSO
1.93
2.00
1.02
4.04
2.01
2.02
2.03
f1 (ppm)

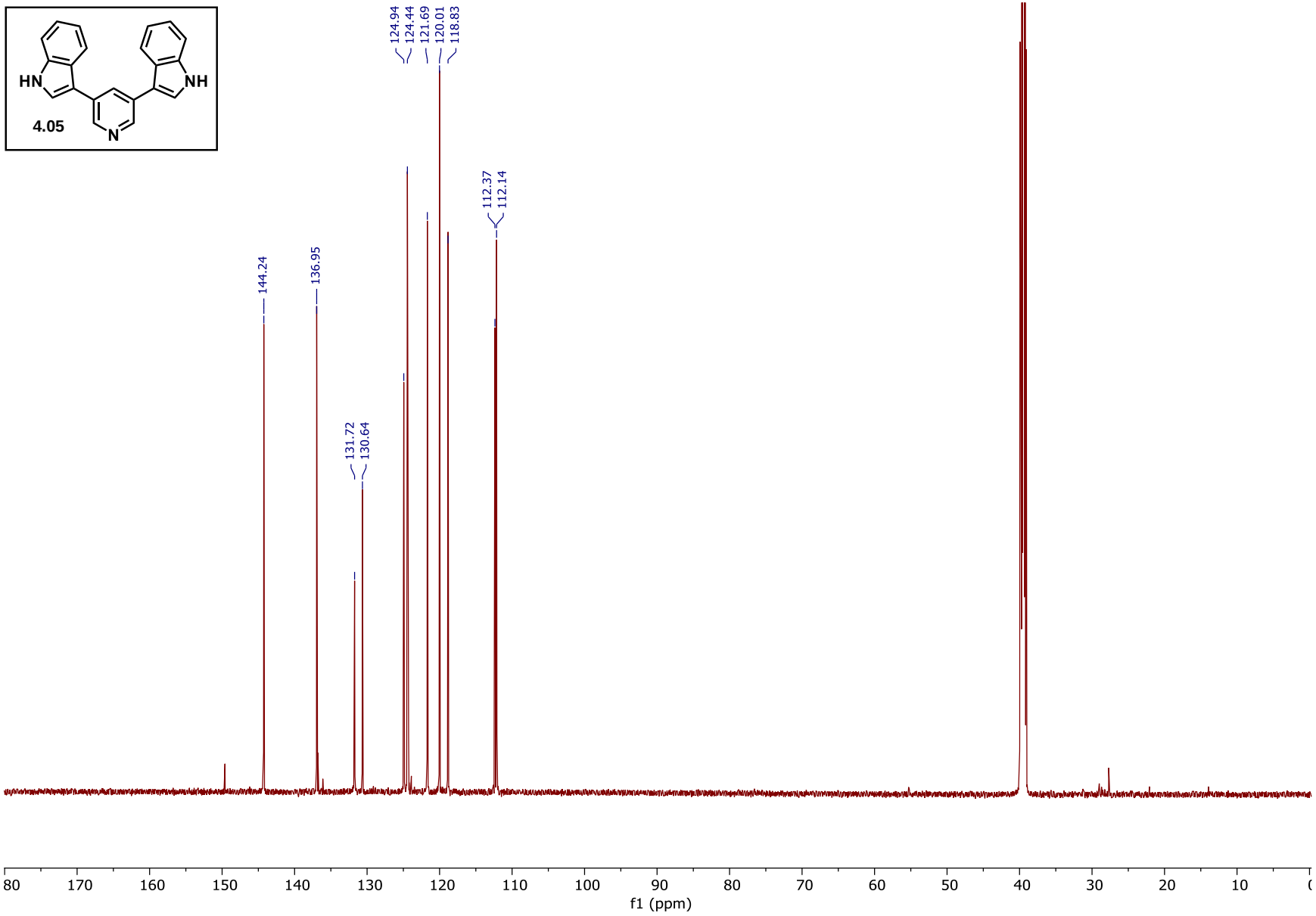
HN
NH
N
4.05
144.24
136.95
131.72
130.64
124.94
124.44
121.69
120.01
118.83
112.37
112.14
80
170
160
150
140
130
120
110
100
90
80
70
60
50
40
30
20
10
f1 (ppm)

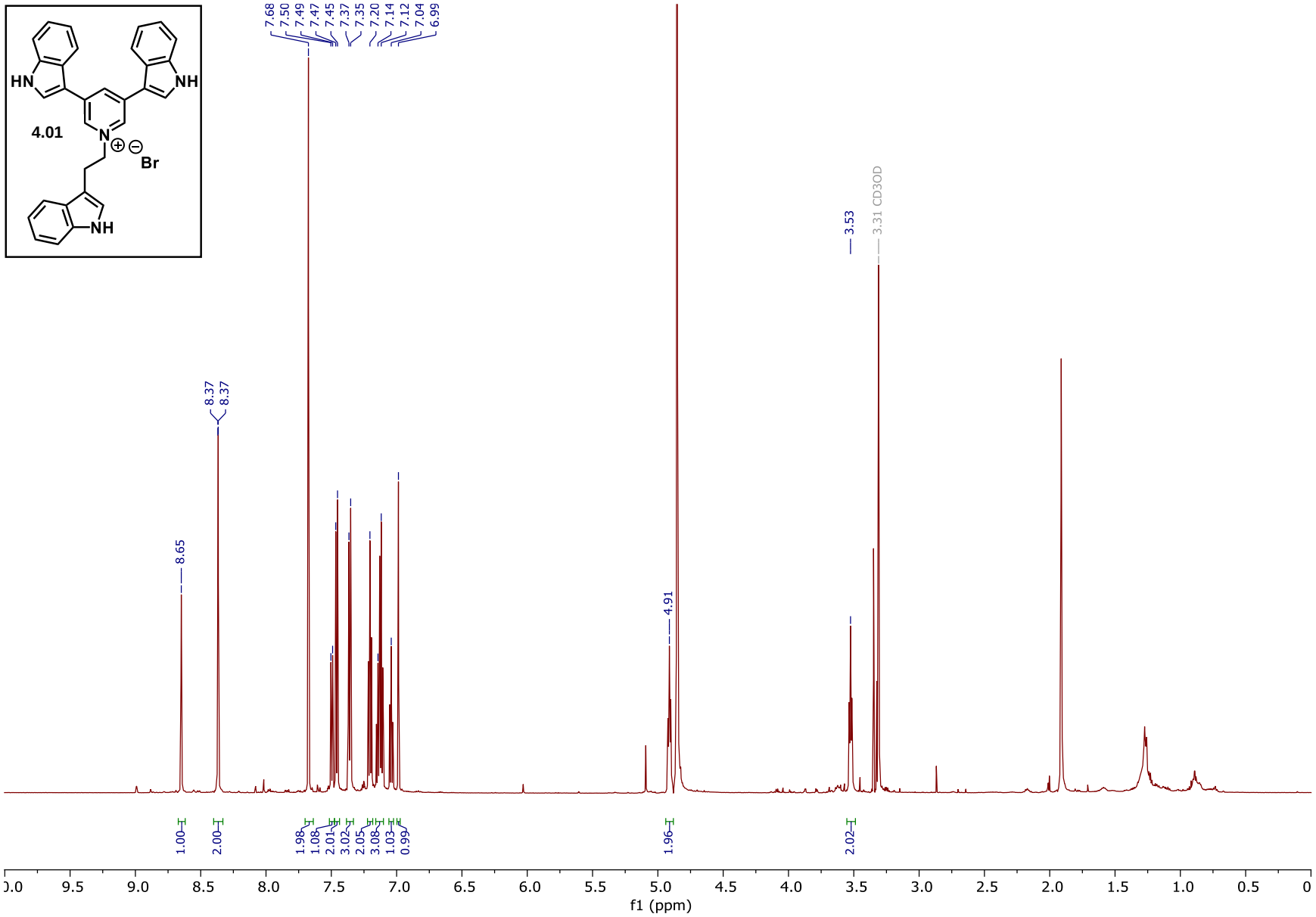
HN
NH
4.01
N
Br
NH
7.68
7.50
7.49
7.47
7.45
7.37
7.35
7.20
7.14
7.12
7.04
6.99
8.37
8.37
8.65
4.91
3.53
3.31 CD3OD
1.00
2.00
1.98
1.08
2.01
3.02
2.05
3.08
1.03
0.99
1.96
2.02
f1 (ppm)

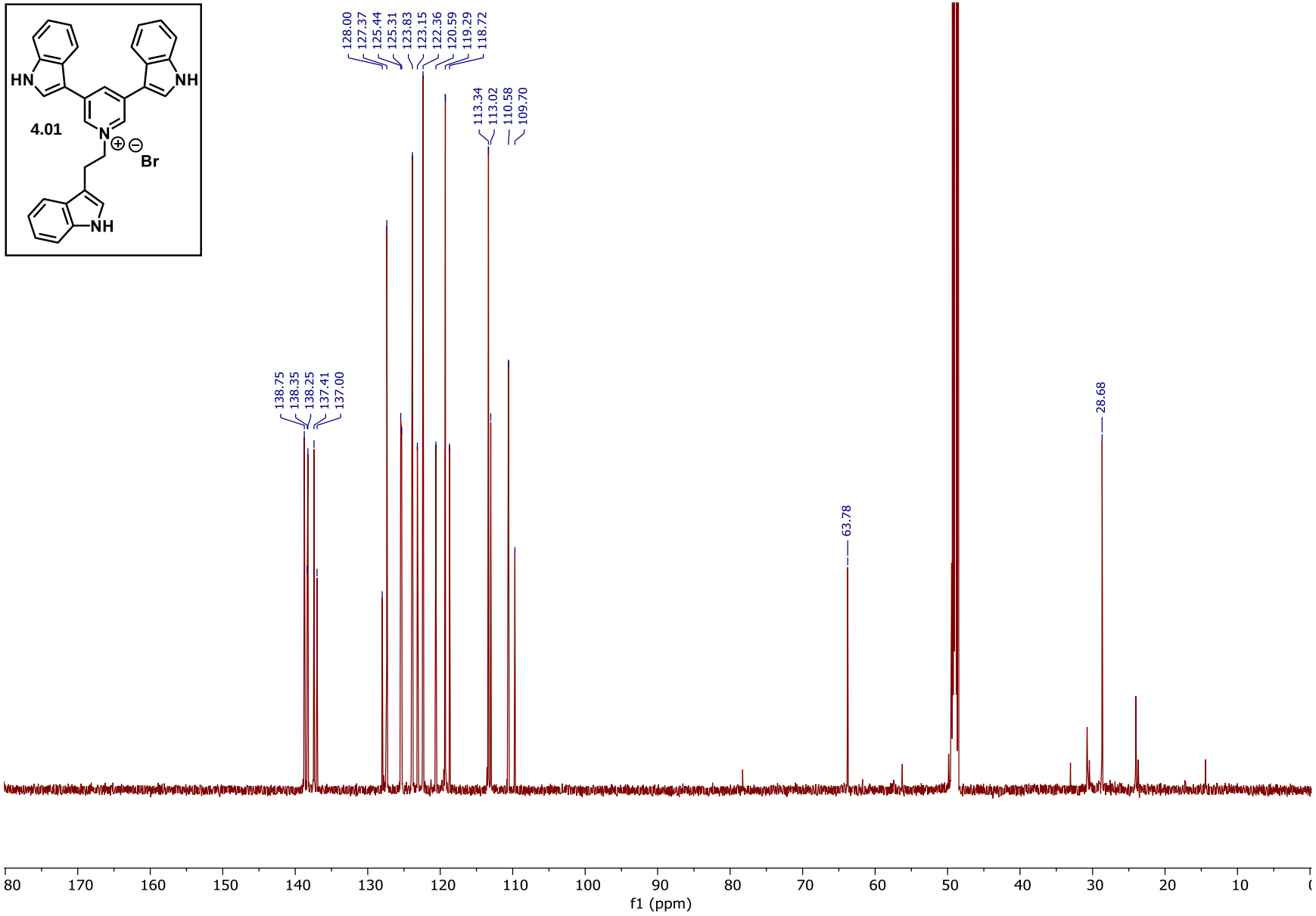
4.01
HN
NH
N
Br
NH
128.00
127.37
125.44
125.31
123.83
123.15
122.36
120.59
119.29
118.72
113.34
113.02
110.58
109.70
138.75
138.35
138.25
137.41
137.00
63.78
28.68
80
170
160
150
140
130
120
110
100
90
80
70
60
50
40
30
20
10
f1 (ppm)

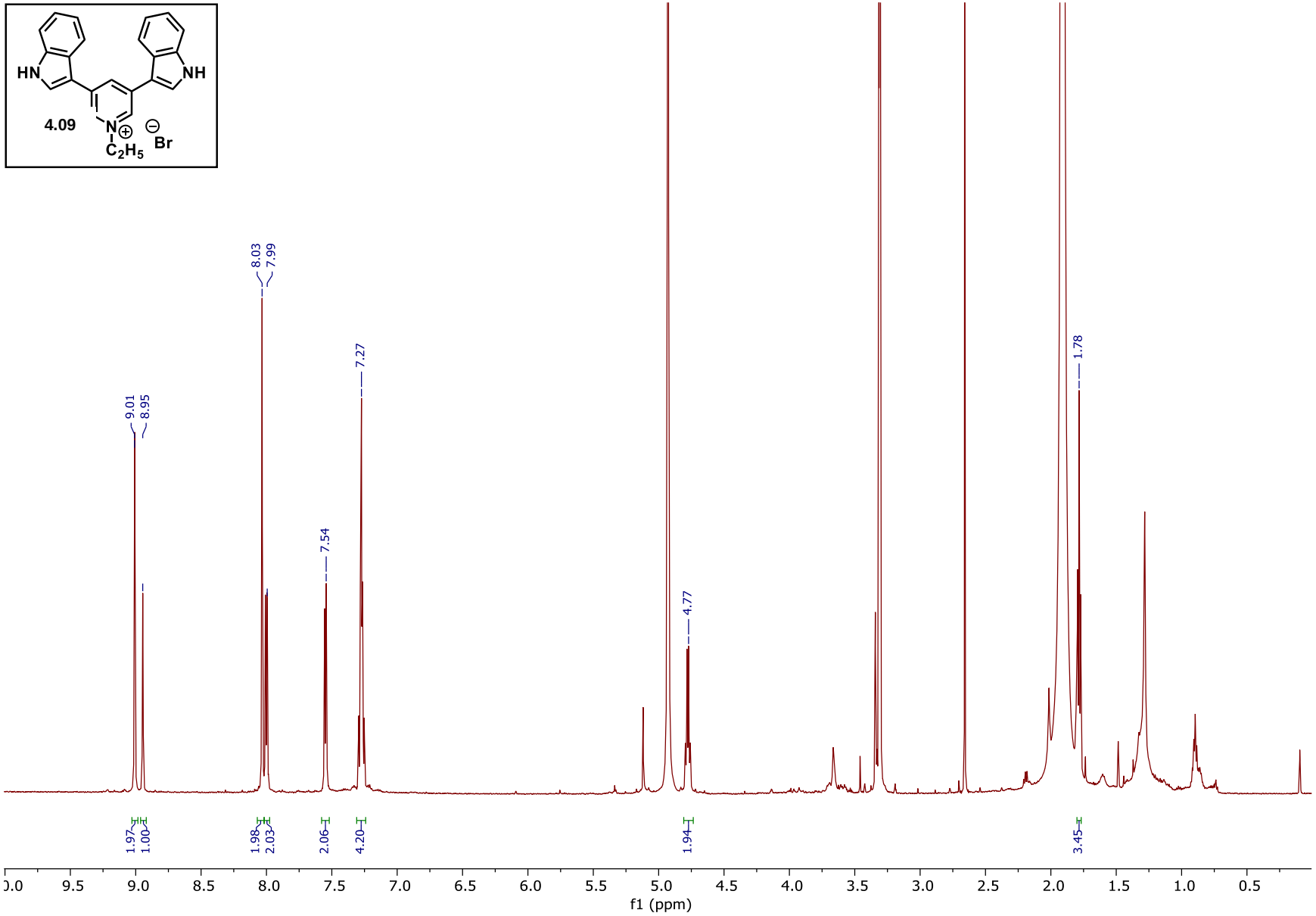
HN
NH
4.09
N
Br
C2H5
9.01
8.95
8.03
7.99
7.54
7.27
4.77
1.78
1.97
1.00
1.98
2.03
2.06
4.20
1.94
3.45
f1 (ppm)

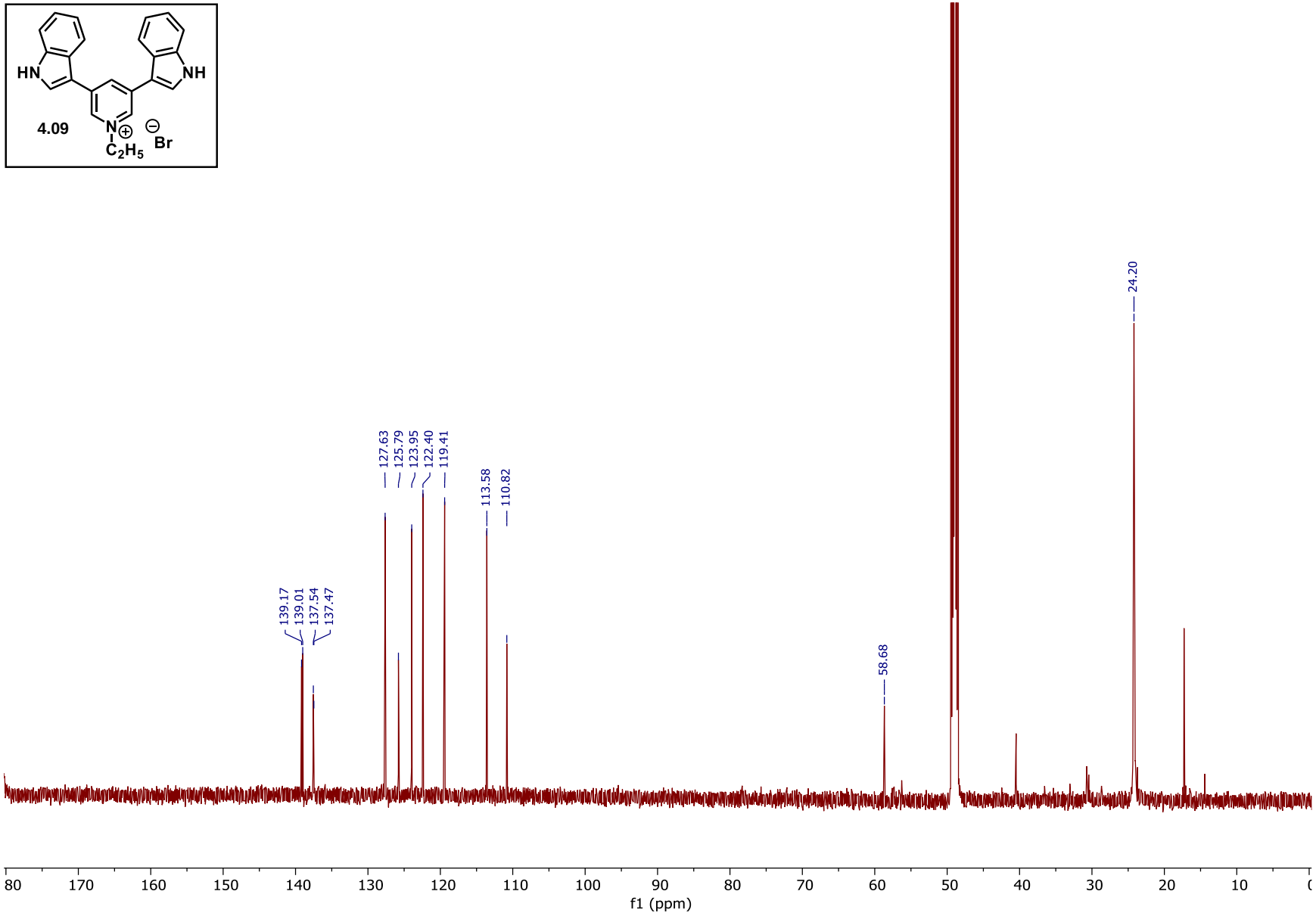
HN
NH
4.09
N
Br
C2H5
139.17
139.01
137.54
137.47
127.63
125.79
123.95
122.40
119.41
113.58
110.82
58.68
24.20
80
170
160
150
140
130
120
110
100
90
80
70
60
50
40
30
20
10
f1 (ppm)

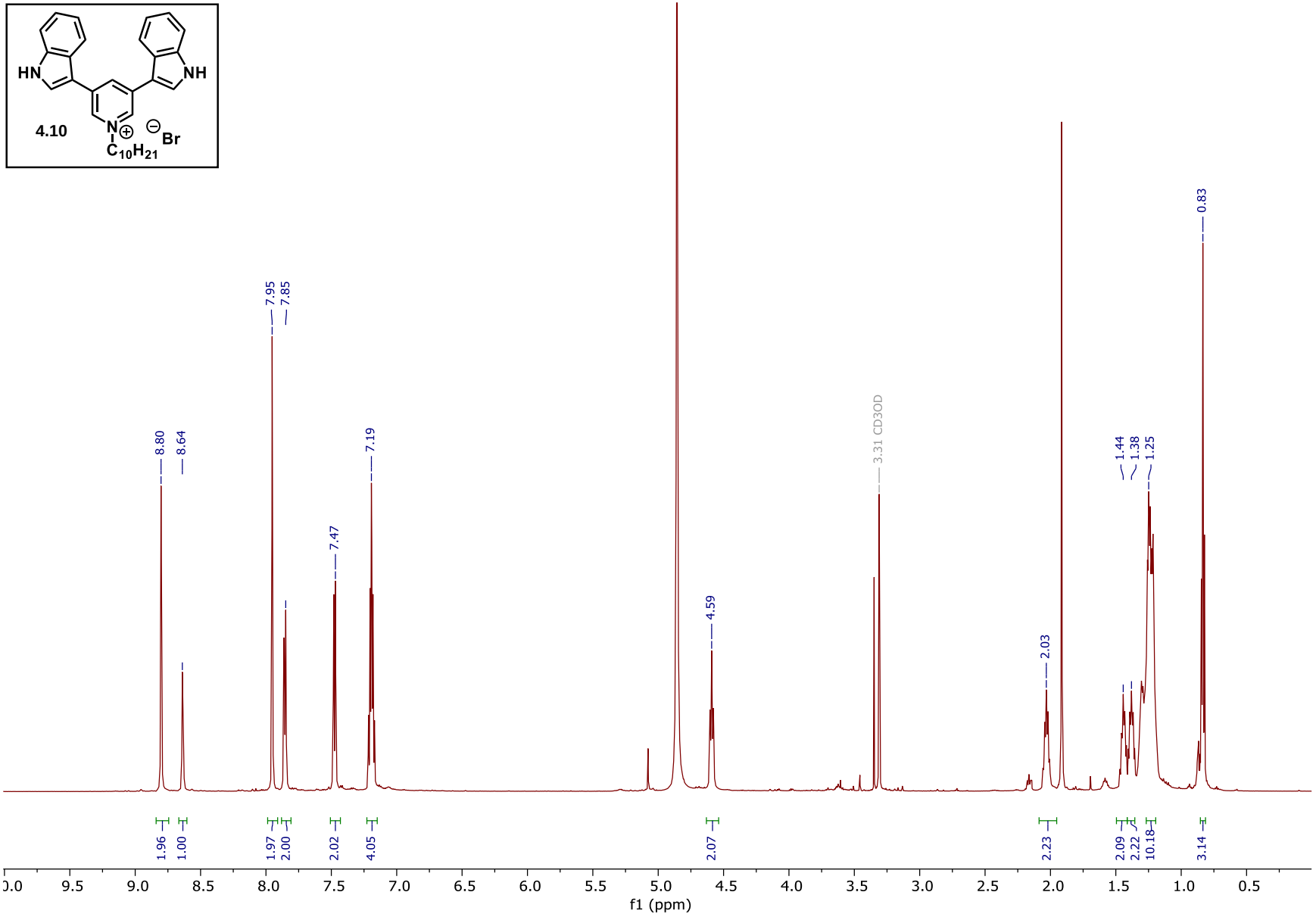
HN
NH
4.10
N
Br
C10H21
8.80
8.64
7.95
7.85
7.47
7.19
4.59
3.31 CD3OD
2.03
1.44
1.38
1.25
0.83
1.96
1.00
1.97
2.00
2.02
4.05
2.07
2.23
2.09
2.22
10.18
3.14
f1 (ppm)

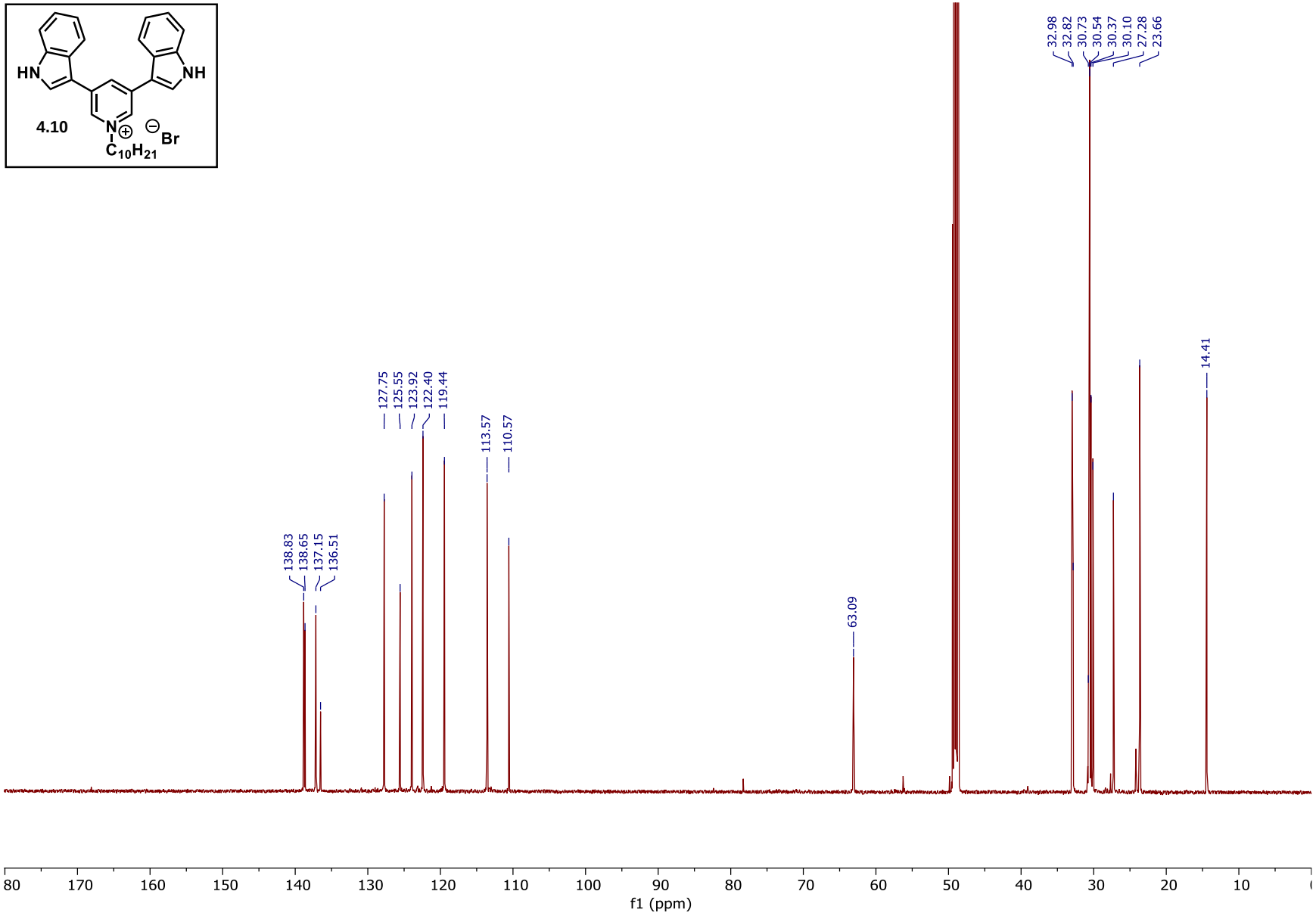
HN
NH
4.10
N
Br
C10H21
32.98
32.82
30.73
30.54
30.37
30.10
27.28
23.66
14.41
127.75
125.55
123.92
122.40
119.44
113.57
110.57
138.83
138.65
137.15
136.51
63.09
80
170
160
150
140
130
120
110
100
90
80
70
60
50
40
30
20
10
f1 (ppm)

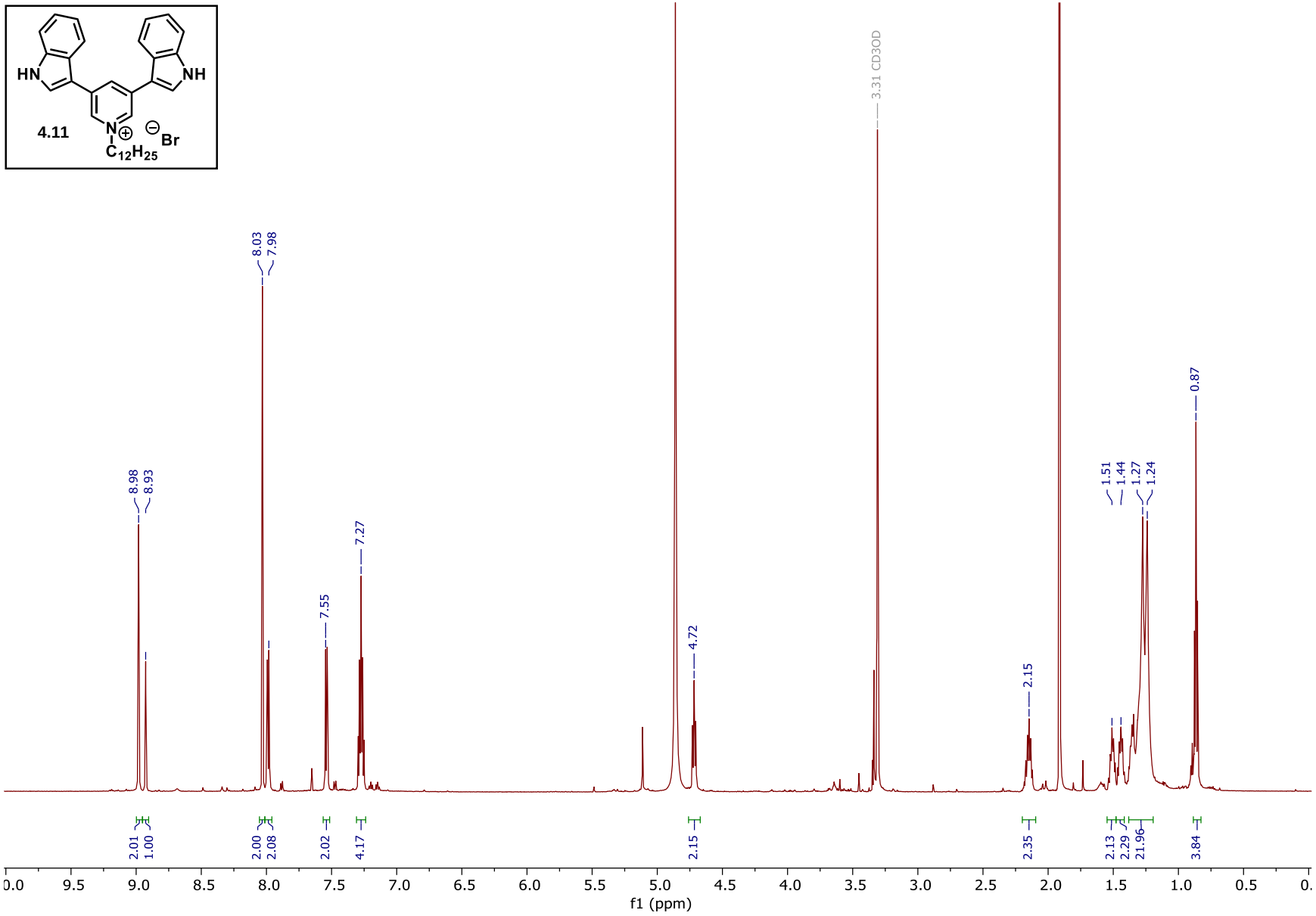
HN
NH
4.11
N
Br
C12H25
8.98
8.93
8.03
7.98
7.55
7.27
4.72
3.31 CD3OD
2.15
1.51
1.44
1.27
1.24
0.87
2.01
1.00
2.00
2.08
2.02
4.17
2.15
2.35
2.13
2.29
21.96
3.84
f1 (ppm)

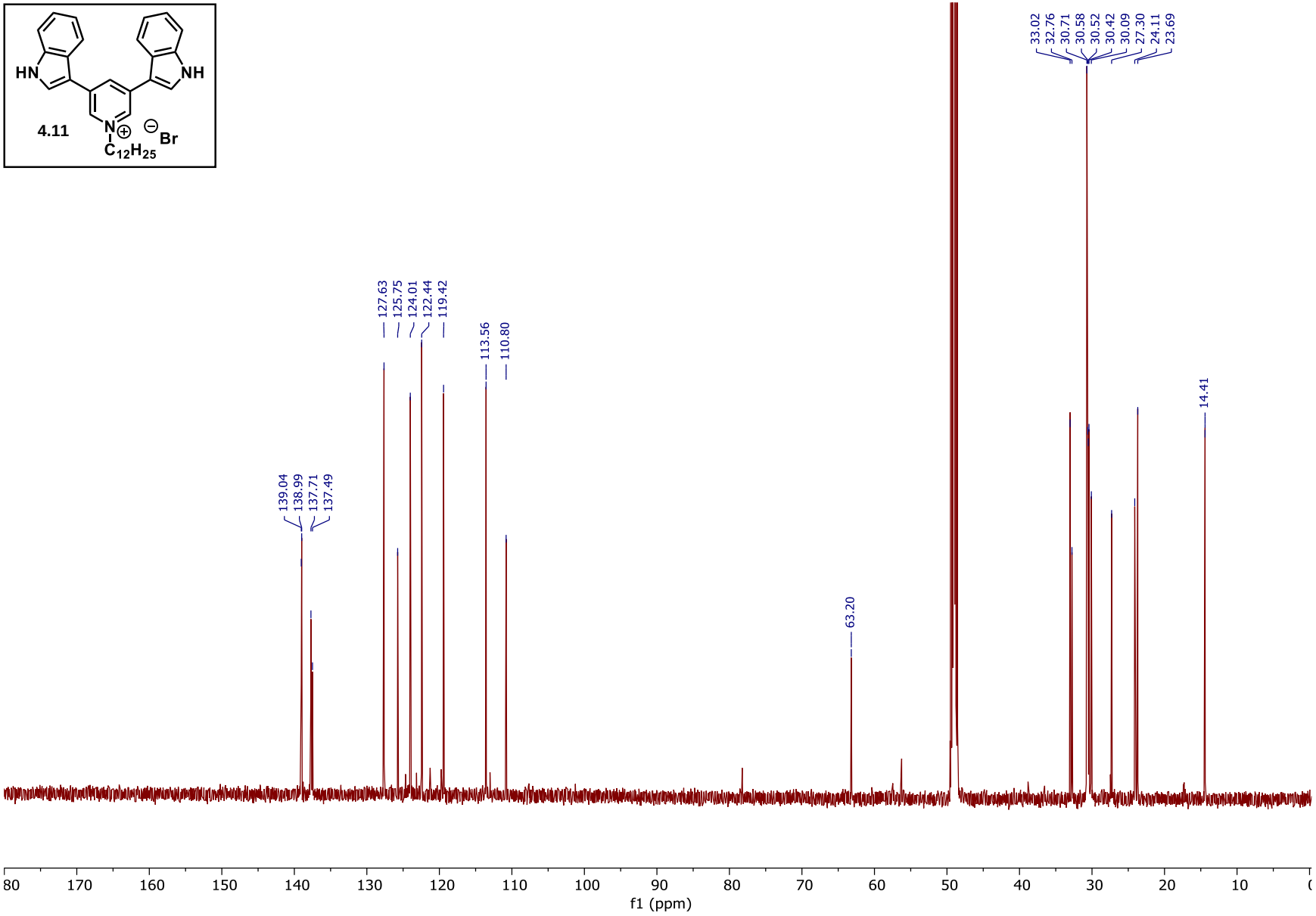
HN
NH
4.11
N
Br
C12H25
33.02
32.76
30.71
30.58
30.52
30.42
30.09
27.30
24.11
23.69
127.63
125.75
124.01
122.44
119.42
113.56
110.80
139.04
138.99
137.71
137.49
63.20
14.41
80
170
160
150
140
130
120
110
100
90
80
70
60
50
40
30
20
10
f1 (ppm)

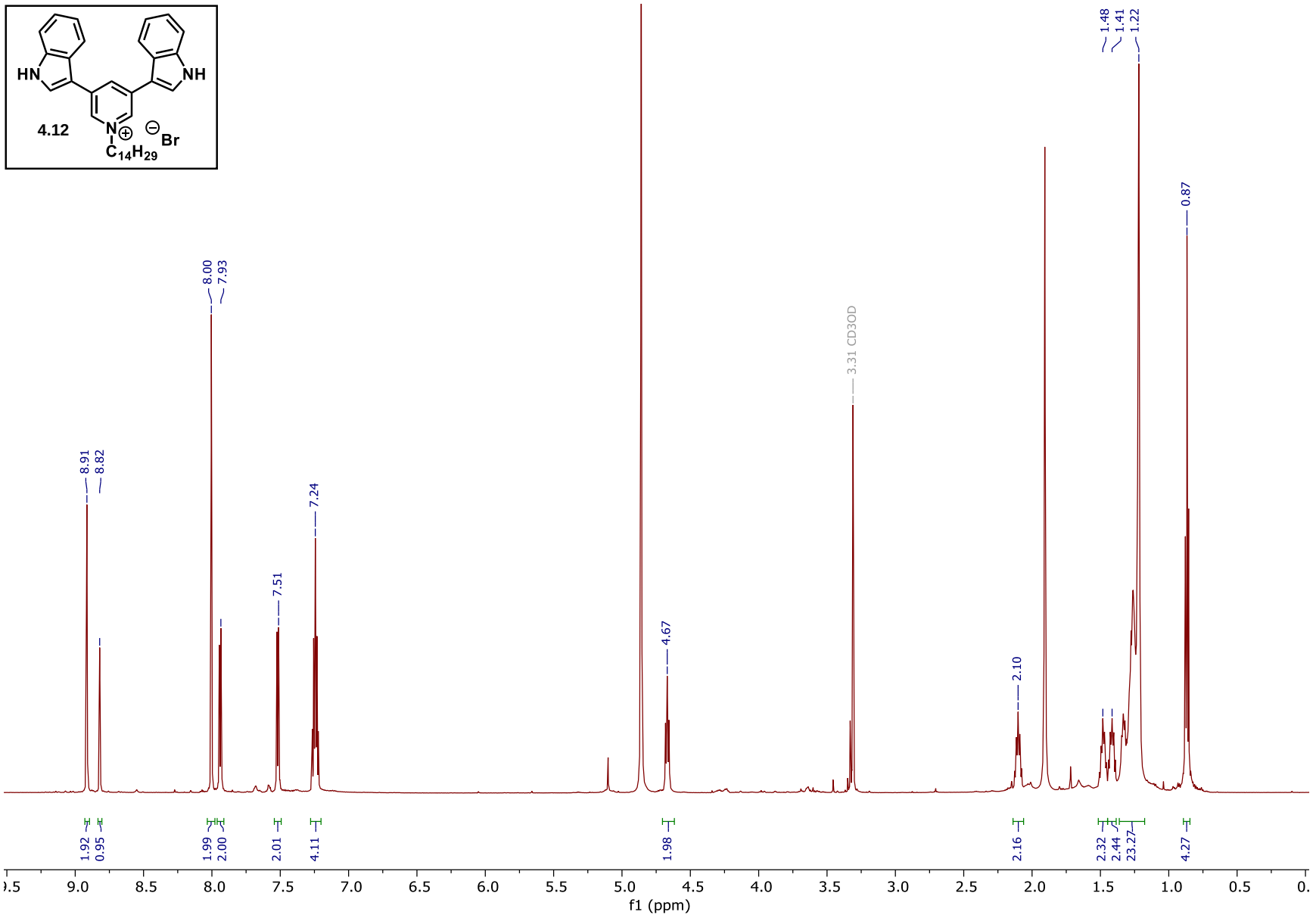
HN
NH
4.12
N
Br
C14H29
8.91
8.82
8.00
7.93
7.51
7.24
4.67
3.31 CD3OD
2.10
1.48
1.41
1.22
0.87
1.92
0.95
1.99
2.00
2.01
4.11
1.98
2.16
2.32
2.44
23.27
4.27
f1 (ppm)

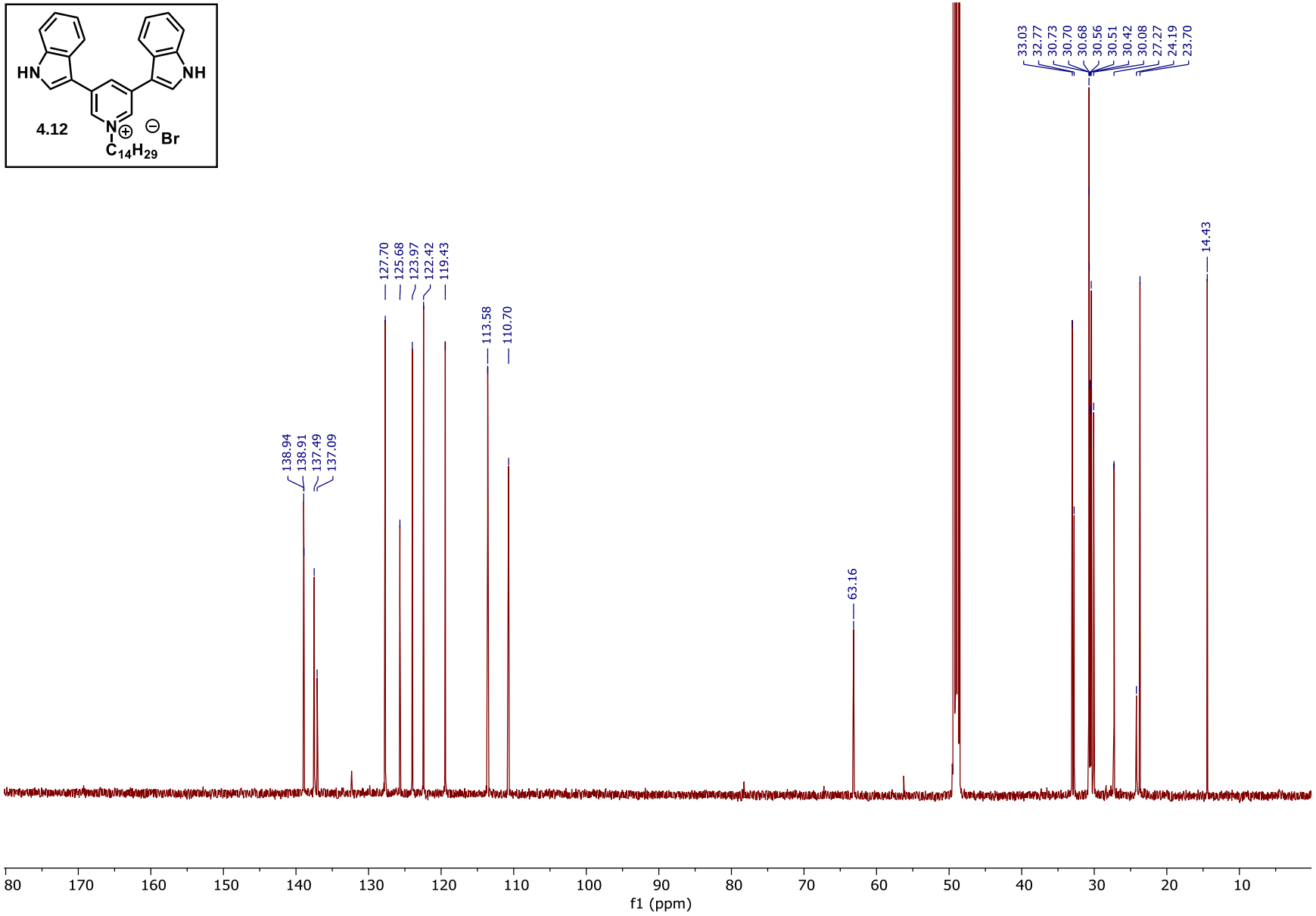
HN
NH
4.12
N
Br
C14H29
138.94
138.91
137.49
137.09
127.70
125.68
123.97
122.42
119.43
113.58
110.70
63.16
33.03
32.77
30.73
30.70
30.68
30.56
30.51
30.42
30.08
27.27
24.19
23.70
14.43
80
170
160
150
140
130
120
110
100
90
80
70
60
50
40
30
20
10
f1 (ppm)

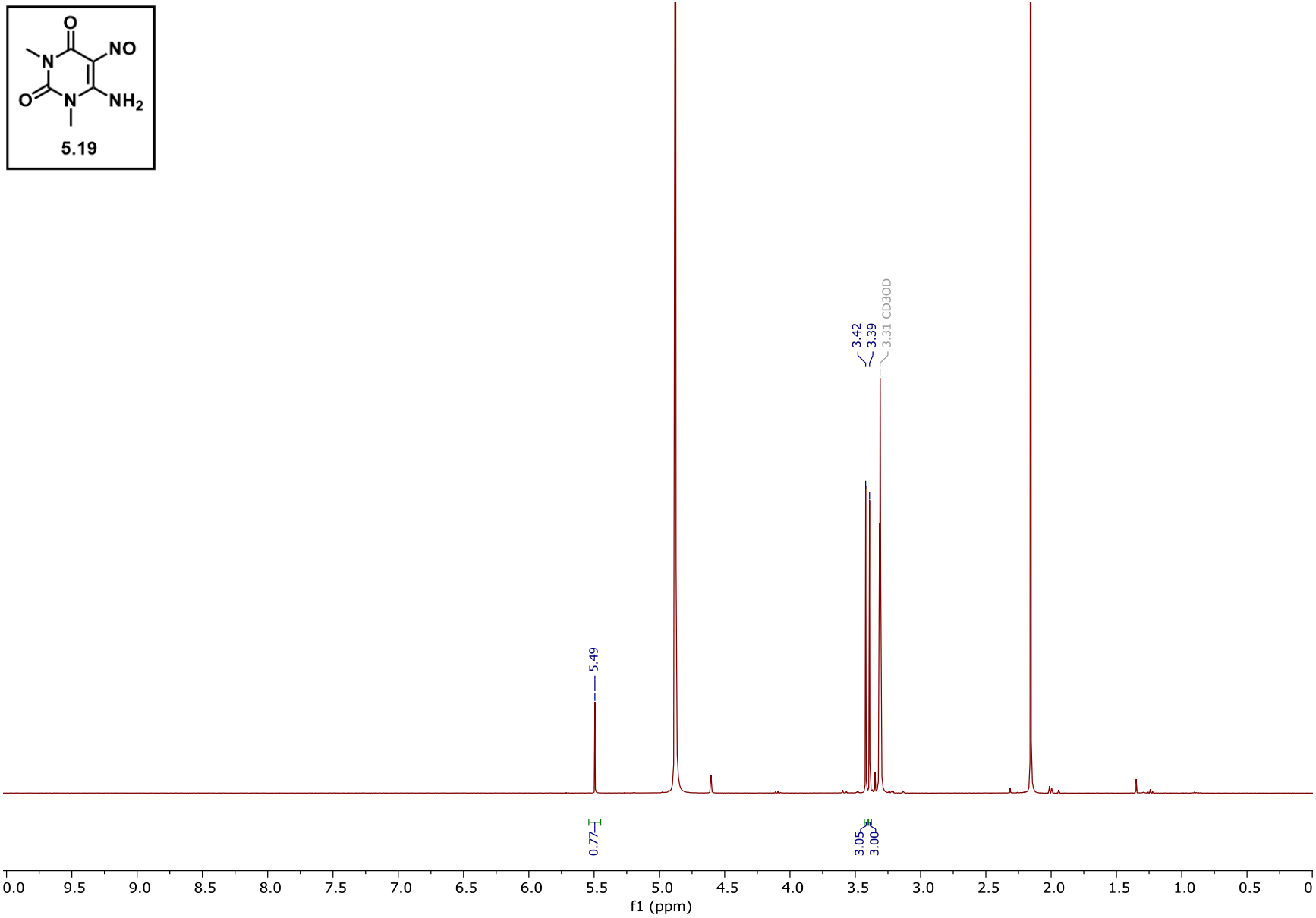
O
NO
N
O
N
NH2
5.19
5.49
3.42
3.39
3.31 CD3OD
0.77
3.05
3.00
0.0
9.5
9.0
8.5
8.0
7.5
7.0
6.5
6.0
5.5
5.0
4.5
4.0
3.5
3.0
2.5
2.0
1.5
1.0
0.5
0
f1 (ppm)

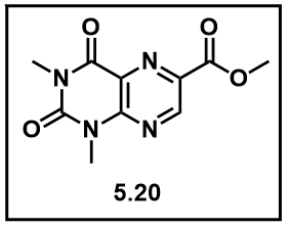
O
O
N
N
O
O
N
N
5.20

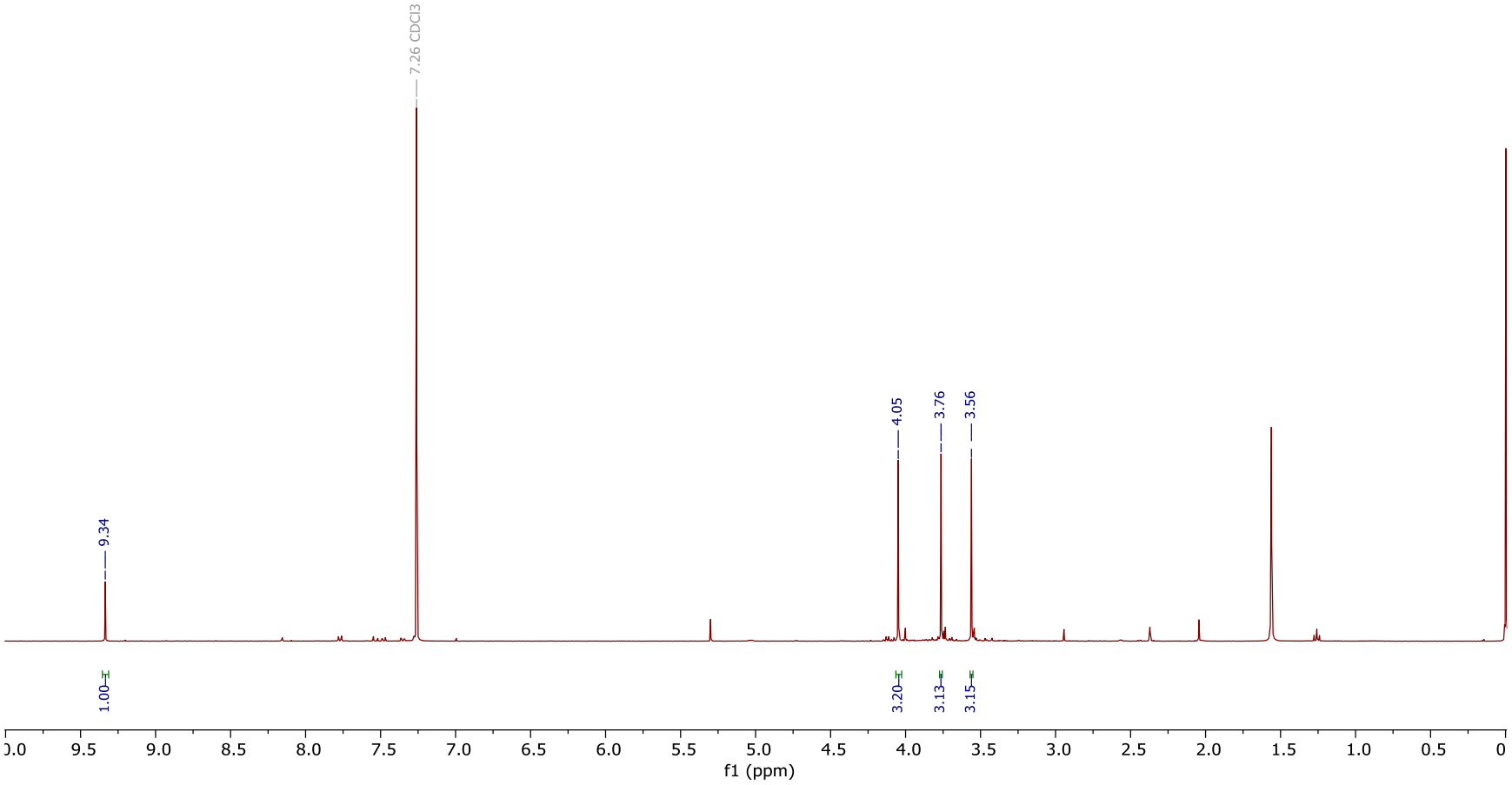
7.26 CDCl3
9.34
4.05
3.76
3.56
1.00
3.20
3.13
3.15
f1 (ppm)

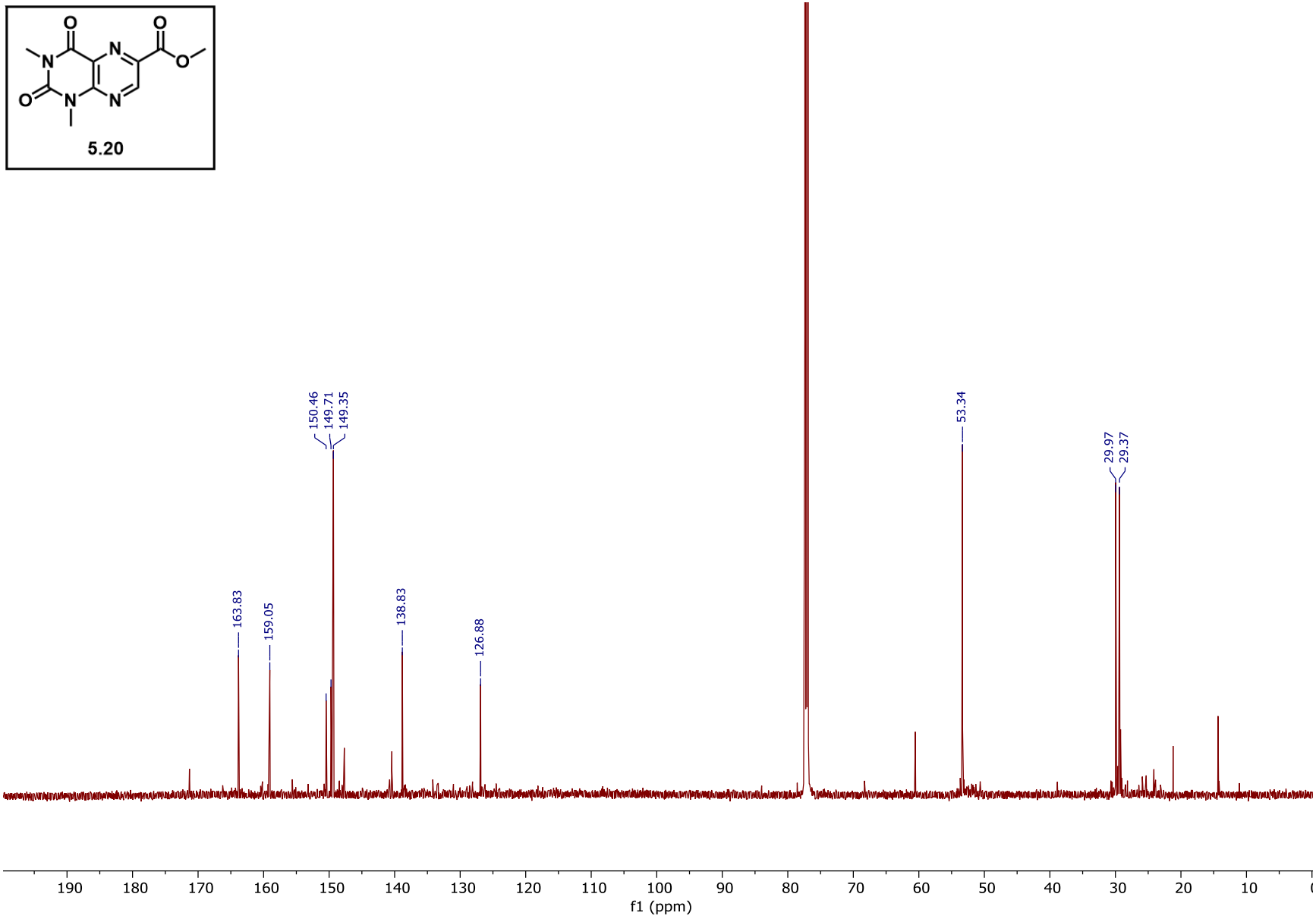
5.20
163.83
159.05
150.46
149.71
149.35
138.83
126.88
53.34
29.97
29.37
190
180
170
160
150
140
130
120
110
100
90
80
70
60
50
40
30
20
10
f1 (ppm)

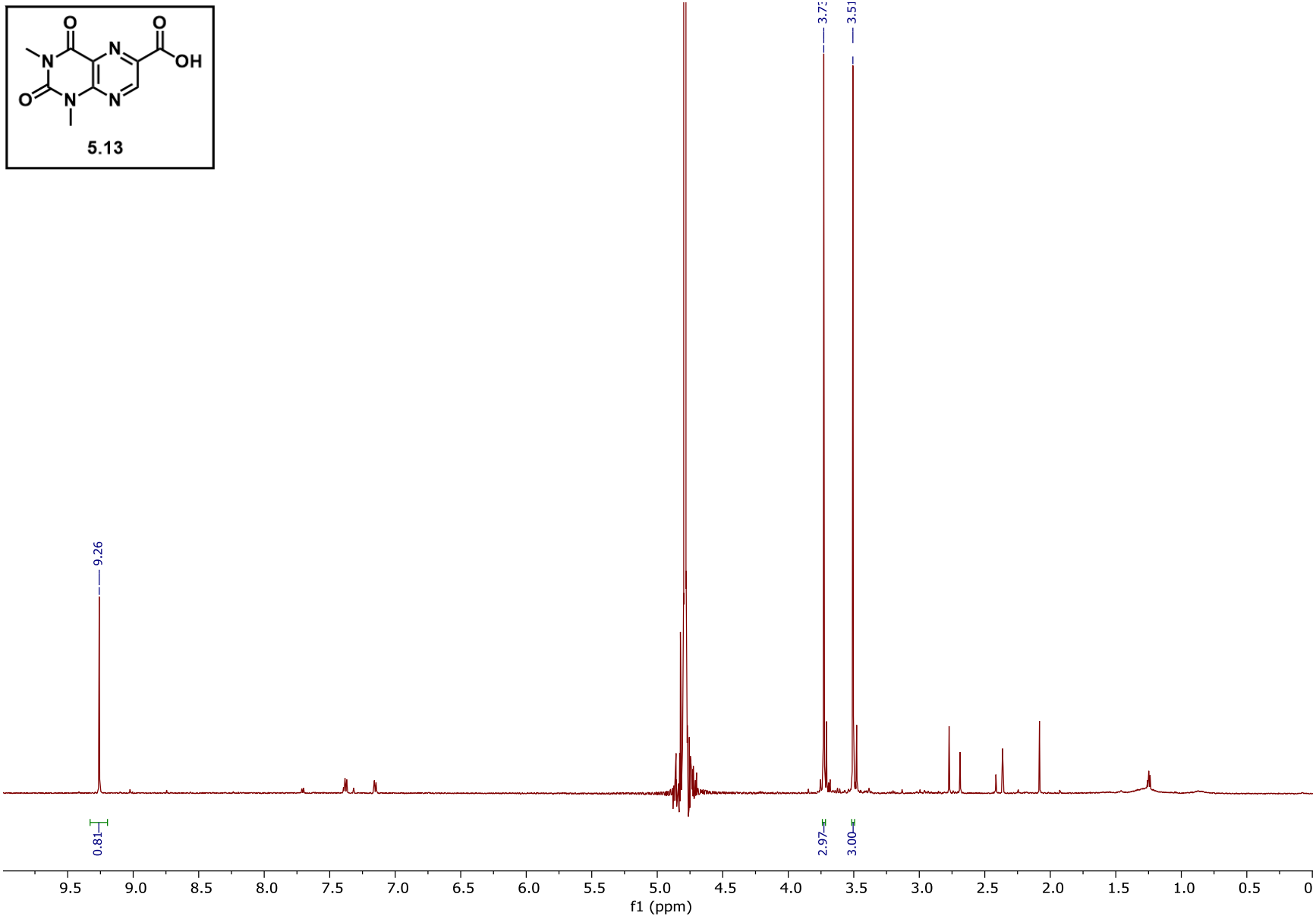
5.13
9.26
3.75
3.51
0.81
2.97
3.00
9.5
9.0
8.5
8.0
7.5
7.0
6.5
6.0
5.5
5.0
4.5
4.0
3.5
3.0
2.5
2.0
1.5
1.0
0.5
0
f1 (ppm)

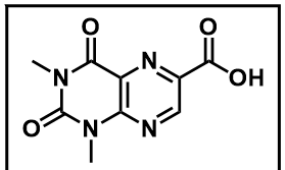
O
O
N
N
OH
O
N
N

5.13

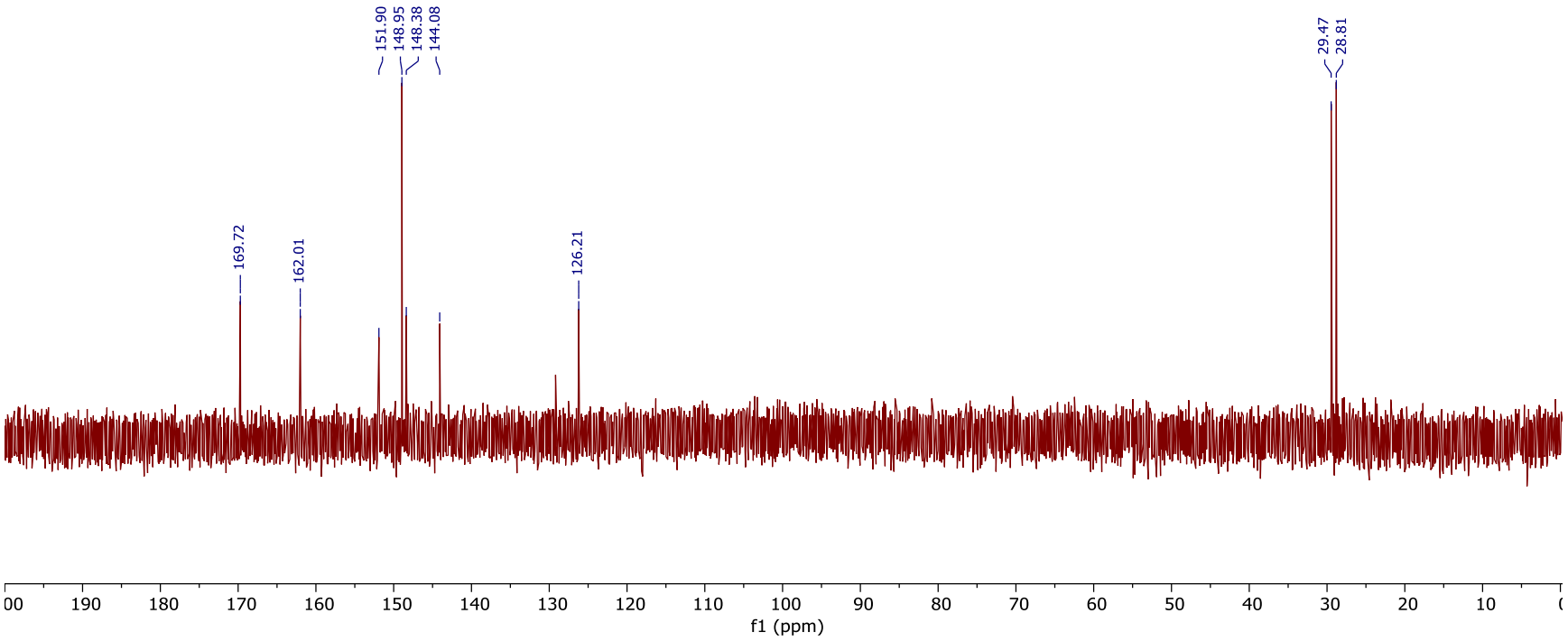
169.72
162.01
151.90
148.95
148.38
144.08
126.21
29.47
28.81
00
190
180
170
160
150
140
130
120
110
100
90
80
70
60
50
40
30
20
10
f1 (ppm)

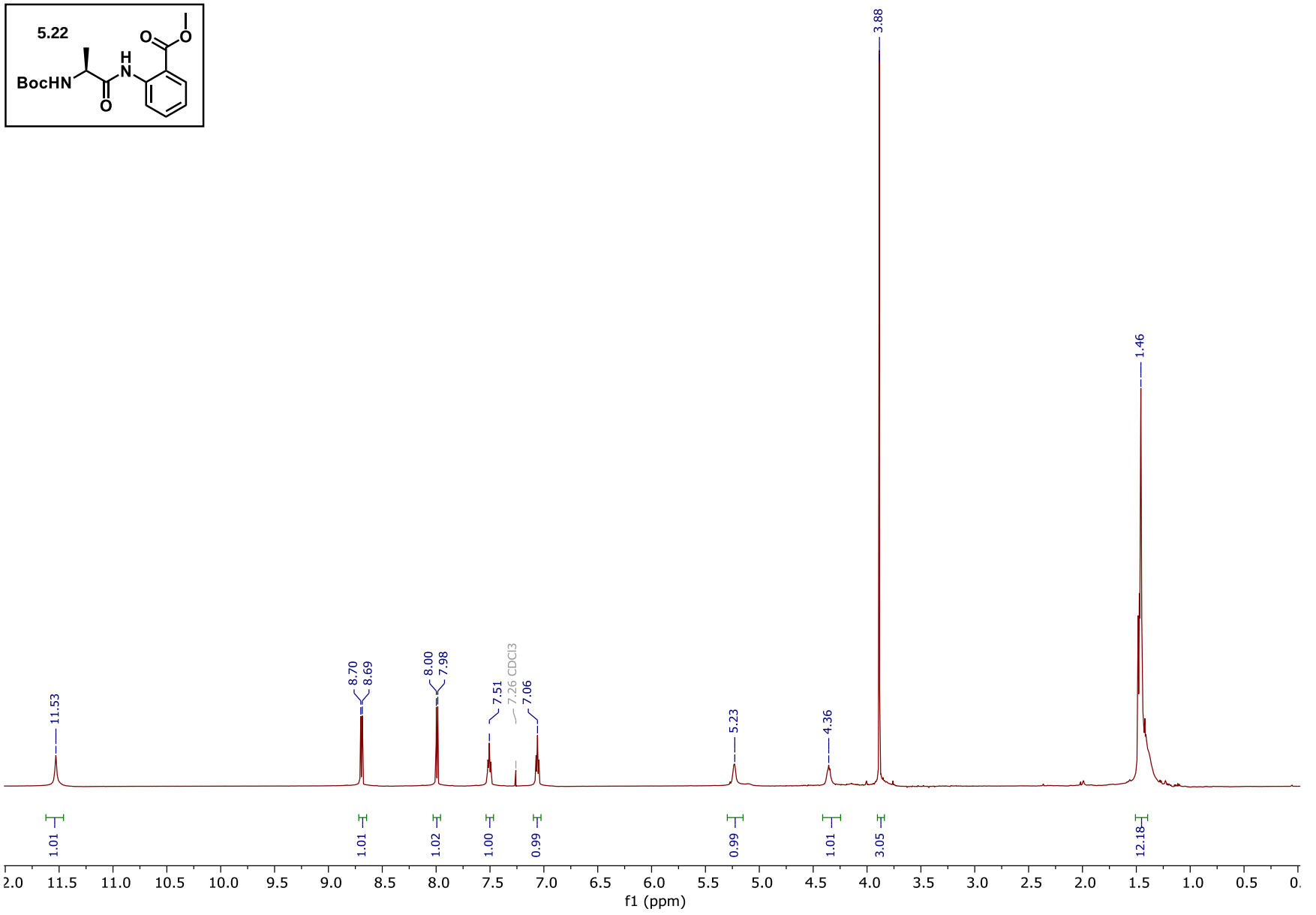
5.22
BocHN
H
N
O
O
O
11.53
8.70
8.69
8.00
7.98
7.51
7.26 CDCl3
7.06
5.23
4.36
3.88
1.46
1.01
1.01
1.02
1.00
0.99
0.99
1.01
3.05
12.18
f1 (ppm)

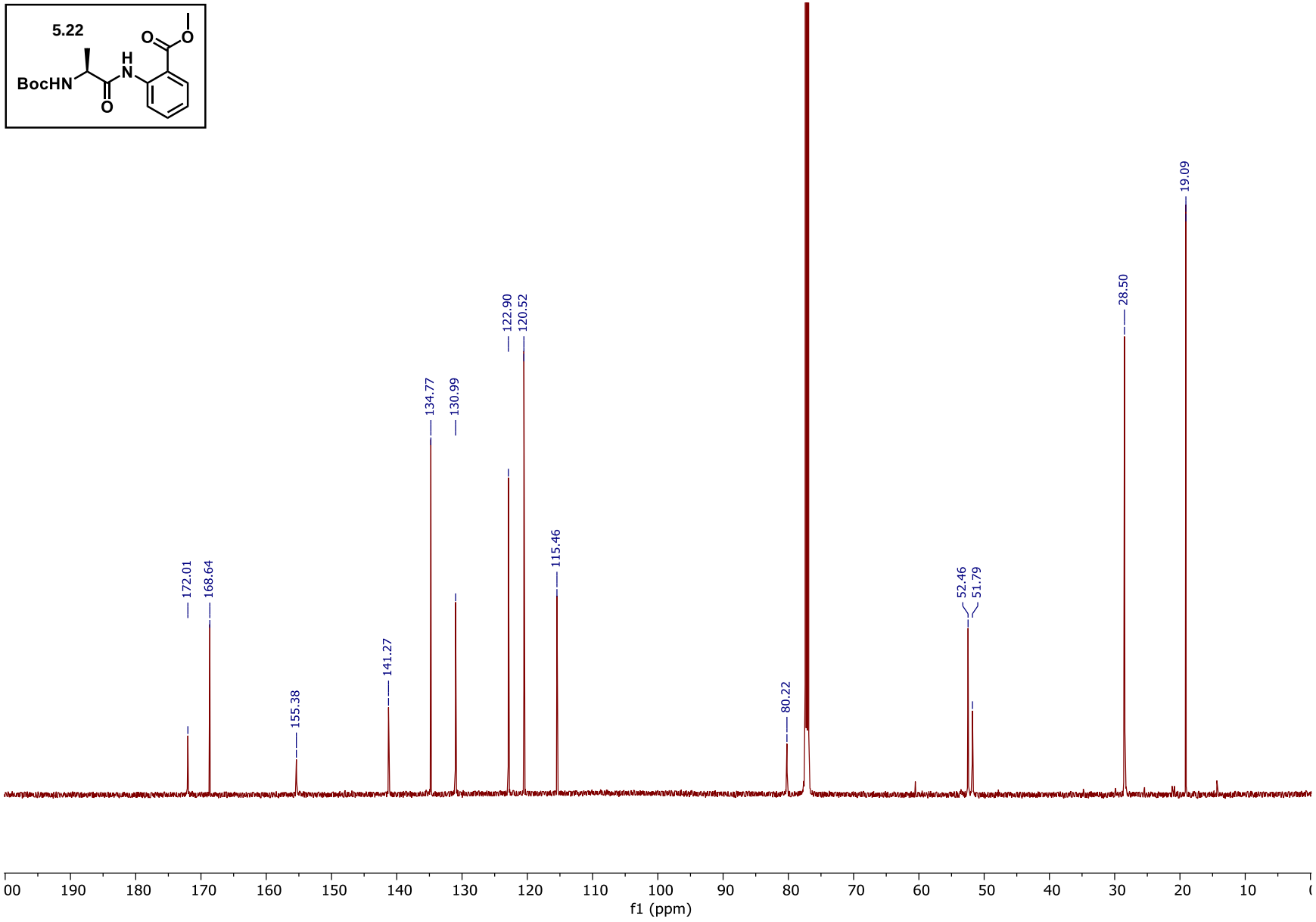
5.22
BocHN
H
N
O
O
O
172.01
168.64
155.38
141.27
134.77
130.99
122.90
120.52
115.46
80.22
52.46
51.79
28.50
19.09
f1 (ppm)

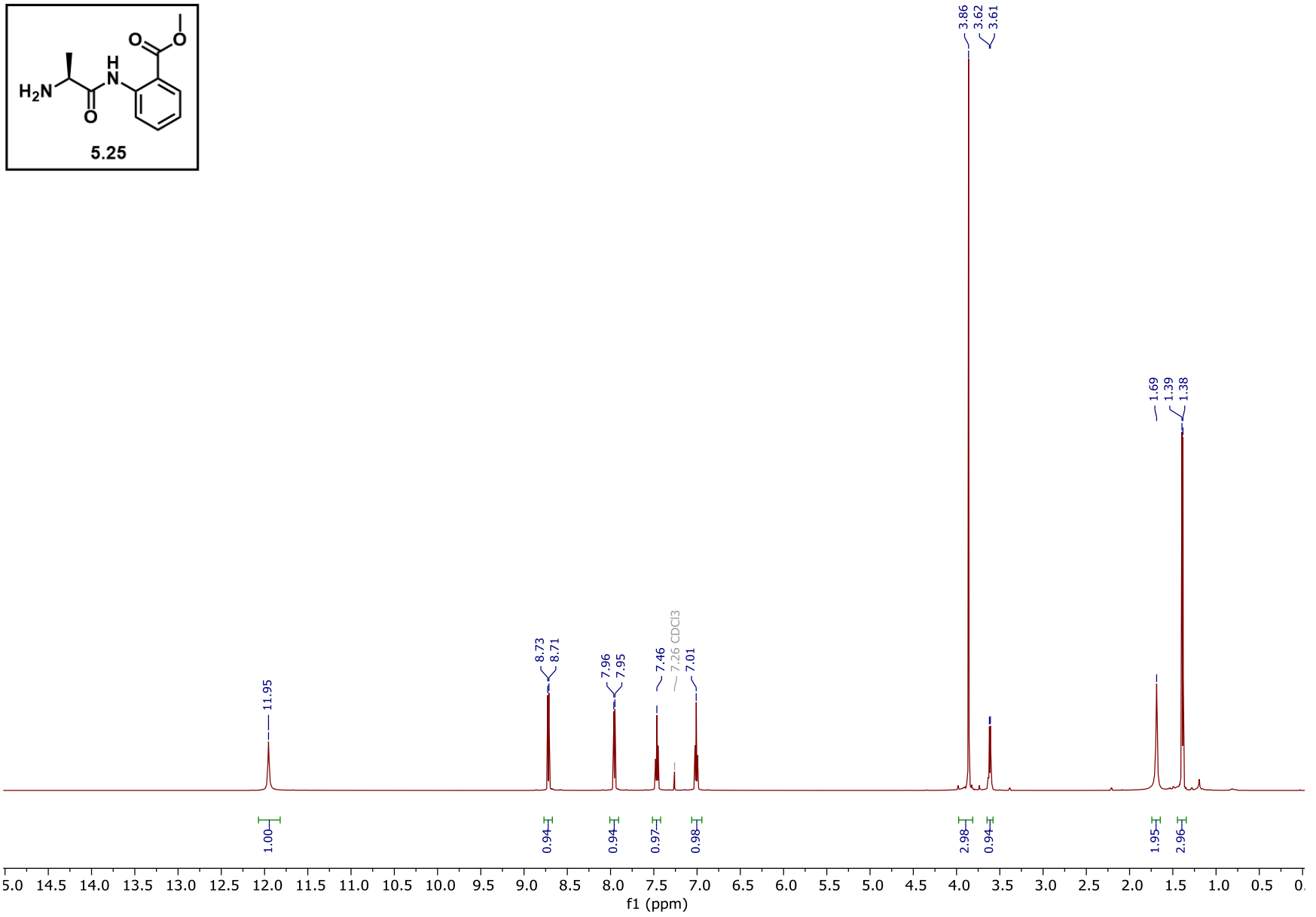
5.25
3.86
3.62
3.61
1.69
1.39
1.38
11.95
8.73
8.71
7.96
7.95
7.46
7.26 CDCl3
7.01
1.00
0.94
0.94
0.97
0.98
2.98
0.94
1.95
2.96
f1 (ppm)

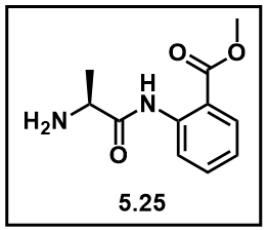
O
O
H
N
H_2N
O

5.25

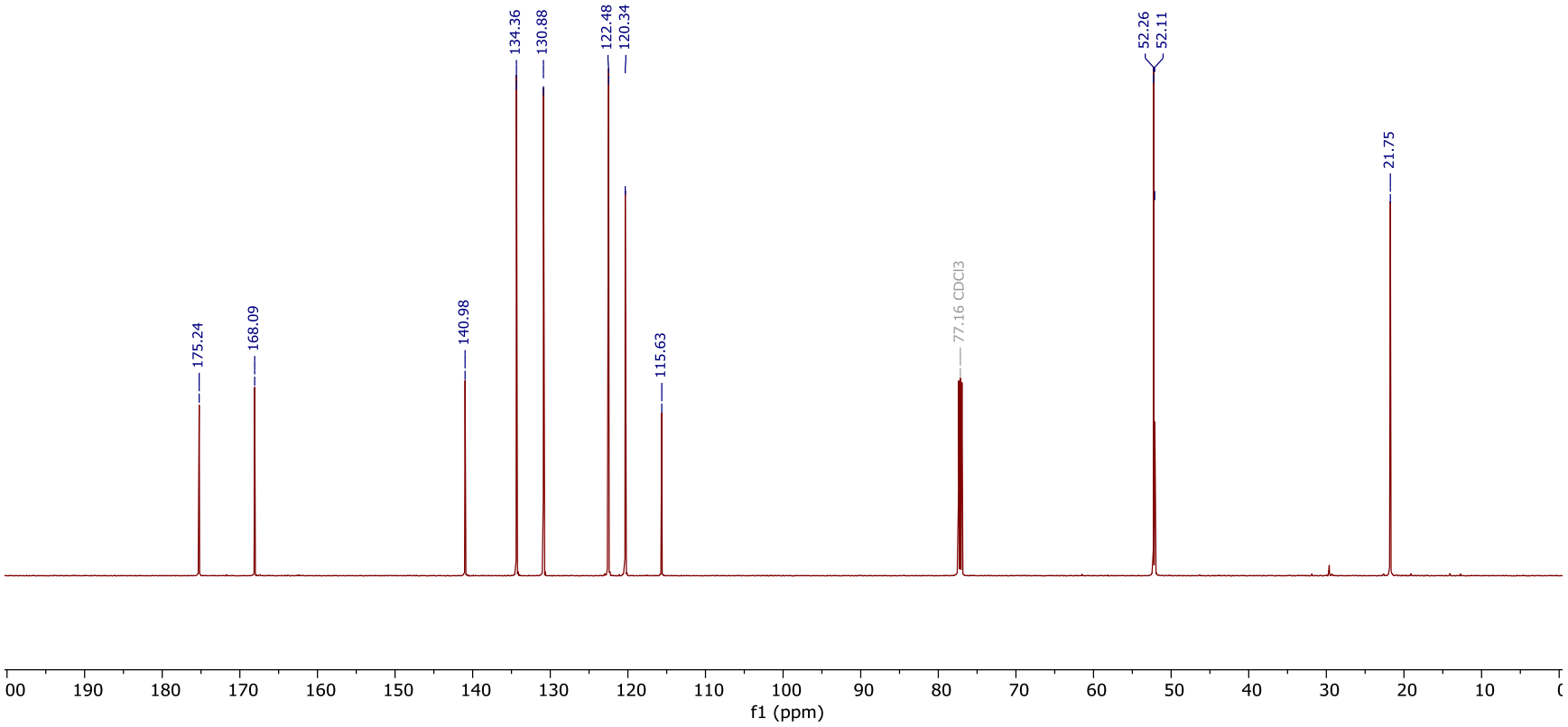
175.24
168.09
140.98
134.36
130.88
122.48
120.34
115.63
77.16 CDCl3
52.26
52.11
21.75
00
190
180
170
160
150
140
130
120
110
100
90
80
70
60
50
40
30
20
10
f1 (ppm)

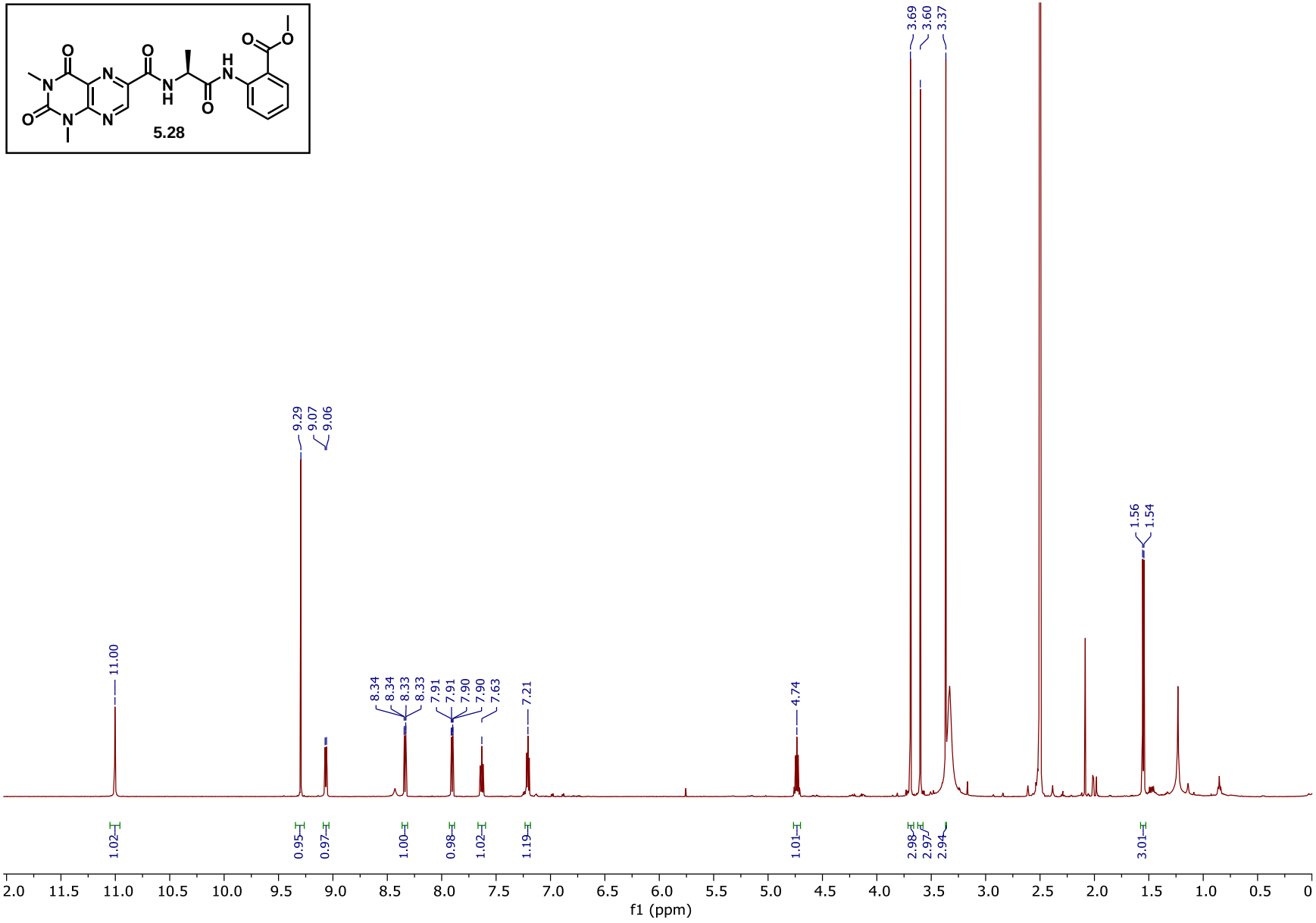
5.28
11.00
9.29
9.07
9.06
8.34
8.34
8.33
8.33
7.91
7.91
7.90
7.90
7.63
7.21
4.74
3.69
3.60
3.37
1.56
1.54
1.02
0.95
0.97
1.00
0.98
1.02
1.19
1.01
2.98
2.97
2.94
3.01
f1 (ppm)

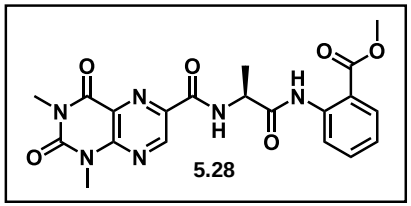
5.28

170.69
167.34
162.50
159.18
150.43
149.53
146.66
139.41
139.24
134.08
130.61
126.25
123.45
120.98
117.67
52.35
49.98
29.40
28.62
17.28
f1 (ppm)

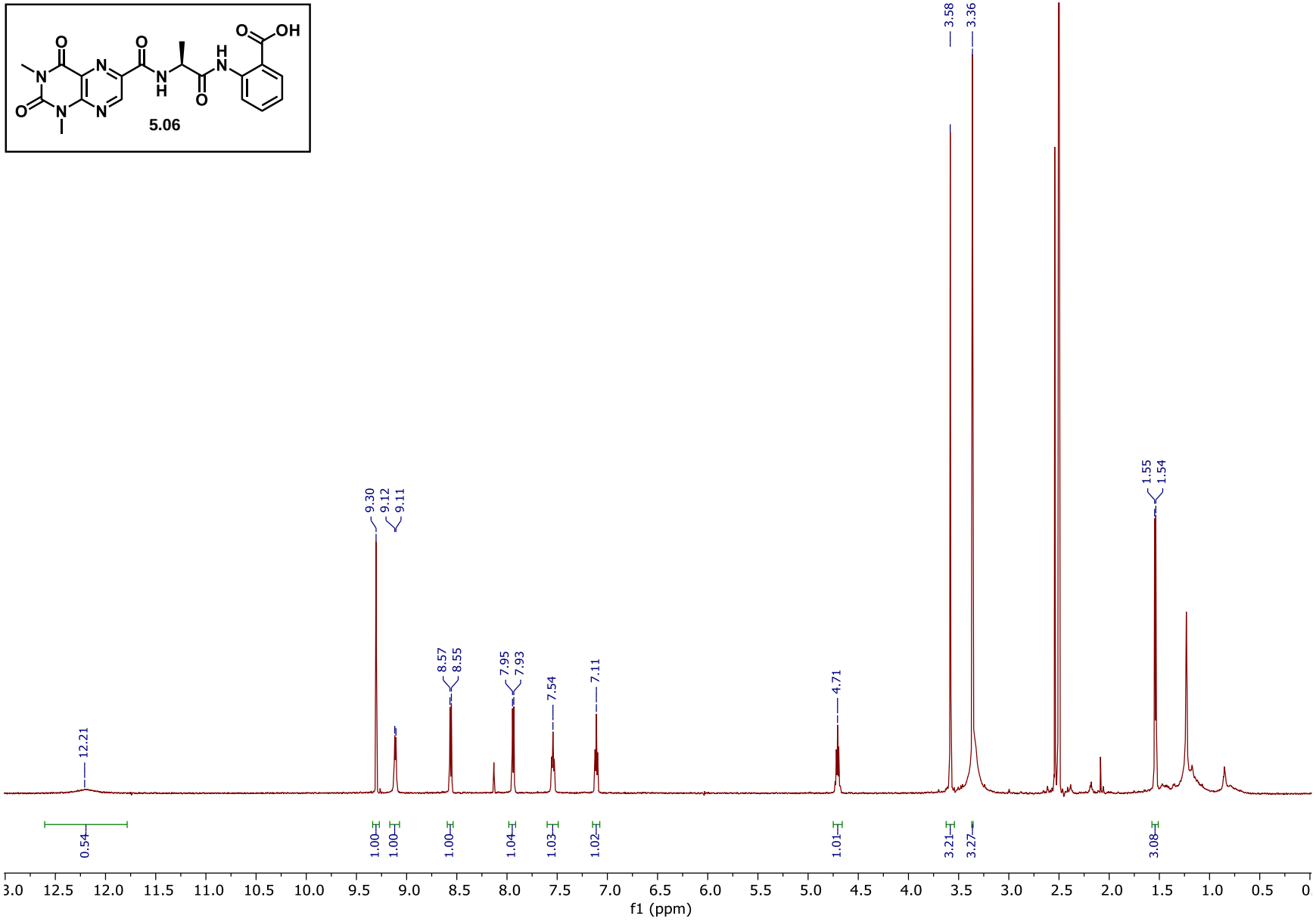
5.06
12.21
9.30
9.12
9.11
8.57
8.55
7.95
7.93
7.54
7.11
4.71
3.58
3.36
1.55
1.54
0.54
1.00
1.00
1.00
1.04
1.03
1.02
1.01
3.21
3.27
3.08
f1 (ppm)

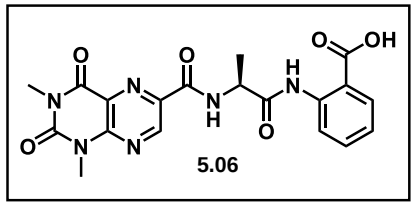
O
O
N
N
O
N
H
N
O
OH
N
N
O
N
H
O
5.06

170.51
169.24
163.10
162.41
159.15
150.37
149.43
146.72
140.44
139.51
133.20
131.15
126.19
122.52
119.36
50.07
29.38
28.64
17.31
00
190
180
170
160
150
140
130
120
110
100
90
80
70
60
50
40
30
20
10
f1 (ppm)

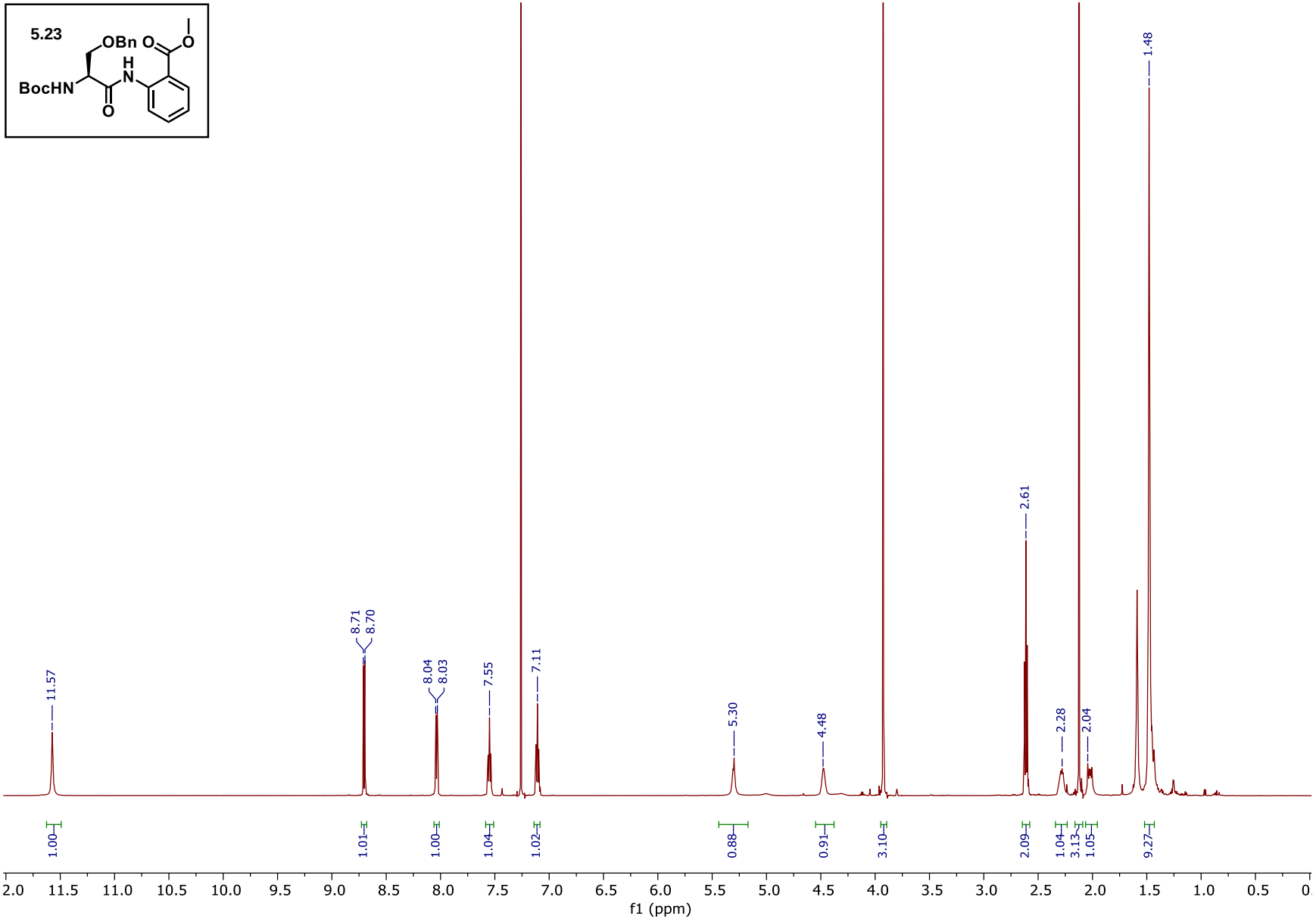
5.23
OBn
O
O
H
N
BocHN
O
11.57
8.71
8.70
8.04
8.03
7.55
7.11
5.30
4.48
2.61
2.28
2.04
1.48
1.00
1.01
1.00
1.04
1.02
0.88
0.91
3.10
2.09
1.04
3.13
1.05
9.27
f1 (ppm)

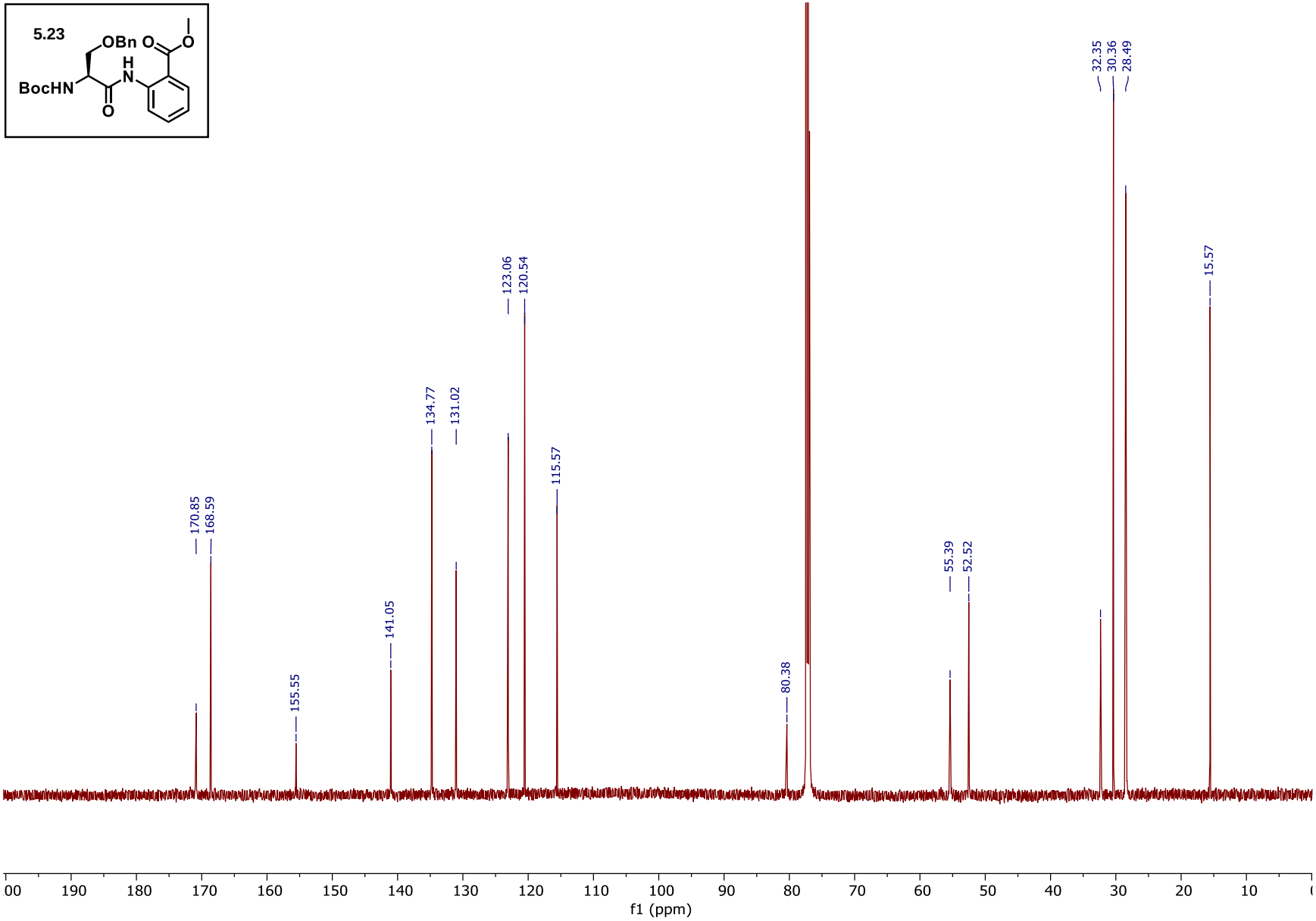
5.23
OBn
O
O
H
N
BocHN
O
170.85
168.59
155.55
141.05
134.77
131.02
123.06
120.54
115.57
80.38
55.39
52.52
32.35
30.36
28.49
15.57
f1 (ppm)

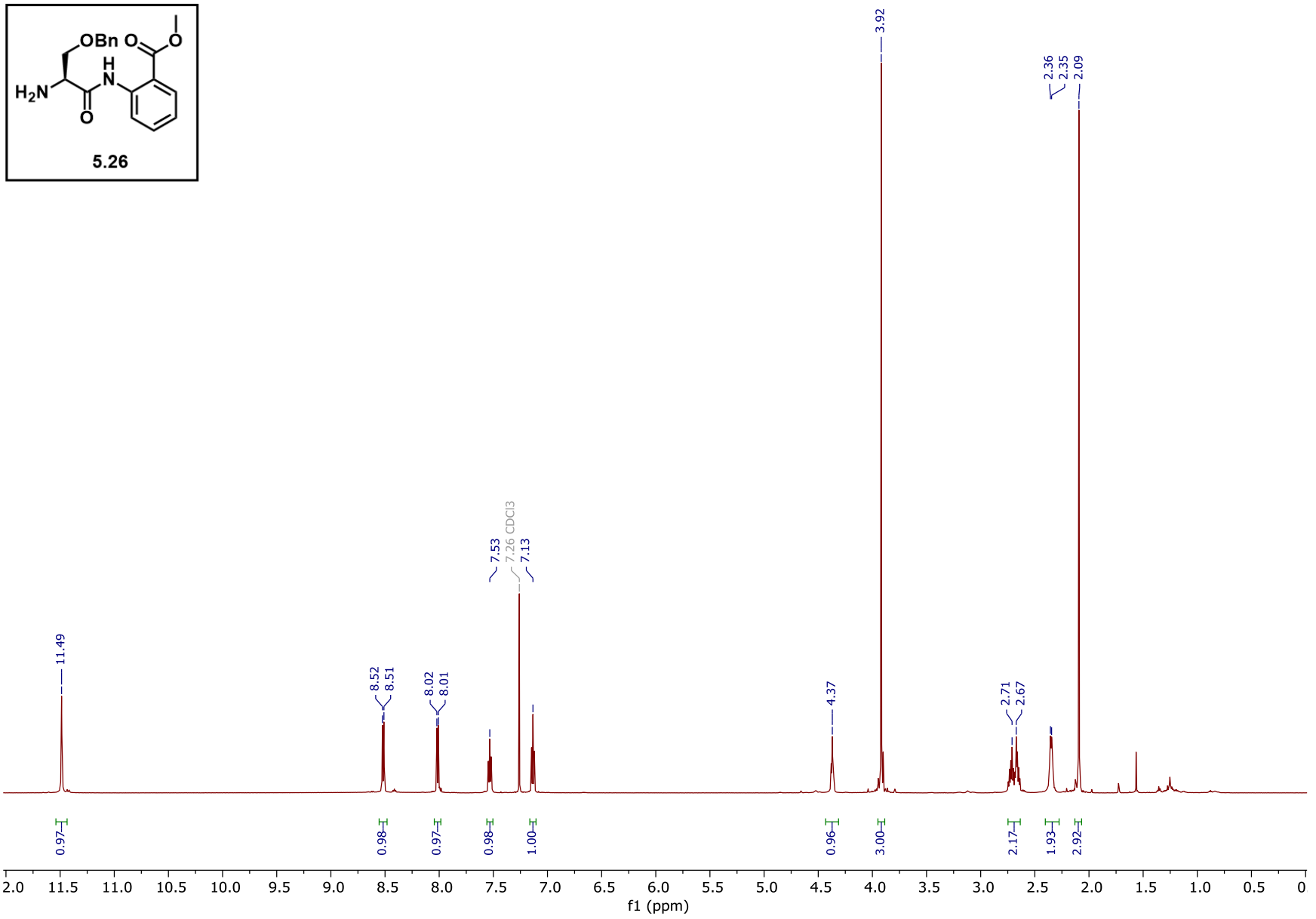
OBn
O
O
H
N
H_2N
O
5.26
11.49
8.52
8.51
8.02
8.01
7.53
7.26 CDCl3
7.13
4.37
3.92
2.71
2.67
2.36
2.35
2.09
0.97
0.98
0.97
0.98
1.00
0.96
3.00
2.17
1.93
2.92
f1 (ppm)

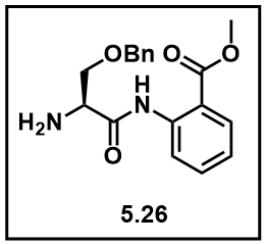
OBn
O
O
H
N
H_2N
O

5.26

168.75
167.15
139.81
134.91
131.05
124.06
121.06
116.04
54.07
52.80
30.42
29.27
14.89
f1 (ppm)

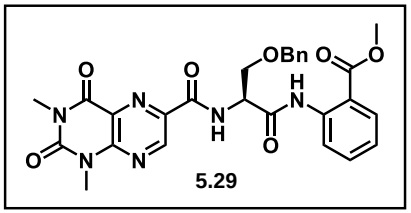
OBn
O
O
H
N
O
N
N
N
N
O
O
N
O
5.29

11.13
9.32
8.89
8.88
8.39
8.37
7.92
7.90
7.64
7.35
7.34
7.30
7.25
7.21
4.94
4.92
4.59
4.58
4.06
4.06
4.05
4.04
3.95
3.95
3.94
3.93
2.50 DMSO
1.03
0.94
1.00
1.01
1.03
1.04
2.04
2.04
1.03
1.02
1.02
2.08
1.01
0.99
2.97
3.01
3.00
2.0
11.5
11.0
10.5
10.0
9.5
9.0
8.5
8.0
7.5
7.0
6.5
6.0
5.5
5.0
4.5
4.0
3.5
3.0
2.5
2.0
1.5
1.0
0.5
0
f1 (ppm)

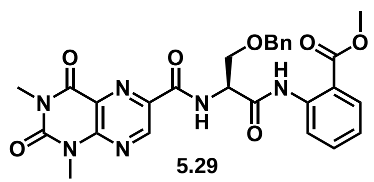

5.29

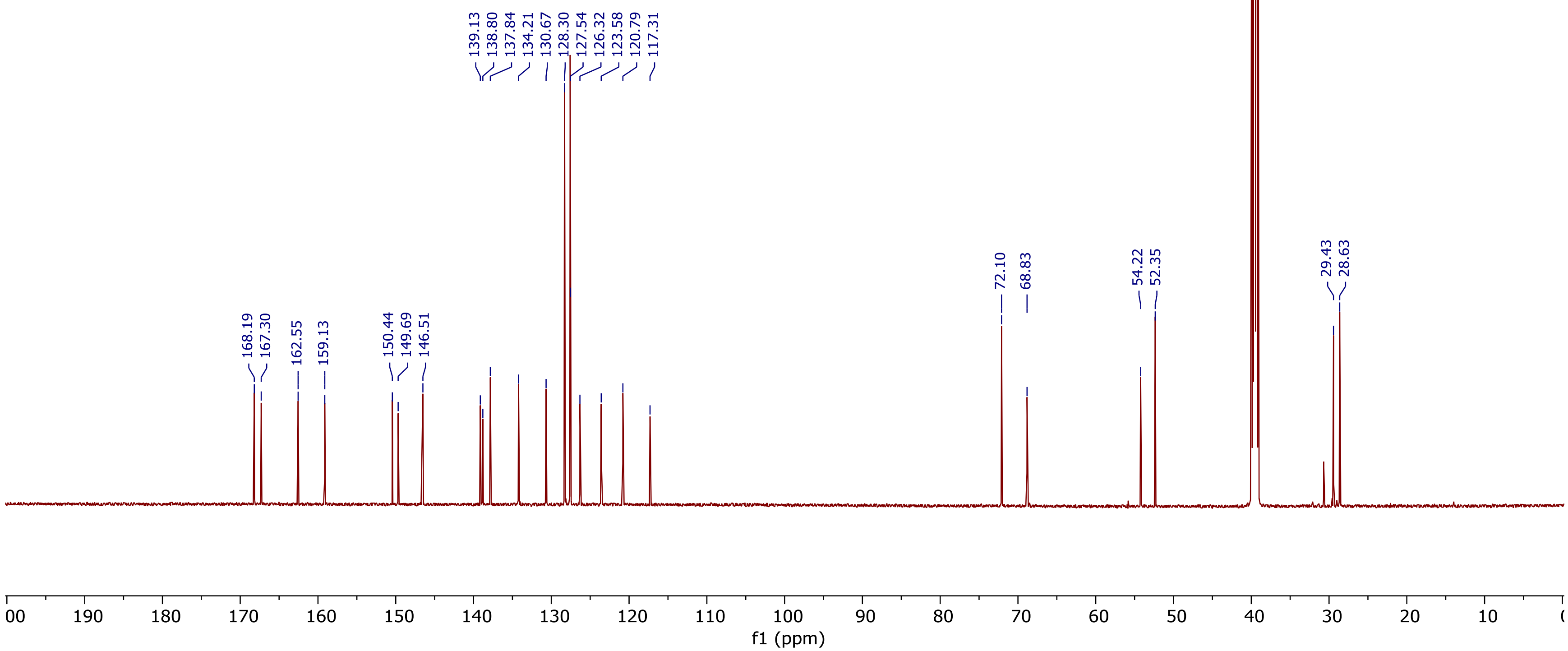

168.19
167.30
162.55
159.13
150.44
149.69
146.51
139.13
138.80
137.84
134.21
130.67
128.30
127.54
126.32
123.58
120.79
117.31
72.10
68.83
54.22
52.35
29.43
28.63
f1 (ppm)

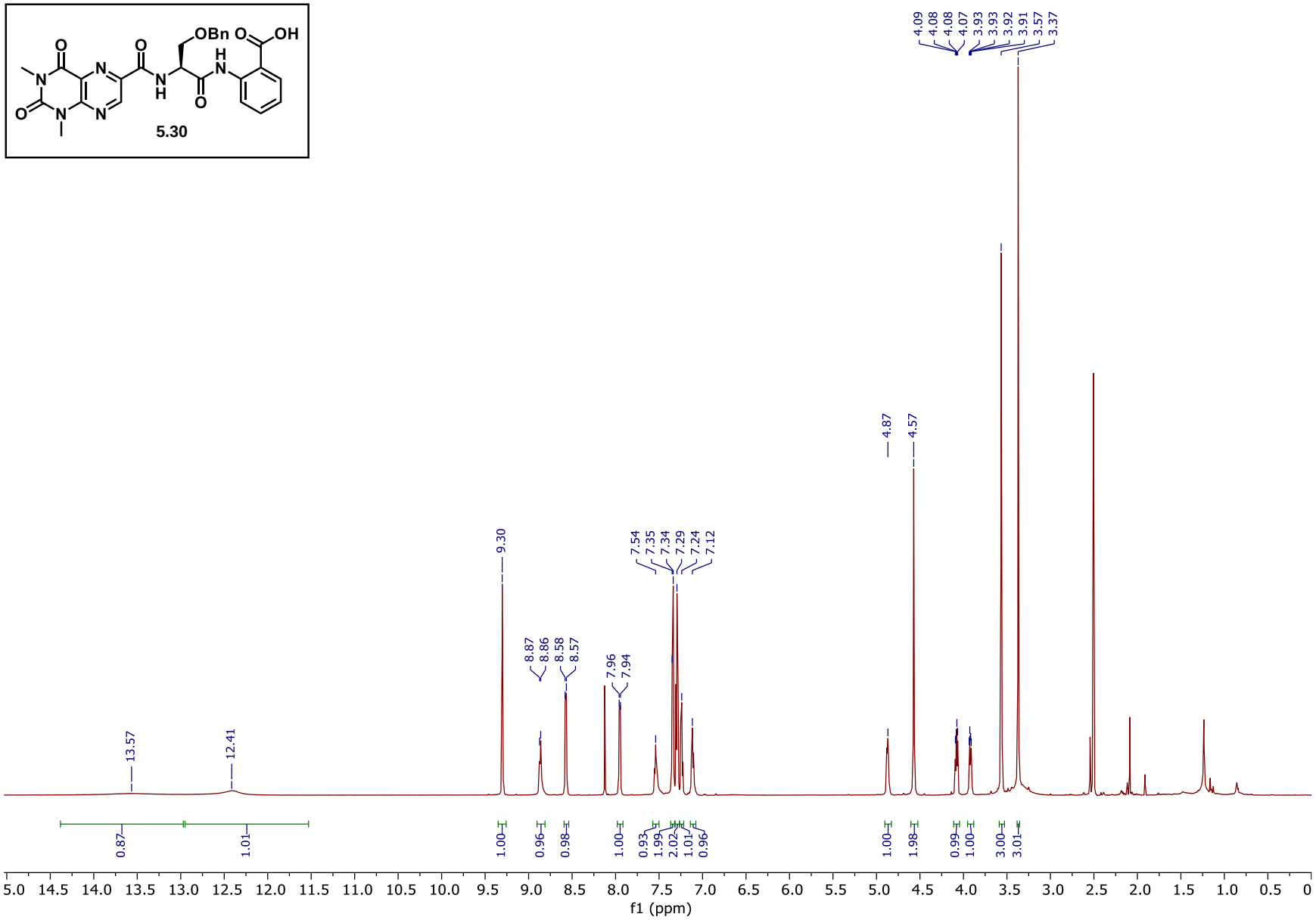
5.30
4.09
4.08
4.08
4.07
3.93
3.93
3.92
3.91
3.57
3.37
4.87
4.57
9.30
8.87
8.86
8.58
8.57
7.96
7.94
7.54
7.35
7.34
7.29
7.24
7.12
13.57
12.41
0.87
1.01
1.00
0.96
0.98
1.00
0.93
1.99
2.02
1.01
0.96
1.00
1.98
0.99
1.00
3.00
3.01
f1 (ppm)

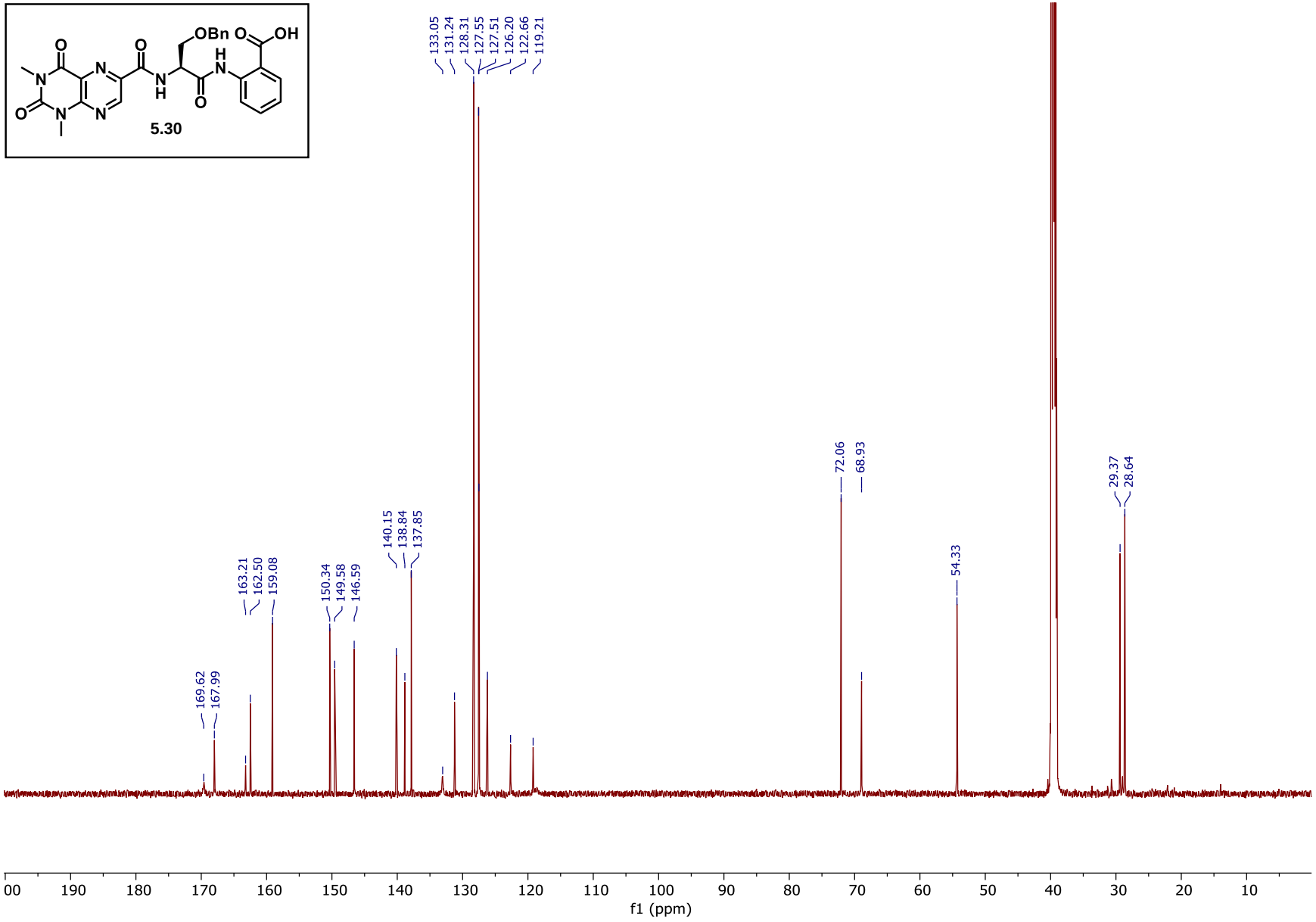
OBn
O
OH
O
N
H
N
O
N
N
N
O
N
5.30
133.05
131.24
128.31
127.55
127.51
126.20
122.66
119.21
72.06
68.93
29.37
28.64
54.33
140.15
138.84
137.85
163.21
162.50
159.08
150.34
149.58
146.59
169.62
167.99
00
190
180
170
160
150
140
130
120
110
100
90
80
70
60
50
40
30
20
10
f1 (ppm)

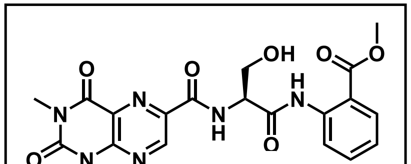

5.10a

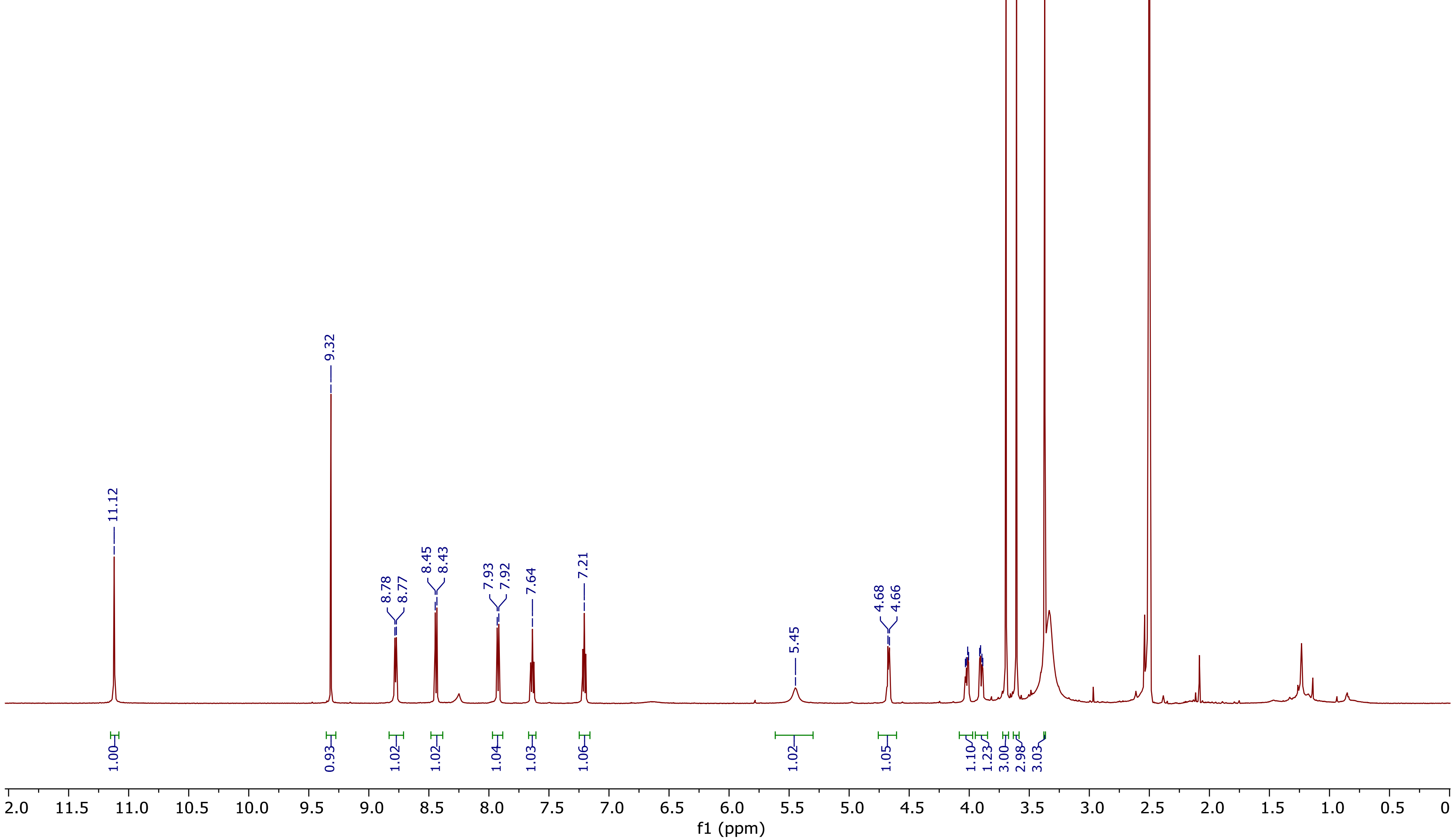

4.03 4.02 4.01 4.01 3.91 3.91 3.89 3.89 3.69 3.61 3.37
11.12
9.32
8.78 8.77
8.45 8.43
7.93 7.92
7.64
7.21
5.45
4.68 4.66
1.00
0.93
1.02
1.02
1.04
1.03
1.06
1.02
1.05
1.10
1.23
3.00
2.98
3.03
2.0 11.5 11.0 10.5 10.0 9.5 9.0 8.5 8.0 7.5 7.0 6.5 6.0 5.5 5.0 4.5 4.0 3.5 3.0 2.5 2.0 1.5 1.0 0.5 0
f1 (ppm)

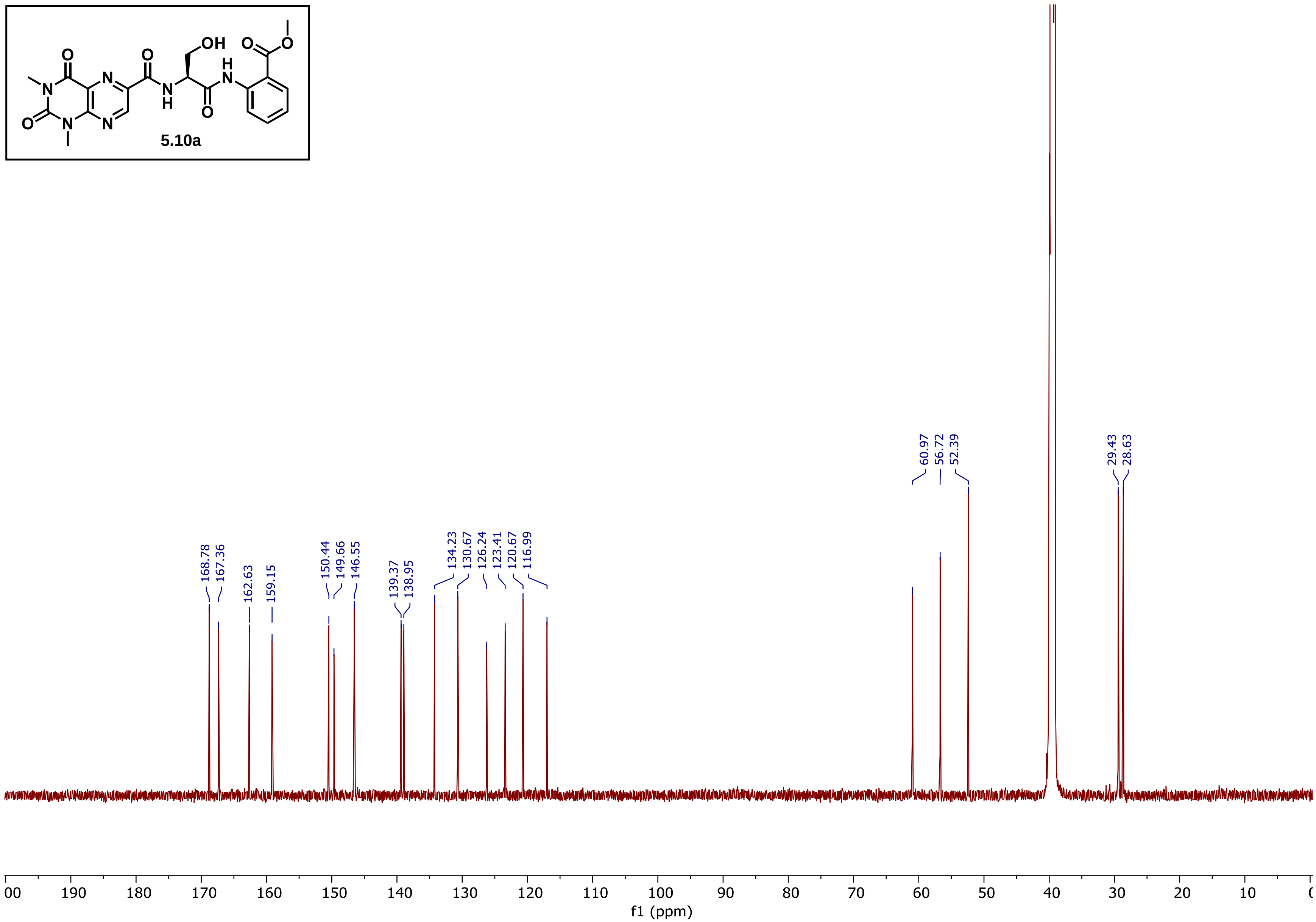
5.10a
168.78
167.36
162.63
159.15
150.44
149.66
146.55
139.37
138.95
134.23
130.67
126.24
123.41
120.67
116.99
60.97
56.72
52.39
29.43
28.63
f1 (ppm)

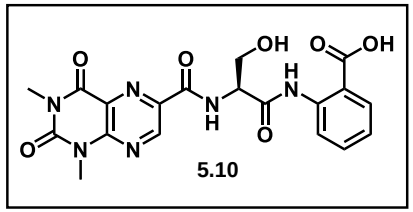
O
O
OH
O
OH
N
N
H
N
N
N
H
O
O
N
5.10

4.05
4.04
3.90
3.88
3.60
3.37
9.32
8.78
8.77
8.60
8.59
7.95
7.94
7.54
7.11
5.41
4.62
4.61
13.64
12.20
0.81
0.72
1.00
0.96
1.09
1.01
0.99
1.03
0.99
0.99
1.01
1.02
3.16
3.02
f1 (ppm)

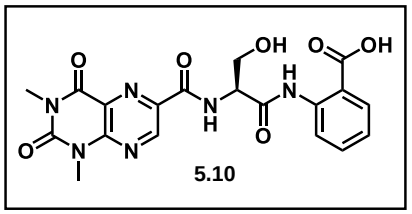
O
O
OH
O
OH
N
N
H
N
N
H
O
O
N
N
5.10

169.21
168.62
163.07
162.60
159.11
150.36
149.56
146.59
140.32
139.02
136.13
131.16
126.15
122.65
119.35
61.04
56.87
29.42
28.65
190
180
170
160
150
140
130
120
110
100
90
80
70
60
50
40
30
20
10
f1 (ppm)

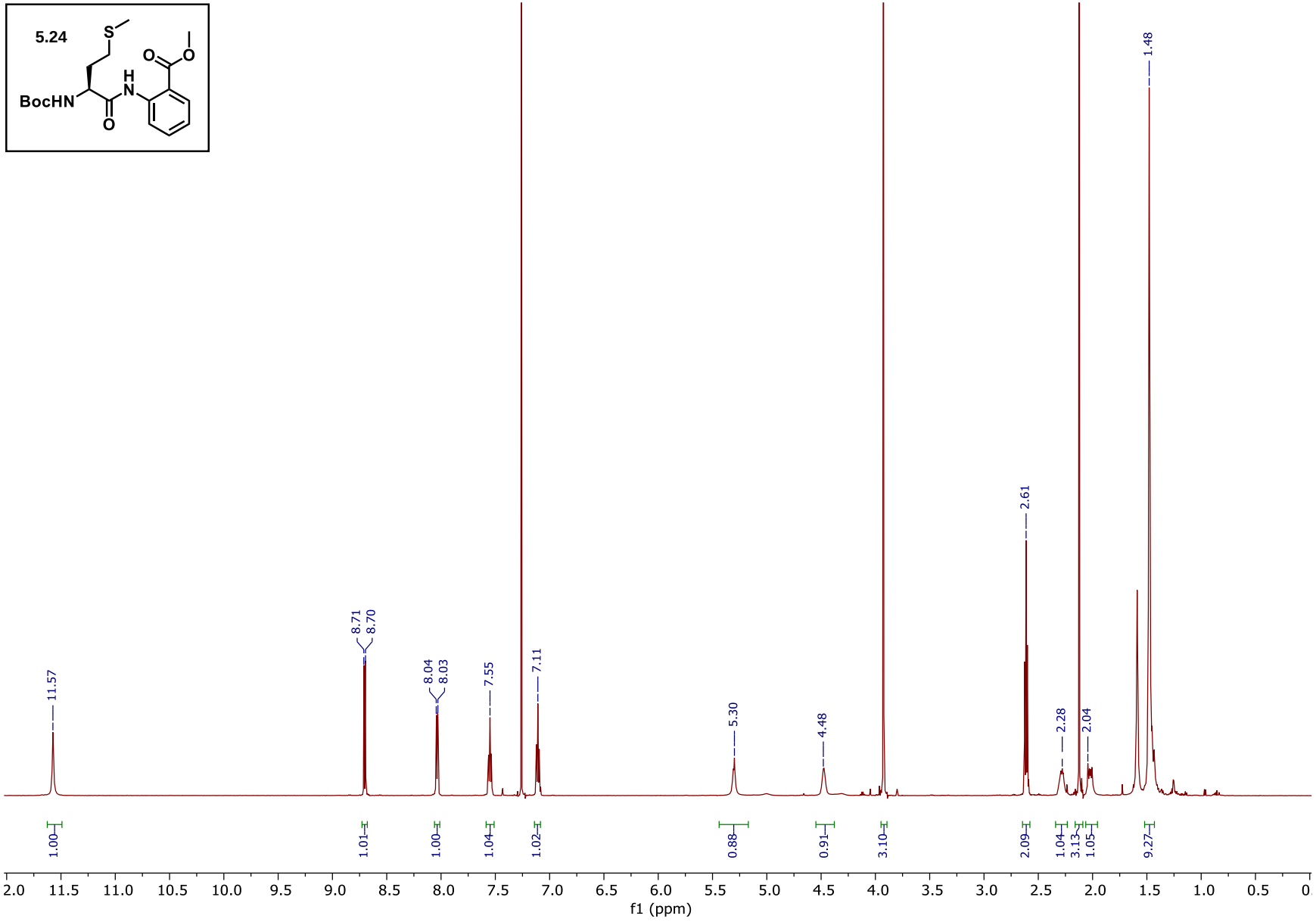
5.24
S
O
O
H
N
BocHN
O
11.57
8.71
8.70
8.04
8.03
7.55
7.11
5.30
4.48
2.61
2.28
2.04
1.48
1.00
1.01
1.00
1.04
1.02
0.88
0.91
3.10
2.09
1.04
3.13
1.05
9.27
f1 (ppm)

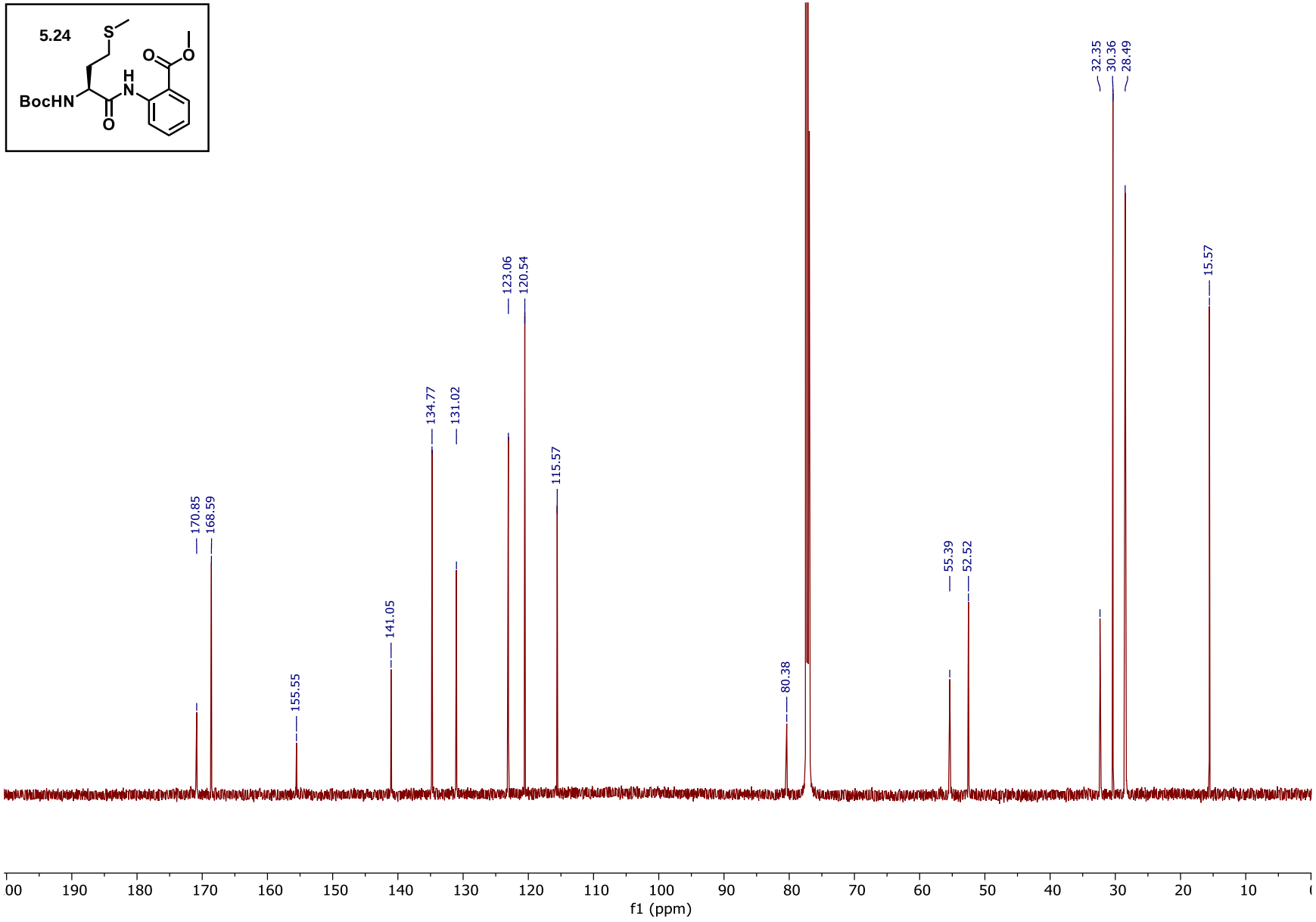
5.24
S
O
O
H
N
BocHN
O
170.85
168.59
155.55
141.05
134.77
131.02
123.06
120.54
115.57
80.38
55.39
52.52
32.35
30.36
28.49
15.57
f1 (ppm)

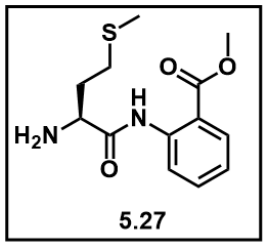
S
O
O
H
N
H_2N
O
5.27

11.49
8.52
8.51
8.02
8.01
7.53
7.26 CDCl3
7.13
4.37
3.92
2.71
2.67
2.36
2.35
2.09
0.97
0.98
0.97
0.98
1.00
0.96
3.00
2.17
1.93
2.92
f1 (ppm)

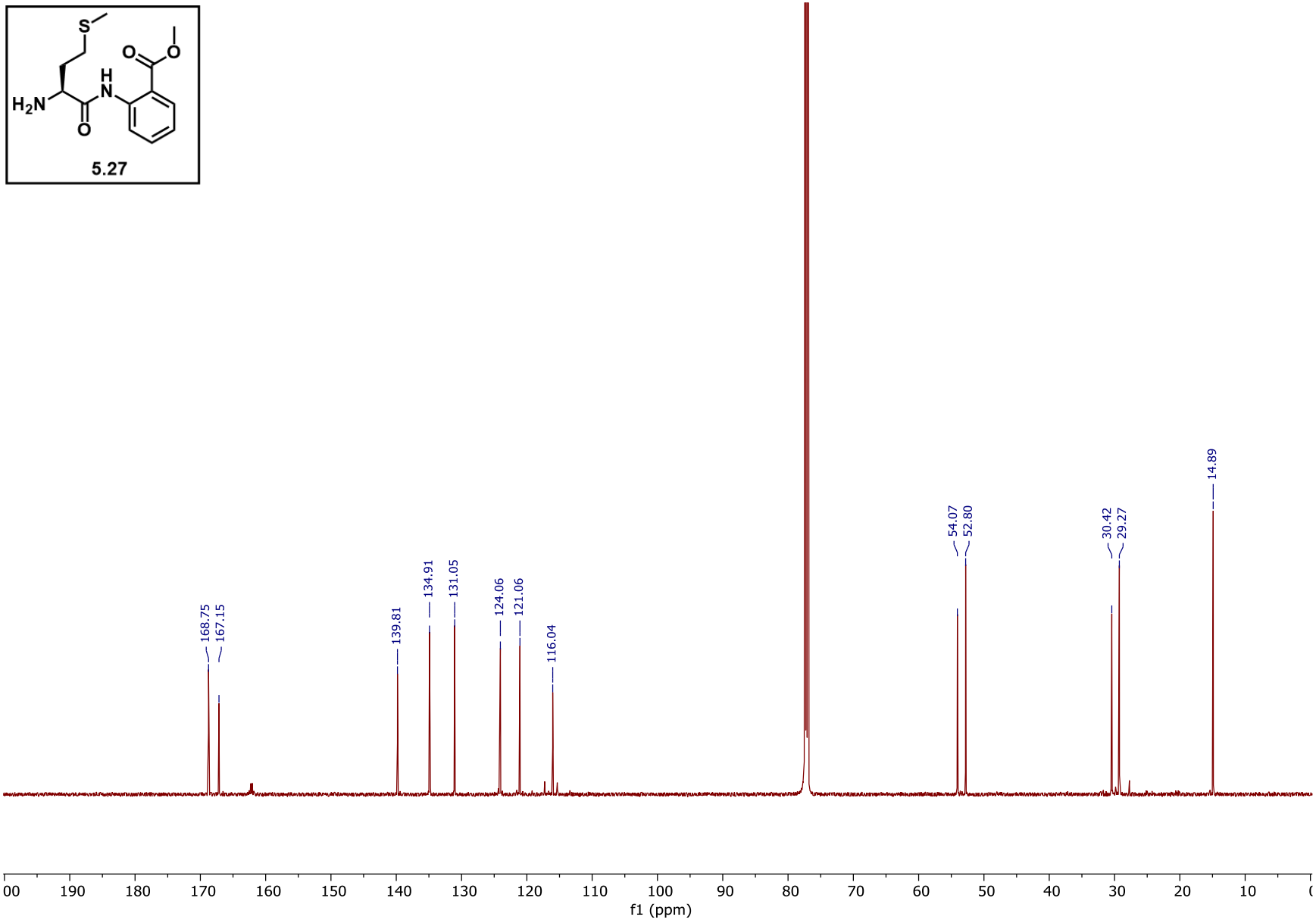
5.27
168.75
167.15
139.81
134.91
131.05
124.06
121.06
116.04
54.07
52.80
30.42
29.27
14.89
f1 (ppm)

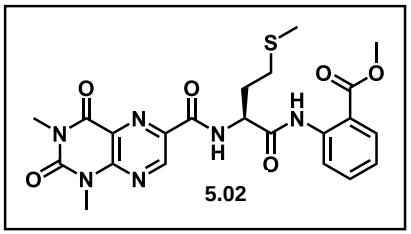
5.02

11.05
9.30
9.18
9.17
8.35
8.33
7.91
7.89
7.63
7.21
4.83
4.82
3.67
3.60
3.36
2.62
2.56
2.30
2.25
2.08
0.97
0.91
0.88
2.09
0.97
1.00
1.00
0.96
2.99
3.00
3.47
0.94
0.96
0.98
0.96
2.95
2.0 11.5 11.0 10.5 10.0 9.5 9.0 8.5 8.0 7.5 7.0 6.5 6.0 5.5 5.0 4.5 4.0 3.5 3.0 2.5 2.0 1.5 1.0 0.5 0
f1 (ppm)

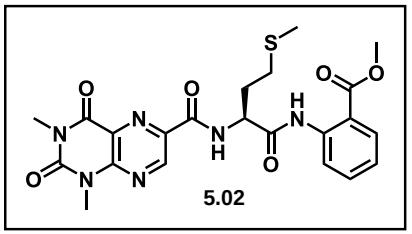
5.02

169.92
167.33
163.05
159.20
150.44
149.53
146.77
139.45
139.14
134.10
130.60
126.27
123.53
121.01
117.68
53.44
52.36
30.25
29.98
29.41
28.63
14.58
f1 (ppm)

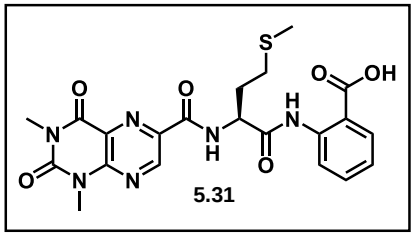
5.31

13.55
11.79
9.31
9.23
9.22
8.58
8.56
7.95
7.94
7.59
7.14
4.82
4.82
3.60
3.37
2.59
2.54
2.35
2.24
2.07
0.86
1.01
1.03
0.84
0.98
1.02
1.00
1.00
0.98
2.97
3.10
0.89
1.40
0.96
0.94
2.80
f1 (ppm)

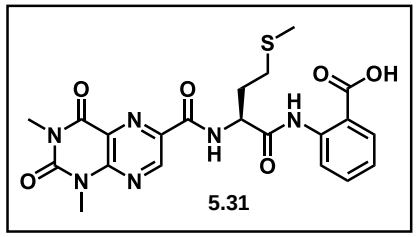
S
O
OH
O
O
N
N
H
N
H
O
O
N
N
5.31

174.50
169.91
169.36
163.01
159.16
150.38
149.47
146.81
140.35
139.47
133.90
131.19
126.25
122.84
119.67
53.44
30.70
30.06
29.41
28.65
14.55
f1 (ppm)

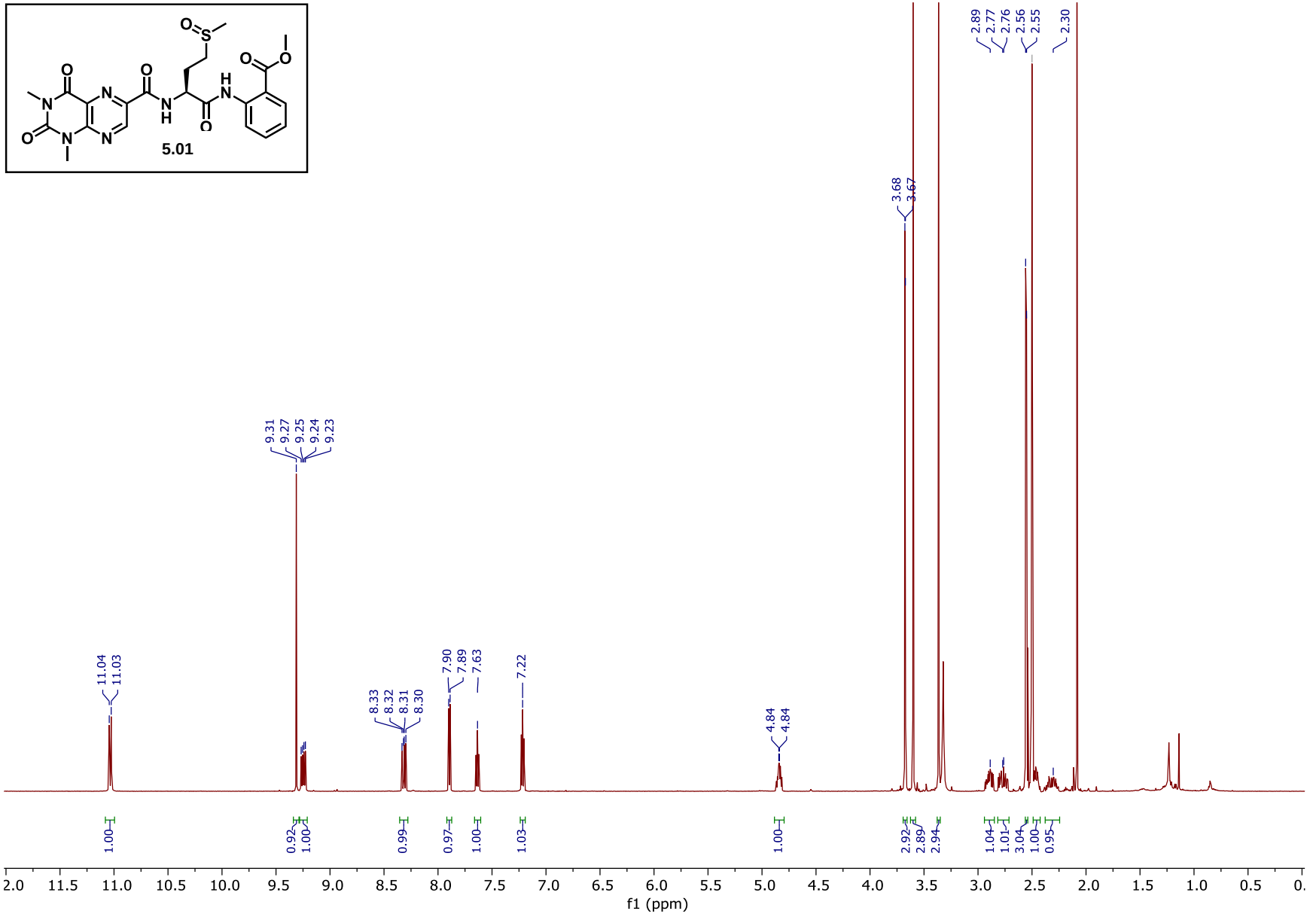
5.01
11.04
11.03
9.31
9.27
9.25
9.24
9.23
8.33
8.32
8.31
8.30
7.90
7.89
7.63
7.22
4.84
4.84
3.68
3.67
2.89
2.77
2.76
2.56
2.55
2.30
1.00
0.92
1.00
0.99
0.97
1.00
1.03
1.00
2.92
2.89
2.94
1.04
1.01
3.04
1.00
0.95
f1 (ppm)

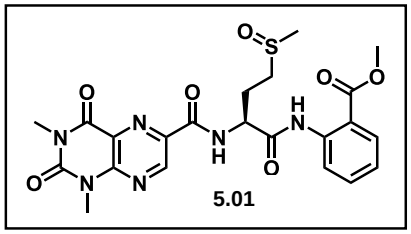
5.01

169.43
169.41
167.28
167.27
163.03
162.97
159.17
159.16
150.43
149.54
146.81
146.78
139.39
139.35
138.99
138.92
134.06
134.02
130.59
130.58
126.26
123.65
123.62
121.27
121.17
118.06
117.91
53.57
53.33
52.37
49.93
49.78
38.10
37.95
29.41
28.63
24.22
23.85
00
190
180
170
160
150
140
130
120
110
100
90
80
70
60
50
40
30
20
10
f1 (ppm)

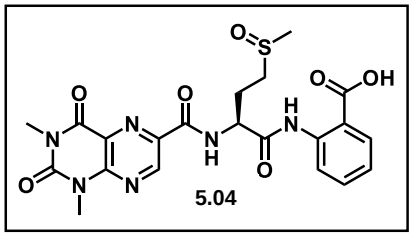
5.04

13.75
12.87
9.32
9.26
9.24
9.23
9.22
8.54
7.93
7.92
7.92
7.48
7.08
4.79
4.78
3.58
3.36
2.86
2.77
2.54
2.48
2.32
0.68
0.92
0.98
0.97
1.00
0.97
1.00
0.97
2.93
3.32
0.99
0.90
3.19
1.03
1.00
f1 (ppm)

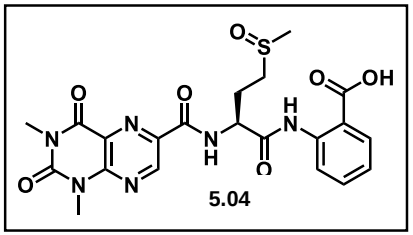
5.04

169.16
169.12
169.07
163.13
162.92
162.85
159.17
150.36
149.41
149.40
146.89
146.87
140.29
140.27
139.58
139.54
131.12
126.21
122.44
119.24
53.70
53.47
50.06
49.95
38.08
37.92
30.70
29.38
28.64
24.27
23.92
f1 (ppm)